

PALACKÝ UNIVERSITY OLOMOUC

Faculty of Science

Laboratory of Growth Regulators



Biological activity of novel auxin synthetic derivatives

Ph.D. thesis

Author:	Mgr. Barbora Pařízková
Study programme:	P1527 / Biology
Field of Study:	Experimental Biology
Form of study:	Daily
Supervisor:	doc. Mgr. Ondřej Novák, Ph.D.
Consultant:	Assoc. Prof. Stéphanie Robert

Bibliographical identification

Author's first name and surname	Mgr. Barbora Pařízková
Title of thesis	Biological activity of novel auxin synthetic derivatives
Type of thesis	Ph.D.
Department	Laboratory of Growth Regulators
Supervisor	doc. Mgr. Ondřej Novák, Ph.D.
The year of presentation	2019
Abstract	<p>Auxin is a crucial hormonal player that in cooperation with other phytohormones regulates proper plant growth and development. Its precise spatiotemporal distribution in specific tissues together with auxin perception at a cellular level underlies a plethora of auxin actions. This thesis presents a characterization of new synthetic structural auxin analogues that can serve as a chemical tool for investigation of the molecular mechanisms of auxin physiology. The fluorescent auxin derivatives can help to determine auxin transport sites within various developmental processes while the selective auxin agonists can elucidate the roles of specific auxin co-receptors in auxin-regulated responses. Sensitive purification and detection methods based on liquid chromatography - mass spectrometry (LC-MS) technique have also been developed to evaluate the metabolization of synthetic auxin analogues <i>in planta</i>. Taken together, the novel synthetic auxin derivatives together with MS-based methods for evaluation of their stability <i>in vivo</i> represent a powerful tool for unravelling the complexity of auxin actions.</p>
Keywords	auxin, fluorescent labelling, LLE, IAC, UHPLC-MS/MS
Number of pages	61
Number of supplements	5
Language	English

Acknowledgement

This work was performed at the Laboratory of Growth Regulators, Palacký University in Olomouc and would not exist without the great patience of my supervisor doc. Mgr. Ondřej Novák, Ph.D., who provided me with advice, support and encouragement. I am also grateful to Assoc. Prof. Stéphanie Robert and her research group from Umeå Plant Science Centre (UPSC) who enabled me to discover the beauties and deceits of plant biology and, more importantly, became very good friends and important people to me. I would like to thank Mgr. Karel Doležal Dr., DSc. for critical reading of this thesis and for a number of very valuable discussions over all four years. I want to acknowledge all my colleagues from both Olomouc and Umeå departments who always created a friendly and supportive working atmosphere, provided me with scientific and technical assistance and did not hesitate to help anytime I needed it. I also thank my family and friends for their never-ending support to finish my Ph.D.

Declaration

Hereby I declare that the thesis summarizes original results obtained during my Ph.D. under the great supervision of doc. Mgr. Ondřej Novák, Ph.D. and Assoc. Prof. Stéphanie Robert using the literature sources listed below

In Olomouc,

.....

Content

List of papers.....	6
Abbreviations.....	8
1 Introduction.....	10
2 Aims and scopes.....	11
3 Literature review.....	12
3.1 Plant hormones.....	12
3.2 Auxins.....	12
3.2.1 Structure-activity relationship – importance of synthetic auxins.....	13
3.2.2 Auxin distribution regulates plant development.....	18
3.2.3 Auxin bioassays.....	28
3.2.4 Analytical methods for auxin analysis.....	31
4 Materials and methods.....	37
4.1 Chemicals.....	37
4.2 Plant materials and growth conditions.....	37
4.3 Methods.....	38
4.3.1 Auxin-responsive bioassays.....	38
4.3.2 Confocal microscopy.....	39
4.3.3 Extraction and purification methods.....	39
4.3.4 UHPLC-MS/MS methods.....	40
5 SURVEY OF RESULTS.....	41
5.1 Biological characterization of new fluorescent auxins analogues.....	41
5.2 Method development for studying the metabolic conversion of synthetic auxin analogues <i>in vivo</i>	42
6 Conclusion and perspectives.....	47
7 References.....	48
8 Supplements I – V.....	61

List of papers

This thesis summarizes and links the following papers that are referred in the text by Roman numerals I-V and attached at the end of the thesis in the Supplementary section.

- I** **Pařízková B.**, Pernisová M., Novák O. (2017) What Has Been Seen Cannot Be Unseen—Detecting Auxin *In Vivo*. *Int. J. Mol. Sci.* **18** (12), 2736.
- II** Bielešová K¹, **Pařízková B**¹, Kubeš M., Husičková A., Kubala M., Sedlářová M., Doležal K., Strnad M., Novák O., Žukauskaitė A. (2018) New fluorescently labeled auxins exhibit promising anti-auxin activity. *N. Biotechnol.* **48**, 44-52.
- III** **Pařízková B.**¹, Žukauskaitė A.¹, Vain T.¹, Grones P.¹, Kubeš M., Kieffer M., Karel Doležal K., Kepinski S., Napier R., Strnad M., Robert S., Novák O. New auxin fluorescent probes for live imaging of auxin sites of action in plants (*in preparation*).
- IV** Vain T.¹, Raggi S.¹, Ferro N., Kumar Barange D., Kieffer M., Ma Q., Doyle S. M., Thelander M., **Pařízková B.**, Novák O., Ismail A., Enquist P-A., Rigal A., Łangowska M., Harborough S. R., Zhang Y., Ljung K., Callis J., Almqvist F., Kepinski S., Estelle M., Pauwels L., Robert S. (2019) Selective auxin agonists induce specific AUX/IAA protein degradation to modulate plant development. *Proc. Natl. Acad. Sci. USA* **116** (13), 6463–6472.
- V** Eyer L., Vain T., **Pařízková B.**, Oklestkova J., Barbez E., Kozubíková H., Pospíšil T., Wierzbicka R., Kleine-Vehn J., Fránek M., Strnad M., Robert S., Novak O. (2016) 2,4-D and IAA Amino Acid Conjugates Show Distinct Metabolism in *Arabidopsis*. *PLoS One* **11** (7), e0159269.

¹ These authors contributed equally to the presented works.

Contribution report

- I** As a first author, BP performed a literature review of traditional and novel methods for visualization of auxin distribution *in vivo*.
- II** As a first author, BP designed and performed the experiments for testing of biological activity of novel auxin fluorescent derivatives and contribute to writing of the manuscript.
- III** As a first author, BP performed the bioassays evaluating the biological activity and *in vivo* distribution of novel fluorescent auxin analogues. BP also developed a purification and detection method for evaluation of metabolization of analogues in plants and wrote the manuscript.
- IV** As a co-author, BP optimized a purification and detection method for determination of stability of tested selective auxin agonists *in planta*.
- V** As a co-author, BP developed a purification method and quantification method for determination of 2,4-D and its metabolites in plant matrix and using the method BP identified two 2,4-D metabolites and their metabolism rates in *Arabidopsis*.

Abbreviations

2,4-D	2,4-dichlorophenoxyacetic acid
2,4,5-T	2,4,5-trichlorophenoxyacetic acid
4-MUG	4-methylumbelliferyl β -D-glucuronide
4-MU	4-methyl umbelliferone
4-Cl-IAA	4-chloroindolyl-3-acetic acid
AA	amino acid
ABA	abscisic acid
ABP1	AUXIN BINDING PROTEIN1
ABCB	ATP-binding cassette B
CAN	acetonitrile
AFB	AUXIN SIGNALING F-BOX
ARF	AUXIN RESPONSE FACTOR
AUX1/LAX	AUXIN RESISTANT 1/LIKE AUX
Aux/IAA	AUXIN/INDOLE-3-ACETIC ACID
AXR	AUXIN- RESISTANT
ATP	adenosine-5'-triphosphate
BRM	BRAHMA
BSA	BOVINE SERUM ALBUMIN
ccvTIR1	concave TIR1
CE	capillary electrophoresis
CK	cytokinin
cvxIAA	convex IAA
DAD	diode array detection
DPB	E2F DIMERIZATION PARTNER B
E2FC	E2 PROMOTER TRANSCRIPTION FACTOR C
ELISA	enzyme-linked immunosorbent assay
ER	endoplasmic reticulum
FITC	fluorescein
GA	gibberellin
GC	gas chromatography
GFP	green fluorescent protein
GH3	GRETCHEN HAGEN 3
GUS	β -glucuronidase
HLB	hydrophilic-lipophilic balance
HRMS	high-resolution mass spectrometry
IAA	indolyl-3-acetic acid
IAC	immunoaffinity chromatography
IAOx	indolyl-3-acetaldoxim
IAM	indol-3-ylacetamid
IAMT1	IAA CARBOXYL METHYLTRANSFERASE1
IAR3	IAA-ALANINE RESISTANT3
IBA	indolyl-3-butyric acid
IBR	INDOL-3-BUTYRIC ACID RESPONSE
ILL2	IAA-LEUCINE RESISTANT-LIKE2
ILR1	IAA-LEUCIN RESISTANT1
IPyA	indolyl-3-pyruvic acid
JA	jasmonic acid
LC	liquid chromatography
LLE	liquid-liquid extraction

LLME	liquid-liquid microextraction
LMr	low molecular weight fraction
MATE	multidrug and toxic compound extrusion
MAX	mixed-mode, strong anion-exchange
MCPA	2-metyl-4-chlorphenoxyacetic acid
MIP	molecularly imprinted polymer
MRM	multiple reaction monitoring
MS	mass spectrometry
NAA	1-naphtalene acetic acid
NBD	7-nitro-2,1,3-benzoxadiazole
NMR	nuclear magnetic resonance
NPA	1-naphthylphthalamic acid
PAA	phenylacetic acid
PAT	polar auxin transport
PEO-IAA	α -(phenylethyl-2-oxo)-IAA
PILS	PIN-LIKES
PIN	PIN-FORMED
PM	plasma membrane
qPCR	quantitative polymerase chain reaction
RFP	RED FLUORESCENT PROTEIN
RITC	rhodamine
RIA	radioimmunoassay
RN1-4	RubNeddin1 - 4
ROP	RHO-LIKE GTPASES OF PLANTS
SA	salicylic acid
SAR	structure-activity relationship
SCF	S-PHASE KINASE ASSOCIATED PROTEIN 1 - CULLIN 1 - F-BOX
SKP2A	S-PHASE KINASE-ASSOCIATED PROTEIN 2A
SPE	solid phase extraction
SPR	surface plasmon resonance
SSF	solid-surface fluorescence
SUR	SUPERROOT
TAA1	TRYPTOPHAN AMINOTRANSFERASE OF ARABIDOPSIS 1/
TAM	tryptamine
TAR	TRYPTOPHAN AMINOTRANSFERASE RELATED
TAZ	thiazolidine
TIR1	TRANSPORT INHIBITOR RESISTANT1
TF	transcription factor
TOF	time-of-flight
Trp	L-tryptophan
VMAE	vacuum microwave-assisted extraction
VPE	vapor phase extraction
WAT1	WALLS ARE THIN1
X-GlcA	X-glucuronide

1 Introduction

Auxins are a class of plant hormones that control almost all physiological processes leading to proper plant growth and development. Indolyl-3-acetic acid (IAA) is considered as the most important naturally occurring auxin. Uneven distribution of auxins within specific tissues regulates organogenesis and plant shape in response to exo- and endogenous stimuli. The auxin maxima establishment and maintenance are regulated by the coordination of auxin biosynthesis, metabolism and active polar transport. Furthermore, a wide array of small synthetic molecules with auxin activities has been produced. The biological activity of compounds such as 2,4-dichlorophenoxyacetic acid (2,4-D) and 1-naphtalene acetic acid (NAA) is concentration dependent and therefore they can be used as growth promoters in tissue culture or inhibiting herbicides in agriculture.

The preparation of auxin synthetic derivatives and the study of their structure-activity relationships (SAR) help to unravel the mechanisms of auxin action. With the knowledge of structural requirements, various auxin analogues can be prepared for specific purposes. For example, selective auxin agonists and antagonists of auxin binding proteins can help to evaluate their role in auxin signalling, biosynthesis and transport. SAR analysis has been extensively used to generate caged and, more importantly, fluorescently labelled plant hormones. Coupling of the auxin molecule with fluorescent probe provides a powerful tool to visualize auxin distribution in plants in a minimal invasive manner. In vivo and in real time visualization of the compounds enable study of the relationship between auxin action and localization in plants with a high spatiotemporal resolution at the tissue, cellular and subcellular levels. Moreover, the evaluation of the chemical stability of auxin derivatives in planta is a crucial step for compound characterization. Development of methods employing sensitive detection techniques such as mass spectrometry enables us to estimate the potential metabolization rates of tested compounds. Accurate identification of possible metabolites also helps to unravel the molecular mechanisms behind the mode of action of new auxin analogues.

2 Aims and scope

The presented Ph.D. thesis deals with SAR study of newly synthesized auxin analogues. A multidisciplinary approach including chemical genomics, reverse genetics and sensitive mass spectrometry (MS)-based methods helped to unravel the mode of action of prepared analogues. Altogether, this work led to the biological characterization of new fluorescent auxin derivatives, selective auxin agonists and to new insights into 2,4-D metabolism *in planta*.

The main aims of the work described in this thesis were as follows:

- to review the traditional and novel methods for visualization of auxin distribution *in vivo*,
- to perform biological and chemical-physical characterization of new synthetic auxin derivatives in different auxin-responsive assays to evaluate their mode of action,
- to study fluorescent properties, tissue-specific distribution and subcellular localization of new fluorescent auxin analogues by confocal microscopy,
- to develop an extraction, purification and detection method for determination and quantification of fluorescently labelled auxin derivatives, novel auxin selective agonists and 2,4-D together with their potential metabolites using MS-based techniques in order to evaluate the metabolization of the compounds *in planta* with respect to their structure.

3 Literature review

3.1 Plant hormones

Proper growth and development of multicellular and complex organisms such as higher plants require an efficient communication system from the subcellular to the whole organism. Plant hormones (phytohormones) are organic substances naturally occurring at extremely low concentrations (Taiz and Zeiger, 2010). Several groups of plant hormones with various physicochemical properties and with wide range of physiological effects have been identified so far including cytokinins (CKs), auxins, ethylene, brassinosteroids (BRs), abscisates (ABAs), jasmonates (JAs), gibberellins (GAs), salicylic acid (SA) and strigolactones (Davies, 2010). Via their specific receptors, each group regulates all aspects of plant development from embryogenesis, organ growth and morphogenesis, reproduction to stress tolerance or responses to environmental stimuli (Davies, 2010). Importantly, the developmental processes are modulated by the dynamic interactions among different plant hormones. Dependent on the biological context, this so-called hormonal cross-talk can be synergistic or antagonistic (Vanstraelen and Benková, 2012).

Besides plant hormones, other endogenous but more abundant compounds play a role of growth regulators such as polyamines, oligosaccharides, polypeptides or phenolic compounds (Taiz and Zeiger, 2010). Moreover, karrikins were recently discovered as a new group of plant morphogenes (Flematti et al., 2004; Van Staden et al., 2004). Karrikins lie on the interface between hormones and growth regulators since they are not endogenously present in plants in physiological conditions but once produced by burning of plant material, molecular mode of action of karrikins shares many components with strigolactone signalling pathways (Chiwocha et al., 2009).

3.2 Auxins

Auxins were the first group of plant hormones to be discovered, when in the 19th century Charles Darwin with his son Francis suggested the presence of moving regulators that control the growth and movement of the plants (Darwin and Darwin, 1880). According to their theory, light triggers the signal in the tip of the coleoptile of etiolated canary grass seedlings (*Avena sativa* L.) which is then transported to the growth zone where

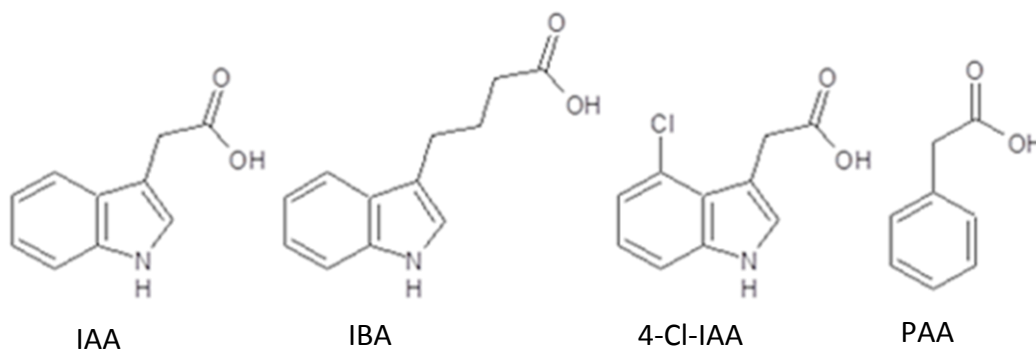


Fig. 1 Chemical structures of naturally occurring auxins.

the bending of the shoot towards the light source occurs (Darwin and Darwin, 1880). Later on, Frits W. Went proved that the asymmetric distribution of signalling molecules results in the more intense cell growth on the shaded side of the coleoptile. This differential growth leads to the phototropic movement towards the source of light (Went, 1926). He called these molecules auxins (from Greek *auxein* – to grow). The first auxin that was isolated was heteroauxin, later identified as indolyl-3-acetic acid (IAA, Fig. 1) (Kögl et al., 1934; Thiman, 1935).

Since then, auxins have been shown to be involved in almost every aspects of plant development such as cell division, expansion and differentiation (Shao, 2016), embryogenesis (Jenik and Barton, 2005), organogenesis and meristem patterning (Hamant et al., 2008), phototropism and gravitropism (Friml, 2003), fruit ripening (De Jong et al., 2009), apical dominance (Leyser, 2005) or leaf abscission (Rubinstein and Leopold, 1963). Besides IAA, which is the most potent naturally occurring auxin, three other auxinic compounds were discovered in plants - indolyl-3-butyric acid (IBA), 4-chloroindolyl-3-acetic acid (4-Cl-IAA) and phenylacetic acid (PAA) (Fig. 1). These exhibit lower biological activity (Simon and Petrášek, 2011). Moreover, recent study elucidating the auxin metabolome in *Arabidopsis thaliana* gave rise to the question of IBA as an endogenous active auxin, since the levels of IBA in *Arabidopsis* have been under the limit of detection until now (Novák et al., 2012; Frick and Strader, 2018).

3.2.1 Structure-activity relationship – importance of synthetic auxins

After the chemical structure of IAA was revealed, the structure-activity relationship (SAR) studies led to the discovery of diverse synthetic derivatives (Zimmerman and Wilcoxon,

1935; Bentley 1950; Peterson 1967) with auxinic activity but with no knowledge on their mode of action. The SAR study indicated that the indole group is not essential for sustaining auxinic activity and can be replaced by a system of one or more condensed aromatic rings (Robert et al., 1967). Years of comprehensive studies resulted in defining the general structural compound characteristics required for auxin-like activity – carboxyl group separated from the planar aromatic ring in the specific position and distance (Ferro et al., 2010). Over the years, a plethora of auxin synthetic analogues with various applications in both basic and applied research were generated (reviewed in Ma et al., 2018).

The 1940s, mainly during World War II, were a very potent period for the development of auxin-like growth regulators. Compounds such as naphthalene-1-acetic acid (NAA); 2,4-dichlorophenoxyacetic acid (2,4-D); 2,4,5-trichlorophenoxyacetic acid (2,4,5-T) and dicamba (Fig. 2) are still broadly used as a chemical tool in basic research as well as herbicides in agriculture and horticulture (Grossman, 2009). At lower concentrations, these compounds display similar developmental responses as IAA, but are more stable due to lower metabolic inactivation and light degradation (Yamakawa et al., 1979, Mithila et al., 2011). Hence, they are used e.g. for promotion of parthenocarpy, protection against leaf and fruit fallout, rooting during plant propagation or auxin-induced ethylene synthesis leading to faster flowering and fruit ripening (Taiz and Zeiger, 2010). At higher concentrations, auxin activity displays a toxic effect and consequent death of the plant (Mithila et al., 2011). Distinct metabolism in monocots and dicots makes these compounds potent herbicides with a selective mode of action to control weed growth (Grossmann, 2009).

Due to the complexity of auxin action, the use of chemical biology approach employing small-molecule probes that help to dissect auxin responses has been on a rise (De Rybel, 2009). Proauxins are synthetic auxin analogues consisting of active auxin compound attached to the hydrophobic heterocyclic moiety with amide or ester bond making the molecule non-active but more lipophilic (Ma et al., 2018). Therefore, such compounds display better uptake to the tissues unreachable for auxin itself. Tissue-specific enzymatic release of active auxin can separate different developmental processes as primary root growth and hypocotyl elongation (Savaldi-Goldsein et al., 2008) and help to unravel molecular mechanisms behind their regulation.

A similar strategy of modulating plant development is represented by caged auxins (Ma et al., 2018). Active auxin is caged with protecting group resulting in the biologically inactive compound. The caging group can be cleaved by light with the desired wavelength. Since the illumination is an easily tunable parameter (in term of intensity, area of irradiation and time frame), the caged auxins represent powerful tools with spatial and temporal resolution of application (Hayashi et al., 2015).

Revealing the mechanisms of auxin perception (Dharmasiri et al., 2005a, b) together with the crystal structure of auxin receptor TRANSPORT INHIBITOR RESISTANT1 (TIR1) (Tan et al., 2007) enabled to employ more effective methods of structural design for various auxin analogues. In the basic auxin perception model described below in more detail (chapter 3.2.2.3), auxin is bound to the TIR1 receptor and promotes the interaction of TIR1 with small peptides AUXIN/INDOLE-3-ACETIC ACID (Aux/IAA), transcriptional inhibitors. The interaction of TIR1 with Aux/IAs releases transcription factors (TF) from repression and the expression of auxin responsive genes is triggered (reviewed in Weijers and Friml, 2009). Moreover, these studies showed that the binding pocket of TIR1 and its analogues AUXIN SIGNALING F-BOX1-5 (AFB1-5) is promiscuous and can accommodate compounds significantly differing in structure with diverse affinities (Lee et al., 2014). These compounds increase the affinity of TIR1/AFBs to Aux/IAs and serve as potent complex or selective agonists. Moreover, the compound structure modification can cause the TIR1/AFBs steric restriction to interact with transcriptional repressors leading into anti-auxin activity (Ma, et al., 2018). The auxin or anti-auxin activity of the structural analogue and the potency of the biological effect is influenced by the chemical character of the side chain modification (Hayashi et al., 2008) and the length of such molecular linker (Bieleszová et al., 2018). *In silico* modelling was used for rational design of auxin antagonists α -(phenylethyl-2-oxo)-IAA (PEO-IAA) and optimized structure of auxinole (α -(2,4-dimethylphenylethyl-2-oxo)-IAA) (Hayashi et al., 2012) (Fig. 2), which are today widely used as a valuable tool for reversible blocking of auxin signalling (Sugawara, 2015; Fendrych et al., 2016). Moreover, such compounds can be very specific in their mode of action inducing the selective interaction between TIR1 and particular Aux/IAs. Selective auxin agonists can separately modulate distinct developmental processes and thus help to discover molecular mechanisms of auxin-regulated responses (Vain et al., 2019).

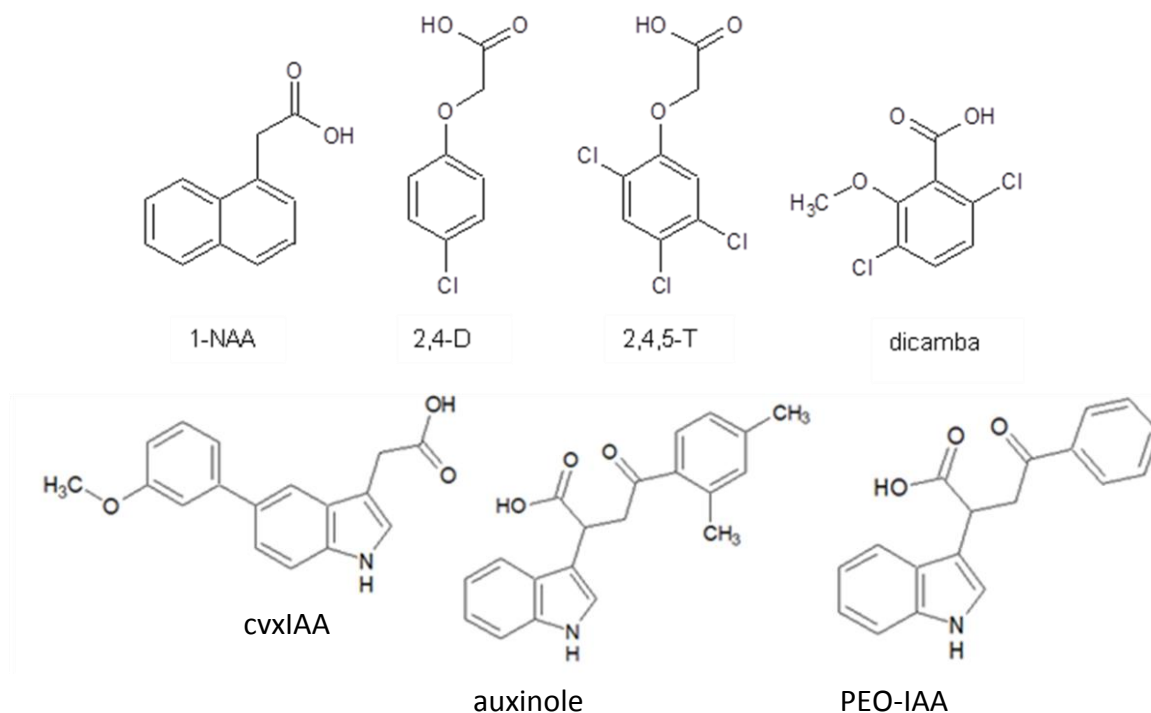


Fig. 2 Chemical structures of synthetic auxin analogues.

A very novel direction of chemical biology was opened by Uchida et al. (2018) who designed an artificial IAA-TIR1 interaction based on bump-and-hole approach. A synthetic auxin derivative with the additional functional group (convex IAA, cvxIAA – bump), not binding into the wild-type TIR1, interacts selectively with engineered TIR1 carrying a single amino acid substitution creating a hole in the binding pocket (concave TIR1, ccvTIR1). Since the cvxIAA triggers the auxin-related responses only in ccvTIR1 expressing seedlings and vice versa ccvTIR1 selectively perceives cvxIAA, this system represents a very elegant tool to investigate the TIR1-regulated processes (Fendrych, 2018). This study has already been updated by a super strong engineered auxin-TIR1 pair with greater affinity between cvxIAA and ccvTIR1 (Yamada et al., 2018).

The discovery of structural groups important for auxinic activity, as a result of SAR studies, has opened new pathways for structural analogue design. In addition, this has helped to identify sites for possible attachment of molecular linkers. For example, coupling auxin molecule with fluorescent dye enables visualization of the auxin distribution with high spatiotemporal resolution and in minimal invasive manner (Muscolo et al., 2007; Sokołowska et al., 2014; Hayashi et al., 2014; Bielešová et al., 2018). The auxin molecule as such is too small to generate immune response in animals,

but can be linked to a carrier protein to efficiently produce antibodies useful e. g. for immunohistochemical localization of IAA in plant tissues (Sauer et al., 2006) or selective purification of IAA and its metabolites from various plant matrices (Marcussen et al., 1989, Pěňčík et al., 2009). Plus, biotinylated or sepharose-linked plant hormones enabled the discovery of phytohormone binding proteins (Pedron et al., 1998; Reizelman et al., 2003), characterization of the of the brassinosteroid receptor binding site (Kinoshita et al., 2005) or visualization of abscisic acid-perception sites in *Vicia faba* stomatal guard cells (Yamazaki et al., 2003).

Taken together, years of extensive SAR studies have been advanced by today's high-throughput screening strategies and *in silico* mathematical modelling for pre-screenings of selective protein-ligand interactions. Such novel approaches helped to generate numerous auxin-derived compounds as well as structures without auxin core but interacting with distinct transport or biosynthetic pathways (Ma and Robert, 2014). Such approach has unravelled most of the key components of auxin transport and signalling and still represent a powerful tool for investigation of the pleiotropic effects and molecular mechanisms behind auxin-regulated plant development (De Rybel et al., 2009).

3.2.1.1 Fluorescent auxin analogues

Since the system of aromatic rings and carboxyl group side chain were investigated as required moieties for auxin-like activity, other parts of the auxin molecule can be attached or modified for respective purposes such as fluorescent labelling to visualize auxin distribution *in vivo* (Pařízková et al., 2017).

The first published structures of fluorescent auxin were conjugates of IAA with fluorescein (FITC) dye used for evaluating of the biological activity of low molecular weight fraction (LMr) of humic substances in *Daucus carota* (Muscoet al., 2007). This study proposed the interaction of LMr with the IAA receptors based on the correlation of the FITC-IAA and FITC-LMr fluorescent patterns on the cell membranes of the carrot cells. More recently, new fluorescent conjugates of IAA with FITC and rhodamine (RITC) dyes via the secondary amino group of the indole ring were published by Sokołowska et al. (2014). Both FITC-IAA and RITC-IAA were shown to sustain

auxinic activity in several auxin-responsive bioassays and auxin-like distribution in comparison to free RITC and FITC labels (Sokołowska et al., 2014). However, neither of these two studies discussed the structures of fluorescent analogues or their stabilities in living system, making the obtained results hard to interpret. In addition, Hayashi et al. (2014) reported a conjugation of 5-hydroxy-IAA and 7-hydroxy-NAA with 7-nitro-2,1,3-benzoxadiazole (NBD) tag based on the previous SAR study of synthetic alkoxy-auxin analogues as inhibitors of auxin transporters (Tsuda et al., 2011). Both NBD-IAA and NBD-NAA displayed a fluorescent pattern of distribution similar to the expression pattern of *pDR5::GUS*, a synthetic auxin-sensitive marker line widely used for visualization of auxin response, induced by free IAA and NAA, respectively. On the other hand, the analogues did not exhibit any auxin bioactivity. Since the compounds are not active via the TIR1/AFB signalling pathway and were shown not to be substrates for auxin inactivating enzymes GRETCHEN HAGEN 3 (GH3), they are considered as probes to precisely visualize natural auxin distribution *in vivo* on tissue and subcellular level (Hayashi et al., 2014). Furthermore, Bielešzová et al. (2018) introduced the NBD tag on a N1 position of IAA indole ring via aliphatic linkers varying in number of carbons in the structure (from C₃ to C₆). Therefore, four IAA fluorescent derivatives with the same structure but different length of linker were generated. Interestingly, the substitution of IAA in the N1 position was shown to change the auxin-like compounds into anti-auxins. Moreover, both physical-chemical and biological properties of the compounds are significantly dependent on the length of the linker. The IAA fluorescent analogue with the longest linker (C₆) shows the best fluorescent properties and exhibited the strongest anti-auxin activity in various auxin bioassays (Bielešzová et al., 2018).

Overall, the need for developing new fluorescently labelled auxins combining good fluorescent properties, *in vivo* stability and biological activity with distribution of natural auxins remains relevant.

3.2.2 Auxin distribution regulates plant development

Auxins are not distributed equally within different plant tissues and organs. Tissue-specific uneven distribution of auxin is necessary for proper plant organogenesis and development (Vanneste and Friml, 2009). The precise concentrations of auxin

in particular time and space are regulated by complex coordination of auxin active transport and local *de novo* biosynthesis (Paque and Weijers, 2016).

3.2.2.1 Auxin biosynthesis and metabolism

During plant growth, the most intense auxin biosynthesis takes place in rapidly developing organs such as young leaves and tips of the shoot or root, but generally, all parts of young seedlings can synthesize IAA (Ljung, 2013). The matured plants keep the biosynthetic machinery active especially in growing leaves and shoot apical meristem. From the areal parts of plant, auxin is then transported basipetally towards the root by the phloem. In the root, auxin is further transported acropetally to the root tip where it accumulates and is consequently redistributed (Friml, 2003). In general, auxin is distributed from the sites of biosynthesis (e.g. young leaves) to sink organs, such as meristems (Paque and Weijers, 2016; Ljung, 2005).

Keeping an intracellular auxin homeostasis relies on the precise coordination of aforementioned *de novo* biosynthesis, degradation and temporal or irreversible inactivation (Ljung et al., 2005). There are two ways of IAA biosynthesis in plants with or without tryptophan (Trp) as a main precursor. Although even if little is known about the Trp-independent pathway, it is thought to be triggered only when the Trp-dependent pathway is blocked (Normanly, 1993, Wang et al., 2015). The Trp-dependent pathway is believed to be the most important source of auxin biosynthesis in diverse plants (Zhao, 2012) (Fig. 3). There are four Trp-dependent pathways participating in the generation of IAA (named according to their main intermediates) – indolyl-3-acetaldoxim (IAOx), indol-3-ylacetamid (IAM), tryptamine (TAM) and indolyl-3-pyruvic acid (IPyA) (Normanly, 2010). It was shown that IPyA is the main pathway of auxin biosynthesis in *Arabidopsis* (Zhao, 2012). In this route, IAA is produced by a two-step reaction when TRYPTOPHAN AMINOTRANSFERASE OF ARABIDOPSIS 1/TRYPTOPHAN AMINOTRANSFERASE RELATED (TAA1/TAR) enzymes transform Trp to IPyA, which is subsequently converted to IAA by decarboxylation and oxidation by YUCCA family of flavin monooxygenases (Mashiguchi et al., 2011) (Fig. 3). Moreover, Trp can also serve as a source of indole glucosinolates, compounds playing an important role in plant defence responses, that are generated through the IAOx pathway by action of oxime-metabolizing enzymes SUPERROOT1 and 2

(SUR1 and SUR2) (Bak et al., 2001). The endogenous levels of free IAA are strictly kept by homeostasis apparatus such as conjugation with sugars, amino acids (AAs), peptides or proteins (Ljung, 2013). The reversible inactivation of IAA by conjugation with AAs, mainly alanine, leucine, aspartic and glutamic acid (Kowalczyk and Sandberg, 2001), is catalysed by the GH3 (GRETCHEN HAGEN 3) protein family (Staswick et al., 2005). Whereas, ILR1 (IAA-LEUCIN RESISTANT1), IAA-LEUCINE RESISTANT (ILR)-LIKE2 (ILL2) and IAA-ALANINE RESISTANT3 (IAR3) aminohydrolyses release free IAA from AA conjugates (Ludwig-Müller, 2011). The UDP-glucosyltransferase UGT84B1 then converts IAA to indol-3-acetyl-1-O- β -D-glucose (Jackson et al., 2001). The irreversible deactivation of active IAA is its oxidation to 2-oxindol-3-acetic acid (oxIAA) (Pěnčík et al., 2013) by DIOXYGENASE FOR AUXIN OXIDATION1 (DAO1) and DAO2 (Porco et al., 2016; Zhang et al., 2016) which can be further glycosylated to oxIAA-glucose by UDP-glucosyltransferase UGT74D1 (Tanaka et al., 2014). Interestingly, IAA oxidation was shown to be more intense in lower auxin concentrations while conjugation via amide or ester bond is more dominant at high auxin levels (Porco et al., 2016; Zhang et al., 2016). In addition, IBA represents another stock form that can be converted to IAA and contrariwise (Woodward and Bartel, 2005). Conversion of IAA to less active IBA is facilitated by IBA synthetase via classical elongation of side chain observed e.g. in biosynthesis of fatty acids (Ludwig-Müller, 2007). A reverse step from IBA to IAA is then driven by INDOL-3-BUTYRIC ACID RESPONSE (IBR) enzymes via β -oxidation in peroxisomes (Zolman et al., 2008). Since IBA has not been detected by today's sensitive detection techniques in *Arabidopsis* (Novák et al., 2012), its role as endogenous hormone remains elusive. Moreover, it was shown that IAA methylation *via* IAA CARBOXYL METHYLTRANSFERASE1 (IAMT1) also plays an important role in maintaining tissue-specific concentration range of IAA. Once the methylation is disrupted, the asymmetric redistribution of IAA is affected and influences the consequent gravitropic response in the hypocotyl (Abbas, 2018).

The metabolism of natural and synthetic auxins displays common features such as direct conjugation of carboxyl group with amino acids or glucose, cleavage of the side-chain or phenol ring hydroxylation (Peterson et al., 2016). In addition, a recent comprehensive study of 2,4-D metabolism identified 16 novel 2,4-D metabolites in *Arabidopsis* T87 cell culture beside the ones already described previously (Tanaka et al., 2018). Despite this fact, it is likely that the lower metabolism rate of 2,4-D compared to

conjugates displayed rapid back conversion to free 2,4-D (Eyer et al., 2016). The 2,4-D metabolism also differs among monocot and dicot plants. This selectivity is used in agriculture as mentioned before. The reversible conjugation of 2,4-D with amino acids or glucose leads to phototoxic metabolic intermediates that are back converted to free 2,4-D. This metabolic pathway is specific for sensitive dicots while tolerant monocots prefer ring hydroxylation resulting in non- or partially phytotoxic products (Peterson et al., 2016).

3.2.2.2 Auxin transport

As mentioned, IAA is mainly produced in the shoot apical meristem and young developing leaves (Ljung, 2005). Within the shoot (long-distance transport), auxin is transported basipetally to the lower parts of the plant through phloem (Cambridge and Morris, 1996). In the root, there are two distinct tissue-specific directions of auxin transport – acropetal distribution in the central cylinder towards the auxin maxima in the root tip and basipetal transport in the outer layers of the root – creating a fountain-like model (van Berkel, 2013) (Fig. 4A). This cell-to-cell auxin flow is called polar auxin transport (PAT). PAT is actively facilitated by specific auxin transport carriers and contributes to establishing and maintaining the concentration gradients (Robert and Friml, 2009). Therefore, the visualization of auxin distribution within different developmental processes at high spatiotemporal resolution is of great interest (Pařízková et al., 2017).

IAA is a weak organic acid ($pK_a = 4,75$), thus its charge is dependent on the pH of its environment. The pH of the apoplast is around 5,5 and it is maintained by the activity of the proton pump H^+ -ATPases pumping the protons out of the cells. At a pH of 5,5, IAA remains in a protonated lipophilic form and can be transported across the phospholipid membrane by passive diffusion. In a neutral pH such as the one inside the cell, IAA dissociates, acquires a negative charge ($IAA-H \rightleftharpoons IAA^- + H^+$) and gets trapped in the cytoplasm. The IAA is then transported outside the cell by PAT. This model combining passive auxin influx with active PAT has been described by the chemiosmotic hypothesis (Fig. 4B; reviewed in Vanneste and Friml, 2009). IAA import is actively facilitated by influx carriers AUXIN RESISTANT 1/LIKE AUX (AUX1/LAX1, 2, 3) (Peer et al.,

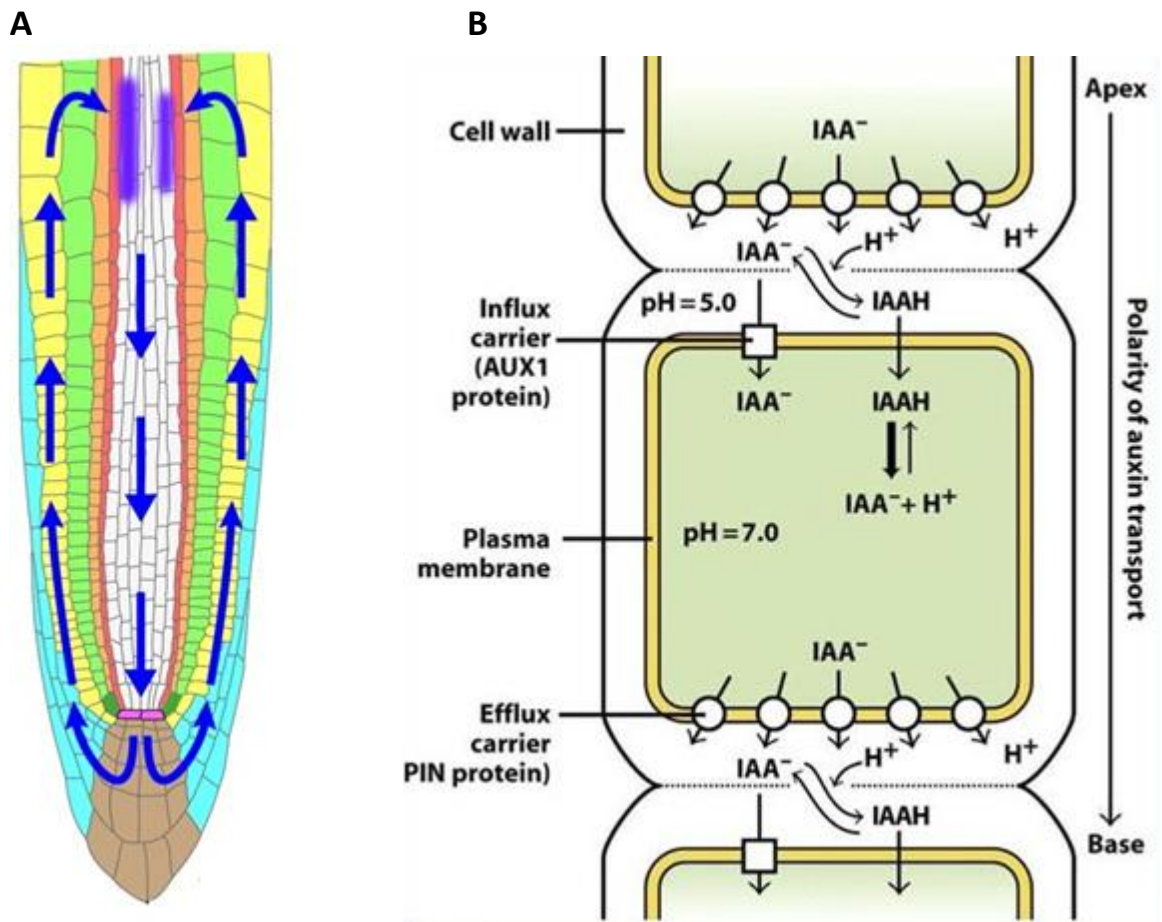


Fig. 4 Polar auxin transport on the tissue-specific (A) and cellular level (B)

- (A) Polar localization of auxin transporters enables one directional tissue-specific auxin flow. Basipetal transport of auxin from the lateral root cap through the epidermis to the basal meristem and acropetally back towards the root tip through the stele creates the fountain-like pattern of distribution in the root tip. (Overvoorde et al., 2010).
- (B) Cell-to-cell polar auxin transport is driven by specific transport carriers. The auxin influx is mediated, apart from passive diffusion of protonated non-polar IAA, by active AUX1/LAX1-3 importers, while export of auxin from cells is facilitated by PIN and ACBC transporters.

2011). AUX1/LAX proteins are plasma membrane (PM)-associated permeases mediating symport of IAA with protons (Bennett et al., 1996, Yang et al., 2006). In the roots of *Arabidopsis*, AUX1/LAX carriers are polarly localized in the PM (Fig. 4B) and contribute to one-directional flux of auxin (Zažímalová et al., 2010). Therefore, they play an important role in various developmental processes such as the gravitropic response (Bennett et al., 1996), root hair growth (Grebe et al., 2002) or lateral root formation (Swarup et al., 2008).

Auxin efflux is driven mainly by PIN (PIN-FORMED) proteins. There are eight types of PINs in *Arabidopsis* which can be divided into two categories based on their structure -

long and short. Long PINs (1–4, 7) are polarly anchored in the PM (Fig. 4B), their specific polar localization and expression significantly differ in different tissues and moreover, PINs can undergo very dynamic cellular redistribution in response to developmental context (Wiśniewska et al., 2006). Short PINs (5, 6 and 8) are localized in the membrane of the endoplasmic reticulum (ER) and facilitate the auxin transport between cytosol and ER lumen (Barbez and Kleine-Vehn, 2013a). In addition, PILS (PIN-LIKE) proteins also contribute to the intracellular auxin flux to the ER (Barbez et al., 2012; Barbez et al., 2013b). Therefore, both short PINs and PILSs participate in the regulation of auxin uptake and consequently auxin signalling and downstream responses (Middleton et al., 2018, Feraru et al. 2019, Béziat et al., 2017). Not surprisingly, PIN transporters play an important role in regulation of various aspects of plant development and mutations in these genes result in developmental defects (Zažímalová, 2010). Additionally, except for PIN and PILS carriers, vacuolar auxin transporter WALLS ARE THIN1 (WAT1) (Ranocha et al., 2013) or endomembrane putative MATE (multidrug and toxic compound extrusion) transporter ADP1 (Li et al., 2014) also participate in the maintenance of intracellular auxin homeostasis.

Besides AUX1/LAX and PIN/PILs auxin carriers, several P-glycoproteins from ABCB (ATP-binding cassette B) subfamily facilitate the auxin transport (Remy and Duque, 2014). The best described are ABCB1, 4, 19 and 21. While ABCB1 and ABCB19 were shown to be auxin efflux carriers (Noh et al., 2001; Lewis, 2007), both ABCB4 and ABCB21 are thought to be facultative transporters playing a role of auxin importers under low auxin concentration and exporting auxin out of the cell in high concentrations as another level of sustaining of auxin homeostasis in cells (Kubeš et al., 2012; Kamimoto et al., 2012).

In the case of synthetic auxins, their affinities for specific transporters differ significantly (Delbarre et al., 1996). In general, NAA is uptaken into cells by passive diffusion and its further redistribution is controlled by efflux carriers. On the other hand, 2,4-D transport into the cell requires influx transporters while it has long been considered as a poor substrate for auxin exporters (Delbarre et al., 1996). Thus, the distinct transport properties of NAA and 2,4-D are used to dissect auxin efflux and influx, respectively. In more detail, NAA bypasses the active auxin influx while its efflux is facilitated by PIN4 and PIN7 (Petrášek et al., 2006) and ABCB4 (Cho et al., 2007). Moreover, NAA was published as a substrate for intracellular PIN proteins 5, 6 and 8 (Petrášek et al., 2006;

Mravec et al., 2009; Ganguly et al., 2010). 2,4-D is actively imported by AUX1, LAX1, and LAX3 (Swarup et al., 2004; Péret et al., 2012; Swarup et al., 2008) and its efflux is driven by PIN2 and 7 (Yang and Murphy, 2009) together with ABCB1, ABCB19 and ABCG37 carriers (Yang and Murphy, 2009; Ito and Gray, 2006).

3.2.2.3 Auxin perception and signalling

Auxin acts as a general coordinator of plant growth and development through intercellular communication. Binding of auxin molecule to the specific receptor triggers intracellular molecular changes resulting in the expression of auxin-responsive genes as a particular response to this stimulus (Weijers and Wagner, 2016). By now, three auxin receptors and associated signalling pathways are known to modulate plant development through cell-type specific transcriptional and cellular responses (Ma et al., 2018).

The best described is the TIR1/AFB signalling pathway. TIR1 was found thanks to a screen searching for mutants resistant to the auxin transport inhibitor 1-naphthylphthalamic acid (NPA) (Ruegger et al. 1997; Ruegger et al. 1998). TIR1 was identified as an auxin receptor few years later (Dharmasiri et al., 2005; Kepinski & Leyser, 2005). TIR1/AFB1-5 are F-box proteins, the auxin-binding components of S-PHASE KINASE ASSOCIATED PROTEIN 1 - CULLIN 1 - F-BOX (SCF)-type E3 ligase (Weijers and Wagner, 2016). In the absence of auxin, Aux/IAA transcriptional repressors heterodimerize with AUXIN RESPONSE FACTOR (ARF) transcription factors and block the auxin signalling (Fig. 5). After perception of the auxin molecule, auxin acts as molecular glue enhancing the affinity between SCF^{TIR1/AFB1-5} and DII degron domain of Aux/IAAs. Such interaction results in polyubiquitylation of Aux/IAA inhibitors and their degradation by 26S proteasome, releasing ARFs and triggering the expression of auxin-responsive genes (Fig. 5) (Tan et al., 2007).

In *Arabidopsis*, there are five functional homologues of TIR1 receptor, AFB1-5 which bind auxin with different affinities (Calderón Villalobos et al., 2012). Aux/IAAs belong to a protein family of 29 members and there are 22 ARFs in *Arabidopsis*. Even though some TIR1-Aux/IAA co-receptor pairs have not been proven, such large combinatorial properties of auxin perception underlie the complexity of auxin responses regulating a plethora of auxin-related developmental processes (Calderón Villalobos et

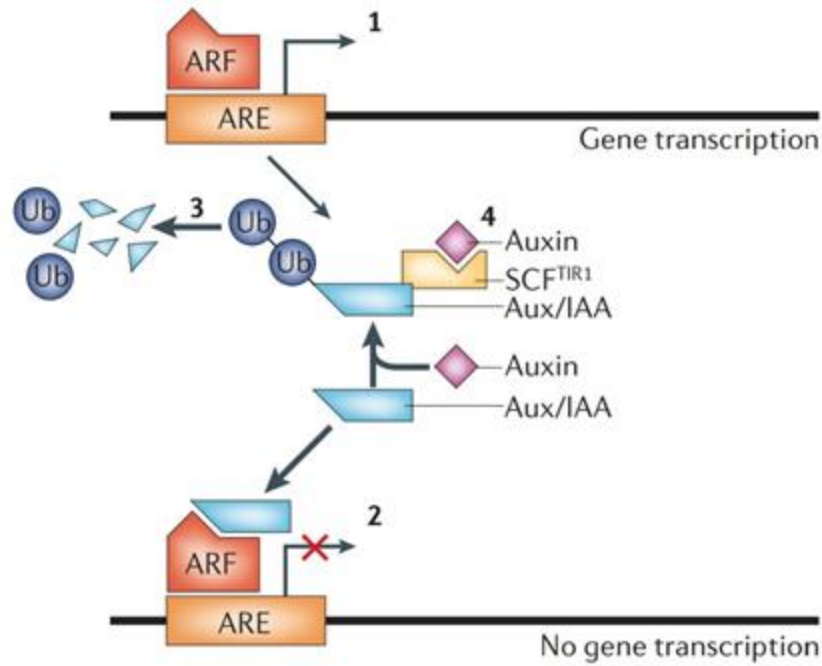


Fig. 5 Scheme of auxin signalling through $SCF^{TIR1/AFB}$ signalling pathway (Taele et al., 2006). Expression of auxin responsive genes is blocked by Aux/IAA repressors of ARF transcription factors. Auxin promotes the interaction of SCF E3 ubiquitin ligase TIR1 with Aux/IAs resulting in ubiquitination and degradation of Aux/IAA inhibitors and triggering transcription of auxin-related gene transcription.

al., 2012). Moreover, recent studies propose a novel non-canonical TIR1/AFB signalling as playing a role in rapid auxin responses (Kubeš and Napier, 2019). Real-time monitoring of the root growth inhibition in response to auxin treatment was shown to be TIR1/AFB-dependent but too fast to be regulated via canonical TIR1/AFB-mediated gene expression (Fendrych et al., 2018).

A similar mechanism of signal transduction is mediated by S-PHASE KINASE-ASSOCIATED PROTEIN 2A (SKP2A). SKP2A is also a F-box protein belonging to a SCF complex involved in the regulation of the cell cycle (specifically of G1/M transition) (Jurado et al., 2010). E2 PROMOTER TRANSCRIPTION FACTOR C (E2FC) and E2F DIMERIZATION PARTNER B (DPB) are negative transcription factors of the cell proliferation initiation. After their degradation, the cell can pass through the G1/M checkpoint and proliferate (del Pozo et al., 2006; del Pozo et al., 2006). E2FC/DPB TFs bind the promoters of cell cycle genes and inhibit their transcription. In the presence of auxin, the SCF^{SKP2A} -E2FB/DPB interaction stimulates the ubiquitination and degradation of phosphorylated E2FB/DPB repressors followed by the expression of cell division-

promoting genes (del Pozo et al., 2006). This function of SKP2A confirms the role of auxin as a positive regulator of cell division.

The first discovered auxin receptor was AUXIN BINDING PROTEIN1 (ABP1) first isolated in 1985 (Löbler a Klämbt, 1985) and as an auxin binding protein identified four years later (Jones a Venis, 1989). ABP1 is located mainly in the ER membrane but a small percentage is assumed to be localized outside the cell as ABP1 displays low affinity for auxin at the pH of the ER (Enders and Strader, 2015). However, its real function remains elusive. For a long time, research on ABP1 was unobtainable because the original *Arabidopsis* mutant line *abp1* was shown to be embryo lethal and was ABP1 was considered an essential gene for plant development (Chen et al., 2001). Several alternative approaches, e.g. TILLING-generated missense point mutation alleles of *abp1*, inducible *ABP1* antisense transcript expression or inducible expression of fragments of antibodies against ABP1, were developed to overcome this issue so that the role of ABP1 could be studied (Chen et al., 2014; Xu et al., 2014; Braun et al., 2008; Paque et al., 2014). Using these methods, it was shown that ABP1 is involved in fast non-transcriptional auxin responses such as rapid cell elongation driven by ion flux, clathrin-mediated endocytosis of PIN transporters defining the cell polarity or RHO-LIKE GTPASES OF PLANTS (ROP)-dependent cytoskeleton rearrangements resulting in asymmetric cell growth and lobbing (reviewed in Sauer and Kleine-Vehn, 2011). In 2015, new null alleles mutant line of *abp1* using Cas9/CRISPR technology was generated and surprisingly showed no molecular or morphological defects compared to the wild-type (Gao et al., 2015). This study gave rise to the question of ABP1 importance in plant development and initiated the re-exploration of observed developmental defects in different *abp1* mutant lines, which were addressed mainly to off-target effects and background mutations of developmentally important genes (Michalko et al., 2015; Michalko et al., 2016; Enders et al., 2015).

Since the binding pocket of TIR1/AFBs is promiscuous enough to accommodate auxin analogues significantly varying in the structure, the SCF^{TIR1/AFB} signalling pathway was shown to be dominant in mediating auxin-related responses induced by synthetic auxins. TIR1 was shown to be the prevailing receptor for 2,4-D action (Parry et al., 2009) even though the binding affinity of 2,4-D with TIR1 is lower compare to the one of IAA. It is due to the absence of the NH group in the structure of both 2,4-D and NAA which is present in the indole ring of IAA and creates an extra hydrogen bond with carbonyl residue of TIR1

(Tan et al., 2007). Interestingly, 2,4-D helped to identify another important player in auxin TRI1/AFB signalling - AUXIN- RESISTANT (AXR). In chemical genetic screening for auxin resistance, 2,4-D was used as probe that enabled to reveal the function of AXRs, including AXR1-3, 5 and 6, in the TIR1 pathway (Ma et al., 2018). Besides 2,4-D and its structural derivatives including 2,4,5-T or 2-methyl-4-chlorophenoxyacetic acid (MCPA) that also prefer TIR1 as a main receptor for their mode of action, other derivatives displaying selectivity in binding to auxin receptors have been generated. For instance, chemical genetic screening revealed that mutations in genes for AFB4 and AFB5 exhibit selective resistance to synthetic picolinate auxins, especially picloram, but not to 2,4-D or IAA. (Walsh et al., 2006; Prigge et al., 2016). Such compounds selectively targeting specific receptors can be used to separate different signalling pathways for the purpose of studying their role in plant development (Fendrych et al., 2016).

3.2.3 Auxin bioassays

Evaluation of the biological activity of synthetic auxin analogues is based on their physiological effect during processes that are typically regulated by auxin, e.g. apical dominance, inhibition of brunching, stimulation of rooting, tropic responses or apical hook formation during dark growth (Davies, 2010). Both natural and synthetic auxins display a bell-shaped dose-response curve where low concentrations promote growth while concentrations above the optimal range result in inhibitory and toxic effects (Woodward and Bartel, 2005). Since very simple to perform, the inhibition of primary root growth (Fig. 6C) is a widely used bioassay in screening for auxin-like candidate structures in *Arabidopsis*.

The first discovered auxin response was the movement of the plant towards the light source named as phototropism (Darwin and Darwin, 1880). In this assay, the shoot of *Avena Sativa* is decapitated in order to remove the source of auxin. An agar block containing the compound exhibiting the auxin activity is placed asymmetrically on the decapitated coleoptile (Fig. 6A). A bending of the coleoptile is then observed as a result of the growth promoting activity even in absence of the light stimulus (Went, 1926; Fig. 6A). After incubation, the curvature mediated by the diffusion and transport of auxin-like compound from the agar block into the coleoptile of *A. sativa* is evaluated

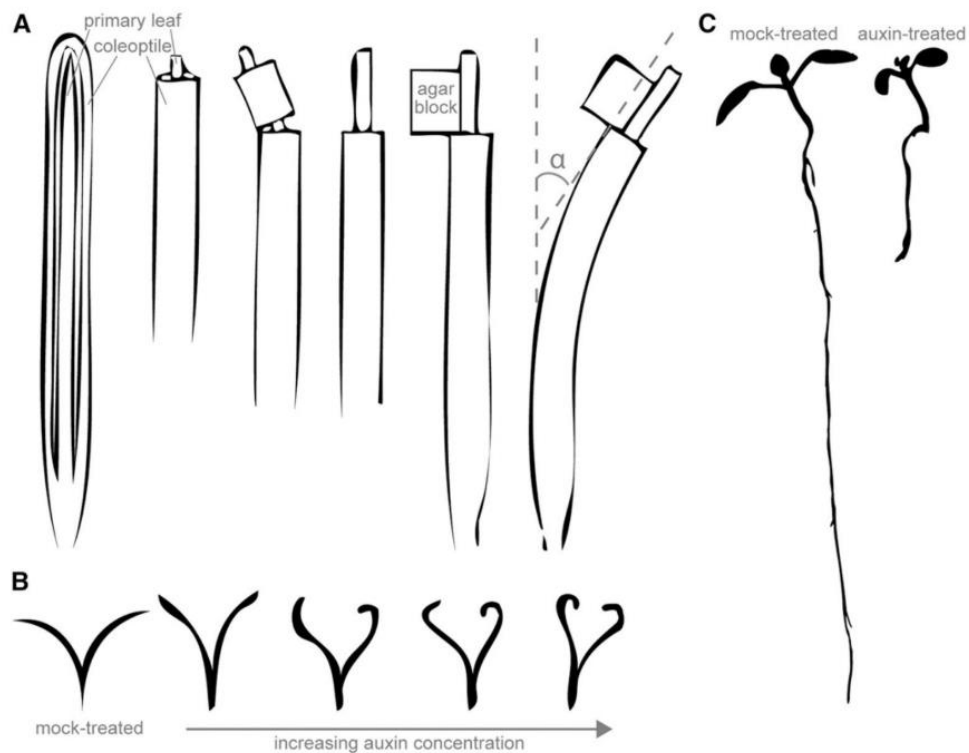


Fig. 6 Bioassays for evaluation of auxinic activity (Modified from Enders and Strader, 2015).

- (A) *Avena* bioassay – asymmetric application of compounds with auxinic activity in agar block promotes the curvature of decapitated coleoptile.
- (B) *Pisum* bioassay - Tops of the *Pisum* seedlings are cut below the terminal bud, split vertically and incubated in solution supplied with tested compound. Auxin-like chemicals trigger the curvature of vertical cuttings towards each other while control stem cuttings grow apart.
- (C) *Arabidopsis* root elongation assay - *Arabidopsis* seedlings are grown on the solid media supplemented with a compounds of interest. The lengths of the primary root of 5-10-day-old seedlings are measured.

(Enders and Strader, 2015). Another model system used to evaluate the auxin activity is *Pisum sativum*. For this assay, the shoot of *P. Sativum* is decapitated, cut longitudinally and incubated in solution containing the compound of interest (Fig. 6B). If the compound possesses auxin activity, both parts of the split stem move towards each other (Fig. 6B), otherwise they move apart (Went and Thimann, 1937; Fig. 6B). Another auxin bioassay was established based on the research of Miller and Skoog (1957) focused on the role of auxins and cytokinins during growth and organ formation in plant tissues cultured *in vitro* (Miller and Skoog, 1957). The bioassay evaluates the ability of tested auxin compounds to stimulate root system architecture from dedifferentiated plant tissue

in tissue culture. All other classical bioassays for testing of auxin activity are reviewed in Gyulai and Heszky (1994).

Today's methods to test auxin activity take advantage of genetic engineering which generates valuable tools as plants expressing reporter genes under the control of specific auxin-responsive promoters. For auxins, the most commonly used is *Arabidopsis* line expressing the auxin-inducible promoter DR5 fused with the β -glucuronidase (GUS) enzyme. This line is called *pDR5::GUS* (Ulmasov et al., 1997). When exogenously applied to the plant, compounds exhibiting auxin activity induces the DR5 expression and the consequent accumulation of the GUS enzyme in the tissue. The GUS enzyme mediates the conversion of colourless substrate X-glucuronide (X-GlcA) to a blue product enabling the histochemical localization of auxin activity at the tissue level. Besides the commonly used histochemical visualization of auxin action, the quantitative determination of GUS activity in plant extracts using 4-methylumbelliferyl β -D-glucuronide (4-MUG) as a GUS substrate converted to the fluorochrome 4-methyl umbelliferone (4-MU) was introduced. By using excitation at 365 nm and measuring emission at 455 nm, the amount of 4-MU can be quantified (Blázquez, 2002). Based on the estimated GUS activity, the potency of auxin compound to promote GUS expression can be determined.

Many auxin-responsive marker genes have been developed over the last decade, combining either natural (e.g. IAA3, IAA12) or synthetic (e.g. DR5, DR5v2, BA3) promoters with different marker genes (GUS; red, green fluorescent proteins – RFP, GFP). These reporters usually display different patterns and intensity of expression and thus they can provide deeper knowledge about the mode of action of tested compounds (Pařízková et al., unpublished). Nevertheless, the overall output of the expression-based markers represents the combination of the auxin activity and other regulatory pathways (Chapman and Estelle, 2009). Therefore, another auxin reporter based on the auxin perception was developed (Brunoud et al., 2012). The degron DII domain of Aux/IAA is fused with fast maturing yellow fluorescent protein VENUS creating DII-VENUS construct. When the auxin compound is perceived, rapid degradation of DII-VENUS results in decrease of the fluorescent signal. Such response occurs in minutes, compared to expression-based systems, and can be used to visualize dynamic changes in auxin distribution with great spatiotemporal resolution (Brunoud et al., 2012). Furthermore, some other auxin-responsive methods based on degradation of labelled Aux/IAs have

been developed (Pařízková et al., 2017). A plethora of very specific assays have been established in the last decade to evaluate auxin roles and modes of action in particular developmental processes (Kleine-Vehn and Sauer, 2017).

3.2.4 Analytical methods for auxin analysis

Plant hormones as signalling molecules act at very low concentrations levels compared to other substances such as sugars, pigments or other secondary metabolites present in far greater concentrations (Du et al. 2012). Therefore, the determination of phytohormones in a complex plant matrix represents a challenging issue. Moreover, to precisely understand all the mechanisms behind the molecular action of hormones and maintaining their homeostasis, profiling of their biosynthetic precursors and metabolites with distinct chemical properties and occurring in a wide range of concentrations is of great interest. Taken together, the phytohormonal analysis places high demands on specific and efficient sample preparation together with selective and sensitive detection techniques (Tarkowská et al., 2014).

3.2.4.1 Sample extraction

Extraction is the first step in sample preparation that may significantly influence the isolation of analytes from the matrix and helps to remove the interference compounds. Therefore, the conditions need to be optimized for the best extraction efficiency of studied analytes while minimizing the yield of ballast compounds (Tarkowská et al., 2014). Prior to extraction, a thorough homogenization of plant tissue is required to break the cell walls and release the compounds into particular extraction solution (Harrison, 2011).

Many organic solvents have been used to extract auxins from plant samples during decades of auxin research, including methanol, acetone, acetonitrile or isopropanol, as well as their different combinations (methanol/water; isopropanol/acetic acid; 1-propanol/water/concentrated hydrochloric acid (HCl); methanol/water/formic acid - modified Bielecki's solvent; isopropanol/imidazole buffer or methanol/isopropanol/acetic acid) (Fig. 7) (reviewed in Novák et al., 2014). Moreover, aqueous buffers, especially

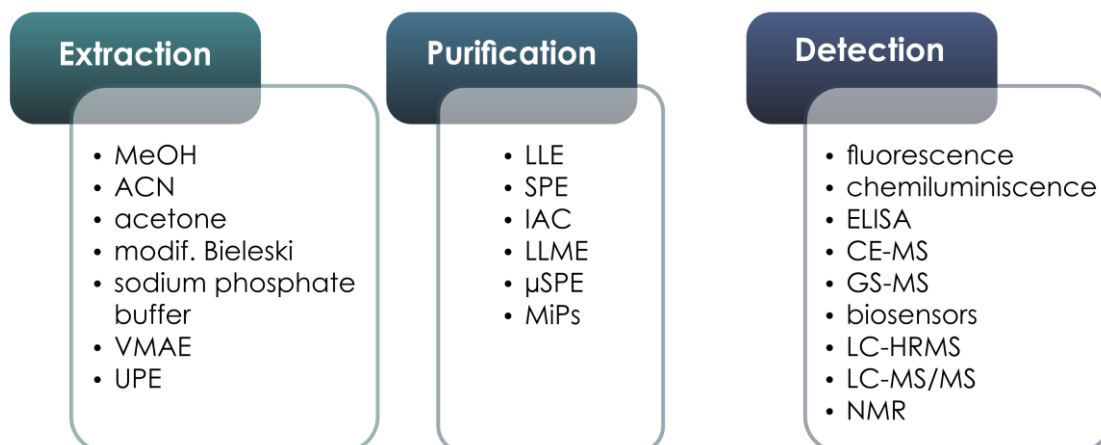


Fig. 7 Combinations of isolation and detection techniques used in auxin analysis.

sodium phosphate buffer at pH 7.0, were shown to be effective solutions for extraction of IAA and its metabolites because of high IAA recovery and low contamination by non-polar interferences (Novák et al. 2012). To increase the stability of analytes during the extraction procedure, chemical decomposition of the compounds should be avoided. Minimizing the degradation can be achieved by performing the extraction at low temperatures between -20 °C to 4 °C or by adding the suitable antioxidant, e.g. sodium diethyldithiocarbamate, to the extraction solution (Pěňčík et al., 2009). Other alternatives for to eluding the analyte breakdown were developed. Using vacuum microwave-assisted extraction (VMAE) (Hu et al., 2011) enables the creation of a low oxygen environment to minimize IAA oxidation while vapor phase extraction (VPE) speeds up the extraction and derivatization by heating the auxin samples to 200 °C (Schmelz et al., 2004). Moreover, the addition of internal isotopically labelled standard (the isotope dilution method) to the extraction solvent before extraction helps to cover the losses of IAA and its metabolites during the whole sample preparation and during analysis, which allows precise final quantification of the compounds in the sample (Rittenberg and Foster 1940; Ljung et al., 2004).

3.2.4.2 Methods for auxin purification

Purification of the sample extract is the main step of separation of analytes from a complex plant matrix. It needs to be optimized to obtain the maximal purification efficiency with the sufficient recoveries of all analytes and with respect to subsequent detection technique (Fig. 7).

The classical method of sample purification is liquid-liquid extraction (LLE) based on the separation of analytes between two liquid phases of different polarities (Nováková and Vlčková, 2009). Different pairs of solvent have been used for isolation of IAA - sodium phosphate buffer/ethyl acetate, aqueous 1-propanol/methylene chloride, acidified 80 % methanol/diethyl ether and potassium sulphate buffer/chloroform (Novák et al., 2014). In addition, to analyse minute samples and also to decrease the consumption of organic solvents, the miniaturized arrangement of LLE such as dispersive and hollow fibre liquid-liquid microextraction (LLME) have been developed (Lu et al. 2010; Wu and Hu 2009). The most commonly used approach to purification these days is solid phase extraction (SPE) using silica or polymer-based sorbents. A plethora of commercially available sorbents with different levels of specificities enables the isolation of analytes from diverse plant matrices by applying various interaction mechanisms such as adsorption, hydrogen bonding, polar and hydrophobic interactions, Van der Waals and dipole–dipole forces, ion-exchange and/or size exclusion (Nováková and Vlčková, 2009). Several methods based on one-step purification of auxin have been established mainly applying hydrophobic interactions by using C₁₈, C₈ or Oasis HLB columns (Kowalczyk and Sandberg 2001; Pěňčík et al. 2009; Liu et al. 2012; Novák et al. 2012). Multistep SPE methods and mixed-mode SPE processes usually combining reverse-phase and ion-exchange interactions can help to increase the sample clean-up efficiency as well as the number of retained IAA metabolites for analysis (Dobrev and Kamínek 2002; Dobrev et al., 2005). A miniaturized alternative was also established for SPE, called in-tip microSPE and enables a rapid and high-throughput screening of IAA metabolome in minute samples (Liu et al., 2012; Pěňčík et al., 2018). In addition to classical SPE, even more selective purification methods are used for auxin isolation employing either mono- or polyclonal antibodies against IAA in immunoaffinity chromatography (IAC) (Sundberg et al. 1986; Pěňčík et al., 2009) or IAA molecularly imprinted polymers (MIPs) (Kugimiya and Takeuchi 1999a,b; Chen et al. 2006). Such specific interaction of phytohormone molecule with sorbent recognising only IAA and its close structural analogues significantly reduces the background noise making the following analysis easier (Tarkowská et al., 2014).

3.2.4.3 Methods of auxin detection, identification and quantification

Together with a long tradition of auxin research also employing the auxin determination in different types of samples, many techniques to detect and quantify IAA have been introduced with different advantages, sensitivities and limitations. Among others, nuclear magnetic resonance (NMR), immunoassays such as radioimmunoassay (RIA) and enzyme-linked immunosorbent assay (ELISA), biosensors, fluorescence and chemiluminescence-based detection or colorimetric methods of detection for IAA and IBA can be mentioned (Fig. 7) (reviewed in Porfírio et al., 2016). With respect to very low concentration levels of phytohormones in plant tissues, mass spectrometry (MS)-based detection techniques are currently the most widely used (Pan and Wang, 2009).

The MS analysis itself is usually preceded by separation of the complex mixture of analytes by one of the separation methods such as capillary electrophoresis (CE) and its alternatives, gas chromatography (GC) or liquid chromatography (LC) (Porfírio et al., 2016). Though GC-MS is a very sensitive method that enables to identification (Kowalczyk and Sandberg 2001) and quantification (Barkawi et al., 2010; Liu et al., 2012) of auxin and its metabolites in different plant species, however, it requires an appropriate chemical derivatization of non-volatile compounds making GC laborious. Therefore, LC-MS has the priority status in auxin analysis, where all IAA metabolites except labile IPyA and IAAlD can be analysed without prior derivatization (Novák et al., 2014). Many derivatization protocols to stabilize IPyA and IAAlD during the isolation procedure were developed. For example, cysteamine can be employed to convert these metabolites into their thiazolidine (TAZ) derivatives (Novák et al., 2012).

MS detection is a very sensitive and versatile method for both qualitative and quantitative auxin determination (Novák et al., 2014). The low-resolution tandem mass spectrometry (MS/MS) can be used for identification of the metabolites by analysing the fragmentation patterns of the ions and isotopic distribution in MS spectrum together with chromatographic properties of the compound ideally compared to particular chemical standard prepared by organic synthesis (Novák et al., 2014). The MS/MS approach helped to identify for instance several auxin amino acid conjugates (Pěňčík et al., 2009), their oxidative metabolites and IAA-glucose conjugates (Kai et al., 2007a, b). Besides MS/MS, high-resolution mass spectrometry (HRMS) based on time-of-flight (TOF)

ion separation or Fourier Transform in Orbitrap technology can be used for compound identification. HRMS spectra provide information about the accurate mass that helps to predict the structure of the compound. HRMS Orbitrap instrument was used for detection of several IAA metabolites in tomato (Van Meulebroek et al. 2012) or rice (Haeck et al., 2018).

Quantification of IAA and auxin metabolites is usually performed by a selected reaction monitoring (SRM) mode which is currently the most sensitive MS detection method (Pan and Wang, 2009). Moreover, highly selective purification method (Pěňčík et al., 2009), appropriate additives in mobile phase (Pěňčík et al., 2009; Novák et al., 2012), using soft ionization techniques with minimal ion fragmentation in the ion source (Pan and Wang, 2009) or the derivatization of the analytes (Novák et al., 2012) can improve the sensitivity of the MS/MS method. Determination of the precise concentrations of all analytes can be achieved by the isotopic dilution method (Rittenberg and Foster 1940). Adding known concentration of the internal standards labelled with stable isotopes (^2H , ^{13}C , ^{15}N or ^{18}O) before the sample extraction covers the losses during sample preparation, ionisation efficiency and matrix effects during MS analysis and therefore enables accurate quantification. A number of very sensitive methods for auxin analysis combining LC-MS or GC-MS has been reported during the last decade (reviewed in Novák et al., 2014). The miniaturizing trends of sample preparation and decreasing limits of detection of MS methods enables analysis of auxin metabolome in minute samples on tissue-specific (Petersson et al., 2009; Novák et al., 2012; Pěňčík et al., 2013) and cell-specific (Petersson et al., 2015) levels and slowly reaching subcellular resolution (Skalický et al., unpublished).

3.2.4.4 Determination and metabolite profiling of 2,4-D

2,4-D is a widely used herbicide in agriculture. It is a water-soluble compound easily penetrating and accumulating in the soil, groundwater and surface water (Jursík et al., 2010) contaminating the ecosystems. Chlorinated derivatives of phenoxyacetic acid were shown to exhibit moderate toxicity to human and aquatic animals (Cserháti and Forgács, 1998) and thus, the number of analytic methods for rapid monitoring of 2,4-D and its metabolites in different types of matrices is increasing.

In general, the purification methods for isolation of 2,4-D, its analogues and metabolites copy the IAA protocols. LLME (Vain et al., 2019; Pařízková et al., unpublished), SPE (Eyer et al., 2016; Qin et al., 2017; Chaves et al., 2018), solid-phase microextraction (Rodríguez et al., 2005; Henneberger et al., 2019), MIPs (Pereira et al., 2018; Hua et al., 2018) and IAC (Eyer et al., 2016) based approaches have been reported to isolate 2,4-D and its derivatives from various sorts of matrix. Detection techniques usually use a classical GC (Santos-Delgado et al., 2000; Rodríguez et al., 2005; Zanella et al., 2012) or LC (Koesukwiwat et al., 2008, Eyer et al., 2016) system coupled with MS or diode array detection (DAD)(Chaves et al., 2018) for routine 2,4-D quantification. On the other hand, a surprisingly large number of alternatives for 2,4-D detection have been developed including electrochemical determination using a modified screen-printed carbon electrode with bismuth film (Niguso et al., 2018), solid-surface fluorescence (SSF) detection of 2,4-D in complex with Rhodamine B (Alesso et al., 2017), surface-enhanced Raman spectroscopy (Hua et al., 2018), competitive immunoassay using covalent immobilization of 2,4-D-bovine serum albumin (2,4-D-BSA) on optofluidic chip (Feng et al., 2017) or chemiluminescent ELISA (Vdovenko et al., 2013). Also identification of 2,4-D metabolites employing MS detection is performed as in the case of IAA by MS/MS and HRMS techniques. For example, comparing mass spectra and chromatographic retention times of unknown metabolites with synthesized standard, amino acid conjugates of 2,4-D with glutamic and aspartic acid were identified in *Arabidopsis* (Eyer et al., 2016). Using HRMS data in combination with NMR analysis led to the identification of glucose ester as a major 2,4-D metabolite in wild radish when the structure was also confirmed by synthesis (Goggin et al., 2018). Recently, a comprehensive LC-HRMS/MS analysis of 2,4-D metabolism in *Arabidopsis* T87 cultured cells was performed by Takahashi et al. (2018). Using a stable isotopic labelling approach, accurate detection of 83 candidates for 2,4-D metabolites resulted in confirmation of 10 previously described and identification 16 novel 2,4-D metabolites (Takahashi et al., 2018).

4 Materials and methods

More detailed information about individual methods and equipment parameters are given in the research papers attached in the Supplement section.

4.1 Chemicals

- All chromatographic solvents and chemicals for hormonal analysis were of hypergrade purity from Sigma-Aldrich Chemie GmbH (Steinheim, Germany), Merck (Darmstadt, Germany) and Roche Diagnostics (Mannheim, Germany) (*Supplement II-V*).
- Standards of tested chemicals were obtained from Olchemim Ltd (Olomouc, Czech Republic), Sigma-Aldrich Chemie GmbH (Steinheim, Germany), CDN Isotopes (Quebec, Canada) (*Supplement II-V*), synthesized at the Department of Chemical Biology and Genetics, Centre of the Region Haná for Biotechnological and Agricultural Research, Palacký University, Olomouc (*Supplement II, II, V*) or newly ordered using the Chembridge identification number (*Supplement IV*).

4.2 Plant materials and growth conditions

- Seeds of *Arabidopsis thaliana* were typically sown on ½ MS medium (2.2 g/L Murashige and Skoog medium - Duchefa Biochemie, 1% sucrose, 0.05 g/L - morpholinoethanesulfonic acid (Sigma Aldrich); and 0.7% agar - Duchefa Biochemie, pH 5.6), stratified for two days at 4 °C in the dark and then transferred to long-day light conditions (22 °C, 16 h light/8 h dark) for five days. To obtain etiolated seedlings, after two days of stratification and 5 h on light (22°C) plates with seeds were packed into aluminium foil and grown in the dark for three days. All the mutant lines used in this work are in Col-0 background and have been described before (for seed references see the Supplements).

4.3 Methods

4.3.1 Auxin-responsive bioassays

Bioassays used to test the auxin activity of synthetic auxin analogues were modified for respective purposes. Times of treatments, concentrations of tested chemicals or concentrations of IAA, used in combination with studied compounds for testing of anti-auxin activity, may differ. More detailed experimental designs of each experiment are described in research papers attached in Supplement sections as mentioned below in brackets. Typically, the assays were performed as follows:

- *Root growth inhibition assay* – Seedlings of *Arabidopsis* Col-0 were grown in the 24-well plates containing solid ½ MS media in the presence of different concentrations of tested compounds in the long-day light conditions. After five days, the lengths of the primary root were measured (*Supplements II-V*).
- *Reverse genetics* – Seeds of *Arabidopsis* mutant lines in signalling, transport or biosynthetic pathways were sown on the vertical square Petri dishes with ½ MS medium supplemented by optimized concentration of tested compound and grown for five days in long-day conditions. After that, the primary root growth and the root phenotype were evaluated (*Supplements II-V*).
- *GUS assays* - Five-day-old *Arabidopsis* seedlings of GUS marker were treated with 10 µM compounds for defined periods of time, fixed with ice-cold acetone for 20 min at -20 °C and washed with distilled water. Plants were incubated in GUS buffer (0.1% triton X100; 10 mM EDTA; 0.5 mM potassium ferrocyanide; 0.5 mM potassium ferricyanide in 0.1 M phosphate buffer) containing 2 mM X-GlcA (Duchefa Biochemie) at 37 °C in the dark for 30 min. The staining reaction was stopped using 70 % ethanol for one h and the samples were then mounted in a mixture of chloral hydrate:glycerol:H₂O (8:3:1). GUS expression was evaluated using a light microscopy (*Supplements II-V*).
- *DII-Venus* - Five-day-old seedlings of *Arabidopsis* DII-Venus marker line were treated with 10 µM chemicals for short time (from 15 to 45 min), the confocal images of the root tips were acquired and the intensity of the Venus signal in the tips was evaluated (*Supplements III-IV*).

- *Real-time qPCR of early auxin-responsive genes* – Five-day-old *Arabidopsis* Col-0 seedlings were treated in 12-well plate containing ½ MS liquid medium treated with compounds at defined concentrations. 20 fresh seedlings were pre-treated with the first compound for one h followed by two h of co-treatment with the second compound. Seedlings were harvested into liquid nitrogen and frozen to -80°C. Total RNA was extracted using the RNeasy Plant Mini Kit (QIAGEN), with genomic DNA removed by on-column digestion using RQ1 RNase-Free DNase (Promega). 2µg total RNAs was reverse transcribed to cDNA using Oligo(dT)20 primer (Invitrogen) and SuperScript® IV Reverse Transcriptase (Invitrogen). Real-time qPCR analysis was performed using a LightCycler® 480 SYBR Green I Master (Roche) on a LightCycler® 480 Instrument II real-time PCR machine (Roche) (*Supplement II*).

4.3.2 Confocal microscopy

- Seedlings were typically treated in liquid ½ MS media supplemented by auxin fluorescent analogues at optimized concentration, transferred on microscopic slide glass with a drop of the media containing tested compounds. Confocal images were taken immediately using Zeiss LSM 780 confocal microscope or Confocal laser scanning microscope FV1000 (Olympus). NBD-labelled auxins and Venus fluorescent protein were excited at 488 nm, m-cherry fluorescent protein at 514 nm and cyan fluorescent protein at 458 nm by an Argon multiline laser. Live imaging of distribution of fluorescent compounds were performed using Nikon vertical macroconfocal (AZ-C2 vertical) in vertical square Petri dishes containing ½ MS media supplemented with fluorescent compounds.

4.3.3 Extraction and purification methods

- For quantification of 2,4-D and its metabolites, 15–20 mg fresh weight of treated plant tissues were extracted in 1ml of cold sodium phosphate buffer (50 mM, pH 7.0). The samples were purified by performing solid-phase extraction (SPE) using a mixed mode reversed phase/strong anion exchange column (Oasis® MAX, 1 ml/30 mg,

Waters) followed by immunoaffinity chromatography (IAC). Isotopically labelled internal standards of each analyte were added to the samples for final quantification.

- For the quantification of fluorescently labelled analogues of 2,4-D and 2,4-D-derived auxin agonists in *Arabidopsis* roots, an one-step extraction and purification method based on a liquid-liquid extraction (LLE) into water:methanol:hexane (1:1:1) mixture was developed. Isotopically labelled internal standards of each analyte were added to the samples for final quantification.

4.3.4 UHPLC-MS/MS methods

- For the quantitative analysis of all tested compounds, ACQUITY UPLC® I-Class system combined with a triple quadrupole mass spectrometer Xevo™ TQ-S (Waters, Manchester, UK) was used. Quantification was obtained by multiple reaction monitoring (MRM) mode of precursor ions ($[M+H]^+$ or $[M-H]^-$) and the appropriate product ions. Concentrations of all compounds were then calculated by an isotopic dilution method using the stable isotope labelled standards by deuterium and/or ^{13}C .
- For the quantification of 2,4-D and its metabolites, the samples were injected onto a reversed-phase column (Acquity UPLC® BEH C18, 1.7 μ m, 2.1x50 mm; temperature 40°C) and eluted with a linear gradient (0–7 min, 35–65% B; 7–8 min, 100% B; 8–10 min, 35% B) of aqueous 0.1% formic acid (A) and 0.1% formic acid in methanol (B) at a flow-rate of 0.25 ml min⁻¹.
- For the quantification of fluorescently labelled analogues of 2,4-D in *Arabidopsis* roots, the samples were injected onto a reversed-phase column (Kinetex™ C18 100A, 50 x 2.1 mm, 1.7 μ m; Phenomenex, Torrance, USA) and eluted with a linear gradient 10:90 to 95:5 A:B using 0.1% acetic acid in methanol (A) and 0.1% acetic acid in water (B) as mobile phases at a flow rate of 0.5 ml·min⁻¹ and column temperature of 40 °C. At the end of the gradient, the column was washed with 95% methanol (0.5 min), and re-equilibrate to initial conditions (1.0 min).

5 SURVEY OF RESULTS

Since the precise regulation of auxin distribution is crucial for proper plant growth and development, a plethora of approaches for visualizing auxin transport sites with particular advantages and limits have been developed and reviewed in *Supplement I*. For this purpose, two groups of synthetic fluorescently labelled auxin analogues derived from IAA (*Supplement II*) and 2,4-D (*Supplement III*) were prepared in the Department of Chemical Biology and Genetics (Centre of the Region Haná for Biotechnological and Agricultural Research, Faculty of Science, Palacký University in Olomouc) and characterized in cooperation with Department of Forest Genetics and Plant Physiology of the Swedish University of Agricultural Sciences (SLU) with the Umeå Plant Science Centre (UPSC). Moreover, sensitive LC/MS-based methods were developed to precisely evaluate the stability and metabolization of the fluorescent auxin analogues (*Supplement II-III*), novel auxin selective agonists RubNeddins (RNs) (*Supplement IV*) and 2,4-D together with its metabolites (*Supplement V*) in plants. Anti-2,4-D monoclonal antibodies (E2/G2) used for efficient isolation of 2,4-D and its analogues from plant matrix were prepared in the Department of Virology, Veterinary Research Institute, Brno.

5.1 Biological characterization of new fluorescent auxins analogues

- The biological activity of four novel fluorescently labelled IAA derivatives (*Supplement II*, Fig. 1), differing by the length of the aliphatic linker (C₃ – C₆) between IAA molecule and NBD fluorophore was determined. N1 substitution of the indole ring of IAA was shown not to possess the activity of auxin but *vice versa*, the activity of auxin antagonists, in different auxin bioassays – *Arabidopsis* root growth assay (*Supplement II*, Fig. 2), inhibition effect on auxin-induced root hair formation (*Supplement II*, Fig. 3), DR5::GUS assay (*Supplement II*, Fig. 4) and transcription of early auxin-responsive genes (*Supplement II*, Fig. 5). The anti-auxin activity was tightly connected with the length of the linker, making the compound with the longest linker (C₆) the most potent fluorescent anti-auxin (*Supplement II*). In addition, the length of the linker had a big impact on the fluorescent properties of the compounds. These characteristics of

IAA analogues, such as the fluorescent intensity, fluorescence decay and fluorescence quantum yield, were measured by the Department of Biophysics, Faculty of Science, Palacký University (*Supplement II*, Fig. S1, S2).

- A library of eleven fluorescent auxin analogues derived from five auxin-like compounds in combination with three types of molecular linkers and NBD fluorophore (*Supplement III*, Fig. S1) was characterized for biological activity, stability and distribution *in planta*. The screening strategy revealed 2,4-D derivatives (FluorA I and II) as the ones with the best fluorescent and biological properties (*Supplement III*, Fig. 1, S2). However, the evaluation of FluorA metabolization (*Supplement III*, Fig. S4A-B) discovered that the biological effect of FluorA compounds is coming from the free 2,4-D released by compound degradation (*Supplement III*, Fig. S4D). Importantly, the confocal studies of fluorescent 2,4-D derivatives indicated that distribution of both analogues, aside of simple diffusion, was regulated by active auxin transport system creating the maxima in tissues where the natural auxin is concentrated, such as quiescent centre, concave side of the apical hook or lateral roots (*Supplement III*, Fig. 3) and the distribution was affected by exogenous stimuli such as light or gravity (*Supplement III*, Fig. 5). Moreover, the subcellular localization of fluorescent analogues was confirmed in the endosomes and ER (*Supplement III*, Fig. 4).

5.2 Method development for studying the metabolic conversion of synthetic auxin analogues *in vivo*

- Purification and detection methods were developed for the investigation of metabolism of different auxin structural analogues (*Supplement III-V*). Methods based on SPE, IAC and LLE together with optimized parameters for LC separation of individual analytes and sensitive MS/MS detection helped to study metabolic conversion and consequent application of auxin derivatives prepared for respective purposes.
- Rapid one-step purification method using LLE of analytes (*Supplement III, IV*) to the water:methanol:hexan (1:1:1) extraction solvent was chosen during optimization based on its high-throughput, availability and efficiency. Several purification protocols combining SPE, LLE and/or IAC were tested. The recoveries of

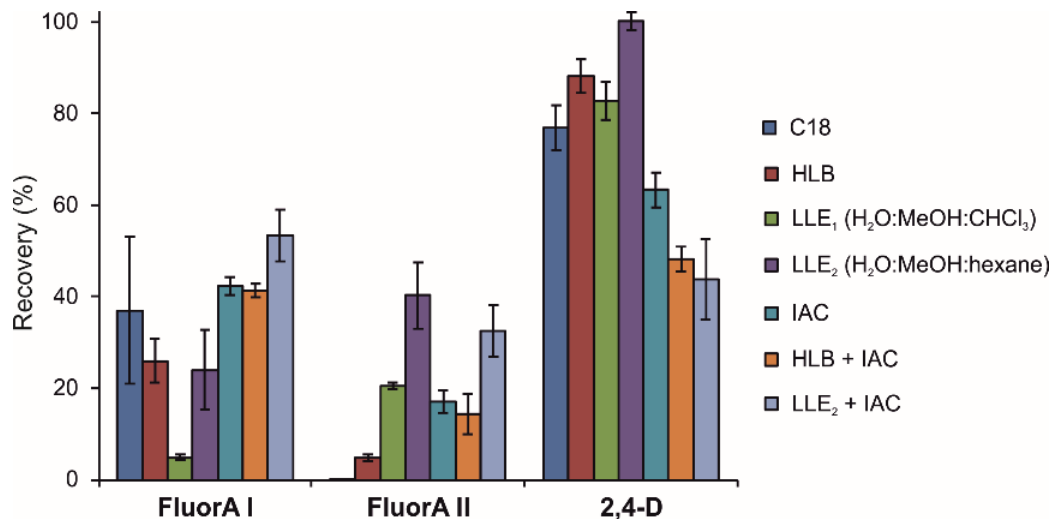


Fig. 9 Recoveries (%) of FluorA compounds and 2,4-D isolated from spiked plant matrices using different purification protocols as follows:

C18 (6ml/500g columns): sample extraction in 1 ml 80% acetonitrile (ACN); column equilibration – 2 ml MeOH and 2x2ml 80% ACN; sample application (1 ml) and column wash (2ml 80% ACN) – flow-throw fraction (3 ml in total) collected in one tube.

HLB (1ml/30 mg columns): sample extraction in 1 ml 70% ACN; column equilibration – 1 ml MeOH, 1 ml H₂O and 1 ml 70% ACN; sample application (1 ml) – flow-throw fraction (1 ml) collected in one tube.

LLE₁: sample extraction in 900 μ l MeOH:H₂O:CHCl₃ (1:1:1); incubation at 4°C for 30 min with continuous shaking; centrifugation; collection of MeOH:H₂O phase.

LLE₂: sample extraction in 1200 μ l MeOH:H₂O:hexane (1:1:1); incubation at 4°C for 30 min with continuous shaking; centrifugation; collection of MeOH:H₂O phase.

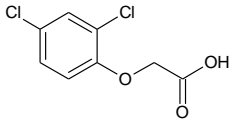
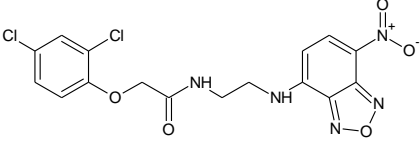
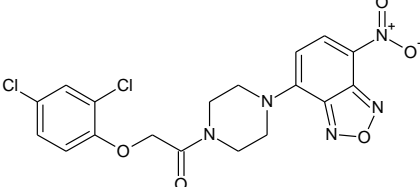
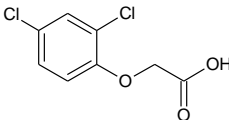
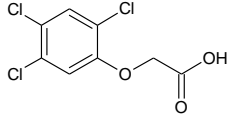
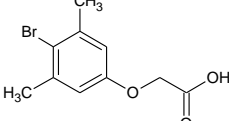
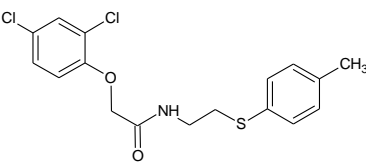
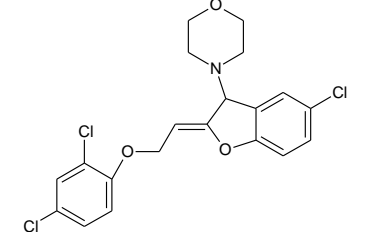
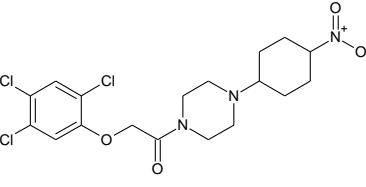
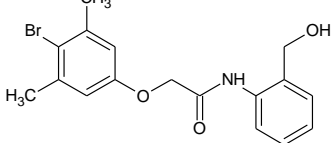
IAC: performed as described in Eyer et al. (2016).

The eluates were then evaporated to dryness, dissolved in 50 μ l of 35% methanol and analysed by UHPLC-MS/MS (10 μ l of sample injected). Each spiking level was determined, compared with the concentration of appropriate standard solution and the recoveries were calculated. Error bars represent mean \pm standard deviations (n=4).

FluorA compounds during the optimized LLE purification are shown in Fig. 9. Moreover, the optimized LLE approach was shown to be with minimal modifications complex enough for efficient extraction and purification of different organic compounds from plant matrix (Tab. 1). Universal LC gradient providing base-line separation of all compounds (Fig. 10) with sensitive MS/MS detection optimized for each group of derivatives (Tab. 2) helped to examine the stability characteristics of studied compounds:

- Fluorescent 2,4-D derivatives FluorA I and II (*Supplement III*) are metabolized *in vivo* to free 2,4-D that provides the auxin response in bioassays (*Supplement III*, Fig. S4).

Tab. 1 Recoveries of studied synthetic organic compounds from plant matrix after using optimized LLE protocol.

Compound	Recovery (%)	Structure	Extraction	Reference
2,4-D	100		H ₂ O:MeOH:hexane 1:1:1	Supplement III
FluorA I	24		H ₂ O:MeOH:hexane 1:1:1	Supplement III
FluorA II	40		H ₂ O:MeOH:hexane 1:1:1	Supplement III
2,4-D	72		H ₂ O:MeOH:hexane 0.1:2:1	Supplement IV
2,4,5-T	64		H ₂ O:MeOH:hexane 0.1:2:1	Supplement IV
RN4-1	74		H ₂ O:MeOH:hexane 0.1:2:1	Supplement IV
RN1	55		H ₂ O:MeOH:hexane 0.1:2:1	Supplement IV
RN2	31		H ₂ O:MeOH:hexane 0.1:2:1	Supplement IV
RN3	48		H ₂ O:MeOH:hexane 0.1:2:1	Supplement IV
RN4	72		H ₂ O:MeOH:hexane 0.1:2:1	Supplement IV

- RN compounds are converted *in planta* to corresponding free auxins partially function as prohormones (*Supplement IV*, Fig. S4). More detailed dose response analysis of RNs bioactivity coupled with MS quantification of endogenous levels of free auxins released from RN3 and RN4 revealed that RN3 and RN4 display different plant response compare to equivalent amount of free 2,4,5-T or RN4-1 respectively (*Supplement IV*, Fig. S5). Additional *in vitro* and *in vivo* evidences showed that RN compounds are selective auxin agonists promoting interaction of TIR1 receptor with specific subset of Aux/IAAs.
- Two-step purification protocol employing ion exchange SPE and immuno-specific sorbent based on anti-2,4-D monoclonal antibodies (E2/G2) was combined with a sensitive LC-MS/MS method (*Supplement V*, Fig. S1 and Tab. S3). Using the target profiling approach, amide-linked metabolites of 2,4-D were detected and identified in 2,4-D treated *Arabidopsis* plants (*Supplement V*, Fig. 2). In addition, the established method helped to unravel that not only the metabolism rates of 2,4-D and IAA, but also metabolisms of their amino acid conjugates (2,4-D-Aspartate and 2,4-D-Glutamate) are distinct. Whereas 2,4-D appeared more stable than IAA with significantly less amino acid conjugation (*Supplement V*, Fig. 4), our results suggested that amide-linked metabolites of 2,4-D, more pronounced with 2,4-D-Asp, are less stable *in vivo*. Further 2,4-D-Asp can be reversibly converted to free 2,4-D or even secondarily metabolized to 2,4-D-Glu (*Supplement V*, Fig. 3). Moreover, 2,4-D-Glu had the potency to affect the root growth in *Arabidopsis* via TIR1/AFB auxin-mediated signalling pathway (*Supplement V*, Fig. 1). Whether the observed auxin effects can be addressed to 2,4-D-Glu itself or to 2,4-D as a hydrolysis product needs to be further investigated.

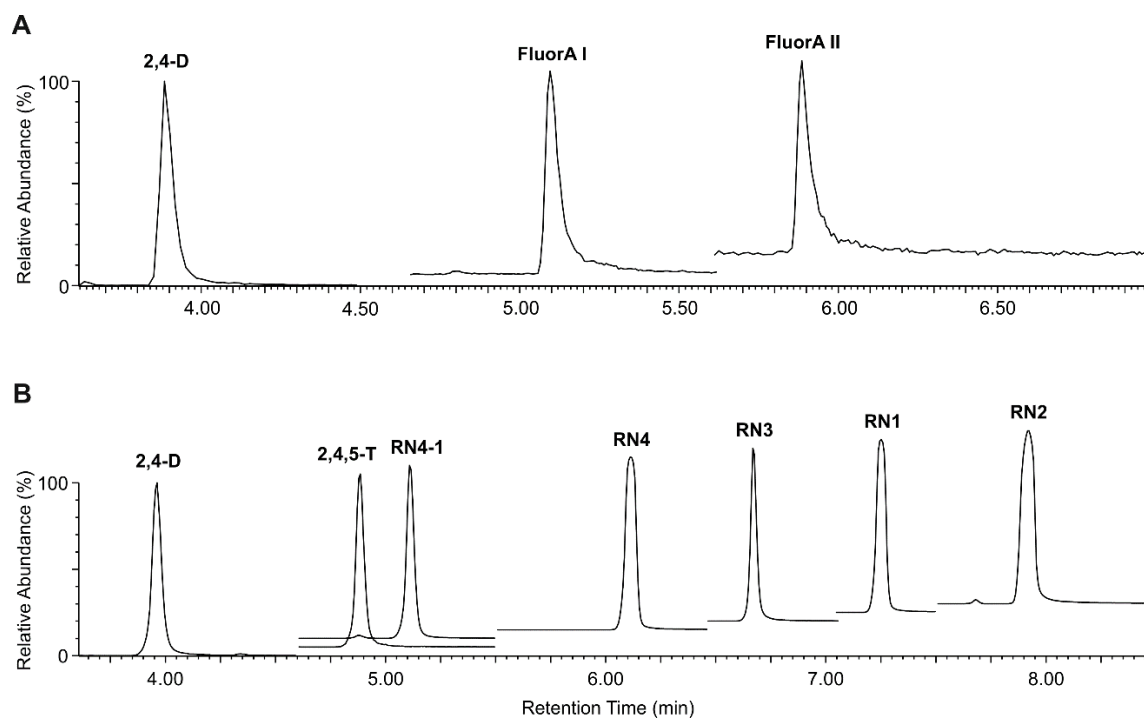


Fig. 10 MRM separations of studied compounds and their potential metabolites by UHPLC-MS/MS method using a Kinetex™ C18 2.1 × 50 mm column and optimized LC gradient (see Chapter 4.3.4). Multi-MRM chromatograms of FluorA compounds (A; Supplement III) and auxin selective agonists RNs (B; Supplement IV).

Tab. 2 Optimized conditions of LC-(ESI)-MS/MS method for each analyte.

Compound	ESI	Retention time [min] ^a	MRM Transition	Capillary voltage [kV]	Cone voltage [V]	Collision energy [V]
2,4-D	-	3.94 ± 0.01	219 > 161	3.0	13	14
FluorA I	+	5.11 ± 0.01	426 > 246	3.0	20	16
FluorA II	+	5.91 ± 0.06	452 > 250	3.0	20	22
2,4,5-T	-	5.09 ± 0.01	253 > 195	3.0	16	14
RN4-1	-	6.65 ± 0.01	257 > 199	3.0	12	15
RN1	+	6.09 ± 0.01	346 > 106	3.0	19	16 / 20
RN2	+	6.65 ± 0.01	444 > 165	3.0	19	33 / 22
RN3	+	7.24 ± 0.01	370 > 151	3.0	19	12 / 12
RN4	+	7.91 ± 0.01	426 > 178	3.0	19	30 / 14

^a The retention time stability is shown as mean ± standard deviations (n=4); ESI, electrospray ionization; MRM, multiple reaction monitoring.

6 Conclusion and perspectives

This thesis deals with the characterization of various novel auxin synthetic analogues with respect to their structure in order they can serve as a useful tool for unravelling the mechanisms of auxin physiology. For this reason, such compounds need to be well investigated in terms of mode of action which includes not only evaluation of biological activity but also their metabolism in model systems.

Overall, the most important outcomes of the work are:

- Novel fluorescent derivatives of IAA that display good fluorescent properties and promising anti-auxin activity due the N1 substitution of indole ring, their precise mode of action and distribution need to be studied in more detail.
- Fluorescent analogues of synthetic auxin 2,4-D that are partially metabolized in to free 2,4-D *in planta*. The fluorescent conjugates as such are not active for auxin signalling but display the auxin-like distribution on both tissue and subcellular levels. This distribution is affected in response to exogenous stimuli. The studies of transport mechanisms with focus on the distribution of fluorescent analogues in apical hook are still in progress.
- New purification and detection methods have been developed to evaluate the metabolism of various auxin analogues *in vivo*. They enabled to estimate the stability of FluorA fluorescent 2,4-D-based derivatives and RN auxin agonists in plants as well as helped to uncover the distinct metabolism of 2,4-D and IAA and their respective amino acid conjugates.

In summary, this thesis provides valuable tools for the field of chemical biology as the form of novel auxin synthetic derivatives and techniques for evaluating their metabolism in plants. The fluorescent auxin analogues with promising biological activity, derivatives mimicking the PAT-driven distribution and selective auxin agonists dissecting different developmental processes together with sensitive MS methods for monitoring their *in vivo* metabolism will be useful tools for investigation of transport and signalling mechanisms underlying plethora of auxin actions.

7 References

- Abbas M., Hernández-García J., Pollmann S., Samodelov S. L., Kolb M., Friml J., Hammes U. Z., Zurbriggen M. D., Blázquez M. A., Alabadí D. (2018) Auxin methylation is required for differential growth in *Arabidopsis*. *Proc Natl Acad Sci USA* **115** (26), 6864–6869.
- Alesso M., Talio M. C., Fernández L. P. (2017) Solid surface fluorescence methodology for fast monitoring of 2,4-dichlorophenoxyacetic acid in seed samples. *Microchem. J.* **135**, 60–65.
- Bak S., Tax F. E., Feldmann K. A., Galbraith D. W., Feyereisen R. (2001) CYP83B1, a cytochrome P450 at the metabolic branch point in auxin and indole glucosinolate biosynthesis in *Arabidopsis*. *Plant Cell* **13**, 101–111.
- Barbez E., Kleine-Vehn J. (2013a) Divide Et Impera--cellular auxin compartmentalization. *Curr. Opin. Plant. Biol.* **16** (1), 78–84.
- Barbez E., Laňková M., Pařezová M., Maizel A., Zařimalová E., Petrášek J., Friml J., Kleine-Vehn J. (2013b) Single-cell-based system to monitor carrier driven cellular auxin homeostasis. *BMC Plant Biol.* **13**, 1–13.
- Barbez E., Kubeš M., Rolčík J., Béziat C., Pěňčík A., Wang B., Rosquet, e M. R., Zhu J., Dobrev P. I., Lee Y., Zařimalová E., Petrášek J., Geisler M., Friml J., Kleine-Vehn J. (2012) A novel putative auxin carrier family regulates intracellular auxin homeostasis in plants. *Nature* **485**, 119–122.
- Barkawi L. S., Tam Y-Y., Tillman J. A., Normanly J., Cohen J. D. (2010) A high-throughput method for the quantitative analysis of auxins. *Nat Protoc* **5**, 1609–1618.
- Bennett M. J., Marchant A., Green H. G., May S. T., Ward S. P., Millner P. A., Walker A. R., Schulz B., Feldmann K. A. (1996) *Arabidopsis* AUX1 gene: a permease-like regulator of root gravitropism. *Science* **273**, 948–950.
- Béziat C., Barbez E., Feraru M. I., Lucyshyn D., Kleine-Vehn J. (2017) Light triggers PILS- dependent reduction in nuclear auxin signalling for growth transition. *Nat. Plants* **3**: 17105
- Bentley J. A. (1950) Growth-regulating effect of certain organic compounds. *Nature* **165**, 449.
- Bieleszová K., Pařízková B., Kubeš M., Husičková A., Kubala M., Sedlářová M., Doleřal K., Strnad M., Novák O., Žukauskaitė A. (2018) New fluorescently labeled auxins exhibit promising anti-auxin activity. *N Biotechnol* **48**, 44–52.
- Blázquez M. (2007) Quantitative GUS Activity Assay of Plant Extracts. *CSH Protoc.* pdb.prot4690.
- Brunoud G., Wells D. M., Oliva M., Larrieu A., Mirabet V., Burrow A. H., Beeckman T., Kepinski S., Traas J., Bennett M. J., Vernoux T. (2012) A novel sensor to map auxin response and distribution at high spatio-temporal resolution. *Nature* **482** (7383), 103–106.
- Calderón Villalobos L. I., Lee S., De Oliveira C., Ivetac A., Brandt W., Armitage L., Sheard L. B., Tan X., Parry G., Mao H., Zheng N., Napier R., Kepinski S., Estelle M. (2012) A combinatorial TIR1/AFB-Aux/IAA co-receptor system for differential sensing of auxin. *Nat. Chem. Biol.* **8** (5), 477–485.
- Cambridge, A., Morris, D. (1996) Transfer of exogenous auxin from the phloem to the polar auxin transport pathway in pea (*Pisum sativum* L.). *Planta* **199**, 583–588.

- Chapman E. J., Estelle M. (2009) Mechanism of auxin-regulated gene expression in plants. *Annu. Rev. Genomics. Hum. Genet.* **43**, 265–285.
- Chaves M. de J. S., Verbinnen R., Diniz M. dos S., Viana J. L. M. (2018) Successful and Robustness of 2,4-D Analysis in Surface Waters. *Revista Virtual de Quimica* **10** (5), 1474–1484.
- Chen C., Chen Y., Zhou J., Wu C. (2006) A 9-vinyladenine-based molecularly imprinted polymeric membrane for the efficient recognition of plant hormone 1H-indole-3-acetic acid. *Anal. Chim. Acta* **569** (1), 58–65.
- Chen J. G., Ullah H., Young J. C., Sussman M. R., Jones A. M. (2001) ABP1 is required for organized cell elongation and division in *Arabidopsis* embryogenesis. *Genes Dev.* **15**, 902–911.
- Chen X., Grandont L., Li H., Hauschild R., Paque S., Abuzeineh A., Rakusová H., Benkova E., Perrot-Rechenmann C., Friml J. (2014) Inhibition of cell expansion by rapid ABP1-mediated auxin effect on microtubules. *Nature* **516**, 90–93.
- Chiwocha S. D., Dixon K. W., Flematti G. R., Ghisalberti E. L., Merritt D. J., Nelson D. C., Riseborough J. M., Smith S., Stevens J. (2009). Karrikins: A new family of plant growth regulators in smoke. *Plant Sci.* **177** (4), 252–256.
- Cho M., Lee S. H., Cho H-T. (2007) P-glycoprotein4 displays auxin efflux transporter-like action in *Arabidopsis* root hair cells and tobacco cells. *Plant Cell.* **19** (12), 3930–3943.
- Cserháti T., Forgács E. (1998) Phenoxyacetic acids: separation and quantitative determination. *J. Chromatogr. B.* **717**, 125–178.
- Darwin C. and Darwin F. (1880) *The power of movement in plants*. John Murray, London.
- Davies P. J. (2010) *Plant Hormones: Biosynthesis, Signal Transduction, Action!* 3rd Edition: The Plant Hormones: Their Nature, Occurrence, and Functions. Kluwer Academic Publishers, Dordrecht, Netherlands, 5–15.
- De Jong M., Wolters-Arts M., Feron R., Mariani C., Vriezen W. H. (2009) The *Solanum lycopersicum* auxin response factor 7 (SIARF7) regulates auxin signaling during tomato fruit set and development. *Plant J.* **57**, 160–170.
- De Rybel B., Audenaert D., Beeckman T., Kepinski S. (2009). The Past, Present, and Future of Chemical Biology in Auxin Research. *ACS Chem. Biol.* **4** (12), 987–998.
- del Pozo J. C., Boniotti M. B., Gutierrez C. (2002) *Arabidopsis* E2FC functions in cell division and is degraded by the ubiquitin-SCFAtSKP2 pathway in response to light. *Plant Cell.* **14**, 3057–3071.
- del Pozo J. C., Diaz-Trivino S., Cisneros N., Gutierrez C. (2006) The balance between cell division and endoreplication depends on E2FC-DPB, transcription factors regulated by the ubiquitin-SCFSKP2A pathway in *Arabidopsis*. *Plant Cell.* **18**, 2224–2235.
- Delbarre A., Muller P., Imhoff V., Guern J. (1996) Comparison of mechanisms controlling uptake and accumulation of 2,4-dichlorophenoxy acetic acid, naphthalene-1-acetic acid, and indole-3-acetic acid in suspension-cultured tobacco cells. *Planta* **198** (4), 532–541.
- Dharmasiri N., Dharmasiri S., Estelle M. (2005a) The F-box protein TIR1 is an auxin receptor. *Nature* **435**, 441–445.

- Dharmasiri N., Dharmasiri S., Weijers D., Lechner E., Yamada M., Hobbie L., Ehrismann J. S., Jürgens G., Estelle M. (2005b) Plant development is regulated by a family of auxin receptor F box proteins. *Dev. Cell* **9**, 109–119.
- Dobrev P. I., Havlíček L., Vágner M., Malbeck J., Kamínek M. (2005) Purification and determination of plant hormones auxin and abscisic acid using solid phase extraction and two-dimensional high performance liquid chromatography. *J. Chromatogr. A* **1075** (1-2), 159–166.
- Dobrev P. I., Kamínek M. (2002) Fast and efficient separation of cytokinins from auxin and abscisic acid and their purification using mixed-mode solid-phase extraction. *J. Chromatogr. A* **950**(1-2), 21–29.
- Du F., Ruan G., Liu H. (2012) Analytical methods for tracing plant hormones. *Anal Bioanal Chem.* **403** (1), 55–74.
- Epel B. L., Erlanger M., Yahalom M. (1987) The etiolated cucumber hypocotyl weight-growth test: A sensitive, easy and ultrafast bioassay for IAA. *Plant Growth Regul.* **5**, 3–14.
- Enders T. A., Oh S., Yang Z., Montgomery B. L., Strader L. C. (2015) Genome Sequencing of *Arabidopsis abp1-5* Reveals Second-Site Mutations That May Affect Phenotypes. *Plant Cell.* **27** (7), 1820–1826.
- Enders T. A., Strader L. C. (2015) Auxin Activity: Past, present, and Future. *Am J Bot.* **102** (2), 180–196.
- Eyer L., Vain T., Pařízková B., Okleštková J., Barbez E., Kozubíková H., Pospíšil T., Wierzbicka R., Kleine-Vehn J., Fránek M., Strnad M., Robert S., Novák O. (2016) *PLoS One* **11** (7), e0159269.
- Fendrych M., Leung J., Friml J. (2016) TIR1/AFB-Aux/IAA auxin perception mediates rapid cell wall acidification and growth of *Arabidopsis* hypocotyls. *eLife* **5**, e19048.
- Fendrych M., Akhmanova M., Merrin J., Glanc M., Hagihara S., Takahashi K., Uchida N., Torii K. U., Friml J. (2018) Rapid and reversible root growth inhibition by TIR1 auxin signalling. *Nat. Plants* **4**, 453–459.
- Feng X., Zhang G., Chin L. K., Liu A. Q., Liedberg B. (2017) Highly Sensitive, Label-Free Detection of 2,4-Dichlorophenoxyacetic Acid Using an Optofluidic Chip. *ACS Sens.* **2** (7), 955–960.
- Feraru E., Feraru M. I., Barbez E., Waidmann S., Sun L., Gaidora A., Kleine-Vehn J. (2019) PILS6 is a temperature-sensitive regulator of nuclear auxin input and organ growth in *Arabidopsis thaliana*. *Proc. Natl. Acad. Sci. USA* **116** (9), 3893–3898.
- Ferro N., Bredow T., Jacobsen H. J., Reinard T. (2010) Route to novel auxin: auxin chemical space toward biological correlation carriers. *Chem. Rev.* **110**, 4690–4708.
- Flematti G. R., Ghisalberti E. L., Dixon K. W., Trengove R. D. (2004) A Compound from Smoke That Promotes Seed Germination. *Science* **305**, 977.
- Frick E. M., Strader L. C. (2018) Roles for IBA-derived auxin in plant development. *J. Exp. Bot.* **69**(2), 169-177.
- Friml, J. (2003) Auxin transport - shaping the plant. *Curr. Opin. Plant. Biol.* **6**, 7–12.
- Ganguly A., Lee S. H., Cho M., Lee O. R., Yoo H., Cho H. T. (2010) Differential auxin-transporting activities of PIN-FORMED proteins in *Arabidopsis* root hair cells. *Plant Physiol.* **153**, 1046–1061

- Gao Y., Zhang Y., Zhang D., Dai X., Estelle M., Zhao Y.: Auxin binding protein 1 (ABP1) is not required for either auxin signaling or *Arabidopsis* development. *Proc. Natl. Acad. Sci. USA* **112**, 2275–2280.
- Goggin D. E., Nealon G. L., Cawthray G. R., Scaffidi A., Howard M. J., Powles S. B., Flematti G. R. (2018) Identity and Activity of 2,4-Dichlorophenoxyacetic Acid Metabolites in Wild Radish (*Raphanus raphanistrum*). *J. Agric. Food. Chem.* **66** (51), 13378–13385.
- Grebe M., Friml J., Swarup K., Ljung K., Sandberg G., Terlouw M., Palme K., Bennett M. J., Scheres B. (2002) Cell polarity signaling in *Arabidopsis* involves a BFA-sensitive auxin influx Pathway. *Curr. Biol.* **12**, 329–334.
- Grossmann K. (2009) Auxin herbicides: current status of mechanism and mode of action. *Pest manag. sci.* **66**, 113–120.
- Gyulai G., Heszky L. E. (1994) Auxin and cytokinin bioassays. A short overview. *Acta Agronomica Hung.* **43**, 185–197.
- Haeck A., Van Langenhove H., Harinck L., Kyndt T., Gheysen G., Höfte M., Demeestere K. (2018) Trace analysis of multi-class phytohormones in *Oryza sativa* using different scan modes in high-resolution Orbitrap mass spectrometry: method validation, concentration levels, and screening in multiple accessions. *Anal. Bioanal. Chem.* **410**, 4527–4539.
- Hamant O., Heisler M. G., Jonsson H., Krupinski P., Uyttewaal M., Bokov P., Corson F., Sahlin P., Boudaoud A., Meyerowitz E. M., Couder Y., Traas J. (2008) Developmental patterning by mechanical signals in *Arabidopsis*. *Science* **322**, 1650–1655.
- Harrison S. T. L. (2011) Comprehensive Biotechnology 2nd Edition: Cell disruption. Elsevier, Oxford, England, 619–640.
- Hayashi K. I., Tan X., Zheng N., Hatate T., Kimura Y., Kepinski S., Nozaki H. (2008) Small-molecule agonists and antagonists of F-box protein– substrate interactions in auxin perception and signaling. *Proc. Natl. Acad. Sci. USA* **105**, 5632–5637.
- Hayashi K. I., Neve J., Hirose M., Kuboki A., Shimada Y., Kepinski S., Nozaki H. (2012) Rational design of an auxin antagonist of the SCF^{TIR1} auxin receptor complex. *ACS Chem. Biol.* **7**, 590–598.
- Hayashi K. I., Nakamura S., Fukunaga S., Nishimura T., Jenness M. K., Murphy A. S., Motose H., Nozaki H., Furutani M., Aoyama T. (2014) Auxin transport sites are visualized in planta using fluorescent auxin analogs. *Proc. Natl. Acad. Sci. USA* **111**: 11557–11562.
- Hayashi K. I., Kusaka N., Yamasaki S., Zhao Y., Nozaki H. (2015) Development of 4-methoxy-7-nitroindolinyI (MNI)-caged auxins which are extremely stable *in planta*. *Bioorg. Med. Chem. Lett.* **25**, 4464–4471.
- Henneberger L., Mühlenbrink M., Fischer F. C., Escher B. I. (2017) C18-Coated Solid-Phase Microextraction Fibers for the Quantification of Partitioning of Organic Acids to Proteins, Lipids, and Cells. *Chem. Res. Toxicol.* **32**, 168–178.
- Hu Y., Li Y., Zhang Y., Li G., Chen Y. (2011) Development of sample preparation method for auxin analysis in plants by vacuum microwave-assisted extraction combined with molecularly imprinted clean-up procedure. *Anal Bioanal Chem.* **399** (10), 3367–3374.

- Hua M. Z., Feng S. L., Wang S., Lu X. N. (2018) Rapid detection and quantification of 2,4-dichlorophenoxyacetic acid in milk using molecularly imprinted polymers-surface-enhanced Raman spectroscopy. *Food Chem.* **258**, 254–259.
- Ito H., Gray W. M. A gain-of-function mutation in the *Arabidopsis* pleiotropic drug resistance transporter PDR9 confers resistance to auxinic herbicides. *Plant Phys.* **142**, 63–74.
- Jackson R. G., Lim E. K., Li Y., Kowalczyk M., Sandberg G., Hoggett J., Ashford D. A., Bowles D. J. (2001) Identification and biochemical characterization of an *Arabidopsis* indole-3-acetic acid glucosyltransferase. *J Biol Chem.* **276** (6), 4350–4356.
- Jenik P. D., Barton M. K. (2005) Surge and destroy: the role of auxin in plant embryogenesis. *Development* **132**, 3577–3585.
- Jones A. M., Venis M. A. (1989) Photoaffinity labeling of indole-3-acetic acid-binding proteins in maize. *Proc. Natl. Acad. Sci. USA* **86**, 6153–6156.
- Jurado S., Abraham Z., Manzano C., Lopez-Torrejon G., Pacios L. F., Del Pozo J. C. (2010) The *Arabidopsis* cell cycle F-box protein SKP2A binds to auxin. *Plant Cell.* **22**, 3891–3904.
- Jursík M., Soukup J., Holec J. (2010) Úvod do problematiky mechanismu působení herbicidů. *Listy cukrovarnické a řepařské* **126**, 14–16.
- Kai K., Horita J., Wakasa K., Miyagawa H. (2007a) Three oxidative metabolites of indole-3-acetic acid from *Arabidopsis thaliana*. *Phytochemistry* **68** (12), 1651–63.
- Kai K., Wakasa K., Miyagawa H. (2007b) Metabolism of indole-3-acetic acid in rice: identification and characterization of N-beta-D-glucopyranosyl indole-3-acetic acid and its conjugates. *Phytochemistry* **68** (20), 2512–2522.
- Kamimoto Y., Terasaka K., Hamamoto M., Takanashi K., Fukuda S., Shitan N., Sugiyama A., Suzuki H., Shibata D., Wang B., Pollmann S., Geisler M., Yazaki K. (2012) *Arabidopsis* ABCB21 is a Facultative Auxin Importer/Exporter Regulated by Cytoplasmic Auxin Concentration. *Plant. Cell. Physiol.* **53** (12), 2090–2100.
- Kepinski S., Leyser O. (2005) The *Arabidopsis* F-box protein TIR1 is an auxin receptor. *Nature* **435** (7041), 446–451.
- Kinoshita T., Cano-Delgado A. C., Seto H., Hiranuma S., Fujioka S., Yoshida S., Chory J. (2005) Binding of brassinosteroids to the extracellular domain of plant receptor kinase BRI1. *Nature* **433**, 167–171.
- Kleine-Vehn J., Sauer M. (2017) *Plant Hormones: Methods and Protocols* 3rd Edition, Humana Press, New York, USA.
- Koesukwiwat U., Sanguankaew K., Leepipatpiboon N. (2008) Rapid determination of phenoxy acid residues in rice by modified QuEChERS extraction and liquid chromatography-tandem mass spectrometry. *Anal Chim Acta* **626**, 10–20.
- Kowalczyk M., Sandberg G. (2001) Quantitative analysis of indole-3-acetic acid metabolites in *Arabidopsis*. *Plant Physiol.* **127**, 1845–1853.
- Kubeš M., Napier R. (2019) Non-canonical auxin signalling: fast and curious. *J. Exp. Bot.* pii: erz111. doi: 10.1093/jxb/erz111. [Epub ahead of print].

- Kubeš M., Yang H., Richter G. L., Cheng Y., Młodzińska E., Wang X., Blakeslee J. J., Carraro N., Petrášek J., Zažímalová E., Hoyerová K., Peer W. A., Murphy A.S. (2012) The *Arabidopsis* concentration-dependent influx/efflux transporter ABCB4 regulates cellular auxin levels in the root epidermis. *Plant J* **69** (4), 640–654.
- Kugimiya A., Takeuchi T. (1999) Application of indoleacetic acid-imprinted polymer to solid phase extraction. *Anal. Chim. Acta* **395** (3), 251–255.
- Lee S., Sundaram S., Armitage L., Evans J. P., Hawkes T., Kepinski S., Ferro N., Napier R. M. (2014) Defining binding efficiency and specificity of auxins for SCF(TIR1/AFB)-Aux/IAA co-receptor complex formation. *ACS Chem. Biol.* **9** (3), 673–82.
- Lewis D. R., Miller N. D., Splitt B. L., Wu G., Spalding E. P. (2007) Separating the roles of acropetal and basipetal auxin transport on gravitropism with mutations in two *Arabidopsis* multidrug resistance-like ABC transporter genes. *Plant Cell.* **19**, 1838–1850.
- Leyser O. (2005) The fall and rise of apical dominance. *Curr. Opin. Genet. Dev.* **15**, 468–471.
- Li R., Li J., Li S., Qin G., Novák O., Pěňčík A., Ljung K., Aoyama T., Liu J., Murphy A. S., Gu H., Tsuge T., Qu L. J. (2014) ADP1 affects plant architecture by regulating local auxin biosynthesis. *PLoS Genet.* **10**(1), e1003954.
- Liu X., Hegeman A. D., Gardner G., Cohen J. D. (2012) Protocol: High-throughput and quantitative assays of auxin and auxin precursors from minute tissue samples. *Plant Methods* **8** (31), 1–17.
- Ljung K. (2013) Auxin metabolism and homeostasis during plant development. *Development* **140**, 943–950.
- Ljung K., Hull A. K., Celenza J., Yamada M., Estelle M., Normanly J., Sandberg G. (2005) Sites and regulation of auxin biosynthesis in *Arabidopsis* roots. *Plant Cell* **17**, 1090–1104.
- Ljung K., Sandberg G., Moritz T. (2004) Methods of plant hormone analysis. *Plant hormones: Biosynthesis, Signal Transduction, Action!*, P.J. Davies, ed., Kluwer Academic Publishers, Dordrecht, Netherlands, 671–694.
- Löbner M., Klämbt D. (1985) Auxin-binding protein from coleoptile membranes of corn (*Zea mays* L.): Purification by immunological methods and characterization. *J. Biol. Chem.* **260**, 9848–9853.
- Lu Q., Chen L., Lu M., Chen G., Zhang L. (2010) Extraction and analysis of auxins in plants using dispersive liquid-liquid microextraction followed by high-performance liquid chromatography with fluorescence detection. *J Agric Food Chem.* **58** (5), 2763–2770.
- Ludwig-Müller J. (2007) Indole-3-butyric acid synthesis in ecotypes and mutants of *Arabidopsis thaliana* under different growth conditions. *J. Plant Physiol.* **164** (1):47–59.
- Ludwig-Müller J. (2011) Auxin conjugates: Their role for plant development and in the evolution of land plants. *J. Exp. Bot.* **62**, 1757–1773.
- Ma Q., Robert S. (2014) Auxin biology revealed by small molecules. *Physiol. Plant.* **151** (1), 25–42.
- Ma Q., Groner P., Robert S. (2017) Auxin signaling: a big question to be addressed by small molecules. *J. Exp. Bot.* **69** (2), 313–328.

- Marcussen J., Ulvskov P., Olsen C. E., Rajagopal R. (1989) Preparation and properties of antibodies against indoleacetic-acid (IAA)-C5-BSA, a novel ring-coupled IAA antigen, as compared to 2 other types of IAA-specific antibodies. *Plant Physiol.* **89**, 1071–1078.
- Mashiguchi K., Tanaka K., Sakai T., Sugawara S., Kawaide H., Natsume M., Hanada A., Yaeno T., Shirasu K., Yao H., McSteen P., Zhao Y., Hayashi K., Kamiya Y., Kasahara H. (2011) The main auxin biosynthesis pathway in *Arabidopsis*. *Proc. Natl. Acad. Sci. USA* **108**, 18512–18517.
- Michalko J., Dravecká M., Bollenbach T., Friml J. (2015) Embryo-lethal phenotypes in early *abp1* mutants are due to disruption of the neighboring *BSM* gene. *F1000Research* **4**:1104, 1–14.
- Michalko J., Glanc M., Perrot-Rechenmann C., Friml J. (2016) Strong morphological defects in conditional *Arabidopsis abp1* knock-down mutants generated in absence of functional ABP1 protein. *F1000Research* **5**:86, 1–13.
- Middleton A. M., Dal Bosco C., Chlap P., Bensch R., Harz H., Ren F., Bergmann S., Wend S., Weber W., Hayashi K. I., Zurbriggen M. D., Uhl R., Ronneberger O., Palme K., Fleck C., Dovzhenko A. (2018) Data-Driven Modeling of Intracellular Auxin Fluxes Indicates a Dominant Role of the ER in Controlling Nuclear Auxin Uptake. *Cell. Rep.* **22** (11), 3044–3057.
- Miller C. O., Skoog F. (1957) Chemical regulation of growth and organ formation in plant tissues cultured *in vitro*. *Symp. Soc. Exp. Biol.* **11**, 118–130.
- Mithila J., Hall Ch. J., Johnson G. W., Kelley K. B., Riechers D. E. (2011) Evolution of Resistance to Auxinic Herbicides: Historical Perspectives, Mechanisms of Resistance, and Implications for Broadleaf Weed Management in Agronomic Crops. *Weed Sci.* **59**: 445–457.
- Mravec J., Skůpa P., Bailly A., Hoyerová K., Křeček P., Bielach A., Petrášek J., Zhang J., Gaykova V., Stierhof Y. D., Dobrev P. I., Schwarzerová K., Rolčík J., Seifertová D., Luschnig C., Benková E., Zažímalová E., Geisler M., Friml J. (2009) Subcellular homeostasis of phytohormone auxin is mediated by the ER-localized PIN5 transporter. *Nature* **459**, 1136–1140.
- Muscolo A., Sidari M., Francioso O., Tugnoli V. a Nardi S. (2007) The auxin-like activity of humic substances is related to membrane interactions in capot cell cultures. *J. Chem. Ecol.* **33**: 115–129.
- Niguso T. T., Soreta T. R., Woldemariam E. T. (2018) Electrochemical Determination of 2,4-Dichlorophenoxyacetic Acid using Bismuth Film Modified Screen-printed Carbon Electrode. *S. Afr. J. Chem.* **71**, 160–165.
- Noh B., Murphy A. S., Spalding E. P. (2001) Multidrug resistance-like genes of *Arabidopsis* required for auxin transport and auxin-mediated development. *Plant Cell* **13**, 2441–2454.
- Normanly J. (2010) Approaching Cellular and Molecular Resolution of Auxin Biosynthesis and Metabolism - *Cold Spring Harb. Perspect. Biol.* **2**, 1–17.
- Normanly J., Cohen J. D., Fink G. R. (1993) *Arabidopsis thaliana* auxotrophs reveal a tryptophan-independent biosynthetic pathway for indole-3-acetic acid. *Proc. Natl. Acad. Sci. USA* **90**, 10355–10359.
- Novák O., Hényková E., Sairanen I., Kowalczyk M., Pospíšil T., Ljung K. (2012) Tissue-specific profiling of the *Arabidopsis thaliana* auxin metabolome. *Plant J.* **72**, 523–536.

- Novák O., Pěňčík A., Blahoušek O., Ljung K. Quantitative Auxin Metabolite Profiling Using Stable Isotope Dilution UHPLC-MS/MS. *Curr. Protoc. Plant Biol.* **1** (2), 419–430.
- Novák O., Pěňčík A., Ljung K. (2014) Auxin and Its Role in Plant Development: Identification and Profiling of Auxin and Auxin Metabolites. Springer-Verlag Wien, Austria, 39–60.
- Nováková L., Vlčková H. (2009) A review of current trends and advances in modern bio-analytical methods: chromatography and sample preparation. *Anal Chim Acta* **656** (1-2), 8–35.
- Overvoorde P., Fukaki H., Beeckman T. (2010) Auxin control of root development. *Cold. Spring Harb. Perspect. Biol.* **2** (6), 1–16.
- Péret B., Swarup K., Ferguson A., Seth M., Yang Y., Dhondt S., James N., Casimiro I., Perry P., Syed A., Yang H., Reemmer J., Venison E., Howells C., Perez-Amador M. A., Yun J., Alonso J., Beemster G. T., Laplace L., Murphy A., Bennett M. J., Nielsen E., Swarup R. AUX/LAX genes encode a family of auxin influx transporters that perform distinct functions during *Arabidopsis* development. *Plant Cell.* **24** (7), 2874–2885.
- Peterson M. A., McMaster S. A., Riechers D. E., Skelton J., Stahlman P. W. (2016) 2,4-D Past, Present, and Future: A Review. *Weed Technol.* **30** (2), 303–345.
- Petersson S. V., Johansson A. I., Kowalczyk M., Makoveychuk A., Wang J. Y., Moritz T., Grebe M., Benfey P. N., Sandberg G., Ljung K. (2009) An auxin gradient and maximum in the *Arabidopsis* root apex shown by high-resolution cell-specific analysis of IAA distribution and synthesis. *Plant Cell.* **21** (6), 1659–1668.
- Petersson S. V., Lindén P., Moritz T., Ljung K. (2015) Cell-type specific metabolic profiling of *Arabidopsis thaliana* protoplasts as a tool for plant systems biology. *Metabolomics* **11** (6), 1679–1689.
- Pan S. X., Wang X. (2009) Profiling of plant hormones by mass spectrometry. *J. Chrom. B* **877** (26), 2806–2813.
- Pařízková B., Pernisová M., Novák O. (2017) What Has Been Seen Cannot Be Unseen—Detecting Auxin *In Vivo*. *Int. J. Mol. Sci.* **18** (12), 2736.
- Paque S., Mouille G., Grandont L., Alabadí D., Gaertner C., Goyallon A., Muller P., Primard-Brisset C., Sormani R., Blázquez M. A., Perrot-Rechenmann C. (2014) AUXIN BINDING PROTEIN1 links cell wall remodeling, auxin signaling, and cell expansion in *Arabidopsis*. *Plant Cell.* **26**, 280–295.
- Paque S., Weijers D. (2016) Q&A: Auxin: the plant molecule that influences almost anything. *BMC Biol.* **14** (1):67, 1–5.
- Parry G., Calderon-Villalobos L. I., Prigge M., Peret B., Dharmasiri S., Itoh H., Lechner E., Gray W. M., Bennett M., Estelle M. (2009) Complex regulation of the TIR1/AFB family of auxin receptors. *Proc Natl Acad Sci USA* **106** (52), 22540–22545.
- Pedron J., Brault M., Nake C., Miginiac E. (1998) Detection of abscisic-acid-binding proteins in the microsomal protein fraction of *Arabidopsis thaliana* with abscisic-acid-protein conjugates used as affinity probes. *Eur. J. Biochem.* **252**, 385–390.
- Peer W. A., Blakeslee J. J., Yang H., Murphy A. S. (2011) Seven things we think we know about auxin transport. *Mol. Plant.* **4**, 487–504.

- Pereira I., Rodrigues M. F., Chaves A. R., Vaz B. G. (2018) Molecularly imprinted polymer (MIP) membrane assisted direct spray ionization mass spectrometry for agrochemicals screening in foodstuffs. *Talanta* **178**, 507–514.
- Peterson G. E. (1967) The discovery and development of 2,4-D. *Agric. Hist.* **41**, 243–253.
- Petrášek J., Mravec J., Bouchard R., Blakeslee J. J., Abas M., Seifertova D., Wisniewska J., Tadele Z., Kubeš M., Covanová M., Dhonukshe P., Skupa P., Benková E., Perry L., Krecek P., Lee O. R., Fink G. R., Geisler M., Murphy A. S., Luschnig C., Zažímalová E., Friml J. (2006) PIN proteins perform a rate-limiting function in cellular auxin efflux. *Science* **312**, 914–918.
- Pěňčík A., Casanova-Sáez R., Pilařová V., Žukauskaite A., Pinto R., Micol J. L., Ljung K., Novák O. (2018) Ultra-rapid auxin metabolite profiling for high-throughput mutant screening in *Arabidopsis*. *J. Exp. Bot.* **69** (10), 2569–2579.
- Pěňčík A., Rolčík J., Novák O., Magnus V., Barták P., Buchtík R., Salopek-Sondi B., Strnad M. (2009) Isolation of novel indole-3-acetic acid conjugates by immunoaffinity extraction. *Talanta* **80** (2), 651–655.
- Pěňčík A., Simonovik B., Petersson S. V., Henyková E., Simon S., Greenham K., Zhang Y., Kowalczyk M., Estelle M., Zažímalová E., Novák O., Sandberg O., Ljung K. (2013) Regulation of auxin homeostasis and gradients in *Arabidopsis* roots through the formation of the indole-3-acetic acid catabolite 2-oxindole-3-acetic acid. *Plant Cell* **25**, 3858–3870.
- Porco S., Pěňčík A., Rashed A., Voß U., Casanova-Sáez R., Bishopp A., Golebiowska A., Bhosale R., Swarup R., Swarup K., Peňáková P., Novák O., Staswick P., Hedden P., Phillips A. L., Vissenberg K., Bennett M. J., Ljung K. (2016) Dioxygenase-encoding AtDAO1 gene controls IAA oxidation and homeostasis in *Arabidopsis*. *Proc. Natl. Acad. Sci. USA.* **113** (39), 11016–21.
- Porfírio S., Gomes da Silva M. D. R., Peixe A., Cabrita M. J., Azadi P. Current analytical methods for plant auxin quantification--A review. *Anal Chim Acta.* **902**, 8–21.
- Prigge M. J., Greenham K., Zhang Y., Santner A., Castillejo C., Mutka A. M., O'Malley R. C., Ecker J. R., Kunkel B. N., Estelle M. (2016) The *Arabidopsis* auxin receptor F-box proteins AFB4 and AFB5 are required for response to the synthetic auxin picloram. *G3 (Bethesda)* **6** (5), 1383–1390.
- Qin G., Zou K., Tian L., Li Y. (2018) Determination of Five Plant Growth Regulator Containing Carboxyl in Bean Sprouts Based on Chemical Derivatization by GC-MS. *Food Anal. Methods* **11** (9), 2628–2635.
- Ranocha P., Dima O., Nagy R., Felten J., Corratgé-Faillie C., Novák O., Morreel K., Lacombe B., Martinez Y., Pfrunder S., Jin X., Renou J. P., Thibaud J. B., Ljung K., Fischer U., Martinoia E., Boerjan W., Goffner D. (2013) *Arabidopsis* WAT1 is a vacuolar auxin transport facilitator required for auxin homeostasis. *Nat Commun* **4**, 2625.
- Reizelman A., Wigchert S. C. M., del-Bianco C., Zwanenburg B. (2003) Synthesis and bioactivity of labelled germination stimulants for the isolation and identification of the strigolactone receptor. *Org. Biomol. Chem.* **1**, 950–959.
- Remy E., Duque P. (2014) Beyond cellular detoxification: A plethora of physiological roles for MDR transporter homologs in plants. *Front. Physiol.* **5** (201), 1–10.

- Rittenberg D., Foster G. L. (1940) A new procedure for quantitative analysis by isotope dilution, with application to the determination of amino acids and fatty acids. *J. Biol. Chem.* **133**, 737–744.
- Robert M. M., Fujita T., Hansch C. (1967) Structure-Activity Relationship in the Auxin Activity of Mono-Substituted Phenylacetic Acids. *Plant Physiol.* **42**: 1519–1526.
- Robert S., Friml J. (2009) Auxin and other signals on the move in plants. *Nat. Chem. Bio.* **5**, 325–332.
- Rodriguez I., Rubi E., Gonzalez R, Quintana J. B., Cela R. (2005) On-fibre silylation following solid-phase microextraction for the determination of acidic herbicides in water samples by gas chromatography. *Anal. Chim. Acta* **537** (1-2), 259–266.
- Ruegger M., Dewey E., Hobbie L., Brown D., Bernasconi P., Turner J., Muday G., Estelle M. (1997) Reduced NPA-binding in the *tir3* mutant of *Arabidopsis* is associated with a reduction in polar auxin transport and diverse morphological defects. *Plant Cell.* **9**, 745–757.
- Ruegger M., Dewey E., Gray W. M., Hobbie L., Turner J., Estelle M. (1998) The TIR1 protein of *Arabidopsis* functions in auxin response and is related to human SKP2 and yeast *grr1p*. *Genes Dev.* **12**, 198–207.
- Rubinstein B., Leopold A. C. (1963) Analysis of the auxin control of bean leaf abscission. *Plant Physiol.* **38**, 262–267.
- Santos-Delgado M. J., Crespo-Corral E., Polo-Díez L. M. (2000) Determination of herbicides in soil samples by gas chromatography: optimization by the simplex method. *Talanta* **53** (2), 367–377.
- Sauer M., Kleine-Vehn J. (2011) AUXIN BINDING PROTEIN1: the outsider. *Plant Cell.* **23** (6), 2033–2043.
- Savaldi-Goldstein S., Baiga T. J., Pojer F., Dabi T., Butterfield C., Parry G., Santner A., Dharmasiri N., Tao Y., Estelle M., Noel J. P., Chory J. (2008) New auxin analogs with growth-promoting effects in intact plants reveal a chemical strategy to improve hormone delivery. *Proc. Natl. Acad. Sci. USA* **105**, 15190–15195.
- Simon S., Petrášek J. (2011) Why plants need more than one type of auxin. *Plant Sci.* **180**, 454–460.
- Schmelz E. A., Engelberth J., Tumlinson J. H., Block A., Alborn H. T. The use of vapor phase extraction in metabolic profiling of phytohormones and other metabolites. *Plant J.* **39** (5), 790–808.
- Shao W., Dong J. (2016) Polarity in plant asymmetric cell division: Division orientation and cell fate differentiation. *Dev. Biol.* **419**, 121–131.
- Sokołowska K., Kizińska J., Szewczuk Z. a Banasiak A. (2014) Auxin conjugated to fluorescent dyes - a tool for the analysis of auxin transport pathways. *Plant Biol.* **16**: 866–877.
- Staswick P. E., Serban B., Rowe M., Tiryaki I., Maldonado M. T., Maldonado M. C., Suza W. (2005) Characterization of an *Arabidopsis* enzyme family that conjugates amino acids to indole-3-acetic acid. *Plant Cell* **17** (2), 616–27.
- Sugawara S., Mashiguchi K., Tanaka K., Hishiyama S., Sakai T., Hanada K., Kinoshita-Tsujimura K., Yu H., Dai X., Takebayashi Y., Takeda-Kamiya N., Kakimoto T., Kawaide H., Natsume M., Estelle M.,

- Zhao Y., Hayashi K. I., Kamiya Y., Kasahara H. (2015) Distinct Characteristics of Indole-3-Acetic Acid and Phenylacetic Acid, Two Common Auxins in Plants. *Plant Cell Physiol* **56** (8), 1641–1654.
- Sundberg B., Sandberg G., Crozier A. (1986) Purification of indol-3-acetic acid in plant extracts by immunoaffinity chromatography. *Phytochemistry* **25**, 295–298.
- Swarup K., Benková E., Swarup R., Casimiro I., Péret B., Yang Y., Parry G., Nielsen E., De Smet I., Vanneste S., Levesque M. P., Carrier D., James N., Calvo V., Ljung K., Kramer E., Roberts R., Graham N., Marillonnet S., Patel K., Jones J. D., Taylor C. G., Schachtman D. P., May S., Sandberg G., Benfey P., Friml J., Kerr I., Beeckman T., Laplace L., Bennett M. J. (2008) The auxin influx carrier LAX3 promotes lateral root emergence. *Nat Cell Biol.* **10** (8) 946–54.
- Sirois J. C. (1966) Studies on growth regulators: Improved *Avena* coleoptile elongation test for auxin. *Plant Physiol.* **41**, 1308–1312.
- Swarup R., Kargul J., Marchant A., Zadik D., Rahman A., Mills R., Yemm A., May S., Williams L., Millner P., Tsurumi S., Moore I., Napier R., Kerr I. D., M, Bennett M. J. (2004) Structure–function analysis of the presumptive *Arabidopsis* auxin permease AUX1. *Plant Cell.* **16**, 3069–3083.
- Tarkowská D., Novák O., Floková K., Tarkowski P., Turečková V., Grúz J., Rolčík J., Strnad M. Quo vadis plant hormone analysis? *Planta.* **240** (1), 55–76.
- Teale W. D., Paponov I. A., Palme K. (2006) Auxin in action: signalling, transport and the control of plant growth and development. *Nat. Rev. Mol. Cell Biol.* **7** (11), 847–859.
- Taiz L. and Zeiger, E. (2010) *Plant Physiology*. 5th Edition, p. 423, Sinauer Associates Inc., Sunderland, the United Kingdom.
- Takahashi M., Izumi Y., Iwahashi F., Nakayama Y., Iwakoshi M., Nakao M., Yamato S., Fukusaki E., Bamba T. Highly Accurate Detection and Identification Methodology of Xenobiotic Metabolites Using Stable Isotope Labeling, Data Mining Techniques, and Time-Dependent Profiling Based on LC/HRMS/MS. *Anal Chem.* **90** (15), 9068–9076.
- Tan X., Calderon-Villalobos L. I., Sharon M., Zheng C., Robinson C. V., Estelle M., Zheng N. (2007) Mechanism of auxin perception by the TIR1 ubiquitin ligase. *Nature* **446**, 640–645.
- Tanaka K., Hayashi K.-I., Natsume M., Kamiya Y., Sakakibara H., Kawaide H., Kasahara H. (2014) UGT74D1 Catalyzes the Glucosylation of 2-Oxindole-3-Acetic Acid in the Auxin Metabolic Pathway in *Arabidopsis*. *Plant Cell Physiol.* **55** (1): 218–228.
- Thimann K. V. (1935) On the plant growth hormone produced by *Rhizopus suinus*. *J. Biol. Chem.* **109**, 279–291.
- Thimann K. V., Schneider C. A. (1939) The relative activities of different auxins. *Am. J. Bot.* **26**, 328–333.
- Uchida N., Takahashi K., Iwasaki R., Yamada R., Yoshimura M., Endo T. A., Kimura S., Zhang H., Nomoto M., Tada Y., Kinoshita T., Itami K., Hagihara S., Torii K. U. (2018) Chemical hijacking of auxin signaling with an engineered auxin–TIR1 pair. *Nat. Chem. Biol.* **14** (3), 299–305.
- Ulmasov T., Murfett J., Hagen G., Guilfoyle T. J. (1997) Aux/IAA Proteins Repress Expression of Reporter Genes Containing Natural and Highly Active Synthetic Auxin Response Elements. *Plant Cell.* **9**, 1963–1971.

- Vain T., Raggi S., Ferro N., Kumar Barange D., Kieffer M., Ma Q., Doyle S. M., Thelander M., Pařízková B., Novák O., Ismail A., Enquist P.-A., Rigal A., Łangowska M., Harborough S. R., Zhang Y., Ljung K., Callis J., Almqvist F., Kepinski S., Estelle M., Pauwels L., Robert S. (2019) Selective auxin agonists induce specific AUX/IAA protein degradation to modulate plant development. *Proc. Natl. Acad. Sci. USA* **116** (13), 6463–6472.
- van Berkel K., de Boer R. J., Scheres B., ten Tusscher K. (2013) Polar auxin transport: models and mechanisms. *Development* **140** (11), 2253–68.
- Van Meulebroek L., Bussche J. V., Steppe K., Vanhaecke L. (2012) Ultra-high performance liquid chromatography coupled to high resolution Orbitrap mass spectrometry for metabolomic profiling of the endogenous phytohormonal status of the tomato plant. *J Chromatogr A* **1260**, 67–80.
- Van Staden J., Jäger A. K., Light M. E., Burger B. V. (2004) Isolation of the major germination cue from plant-derived smoke. *South African J. Bot.* **70**, 654–659.
- Vanneste S., Friml J. (2009) Auxin: A Trigger for Change in Plant Development. *Cell* **136**, 1005–1016.
- Vanstraelen M., Benková E. (2012) Hormonal interactions in the regulation of plant development. *Annu. Rev. Cell. Dev. Biol.* **28**, 463–487.
- Vdovenko M. M., Stepanova A. S., Eremin S. A., Cuong N. V., Uskova N. A., Sakharov I. Y. (2013) Quantification of 2,4-dichlorophenoxyacetic acid in oranges and mandarins by chemiluminescent ELISA. *Food Chem.* **141** (2), 865–868.
- Walsh T. A., Neal R., Merlo A. O., Honma M., Hicks G. R., Wolff K., Matsumura W., Davies J. P. (2006) Mutations in an auxin receptor homolog AFB5 and in SGT1b confer resistance to synthetic picolinate auxins and not to 2,4-dichlorophenoxyacetic acid or indole-3-acetic acid in *Arabidopsis*. *Plant Phys.* **142**, 542–552.
- Wang B., Chu J., Yu T., Xu Q., Sun X., Yuan J., Xiong G., Wang G., Wang Y., Li J. (2015) Tryptophan-independent auxin biosynthesis contributes to early embryogenesis in *Arabidopsis*. *Proc. Natl. Acad. Sci. USA* **112**, 4821–4826.
- Weijers D., Friml J. (2009) SnapShot: auxin signaling and transport. *Cell* **136**, 1172.
- Weijers D., Wagner D. (2016) Transcriptional Responses to the Auxin Hormone. *Annu. Rev. Plant. Biol.* **67**, 539–574.
- Went F. W. (1926) On growth-accelerating substances in the coleoptile of *Avena sativa*. *Proc. K. Ned. Akad. Wet. C.* **30**, 10–19.
- Went F. W., Thimann K. V. (1937) *Phytohormones*. New York: The Macmillan Company.
- Wisniewska J., Xu J., Seifertová D., Brewer P. B., Ruzicka K., Blilou I., Rouquié D., Benková E., Scheres B., Friml J. (2006) Polar PIN localization directs auxin flow in plants. *Science* **312** (5775):883.
- Woodward A. W., Bartel B. (2005) Auxin: regulation, action, and interaction. *Ann. Bot.* **95**, 707–735.

- Wu Y., Hu B. (2009) Simultaneous determination of several phytohormones in natural coconut juice by hollow fiber-based liquid-liquid-liquid microextraction-high performance liquid chromatography. *J Chromatogr A* **1216**, 7657–7663.
- Xu T., Dai N., Chen J., Nagawa S., Cao M., Li H., Zhou Z., Chen X., De Rycke R., Rakusová H., Wang W., Jones A. M., Friml J., Patterson S. E., Bleecker A. B., Yang Z. (2014) Cell surface ABP1-TMK auxin-sensing complex activates ROP GTPase signaling. *Science* **343**, 1025–1028.
- Yamada R., Murai K., Uchida N., Takahashi K., Iwasaki R., Tada Y., Kinoshita T., Itami K., Torii K. U., Hagihara S. (2018) A Super Strong Engineered Auxin-TIR1 Pair. *Plant Cell. Physiol.* **9** (8), 1538–1544.
- Yamakawa T., Kurahashi O., Ishida K., Kato S., Kodama T., Minoda Y. (1979) Stability of indole-3-acetic acid to autoclaving, aeration and light illumination. *Agric. Biol. Chem.* **43**, 879–880.
- Yamazaki D., Yoshida S., Asami T., Kuchitsu K. (2003) Visualization of abscisic acid-perception sites on the plasma membrane of stomatal guard cells. *Plant J.* **35**, 129–139.
- Yang H., Murphy A. S. Functional expression and characterization of *Arabidopsis* ABCB, AUX 1 and PIN auxin transporters in *Schizosaccharomyces pombe*. *Plant J.* **59**, 179–191.
- Yang Y., Hammes U. Z., Taylor C. G., Schachtman D. P., Nielsen E. (2006) High-affinity auxin transport by the AUX1 influx carrier protein. *Curr. Biol.* **16**, 1123–1127.
- Zanella R., Prestes O. D., Friggi C. A., Martins M. L., Adaime M. B. (2018) The Impact of Pesticides: Modern sample preparation methods for pesticide multiresidue determination in foods of animal origin by chromatographic-mass spectrometric techniques. Academy Publishing, New York, USA 355–379.
- Zažímalová E., Murphy A. S., Yang H., Hoyerova K., Hosek P. (2010) Auxin transporters—Why so many? *Cold Spring Harb Perspect Biol.* **2** (3), 1–14.
- Zhang J., Lin J. E., Harris C., Campos Mastrotti Pereira F., Wu F., Blakeslee J. J., Peer W. A. (2016) DAO1 catalyzes temporal and tissue-specific oxidative inactivation of auxin in *Arabidopsis thaliana*. *Proc. Natl. Acad. Sci. USA*, **113** (39), 11010–11015.
- Zhao Y. (2012) Auxin biosynthesis: a simple two-step pathway converts tryptophan to indole-3-acetic acid in plants. *Mol. Plant* **5**(2), 334–338.
- Zimmerman P. W., Wilcoxon F. (1935) Several chemical growth substances which cause initiation of roots and other responses in plants. *Contr. Boyce Thomps. Inst. Plant Res.* **7**, 209–229.
- Zolman B. K., Martinez N., Millius A., Adham A. R., Bartel B. (2008) Identification and characterization of *Arabidopsis* indole-3-butyric acid response mutants defective in novel peroxisomal enzymes. *Genetics* **180**, 237–251.

8 Supplements I – V

Supplement I

Pařízková B., Pernisová M., Novák O. (2017) What Has Been Seen Cannot Be Unseen—Detecting Auxin *In Vivo*. *Int. J. Mol. Sci.* **18** (12), 2736.

Supplement II

Bieleszová K., **Pařízková B.**, Kubeš M., Husičková A., Kubala M., Sedlářová M., Doležal K., Strnad M., Novák O., Žukauskaitė A. (2018) New fluorescently labeled auxins exhibit promising anti-auxin activity. *N. Biotechnol.* **48**, 44-52.

Supplement III

Pařízková B., Žukauskaitė A., Vain T., Grones P., Kubeš M., Kiefferd M., Karel Doležal K., Kepinski S., Napier R., Strnad M., Robert S., Novák O. New auxin fluorescent probes for live imaging of auxin sites of action in plants (*in preparation*).

Supplement IV

Vain T.¹, Raggi S.¹, Ferro N., Kumar Barange D., Kieffer M., Ma Q., Doyle S. M., Thelander M., **Pařízková B.**, Novák O., Ismail A., Enquist P-A., Rigal A., Łangowska M., Harborough S. R., Zhang Y., Ljung K., Callis J., Almqvist F., Kepinski S., Estelle M., Pauwels L., Robert S. (2019) Selective auxin agonists induce specific AUX/IAA protein degradation to modulate plant development. *Proc. Natl. Acad. Sci. USA* **116** (13), 6463–6472.

Supplement V

Eyer L., Vain T., **Pařízková B.**, Oklestkova J., Barbez E., Kozubíková H., Pospíšil T., Wierzbicka R., Kleine-Vehn J., Fránek M., Strnad M., Robert S., Novak O. (2016) 2,4-D and IAA Amino Acid Conjugates Show Distinct Metabolism in *Arabidopsis*. *PLoS One* **11** (7), e0159269.



Review

What Has Been Seen Cannot Be Unseen—Detecting Auxin In Vivo

Barbora Pařízková^{1,2}, Markéta Pernisová^{2,3}  and Ondřej Novák^{1,*} 

¹ Laboratory of Growth Regulators, Centre of the Region Haná for Biotechnological and Agricultural Research, Faculty of Science of Palacký University & Institute of Experimental Botany of the Czech Academy of Sciences, Šlechtitelů 27, CZ-783 71 Olomouc, Czech Republic; barbora.parizkova@upol.cz

² Department of Chemical Biology and Genetics, Centre of the Region Haná for Biotechnological and Agricultural Research, Faculty of Science of Palacký University, Šlechtitelů 27, CZ-783 71 Olomouc, Czech Republic; pernisov@sci.muni.cz

³ Functional Genomics and Proteomics, National Centre for Biomolecular Research, Faculty of Science, Masaryk University, Kamenice 5, CZ-62500 Brno, Czech Republic

* Correspondence: novako@ueb.cas.cz; Tel.: +420-585-634-853

Received: 14 November 2017; Accepted: 12 December 2017; Published: 16 December 2017

Abstract: Auxins mediate various processes that are involved in plant growth and development in response to specific environmental conditions. Its proper spatio-temporal distribution that is driven by polar auxin transport machinery plays a crucial role in the wide range of auxins physiological effects. Numbers of approaches have been developed to either directly or indirectly monitor auxin distribution in vivo in order to elucidate the basis of its precise regulation. Herein, we provide an updated list of valuable techniques used for monitoring auxins in plants, with their utilities and limitations. Because the spatial and temporal resolutions of the presented approaches are different, their combination may provide a comprehensive outcome of auxin distribution in diverse developmental processes.

Keywords: auxin; auxin signalling; auxin distribution; auxin transport; indirect visualization; direct visualization; receptor; sensor

1. Introduction

Auxin, which was the first-identified plant hormone, plays a fundamental role in plant growth and development (e.g., inducing vascular tissue differentiation, tropic responses, and promoting root development). Indole-3-acetic acid (IAA) is the main natural auxin, but some plants contain other compounds that display weak auxin activity (e.g., phenylacetic acid). Several synthetic auxins (e.g., 1-naphthaleneacetic acid, 1-NAA) are often used in commercial applications [1]. The functionality of all components of auxin signalling and homeostasis is essential for proper plant development.

The cellular presence of an endogenous or exogenous (e.g., synthetic) auxin is perceived by the TRANSPORT INHIBITOR RESPONSE1/AUXIN SIGNALING F-BOX (TIR1/AFB) signalling pathway, and triggers the expression of the target genes, which induce biological responses to the received stimulus. The auxin signalling TIR1/AFB pathway comprises three major families of proteins: (i) auxin nuclear receptor TIR1/AFB F-box proteins; (ii) AUXIN RESPONSE FACTOR (ARF) transcription factors; and, (iii) AUXIN/INDOLE 3-ACETIC ACID INDUCIBLE (Aux/IAA) repressor proteins [2]. In the absence of auxin, Aux/IAAs bind ARF transcription factors disabling their function. Auxin binding to TIR1/AFB induces the proteasomal-dependent degradation of Aux/IAA by targeting the domain II for ubiquitination, and thus releases ARFs from repression enabling auxin response.

While the TIR1/AFB signalling pathway is fully explained at the molecular level [3], the function of other factors playing a role in response to auxin stimuli has not yet been fully understood [4].

These factors include, for example, (i) the S-PHASE KINASE-ASSOCIATED PROTEIN 2A (SKP2A) protein that could bind auxins in order to regulate cell division; (ii) SMALL AUXIN UP RNA (SAUR) proteins that are likely involved in cell elongation; (iii) INDOLE 3-BUTYRIC ACID RESPONSE 5 (IBR5); and, (iv) AUXIN BINDING PROTEIN 1 (ABP1), which is the oldest known putative auxin receptor [5,6]; however, these latest findings were put into question when ABP1 was found to have little, if none, prominent role in *Arabidopsis* development [7].

The differential and dynamic distribution of auxins within individual plant tissues depends on auxin homeostasis (metabolism and transport). Free auxin levels are maintained by its metabolism (biosynthesis, conjugation, and degradation), which occur predominantly in rapidly growing meristematic areas or organs, such as a shoot tip, a root tip, or emerging leaves [8]. The IAA is de novo synthesised through two biosynthetic pathways: (i) L-tryptophan (L-Trp) independent, well described in microorganisms [9]; and (ii) Trp-dependent, which includes four biosynthetic pathways that are named according to their first intermediates, and which is a significant source of endogenous IAA for higher plants [10]. The auxin metabolism comprises (i) an oxidative catabolism leading to the inactive 2-oxindole-3-yl acetic acid (oxIAA) [11]; and, (ii) a conjugation with sugars, amino acids, peptides, or proteins [12]. IAA conjugates have transport, storage, and deactivation functions, which ensure the maintenance of auxin homeostasis [13].

Another important process that is involved in the concentration gradient is passive and active auxin transport. In higher plants, auxins are transported together with assimilates through the vascular system at long distances (phloem). At a short distance (cell-to-cell), a polar active movement combines the chemiosmotic force, ATP hydrolysis and auxin transporters [14]. Major protein carriers that are present in the auxin transport are (i) AUXIN RESISTANT 1 (AUX1) and LIKE-AUX1 (LAX) from the subfamily of amino acid permeases contributing to auxin influx [15]; (ii) PIN-FORMED (PIN) transmembrane proteins specifically delivering auxin molecules out of the cell and regulating intracellular auxin homeostasis [16]; (iii) P-GLYCOPROTEINS/ATP-BINDING CASSETTE SUBFAMILY B (PGP/ABCB) transmembrane transporters [17]; and, (iv) PIN-LIKES (PILS) proteins with structural similarity to PIN proteins that are localised in the membrane of the endoplasmic reticulum [18]. The loss of the asymmetric distribution of auxin due to the genetic alteration of PIN function affects many developmental processes, e.g., embryogenesis, organogenesis, tissue differentiation, and various tropisms [19–21]. It has also been shown several times that auxin influx carriers (AUX1/LAX) play an important role during gravitropism, phototropism, lateral root, and root-hair development [22–25]. Furthermore, additional substances, such as flavonols, have been recently proposed as endogenous auxin transport regulators [26,27]. Flavonols are plant phenolic secondary metabolites that have been suggested as auxin transport inhibitors [28]. Based on the fact that auxin transport is elevated in the absence of flavonoids and is reduced in the presence of excess flavonols, they are thought to act as auxin efflux modulators [29] that are targeting both PIN [30,31] and ABCB [32,33] auxin efflux facilitators. Nevertheless, the regulation of auxin distribution by flavonols seems to be more complex, involving auxin signalling [34,35], changes in vesicular trafficking [31], or protein phosphorylation [36].

In this review, we focus on the indirect and direct methods for visualization of auxin signalling, metabolism, and transport. We describe the recent advances in monitoring auxin distribution and signalling, as well as bioanalytical tools for the quantification and visualisation of auxin metabolites at tissue and cellular level.

2. Indirect Auxin Visualization—Methods Based on Detection of Auxin Action

2.1. Reporters Based on Auxin Signalling

Visualisation of auxin in plants, direct or indirect, has attracted a lot of interest in phytohormone research for many years. The first auxin reporters were made of promoters of auxin inducible genes that were fused to a β -glucuronidase (*GUS*) reporter gene, such as *SAUR:GUS* transformed into tobacco [37] or soybean GRETCHEN HAGEN 3 (GH3)-derived *GH3:GUS* used in white clover (*Trifolium repens*) [38].

Both of the reporters were able to show an asymmetric pattern of the auxin action during gravitropism or phototropism.

Going more into details on the DNA sequence, a 183-bp auxin-responsive region (AuxRR) of the *PsIAA4/5* promoter was identified in *Pisum sativum* containing two auxin-responsive domains (AuxRD) A and B defined by linker scanning mutagenesis [39,40]. AuxRD A possesses a conserved sequence $^T/C$ GTCCCAT and has been described as an auxin switch, while AuxRD B was hypothesised to have an enhancer-like activity, with $^C/A$ ACATGGN $^C/A$ $^A/G$ TGT $^T/C$ $^T/C$ $^C/A$ nucleotide sequence [39]. Domains A and B were cloned to control *GUS* expression in a *BA:GUS* construct and tested in *Arabidopsis* for their functionality [41]. In the root elongation zone, the expression of *BA:GUS* was induced by active auxins such as IAA, NAA or 2,4-dichlorophenoxyacetic acid (2,4-D); and, less by indole-3-butyric acid (IBA). Moreover, other tested compounds, such as inactive auxin analogue, IAA metabolic precursors, IAA transport inhibitors, or phytohormones, were unable to induce *GUS* expression. *In planta*, the inducibility of the *BA:GUS* reporter gene by IAA was increased from 10^{-7} M to 10^{-4} M, but was inhibited at 10^{-3} M. In addition, *BA:GUS* expression pattern was confirmed by introducing the second reporter gene, encoding the green fluorescent protein (GFP), under the control of BA sequence. *BA:GFP* expression displayed a similar pattern to that of *BA:GUS*, and was inducible by auxin as well [41]. Using chemical genetics in *Arabidopsis*, *BA:GUS* reporter has been successfully used as bait for the identification of inhibitors of auxin transcriptional activation [42].

2.1.1. The Signalling Reporter *DR5* and Variants

The most popular auxin reporter to indirectly visualise auxin in plants is the artificial auxin-response promoter *DR5* [43], whose activity reflects an auxin response maximum [44]. Among several auxin inducible genes, *GH3* from a soybean was identified as rapidly and specifically induced by auxins [45]. Transcriptional activation of this gene was observed within 5 min after auxin application [46]. Within the *GH3* promoter, the smallest composite natural auxin response element (AuxRE) with strict auxin specificity was identified and named *D1-4* element [47]. The *D1-4* represents an 11 bp 5'-CCTCGTGTCTC-3' sequence, and contains a coupling element that overlaps with the TGTCTC motif required for auxin inducibility [48]. The TGTCTC sequence occurs in many promoters of early auxin responsive genes, bound by ARFs and responding rapidly to active auxins only [47] (Figure 1a). Together with the GGTCCCAT sequence that was identified in a pea [39], it is also present as a TGTCTCtatttGGTCCCAT sequence in *SAUR* promoters [49].

Thymidine substitutions in the natural *D1-4* AuxRE (CCTCGTGTCTC) provided the synthetic *DR5* AuxRE 5'-CCTtTGTCTC-3', with an exceptionally strong auxin response when cloned upstream of a minimal -46 *cauliflower mosaic virus* (*CaMV*) 35S promoter [43]. Eight repeats of the synthetic *DR5* (8x) AuxRE displayed up to 10-fold higher inducibility by NAA when compared with the eight repeats of natural *D1-4* (8x) AuxRE. In addition, the spacing between TGTCTC elements and nucleotide composition upstream of TGTCTC elements was suggested to be important for the auxin inducibility in the *DR5* construct [43]. Several variants of *DR5* element were prepared to monitor auxin signalling action in plants (Figure 1). Seven tandem repeats of the 11 bp sequence 5'-CCTTTTGTCTC-3' fused to a -46 bp *CaMV35S* minimal promoter and driving the *GUS* gene gave a rise to the *DR5:GUS* reporter [50]. Nine inverted repeats of the 11 bp element, a *CaMV35S* minimal promoter and a *TMV* leader sequence were used to create a *DR5rev* version of the auxin responsive promoter. Different reporter genes were combined with *DR5rev* promoter, such as phosphonate monoester hydrolase *PEH A* gene in *DR5rev:PEHA* [51], an endoplasmic reticulum-targeted green fluorescent protein in *DR5rev:GFP* [44] (Figure 1b), three tandem copies of Venus, a fast maturing variant of the yellow fluorescent protein, fused to a nuclear localization signal (NLS) in *DR5rev:3xVenus-N7* [52] (Figure 1b), a red fluorescent protein (RFP) targeted to the endoplasmic reticulum in *DR5rev:mRFP* [53] and *DR5rev:erRFP* [54] (Figure 1b), or a luciferase coding region in *DR5:Luciferase* [55]. Overall, transgenic *Arabidopsis* plants that were carrying these reporters displayed a similar pattern, with visible staining in root quiescent centre (QC), columella cells, protoxylem, the most distal domain of developing shoot

primordia with an incipient leaf vein and in root primordia tips. It has been shown that the activity of *DR5* correlates with auxin accumulation detected by immunolocalisation in *Arabidopsis* [56].

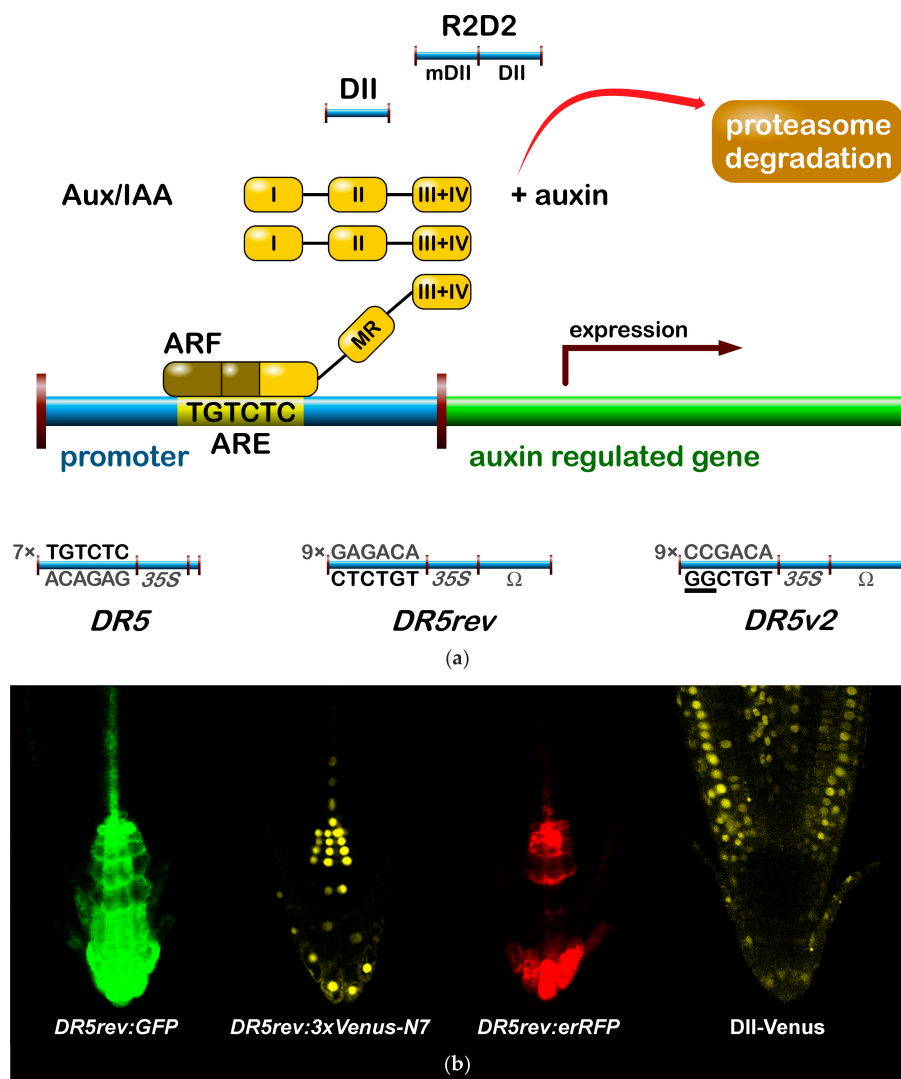


Figure 1. Indirect auxin reporters. (a) *DR5* reporters were derived from auxin response element (ARE) sequence for binding of ARF transcription factors in auxin responsive promoters. (b) The expression of *DR5rev:GFP*, *DR5rev:3xVenus-N7* and *DR5rev:erRFP* reflects similar auxin signalling output in *Arabidopsis* root tip. Degradation based reporters *DII* and *R2D2* contain degron domain from Aux/IAA repressors leading to ubiquitination and degradation in the presence of auxin. They represent auxin signalling input. 35S, *CaMV35S* minimal promoter; ARE, auxin response element; ARF, AUXIN RESPONSE FACTOR; Aux/IAA, AUXIN/INDOLE-3-ACETIC ACID; GFP, green fluorescent protein; RFP, red fluorescent protein; Venus, yellow fluorescent protein; and, Ω , tobacco mosaic virus leader sequence.

To create a more sensitive auxin responsive promoter, two bases in the original *DR5* binding sequence TGTCTC were exchanged to make a TGTCCG with higher binding affinity to ARF, as identified by protein binding microarrays [57]. Interestingly, the TGTCCG sequence occurs also in a promoter of *Agrobacterium tumefaciens* T-DNA of *Ach5 Ti* plasmid [58]. Nine original AuxREs in the *DR5rev* promoter were replaced with new binding site elements producing a *DR5v2* promoter [59] (Figure 1a). The expression pattern of *DR5v2* matches more precisely the auxin accumulation sites, as predicted from the localisation of the polar auxin transporters [60]. Moreover, *DR5v2*

showed a weak activity in the dividing cells of the embryo, leaf, or shoot meristem corresponding to an auxin function in cell division processes [61]. When comparing the activity of *DR5* and *DR5v2* in a *DR5v2::ntdTomato-DR5::n3EGFP* double reporter [59], all of the expression sites of *DR5* were overlapped by a *DR5v2* expression and the additional *DR5v2* signal appeared in other cell types (cotyledons and vasculature during embryogenesis, in metaxylem, pericycle, lateral root cap, epidermal cells of root, and in the cells surrounding the shoot primordia and the L1 layer of the shoot apical meristem). The difference in *DR5* and *DR5v2* sensitivity and localisation can be useful for the identification of unique regulatory factors, preferring specific AuxRE binding sequences in both promoters.

2.1.2. Degradation-Based Auxin Reporters

In addition to *DR5*, another type of auxin responsive promoter was constructed to monitor auxin signalling input [62]. The auxin interacting domain II (DII) [63] of IAA28 protein was cloned under a constitutive promoter and was fused to Venus with a NLS sequence [64] to generate the DII-Venus auxin sensor (Figure 1). The DII domain is the Aux/IAA domain that is ubiquitinated and induces degradation of the protein in response to the auxin dose-dependent presence. Therefore, DII-Venus monitors the input into the auxin signalling pathway by the degradation of fusion protein, thus switching off the signal in the presence of auxin, in an opposite manner to *DR5* principle. Two promoter variants were used for the sensor: a *CaMV35S* promoter [64] or a *RPS5A* promoter [59]. The need of “auxin input” quantification led to the development of an innovated reporter. The combination of DII-Venus and mDII-ntdTomato, a mutated auxin insensitive variant of DII, into one construct gave a rise to the ratiometric version of the auxin input—R2D2 [59] (Figure 1a). Two fluorophores allow for a semiquantitative measurement of auxin accumulation as a ratio of yellow and red signal. Auxin sensitive DII and R2D2 reporters enable the observation of fast changes in auxin accumulation at cellular resolution in real-time [59,64–67]. Based on DII degradation, another quantitative ratiometric sensor for analysis of auxin dynamics in real-time was developed and optimised for the use in single cell systems combining a luminescent reporter with an internal normalization element [68].

Interestingly, DII and R2D2 reporters showed partial auxin insensitivity in the root tip, particularly in the epidermis, cortex, and endodermis cell files that are close to the QC [59,64,65]. After the gravistimulation or exogenous auxin application, the DII-Venus signal of both the reporters is not switched off completely in these cells, suggesting a distinct type of regulation when compared to cells without signal. Moreover, the comparison of *DR5* and DII signals revealed discrepancies between the auxin signalling response input and output, suggesting the presence of the auxin, but the absence of a signalling response in particular parts of the growing plant [59]. It would be useful to combine *DR5v2* and R2D2 in a single three-colour reporter to inspect the auxin input and output in one plant.

2.1.3. Dissecting the Specificity of the Auxin Signalling

To follow the specificity of the auxin signalling, a set of Aux/IAA and ARF reporters were fused with *GUS* or *GFP* tag to report signalling pathways with particular sets of Aux/IAA and ARF proteins. An ARF collection using transcriptional fusion with nuclear localised 3xGFP mapped their different, as well as overlapping expression pattern in embryo and in the root tip [69]. Analogically, members of Aux/IAA family possess a wide range of localization patterns in *Arabidopsis*, suggesting their spatiotemporal specificity [70–78]. When combining the members of Aux/IAA and/or ARF families provides a huge set of possible mutual interactions pointing to variability and complexity of the auxin signalling in plant development [62,79] and waiting to be revealed.

2.2. Focused on Auxin Source

Inspecting auxin production by the activity of auxin biosynthetic genes provides us another approach how to visualize auxin indirectly. Indeed, auxin biosynthesis pathways are represented by a wide scale of participating enzymes [80]. Several biosynthetic pathways produce free IAA most probably

in the tissue-, cell-, or time-dependent manner, reflecting plant development plasticity and adaptability. The expression patterns of two related enzymes in the probably essential Trp-dependent auxin biosynthetic pathway, *TAA1p::GFP-TAA1* (TRYPTOPHAN AMINOTRANSFERASE OF ARABIDOPSIS 1), and *TAR2p::GUS* (TRYPTOPHAN AMINOTRANSFERASE RELATED 2), are complementary in stele, QC, and columella cells [81]. Subsequent enzymatic step to produce IAA is catalysed by flavin-containing monooxygenases from the YUCCA (YUC) family. Several fusion variants of the *YUC1* to *YUC11* to a *GUS*, nuclear-targeted *3xGFP*, or a cytosolic *GFP-GUS* tag showed auxin production specificity in flower organs [82], during embryo development [83,84] and leaf formation [83], or in the root tip [85]. The expression patterns of these genes point to the root meristem as a very active place for auxin biosynthesis [81,85].

2.3. Following Auxin Flow

Auxin biosynthesis reporters in combination with the reporters of the auxin transport machinery mark the auxin source and subsequent auxin flow. As auxin efflux carriers from the PIN family represent limiting factors of auxin transport [86], they can serve as an arrow of auxin flow direction by their polar cell localisation, and sites with high auxin concentration can be therefore predicted. Grouped by their structure [87], “long” PINs (1–4, 7) enable intercellular auxin transport with partially redundant function [88,89], while “short” PINs (5, 6, 8) participate mainly in intracellular auxin distribution. Over the years, an almost complete set of PIN transporters translational reporters with fluorescent proteins were generated (PIN1 [56], PIN2 [90], PIN3 [91], PIN4 [89], PIN6 [92–94], PIN7 [88], and PIN8 [94–96]; Figure 2). In case of PIN5, the translational fusion with the *GUS* reporter was published [92]. Particularly, the PIN1 protein localization in combination with the *DR5* reporter served to predict auxin accumulation as a common modulator for organ formation in many plant developmental processes [56], e.g., embryo development [44,56], defining apical-basal axis in embryo [84,97], lateral root primordia formation [98], primordia development of inflorescence meristem [52], vascular pattern development in leaves [60], leaf shape [99,100], or de novo organ formation from explants [101]. In addition, in the root apical meristem, combined action of PIN1, PIN2, PIN3, PIN4, and PIN7 is considered to establish a local auxin “reflux loop”, thus maintaining the activity of the root apical meristem [88].

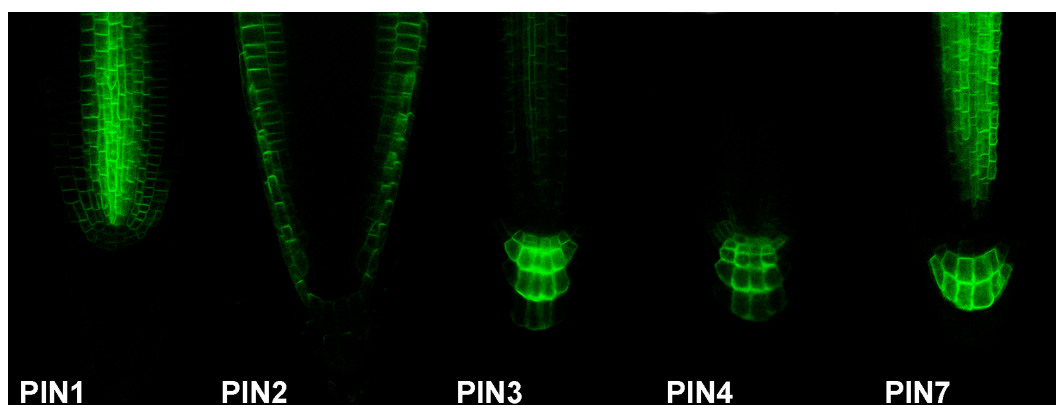


Figure 2. Visualisation of auxin flow. Functional translational fusion of auxin transport proteins enables to predict auxin distribution in *Arabidopsis* root tip. Auxin efflux carriers from the PIN family were fused with GFP. PIN, PIN-FORMED.

2.4. Immunolocalisation and In Situ Hybridisation Approaches

A complex expression pattern of ARFs and Aux/IAAs in the shoot apical meristem was provided by RNA in situ hybridization [62]. Whole-mount in situ hybridisation and immunolocalisation techniques served to detect mRNA and proteins of PIN efflux carriers in *Arabidopsis* seedlings [88,102,103].

Together with GFP reporters, the antibodies against auxin transporters helped to define their cellular localization, particularly anti-PIN1 [104], anti-PIN2 [105], anti-PIN3 [106], and anti-PIN4 [51].

3. Direct Methods for Tracking Auxin Distribution

3.1. Immunolocalisation of IAA

A high amount effort was also invested to directly visualise IAA by specific antibodies *in planta*. In *Arabidopsis*, the successful use of IAA antibodies confirmed IAA accumulation in accordance to DR5 reporter in columella initials and the QC region of the mature root and in lateral roots [56,107]. In addition to *Arabidopsis*, immunolocalisation of IAA was applied in several other plant species to monitor auxin levels during development, e.g., in developing peach leaf cells [108], sunflower embryos [109], tobacco embryo [110], maize coleoptile tips [111], or during the adventitious root formation from cotyledon explants of walnut [112]. Nevertheless, even if the IAA visualisation using antibodies can show auxin accumulation in plants, it seems that the immunolocalisation of such small molecule, like IAA, is not a suitable approach on the sub-cellular level [113].

3.2. Radiolabelling

3.2.1. Traditional Methods for Studying Polar Auxin Transport in Plants

One of the original methods how to directly track auxin movements in plants employs radioactively labelled molecules of IAA or other natural and synthetic auxins. Different strategies for different purposes in various plant species and cell cultures have been developed in order to investigate the basics of polar auxin transport and its role in plant development [114]. This methodology has been also used for the functional characterisation of auxin transport carriers [115,116]. Although having the advantage of being possibly carried out in any desired mutant background, this approach has certain limitations. Despite the progress in the development of microscale manipulator techniques, the spatial resolution of the method still remains the major limit. The radioactively supplemented source of auxin is applied on plant tissue segments that are covering several cell types. Moreover, tissue-specific dissection of plant organs for scintillation quantification has not been achieved. Thus, the method is not suitable for determination of local auxin changes in specific tissues [26]. The second major limitation is represented by passive diffusion of auxin through cell plasma membranes from the donor source, which may influence the overall outcome of the transport evaluation. For this reason, proper controls have to be performed to minimize the impact of this background process, e.g., simultaneous application of labelled auxin with the compound of similar size and polarity, which is not transportable by the active auxin transport machinery. Also, the treatment with auxin transport inhibitors helps to reveal background diffusion by blocking active transport [115].

The fundamentals of the complex polar auxin distribution in roots and its influence on root elongation and georeaction were laid in 1980's, when evidences of two-directional IAA transport were exposed—the acropetal transport towards the root apex in stele and basipetal transport from the apex towards the base in the outer root cell layers [117–121]. Auxin is transported basipetally in a single polarity in stems including hypocotyls and inflorescences [122–125]. In the very first assays, lanolin paste or agar blocks were used as a donors of radiolabelled IAA and the radioactivity was measured in receiver agar blocks in the opposite site of the examined segment [121]. The spatial resolution of this approach was sufficient only for bigger plant species, such as *Zea mays* [117], *Phaseolus coccineus* [118,119,122,123], or *Vicia faba* [120,121,126]. The first attempt to measure direct auxin transport in *Arabidopsis thaliana* was performed by Okada [127], who transferred cut inflorescence segments of *Arabidopsis* into microtubes with a small amount of liquid source of ¹⁴C-IAA, while measuring radioactivity at the other end of the inflorescence. This study confirmed the basipetal transport of auxin in the plant shoot, and revealed the importance of PIN1 transport carrier in this process as playing a role in proper floral bud formation [127]. For the root polar auxin transport

mechanisms, optimised handling of this assay was developed using ^3H -IAA-supplemented agar cylinders made with a narrow stem transfer pipette to only locally apply ^3H -IAA to the root tip. By that means it was found that the basipetal auxin transport in a gravitropic mutant of *pin2* allele *eir1-1* is altered, while the acropetal auxin transport remains undistinguishable from the wild-type. This experiment demonstrated that the apex-to-base direction of IAA flux is responsible for gravitropic responses in *Arabidopsis* [128]. The measurements of auxin in hypocotyls can be more difficult because of the weak uptake of IAA from the aqueous media into the intact hypocotyl, and therefore it is helpful to dissect the shoot apex and place the agar block on the decapitated site [115].

With these methods auxin movement was measured as the amount of IAA transported between the donor and the receiver site of the plant segment over a defined period of time. It defined an auxin flux, while the quantification of radioactive auxin in several loci with an increasing distance from its source will determine the rate of the auxin transport [115]. This was done by performing the “pulse-chase” assay when the plant tissue is treated for a short time with radioactive auxin, followed by a longer treatment with non-labelled auxin for defined periods of time. The tissue is then cut into segments, and the level of radiolabelled IAA in each segment is quantified [129]. This method helped to determine the differences between transport rates of IAA and IBA in both *Arabidopsis* root and inflorescence tissues. No IBA movement was detected in the inflorescence when compared to basipetal IAA transport at the rate of 13–15 mm per hour. In roots the basipetal transport of both IBA and IAA displayed the same rate of 8–10 mm per hour [129].

All of the protocols and methods of radiolabelled auxin applications for determination fluxes and rates of auxin transport in roots, hypocotyls, and inflorescences are reviewed in Lewis and Muday [115]. Taken together, the measurement of radioactively labelled auxins represents a very sensitive and fast technique for the direct tracking of auxin *in planta*. These methodologies have significantly contributed to the elucidation of the basic principles of the polar auxin transport in different developmental processes [127–132]. It also has been crucial for the determination of the functionality of auxin transport carriers responsible for the precise regulation of the auxin polar transport in plants [32,133–137].

3.2.2. Cellular Polar Auxin Transport Matters

The above-mentioned methods that are based on the detection of movement of radioactively labelled auxins provided information about overall auxin polar transport within distinct organs and tissues and its impact on plant morphogenesis. However, suspension-cultured cell lines may represent a sensitive system for evaluation of kinetic parameters of individual auxin transporters, their substrate specificity or the role in promoting and regulating auxin fluxes from and into the cell. Based on the accumulation of radioactivity in the tobacco cell culture, Delbarre et al. [138] published comparative data on two synthetic auxins ^3H -NAA and ^{14}C -2,4-D. This study showed that these two analogues behaved differently across the plasma membrane. 1-NAA appeared to be transported by passive diffusion into the cell, but required carriers for active efflux. On the contrary, 2,4-D required active auxin influx to get into the cell while it was shown as a weak substrate for auxin efflux transporters [138]. Based on these findings, these two molecules are used to dissect these two processes and to study auxin influx and efflux independently. The selective affinities of 2,4-D and 1-NAA to auxin transporters have been later confirmed in *Arabidopsis* suspension-cultured cells [139,140]. Nevertheless, Hošek et al. [141] detected an increased accumulation of 2,4-D in BY-2 tobacco cells after 1-naphthylphthalamic acid (NPA) treatment suggesting its role as a substrate for auxin exporters. Moreover, a proposed mathematical model for 2,4-D transport includes possible passive diffusion contributing to its influx and efflux. It is in concert with previously published evidence demonstrating a contribution of diffusion (influx/efflux) and active efflux to 2,4-D transport in *Nicotiana tabacum* L. cv. Virginia Bright Italia (VBI-0) cells [142,143], and BY-2 over-expressors of the *Arabidopsis* gene *PIN7* [86].

In addition, expressing auxin transporters in heterologous systems helps to overcome certain limitations of this approach. Due to metabolic changes such as conjugation or inactivation of auxin in the plant cell systems, it is hard to determine the precise pool of free auxin to be transported [114]. Moreover, because the regulation of auxin transport is a very complex process that is driven by multiple carriers, which may be functionally redundant, expression of the desired transporters in a non-plant system will separate auxin influx and efflux, and solve the problem of redundancy. So far, several heterologous systems, such as yeast [32,33,86,137,144–147], mammalian cells [32,33,86,144,146], or oocytes of *Xenopus laevis* [148] have been prepared to evaluate specific roles of desired transport proteins in the auxin transport machinery. However, some substrate specificity, inhibitory sensitivity, and kinetic parameters of heterologously expressed proteins were observed [32,86,146], and have to be kept in mind for further studies in plants.

3.3. Fluorescent Labelling

3.3.1. Strategies to Label Plant Hormones

Even though the indirect detection of the auxin action using auxin-sensitive reporters provides a powerful tool, which has been widely exploited for several years to study the modes of auxin distribution, these methods have certain limitations. Firstly, the overall signal output from the reporter expression is an indicator of the presence of auxin, including local biosynthesis and metabolism, to the transport contribution. Likewise, the cells promoting auxin transport are not necessarily sensitive for auxin signalling. Moreover, these reporter transgenes are not available for all of the model species and the introgression of the reporters in mutant lines is time-consuming. Finally, since the regulation of the auxin transport machinery is a very dynamic and complicated process, all of the indirect and invasive methods for auxin detection are no longer sufficient for both temporal and spatial resolution of auxin monitoring. Consequently, the efforts are made to develop microscale techniques to visualise auxin tissue-specific, as well as inter- and intracellular transport in real time [149].

The current conception of studying molecular and structural insights of plant hormone modes of action is based on the interplay between biology and chemistry. Libraries of diverse structural analogues of phytohormones led to discoveries on the relationships between their structure and their biological effect (structure-activity relationship—SAR) [150]. It helped to unravel the essential parts of the molecule responsible for its biological activity from the non-essential moieties, which can be modified for different purposes. This chemical biology approach opened a new field how to study the biological properties of small compounds that are involved in plant growth and development. Employing fluorescent labels that are conjugated with hormone molecules provides very useful tools to visualize their distribution in vivo in real time in all organs and tissues at cellular and sub-cellular levels. They can also help to identify the sites of their perception by creating detectable receptor-ligand complexes [151]. In combination with rapidly developing and very sensitive microscopic imaging techniques, fluorescently labelled phytohormones represent a modern approach with high spatio-temporal resolution to investigate the coordination of their transport, perception and mode of action regulating all the aspects of plant development and responses to various environmental stimuli. Moreover, regarding the usage of fluorescent compounds, no transformation of reporter construct is needed to detect the presence of the hormone. Thus, the determination of its distribution can be elucidated in any chosen plant line [149].

The synthesis of the fluorescent analogues is preceded by the selection of the optimal structure design. This can be achieved based on the structure-activity relationship information coupled with computational modelling, which provides structural information about the target protein based on its crystal structure. In silico screening of proposed structures with the protein binding site can help to predict the best option of modification when considering the theoretical binding interactions. Nevertheless, the real overall chemical features of the derived molecules influenced by both the used linker and the fluorescent label have to be borne in mind. The position of the labelling site [152], and the

character and the length of the linker [153–155] play a crucial role in the bioactivity of the new hormone analogues. Also, the choice of the fluorescent probe has to be considered. In general, there are three possible ways how to fluorescently label and visualise the object of interest for imaging: (i) fluorescent proteins; (ii) small organic fluorophores (Figure 3); and, (iii) quantum dots—QDs [156]. Talking about hormones, small bioactive molecules, only the last two approaches can be taken into account. QDs are not very often used in phytohormone field [157–159]. Small organic fluorophores are still the most important players with the commonly used fluoresceins (FITC), rhodamines (RITC), coumarins, NBD (7-nitro-2,1,3-benzoxadiazole), and BODIPY (boron-dipyrromethens) dyes. Furthermore, a plethora of their structural analogues covers the whole UV-VIS spectra of emission wavelengths, so one can choose according to their application needs [156]. Because of the distinct pH conditions inside the cells, in apoplast and different organelles, pH sensitivity of the labels has to be taken into account. For example fluorescein is very sensitive to pH changes and gets protonated below pH 7, resulting in significant decline of its fluorescent intensity due to a reconfiguration of the fluorophore's π -electron system after protonation [160]. On the contrary, BODIPY and Alexa Fluor dyes lack pH-dependent ionizable substituents, making them pH-insensitive alternative to FITC [161,162]. In addition, rhodamine-based labels are more photo- and pH-stable, but they suffer from bad water solubility [163]. Nevertheless, Alexa Fluor dyes are negatively charged, which may influence the distribution of their conjugates [161].

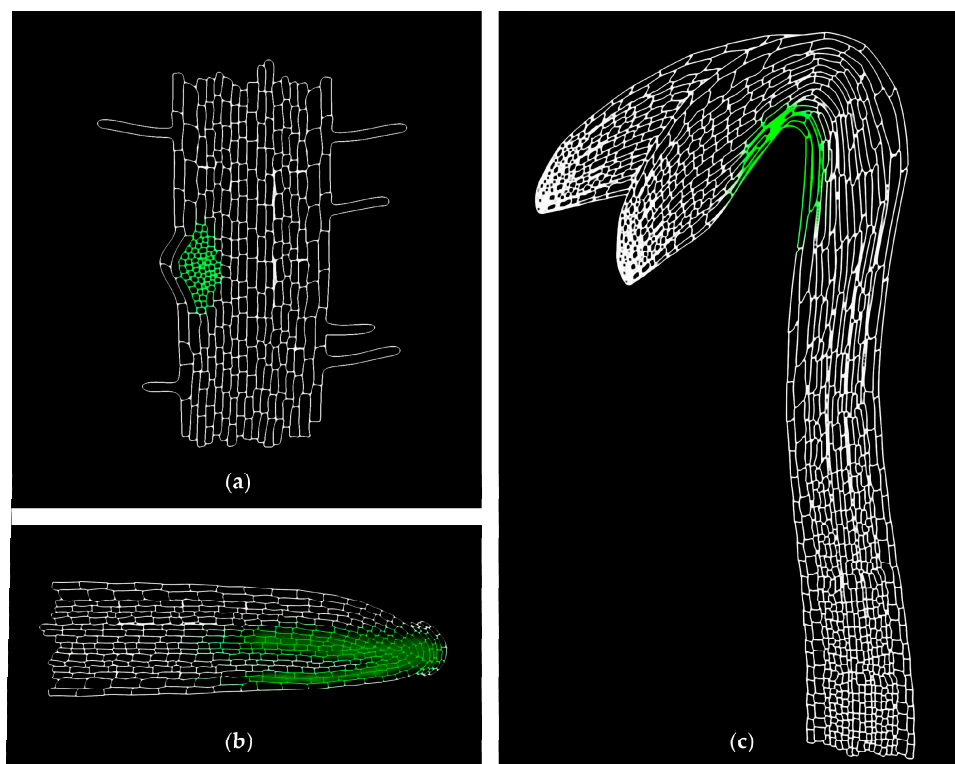


Figure 3. Scheme of tissue-specific localization of fluorescent auxin analogues. The active auxin transport carriers regulate the asymmetric distribution of auxins within different developmental processes. The distribution pattern of fluorescently labelled auxins should mimic the native IAA gradients in specific tissues such as (a) lateral root initiation sites, (b) the lower side of gravistimulated roots, or (c) the concave side of apical hook. Moreover, the non-specific fluorescent signal needs to be investigated, for instance by using a fluorescent analogue non-specific for polar auxin transport machinery. Green color represents localization of auxin analogue labeled with green fluorophore, e.g., NBD (7-nitro-2,1,3-benzoxadiazole).

As indicated above, the tracers together with the linkers significantly differ in chemical and physical properties, and therefore their application may change the behaviour of the tagged molecules,

such as solubility, charge, hydrophobicity, or fluorescent intensity, resulting in altered physiological properties, e.g., the speed of uptake, perception, transport dynamics, or metabolism [156]. Hence, before the fluorescent analogues of endogenous hormones can be used as a tool to study molecular insight of their activity, all of the mentioned details should be investigated using *in vitro* and *in vivo* bioassays to confirm that the addition of the fluorophore and the linker counterparts does not alter the physiological properties of the hormone. Moreover, the possible enzymatic degradation of the fluorescent construct in living systems has to be considered and elucidated with sensitive methods to (i) minimize misinterpretations of data obtained when using fluorescent hormone analogues; and, to (ii) obtain credible data of the hormone distribution based on the fluorescent pattern. Additionally, since the fluorescent hormone analogues are applied exogenously in non-physiological concentrations, the artificial non-specific fluorescent signal and the real tissue-specific accumulation need to be distinguished properly. For that purpose, negative fluorescent controls that provide a fluorescent signal but are not recognised by auxin transport carriers can be used [164]. If the uneven distribution of the compounds during auxin-related developmental processes is driven by the polar auxin transport, then the fluorescent maxima in the specific tissues can be expected (Figure 3). Negative controls should not exhibit this accumulation.

3.3.2. Up-To-Date Labelling of Auxins

The SAR analysis investigating auxin structural insights revealed only two moieties crucial for its biological activity—system of one or more aromatic rings and carboxyl group side chain [165,166]. The ring structure can be modified significantly, showing a high level of promiscuity of the auxin receptor binding site [63]. Despite the secondary amino group of the indole ring of IAA contributes to the interaction with the receptor by creating hydrogen bonds, it is not needed for the proper binding of auxin into the binding pocket of the receptor [63,167,168]. Unlike the carboxylic group, different positions in the aromatic ring structure can be used for the attachment of fluorescent moiety. The first published fluorescently labeled IAA was used to study the biological activity of humic substances and their possible interactions with the receptor for IAA in carrot cell culture [169]. The conjugation of FITC with both IAA and low molecular weight fraction (LMr) of humic substances revealed a correlation between the fluorescent patterns of FITC-IAA and FITC-LMr on cell membranes of *Daucus carota*, suggesting that IAA and LMr fractions bind the receptor in the same way [169]. However, neither the structure of the FITC-IAA conjugate, nor its stability in carrot cells were discussed, which makes the observed results hard to interpret. More recently, Sokołowska et al. [170] have presented new fluorescent conjugates of RITC and FITC fluorophores with IAA via the secondary amino group of the indole ring. These compounds have been shown to retain auxin-like biological activity and its distribution pattern has been driven by auxin transport system. Even though the used dyes themselves are thought to be transported differently (RITC by apoplastic, FITC by symplastic transport), the fluorescent compounds exhibited a similar distribution pattern to the one of free auxin [170]. Nevertheless, a mass spectrometry (MS) analysis of the tested compounds revealed the cleavage of the conjugates with a release of fluorophore from IAA. The fragmentation is discussed to take place during the MS analysis. But, the fact that it may be due to enzymatic degradation *in planta* still needs to be taken into consideration while interpreting the data based on the biological activity and of the observed fluorescent pattern. To our knowledge, the last published attempt to produce fluorescently labelled auxin was performed by coupling of two different auxin compounds—IAA and NAA—with NBD tag [164]. Based on the previous research of alkoxy-auxin analogues as competitive inhibitors of auxin transporters [171], the new fluorescent analogues were synthesised with NBD introduced on 5-hydroxy-IAA and 7-hydroxy-NAA. These compounds were designed to be active for auxin transport machinery, but neither for the auxin signalling TIR1/AFB pathway, nor for the GH3-dependent metabolism pathway. Both NBD-IAA and NBD-NAA have been shown to exhibit the pattern of distribution similar to the DR5 pattern in free auxin-treated roots. Moreover, the presence

of NBD-auxins in endoplasmic reticulum of cultured cells confirmed that such compounds enable tracking auxin gradients with high spatio-temporal resolution on the subcellular level [156,164].

3.4. Microelectrodes

Another method for direct non-invasive monitoring of auxin fluxes in vivo employs IAA-selective microelectrodes [172,173]. Organogenesis and reactions of plants to environmental stimuli are driven by dynamic auxin transport generating auxin gradients in specific tissues [174]. This uneven auxin distribution creates an electrical potential across the organ [175,176], where the side with higher auxin concentration is considered as positive (secreting more H⁺ ions) compared to the side with lower auxin levels. These electrical potentials can be surface-measured using microelectrodes [124]. To be used for continuous recording of auxin transport and the quantification of the local IAA levels, the electrochemical sensors must display a high selectivity for IAA, sensitivity, fast response times, and calibration stability. Mancuso et al. [172] used a platinum electrode with surface-immobilised multiwalled carbon nanotubes (MWNTs) and with a small planar sensing tip for good spatial resolution in combination with a self-referencing electrode to measure auxin transport in root apices of *Zea mays*. Even though the usage of MWNTs enhanced the method sensitivity when compared to a bare platinum electrode, the detection limit of only 0.1 μM IAA was achieved, and thus an exogenous application of IAA had to be performed. Nevertheless, this method was presented as a useful approach for the direct determination of IAA in root samples, direct measurements of its local concentrations, and measurement of IAA fluxes in different positions along the maize root. The study demonstrated that the most intensive influx rate is in the transition zone. This peak in flux (expressed in fmol·cm⁻²·s⁻¹) at 1.0–1.5 mm above the root apex corresponds to the auxin reflux loop model [88]. Moreover, the application of auxin uptake inhibitors significantly decreased the influx of IAA into the cells, resulting in a drop of the flux peak for this zone [172]. Although this microelectrode method is applicable only on cells at the root surface or on a thin cell layer, it appears to be a valuable tool for detecting auxin fluxes and has helped to discover and characterise several auxin transport mutants and inhibitors of auxin transport carriers [146,177–181]. This method has been improved by using platinum black and carbon nanotube surface modifications, which helped to increase signal-to-noise ratio [173]. Together with better signal processing and data integration, it enabled directly and non-invasively measuring endogenous IAA transport parameters, with no external source of IAA needed. This enhanced method was used to determine the differences in IAA movements in roots of wild-type maize and auxin transport mutant maize [147,182]. The most intense transport of endogenous IAA was detected in the distal elongation zone of maize roots. Expectedly, the flux of auxin in transport mutant was significantly reduced [173], which correlates with the effect observed in *Arabidopsis thaliana* that is caused by the loss of function mutant of orthologue transporter in *Arabidopsis* [32]. Furthermore, the detection of inhibition of both IAA efflux and influx after treatment with auxin transport inhibitors points out the potential of self-referencing microsensors as a valuable approach for in vivo non-invasive monitoring of IAA transport despite it is still limited to the root surface layers and epidermal cell [173].

4. New Valuable Tools to Visualize Auxin Metabolites

The regulation of bioactive auxin levels is complex, and cell- and tissue-specific metabolic profiling can help to answer many questions about local IAA biosynthesis and degradation, as well as auxin transport and the formation of auxin gradients. This short summary does not present the whole picture of auxin profiling methods. For more recent and specific overviews of novel bioanalytical approaches, including the advances of mass spectrometry (MS) and biosensors, we refer the reader to other publications [183–186].

4.1. Cell-Type Specific Mass Spectrometric Analysis

MS-based quantitative measurement of auxins on a tissue and at a cellular level is a difficult task, not only due to extremely low concentrations (fmol–pmol/g of fresh weight), but also due to

the presence of interfering substances in the plant matrix (e.g., pigments, lipids, phenolic compounds, or proteins) [187]. Together with chemical/thermal/light lability and enzymatic/oxidative degradation of auxins during the extraction and isolation steps, accurate and precise determination is highly challenging [184]. Recent technical advances in analytical methods helped to detect more IAA metabolites (precursors, catabolites, and conjugates) in one sample, and thus to obtain information about the overall pattern of auxin metabolome. Gas chromatography (GC) and liquid chromatography (LC), coupled to tandem mass spectrometry (MS/MS) are often used in the analysis of the most known auxin metabolites, the substances with very different physicochemical properties [188,189]. Several MS-based measurements confirmed the auxin gradients in meristematic tissue sections, such as cambial meristem [190,191] and isolated cell types of the *Arabidopsis* root apical meristem [11,113] (Figure 4). Moreover, a single-cell-resolution analysis of IAA and other phytohormone metabolites in the *Arabidopsis* guard cell protoplasts has been recently published [192].

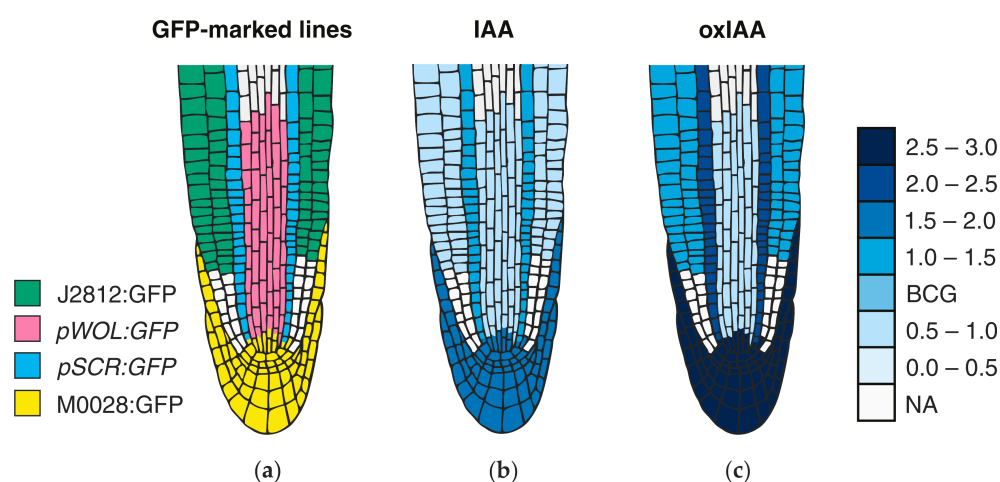


Figure 4. Auxin distribution map within the *Arabidopsis* root tip. (a) The data presented in the map was derived from four green fluorescent protein (GFP)-tagged *Arabidopsis* lines (J2812:GFP, *pWOL:GFP*, *pSCR:GFP* and M0028:GFP), covering almost all of the different cell types of the root apex. (b,c) Roots from eight-day-old *Arabidopsis* seedlings were protoplasted and sorted using FACS, and the concentrations of IAA (b) and oxIAA (c) were quantified in the separated GFP-expressing cell populations using LC-MS/MS. Cell type-specific concentrations of both auxins were calculated in fmol per 100,000 isolated GFP-expressing protoplasts and then normalised to the non-GFP-expressing reference population for each GFP cell line. “NA” represents cell populations that were not analysed; “BCG” means the background level. The maps were constructed based on the IAA and oxIAA levels published in [11].

Cryo-sectioning is a popular method of minute plant tissue sampling, which often provides sufficient cell-type-specific resolution for hormone profiling. For example, the IAA distribution in 30- μ m tangential sections that were obtained across the cambial region was measured by GC-MS [190]. To connect the hormone distributions to the status of hormonal signalling and homeostasis, a genome-wide gene expression profiling at a high resolution across the cambial zone were performed [191]. These results suggest that most of the auxin response genes showed maximal expression in the middle of the cambial zone, coinciding with the peak in auxin content.

Another possible high-resolution cell-type specific method is based on the auxin quantification in root cell populations that are sorted by fluorescence-activated cell sorting (FACS). This approach enables the recognition of isolated protoplasts of similar size and granularity, followed by their sorting into homogenous cell-type groups according to the presence or absence of internal fluorochromes (e.g., GFP). In isolated protoplasts that are derived from *Arabidopsis* mutant lines expressing GFP in specific root cell types, the presence of IAA concentration gradients within the root tip with

a distinct maximum in the organizing QC of the root apex has been confirmed [113]. Interestingly, cell type-specific auxin measurements do not effectively match DR5 expression in the root apex, however, graded auxin response more closely fits measured auxin concentrations [193]. The found auxin distribution also confirms the hypothesis of different polarisation of PIN proteins at the root apex, resulting in auxin accumulation in the root cap [194]. In Figure 4, the IAA distribution map shows a concentration maximum in the lateral root cap, columella, columella initials, and QC cells. A similar gradient was also found at concentration levels of oxIAA, the primary auxin catabolite formed in the *Arabidopsis* roots [11]. Its origin at the cellular level contributes, in addition to active transport, to maintaining the correct IAA minima/maxima ratios that are necessary for proper root growth and development.

4.2. Auxin Monitoring by Solid-State Biosensors

As mentioned above, hormonal signalling reporters and sensors are preferred for in vivo and real-time detection of auxin in living tissues [195]; nevertheless, other biosensors also offer real-time and in vivo quantitation of auxin [186]. Generally, a biosensor is a sensitive analytical device combining a biological component module for the analyte's recognition with a physicochemical detector, which converts a biological response (e.g., immunochemical or electrochemical reactions) into a signal that can be captured and interrogated [183]. Several reviews have discussed the applications of solid-state biosensors that are used for ex vivo and in vivo monitoring of auxin metabolites [183,185,186]. For example, immunosensors designed for IAA detection can be classified based on the type of the detector: (i) electrochemical [196,197]; (ii) photoelectrochemical [198]; and, (iii) piezoelectric [199]. Other types of biosensors make use of molecular imprinted materials (MIPs), which also selectively recognize a template molecule. Several examples of the MIPs application to auxin quantification can be found in the literature [200,201]. However, affinity-based sensors often required an analyte extraction from plant tissues and one or more steps of pre-concentration. A non-enzymatic electrochemical biosensor system that is based on the direct oxidation of IAA by a graphite paste electrode was also introduced [202], and then modified to carbon nanotube-coated platinum electrodes [203]. Moreover, Mancuso et al. [172] and McLamore et al. [173] used a self-referencing vibrating microelectrode technique for the study of auxin fluxes in root apices (for more details see Section 3.3).

In summary, the solid-state biosensors, together with development of genetically encoded reporters and sensors and advances in fluorescent labelling, facilitate the study of auxin signalling and distribution in living intact plants. Several bioanalytical approaches, such as FACS and LC-MS/MS methods, can be equally used for cell-specific analysis of auxins, and thus provides ideas about the coordination of plant hormone metabolism and transport, and the regulation of core signalling component expression.

5. Future Prospects

Diverse plant developmental events that are triggered by auxin trafficking, redistribution, and tissue-specific accumulation as a response to ambient conditions represent very dynamic and highly regulated processes. Moreover, the microenvironment in plant tissues is very complex and two neighbouring cells can be in a different state of development, and thus have a distinct function. For those reasons, claims on spatial and temporal resolutions of detecting techniques are increasing. Therefore, the application of mass spectrometry imaging (MSI) and living single-cell MS analysis could soon provide a powerful tool for studying of auxin distribution, even though it is still limited for hormone profiling [186]. Moreover, very little is known about extra- and intracellular distributions of auxins and their metabolites, as well as their levels in individual cell compartments. Separation of organelles for auxin profiling was recently carried out by porous-specific filtration (e.g., gradual separation of chloroplasts and mitochondria [204]) or density-based fractionation (e.g., chloroplasts separation in percol solution [205]). However, a detailed organelle-specific analysis of auxin levels is

still lacking. Therefore, we are looking forward to developing new analytical methods and periods of innovative approaches to work at the intracellular level.

To detect and monitor auxin distribution with sufficient spatial and temporal resolution in minimal invasive manner, improvement of above-mentioned methods employing genetic biosensors, as well as novel approaches of live imaging to capture extra- and intracellular hormone dynamics are also demanded. Aside from the development of new expression reporters with high selectivity for auxin molecules responding rapidly to physiological levels of hormones in linear manner so that the response can be quantified [206], new genetically encoded biosensors for the quantitative distribution of biomolecules based on (i) fluorescent translocation sensors; (ii) fluorescence-intensity-based nanosensors; and, (iii) Förster resonance energy transfer (FRET)-based nanosensors are on the rise [207]. Also, the preparation of new fluorescent auxin analogues, which would display biological activity, auxin transporters-dependent distribution, and enzymatic stability, remains a challenging issue. The rapid progress of different microscopic imaging techniques [208] goes hand in hand with inventions of devices allowing for the long-term monitoring of plant growth in vertical position to maintain physiological growing conditions [67,209–212]. Moreover, employing of microfluidic perfusion system that is controlled by micromechanical valves provides precise and fast control and modulation of the plant environment when reversible delivery of the chemicals of interest is enabled [213,214]. This set of devices, together, in combination with rapid-response and sensitive genetic reporters of auxin action or reliable fluorescent auxin derivative treatment could offer a powerful method to visualize in vivo auxin distribution with real time resolution on all organs and tissues, at the cellular and subcellular levels. In addition, label-free imaging techniques, which have been used for metabolic imaging of high abundant molecules in mammalian cells, such as lipids monitored with coherent anti-Stokes Raman scattering (CARS) microscopy [215] or ω -3 fatty acids by stimulated Raman scattering (SRS) [216], may soon achieve adequate sensitivity for selective monitoring of plant hormones without any needs of indirect visualization or structure modification, which would enable to track their distribution in different processes in the most natural manner.

Acknowledgments: We are thankful to Helene Robert Boisivon for critical reading of the manuscript, Ota Blahoušek for drawing Figure 3 and Helena Mazáčová for careful revision of the manuscript. This work was supported by the Ministry of Education, Youth and Sports of the Czech Republic—NPU I program with project LO1204 (Barbora Pařízková, Markéta Pernisová and Ondřej Novák), by the Internal Grant Agency of Palacký University (IGA_PrF_2017_010; Barbora Pařízková), by the Endowment Fond of Palacký University in Olomouc (Barbora Pařízková), and by the Czech Science Foundation GACR 16-01137S (Markéta Pernisová).

Author Contributions: All authors developed the idea and outline of the paper. Barbora Pařízková wrote the manuscript in detail. Markéta Pernisová wrote the reporter section of the manuscript. Ondřej Novák revised the manuscript thoroughly and finalised it. All authors have read the manuscript before submission.

Conflicts of Interest: The authors declare no conflict of interest.

References

1. Davies, P.J. *Plant Hormones—Biosynthesis, Signal Transduction, Action!*, 3rd ed.; Springer: London, UK, 2010; pp. 16–35, ISBN 9788578110796.
2. Korasick, D.A.; Westfall, C.S.; Lee, S.G.; Nanao, M.H.; Dumas, R.; Hagen, G.; Guilfoyle, T.J.; Jez, J.M.; Strader, L.C. Molecular basis for AUXIN RESPONSE FACTOR protein interaction and the control of auxin response repression. *Proc. Natl. Acad. Sci. USA* **2014**, *111*, 5427–5432. [[CrossRef](#)] [[PubMed](#)]
3. Wang, R.; Estelle, M. Diversity and specificity: Auxin perception and signaling through the TIR1/AFB pathway. *Curr. Opin. Plant Biol.* **2014**, *21*, 51–58. [[CrossRef](#)] [[PubMed](#)]
4. Powers, S.K.; Strader, L.C. Up in the air: Untethered Factors of Auxin Response. *F1000Research* **2016**, *5*. [[CrossRef](#)] [[PubMed](#)]
5. Löbler, M.; Klämbt, D. Auxin-binding protein from coleoptile membranes of corn (*Zea mays* L.). I. Purification by immunological methods and characterization. *J. Biol. Chem.* **1985**, *260*, 9848–9853. [[PubMed](#)]
6. Jones, A.M.; Venis, M.A. Photoaffinity labeling of indole-3-acetic acid-binding proteins in maize. *Proc. Natl. Acad. Sci. USA* **1989**, *86*, 6153–6156. [[CrossRef](#)] [[PubMed](#)]

7. Gao, Y.; Zhang, Y.; Zhang, D.; Dai, X.; Estelle, M.; Zhao, Y. Auxin binding protein 1 (ABP1) is not required for either auxin signaling or *Arabidopsis* development. *Proc. Natl. Acad. Sci. USA* **2015**, *112*, 2275–2280. [[CrossRef](#)] [[PubMed](#)]
8. Paque, S.; Weijers, D. Q&A: Auxin: The plant molecule that influences almost anything. *BMC Biol.* **2016**, *14*, 67. [[CrossRef](#)]
9. Spaepen, S.; Vanderleyden, J.; Remans, R. Indole-3-acetic acid in microbial and microorganism-plant signaling. *FEMS Microbiol. Rev.* **2007**, *31*, 425–448. [[CrossRef](#)] [[PubMed](#)]
10. Ljung, K. Auxin metabolism and homeostasis during plant development. *Development* **2013**, *140*, 943–950. [[CrossRef](#)] [[PubMed](#)]
11. Pěňčík, A.; Simonovik, B.; Petersson, S.V.; Henyková, E.; Simon, S.; Greenham, K.; Zhang, Y.; Kowalczyk, M.; Estelle, M.; Zažímalová, E.; et al. Regulation of auxin homeostasis and gradients in *Arabidopsis* roots through the formation of the indole-3-acetic acid catabolite 2-oxindole-3-acetic acid. *Plant Cell* **2013**, *25*, 3858–3870. [[CrossRef](#)] [[PubMed](#)]
12. Normanly, J. Approaching cellular and molecular resolution of auxin biosynthesis and metabolism. *Cold Spring Harb. Perspect. Biol.* **2010**, *2*, a001594. [[CrossRef](#)] [[PubMed](#)]
13. Ludwig-Müller, J. Auxin conjugates: Their role for plant development and in the evolution of land plants. *J. Exp. Bot.* **2011**, *62*, 1757–1773. [[CrossRef](#)] [[PubMed](#)]
14. Reemmer, J.; Murphy, A.S. Intercellular Transport of Auxin. In *Auxin and Its Role in Plant Development*, 1st ed.; Zažímalová, E., Petrášek, J., Benková, E., Eds.; Springer: London, UK, 2014; Volume 33, pp. 75–101, ISBN 978-3-7091-1526-8.
15. Swarup, R.; Péret, B. AUX/LAX family of auxin influx carriers—An overview. *Front. Plant Sci.* **2012**, *3*, 225. [[CrossRef](#)] [[PubMed](#)]
16. Adamowski, M.; Friml, J. PIN-Dependent Auxin Transport: Action, Regulation, and Evolution. *Plant Cell* **2015**, *27*, 20–32. [[CrossRef](#)] [[PubMed](#)]
17. Do, T.H.T.; Martinoia, E.; Lee, Y. Functions of ABC transporters in plant growth and development. *Curr. Opin. Plant Biol.* **2018**, *41*, 32–38. [[CrossRef](#)] [[PubMed](#)]
18. Barbez, E.; Kubeš, M.; Rolčík, J.; Béziat, C.; Pěňčík, A.; Wang, B.; Rosquete, M.R.; Zhu, J.; Dobrev, P.I.; Lee, Y.; et al. A novel putative auxin carrier family regulates intracellular auxin homeostasis in plants. *Nature* **2012**, *485*, 119–122. [[CrossRef](#)] [[PubMed](#)]
19. Vieten, A.; Sauer, M.; Brewer, P.B.; Friml, J. Molecular and cellular aspects of auxin-transport-mediated development. *Trends Plant Sci.* **2007**, *12*, 160–168. [[CrossRef](#)] [[PubMed](#)]
20. Grunewald, W.; Friml, J. The march of the PINs: Developmental plasticity by dynamic polar targeting in plant cells. *EMBO J.* **2010**, *29*, 2700–2714. [[CrossRef](#)] [[PubMed](#)]
21. Petrášek, J.; Friml, J. Auxin transport routes in plant development. *Development* **2009**, *136*, 2675–2688. [[CrossRef](#)] [[PubMed](#)]
22. Bennett, M.J.; Marchant, A.; Green, H.G.; May, S.T.; Ward, S.P.; Millner, P.A.; Walker, A.R.; Schulz, B.; Feldmann, K.A. *Arabidopsis* AUX1 Gene: A Permease-Like Regulator of Root Gravitropism. *Science* **1996**, *273*, 948–950. [[CrossRef](#)] [[PubMed](#)]
23. Stone, B.B.; Stowe-Evans, E.L.; Harper, R.M.; Brandon Celaya, R.; Ljung, K.; Sandberg, G.; Liscum, E. Disruptions in AUX1-dependent auxin influx alter hypocotyl phototropism in *Arabidopsis*. *Mol. Plant* **2008**, *1*, 129–144. [[CrossRef](#)] [[PubMed](#)]
24. Swarup, K.; Benková, E.; Swarup, R.; Casimiro, I.; Péret, B.; Yang, Y.; Parry, G.; Nielsen, E.; De Smet, I.; Vanneste, S.; et al. The auxin influx carrier LAX3 promotes lateral root emergence. *Nat. Cell Biol.* **2008**, *10*, 946–954. [[CrossRef](#)] [[PubMed](#)]
25. Jones, A.R.; Kramer, E.M.; Knox, K.; Swarup, R.; Bennett, M.J.; Lazarus, C.M.; Leyser, H.M.O.; Grierson, C.S. Auxin transport through non-hair cells sustains root-hair development. *Nat. Cell Biol.* **2009**, *11*, 78–84. [[CrossRef](#)] [[PubMed](#)]
26. Peer, W.A.; Murphy, A.S. Flavonoids and auxin transport: Modulators or regulators? *Trends Plant Sci.* **2007**, *12*, 556–563. [[CrossRef](#)] [[PubMed](#)]
27. Steenackers, W.; Klíma, P.; Quareshy, M.; Cesarino, I.; Kumpf, R.P.; Corneillie, S.; Araújo, P.; Viaene, T.; Goeminne, G.; Nowack, M.K.; et al. *cis*-Cinnamic Acid Is a Novel, Natural Auxin Efflux Inhibitor that Promotes Lateral Root Formation. *Plant Physiol.* **2017**, *173*, 552–565. [[CrossRef](#)] [[PubMed](#)]

28. Brown, D.E.; Rashotte, A.M.; Murphy, A.S.; Normanly, J.; Tague, B.W.; Peer, W.A.; Taiz, L.; Mudaye, G.K. Flavonoids act as negative regulators of auxin transport in vivo in *Arabidopsis*. *Plant Physiol.* **2001**, *126*, 524–535. [[CrossRef](#)] [[PubMed](#)]
29. Kuhn, B.M.; Geisler, M.; Bigler, L.; Ringli, C. Flavonols Accumulate Asymmetrically and Affect Auxin Transport in *Arabidopsis*. *Plant Physiol.* **2011**, *156*, 585–595. [[CrossRef](#)] [[PubMed](#)]
30. Santelia, D.; Henrichs, S.; Vincenzetti, V.; Sauer, M.; Bigler, L.; Klein, M.; Bailly, A.; Lee, Y.; Friml, J.; Geisler, M.; et al. Flavonoids redirect PIN-mediated polar auxin fluxes during root gravitropic responses. *J. Biol. Chem.* **2008**, *283*, 31218–31226. [[CrossRef](#)] [[PubMed](#)]
31. Peer, W.A.; Bandyopadhyay, A.; Blakeslee, J.J.; Makam, S.N.; Chen, R.J.; Masson, P.H.; Murphy, A.S. Variation in Expression and Protein Localization of the PIN Family of Auxin Efflux Facilitator Proteins in Flavonoid Mutants with Altered Auxin Transport in *Arabidopsis thaliana*. *Plant Cell* **2004**, *16*, 1898–1911. [[CrossRef](#)] [[PubMed](#)]
32. Geisler, M.; Blakeslee, J.J.; Bouchard, R.; Lee, O.R.; Vincenzetti, V.; Bandyopadhyay, A.; Titapiwatanakun, B.; Peer, W.A.; Bailly, A.; Richards, E.L.; et al. Cellular efflux of auxin catalyzed by the *Arabidopsis* MDR/PGP transporter AtPGP1. *Plant J.* **2005**, *44*, 179–194. [[CrossRef](#)] [[PubMed](#)]
33. Blakeslee, J.J.; Bandyopadhyay, A.; Lee, O.R.; Mravec, J.; Titapiwatanakun, B.; Sauer, M.; Makam, S.N.; Cheng, Y.; Bouchard, R.; Adamec, J.; et al. Interactions among PIN-FORMED and P-glycoprotein auxin transporters in *Arabidopsis*. *Plant Cell* **2007**, *19*, 131–147. [[CrossRef](#)] [[PubMed](#)]
34. Grunewald, W.; De Smet, I.; Lewis, D.R.; Löfke, C.; Jansen, L.; Goeminne, G.; Bosschea, R.V.; Karimi, M.; De Rybela, B.; Vanholmea, B.; et al. Transcription factor WRKY23 assists auxin distribution patterns during *Arabidopsis* root development through local control on flavonol biosynthesis. *Proc. Natl. Acad. Sci. USA* **2011**, *109*, 1554–1559. [[CrossRef](#)] [[PubMed](#)]
35. Lewis, D.R.; Ramirez, M.V.; Miller, N.D.; Vallabhaneni, P.; Ray, W.K.; Helm, R.F.; Winkel, B.S.J.; Muday, G.K. Auxin and Ethylene Induce Flavonol Accumulation through Distinct Transcriptional Networks. *Plant Physiol.* **2011**, *156*, 144–164. [[CrossRef](#)] [[PubMed](#)]
36. Titapiwatanakun, B.; Murphy, A.S. Post-transcriptional regulation of auxin transport proteins: Cellular trafficking, protein phosphorylation, protein maturation, ubiquitination, and membrane composition. *J. Exp. Bot.* **2009**, *60*, 1093–1107. [[CrossRef](#)] [[PubMed](#)]
37. Li, Y.; Hagen, G.; Guilfoyle, T. An Auxin-Responsive Promoter Is Differentially Induced by Auxin Gradients during Tropisms. *Plant Cell* **1991**, *3*, 1167–1175. [[CrossRef](#)] [[PubMed](#)]
38. Larkin, P.J.; Gibson, J.M.; Mathesius, U.; Weinman, J.J.; Gartner, E.; Hall, E.; Tanner, G.J.; Rolfe, B.G.; Djordjevic, M.A. Transgenic white clover. Studies with the auxin-responsive promoter, GH3, in root gravitropism and lateral root development. *Transgenic Res.* **1996**, *5*, 443–450. [[CrossRef](#)]
39. Ballas, N.; Wong, L.M.; Theologis, A. Identification of the Auxin-responsive Element, *AuxRE*, in the Primary indoleacetic Acid-inducible Gene, *PS-IAA4/5*, of Pea (*Pisum sativum*). *J. Mol. Biol.* **1993**, *233*, 580–596. [[CrossRef](#)] [[PubMed](#)]
40. Ballas, N.; Wong, L.M.; Ke, M.; Theologis, A. Two auxin-responsive domains interact positively to induce expression of the early indoleacetic acid-inducible gene *PS-IAA4/5*. *Proc. Natl. Acad. Sci. USA* **1995**, *92*, 3483–3487. [[CrossRef](#)] [[PubMed](#)]
41. Oono, Y.; Chen, Q.G.; Overvoorde, P.J.; Köhler, C.; Theologis, A. *age* Mutants of *Arabidopsis* exhibit altered auxin-regulated gene expression. *Plant Cell* **1998**, *10*, 1649–1662. [[CrossRef](#)] [[PubMed](#)]
42. Armstrong, J.I.; Yuan, S.; Dale, J.M.; Tanner, V.N.; Theologis, A. Identification of inhibitors of auxin transcriptional activation by means of chemical genetics in *Arabidopsis*. *Proc. Natl. Acad. Sci. USA* **2004**, *101*, 14978–14983. [[CrossRef](#)] [[PubMed](#)]
43. Ulmasov, T.; Murfett, J.; Hagen, G.; Guilfoyle, T.J. Aux/IAA proteins repress expression of reporter genes containing natural and highly active synthetic auxin response elements. *Plant Cell* **1997**, *9*, 1963–1971. [[CrossRef](#)] [[PubMed](#)]
44. Friml, J.; Vieten, A.; Sauer, M.; Weijers, D.; Schwarz, H.; Hamann, T.; Offringa, R.; Jürgens, G. Efflux-dependent auxin gradients establish the apical–basal axis of *Arabidopsis*. *Nature* **2003**, *426*, 147–153. [[CrossRef](#)] [[PubMed](#)]
45. Hagen, G.; Martin, G.; Li, Y.; Guilfoyle, T.J. Auxin-induced expression of the soybean *GH3* promoter in transgenic tobacco plants. *Plant Mol. Biol.* **1991**, *17*, 567–579. [[CrossRef](#)] [[PubMed](#)]

46. Hagen, G.; Guilfoyle, T.J. Rapid induction of selective transcription by auxins. *Mol. Cell. Biol.* **1985**, *5*, 1197–1203. [[CrossRef](#)] [[PubMed](#)]
47. Ulmasov, T.; Liu, Z.B.; Hagen, G.; Guilfoyle, T.J. Composite structure of auxin response elements. *Plant Cell* **1995**, *7*, 1611–1623. [[CrossRef](#)] [[PubMed](#)]
48. Liu, Z.B.; Ulmasov, T.; Shi, X.; Hagen, G.; Guilfoyle, T.J. Soybean *GH3* promoter contains multiple auxin-inducible elements. *Plant Cell* **1994**, *6*, 645–657. [[CrossRef](#)] [[PubMed](#)]
49. Li, Y.; Liu, Z.B.; Shi, X.; Hagen, G.; Guilfoyle, T.J. An auxin-inducible element in soybean SAUR promoters. *Plant Physiol.* **1994**, *106*, 37–43. [[CrossRef](#)] [[PubMed](#)]
50. Sabatini, S.; Beis, D.; Wolkenfelt, H.; Murfett, J.; Guilfoyle, T.; Malamy, J.; Benfey, P.; Leyser, O.; Bechtold, N.; Weisbeek, P.; et al. An auxin-dependent distal organizer of pattern and polarity in the *Arabidopsis* root. *Cell* **1999**, *99*, 463–472. [[CrossRef](#)]
51. Friml, J.; Benková, E.; Blilou, I.; Wisniewska, J.; Hamann, T.; Ljung, K.; Woody, S.; Sandberg, G.; Scheres, B.; Jürgens, G.; et al. AtPIN4 mediates sink driven auxin gradients and patterning in *Arabidopsis* roots. *Cell* **2002**, *108*, 661–673. [[CrossRef](#)]
52. Heisler, M.G.; Ohno, C.; Das, P.; Sieber, P.; Reddy, G.V.; Long, J.A.; Meyerowitz, E.M. Patterns of auxin transport and gene expression during primordium development revealed by live imaging of the *Arabidopsis* inflorescence meristem. *Curr. Biol.* **2005**, *15*, 1899–1911. [[CrossRef](#)] [[PubMed](#)]
53. Gallavotti, A.; Yang, Y.; Schmidt, R.J.; Jackson, D. The Relationship between Auxin Transport and Maize Branching. *Plant Physiol.* **2008**, *147*, 1913–1923. [[CrossRef](#)] [[PubMed](#)]
54. Marin, E.; Jouannet, V.; Herz, A.; Lokerse, A.S.; Weijers, D.; Vaucheret, H.; Nussaume, L.; Crespi, M.D.; Maizel, A. miR390, *Arabidopsis* TAS3 tasiRNAs, and Their AUXIN RESPONSE FACTOR Targets Define an Autoregulatory Network Quantitatively Regulating Lateral Root Growth. *Plant Cell* **2010**, *22*, 1104–1117. [[CrossRef](#)] [[PubMed](#)]
55. Moreno-Risueno, M.A.; Van Norman, J.M.; Moreno, A.; Zhang, J.; Ahnert, S.E.; Benfey, P.N. Oscillating Gene Expression Determines Competence for Periodic *Arabidopsis* Root Branching. *Science* **2010**, *329*, 1306–1311. [[CrossRef](#)] [[PubMed](#)]
56. Benková, E.; Michniewicz, M.; Sauer, M.; Teichmann, T.; Seifertová, D.; Jürgens, G.; Friml, J. Local, Efflux-Dependent Auxin Gradients as a Common Module for Plant Organ Formation. *Cell* **2003**, *115*, 591–602. [[CrossRef](#)]
57. Boer, D.R.; Freire-Rios, A.; van den Berg, W.A.M.; Saaki, T.; Manfield, I.W.; Kepinski, S.; López-Vidriero, I.; Franco-Zorrilla, J.M.; de Vries, S.C.; Solano, R.; et al. Structural basis for DNA binding specificity by the auxin-dependent ARF transcription factors. *Cell* **2014**, *156*, 577–589. [[CrossRef](#)] [[PubMed](#)]
58. Korber, H.; Strizhov, N.; Staiger, D.; Feldwisch, J.; Olsson, O.; Sandberg, G.; Palme, K.; Schell, J.; Koncz, C. T-DNA gene 5 of *Agrobacterium* modulates auxin response by autoregulated synthesis of a growth hormone antagonist in plants. *EMBO J.* **1991**, *10*, 3983–3991. [[PubMed](#)]
59. Liao, C.Y.; Smet, W.; Brunoud, G.; Yoshida, S.; Vernoux, T.; Weijers, D. Reporters for sensitive and quantitative measurement of auxin response. *Nat. Methods* **2015**, *12*, 207–210. [[CrossRef](#)] [[PubMed](#)]
60. Scarpella, E.; Marcos, D.; Friml, J.; Berleth, T. Control of leaf vascular patterning by polar auxin transport. *Genes Dev.* **2006**, *20*, 1015–1027. [[CrossRef](#)] [[PubMed](#)]
61. Perrot-Rechenmann, C. Cellular responses to auxin: Division versus expansion. *Cold Spring Harb. Perspect. Biol.* **2010**, *2*, a001446. [[CrossRef](#)] [[PubMed](#)]
62. Vernoux, T.; Brunoud, G.; Farcot, E.; Morin, V.; van den Daele, H.; Legrand, J.; Oliva, M.; Das, P.; Larrieu, A.; Wells, D.; et al. The auxin signalling network translates dynamic input into robust patterning at the shoot apex. *Mol. Syst. Biol.* **2011**, *7*, 1–15. [[CrossRef](#)] [[PubMed](#)]
63. Tan, X.; Calderon-Villalobos, L.I.A.; Sharon, M.; Zheng, C.; Robinson, C.V.; Estelle, M.; Zheng, N. Mechanism of auxin perception by the TIR1 ubiquitin ligase. *Nature* **2007**, *446*, 640–645. [[CrossRef](#)] [[PubMed](#)]
64. Brunoud, G.; Wells, D.M.; Oliva, M.; Larrieu, A.; Mirabet, V.; Burrow, A.H.; Beeckman, T.; Kepinski, S.; Traas, J.; Bennett, M.J.; et al. A novel sensor to map auxin response and distribution at high spatio-temporal resolution. *Nature* **2012**, *482*, 103–106. [[CrossRef](#)] [[PubMed](#)]
65. Band, L.R.; Wells, D.M.; Larrieu, A.; Sun, J.; Middleton, A.M.; French, A.P.; Brunoud, G.; Sato, E.M.; Wilson, M.H.; Peret, B.; et al. Root gravitropism is regulated by a transient lateral auxin gradient controlled by a tipping-point mechanism. *Proc. Natl. Acad. Sci. USA* **2012**, *109*, 4668–4673. [[CrossRef](#)] [[PubMed](#)]

66. Pernisova, M.; Prat, T.; Grones, P.; Harustiaková, D.; Matonohova, M.; Spichal, L.; Nodzynski, T.; Friml, J.; Hejatko, J. Cytokinins influence root gravitropism via differential regulation of auxin transporter expression and localization in *Arabidopsis*. *New Phytol.* **2016**, *212*, 497–509. [[CrossRef](#)] [[PubMed](#)]
67. Von Wangenheim, D.; Hauschild, R.; Friml, J. Light Sheet Fluorescence Microscopy of Plant Roots Growing on the Surface of a Gel. *J. Vis. Exp.* **2017**. [[CrossRef](#)] [[PubMed](#)]
68. Wend, S.; Bosco, C.D.; Kämpf, M.M.; Ren, F.; Palme, K.; Weber, W.; Dovzhenko, A.; Zurbriggen, M.D. A quantitative ratiometric sensor for time-resolved analysis of auxin dynamics. *Sci. Rep.* **2013**, *3*, 2052. [[CrossRef](#)] [[PubMed](#)]
69. Rademacher, E.H.; Möller, B.; Lokerse, A.S.; Llavata-Peris, C.I.; van Den Berg, W.; Weijers, D. A cellular expression map of the *Arabidopsis* AUXIN RESPONSE FACTOR gene family. *Plant J.* **2011**, *68*, 597–606. [[CrossRef](#)] [[PubMed](#)]
70. Abel, S.; Oeller, P.W.; Theologou, A. Early auxin-induced genes encode short-lived nuclear proteins. *Biochemistry* **1994**, *91*, 326–330. [[CrossRef](#)]
71. Gray, W.M.; Kepinski, S.; Rouse, D.; Leyser, O.; Estelle, M. Auxin regulates SCFTIR1-dependent degradation of AUX/IAA proteins. *Nature* **2001**, *414*, 271–276. [[CrossRef](#)] [[PubMed](#)]
72. Swarup, R.; Friml, J.; Marchant, A.; Ljung, K.; Sandberg, G.; Palme, K.; Bennett, M. Localization of the auxin permease AUX1 suggests two functionally distinct hormone transport pathways operate in the *Arabidopsis* root apex. *Genes Dev.* **2001**, *15*, 2648–2653. [[CrossRef](#)] [[PubMed](#)]
73. Tian, Q.; Uhlir, N.J.; Reed, J.W. Arabidopsis SHY2/IAA3 Inhibits Auxin-Regulated Gene Expression. *Plant Cell* **2002**, *14*, 301–319. [[CrossRef](#)] [[PubMed](#)]
74. Weijers, D.; Benkova, E.; Jäger, K.E.; Schlereth, A.; Hamann, T.; Kientz, M.; Wilmoth, J.C.; Reed, J.W.; Jürgens, G. Developmental specificity of auxin response by pairs of ARF and Aux/IAA transcriptional regulators. *EMBO J.* **2005**, *24*, 1874–1885. [[CrossRef](#)] [[PubMed](#)]
75. Ploense, S.E.; Wu, M.F.; Nagpal, P.; Reed, J.W. A gain-of-function mutation in IAA18 alters *Arabidopsis* embryonic apical patterning. *Development* **2009**, *136*, 1509–1517. [[CrossRef](#)] [[PubMed](#)]
76. De Rybel, B.; Vassileva, V.; Parizot, B.; Demeulenaere, M.; Grunewald, W.; Audenaert, D.; Van Campenhout, J.; Overvoorde, P.; Jansen, L.; Vanneste, S.; et al. A novel Aux/IAA28 signaling cascade activates GATA23-dependent specification of lateral root founder cell identity. *Curr. Biol.* **2010**, *20*, 1697–1706. [[CrossRef](#)] [[PubMed](#)]
77. Müller, C.J.; Valdés, A.E.; Wang, G.; Ramachandran, P.; Beste, L.; Uddenberg, D.; Carlsbecker, A. PHABULOSA Mediates an Auxin Signaling Loop to Regulate Vascular Patterning in *Arabidopsis*. *Plant Physiol.* **2016**, *170*, 956–970. [[CrossRef](#)] [[PubMed](#)]
78. Winkler, M.; Niemeyer, M.; Hellmuth, A.; Janitza, P.; Christ, G.; Samodelov, S.L.; Wilde, V.; Majovsky, P.; Trujillo, M.; Zurbriggen, M.D.; et al. Variation in auxin sensing guides AUX/IAA transcriptional repressor ubiquitylation and destruction. *Nat. Commun.* **2017**, *8*, 15706. [[CrossRef](#)] [[PubMed](#)]
79. Piya, S.; Shrestha, S.K.; Binder, B.; Stewart, C.N.; Hewezi, T. Protein-protein interaction and gene co-expression maps of ARFs and Aux/IAAs in *Arabidopsis*. *Front. Plant Sci.* **2014**, *5*, 744. [[CrossRef](#)] [[PubMed](#)]
80. Kasahara, H. Current aspects of auxin biosynthesis in plants. *Biosci. Biotechnol. Biochem.* **2016**, *80*, 34–42. [[CrossRef](#)] [[PubMed](#)]
81. Stepanova, A.N.; Robertson-Hoyt, J.; Yun, J.; Benavente, L.M.; Xie, D.Y.; Doležal, K.; Schlereth, A.; Jürgens, G.; Alonso, J.M. TAA1-Mediated Auxin Biosynthesis Is Essential for Hormone Crosstalk and Plant Development. *Cell* **2008**, *133*, 177–191. [[CrossRef](#)] [[PubMed](#)]
82. Cheng, Y.; Dai, X.; Zhao, Y. Auxin biosynthesis by the YUCCA flavin monooxygenases controls the formation of floral organs and vascular tissues in *Arabidopsis*. *Genes Dev.* **2006**, *20*, 1790–1799. [[CrossRef](#)] [[PubMed](#)]
83. Cheng, Y.; Dai, X.; Zhao, Y. Auxin Synthesized by the YUCCA Flavins Monooxygenases Is Essential for Embryogenesis and Leaf Formation in *Arabidopsis*. *Plant Cell* **2007**, *19*, 2430–2439. [[CrossRef](#)] [[PubMed](#)]
84. Robert, H.S.; Grones, P.; Stepanova, A.N.; Robles, L.M.; Lokerse, A.S.; Alonso, J.M.; Weijers, D.; Friml, J. Local auxin sources orient the apical-basal axis in *Arabidopsis* embryos. *Curr. Biol.* **2013**, *23*, 2506–2512. [[CrossRef](#)] [[PubMed](#)]
85. Chen, Q.; Dai, X.; de-Paoli, H.; Cheng, Y.; Takebayashi, Y.; Kasahara, H.; Kamiya, Y.; Zhao, Y. Auxin Overproduction in Shoots Cannot Rescue Auxin Deficiencies in *Arabidopsis* Roots. *Plant Cell Physiol.* **2014**, *55*, 1072–1079. [[CrossRef](#)] [[PubMed](#)]

86. Petrášek, J.; Mravec, J.; Bouchard, R.; Blakeslee, J.J.; Abas, M.; Seifertová, D.; Wisniewska, J.; Tadele, Z.; Kubeš, M.; Covanová, M.; et al. PIN proteins perform a rate-limiting function in cellular auxin efflux. *Science* **2006**, *312*, 914–918. [[CrossRef](#)] [[PubMed](#)]
87. Zažímalová, E.; Murphy, A.S.; Yang, H.; Hoyerova, K.; Hošek, P. Auxin Transporters—Why So Many? *Cold Spring Harb. Perspect. Biol.* **2010**, *2*, a001552. [[CrossRef](#)] [[PubMed](#)]
88. Blilou, I.; Xu, J.; Wildwater, M.; Willemsen, V.; Paponov, I.; Friml, J.; Heidstra, R.; Aida, M.; Palme, K.; Scheres, B. The PIN auxin efflux facilitator network controls growth and patterning in *Arabidopsis* roots. *Nature* **2005**, *433*, 39–44. [[CrossRef](#)] [[PubMed](#)]
89. Vieten, A.; Vanneste, S.; Wis, J.; Benková, E.; Benjamins, R.; Beeckman, T.; Luschnig, C. Functional redundancy of PIN proteins is accompanied by auxin-dependent cross-regulation of PIN expression. *Development* **2005**, *132*, 4521–4531. [[CrossRef](#)] [[PubMed](#)]
90. Xu, J. Dissection of *Arabidopsis* ADP-RIBOSYLATION FACTOR 1 Function in Epidermal Cell Polarity. *Plant Cell* **2005**, *17*, 525–536. [[CrossRef](#)] [[PubMed](#)]
91. Zadnikova, P.; Petrasek, J.; Marhavy, P.; Raz, V.; Vandenbussche, F.; Ding, Z.; Schwarzerova, K.; Morita, M.T.; Tasaka, M.; Hejatkó, J.; et al. Role of PIN-mediated auxin efflux in apical hook development of *Arabidopsis thaliana*. *Development* **2010**, *137*, 607–617. [[CrossRef](#)] [[PubMed](#)]
92. Mravec, J.; Skůpa, P.; Bailly, A.; Hoyerová, K.; Křeček, P.; Bielach, A.; Petrášek, J.; Zhang, J.; Gaykova, V.; Stierhof, Y.-D.; et al. Subcellular homeostasis of phytohormone auxin is mediated by the ER-localized PIN5 transporter. *Nature* **2009**, *459*, 1136–1140. [[CrossRef](#)] [[PubMed](#)]
93. Bender, R.L.; Fekete, M.L.; Klinkenberg, P.M.; Hampton, M.; Bauer, B.; Malecha, M.; Lindgren, K.; Maki, J.A.; Perera, M.A.D.N.; Nikolau, B.J.; et al. PIN6 is required for nectary auxin response and short stamen development. *Plant J.* **2013**, *74*, 893–904. [[CrossRef](#)] [[PubMed](#)]
94. Sawchuk, M.G.; Edgar, A.; Scarpella, E. Patterning of leaf vein networks by convergent auxin transport pathways. *PLoS Genet.* **2013**, *9*, e1003294. [[CrossRef](#)] [[PubMed](#)]
95. Dal Bosco, C.; Dovzhenko, A.; Liu, X.; Woerner, N.; Rensch, T.; Eismann, M.; Eimer, S.; Hegermann, J.; Paponov, I.A.; Ruperti, B.; et al. The endoplasmic reticulum localized PIN8 is a pollen-specific auxin carrier involved in intracellular auxin homeostasis. *Plant J.* **2012**, *71*, 860–870. [[CrossRef](#)] [[PubMed](#)]
96. Ding, Z.; Wang, B.; Moreno, I.; Dupláková, N.; Simon, S.; Carraro, N.; Reemmer, J.; Pěňčík, A.; Chen, X.; Tejos, R.; et al. ER-localized auxin transporter PIN8 regulates auxin homeostasis and male gametophyte development in *Arabidopsis*. *Nat. Commun.* **2012**, *3*, 941. [[CrossRef](#)] [[PubMed](#)]
97. Wabnik, K.; Robert, H.S.; Smith, R.S.; Friml, J. Modeling framework for the establishment of the apical-basal embryonic axis in plants. *Curr. Biol.* **2013**, *23*, 2513–2518. [[CrossRef](#)] [[PubMed](#)]
98. Dubrovsky, J.G.; Sauer, M.; Napsucially-Mendivil, S.; Ivanchenko, M.G.; Friml, J.; Shishkova, S.; Celenza, J.; Benkova, E. Auxin acts as a local morphogenetic trigger to specify lateral root founder cells. *Proc. Natl. Acad. Sci. USA* **2008**, *105*, 8790–8794. [[CrossRef](#)] [[PubMed](#)]
99. Hay, A. ASYMMETRIC LEAVES1 and auxin activities converge to repress BREVIPEDICELLUS expression and promote leaf development in *Arabidopsis*. *Development* **2006**, *133*, 3955–3961. [[CrossRef](#)] [[PubMed](#)]
100. Barkoulas, M.; Hay, A.; Kougioumoutzi, E.; Tsiantis, M. A developmental framework for dissected leaf formation in the *Arabidopsis* relative *Cardamine hirsuta*. *Nat. Genet.* **2008**, *40*, 1136–1141. [[CrossRef](#)] [[PubMed](#)]
101. Pernisova, M.; Klima, P.; Horak, J.; Valkova, M.; Malbeck, J.; Soucek, P.; Reichman, P.; Hoyerova, K.; Dubova, J.; Friml, J.; et al. Cytokinins modulate auxin-induced organogenesis in plants via regulation of the auxin efflux. *Proc. Natl. Acad. Sci. USA* **2009**, *106*, 3609–3614. [[CrossRef](#)] [[PubMed](#)]
102. Hejatkó, J.; Blilou, I.; Brewer, P.B.; Friml, J.; Scheres, B.; Benková, E. In situ hybridization technique for mRNA detection in whole mount *Arabidopsis* samples. *Nat. Protoc.* **2006**, *1*, 1939–1946. [[CrossRef](#)] [[PubMed](#)]
103. Sauer, M.; Paciorek, T.; Benková, E.; Friml, J. Immunocytochemical techniques for whole-mount in situ protein localization in plants. *Nat. Protoc.* **2006**, *1*, 98–103. [[CrossRef](#)] [[PubMed](#)]
104. Gälweiler, L.; Guan, C.; Müller, A.; Wisman, E.; Mendgen, K.; Yephremov, A.; Palme, K. Regulation of Polar Auxin Transport by AtPIN1 in *Arabidopsis* Vascular Tissue. *Science* **1998**, *282*, 2226–2230. [[CrossRef](#)] [[PubMed](#)]
105. Müller, A.; Guan, C.; Gälweiler, L.; Tänzler, P.; Huijser, P.; Marchant, A.; Parry, G.; Bennett, M.; Wisman, E.; Palme, K. AtPIN2 defines a locus of *Arabidopsis* for root gravitropism control. *EMBO J.* **1998**, *17*, 6903–6911. [[CrossRef](#)] [[PubMed](#)]

106. Friml, J.; Wiśniewska, J.; Benková, E.; Mendgen, K.; Palme, K. Lateral relocation of auxin efflux regulator PIN3 mediates tropism in *Arabidopsis*. *Nature* **2002**, *415*, 806–809. [[CrossRef](#)] [[PubMed](#)]
107. Krouk, G.; Lacombe, B.; Bielach, A.; Perrine-Walker, F.; Malinska, K.; Mounier, E.; Hoyerova, K.; Tillard, P.; Leon, S.; Ljung, K.; et al. Nitrate-Regulated Auxin Transport by NRT1.1 Defines a Mechanism for Nutrient Sensing in Plants. *Dev. Cell* **2010**, *18*, 927–937. [[CrossRef](#)] [[PubMed](#)]
108. Ohmiya, A.; Hayashi, T. Immuno-gold localization of IAA in leaf cells of *Prunus persica* at different stages of development. *Physiol. Plant.* **1992**, *85*, 439–445. [[CrossRef](#)]
109. Thomas, C.; Bronner, R.; Molinier, J.; Prinsen, E.; Van Onckelen, H.; Hahne, G. Immuno-cytochemical localization of indole-3-acetic acid during induction of somatic embryogenesis in cultured sunflower embryos. *Planta* **2002**, *215*, 577–583. [[CrossRef](#)] [[PubMed](#)]
110. Chen, D.; Ren, Y.; Deng, Y.; Zhao, J. Auxin polar transport is essential for the development of zygote and embryo in *Nicotiana tabacum* L. and correlated with ABP1 and PM H⁺-ATPase activities. *J. Exp. Bot.* **2010**, *61*, 1853–1867. [[CrossRef](#)] [[PubMed](#)]
111. Nishimura, T.; Toyooka, K.; Sato, M.; Matsumoto, S.; Lucas, M.M.; Strnad, M.; Baluška, F.; Koshiba, T. Immunohistochemical observation of indole-3-acetic acid at the IAA synthetic maize coleoptile tips. *Plant Signal. Behav.* **2011**, *6*, 2013–2022. [[CrossRef](#)] [[PubMed](#)]
112. Dong, N.; Wang, Q.; Zhang, J.; Pei, D. Immunohistochemical localization of indole-3-acetic acid during induction of adventitious root formation from cotyledon explants of walnut. *J. Am. Soc. Hortic. Sci.* **2011**, *136*, 315–319.
113. Petersson, S.V.; Johansson, A.I.; Kowalczyk, M.; Makoveychuk, A.; Wang, J.Y.; Moritz, T.; Grebe, M.; Benfey, P.N.; Sandberg, G.; Ljung, K. An Auxin Gradient and Maximum in the *Arabidopsis* Root Apex Shown by High-Resolution Cell-Specific Analysis of IAA Distribution and Synthesis. *Plant Cell* **2009**, *21*, 1659–1668. [[CrossRef](#)] [[PubMed](#)]
114. Geisler, M.; Wang, B.; Zhu, J. Auxin transport during root gravitropism: Transporters and techniques. *Plant Biol.* **2014**, *16*, 50–57. [[CrossRef](#)] [[PubMed](#)]
115. Lewis, D.R.; Muday, G.K. Measurement of auxin transport in *Arabidopsis thaliana*. *Nat. Protoc.* **2009**, *4*, 437–451. [[CrossRef](#)] [[PubMed](#)]
116. Petrášek, J.; Laňková, M.; Zažímalová, E. Determination of Auxin Transport Parameters on the Cellular Level. *Methods Mol. Biol.* **2014**, *1056*, 241–253. [[CrossRef](#)] [[PubMed](#)]
117. Pernet, J.J.; Pilet, P.E. Indoleacetic acid movement in the root cap. *Planta* **1976**, *128*, 183–184. [[CrossRef](#)] [[PubMed](#)]
118. Davies, P.J.; Mitchell, E.K. Transport of indoleacetic acid in intact roots of *Phaseolus coccineus*. *Planta* **1972**, *105*, 139–154. [[CrossRef](#)] [[PubMed](#)]
119. Mitchell, E.K.; Davies, P.J. Evidence for Three Different Systems of Movement of Indoleacetic Acid in Intact Roots of *Phaseolus coccineus*. *Physiol. Plant.* **1975**, *33*, 290–294. [[CrossRef](#)]
120. Nagao, M.; Ohwaki, Y. Auxin transport in the elongation zone of *Vicia* roots. *Bot. Mag. Tokyo* **1968**, *81*, 44–45. [[CrossRef](#)]
121. Tsurumi, S.; Ohwaki, Y. Transport of ¹⁴C-labeled indoleacetic acid in *Vicia* root segments. *Plant Cell Physiol.* **1978**, *19*, 1195–1206.
122. McCready, C.C. The polarity of auxin movement in segments excised from *Phaseolus vulgaris* L. In *Biochemistry and Physiology of Plant Growth Substances*; Wightman, F., Setterfield, G., Eds.; Runge Press: Ottawa, ON, Canada, 1968; pp. 1005–1023.
123. Smith, C.W.; Jacobs, W.P. The movement of ¹⁴C-IAA in the hypocotyl of *Phaseolus vulgaris*. *Am. J. Bot.* **1969**, *56*, 492–497. [[CrossRef](#)]
124. Goldsmith, M.H.M. The Polar Transport of Auxin. *Annu. Rev. Plant Physiol.* **1977**, *28*, 439–478. [[CrossRef](#)]
125. Boot, K.J.M.; Hille, S.C.; Libbenga, K.R.; Peletier, L.A.; Van Spronsen, P.C.; Van Duijn, B.; Offringa, R. Modelling the dynamics of polar auxin transport in inflorescence stems of *Arabidopsis thaliana*. *J. Exp. Bot.* **2016**, *67*, 649–666. [[CrossRef](#)] [[PubMed](#)]
126. Ohwaki, Y.; Tsurumi, S. Auxin, transport and growth in intact roots of *Vicia faba*. *Plant Cell Physiol.* **1976**, *17*, 1329–1342. [[CrossRef](#)]
127. Okada, K.; Ueda, J.; Komaki, M.K.; Bell, C.J.; Shimura, Y. Requirement of the Auxin Polar Transport System in Early Stages of *Arabidopsis* Floral Bud Formation. *Plant Cell* **1991**, *3*, 677–684. [[CrossRef](#)] [[PubMed](#)]

128. Rashotte, A.M.; Brady, S.R.; Reed, R.C.; Ante, S.J.; Muday, G.K. Basipetal Auxin Transport Is Required for Gravitropism in Roots of *Arabidopsis*. *Plant Physiol.* **2000**, *122*, 481–490. [[CrossRef](#)] [[PubMed](#)]
129. Rashotte, A.M.; Poupart, J.; Waddell, C.S.; Muday, G.K. Transport of the two natural auxins, indole-3-butyric acid and indole-3-acetic acid, in *Arabidopsis*. *Plant Physiol.* **2003**, *133*, 761–772. [[CrossRef](#)] [[PubMed](#)]
130. Muday, G.K.; Brady, S.R.; Argueso, C.; Deruère, J.; Kieber, J.J.; DeLong, A. RCN1-regulated phosphatase activity and EIN2 modulate hypocotyl gravitropism by a mechanism that does not require ethylene signaling. *Plant Physiol.* **2006**, *141*, 1617–1629. [[CrossRef](#)] [[PubMed](#)]
131. Marchant, A.; Kargul, J.; May, S.T.; Muller, P.; Delbarre, A.; Perrot-Rechenmann, C.; Bennett, M.J. AUX1 regulates root gravitropism in *Arabidopsis* by facilitating auxin uptake within root apical tissues. *EMBO J.* **1999**, *18*, 2066–2073. [[CrossRef](#)] [[PubMed](#)]
132. Casimiro, I.; Marchant, A.; Bhalerao, R.P.; Beeckman, T.; Dhooge, S.; Swarup, R.; Graham, N.; Inzé, D.; Sandberg, G.; Casero, P.J.; et al. Auxin transport promotes *Arabidopsis* lateral root initiation. *Plant Cell* **2001**, *13*, 843–852. [[CrossRef](#)] [[PubMed](#)]
133. Murphy, A.; Peer, W.A.; Taiz, L. Regulation of auxin transport by aminopeptidases and endogenous flavonoids. *Planta* **2000**, *211*, 315–324. [[CrossRef](#)] [[PubMed](#)]
134. Noh, B.; Bandyopadhyay, A.; Peer, W.A.; Spalding, E.P.; Murphy, A.S. Enhanced gravi- and phototropism in plant *mdr* mutants mislocalizing the auxin efflux protein PIN1. *Nature* **2003**, *423*, 999–1002. [[CrossRef](#)] [[PubMed](#)]
135. Geisler, M.; Murphy, A.S. The ABC of auxin transport: The role of p-glycoproteins in plant development. *FEBS Lett.* **2006**, *580*, 1094–1102. [[CrossRef](#)] [[PubMed](#)]
136. Lewis, D.R.; Miller, N.D.; Splitt, B.L.; Wu, G.; Spalding, E.P. Separating the Roles of Acropetal and Basipetal Auxin Transport on Gravitropism with Mutations in Two *Arabidopsis* Multidrug Resistance-Like ABC Transporter Genes. *Plant Cell* **2007**, *19*, 1838–1850. [[CrossRef](#)] [[PubMed](#)]
137. Chen, R.; Hilson, P.; Sedbrook, J.; Rosen, E.; Caspar, T.; Masson, P.H. The *Arabidopsis thaliana* AGRAVITROPIC 1 gene encodes a component of the polar-auxin-transport efflux carrier. *Plant Biol.* **1998**, *95*, 15112–15117. [[CrossRef](#)]
138. Delbarre, A.; Muller, P.; Imhoff, V.; Guern, J. Comparison of mechanisms controlling uptake and accumulation of 2,4-dichlorophenoxy acetic acid, naphthalene-1-acetic acid, and indole-3-acetic acid in suspension-cultured tobacco cells. *Planta* **1996**, *198*, 532–541. [[CrossRef](#)] [[PubMed](#)]
139. Seifertová, D.; Skůpa, P.; Rychtář, J.; Laňková, M.; Pařezová, M.; Dobrev, P.I.; Hoyerová, K.; Petrášek, J.; Zažímalová, E. Characterization of transmembrane auxin transport in *Arabidopsis* suspension-cultured cells. *J. Plant Physiol.* **2014**, *171*, 429–437. [[CrossRef](#)] [[PubMed](#)]
140. Simon, S.; Kubeš, M.; Baster, P.; Robert, S.; Dobrev, P.I.; Friml, J.; Petrášek, J.; Zažímalová, E. Defining the selectivity of processes along the auxin response chain: A study using auxin analogues. *New Phytol.* **2013**, *200*, 1034–1048. [[CrossRef](#)] [[PubMed](#)]
141. Hošek, P.; Kubeš, M.; Laňková, M.; Dobrev, P.I.; Klíma, P.; Kohoutová, M.; Petrášek, J.; Hoyerová, K.; Jiřina, M.; Zažímalová, E. Auxin transport at cellular level: New insights supported by mathematical modelling. *J. Exp. Bot.* **2012**, *63*, 3815–3827. [[CrossRef](#)] [[PubMed](#)]
142. Paciorek, T.; Zažímalová, E.; Ruthardt, N.; Petrášek, J.; Stierhof, Y.D.; Kleine-Vehn, J.; Morris, D.A.; Emans, N.; Jürgens, G.; Geldner, N.; et al. Auxin inhibits endocytosis and promotes its own efflux from cells. *Nature* **2005**, *435*, 1251–1256. [[CrossRef](#)] [[PubMed](#)]
143. Petrášek, J.; Elčknér, M.; Morris, D.; Zažímalová, E. Auxin efflux carrier activity and auxin accumulation regulate cell division and polarity in tobacco cells. *Planta* **2002**, *216*, 302–308. [[CrossRef](#)] [[PubMed](#)]
144. Carrier, D.J.; Abu Bakar, N.T.; Lawler, K.; Dorrian, J.M.; Haider, A.; Bennett, M.J.; Kerr, I.D. Heterologous expression of a membrane-spanning auxin importer: Implications for functional analyses of auxin transporters. *Int. J. Plant Genom.* **2009**, *2009*, 848145. [[CrossRef](#)] [[PubMed](#)]
145. Yang, H.; Murphy, A.S. Functional expression and characterization of *Arabidopsis* ABCB, AUX 1 and PIN auxin transporters in *Schizosaccharomyces pombe*. *Plant J.* **2009**, *59*, 179–191. [[CrossRef](#)] [[PubMed](#)]
146. Bouchard, R.; Bailly, A.; Blakeslee, J.J.; Oehring, S.C.; Vincenzetti, V.; Lee, O.R.; Paponov, I.; Palme, K.; Mancuso, S.; Murphy, A.S.; et al. Immunophilin-like TWISTED DWARF1 modulates auxin efflux activities of *Arabidopsis* P-glycoproteins. *J. Biol. Chem.* **2006**, *281*, 30603–30612. [[CrossRef](#)] [[PubMed](#)]

147. Multani, D.S.; Briggs, S.P.; Chamberlin, M.A.; Blakeslee, J.J.; Murphy, A.S.; Johal, G.S. Loss of an MDR Transporter in Compact Stalks of Maize *br2* and Sorghum *dw3* Mutants. *Science* **2003**, *302*, 81–84. [[CrossRef](#)] [[PubMed](#)]
148. Yang, Y.; Hammes, U.Z.; Taylor, C.G.; Schachtman, D.P.; Nielsen, E. High-Affinity Auxin Transport by the AUX1 Influx Carrier Protein. *Curr. Biol.* **2006**, *16*, 1123–1127. [[CrossRef](#)] [[PubMed](#)]
149. Blakeslee, J.J.; Murphy, A.S. Microscopic and Biochemical Visualization of Auxins in Plant Tissues. *Methods Mol. Biol.* **2016**, *1398*, 37–53. [[CrossRef](#)] [[PubMed](#)]
150. Sauer, M.; Robert, S.; Kleine-Vehn, J. Auxin: Simply complicated. *J. Exp. Bot.* **2013**, *64*, 2565–2577. [[CrossRef](#)] [[PubMed](#)]
151. Rigal, A.; Ma, Q.; Robert, S. Unraveling plant hormone signaling through the use of small molecules. *Front. Plant Sci.* **2014**, *5*, 373. [[CrossRef](#)] [[PubMed](#)]
152. Malachowska-Ugarte, M.; Sperduto, C.; Ermolovich, Y.V.; Sauchuk, A.L.; Jurášek, M.; Litvinovskaya, R.P.; Straltsova, D.; Smolich, I.; Zhabinskii, V.N.; Drašar, P.; et al. Brassinosteroid-BODIPY conjugates: Design, synthesis, and properties. *Steroids* **2015**, *102*, 53–59. [[CrossRef](#)] [[PubMed](#)]
153. Prandi, C.; Ghigo, G.; Occhiato, E.G.; Scarpi, D.; Begliomini, S.; Lace, B.; Alberto, G.; Artuso, E.; Blangetti, M. Tailoring fluorescent strigolactones for in vivo investigations: A computational and experimental study. *Org. Biomol. Chem.* **2014**, *12*, 2960–2968. [[CrossRef](#)] [[PubMed](#)]
154. Enciso, A.E.; Garzoni, M.; Pavan, G.M.; Simanek, E.E. Influence of linker groups on the solubility of triazine dendrimers. *New J. Chem.* **2015**, *39*, 1247–1252. [[CrossRef](#)]
155. Bielezová, K.; Pařízková, B.; Kubeš, M.; Husičková, A.; Kubala, M.; Sedlářová, M.; Doležal, K.; Strnad, M.; Novák, O.; Žukauskaite, A. New fluorescently labeled auxins exhibit promising anti-auxin activity. *N. Biotechnol.* **2017**, Under review.
156. Lace, B.; Prandi, C. Shaping Small Bioactive Molecules to Untangle Their Biological Function: A Focus on Fluorescent Plant Hormones. *Mol. Plant* **2016**, *9*, 1099–1118. [[CrossRef](#)] [[PubMed](#)]
157. Li, J.; Zhu, J.J. Quantum dots for fluorescent biosensing and bio-imaging applications. *Analyst* **2013**, *138*, 2506–2515. [[CrossRef](#)] [[PubMed](#)]
158. Wegner, K.D.; Hildebrandt, N. Quantum dots: Bright and versatile in vitro and in vivo fluorescence imaging biosensors. *Chem. Soc. Rev.* **2015**, *44*, 4792–4834. [[CrossRef](#)] [[PubMed](#)]
159. Cao, Y.; Wei, J.; Liao, Q.; Yu, Y.; Lin, B. In situ fluorescence labelling of jasmonic acid binding sites in plant tissues with cadmium-free quantum dots. *IET Nanobiotechnol.* **2015**, *9*, 35–42. [[CrossRef](#)]
160. Lavis, L.D.; Thomas, J.; Rutkoski, A.; Ronald, T. Raines Tuning the pKa of Fluorescein to Optimize Binding Assays. *Anal. Chem.* **2007**, *79*, 6775–6782. [[CrossRef](#)] [[PubMed](#)]
161. Panchuk-Voloshina, N.; Haugland, R.P.; Bishop-Stewart, J.; Bhalgat, M.K.; Millard, P.J.; Mao, F.; Leung, W.-Y.; Haugland, R.P. Alexa Dyes, a Series of New Fluorescent Dyes that Yield Exceptionally Bright, Photostable Conjugates. *J. Histochem. Cytochem.* **1999**, *47*, 1179–1188. [[CrossRef](#)] [[PubMed](#)]
162. Lavis, L.D.; Raines, R.T. Bright Ideas for Chemical Biology. *ACS Chem. Biol.* **2008**, *3*, 142–155. [[CrossRef](#)] [[PubMed](#)]
163. Beija, M.; Afonso, C.A.M.; Martinho, J.M.G. Synthesis and applications of Rhodamine derivatives as fluorescent probes. *Chem. Soc. Rev.* **2009**, *38*, 2410–2433. [[CrossRef](#)] [[PubMed](#)]
164. Hayashi, K.-I.; Nakamura, S.; Fukunaga, S.; Nishimura, T.; Jenness, M.K.; Murphy, A.S.; Motose, H.; Nozaki, H.; Furutani, M.; Aoyama, T. Auxin transport sites are visualized in *planta* using fluorescent auxin analogs. *Proc. Natl. Acad. Sci. USA* **2014**, *111*, 11557–11562. [[CrossRef](#)] [[PubMed](#)]
165. Muir, R.M.; Fujita, T.; Hansch, C. Structure-activity relationship in the auxin activity of mono-substituted phenylacetic acids. *Plant Physiol.* **1967**, *42*, 1519–1526. [[CrossRef](#)] [[PubMed](#)]
166. Kaethner, T.M. Conformational change theory for auxin structure-activity relationships. *Nature* **1977**, *267*, 19–23. [[CrossRef](#)]
167. Calderon-Villalobos, L.I.; Tan, X.; Zheng, N.; Estelle, M. Auxin Perception-Structural Insights. *Cold Spring Harb. Perspect. Biol.* **2010**, *2*, a005546. [[CrossRef](#)] [[PubMed](#)]
168. Grossmann, K. Auxin herbicides: Current status of mechanism and mode of action. *Pest Manag. Sci.* **2010**, *66*, 113–120. [[CrossRef](#)] [[PubMed](#)]
169. Muscolo, A.; Sidari, M.; Francioso, O.; Tugnoli, V.; Nardi, S. The auxin-like activity of humic substances is related to membrane interactions in carrot cell cultures. *J. Chem. Ecol.* **2007**, *33*, 115–129. [[CrossRef](#)] [[PubMed](#)]

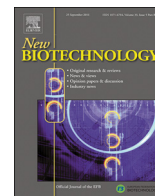
170. Sokołowska, K.; Kizińska, J.; Szewczuk, Z.; Banasiak, A. Auxin conjugated to fluorescent dyes—A tool for the analysis of auxin transport pathways. *Plant Biol.* **2014**, *16*, 866–877. [[CrossRef](#)] [[PubMed](#)]
171. Tsuda, E.; Yang, H.; Nishimura, T.; Uehara, Y.; Sakai, T.; Furutani, M.; Koshiba, T.; Hirose, M.; Nozaki, H.; Murphy, A.S.; et al. Alkoxy-auxins are selective inhibitors of auxin transport mediated by PIN, ABCB, and AUX1 transporters. *J. Biol. Chem.* **2011**, *286*, 2354–2364. [[CrossRef](#)] [[PubMed](#)]
172. Mancuso, S.; Marras, A.M.; Magnus, V.; Baluška, F. Noninvasive and continuous recordings of auxin fluxes in intact root apex with a carbon nanotube-modified and self-referencing microelectrode. *Anal. Biochem.* **2005**, *341*, 344–351. [[CrossRef](#)] [[PubMed](#)]
173. McLamore, E.S.; Diggs, A.; Calvo Marzal, P.; Shi, J.; Blakeslee, J.J.; Peer, W.A.; Murphy, A.S.; Porterfield, D.M. Non-invasive quantification of endogenous root auxin transport using an integrated flux microsensor technique. *Plant J.* **2010**, *63*, 1004–1016. [[CrossRef](#)] [[PubMed](#)]
174. Tanaka, H.; Dhonukshe, P.; Brewer, P.B.; Friml, J. Spatiotemporal asymmetric auxin distribution: A means to coordinate plant development. *Cell. Mol. Life Sci.* **2006**, *63*, 2738–2754. [[CrossRef](#)] [[PubMed](#)]
175. Graham, L. Measurements of Geoelectric and Auxin-Induced Potentials in Coleoptiles with a Refined Vibrating Electrode Technique. *Physiol. Plant.* **1964**, *17*, 231–261. [[CrossRef](#)]
176. Johnsson, A. Photoinduced Lateral Potentials in *Zea mays*. *Physiol. Plant.* **1965**, *18*, 574–576. [[CrossRef](#)]
177. Bailly, A.; Sovero, V.; Vincenzetti, V.; Santelia, D.; Bartnik, D.; Koenig, B.W.; Mancuso, S.; Martinoia, E.; Geisler, M. Modulation of P-glycoproteins by auxin transport inhibitors is mediated by interaction with immunophilins. *J. Biol. Chem.* **2008**, *283*, 21817–21826. [[CrossRef](#)] [[PubMed](#)]
178. Kim, J.-Y.; Henrichs, S.; Bailly, A.; Vincenzetti, V.; Sovero, V.; Mancuso, S.; Pollmann, S.; Kim, D.; Geisler, M.; Nam, H.-G. Identification of an ABCB/P-glycoprotein-specific inhibitor of auxin transport by chemical genomics. *J. Biol. Chem.* **2010**, *285*, 23309–23317. [[CrossRef](#)] [[PubMed](#)]
179. Santelia, D.; Vincenzetti, V.; Azzarello, E.; Bovet, L.; Fukao, Y.; Düchtig, P.; Mancuso, S.; Martinoia, E.; Geisler, M. MDR-like ABC transporter AtPGP4 is involved in auxin-mediated lateral root and root hair development. *FEBS Lett.* **2005**, *579*, 5399–5406. [[CrossRef](#)] [[PubMed](#)]
180. Wang, B.; Bailly, A.; Zwiewka, M.; Henrichs, S.; Azzarello, E.; Mancuso, S.; Maeshima, M.; Friml, J.; Schulz, A.; Geisler, M. *Arabidopsis* TWISTED DWARF1 functionally interacts with auxin exporter ABCB1 on the root plasma membrane. *Plant Cell* **2013**, *25*, 202–214. [[CrossRef](#)] [[PubMed](#)]
181. Schlicht, M.; Strnad, M.; Scanlon, M.J.; Mancuso, S.; Hochholdinger, F.; Palme, K.; Volkmann, D.; Menzel, D.; Baluška, F. Auxin immunolocalization implicates vesicular neurotransmitter-like mode of polar auxin transport in root apices. *Plant Signal. Behav.* **2006**, *1*, 122–133. [[CrossRef](#)] [[PubMed](#)]
182. Knöllner, A.S.; Blakeslee, J.J.; Richards, E.L.; Peer, W.A.; Murphy, A.S. Brachytic2/ZmABCB1 functions in IAA export from intercalary meristems. *J. Exp. Bot.* **2010**, *61*, 3689–3696. [[CrossRef](#)] [[PubMed](#)]
183. Sadanandom, A.; Napier, R.M. Biosensors in plants. *Curr. Opin. Plant Biol.* **2010**, *13*, 736–743. [[CrossRef](#)] [[PubMed](#)]
184. Novák, O.; Pěňčík, A.; Ljung, K. Identification and Profiling of Auxin and Auxin Metabolites. In *Auxin and Its Role in Plant Development*, 1st ed.; Zažímalová, E., Petrášek, J., Benková, E., Eds.; Springer: London, UK, 2014; Volume 33, pp. 39–60, ISBN 978-3-7091-1526-8.
185. Porfírio, S.; Gomes da Silva, M.D.R.; Peixe, A.; Cabrita, M.J.; Azadi, P. Current analytical methods for plant auxin quantification—A review. *Anal. Chim. Acta* **2016**, *902*, 8–21. [[CrossRef](#)] [[PubMed](#)]
186. Novák, O.; Napier, R.; Ljung, K. Zooming In on Plant Hormone Analysis: Tissue- and Cell-Specific Approaches. *Annu. Rev. Plant Biol.* **2017**, *68*, 323–348. [[CrossRef](#)] [[PubMed](#)]
187. Tarkowská, D.; Novák, O.; Floková, K.; Tarkowski, P.; Turečková, V.; Grúz, J.; Rolčík, J.; Strnad, M. Quo vadis plant hormone analysis? *Planta* **2014**, *240*, 55–76. [[CrossRef](#)] [[PubMed](#)]
188. Liu, X.; Hegeman, A.D.; Gardner, G.; Cohen, J.D. Protocol: High-throughput and quantitative assays of auxin and auxin precursors from minute tissue samples. *Plant Methods* **2012**, *8*, 31. [[CrossRef](#)] [[PubMed](#)]
189. Novák, O.; Hényková, E.; Sairanen, I.; Kowalczyk, M.; Pospíšil, T.; Ljung, K. Tissue-specific profiling of the *Arabidopsis thaliana* auxin metabolome. *Plant J.* **2012**, *72*, 523–536. [[CrossRef](#)] [[PubMed](#)]
190. Uggla, C.; Moritz, T.; Sandberg, G.; Sundberg, B. Auxin as a positional signal in pattern formation in plants. *Proc. Natl. Acad. Sci. USA* **1996**, *93*, 9282–9286. [[CrossRef](#)] [[PubMed](#)]
191. Immanen, J.; Nieminen, K.; Smolander, O.P.; Kojima, M.; Alonso Serra, J.; Koskinen, P.; Zhang, J.; Elo, A.; Mähönen, A.P.; Street, N.; et al. Cytokinin and Auxin Display Distinct but Interconnected Distribution and Signaling Profiles to Stimulate Cambial Activity. *Curr. Biol.* **2016**, *26*, 1990–1997. [[CrossRef](#)] [[PubMed](#)]

192. Jin, X.; Wang, R.-S.; Zhu, M.; Jeon, B.W.; Albert, R.; Chen, S.; Assmann, S.M. Abscisic Acid-Responsive Guard Cell Metabolomes of *Arabidopsis* Wild-Type and *gpa1* G-Protein Mutants. *Plant Cell* **2013**, *25*, 4789–4811. [[CrossRef](#)] [[PubMed](#)]
193. Bargmann, B.O.R.; Vanneste, S.; Krouk, G.; Nawy, T.; Efroni, I.; Shani, E.; Choe, G.; Friml, J.; Bergmann, D.C.; Estelle, M.; et al. A map of cell type-specific auxin responses. *Mol. Syst. Biol.* **2014**, *9*, 688. [[CrossRef](#)] [[PubMed](#)]
194. Rosquete, R.M.; Barbez, E.; Kleine-Vehn, J. Cellular auxin homeostasis: Gatekeeping is housekeeping. *Mol. Plant* **2012**, *5*, 772–786. [[CrossRef](#)] [[PubMed](#)]
195. Uslu, V.V.; Grossmann, G. The biosensor toolbox for plant developmental biology. *Curr. Opin. Plant Biol.* **2016**, *29*, 138–147. [[CrossRef](#)] [[PubMed](#)]
196. Zhou, Y.; Xu, Z.; Wang, M.; Meng, X.; Yin, H. Electrochemical immunoassay platform for high sensitivity detection of indole-3-acetic acid. *Electrochim. Acta* **2013**, *96*, 66–73. [[CrossRef](#)]
197. Yin, H.; Xu, Z.; Zhou, Y.; Wang, M.; Ai, S. An ultrasensitive electrochemical immunosensor platform with double signal amplification for indole-3-acetic acid determinations in plant seeds. *Analyst* **2013**, *138*, 1851–1857. [[CrossRef](#)] [[PubMed](#)]
198. Sun, B.; Chen, L.; Xu, Y.; Liu, M.; Yin, H.; Ai, S. Ultrasensitive photoelectrochemical immunoassay of indole-3-acetic acid based on the MPA modified CdS/RGO nanocomposites decorated ITO electrode. *Biosens. Bioelectron.* **2014**, *51*, 164–169. [[CrossRef](#)] [[PubMed](#)]
199. Li, J.; Wu, Z.-Y.; Xiao, L.-T.; Zeng, G.-M.; Huang, G.-H.; Shen, G.-L.; Yu, R.-Q. A novel piezoelectric biosensor for the detection of phytohormone beta-indole acetic acid. *Anal. Sci.* **2002**, *18*, 403–407. [[CrossRef](#)] [[PubMed](#)]
200. Wei, C.; Zhou, H.; Chen, C.; Li, Z.; Zhou, J. On-Line Monitoring ¹H-Indole-3-Acetic Acid in Plant Tissues Using Molecular Imprinting Monolayer Techniques on a Surface Plasmon Resonance Sensor. *Anal. Lett.* **2011**, *44*, 2911–2921. [[CrossRef](#)]
201. Li, J.; Yin, W.; Tan, Y.; Pan, H. A sensitive electrochemical molecularly imprinted sensor based on catalytic amplification by silver nanoparticles for 3-indoleacetic acid determination. *Sens. Actuators B Chem.* **2014**, *197*, 109–115. [[CrossRef](#)]
202. Hernández, P.; Galán, F.; Nieto, O.; Hernández, L. Direct determination of indole-3-acetic acid in plant tissues by electroanalytical techniques using a carbon paste modified with OV-17 electrode. *Electroanalysis* **1994**, *6*, 577–583. [[CrossRef](#)]
203. Wu, K.; Sun, Y.; Hu, S. Development of an amperometric indole-3-acetic acid sensor based on carbon nanotubes film coated glassy carbon electrode. *Sens. Actuators B Chem.* **2003**, *96*, 658–662. [[CrossRef](#)]
204. Sandberg, G. Presence of indole-3-acetic acid in chloroplasts of *Nicotiana tabacum* and *Pinus sylvestris*. *Planta* **1990**, *180*, 562–568. [[CrossRef](#)] [[PubMed](#)]
205. Polanská, L.; Vičánková, A.; Nováková, M.; Malbeck, J.; Dobrev, P.I.; Brzobohatý, B.; Vaňková, R.; Macháčková, I. Altered cytokinin metabolism affects cytokinin, auxin, and abscisic acid contents in leaves and chloroplasts, and chloroplast ultrastructure in transgenic tobacco. *J. Exp. Bot.* **2007**, *58*, 637–649. [[CrossRef](#)] [[PubMed](#)]
206. Wells, D.M.; Laplaze, L.; Bennett, M.J.; Vernoux, T. Biosensors for phytohormone quantification: Challenges, solutions, and opportunities. *Trends Plant Sci.* **2013**, *18*, 244–249. [[CrossRef](#)] [[PubMed](#)]
207. Okumoto, S.; Jones, A.; Frommer, W.B. Quantitative Imaging with Fluorescent Biosensors. *Annu. Rev. Plant Biol.* **2012**, *63*, 663–706. [[CrossRef](#)] [[PubMed](#)]
208. Reddy, G.V.; Gordon, S.P.; Meyerowitz, E.M. Unravelling developmental dynamics: Transient intervention and live imaging in plants. *Nat. Rev. Mol. Cell Biol.* **2007**, *8*, 491–501. [[CrossRef](#)] [[PubMed](#)]
209. Kirchhelle, C.; Moore, I. A Simple Chamber for Long-term Confocal Imaging of Root and Hypocotyl Development. *J. Vis. Exp.* **2017**, *123*, 55331. [[CrossRef](#)] [[PubMed](#)]
210. Von Wangenheim, D.; Hauschild, R.; Fendrych, M.; Barone, V.; Friml, J. Live Tracking of Moving Samples in Confocal Microscopy for Vertically Grown Plant Roots. *eLife* **2017**, *6*, e26792. [[CrossRef](#)] [[PubMed](#)]
211. Maizel, A.; von Wangenheim, D.; Federici, F.; Haseloff, J.; Stelzer, E.H.K. High-resolution live imaging of plant growth in near physiological bright conditions using light sheet fluorescence microscopy. *Plant J.* **2011**, *68*, 377–385. [[CrossRef](#)] [[PubMed](#)]
212. Ovečka, M.; Vaškebová, L.; Komis, G.; Luptovciak, I.; Smertenko, A.; Šamaj, J. Preparation of plants for developmental and cellular imaging by light-sheet microscopy. *Nat. Protoc.* **2015**, *10*, 1234–1247. [[CrossRef](#)] [[PubMed](#)]

213. Grossmann, G.; Guo, W.-J.; Ehrhardt, D.W.; Frommer, W.B.; Sit, R.V.; Quake, S.R.; Meier, M. The RootChip: An Integrated Microfluidic Chip for Plant Science. *Plant Cell* **2011**, *23*, 4234–4240. [[CrossRef](#)] [[PubMed](#)]
214. Grossmann, G.; Meier, M.; Cartwright, H.N.; Sosso, D.; Quake, S.R.; Ehrhardt, D.W.; Frommer, W.B. Time-lapse Fluorescence Imaging of Arabidopsis Root Growth with Rapid Manipulation of The Root Environment Using The RootChip. *J. Vis. Exp.* **2012**, *65*, 4290. [[CrossRef](#)] [[PubMed](#)]
215. Evans, C.L.; Xie, X.S. Coherent anti-Stokes Raman scattering microscopy: Chemical imaging for biology and medicine. *Annu. Rev. Anal. Chem.* **2008**, *1*, 883–909. [[CrossRef](#)] [[PubMed](#)]
216. Freudiger, C.W.; Min, W.; Saar, B.G.; Lu, S.; Holtom, G.R.; Tsai, J.C.; Kang, J.X.; Xie, X.S. Label-Free Biomedical Imaging with High Sensitivity by Stimulated Raman Scattering Microscopy. *Science* **2013**, *322*, 1857–1861. [[CrossRef](#)] [[PubMed](#)]



© 2017 by the authors. Licensee MDPI, Basel, Switzerland. This article is an open access article distributed under the terms and conditions of the Creative Commons Attribution (CC BY) license (<http://creativecommons.org/licenses/by/4.0/>).



Full length Article

New fluorescently labeled auxins exhibit promising anti-auxin activity

Kristýna Bielešová^{a,b,1}, Barbora Pařízková^{a,b,1}, Martin Kubeš^{b,1}, Alexandra Husičková^c,
 Martin Kubala^c, Qian Ma^d, Michaela Sedlářová^e, Stéphanie Robert^d, Karel Doležal^{a,b},
 Miroslav Strnad^{a,b}, Ondřej Novák^{a,b}, Asta Žukauskaitė^{a,b,*}

^a Laboratory of Growth Regulators, Centre of the Region Haná for Biotechnological and Agricultural Research, Faculty of Science of Palacký University & Institute of Experimental Botany of the Czech Academy of Sciences, Šlechtitelů 27, CZ-783 71, Olomouc, Czech Republic

^b Department of Chemical Biology and Genetics, Centre of the Region Haná for Biotechnological and Agricultural Research, Faculty of Science, Palacký University, Šlechtitelů 27, CZ-783 71, Olomouc, Czech Republic

^c Department of Biophysics, Centre of the Region Haná for Biotechnological and Agricultural Research, Faculty of Science, Palacký University, Šlechtitelů 27, CZ-783 71 Olomouc, Czech Republic

^d Umeå Plant Science Centre, Department of Forest Genetics and Plant Physiology, Swedish University of Agricultural Sciences, SE-901 83 Umeå, Sweden

^e Department of Botany, Faculty of Science, Palacký University, Šlechtitelů 27, CZ-783 71 Olomouc, Czech Republic

ARTICLE INFO

Keywords:

Anti-auxin
 Arabidopsis
 Biological activity
 DR5::GUS
 Fluorescent labeling
 Indole-3-acetic acid (IAA)

ABSTRACT

The plant hormone auxin is a key player in the regulation of plant growth and development. Despite numerous studies devoted to understanding its role in a wide spectrum of physiological processes, full appreciation of its function is linked to a comprehensive determination of its spatio-temporal distribution, which plays a crucial role in its mode of action. Conjugation of fluorescent tracers to plant hormones enables sensitive and specific visualization of their subcellular and tissue-specific localization and transport *in planta*, which represents a powerful tool for plant physiology. However, to date, only a few fluorescently labeled auxins have been developed. We report the synthesis of four novel fluorescently labeled derivatives of indole-3-acetic acid (IAA) in the form of a conjugate with a nitrobenzoxadiazole (NBD) fluorophore together with validation of their biological activity. These compounds, unlike other previously reported auxins fluorescently labeled at N1 position (nitrogen of the indole ring), do not possess auxin activity but rather show dose-dependent inhibition of auxin-induced effects, such as primary root growth inhibition, root hair growth and the auxin reporter DR5::GUS expression. Moreover, the study demonstrates the importance of the character of the linker and optimal choice of the labeling site in the preparation of fluorescently labeled auxins as important variables influencing their biological activity and fluorescent properties.

Introduction

Auxins are a class of plant hormones influencing nearly every stage of plant life cycle, from germination to senescence [1]. In addition to indole-3-acetic acid (IAA), which is the most common, naturally occurring auxin, only three other plant auxins have been described, namely indole-3-butyric acid (IBA), 4-chloroindole-3-acetic acid (4-Cl-IAA), and phenylacetic acid (PAA) [2]. Besides naturally occurring auxins, many of their synthetic analogues possess auxin-like activity [2–4], and some, mainly 1-naphthaleneacetic acid (NAA), 2-methyl-4-

chlorophenoxyacetic acid (MCPA) and 2,4-dichlorophenoxyacetic acid (2,4-D), have found application in agriculture [5,6]. Current phytohormone research also greatly benefits from the development of new auxin mimics, which are used as valuable tools to study and control phytohormone action and signaling [7–10].

The determination of plant hormone transport and binding sites is essential to understand the mechanisms behind hormone function. Fluorescently labeled plant hormones are ideal tools enabling precise and specific visualisation of subcellular plant hormone localization and distribution *in planta*, and numerous efforts have been made to their

Abbreviations: CDCl₃, deuterated chloroform; DAG, days after germination; DIPEA, *N,N*-diisopropylethylamine; DMF, dimethylformamide; DMSO, dimethyl sulfoxide; EDTA, ethylenediaminetetraacetic acid; EtOAc, ethyl acetate; GUS, β-glucuronidase; HMPA, hexamethylphosphoramide; IAA, indole-3-acetic acid; IAA5, *indole-3-acetic acid inducible 5*; LBD29, *lateral organ boundaries-domain 29*; LDA, lithium diisopropylamide; LiHMDS, lithium bis(trimethylsilyl)amide; N1, nitrogen of the indole ring; NBD, nitrobenzoxadiazole; NMR, nuclear magnetic resonance; PE, petroleum ether; qPCR, quantitative polymerase chain reaction; QY, quantum yield; R_f, retention factor; RT, room temperature; TFA, trifluoroacetic acid; THF, tetrahydrofuran; TIR1, Transport Inhibitor Resistant 1; TLC, thin layer chromatography

* Corresponding author.

E-mail address: asta.zukauskaite@upol.cz (A. Žukauskaitė).

¹ These authors contributed equally to this work.

<https://doi.org/10.1016/j.nbt.2018.06.003>

Available online 25 June 2018

1871-6784/ © 2018 Elsevier B.V. All rights reserved.

development. Fluorescently labeled versions of nearly all phytohormones are available [11], some of which, e.g. nitrobenzoxadiazole (NBD) labeled auxins NBD-IAA and NBD-NAA [12] or fluorescein (FI) labeled gibberellins GA₃-FI and GA₄-FI [13] are valuable tools to study various aspects of plant growth and development [14–16].

Three reports on the fluorescently labeled auxins have appeared so far. Fluorescein isothiocyanate (FITC) conjugates of IAA and humic substances are reported to potentially interact with auxin receptors [17]. Two fluorescent auxin conjugates IAA-FITC and IAA-RITC have also been prepared by directly coupling IAA with FITC or rhodamine isothiocyanate (RITC) at the N1 position [18]. These two conjugates are reported to retain auxin-like activity and to be transported via the auxin transport machinery, but without unambiguous proof of their stability in plants. More recently, several IAA and NAA based fluorescently labeled auxins have been developed [12]. The two most potent, NBD-IAA and NBD-NAA, are active for auxin transport, but inactive in auxin signalling and metabolism. Thus, despite these valuable examples, the need of developing new fluorescently labeled auxins remains highly relevant.

It has been shown in numerous previous examples that, in order to retain sufficient biological activity, stability and solubility of fluorescently labeled substances, optimal choices of the labeling site [19], proper fluorophore [12,20], type and/or length of spacer [12,13,20] are crucial. Two common features considered to be critical for auxin activity are a planar aromatic ring and a carboxyl group side chain, while ring structure and its attached atoms in known auxin-like compounds vary significantly, suggesting a large degree of structural freedom [21]. Although the NH moiety of the indole ring does not seem to be crucial for auxin activity, as demonstrated by the number of synthetic auxins lacking such functionality [2], in the particular case of IAA, the NH group is involved in hydrogen bonding with the amide group of Leu439 in the Transport Inhibitor Resistant 1 (TIR1) receptor [22], making it unclear how essential this binding is for the auxin potency of IAA. It has been reported that *N*-alkylation of auxin antagonist 4-(2,4-dimethylphenyl)-2-(1*H*-indol-3-yl)-4-oxobutanoic acid (auxinole) dramatically reduced its anti-auxin activity [9], but it cannot be ruled out that the effect was caused by overall steric hindrance of the molecule rather than by N1 functionalization alone. Indeed, previously reported IAA derivatives fluorescently labeled at N1, RITC-IAA and FITC-IAA [18], were found to possess IAA activity. This supports the idea that some N1 modified IAA derivatives could potentially be accommodated in other than the native binding orientation in the TIR1 active site, which is known to be promiscuous [21]. Depending on the overall degree of modification, N1 derivatisation of IAA could give rise not only to inactive compounds but also to new auxins and anti-auxins.

Thus, derivatizing and fluorescent labeling of IAA at N1 were investigated here, together with the elucidation of the biological activity of newly prepared derivatives.

Materials and methods

Reagents and general synthetic methods

Reagents were purchased from Acros, Aldrich, Alfa Aesar, Fluka, Lach-Ner and Penta and were used without further purification. Methyl 2-(1*H*-indol-3-yl)acetate **1**, *N*-Boc protected amine alkyl iodides **2a-d** (Fig. 1) and 4-(2,4-dimethylphenyl)-2-(1*H*-indol-3-yl)-4-oxobutanoic acid (auxinole) were prepared following procedures in [9,23]. All reactions were performed in flame-dried glassware under argon atmosphere using dry solvents unless otherwise noted. Acetonitrile (CH₃CN) and dichloromethane (CH₂Cl₂) were distilled over calcium hydride, while *N,N*-dimethylformamide (DMF) and dimethyl sulfoxide (DMSO) were kept over molecular sieves for at least 48 h prior to use. The conversion of starting materials was monitored by thin layer chromatography (TLC) on aluminum plates coated with silica gel 60 F254 (Merck, USA) and the components were visualized by UV light (254 and

365 nm) and staining solutions (vanillin, ninhydrin and potassium permanganate). The purification of the reaction mixtures was performed by column chromatography on silica gel (40–63 micron Davisil LC60 A, Grace Davison, UK). Eluent composition is given for each substance.

NMR spectroscopy

¹H (500 MHz) and ¹³C (126 MHz) NMR spectra were recorded in CDCl₃ or acetone-d₆ as solvents at room temperature (Jeol ECA-500 NMR, Japan). Peak assignments were elucidated via APT, HMQC and HMBC techniques when necessary.

Determination of purities using LC-PDA-MS

Compounds **3a-d**, **4a-d** and **5a-d** (Fig. 1) were dissolved in 100% methanol to a final concentration of 1×10^{-4} M each. Subsequently, 2 μL of the solution was injected onto a reversed-phase column (ACQUITY UPLC[®] BEH C18 1.7 μm, 2.1 × 150 mm – Waters, Manchester, UK) and analyzed by liquid chromatography – photodiode array – mass spectrometry (LC-PDA-MS) using an ACQUITY UPLC[®] H-Class system combined with UPLC[®] PDA detector and a single quadrupole mass spectrometer QDa[™] (Waters, Manchester, UK). The chromatographic separation, using 0.1% formic acid in methanol (A) and 0.1% formic acid in water (B) as mobile phases, was performed by 15 min linear gradient of 5:95 to 90:10 A:B at a flow rate of 0.25 mL·min⁻¹ and column temperature of 40 °C. Thereafter, the column was washed with 99% methanol (2.0 min), and re-equilibrated to initial conditions (4.0 min). The analytes were detected using PDA detector (range 190–400 nm, resolution 1.2 nm; Waters) in combination with MS detection in both positive and negative FullScan mode (ESI+/-) as [M+H]⁺ and [M-H]⁻. The optimized settings for MS analysis were: Source Temperature, 120 °C; Desolvation Temperature, 600 °C; Capillary voltage, 0.81 kV. Chromatograms were processed by MassLynx[™] V4.1 software (Waters) and purity was evaluated by comparison to a blank represented by pure solvent.

Elucidation of elementary composition using LC-HRMS

Standards of tested fluorescent IAA analogues **5a-d** were dissolved in 100% methanol to a final concentration of 2.5×10^{-6} M each. Subsequently, 2 μL of the solution was injected onto a reversed-phase column (Kinetex[™] C18 100 A, 50 × 2.1 mm, 1.7 μm; Phenomenex, Torrance, USA) and separated by ultra-high performance liquid chromatography ACQUITY UPLC[®] H-Class system by 9 min linear gradient of 10:90 to 95:5 A:B using 0.1% acetic acid in methanol (A) and 0.1% acetic acid in water (B) as mobile phases at a flow rate of 0.5 mL·min⁻¹ and column temperature of 40 °C. Finally, the column was washed with 95% methanol (0.5 min) followed by re-equilibration to initial conditions (1.0 min). Detection was performed by a Synapt[®] G2-Si High Definition MS System (Waters, Manchester, UK) with electrospray ionization in positive FullScan mode (ESI+) (range *m/z* 40–1200) in combination with UPLC[®] PDA detector (range 210–400 nm, resolution 1.2 nm; Waters). The effluent was introduced into the MS system with the optimized settings: Source Offset, 80 V; Source Temperature, 120 °C; Desolvation Temperature, 450 °C; Cone Gas Flow, 50 L·h⁻¹; Nebuliser Gas Flow, 6 bar; Cone Voltage, 25 V; Capillary voltage, 0.5 kV. The analytes were detected as [M+H]⁺. High-resolution mass spectra were used to determine an elemental composition of derivatives **5a-d**. During every analysis the external instrument calibration was performed using a leucine-enkephalin mixture (1 ng·μL⁻¹) for exact mass acquisition. The exact masses of each standard were obtained by MassLynx[™] V4.1 software (Waters) with tolerance better than 1.0 ppm.

General alkylation procedure for the synthesis of 3a-d

Synthesis of methyl 2-(1-(5-((*tert*-butoxycarbonyl)amino)pentyl)-1*H*-indol-3-yl)acetate **3d** is representative. To a suspension of NaH (60% in mineral oil, 34 mg, 0.84 mmol) in dry DMSO (2.5 mL), methyl 2-(1*H*-indol-3-yl)acetate **1** (122 mg, 0.65 mmol), dissolved in dry DMSO (2 mL), was added at room temperature (RT). The resulting reaction mixture was stirred at RT for 1 h. *tert*-Butyl (5-iodopentyl)carbamate **2d** (243 mg, 0.78 mmol), dissolved in dry DMSO (2.5 mL), was added and the reaction mixture stirred at RT for 21 h. The reaction mixture was then cooled to 0 °C, quenched with water (8 mL) and extracted with EtOAc (3 × 10 mL). The combined organic extracts were washed with saturated NaCl solution (2 × 5 mL). Drying with Na₂SO₄, filtration and evaporation of the solvent under reduced pressure and purification of the residue by flash chromatography on silica gel (PE/EtOAc 8.5/1.5) afforded pure compound **3d**.

General fluorescent labeling procedure for the synthesis of 4a-d

Synthesis of methyl 2-(1-(3-((7-nitrobenzo[*c*][1,2,5]oxadiazol-4-yl)amino)propyl)-1*H*-indol-3-yl)acetate **4a** is representative. Methyl 2-(1-(3-((*tert*-butoxycarbonyl)amino)propyl)-1*H*-indol-3-yl)acetate **3a** (48 mg, 0.14 mmol) was dissolved in dry CH₂Cl₂ (2.6 mL) and TFA (0.35 mL) was added dropwise at 0 °C. Resulting reaction mixture was warmed to RT. After 15 min, reaction mixture was cooled to 0 °C, quenched by slow addition of aqueous saturated NaHCO₃ solution until pH = 7 and extracted with EtOAc (3 × 10 mL). The combined organic extracts were washed with saturated NaCl solution (2 × 5 mL). Drying with Na₂SO₄, filtration and evaporation of the solvent under reduced pressure afforded crude methyl 2-(1-(3-aminopropyl)-1*H*-indol-3-yl)acetate, which was dissolved in CH₃CN (5 mL) and cooled to 0 °C. To the resulting solution, Et₃N (0.04 mL, 0.28 mmol) was added dropwise, followed by addition of NBD-Cl in small portions (28 mg, 0.14 mmol). The reaction mixture was stirred at RT for 1 h. The reaction mixture was cooled to 0 °C, quenched with saturated NH₄Cl solution (10 mL) and extracted with EtOAc (3 × 20 mL). The combined organic extracts were washed with saturated NaCl solution (2 × 10 mL). Drying with Na₂SO₄, filtration, evaporation of the solvent under the reduced pressure and purification of the residue by flash chromatography on silica gel (CH₂Cl₂/acetone 50/1) afforded pure methyl 2-(1-(3-((7-nitrobenzo[*c*][1,2,5]oxadiazol-4-yl)amino)propyl)-1*H*-indol-3-yl)acetate **4a**.

General hydrolysis procedure for the synthesis of 5a-d

Synthesis of 2-(1-(3-((7-nitrobenzo[*c*][1,2,5]oxadiazol-4-yl)amino)propyl)-1*H*-indol-3-yl)acetic acid **5a** is representative. Methyl 2-(1-(3-((7-nitrobenzo[*c*][1,2,5]oxadiazol-4-yl)amino)propyl)-1*H*-indol-3-yl)acetate **4a** (20 mg, 0.05 mmol) was dissolved in MeOH (2 mL) and 1 M LiOH solution (0.5 mL) was added at 0 °C. The reaction mixture was brought to 50 °C and stirred for 4 h. The reaction mixture was then cooled to 0 °C and acidified with 1 M HCl solution to pH = 6. The resulting reaction mixture was extracted with EtOAc (3 × 10 mL). The combined organic extracts were washed with saturated NaCl solution (2 × 5 mL). Drying with Na₂SO₄, filtration and evaporation of the solvent under reduced pressure and the purification of the residue by flash chromatography on silica gel (CH₂Cl₂/acetone 50/3), followed by recrystallization (Et₂O/acetone) afforded pure compound **5a**.

Absorption spectra

Absorption spectra of 2 μM solutions of compounds **5a-d** in methanol or distilled water were recorded on a spectrometer (Specord 250Plus, Analytik Jena, Germany) in a quartz cuvette with 1 cm optical path, using a pure solvent as a reference. The spectra were measured in the 250–550 nm interval with steps of 1 nm, 1-nm bandpass and integration time 0.5 s per data point. The extinction coefficient $\varepsilon(\lambda)$ was

calculated from the formula:

$$\varepsilon(\lambda) = \frac{A(\lambda)}{cl} \quad (1)$$

where $A(\lambda)$ is the estimated absorbance, c is the sample concentration and l is the optical path.

Steady-state fluorescence spectra

Steady-state excitation and emission spectra of 2 μM solutions of compounds **5a-d** in methanol or distilled water were recorded on a fluorometer (Fluorolog-3 Jobin-Yvon, France) in a quartz cuvette with 1 cm optical path (both in excitation and emission). The absorbance of the sample at the excitation wavelength should be below 0.05 in all cases, and therefore the inner-filter effect could be neglected. Bandpasses in both the excitation and emission monochromator were set to 3 nm, the spectra were scanned with 1 nm steps and integration time 0.5 s per data point at 22 °C. Emission spectra were recorded with excitation at 480 nm.

Quantum yield (QY) estimation

Emission spectra were acquired under conditions described above. The fluorescence intensity was integrated in the 485–700 nm interval, and the quantum yield (QY) was calculated from the formula:

$$QY = \frac{\varepsilon_S F n^2}{\varepsilon F_S n_S^2} QY_S \quad (2)$$

where ε , F and n refer to the extinction coefficient at 480 nm, integrated fluorescence intensity and refractive index, respectively, the subscript „S“ refers to the standard (1 nM fluorescein in 0.1 M NaOH, $QY_S = 0.95$) [24].

Time-resolved fluorescence measurements

Fluorescence decays of 2 μM solutions of species **5a-d** were measured on a TCSPC fluorometer (PicoHarp300, Picoquant, Germany), using pulsed laser LED centered at 480.5 nm as the source of excitation light and operated at 20 MHz. Data were plotted as a histogram on a time-scale 0–50 ns, where the time-width of one channel was 8 ps. The instrument response function (IRF) was obtained using distilled water as a scatterer, estimated FWHM(IRF) was 0.55 ns. Emission was detected under magic-angle conditions at 545 nm, the emission bandpass was 16 nm. Data were acquired at 22 °C until 20,000 counts in the peak-channel were achieved. Fluorescence decays were fitted using the FluoFit 4.2.1 software (PicoQuant) as a sum of exponentials:

$$I(t) = IRF \otimes \sum_{i=1}^n A_i e^{-\frac{t}{\tau_i}} \quad (3)$$

The quality of fit was evaluated by the χ^2_R and distribution of residuals. The intensity-weighted mean fluorescence lifetime was calculated as previously described [25] using formula:

$$\tau_M = \frac{\sum A_i \tau_i^2}{\sum A_i \tau_i} \quad (4)$$

Plant material and experimental growth conditions

Seeds of *Arabidopsis thaliana* ecotype Col-0 were surface-sterilized using a 0.01% solution of Tween 21 and 70% ethanol. After 2 days of stratification (4 °C in dark), seeds germinated on sterile ½ MS medium (2.2 g/L Murashige and Skoog medium, 1% sucrose and 0.7% agar – all from Duchefa Biochemie, Netherland, pH 5.6) supplemented with 0.1% DMSO as a mock, 1 μM IAA as a positive control, and tested fluorescent auxin analogues **5a-d** in defined concentrations (1, 5, 10, 20, μM) with

or without presence of 1 μM IAA for 5 days in long-day light conditions (22 °C/20 °C, 16 h light / 8 h dark, 100 $\mu\text{mol m}^{-2}\text{s}^{-1}$).

Histochemical localization of auxin activity

Five-day old (5 DAG) seedlings of the *Arabidopsis thaliana* transgenic DR5::GUS reporter line on a (Col-0) background [26] were incubated at RT in 24-well plates containing 1 mL of 1/2 MS liquid media supplemented by fluorescently labeled auxin derivatives **5a-d** in defined final concentrations (5, 10, 15, 20, 25, 50 μM). The compounds were applied for either 5 h on their own or for 2 h followed by wash-out and treatment with 2 μM IAA for a further 3 h. Seedlings were then incubated in the presence of 500 μL of GUS staining solution – 2 mM X-GlcA (Duchefa Biochemie) in GUS buffer (0.1% triton X100; 10 mM EDTA; 0.5 mM potassium ferrocyanide; 0.5 mM potassium ferricyanide in 0.1 M phosphate buffer) – at 37 °C in the dark for 20 min. To stop the staining reaction, seedlings were transferred to 500 μL of 70% ethanol. Finally, GUS expression was evaluated using an inverted light microscope (Olympus IX51) with transmission light mode and phase contrast.

Real-time qPCR

Col-0 seedlings (5 DAG) grown on sterile 1/2 MS solid medium under long-day conditions were treated in sterile 1/2 MS liquid medium with various combinations of compounds at defined concentrations (Fig. 5) under light at 22 °C. All the compounds were dissolved and diluted in DMSO at 1000 \times final concentrations to keep the amount of DMSO used constant at 0.1% (v/v). For each treatment, 20 fresh seedlings were transferred into one well of a 12-well plate containing 2 mL liquid medium and pre-treated with the first compound (Fig. 5) for 1 h. At the end of the pre-treatment, the second compound (Fig. 5) was added immediately and the seedlings were continuously treated for another 2 h before harvesting by flash-freezing in liquid nitrogen. All the treatments were completely randomized on the plate and a total of four independent biological replicates were prepared.

Total RNA was extracted using the RNeasy Plant Mini Kit (QIAGEN), with genomic DNA removed by on-column digestion using RQ1 RNase-Free DNase (Promega). 2 μg total RNAs was reverse transcribed to cDNA using Oligo(dT)₂₀ primer (Invitrogen) and SuperScript[®] IV Reverse Transcriptase (Invitrogen). Real-time qPCR analysis was performed using a LightCycler[®] 480 SYBR Green I Master (Roche) on a LightCycler[®] 480 Instrument II real-time PCR machine (Roche). Transcript levels of two early auxin-responsive genes, lateral organ boundaries-domain 29 - *LBD29* (At3g58190) and indole-3-acetic acid inducible 5 - *IAA5* (At1g15580), were quantified, and glyceraldehyde-3-phosphate dehydrogenase C2 - *GAPDH* (At1g13440) - was used as an internal control. The primer pairs used for qPCR were: *LBD29* forward 5'-GGGATGCCACAGAGAGTAGTTACCA-3' and reverse 5'-TTCAGGTGTGTTCCAAGTCAGAGT-3'; *IAA5* forward 5'-CGGCGAAAAAGAGTCAA GTTGTG-3' and reverse 5'-TTGGTCCGTTTCGAGACTGTTC-3'; *GAPDH* forward 5'-TTGGTGACAACAGGTCAAGCA-3' and reverse 5'-AAACTTG

TCGCTCAATGCAATC-3'. The relative quantification expressed as the fold change relative to the mock control was carried out by LightCycler[®] 480 software provided by the manufacturer. Values presented are means \pm S.E. of 4 biological replicates. Statistical significance between treatments was determined by one-way ANOVA followed by Duncan Post Hoc Tests using SPSS software. Statistical details are reported in Fig. 5 legend.

Confocal microscopy

Seedlings (5 DAG) of *Arabidopsis thaliana* (Col-0) were incubated in 24-well plates containing 1 mL of 1/2 MS liquid medium supplemented with 1% sucrose and were subsequently treated with compound **5d** in defined final concentrations (1 μM , 2 μM , 5 μM , 10 μM) for 10 min. Whole mount plants were subsequently visualized by an IX81 microscope attached to a confocal laser scanning unit FV1000 (Olympus, Japan). Fluorescence was excited by a 488 nm line of argon laser and emission was recorded at 505–605 nm. Experimental set up involved 10 \times and 20 \times objective, resolution 1024 \times 1024 px, integration time 10 or 12.5 μs per pixel, pinhole size 180 μm . A negative control (DMSO) was used to set up the optimal intensity of the laser at the start of experiments.

Results and discussion

Synthesis of the library

It was envisaged that regioselective N1 alkylation of IAA could be achieved by stepwise deprotonation of the indole nitrogen with strong base and subsequent treatment with appropriately protected amino halides. As a model reaction, coupling of commercially available or easily accessible IAA methyl ester **1** [9] with *N*-Boc-protected iodo-propylamine **2a** [23], mediated by various bases was investigated (Supplementary Table S1). This approach, however, was not as straightforward as anticipated. In the first attempt, *N,N*-diisopropylethylamine (DIPEA) was used as a base, however, upon addition of **2a**, no reaction was achieved even after heating the reaction mixture in acetonitrile for 3 h, resulting in full recovery of the starting material (Supplementary Table S1, Entry 1). Then, *N*-alkylation of IAA methyl ester **1** was attempted by pre-forming its lithium salt. In the first attempt, **1** was deprotonated by treatment with lithium bis(trimethylsilyl) amide (LiHMDS) in THF however, subsequent treatment of the active intermediate with **2a** gave no reaction (Supplementary Table S1, Entry 2). In contrast, using lithium diisopropylamide (LDA) as a base with hexamethylphosphoramide (HMPA) as an additive, resulted, after treatment with **2a** at $-78\text{ }^\circ\text{C}$, in formation of the desired product **3a**, however in a low 10% yield (Supplementary Table S1, Entry 3). Without much success in using the lithium salt of **1** as an active intermediate for the alkylation reaction, attention was focused on activating it into a sodium salt. Surprisingly, using one or 1.5 equivalents of sodium hydride as a base in DMF at RT resulted in no reaction

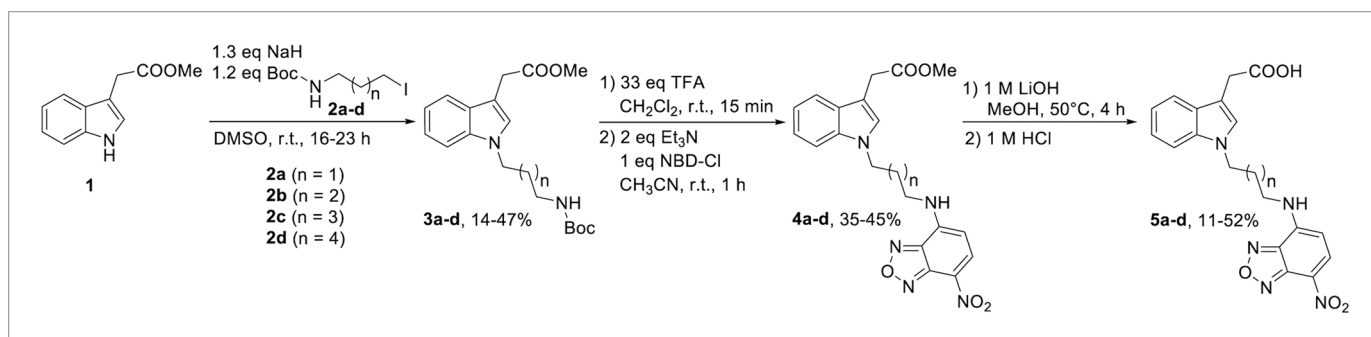


Fig. 1. Synthesis of fluorescently labeled IAA derivatives **5a-d**.

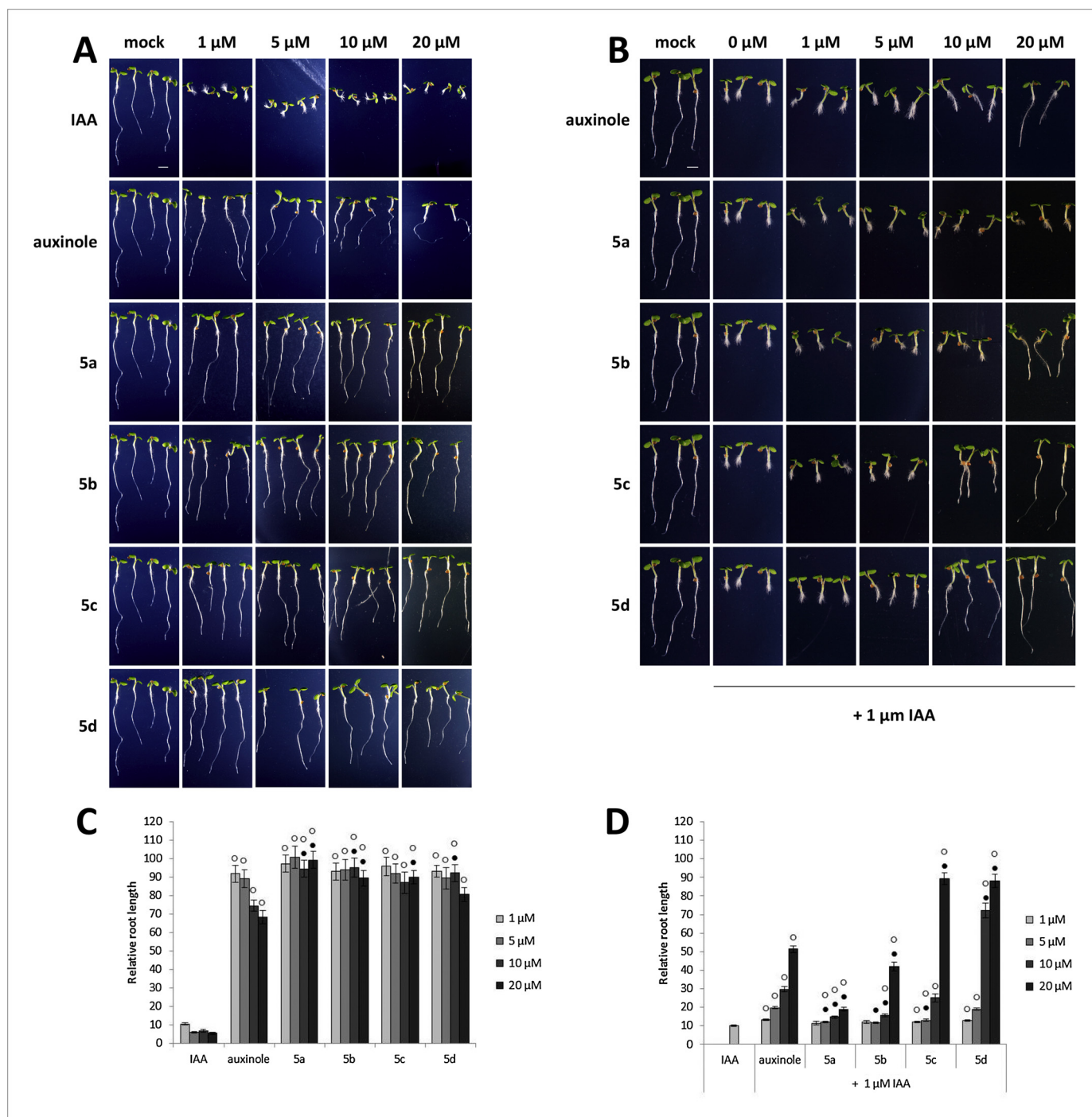


Fig. 2. The effect of derivatives **5a–d** on *Arabidopsis thaliana* (Col-0) primary root growth. Phenotype of primary root was determined on seedlings (5 DAG) grown on 1, 5, 10, 20 μM **5a–d** (A) in the absence or (B) presence of 1 μM IAA. Scale bar represents 1 mm. The length of primary root normalized to DMSO treatment was quantified for both treatments (C and D). Auxinole (1, 5, 10, 20 μM) and IAA (1 μM) were used as controls. Statistical analyses were performed using the t-test, values are means ± S.E., n = ~ 45 from 3 independent replicates. White circles (○) indicate statistically significant differences between the effect of **5a–d** compared to 1 μM IAA treatment, while black circles (●) indicate statistically significant differences between the effect of **5a–d** and auxinole treatments at corresponding concentrations. ○ and ● correspond to P < 0.01.

(Supplementary Table S1, Entries 4–5), even though such reaction conditions are typically used to effectively yield *N*-alkylated indolic derivatives [27,28]. Increasing reaction temperature to 50 °C afforded target product **3a** in 19% yield (Supplementary Table S1, Entry 6). Further increase of reaction temperature to 75 °C did not improve the reaction outcome, but on the contrary the reaction yield fell to 5% (Supplementary Table S1, Entry 7). Changing solvent to DMSO and performing the reaction at RT using 1.3 equivalents of NaH produced

3a in 28% yield (Supplementary Table S1, Entry 8). Increasing amount of the linker to 1.2 equivalent allowed to further increase the yield of **3a** to 47% (Supplementary Table S1, Entry 9).

Optimized reaction conditions were applied for the synthesis of all derivatives **3a–d** producing them in yields of 14–47%. Subsequent cleavage of the Boc-protecting group in the presence of TFA [29,30] quantitatively produced intermediate primary amines, which were subjected to fluorescent labeling. As the use of bulky fluorophores may

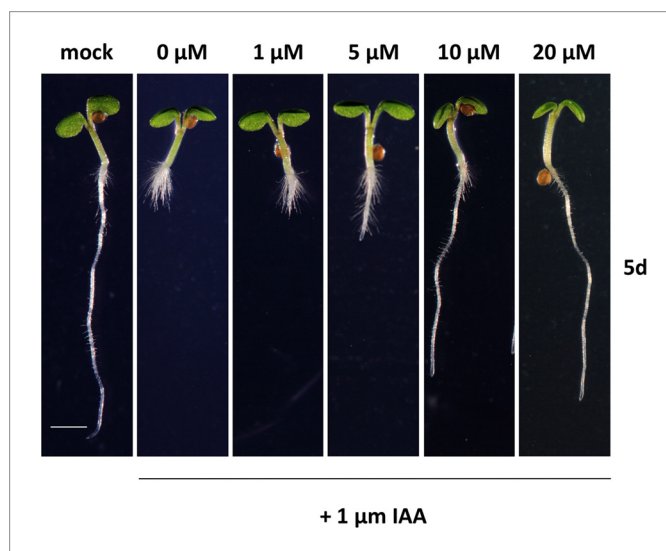


Fig. 3. Inhibitory effect of **5d** on auxin-induced root hair formation in *Arabidopsis thaliana* (Col-0) roots. Root hair formation was evaluated in seedlings (5 DAG) grown on 1, 5, 10, 20 μM **5d** in the presence of 1 μM IAA. Scale bar represents 1 mm.

result in partial or complete loss of biological activity of the auxins, a small heterocyclic fluorophore, 7-nitro-2,1,3-benzoxadiazole chloride (NBD-Cl) was chosen, being readily reactive towards primary and secondary amines and due to its low molecular weight is suitable for labeling of small molecules without affecting their biological activity [31]. Among the reaction conditions typically used to NBD-label primary amines [32], the best results were obtained by treating the freshly prepared intermediate amine with 2 equivalents of triethylamine as a base and one equivalent of NBD chloride in acetonitrile at RT for 1 h, producing fluorescently labeled IAA methyl esters **4a–d** in 35–45% yield. Finally, the hydrolysis of fluorescently labeled IAA methyl esters **4a–d** was performed by simple alkaline hydrolysis [12,33]. Notably, to achieve complete conversion, reaction mixtures needed to be heated at 50 °C for 4 h. Subsequent acidification with 1 M HCl solution, led to the formation of final products **5a–d** in 11–52% yield (Fig. 1).

Absorption and fluorescence measurements

Absorption and emission spectra upon excitation at 480 nm of compounds **5a–d** in water, essentially to mimic the solutions used for the biological testing, and in methanol (Supplementary Fig. S1), were recorded. As expected, fluorescence parameters were sensitive to solvent effects [34,35]. In methanol, being less polar than water [36], all four compounds **5a–d** had absorption maxima between 465–467 nm, and emission maxima at 525–532 nm, resulting in 60–66 nm Stokes shifts, typical for NBD-labeled molecules [37]. Both the absorption and emission spectra in water were bathochromically shifted compared to methanol, with maxima at 486–489 nm and 540–547 nm range, respectively, also resulting in slightly lower 52–59 nm Stokes shifts. Quantum yield of all compounds was significantly lower in water, while in methanol being higher by factor 3.5–7.5. Moreover, fluorescence quantum yield of the compounds increased with the length of the linker between IAA and the NBD-label, i.e. compound **5d**, bearing the longest 6-C linker, exhibited the highest fluorescence quantum yield (insets in Supplementary Fig. S1).

Fluorescence decay of all the compounds was complex with significant contribution of very fast components, making the analyses difficult. In all cases, four exponentials were necessary to describe the decay curve adequately (Supplementary Fig. S2, Supplementary Table

S2). Moreover, the decay of **5a** in methanol was so complex that it could not be fitted even with four components, which is the limit of the software used. Nevertheless, the mean fluorescence lifetime is a very robust characteristic and thus could be estimated for **5a** in methanol with good accuracy from the TCSPC histogram, as previously described [25]. Notably, for all compounds **5a–d**, the decay was significantly faster in water than in methanol (Supplementary Fig. S3, Supplementary Table S3); however, in contrast to the steady-state fluorescence, there was no clear correlation with the length of the linker.

Determination of biological activity

In order to verify the biological activity of the fluorescently labeled auxin derivatives **5a–d**, their effect on primary root growth of *Arabidopsis thaliana* (Col-0) was tested. Typically, auxins inhibit primary root growth regulate responses to gravity and promote root hair formation [1,38]. However, as expected, introduction of alkyl chains at the N1-position of IAA highly altered the biological activity of the resulting compounds. Despite being IAA derivatives, **5a–d** did not inhibit primary root growth (Fig. 2A and C). Moreover, unlike auxins and similarly to auxinole, **5a–d** diminished root hair formation, implying their possible activity as anti-auxins. To further examine this observation, the ability of **5a–d** to block auxin-induced (1 μM IAA) primary root growth inhibition was evaluated. All compounds, to a lesser or greater extent, were able to revert such auxin-induced effects in a dose-dependent manner (Fig. 2B and D). The efficacy of the compounds was highly related to the length of the linker between IAA and NBD. While **5a**, the compound with the shortest linker, had barely any noticeable effect, **5c** and **5d**, with the longest linkers, at 20 μM concentration were able to almost completely counteract IAA-induced primary root growth inhibition. Interestingly, in the experimental design of long day light conditions 16 h/8 h, the effects of **5c** and **5d** at high concentrations were even more pronounced than that of auxinole (Fig. 2B and D). Moreover, the most active derivative **5d** effectively inhibited auxin-induced (1 μM IAA) root hair formation from 10 μM concentration (Fig. 3), while the effect of derivatives **5a–c** was milder, gradually depending on the length of the linker (data not shown).

To further examine the auxin and anti-auxin activities of **5a–d** acting through the SCF^{TIR1} auxin signalling pathway, their ability to induce

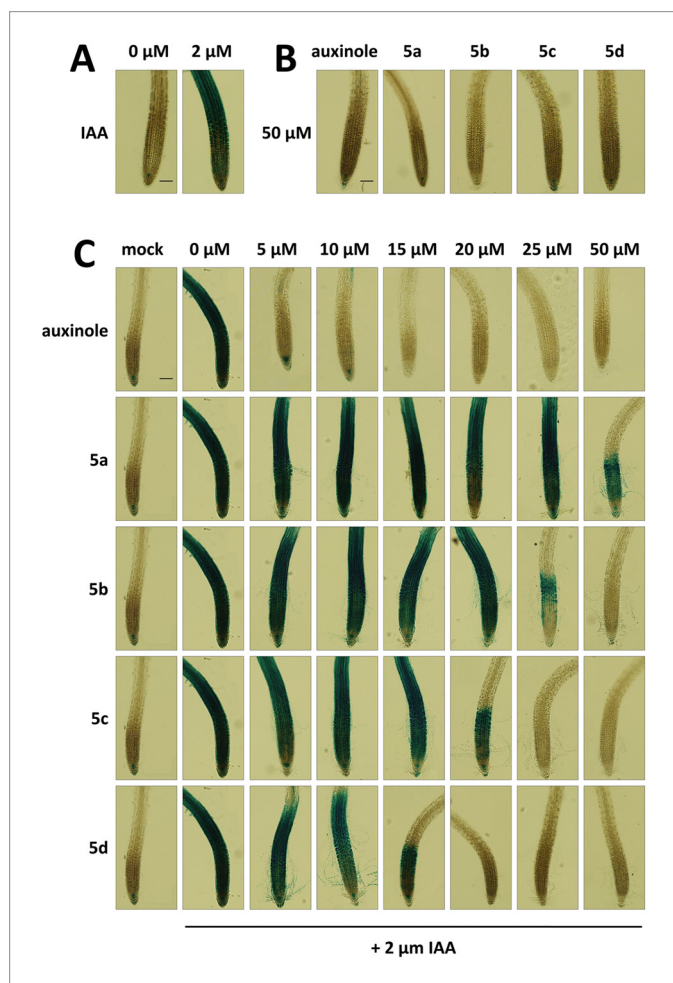


Fig. 4. Effect of compounds **5a–d** on GUS expression in the *DR5::GUS* transgenic plants of *Arabidopsis thaliana*. Seedlings (5 DAG) were treated (A) with IAA at 2 μM and (B) with auxinole and compounds **5a–d** at given concentrations (5, 10, 15, 20, 25 and 50 μM) for 5 h. **5a–d** derivatives showed no GUS expression pattern even at 50 μM concentration compared to control (2 μM IAA). (C) Seedlings (5 DAG) were treated with **5a–d** at given concentrations (5, 10, 15, 20, 25 and 50 μM) for 2 h followed by wash-out and treatment with 2 μM IAA for 3 h. Figures were chosen as representatives from two independent repetitions. Scale bars represent 200 μm.

GUS expression under the control of the *DR5* auxin-sensitive promoter in primary roots of the *DR5::GUS* marker line of *Arabidopsis thaliana* were evaluated. As anticipated, the previously observed anti-auxin effect of **5a–d** in root growth assays was consistent with their inhibitory activity of *DR5::GUS* expression. Compounds **5a–d**, similarly to auxinole, did not induce GUS expression even at the highest concentrations (50 μM), confirming the absence of auxin activity. In contrast, **5a–d** blocked auxin-induced GUS expression in a dose-dependent manner. Analogously to the previous experiment, the strength of the auxin antagonist effect of **5a–d** was also linker-dependent. At 20 μM concentration the most potent compound **5d** completely inhibited *DR5::GUS* expression induced by 2 μM IAA. Likewise, other tested compounds **5a–c** also inhibited *DR5::GUS* expression, but to a lesser extent (Fig. 4A–C).

Subsequently, qPCR analysis was performed of two early auxin-responsive genes, *IAA5* and *LBD29*, upon treatment with the most active

compound **5d** alone or in combination with IAA. Despite showing distinct anti-auxin effects in the previous bioassays, when applied alone at high concentration, compound **5d** exhibited weak auxin-like activity by moderately inducing the expression of both *IAA5* and *LBD29* (Fig. 5). However, in the co-treatment with IAA, **5d** significantly suppressed the IAA-induced *LBD29* expression in a dose-dependent manner (Fig. 5A), confirming its anti-auxin activity. In contrast, this anti-auxin effect was not observed on IAA-induced *IAA5* expression, where no statistical difference was observed between IAA treatment and **5d**-IAA co-treatments (Fig. 5B). These results, even though not anticipated, are not surprising. Different profiles of *IAA5* and *LBD29* gene expression in co-treatment studies might imply the possibly diverse levels of perception of **5d** by different auxin receptor–co-receptor systems [39]. Moreover, the observation that **5d** at high concentration slightly induced auxin-responsive gene expression in *LBD29* and *IAA5*, might suggest that **5d**, while otherwise showing anti-auxin effects, can at some extent trigger slight auxin-like response. A similar effect of ABA agonists and antagonists on ABA-responsive genes has been observed before [40]. Hence, it is possible that the auxin-binding pockets of different auxin receptors could accommodate **5d** to different extents, while it may be the co-receptors that mainly define if the compound is perceived as an anti-auxin. To further dissect recognition of **5d** by different auxin co-receptor systems, additional experiments, such as molecular docking and pull-down assays, would be needed.

Finally, the uptake and distribution of **5d**, the most active fluorescently labeled IAA derivative with the highest fluorescence intensity, in the root of *Arabidopsis* was observed by confocal microscopy. At the concentrations tested, **5d** was taken up by roots within 10 min (Fig. 6). It was distributed along the root, from the root cap to the differentiation zone, mainly in the outer tissues of the root (Fig. 6). Notably, upon increasing concentration and treatment time, the distribution pattern of **5d** was completely lost due to oversaturation of the root with the fluorescent signal (Supplementary Fig. S3).

Conclusions

Four novel fluorescently labeled IAA derivatives were designed and synthesized. These compounds, unlike fluorescently labeled auxins published hitherto, do not possess auxin activity, but in contrast they show dose-dependent inhibition of auxin-induced effects, such as primary root growth inhibition, root hair formation and *DR5::GUS* expression. Importantly, the biological experiments complemented by fluorescence measurements demonstrate the importance of the character of the linker used and the optimal choice of the labeling site as key variables influencing the biological activity and fluorescent properties of these compounds. Among the compounds prepared, derivative **5d**, bearing the longest linker, had the most pronounced anti-auxin effect and fluorescent properties and thus is the most suitable novel fluorescently labeled auxin for further studies, already ongoing. Distinct expression of two early auxin-responsive genes (*IAA5* and *LBD29*) points to the possibility that **5d** might be recognised differentially by various auxin receptors. Considering the different extent of the physicochemical and biological properties of these novel probes, directly related to the length of the linker between IAA and the fluorophore, they could be used to study their interaction with known auxin receptors. This structure-activity relationship may result in the generation or revealing of fluorescently-labeled, full or partial agonists and antagonists of various auxin receptor systems. Such compounds could serve as powerful tools to study the selectivity of auxin recognition within different developmental processes, which could find application in agriculture, horticulture, biotechnology, etc., for example in development of new specific auxin-based herbicides.

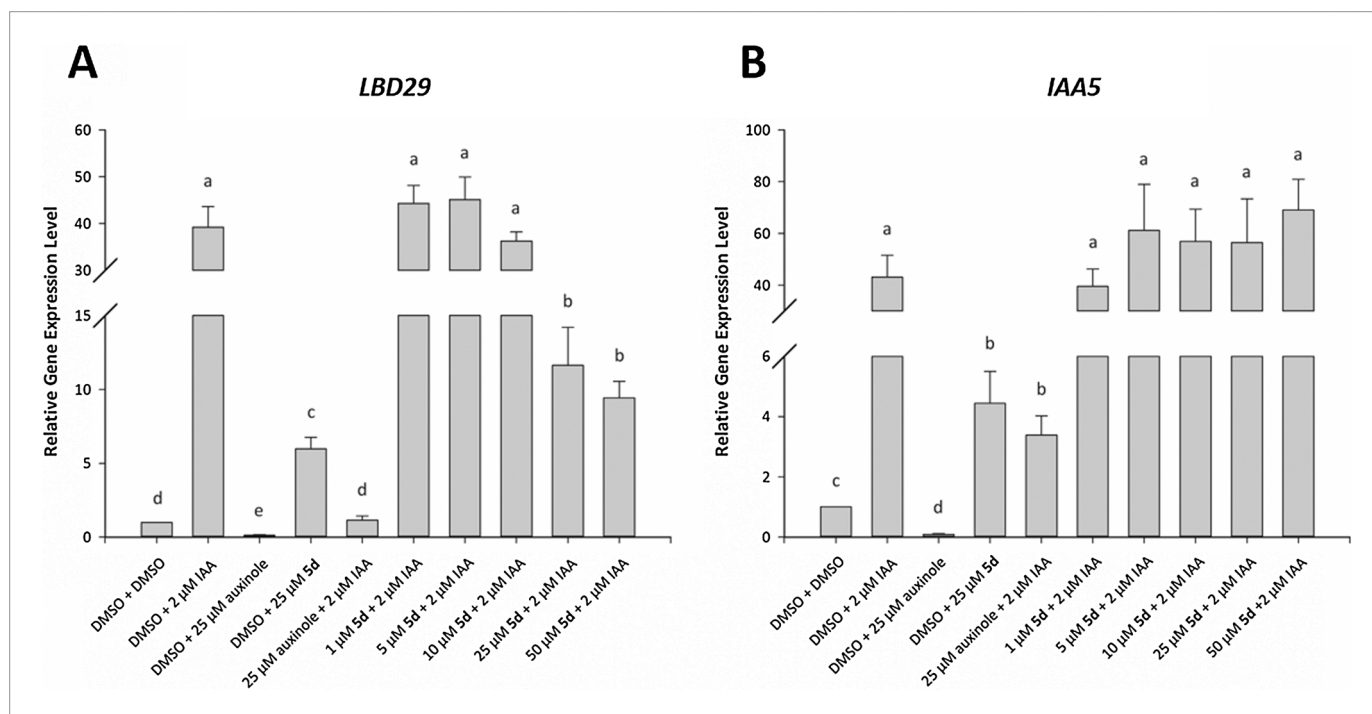


Fig. 5. Transcriptional response of early auxin-responsive genes to treatment with compound **5d**. Col-0 seedlings (5 DAG) grown on solid medium were treated in liquid medium supplemented with the indicated compounds at the specified concentrations under light at 22 °C. All compounds were dissolved and diluted in DMSO at 1000×, keeping the final DMSO concentration at 0.1% (v/v). 20 whole seedlings were mixed and pre-treated with the first compound for 1 h. The second compound was immediately added and the treatment continued for another 2 h before directly harvesting into liquid nitrogen. Transcript levels of two early auxin-responsive genes, *LBD29* (At3g58190) (A) and *IAA5* (At1g15580) (B), were quantified by real-time PCR, normalized to that of *GAPDH* (At1g13440), and presented as fold changes relative to mock (DMSO + DMSO) control. Values are means \pm S.E., $n = 4$ independent replicates. Note that breaks were made in the y-axes to show the values in an appropriate scale. Statistical analysis was performed using one-way ANOVA, followed by Duncan Post Hoc Tests. Different letters indicate statistically significant differences at $P < 0.05$.

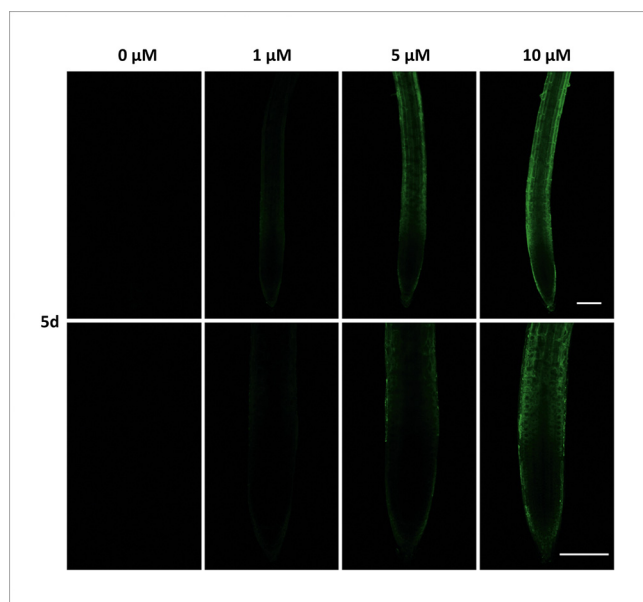


Fig. 6. Uptake of fluorescently labeled IAA derivative **5d** in *Arabidopsis thaliana* roots. Seedlings (5 DAG) were treated with **5d** at given concentrations (1, 5 and 10 μ M) for 10 min. Upper panel: 10× zoom. Lower panel: 20× zoom. Figures were chosen as representatives from 2 independent repetitions. Scale bars represent 100 μ m.

Acknowledgements

We are thankful to Ota Blahoušek for technical assistance with the preparation of the figures. This work was supported by the Ministry of Education, Youth and Sports of the Czech Republic – NPU I program with project LO1204 and by the Internal Grant Agency of Palacký University (IGA_PrF_2018_023 to K.B. and B.P.). This work was also supported by VetenskapsrådetVR2016-00768 (Q.M.), VINNOVA (S.R.), the Knut and Alice Wallenberg Foundation Shapessystem 2012-0050 (S.R., Q.M.), Kempestiftelserna (Q.M.), Carl Tryggers Foundation (Q.M.). B.P. was partially supported by the Endowment Fund of Palacký University in Olomouc.

Appendix A. Supplementary data

Supplementary material related to this article can be found, in the online version, at doi:<https://doi.org/10.1016/j.nbt.2018.06.003>.

References

- [1] Woodward AW, Bartel B. Auxin: regulation, action, and interaction. *Ann Bot* 2005;95:707–35. <http://dx.doi.org/10.1093/aob/mci083>.
- [2] Sauer M, Robert S, Kleine-Vehn JJ. Auxin: simply complicated. *J Exp Bot* 2013;64:2565–77. <http://dx.doi.org/10.1093/jxb/ert139>.
- [3] Simon S, Kubes M, Baster P, Robert S, Dobrev PI, Friml J, et al. Defining the selectivity of processes along the auxin response chain: a study using auxin analogues. *New Phytol* 2013;200:1034–48. <http://dx.doi.org/10.1111/nph.12437>.
- [4] Do-Thanh CL, Vargas JJ, Thomas JW, Armel GR, Best MD, Chi-Linh D-T, et al. Design, synthesis, and evaluation of novel auxin mimic herbicides. *J Agric Food Chem* 2016;64:3533–7. <http://dx.doi.org/10.1021/acs.jafc.6b00675>.
- [5] Song Y. Insight into the mode of action of 2,4-dichlorophenoxyacetic acid (2,4-D) as an herbicide. *J Integr Plant Biol* 2014;56:106–13. <http://dx.doi.org/10.1111/jipb.12131>.
- [6] Grossmann K. Auxin herbicides: current status of mechanism and mode of action.

- Pest Manag Sci 2010;66:113–20. <http://dx.doi.org/10.1002/ps.1860>.
- [7] Fonseca S, Rosado A, Vaughan-Hirsch J, Bishopp A, Chini A. Molecular locks and keys: the role of small molecules in phytohormone research. *Front Plant Sci* 2014;5:709. <http://dx.doi.org/10.3389/fpls.2014.00709>.
- [8] Rigal A, Ma Q, Robert S. Unraveling plant hormone signaling through the use of small molecules. *Front Plant Sci* 2014;5:373. <http://dx.doi.org/10.3389/fpls.2014.00373>.
- [9] Hayashi K, Neve J, Hirose M, Kuboki A, Shimada Y, Kepinski S, et al. Rational design of an auxin antagonist of the SCFTIR1 auxin receptor complex. *ACS Chem Biol* 2012;7:590–8. <http://dx.doi.org/10.1021/cb200404c>.
- [10] Hayashi K, Tan X, Zheng N, Hatate T, Kimura Y, Kepinski S, et al. Small-molecule agonists and antagonists of F-box protein-substrate interactions in auxin perception and signaling. *Proc Natl Acad Sci U S A* 2008;105:5632–7. <http://dx.doi.org/10.1073/pnas.0711146105>.
- [11] Lace B, Prandi C. Shaping small bioactive molecules to untangle their biological function: a focus on fluorescent plant hormones. *Mol Plant* 2016;9:1099–118. <http://dx.doi.org/10.1016/j.molp.2016.06.011>.
- [12] Hayashi K-I, Nakamura S, Fukunaga S, Nishimura T, Jenness MK, Murphy AS, et al. Auxin transport sites are visualized in planta using fluorescent auxin analogs. *Proc Natl Acad Sci U S A* 2014;111:11557–62. <http://dx.doi.org/10.1073/pnas.1408960111>.
- [13] Shani E, Weinstain R, Zhang Y, Castillejo C, Kaiserli E, Chory J, et al. Gibberellins accumulate in the elongating endodermal cells of Arabidopsis root. *Proc Natl Acad Sci U S A* 2013;110:4834–9. <http://dx.doi.org/10.1073/pnas.1300436110>.
- [14] Tal I, Zhang Y, Jorgensen ME, Pisanty O, Barbosa ICR, Zourelidou M, et al. The Arabidopsis NPF3 protein is a GA transporter. *Nat Commun* 2016;7. <http://dx.doi.org/10.1038/ncomms11486>.
- [15] Buskila Y, Sela N, Teper-Bamnolker P, Tal I, Shani E, Weinstain R, et al. Stronger sink demand for metabolites supports dominance of the apical bud in etiolated growth. *J Exp Bot* 2016;67:5495–508. <http://dx.doi.org/10.1093/jxb/erw315>.
- [16] Haga K, Hayashi K, Sakai T. PINOID AGC kinases are necessary for phytochrome-mediated enhancement of hypocotyl phototropism in Arabidopsis. *Plant Physiol* 2014;166. <http://dx.doi.org/10.1104/pp.114.244434>. 1535–+.
- [17] Muscolo A, Sidari M, Francioso O, Tugnoli V, Nardi S. The auxin-like activity of humic substances is related to membrane interactions in carrot cell cultures. *J Chem Ecol* 2007;33:115–29. <http://dx.doi.org/10.1007/s10886-006-9206-9>.
- [18] Sokolowska K, Kizinska J, Szewczuk Z, Banasiak A. Auxin conjugated to fluorescent dyes - a tool for the analysis of auxin transport pathways. *Plant Biol* 2014;16:866–77. <http://dx.doi.org/10.1111/plb.12144>.
- [19] Malachowska-Ugarte M, Sperduto C, Ermolovich YV, Sauchuk AL, Jurasek M, Litvinovskaya RP, et al. Brassinosteroid-BODIPY conjugates: design, synthesis, and properties. *Steroids* 2015;102:53–9. <http://dx.doi.org/10.1016/j.steroids.2015.07.002>.
- [20] Prandi C, Ghigo G, Occhiato EG, Scarpi D, Begliomini S, Lace B, et al. Tailoring fluorescent strigolactones for in vivo investigations: a computational and experimental study. *Org Biomol Chem* 2014;12:2960–8. <http://dx.doi.org/10.1039/c3ob42592d>.
- [21] Calderon-Villalobos LI, Tan X, Zheng N, Estelle M. Auxin perception-structural insights. *Cold Spring Harb Perspect Biol* 2010;2. <http://dx.doi.org/10.1101/cshperspect.a005546>.
- [22] Tan X, Calderon-Villalobos LIA, Sharon M, Zheng CX, Robinson CV, Estelle M, et al. Mechanism of auxin perception by the TIR1 ubiquitin ligase. *Nature* 2007;446:640–5. <http://dx.doi.org/10.1038/nature05731>.
- [23] Ensch C, Hesse M. Total syntheses of the spermine alkaloids (-)-(R,R)-hoppromine and (+/-)-homaline. *Helv Chim Acta* 2002;85:1659–73. [http://dx.doi.org/10.1002/1522-2675\(200206\)85:6<1659::aid-hlca1659>3.0.co;2-d](http://dx.doi.org/10.1002/1522-2675(200206)85:6<1659::aid-hlca1659>3.0.co;2-d).
- [24] Brannon JH, Magde D. Absolute quantum yield determination by thermal blooming fluorescence. *J Phys Chem* 1978;82:705–9. <http://dx.doi.org/10.1021/j100495a018>.
- [25] Fiserova E, Kubala M. Mean fluorescence lifetime and its error. *J Lumin* 2012;132:2059–64. <http://dx.doi.org/10.1016/j.jlumin.2012.03.038>.
- [26] Ulmasov T, Murfett J, Hagen G, Guilfoyle TJ. Aux/IAA proteins repress expression of reporter genes containing natural and highly active synthetic auxin response elements. *Plant Cell* 1997;9:1963–71.
- [27] Ye Q, Mao WL, Zhou YB, Xu L, Li Q, Gao YX, et al. Synthesis and biological evaluation of 3-([1,2,4]triazolo[4,3-a]pyridin-3-yl)-4-(indol-3-yl)-maleimides as potent, selective GSK-3 beta inhibitors and neuroprotective agents. *Bioorg Med Chem* 2015;23:1179–88. <http://dx.doi.org/10.1016/j.bmc.2014.12.026>.
- [28] Grumel V, Mérou J-Y, Lesur B, Giboulot T, Frydman A, Guillaumet G. Design and synthesis of a series of indole glycoprotein IIb/IIIa inhibitors. *Eur J Med Chem* 2002;37:45–62. [http://dx.doi.org/10.1016/S0223-5234\(01\)01325-3](http://dx.doi.org/10.1016/S0223-5234(01)01325-3).
- [29] Semina E, Žukauskaitė A, Šačkus A, De Kimpe N, Mangelinckx S. Selective elaboration of aminodiols towards small ring α - and β -amino acid derivatives that incorporate an aziridine, azetidone, or epoxide scaffold. *Eur J Org Chem* 2016;2016:1720–31. <http://dx.doi.org/10.1002/ejoc.201600036>.
- [30] Žukauskaitė A, Mangelinckx S, Callebaut G, Wybon C, Šačkus A, De Kimpe N. Synthesis of 1,5-diazaspiro[2.3]hexanes, a novel diazaspirocyclic system. *Tetrahedron* 2013;69:3437–43. <http://dx.doi.org/10.1016/J.TET.2013.02.065>.
- [31] Lavis LD, Raines RT. Bright ideas for chemical biology. *ACS Chem Biol* 2008;3:142–55. <http://dx.doi.org/10.1021/cb700248m>.
- [32] Sahoo H. Fluorescent labeling techniques in biomolecules: a flashback. *Rsc Adv* 2012;2:7017–29. <http://dx.doi.org/10.1039/c2ra20389h>.
- [33] Žukauskaitė A, Moretto A, Peggion C, De Zotti M, Šačkus A, Formaggio F, et al. Synthesis and conformational study of model peptides containing N-substituted 3-aminoazetidone-3-carboxylic acids. *Eur J Org Chem* 2014;2014:2312–21. <http://dx.doi.org/10.1002/ejoc.201301741>.
- [34] Lakowicz JR. Principles of fluorescence spectroscopy. New York: Springer; 2006.
- [35] Feryforques S, Fayet JP, Lopez A. Drastic changes in the fluorescence properties of NBD probes with the polarity of the medium - involvement of a TICT state. *J Photochem Photobiol A Chem* 1993;70:229–43. [http://dx.doi.org/10.1016/1010-6030\(93\)85048-d](http://dx.doi.org/10.1016/1010-6030(93)85048-d).
- [36] Reichardt C, Welton T. Solvents and solvent effects in organic chemistry. Wiley-VCH Verlag GmbH & Co. KGaA; 2010.
- [37] Lancet D, Pecht I. Spectroscopic and immunochemical studies with nitrobenzoxadiazolealanine, a fluorescent dinitrophenyl analog. *Biochemistry* 1977;16:5150–7. <http://dx.doi.org/10.1021/bi00642a031>.
- [38] Muday GK. Auxins and tropisms. *J Plant Growth Regul* 2001;20:226–43. <http://dx.doi.org/10.1007/s003440010027>.
- [39] Calderón Villalobos LIA, Lee S, De Oliveira C, Ivetac A, Brandt W, Armitage L, et al. A combinatorial TIR1/AFB-Aux/IAA co-receptor system for differential sensing of auxin. *Nat Chem Biol* 2012;8:477–85. <http://dx.doi.org/10.1038/nchembio.926>.
- [40] Takeuchi J, Okamoto M, Akiyama T, Muto T, Yajima S, Sue M, et al. Designed abscisic acid analogs as antagonists of PYL-PP2C receptor interactions. *Nat Chem Biol* 2014;10:477–82.

APPENDIX A. SUPPLEMENTARY DATA

New fluorescently labeled auxins exhibit promising anti-auxin activity

Kristýna Bieleszová,^{a,b,1} Barbora Pařízková,^{a,b,1} Martin Kubeš,^{b,1} Alexandra Husičková,^c Martin Kubala,^c Qian Ma,^d Michaela Sedlářová,^e Stéphanie Robert,^d Karel Doležal,^{a,b} Miroslav Strnad,^{a,b} Ondřej Novák,^{a,b} Asta Žukauskaitė^{a,b,*}

^aLaboratory of Growth Regulators, Centre of the Region Haná for Biotechnological and Agricultural Research, Faculty of Science of Palacký University & Institute of Experimental Botany of the Czech Academy of Sciences, Šlechtitelů 27, CZ-783 71, Olomouc, Czech Republic

^bDepartment of Chemical Biology and Genetics, Centre of the Region Haná for Biotechnological and Agricultural Research, Faculty of Science, Palacký University, Šlechtitelů 27, CZ-783 71, Olomouc, Czech Republic

^cDepartment of Biophysics, Centre of the Region Haná for Biotechnological and Agricultural Research, Faculty of Science, Palacký University, Šlechtitelů 27, CZ-783 71 Olomouc, Czech Republic

^dUmeå Plant Science Centre, Department of Forest Genetics and Plant Physiology, Swedish University of Agricultural Sciences, SE-901 83 Umeå, Sweden

^eDepartment of Botany, Faculty of Science, Palacký University, Šlechtitelů 27, CZ-783 71 Olomouc, Czech Republic

¹ These authors contributed equally to this work.

* Corresponding author.

E-mail address: asta.zukauskaite@upol.cz

Alternative methods for the synthesis of compound 3a

METHOD A (Supplementary Table 1, Entry 3)

To a solution of methyl 2-(1*H*-indol-3-yl)acetate **1** (94 mg, 0.50 mmol), dissolved in dry THF (3 mL), HMPA (0.4 mL) and LDA (2 M in THF, 374 μ L, 0.75 mmol) were added at -78°C and the reaction mixture was stirred for 30 min. Then, *tert*-butyl(3-iodopropyl)carbamate **2a** (156 mg, 0.55 mmol), dissolved in dry THF (0.5 mL), was added dropwise and the mixture was stirred at -78°C for 1 h. Then, the reaction mixture was warmed up to 0°C and additionally stirred for 15 min. Subsequently, reaction mixture was quenched with water (30 mL) at 0°C and extracted with EtOAc (3×20 mL). The combined organic extracts were washed with saturated NH_4Cl solution (10 mL), and saturated NaCl solution (10 mL). Drying with Na_2SO_4 , filtration and evaporation of the solvent under reduced pressure and purification of the residue by flash chromatography on silica gel (PE/EtOAc 8.5/1.5) afforded pure compound **3a** in 10% yield.

METHOD B (Supplementary Table 1, Entry 6)

To a solution of methyl 2-(1*H*-indol-3-yl)acetate **1** (75 mg, 0.40 mmol), dissolved in dry DMF (1 mL), NaH (60% in mineral oil, 24 mg, 0.60 mmol) was added at 0°C . The reaction mixture was stirred at 0°C for 15 min. Then, *tert*-butyl (3-iodopropyl)carbamate **2a** (114 mg, 0.40 mmol), dissolved in dry DMF (1 mL), was added and the reaction mixture was stirred at 50°C for 24 h. Subsequently, reaction mixture was cooled down to 0°C , quenched with water (4 mL) and extracted with Et_2O (3×10 mL). The combined organic extracts were washed with saturated NaCl solution (5×5 mL). Drying with Na_2SO_4 , filtration and evaporation of the solvent under reduced pressure and purification of the residue by flash chromatography on silica gel (PE/EtOAc 8.5/1.5) afforded pure compound **3a** in 19% yield.

METHOD C (Supplementary Table 1, Entry 7)

To a solution of methyl 2-(1*H*-indol-3-yl)acetate **1** (194 mg, 1.03 mmol), dissolved in dry DMF (1.5 mL), NaH (60% in mineral oil, 82 mg, 2.05 mmol) was added at 0°C . The reaction mixture was stirred at 0°C for 15 min. Then, *tert*-butyl (3-iodopropyl)carbamate **2a** (324 mg, 1.13 mmol), dissolved in dry DMF (1.5 mL), was added and the reaction mixture was stirred at 75°C for 20 h. Subsequently, reaction mixture was cooled down to 0°C , quenched with water (5 mL) and extracted with Et_2O (4×10 mL). The combined organic extracts were washed with saturated NaCl solution (5×5 mL). Drying with Na_2SO_4 , filtration and evaporation of the

solvent under reduced pressure and purification of the residue by flash chromatography on silica gel (PE/EtOAc 8.5/1.5) afforded pure compound **3a** in 5% yield.

METHOD D (Supplementary Table 1, Entry 8)

To a suspension of NaH (60% in mineral oil, 21 mg, 0.53 mmol) in dry DMSO (1 mL), solution of methyl 2-(1*H*-indol-3-yl)acetate **1** (77 mg, 0.41 mmol), dissolved in dry DMSO (1.5 mL), was added at room temperature (RT). The resulting reaction mixture was stirred at RT for 1 h. Then, *tert*-butyl (3-iodopropyl)carbamate **2a** (117 mg, 0.41 mmol), dissolved in dry DMSO (2 mL), was added and the reaction mixture was stirred at RT for 23 h. Subsequently, reaction mixture was cooled down to 0°C, quenched with water (5 mL) and extracted with EtOAc (3 × 10 mL). The combined organic extracts were washed with saturated NaCl solution (2 × 5 mL). Drying with Na₂SO₄, filtration, evaporation of the solvent under reduced pressure and purification of the residue by flash chromatography on silica gel (PE/EtOAc 8.5/1.5) afforded pure compound **3a** in 28% yield.

METHOD E (Supplementary Table 1, Entry 9)

To a suspension of NaH (60% in mineral oil, 110 mg, 2.75 mmol) in dry DMSO (4 mL), methyl 2-(1*H*-indol-3-yl)acetate **1** (400 mg, 2.12 mmol), dissolved in dry DMSO (7 mL), was added at RT. The resulting reaction mixture was stirred at RT for 1 h. Then, *tert*-butyl (3-iodopropyl)carbamate **2a** (729 mg, 2.54 mmol), dissolved in dry DMSO (8 mL), was added and the reaction mixture stirred at RT for 22 h. The reaction mixture was then cooled to 0°C, quenched with water (24 mL) and extracted with EtOAc (3 × 30 mL). The combined organic extracts were washed with saturated NaCl solution (2 × 15 mL). Drying with Na₂SO₄, filtration and evaporation of the solvent under reduced pressure and purification of the residue by flash chromatography on silica gel (PE/EtOAc 8.5/1.5) afforded pure compound **3a** in 47% yield.

Spectral data of compounds 3a-d, 4a-d, 5a-d

Methyl 2-(1-(3-((*tert*-butoxycarbonyl)amino)propyl)-1*H*-indol-3-yl)acetate **3a**. Yellow oil, yield 47%, *R_f* = 0.14 (PE/EtOAc 4/1). ¹H NMR (500 MHz, CDCl₃): δ 1.43 (9H, s, (CH₃)₃), 2.00 (2H, p, *J* = 6.9 Hz, CH₂), 3.01-3.17 (2H, m, CH₂), 3.69 (3H, s, OCH₃), 3.76 (2H, s, CH₂), 4.12 (2H, t, *J* = 6.9 Hz, CH₂), 4.48-4.56 (1H, br s, NH), 7.08 (1H, s, CH), 7.11 (1H, t, *J* = 7.5 Hz, CH), 7.21 (1H, t, *J* = 7.6 Hz, CH), 7.29 (1H, d, *J* = 8.2 Hz, CH), 7.59 (1H, d, *J* = 7.7 Hz, CH). ¹³C

NMR (126 MHz, CDCl₃): δ 28.5 ((CH₃)₃), 30.6 (CH₂), 31.2 (CH₂), 38.3 (CH₂), 43.8 (CH₂), 52.1 (OCH₃), 79.5 (C), 107.3 (C), 109.4 (CH), 119.2 (CH), 119.4 (CH), 121.9 (CH), 126.7 (CH), 127.9 (C), 136.2 (C), 156.1 (C=O), 172.6 (C=O). MS (ESI⁺): m/z (%): 247.25 [M - Boc + H⁺, 100], purity: 97%.

Methyl 2-(1-(4-((*tert*-butoxycarbonyl)amino)butyl)-1*H*-indol-3-yl)acetate **3b**. Yellow oil, yield 14%, R_f = 0.65 (PE/EtOAc 4/1). ¹H NMR (500 MHz, CDCl₃): δ 1.43 (9H, s, (CH₃)₃), 1.48 (2H, p, J = 6.9 Hz, CH₂), 1.84 (2H, p, J = 7.3, CH₂), 3.06-3.15 (2H, m, CH₂), 3.69 (3H, s, OCH₃), 3.76 (2H, s, CH₂), 4.10 (2H, t, J = 7.1 Hz, CH₂), 4.42-4.57 (1H, br s, NH), 7.07 (1H, s, CH), 7.11 (1H, t, J = 7.3 Hz, CH), 7.21 (1H, t, J = 7.6 Hz, CH), 7.31 (1H, d, J = 8.3 Hz, CH), 7.59 (1H, d, J = 8.0 Hz, CH). ¹³C NMR (126 MHz, CDCl₃): δ 27.5 (CH₂), 27.7 (CH₂), 28.5 ((CH₃)₃), 31.2 (CH₂), 40.2 (CH₂), 45.9 (CH₂), 52.1 (OCH₃), 79.4 (C), 107.0 (C), 109.5 (CH), 119.2 (CH), 119.3 (CH), 121.8 (CH), 126.7 (CH), 127.8 (C), 136.2 (C), 156.1 (C=O), 172.7 (C=O). MS (ESI⁺): m/z (%): 261.28 [M - Boc + H⁺, 100], purity: 93%.

Methyl 2-(1-(5-((*tert*-butoxycarbonyl)amino)pentyl)-1*H*-indol-3-yl)acetate **3c**. Yellow oil, yield 37%, R_f = 0.33 (PE/EtOAc 4/1). ¹H NMR (500 MHz, CDCl₃): δ 1.28-1.37 (2H, m, CH₂), 1.44 (9H, s, (CH₃)₃), 1.43-1.51 (2H, m, CH₂), 1.83 (2H, p, J = 7.8 Hz, CH₂), 3.00-3.14 (2H, m, CH₂), 3.69 (3H, s, OCH₃), 3.77 (2H, s, CH₂), 4.06 (2H, t, J = 7.0 Hz, CH₂), 4.37-4.70 (1H, br s, NH), 7.07 (1H, s, CH), 7.11 (1H, t, J = 7.5 Hz, CH), 7.21 (1H, t, J = 7.6 Hz, CH), 7.30 (1H, d, J = 8.3 Hz, CH), 7.60 (1H, d, J = 8.0 Hz, CH). ¹³C NMR (126 MHz, CDCl₃): δ 24.3 (CH₂), 28.5 ((CH₃)₃), 29.9 (CH₂), 30.0 (CH₂), 31.2 (CH₂), 40.5 (CH₂), 46.3 (CH₂), 52.1 (OCH₃), 79.2 (C), 106.9 (C), 109.5 (CH), 119.1 (CH), 119.2 (CH), 121.8 (CH), 126.8 (CH), 127.8 (C), 136.2 (C), 156.1 (C=O), 172.7 (C=O). MS (ESI⁺): m/z (%): 275.17 [M - Boc + H⁺, 100], 397.26 [M + Na⁺, 48], purity: 91%.

Methyl 2-(1-(6-((*tert*-butoxycarbonyl)amino)hexyl)-1*H*-indol-3-yl)acetate **3d**. Yellow oil, yield 37%, R_f = 0.18 (PE/EtOAc 4/1). ¹H NMR (500 MHz, CDCl₃): δ 1.27-1.37 (4H, m, 2 \times CH₂), 1.39-1.48 (11H, m, (CH₃)₃ and CH₂), 1.76-1.86 (2H, m, CH₂), 3.01-3.12 (2H, m, CH₂), 3.69 (3H, s, OCH₃), 3.77 (2H, s, CH₂), 4.06 (2H, t, J = 7.0 Hz, CH₂), 4.38-4.60 (1H, br s, NH), 7.07 (1H, s, CH), 7.11 (1H, t, J = 7.5 Hz, CH), 7.21 (1H, t, J = 7.6 Hz, CH), 7.30 (1H, d, J = 8.3 Hz, CH), 7.60 (1H, d, J = 8.0 Hz, CH). ¹³C NMR (126 MHz, CDCl₃): δ 26.5 (CH₂), 26.8 (CH₂), 28.5 ((CH₃)₃), 30.0 (CH₂), 30.3 (CH₂), 31.2 (CH₂), 40.5 (CH₂), 46.3 (CH₂), 52.1 (OCH₃), 79.2 (C), 106.8 (C), 109.5 (CH), 119.1 (CH), 119.2 (CH), 121.7 (CH), 126.8 (CH), 127.8 (C), 136.2

(C), 156.1 (C=O), 172.7 (C=O). MS (ESI+): m/z (%): 289.20 [M - Boc + H⁺, 65], 411.37 [M + Na⁺, 100], purity: 92%.

Methyl 2-(1-(3-((7-nitrobenzo[*c*][1,2,5]oxadiazol-4-yl)amino)propyl)-1*H*-indol-3-yl)acetate **4a**. Red oil, yield 35%, R_f = 0.82 (CH₂Cl₂/Ac/MeOH 5/0.1/0.1). ¹H NMR (500 MHz, CDCl₃): δ 2.32 (2H, p, J = 6.5 Hz, CH₂), 3.38-3.45 (2H, m, CH₂), 3.72 (3H, s, OCH₃), 3.78 (2H, s, CH₂), 4.31 (2H, t, J = 6.3 Hz, CH₂), 5.86 (1H, d, J = 8.6 Hz, CH), 5.94-6.01 (1H, br s, NH), 7.07 (1H, t, J = 7.5 Hz, CH), 7.11 (1H, s, CH), 7.14 (1H, t, J = 7.7 Hz, CH), 7.23 (1H, d, J = 8.3 Hz, CH), 7.55 (1H, d, J = 8.0 Hz, CH), 8.32 (1H, d, J = 8.6 Hz, CH). ¹³C NMR (126 MHz, CDCl₃): δ 28.3 (CH₂), 30.8 (CH₂), 41.4 (CH₂), 43.8 (CH₂), 52.2 (OCH₃), 98.8 (CH), 108.5 (C), 109.2 (CH), 119.5 (CH), 119.8 (CH), 122.4 (CH), 124.3 (C), 126.4 (CH), 128.2 (C), 136.1 (C), 136.3 (CH), 143.4 (C), 143.8 (C), 144.1 (C), 172.7 (C=O). MS (ESI+): m/z (%): 410.00 [M + H⁺, 100], purity: 96%.

Methyl 2-(1-(4-((7-nitrobenzo[*c*][1,2,5]oxadiazol-4-yl)amino)butyl)-1*H*-indol-3-yl)acetate **4b**. Red oil, yield 45%, R_f = 0.60 (CH₂Cl₂/Ac 5/0.1). ¹H NMR (500 MHz, CDCl₃): δ 1.76 (2H, p, J = 7.5 Hz, CH₂), 2.00 (2H, p, J = 7.2 Hz, CH₂), 3.25-3.35 (2H, m, CH₂), 3.70 (3H, s, OCH₃), 3.76 (2H, s, CH₂), 4.18 (2H, t, J = 6.6 Hz, CH₂), 5.94 (1H, d, J = 8.6 Hz, CH), 6.26-6.34 (1H, br s, NH), 7.08-7.11 (2H, m, 2 \times CH), 7.18 (1H, t, J = 7.6 Hz, CH), 7.28 (1H, d, J = 8.3 Hz, CH), 7.56 (1H, d, J = 7.6 Hz, CH), 8.36 (1H, d, J = 8.6 Hz, CH). ¹³C NMR (126 MHz, CDCl₃): δ 26.0 (CH₂), 27.3 (CH₂), 30.9 (CH₂), 43.5 (CH₂), 45.8 (CH₂), 52.2 (OCH₃), 98.7 (CH), 107.5 (C), 109.4 (CH), 119.3 (CH), 119.6 (CH), 122.1 (CH), 124.0 (C), 126.7 (CH), 128.0 (C), 136.1 (C), 136.6 (CH), 143.7 (C), 143.9 (C), 144.2 (C), 172.8 (C=O). MS (ESI+): m/z (%): 424.00 [M + H⁺, 100], purity: 93%.

Methyl 2-(1-(5-((7-nitrobenzo[*c*][1,2,5]oxadiazol-4-yl)amino)pentyl)-1*H*-indol-3-yl)acetate **4c**. Red oil, yield 39%, R_f = 0.80 (CH₂Cl₂/Ac 5/0.1). ¹H NMR (500 MHz, CDCl₃): δ 1.41-1.49 (2H, m, CH₂), 1.70 (2H, p, J = 7.5 Hz, CH₂), 1.90 (2H, p, J = 7.2 Hz, CH₂), 3.33-3.43 (2H, m, CH₂), 3.70 (3H, s, OCH₃), 3.76 (2H, s, CH₂), 4.12 (2H, t, J = 6.7 Hz, CH₂), 6.03 (1H, d, J = 8.9 Hz, CH), 6.37-6.47 (1H, br s, NH), 7.06-7.09 (2H, m, 2 \times CH), 7.17 (1H, t, J = 7.6 Hz, CH), 7.27 (1H, d, J = 8.3 Hz, CH), 7.55 (1H, d, J = 8.0 Hz, CH), 8.39 (1H, d, J = 8.6 Hz, CH). ¹³C NMR (126 MHz, CDCl₃): δ 24.5 (CH₂), 28.3 (CH₂), 29.6 (CH₂), 31.0 (CH₂), 43.8 (CH₂), 46.1 (CH₂), 52.2 (OCH₃), 98.6 (CH), 107.3 (C), 109.4 (CH), 119.2 (CH), 119.4 (CH), 121.9 (CH), 124.1 (C),

126.8 (CH), 127.9 (C), 136.1 (C), 136.5 (CH), 143.8 (C), 144.0 (C), 144.3 (C), 172.8 (C=O). MS (ESI⁺): *m/z* (%): 438.33 [M + H⁺, 100], purity: 83%.

Methyl 2-(1-(6-((7-nitrobenzo[*c*][1,2,5]oxadiazol-4-yl)amino)hexyl)-1*H*-indol-3-yl)acetate **4d**. Red oil, yield 39%, *R_f* = 0.52 (PE/EtOAc 1/1). ¹H NMR (500 MHz, CDCl₃): δ 1.32-1.46 (4H, m, 2 × CH₂), 1.71 (2H, p, *J* = 7.2 Hz, CH₂), 1.84 (2H, p, *J* = 7.1 Hz, CH₂), 3.31-3.42 (2H, m, CH₂), 3.70 (3H, s, OCH₃), 3.77 (2H, s, CH₂), 4.08 (2H, t, *J* = 6.9 Hz, CH₂), 6.04 (1H, d, *J* = 8.6 Hz, CH), 6.47-6.56 (1H, br s, NH), 7.06-7.09 (2H, m, 2 × CH), 7.18 (1H, t, *J* = 7.5 Hz, CH), 7.27 (1H, d, *J* = 8.3 Hz, CH), 7.55 (1H, d, *J* = 8.0 Hz, CH), 8.40 (1H, d, *J* = 8.6 Hz, CH). ¹³C NMR (126 MHz, CDCl₃): δ 26.5 (CH₂), 26.6 (CH₂), 28.3 (CH₂), 30.0 (CH₂), 31.1 (CH₂), 43.8 (CH₂), 46.2 (CH₂), 52.1 (OCH₃), 98.6 (CH), 107.0 (C), 109.5 (CH), 119.1 (CH), 119.2 (CH), 121.8 (CH), 123.6 (C), 126.9 (CH), 127.8 (C), 136.2 (C), 136.8 (CH), 144.0 (C), 144.1 (C), 144.3 (C), 172.9 (C=O). MS (ESI⁺): *m/z* (%): 452.29 [M + H⁺, 100], purity: 92%.

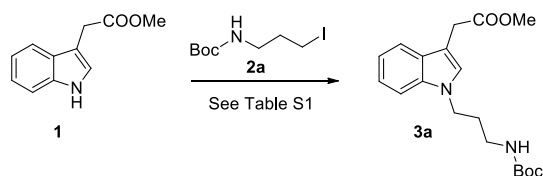
2-(1-(3-((7-Nitrobenzo[*c*][1,2,5]oxadiazol-4-yl)amino)propyl)-1*H*-indol-3-yl)acetic acid **5a**. Red solid, yield 52%, *R_f* = 0.20 (CH₂Cl₂/acetone 5/1). ¹H NMR (500 MHz, acetone-*d*₆): δ 2.38 (2H, p, *J* = 7.0 Hz, CH₂), 3.56-3.67 (2H, m, CH₂), 3.71 (2H, s, CH₂), 4.41 (2H, t, *J* = 6.7 Hz, CH₂), 6.23 (1H, d, *J* = 8.9 Hz, CH), 7.00 (1H, t, *J* = 7.5 Hz, CH), 7.08 (1H, t, *J* = 8.0 Hz, CH), 7.30 (1H, s, CH), 7.41 (1H, d, *J* = 8.3 Hz, CH), 7.56 (1H, d, *J* = 7.6 Hz, CH), 8.17-8.27 (1H, br s, NH), 8.40 (1H, d, *J* = 8.9 Hz, CH), 10.45-10.94 (1H, br s, OH). ¹³C NMR (126 MHz, acetone-*d*₆): δ 28.6 (CH₂), 30.3 (CH₂), 41.2 (CH₂), 43.2 (CH₂), 98.8 (CH), 107.9 (C), 109.6 (CH), 118.9 (CH), 119.1 (CH), 121.5 (CH), 122.7 (C), 127.1 (CH), 128.3 (C), 136.4 (C), 137.0 (CH), 144.3 (C), 144.7 (C), 144.9 (C), 172.4 (C=O). MS (ESI⁻): *m/z* (%): 394.25 [M - H⁻, 100], purity: 98%. HRMS: calcd. for C₁₉H₁₈N₅O₅: 396.1308 [M + H]⁺, found 396.1304 [M + H]⁺; calcd. for C₁₉H₁₇N₅O₅Na: 418.1127 [M + Na]⁺, found 418.1124 [M + Na]⁺.

2-(1-(4-((7-Nitrobenzo[*c*][1,2,5]oxadiazol-4-yl)amino)butyl)-1*H*-indol-3-yl)acetic acid **5b**. Red solid, yield 20%, *R_f* = 0.09 (CH₂Cl₂/acetone 5/1). ¹H NMR (500 MHz, acetone-*d*₆): δ 1.83 (2H, p, *J* = 7.4 Hz, CH₂), 1.98-2.06 (2H, m, CH₂), 3.53-3.64 (2H, m, CH₂), 3.69 (2H, s, CH₂), 4.25 (2H, t, *J* = 6.9 Hz, CH₂), 6.31 (1H, d, *J* = 8.6 Hz, CH), 7.00 (1H, t, *J* = 7.5 Hz, CH), 7.08 (1H, t, *J* = 8.0 Hz, CH), 7.24 (1H, s, CH), 7.38 (1H, t, *J* = 8.3 Hz, CH), 7.54 (1H, d, *J* = 7.9 Hz, CH), 8.20-8.34 (1H, br s, NH), 8.42 (1H, d, *J* = 8.9 Hz, CH), 10.00-11.20 (1H, br s, OH). ¹³C NMR (126 MHz, acetone-*d*₆): δ 25.5 (CH₂), 27.5 (CH₂), 30.4 (CH₂), 43.3 (CH₂), 45.4 (CH₂), 98.7 (CH), 107.6 (C), 109.6 (CH), 118.7 (CH), 119.1 (CH), 121.3 (CH), 122.4 (C), 127.1 (CH),

128.2 (C), 136.4 (C), 137.0 (CH), 144.3 (C), 144.7 (C), 144.8 (C), 172.4 (C=O). MS (ESI⁻): *m/z* (%): 408.36 [M - H⁻, 100], purity: 98%. HRMS: calcd. for C₂₀H₂₀N₅O₅: 410.1462 [M + H]⁺, found 410.1461 [M + H]⁺; calcd. for C₂₀H₁₉N₅O₅Na 432.1284 [M + Na]⁺, found 432.1277 [M + Na]⁺.

2-(1-(5-((7-Nitrobenzo[*c*][1,2,5]oxadiazol-4-yl)amino)pentyl)-1*H*-indol-3-yl)acetic acid **5c**. Red solid, yield 27%, *R_f* = 0.20 (CH₂Cl₂/acetone 5/1). ¹H NMR (500 MHz, acetone-*d*₆): δ 1.43-1.53 (2H, m, CH₂), 1.78-1.94, (4H, m, 2 × CH₂), 3.50-3.65 (2H, m, CH₂), 3.68 (2H, s, CH₂), 4.15-4.19 (2H, m, CH₂), 6.36 (1H, d, *J* = 8.6 Hz, CH), 6.95-7.00 (1H, m, CH), 7.04-7.10 (1H, m, CH), 7.21 (1H, s, CH), 7.35 (1H, d, *J* = 8.3 Hz, CH), 7.54 (1H, d, *J* = 7.6 Hz, CH), 8.20-8.28 (1H, br s, NH), 8.44 (1H, d, *J* = 8.6 Hz, CH), 10.40-10.85 (1H, br s, OH). ¹³C NMR (126 MHz, acetone-*d*₆): δ 24.1 (CH₂), 27.8 (CH₂), 29.8 (CH₂), 30.4 (CH₂), 43.5 (CH₂), 45.6 (CH₂), 98.6 (CH), 107.4 (C), 109.5 (CH), 118.7 (CH), 119.1 (CH), 121.3 (CH), 122.4 (C), 127.1 (CH), 128.1 (C), 136.4 (C), 137.1 (CH), 144.3 (C), 144.7 (C), 144.9 (C), 172.4 (C=O). MS (ESI⁻): *m/z* (%): 422.32 [M - H⁻, 100], purity: 97%. HRMS: calcd. for C₂₁H₂₂N₅O₅: 424.1621 [M + H]⁺, found 424.1620 [M + H]⁺; calcd. for C₂₁H₂₁N₅O₅Na: 446.1440 [M + Na]⁺, found 446.1440 [M + Na]⁺.

2-(1-(6-((7-Nitrobenzo[*c*][1,2,5]oxadiazol-4-yl)amino)hexyl)-1*H*-indol-3-yl)acetic acid **5d**. Red solid, yield 11%, *R_f* = 0.09 (CH₂Cl₂/acetone 5/1). ¹H NMR (500 MHz, acetone-*d*₆): δ 1.35-1.42 (2H, m, CH₂), 1.46-1.52 (2H, m, CH₂), 1.79 (2H, p, *J* = 7.3 Hz, CH₂), 1.83 (2H, p, *J* = 7.3 Hz, CH₂), 3.52-3.63 (2H, m, CH₂), 3.70 (2H, s, CH₂), 4.16 (2H, t, *J* = 7.0 Hz, CH₂), 6.38 (1H, d, *J* = 8.9 Hz, CH), 7.00 (1H, t, *J* = 7.5 Hz, CH), 7.10 (1H, t, *J* = 7.5 Hz, CH), 7.22 (1H, s, CH), 7.36 (1H, t, *J* = 8.3 Hz, CH), 7.55 (1H, d, *J* = 7.9 Hz, CH), 8.23-8.33 (1H, br s, NH), 8.47 (1H, d, *J* = 8.9 Hz, CH), 10.42-10.93 (1H, br s, OH). ¹³C NMR (126 MHz, acetone-*d*₆): δ 26.3 (CH₂), 26.4 (CH₂), 28.7 (CH₂), 30.0 (CH₂), 30.4 (CH₂), 43.4 (CH₂), 45.7 (CH₂), 98.5 (CH), 107.4 (C), 109.7 (CH), 118.7 (CH), 119.3 (CH), 121.3 (CH), 122.4 (C), 127.1 (CH), 128.2 (C), 136.5 (C), 137.0 (CH), 144.4 (C), 144.7 (C), 144.9 (C), 172.3 (C=O). MS (ESI⁻): *m/z* (%): 436.35 [M - H⁻, 100], purity: 100%. HRMS: calcd. for C₂₂H₂₄N₅O₅: 438.1777 [M + H]⁺, found 438.1779 [M + H]⁺; calcd. for C₂₂H₂₃N₅O₅Na: 460.1597 [M + Na]⁺, found 418.1597 [M + Na]⁺.

Table S1. Optimization of the reaction conditions for the synthesis of **3a**.

Entry	Linker	Base	Solvent	Temperature	Time	Result
1	1 eq 2a	1.5 eq DIPEA	CH ₃ CN	70°C	3 h	-
2	1.2 eq 2a	1.2 eq LiHMDS (1 M)	THF	r.t.	17 h	-
3	1.1 eq 2a	1.5 eq LDA (2 M)	HMPA, THF	-78°C, 0°C	1.5 h, 15 min	3a (10%)
4	1 eq 2a	1 eq NaH	DMF	r.t.	18 h	-
5	1.1 eq 2a	1.5 eq NaH	DMF	r.t.	22 h	-
6	1 eq 2a	1.5 eq NaH	DMF	50°C	24 h	3a (19%)
7	1.1 eq 2a	2 eq NaH	DMF	75°C	20 h	3a (5%)
8	1 eq 2a	1.3 eq NaH	DMSO	r.t.	23 h	3a (28%)
9	1.2 eq 2a	1.3 eq NaH	DMSO	r.t.	22 h	3a (47%)

Table S2. Fundamental absorption and fluorescence characteristics of compounds **5a-d**.

Solvent	Compound	λ_{abs} (nm)	λ_{em} (nm)	SS (nm)	ϵ_{480} (cm ⁻¹ ·M ⁻¹)	τ_{M} (ns)	QY
Water	5a	488	540	52	21200	0.39	0.00003
	5b	488	547	59	20700	0.23	0.00013
	5c	489	544	55	20600	0.22	0.00028
	5d	486	545	59	16700	0.60	0.00102
Methanol	5a	465	525	60	20100	2.07	0.00022
	5b	467	530	63	17500	1.41	0.00069
	5c	467	531	64	18600	0.98	0.00188
	5d	466	532	66	16200	2.35	0.00358

SS – Stokes shift, τ_{M} – intensity-weighted mean fluorescence lifetime, QY – fluorescence quantum yield.

Table S3. Parameters of fluorescence decays.

Solvent	Compound	τ_1 (ns)	τ_2 (ns)	τ_3 (ns)	τ_4 (ns)	A_1	A_2	A_3	A_4	τ_M	χ^2_R
Water	5a	11.94	1.41	0.84	0.01	$7.10 \cdot 10^{-6}$	0.001	0.003	0.99	0.37	1.09
	5b	5.42	1.08	0.14	0.01	$1.10 \cdot 10^{-5}$	0.002	0.006	0.99	0.23	1.11
	5c	4.60	1.06	0.17	0.01	$4.10 \cdot 10^{-5}$	0.002	0.07	0.93	0.22	1.06
	5d	3.24	0.92	0.38	0.02	$4.10 \cdot 10^{-4}$	0.04	0.17	0.79	0.54	0.99
Methanol	5a	n.d.								2.07*	
	5b	5.68	1.86	0.22	0.02	0.001	0.002	0.06	0.94	1.41	1.00
	5c	4.88	1.15	0.37	0.04	0.004	0.04	0.27	0.69	0.98	0.98
	5d	5.24	1.50	0.51	0.01	0.01	0.04	0.13	0.81	2.35	0.97

Parameters τ_1 , τ_2 , τ_3 and τ_4 denote fluorescence lifetime components in the fluorescence decay, A_1 , A_2 , A_3 and A_4 - corresponding pre-exponential factors, respectively, χ^2_R - reduced χ^2 for the best fit, *estimate from the TCSPC histogram, n.d. - not determined.

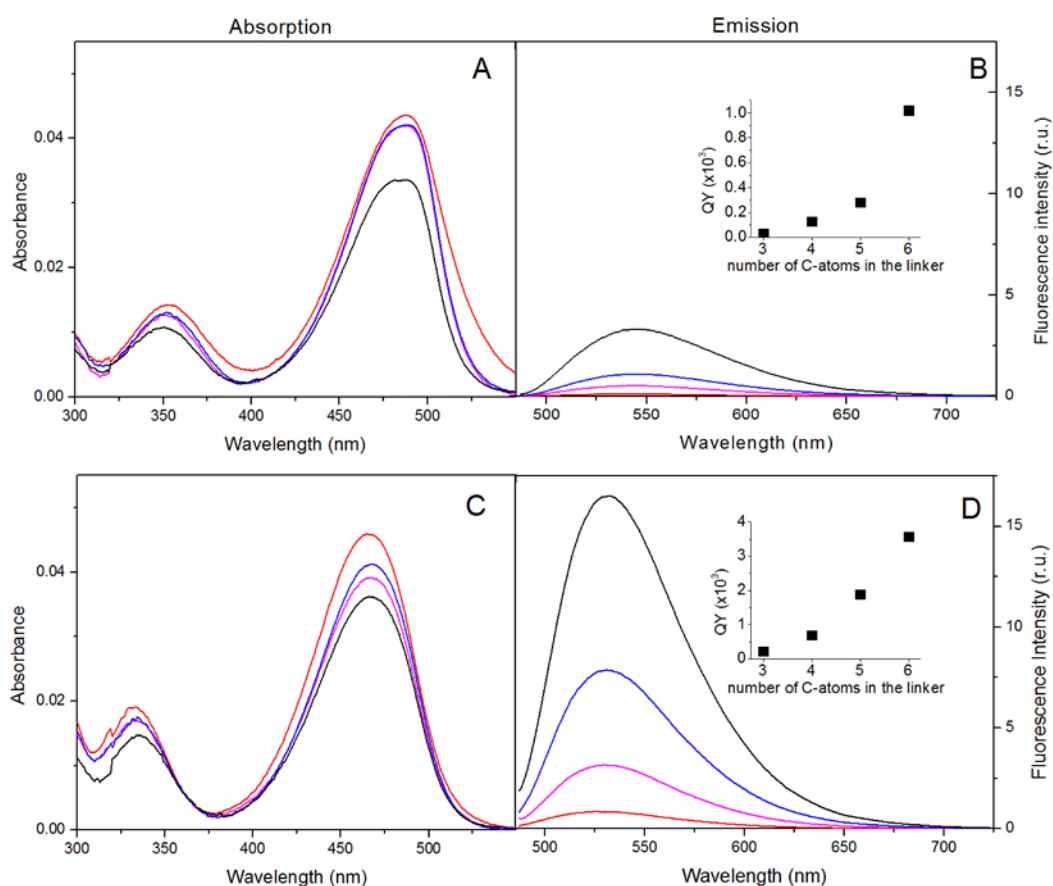


Figure S1. Absorption and emission spectra of 2 μ M solutions of compounds **5a** (red), **5b** (magenta), **5c** (blue) and **5d** (black) in water (**A**, **B**) and methanol (**C**, **D**). Insets: Dependence of fluorescence quantum yield on the length of the linker.

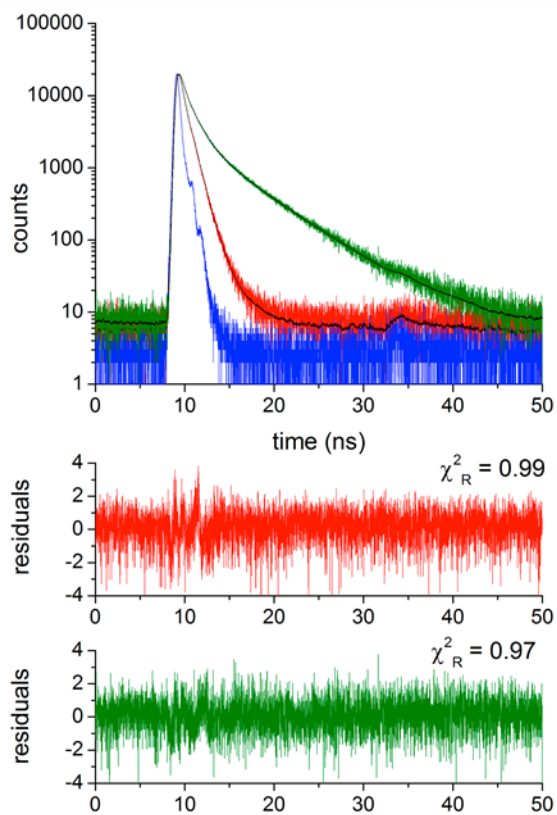


Figure S2. Upper panel: Instrument response function (blue) and fluorescence decay of compound **5d** in water (red) and methanol (green), black lines represent the best fits of data. Lower panels: Plots of corresponding distributions of residuals.

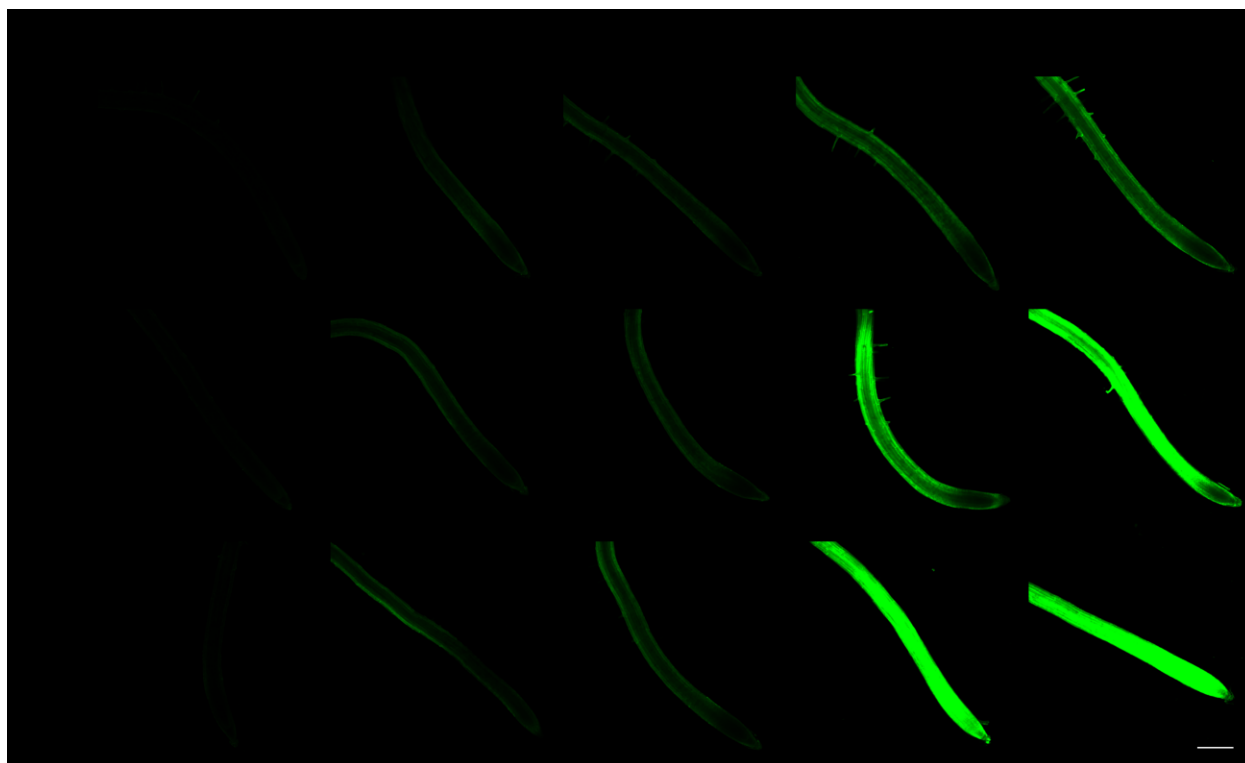


Figure S3. Uptake of fluorescently labeled IAA derivative 5d in *Arabidopsis thaliana* roots. Seedlings (5DAG) were treated with compound **5d** at given concentrations (1, 2, 5 and 10 μM) for 10, 20 and 30 min. Figures were chosen as representatives from 2 independent biological repetitions. Scale bar represent 200 μm .

New auxin fluorescent probes for live imaging of auxin sites of action in plants

Barbora Pařízková^{a,b,1}, Asta Žukauskaitė^{a,b,1}, Thomas Vain^{c,1,2}, Peter Grones^{c,1,3}, Sara Raggi^c, Martin Kubeš^{b,d}, Martin Kieffer^e, Miroslav Strnad^a, Stefan Kepinski^e, Richard Napier^d, Karel Doležal^{a,b}, Stéphanie Robert^{c,4,5}, and Ondřej Novák^{a,4,5}

^a*Laboratory of Growth Regulators, Faculty of Science, Palacký University and Institute of Experimental Botany, The Czech Academy of Sciences, Šlechtitelů 27, CZ-78371 Olomouc, Czech Republic*

^b*Department of Chemical Biology and Genetics, Centre of the Region Haná for Biotechnological and Agricultural Research, Faculty of Science, Palacký University, Šlechtitelů 27, CZ-78371 Olomouc, Czech Republic*

^c*Department of Forest Genetics and Plant Physiology, Umeå Plant Science Centre, Swedish University of Agricultural Sciences, SE-90183 Umeå, Sweden*

^d*School of Life Sciences, The University of Warwick, Coventry, United Kingdom*

^e*Centre for Plant Sciences, University of Leeds, Leeds, LS2 9JT, United Kingdom*

Author contributions: B.P., A.Ž., T.V., P.G., K.D., S.Ro., and O.N. designed research; B.P., A.Ž., T.V., P.G., S.Ra, M.Ku. and M.Ki. performed research; B.P., A.Ž., T.V., P.G. S. Ra, M.Ku., M.Ki., S.K., K.D., M.S., S.Ro., and O.N. analyzed data; and B.P., A.Ž., T.V., S.Ro., and O.N. wrote the paper with contributions of all the authors; K.D., S.K., R.N., M.S., S.Ro. and O.N. supervised the research.

The authors declare no conflict of interest.

¹B.P., A. Ž., T.V. and P. G. contributed equally to this work.

²Present address: DIADE, University of Montpellier, IRD, 911 avenue Agropolis, 34394 Montpellier, France

³Present address: VIB Center for Plant Systems Biology, Technologiepark 927, 9052, Ghent, Belgium.

⁴S.Ro. and O.N. contributed equally to this work

⁵To whom correspondence may be addressed. Email: stephanie.robert@slu.se or novako@ueb.cas.cz

Abstract

The phytohormone auxin mediates most aspects of plant growth and development. The regulation of its spatiotemporal concentration is crucial for plant morphogenesis and response to endo- and exogenous stimuli. Coupling of an auxin molecule with a fluorescent probe provides a tool to visualize *in vivo* auxin distribution in plants, which is essential to study this dynamic process with high spatiotemporal resolution. Here, we present the synthesis, functional characterization and *in planta* stability time-course analysis for new fluorescently labeled auxin-like analogues derived from 2,4-dichlorophenoxyacetic acid (2,4-D). These fluorescent auxins, despite the partial metabolization *in vivo*, display an uneven and dynamic distribution leading to the formation of fluorescence maxima in tissues known to concentrate natural auxin, such as the inner side of the apical hook or the quiescent center (QC) cells of the root. Taken together, our work provides powerful tools for visualization of native auxin distribution within different plant tissues and during various developmental processes in response to both internal and environmental stimuli.

Significance

The introduction of a fluorophore to an auxin molecule represents a sensitive and non-invasive method to directly visualize auxin localization with high spatiotemporal resolution. The presented fluorescently labeled auxin analogues have been shown to display an uneven and dynamic distribution, which appears to be regulated in auxin-related developmental processes. *In vivo* and real-time visualizations of the compounds enable the study of the relationship between auxin action and localization in plants with high spatial resolution.

Keywords

fluorescent auxin, *in vivo* visualization, distribution, subcellular localization

Short title

Fluorescent auxin-based live imaging

Introduction

Auxin is a phytohormone with morphogen-like characteristics, which plays an essential role in controlling plant growth and development. The basic aspect of auxin action lies in its uneven distribution creating local concentration maxima in specific cells or tissues (1). Generating such concentration gradients and regulating precise spatiotemporal auxin levels are driven by auxin biosynthesis, active polar auxin transport (PAT) and conjugation and degradation processes (2). This uneven auxin distribution together with auxin perception at the cellular level coordinates plant morphogenesis including embryogenesis, lateral root and root hair formation (3) as well as responses to exo- and endogenous stimuli such as light or gravity (4).

Indole-3-acetic acid (IAA) is considered as the most important naturally occurring auxin (5). Furthermore, a wide array of small synthetic molecules with auxin activity has been produced (6). Such compounds, such as 2,4-dichlorophenoxyacetic acid (2,4-D) or 1-naphthaleneacetic acid (NAA) are more stable than endogenous auxins and are widely used as growth regulators (7) and herbicides in horticulture and agriculture.

IAA is a weak acid adopting a protonated form in the acidic environment of the apoplast, which allows cellular uptake by passive diffusion (8). In the neutral pH of the cytoplasm, IAA dissociates into a deprotonated form reducing its passive transport through the plasma membrane (9) and an active transport is thus needed to generate cell-to-cell auxin flux (10). The tissue specificity and polar localization of auxin influx and efflux carriers are essential in generating auxin maxima (11). The main family of proteins contributing to auxin uptake into the cell is AUXIN RESISTANT 1/LIKE AUX (AUX1/LAX) carriers (12, 13) whereas PIN-FORMED (PIN) proteins act as auxin efflux facilitators (9). Moreover, the members of the ATP-binding cassette subfamily B (ABCB) also contribute to direct auxin transport (14). Among these, ABCB1 and ABCB19 act as auxin exporters (15), but the function of ABCB4 and ABCB21 has been shown to be facultative (16). These ABCB4 and ABCB21 close homologues play a role as auxin influx carriers under low auxin concentrations whereas in high auxin levels both ABCB4 and ABCB21 are converted to auxin efflux transporters (17, 18). In addition, PIN-like (PILS) putative auxin carriers (19) localized on ER membranes, and vacuolar auxin transporter WALLS ARE THIN1 (WAT1) (20) also participate in the maintenance of intracellular auxin homeostasis.

Synthetic auxins such as 2,4-D and NAA are considered as useful tools to study auxin transport regulation by dissecting influx and efflux thanks to their different transport properties (21). While NAA enters the cells by passive diffusion (22), the uptake of 2,4-D is mediated by the AUX1, LAX1 and LAX3 active auxin carriers (13, 23–25). NAA also represents a good substrate for auxin exporters, especially PIN4 and PIN7 (26) whereas 2,4-D was long thought to be poorly recognized by auxin efflux carriers (22). However, more recent studies showed that 2,4-D can also act as a substrate for the efflux transporters (27), mainly for PIN2 and PIN7 (28) with lower affinity than IAA or NAA. In addition, ABCB1 and ABCB19 contribute to the efflux of 2,4-D (28) while ABCB4 facilitates the efflux of NAA (29).

Auxin action is triggered via its perception by specific receptors controlling the expression of auxin-responsive genes (32). The best-described auxin perception system is based on auxin-dependent degradation of AUXIN/IAA INDUCIBLE (AUX/IAA) transcription repressors by the 26S proteasome. The binding of IAA to the TRANSPORT INHIBITOR RESPONSE 1 (TIR1) or AUXIN SIGNALING F-BOX (AFB) receptors promotes the interaction of TIR1/AFB1-5 with AUX/IAA transcription inhibitors. The subsequent degradation of AUX/IAs leads to the release of AUXIN RESPONSE FACTOR (ARF) transcription factors and expression of auxin-responsive genes (30). Compared to IAA, 2,4-D displays lower affinity to the TIR1 auxin binding site (31), but this receptor still plays a dominant role in the 2,4-D mode of action (32).

Several methods have been developed to study the regulation of auxin distribution during plant development. Auxin reporters enable detection of tissue-specific localization of auxin activity as a result of the expression of markers (e. g. β -glucuronidase (GUS) or fluorescent proteins) fused to auxin-sensitive promoters (33). In addition, degradation-based reporters have been constructed to provide sensitive and rapid responses to the presence of auxin at a cellular resolution. The fluorescently tagged DII domain of the AUX/IAA repressors (DII-Venus) undergoes rapid degradation in response to auxin (34). The loss of the fluorescent signal can be used to detect the dynamic changes in auxin distribution (35). The cellular localization of auxin carriers also helps to predict the auxin fluxes during different developmental processes. These transporters are commonly visualized *in vivo* using fluorescent protein tags or monoclonal antibodies (33). Approaches employing microelectrodes, scintillation detection of radiolabeled IAA molecules or IAA targeted monoclonal antibodies provide the potential for direct detection of auxin distribution in plants. In addition, auxin fluorescent labeling has recently become a popular method, which represents a real-time and relatively non-invasive technique of detecting auxin distribution directly *in vivo*.

Here we present new tools to monitor auxin distribution using 2,4-D analogues labeled with the 7-nitro-2,1,3-benzoxadiazole (NBD) fluorophore. These fluorescently labeled 2,4-D derivatives specifically accumulate in the tissues where auxin maxima are expected, such as the quiescent center (QC) of root tips or concave side of apical hooks. Moreover, at the subcellular level we discovered the presence of the fluorescent analogues in specific organelles such as endosomes and endoplasmic reticulum (ER). Such a toolset represents high spatiotemporal resolution support for revealing the mechanisms behind the precise regulation of auxin distribution in live material.

Results

Design strategy for generation of the fluorescent auxin library

The intention of this study was to develop fluorescently labeled auxins, which would maintain the original hormone activity and would display auxin-like distribution in plant tissues. Since 2,4-D is not uptaken by passive diffusion, it has long been used to study auxin influx mechanisms (36). Additionally, this auxin agonist was also recently shown to be transported via auxin exporters (27) and thus represents an eligible candidate for auxin transport research. As a synthetic auxin, 2,4-D shows lower sensitivity to inactivating enzymes than IAA, explaining its higher metabolic stability *in planta* (37). For auxins, the carboxyl group moiety together with the planar aromatic ring are considered to be essential for binding to the hydrophobic binding site of TIR1 (38, 39) and thus for perception of the auxin signal. However, our parallel study (40) demonstrated that 2,4-D analogues bearing various phenylpiperazines or phenylthioethylamines coupled to its carboxyl group via an amide bond promote a specific interaction of TIR1 with different AUX/IAAs and accordingly influence different developmental processes. Inspired by these results, 2,4-D was fluorescently labeled with an NBD fluorophore via its carboxyl group side chain using three different linkers – ethylenediamine (EDA), piperazine (PIP) and 1,3-dimercaptopropane (DMP) and collectively named as FluorAs (from Fluorescent Auxins) (Fig. S1 A). Based on a screening strategy (Fig. S1 B), EDA and PIP linkers were chosen for the labeling of other synthetic auxin analogues (4-bromophenoxyacetic acid, 4-Br-POA; 2,4,5-trichlorophenoxyacetic acid, 2,4,5-T; 4-chlorophenoxyacetic acid, 4-Cl-POA and 2-phenoxyacetic acid, POA) with an NBD tag (Fig. S1 A) to obtain a wide portfolio of possible promising candidates and their biological function was characterized *in planta* (Fig. S2).

Searching for candidates – the structure–activity relationships of FluorAs

The best aspirants for detailed biological characterization were chosen based on their biological activity, fluorescent properties and stability *in planta* (Fig. 1, Fig. S1 B). In order to rapidly investigate whether the prepared compounds (Fig. S1 A) were active, their ability to inhibit primary root growth of *Arabidopsis* Col-0 seedlings (Fig. 1 A, Fig. S2 A) and to induce the expression of *Arabidopsis* auxin response marker *pDR5::GUS* were evaluated (Fig. 1 B, Fig. S2 B). Remarkably, the most active fluorescent analogues were the ones derived from 2,4-D regardless of the linker, showing a dose-dependent bioactivity from 1 μ M (Fig. 1 A) and promoting the expression of *pDR5::GUS* in roots at 10 μ M within 5 h of treatment (Fig. 1 B). Other fluorescent derivatives exhibited lower or no activity in both auxin-responsive assays (Fig. S2 A and B). In addition, the fluorescent properties of the 2,4-D analogues bearing three different linkers (EDA, PIP and DMP; Fig. S1 A) were evaluated. The strongest fluorescent signal was provided by FluorA II (Fig. 1 C). Using the confocal settings optimized for FluorA II, FluorA I displayed lower fluorescence intensity in roots after 15 min uptake at 2 μ M while FluorA III

did not provide any fluorescent output (Fig. 1 C). The intensity of the fluorescence is therefore likely to be influenced by the linker, with the strongest signals associated with the PIP linker followed by the EDA linker, but weak or no signals associated with the DMP linker. Unfortunately, this results in FluorA III, the most active analogue in the auxin bioassays (Fig. 1 A and B), being non-suitable for visualizing auxin distribution. On the other hand, both FluorA I and FluorA II generated a fluorescent pattern similar to that of the *pDR5::GUS* expression pattern in the roots treated with free 2,4-D (Fig. 1 B and C), with strong signals in the root columella and elongation zone. Therefore, our compound screening revealed FluorA I and FluorA II as two promising fluorescent candidates derived from 2,4-D suitable for advanced characterization of their biological functions. In addition, FluorA XI derived from POA, which did not affect root growth nor *pDR5::GUS* expression (Fig. S2 A and B), was suitable as a putative negative control, primarily for excluding non-specific fluorescent signal during investigation of FluorA distribution.

To better characterize the activity of the selected compounds, the expression of the auxin-responsive reporter lines *pIAA3::GUS* and *pIAA12::GUS* (41) and *pBA3::GUS* (42), were analyzed after chemical treatments. Both FluorA I and FluorA II stimulated the expression of all three reporters, while FluorA II was more potent in this regard (Fig. 2 A-C). To further characterize the activity of these two FluorA compounds, a reverse genetic approach was conducted by challenging *Arabidopsis* Col-0 WT and auxin signaling (*tir1-1*) and biosynthetic (*weak ethylene insensitive - wei2-1wei7-1*) deficient mutants with increasing FluorA concentrations. Both FluorA I and FluorA II inhibited root elongation of Col-0 WT in a dose dependent manner from 0.5 μ M treatment concentration (Fig. 2 D). At 0.5-1 μ M treatment concentration, *tir1-1* displayed lower sensitivity to both FluorA compounds than Col-0 (Fig. 2 D and Fig. S3), suggesting the importance of the TIR1 receptor in their mode of action. In both Col-0 and *tir1-1*, higher FluorA concentrations had an inhibitory effect on primary root growth. Similarly to *tir1-1*, *wei2-1wei7-1* displayed lower sensitivity to the root growth inhibitory effects of 2,4-D and both FluorAs (Fig. 2D). Moreover, similar to 2,4-D treatment from 0.05 μ M, both FluorA compounds were capable of rescuing the agravitropic phenotype of *wei2-1wei7-1* primary roots from 0.5 μ M (Fig. S3), indicating their auxin-like activity. Taken together, the fluorescent 2,4-D analogues FluorA I and II are biologically active auxins and are likely act through the TIR1 auxin signaling pathway.

Biological activity of FluorAs in shade of metabolization *in planta*

Since our results suggest that the 2,4-D-derived FluorA analogues actively affect plant growth in an auxin-dependent manner as well as triggering early auxin-responsive genes, we investigated their uptake and stability dynamics *in vivo*. For this purpose, a rapid analytical approach using a one-step purification method coupled with liquid chromatography-tandem mass spectrometry (LC-MS/MS) was developed to perform an absolute quantification of all analytes. To address the observed biological activity to FluorA compounds, this method

was employed for determination of time-dependent metabolization dynamics of fluorescent 2,4-D derivatives in roots of *Arabidopsis* Col-0 seedlings. As there was a slight metabolization detected after 15 min of FluorA treatment, we performed a dose-response analysis on Col-0 WT seedlings with various 2,4-D concentrations and quantified the endogenous levels of 2,4-D after 15 min of treatment. The exogenous concentration of 2,4-D providing the equivalent amount of 2,4-D endogenously released after 15 min of FluorA treatment was then calculated. Seedlings of the *Arabidopsis* reporter line *p35S::DII-Venus*, which expresses auxin-sensitive fluorescently labeled DII domains of AUX/IAAs (35), were then treated for 15 min with the 10 μ M FluorA compounds and estimated amount of 2,4-D and the fluorescent signals in response to the treatments were compared.

From the time-course experiment it was calculated that after 15 min of 10 μ M FluorA treatment approximately 2.5 pmol/50 roots of free 2,4-D was released (Fig. S4 A-B). To achieve this level of endogenous 2,4-D, exogenous application was calculated to approx. 230 nM 2,4-D (Fig. S4 C). Subsequently, *p35S::DII-Venus* seedlings were treated with 10 μ M FluorAs and 230 nM free 2,4-D assuming the equivalent amount of endogenous 2,4-D after 15 min. The quantification of Venus signal showed that the above mention treatments display the similar extend of degradation of the Venus signal (Fig. S4 D). This strongly suggest that observed auxinic activity comes from metabolization of FluorAs to 2,4-D. This fact was supported by surface plasmon resonance (SPR) analysis, which revealed that FluorA derivatives are not bound to TIR1 receptor *in vitro* and thus do not display auxin, and only a very weak anti-auxin, activity (Fig. S4 E).

Tissue-specific distribution of FluorAs

Although the biological effects of FluorAs were not confirmed, they can still act as active auxins for the auxin transport system. Hence, the impact of the auxin transport mechanisms on the distribution of fluorescent compounds chosen from the screening (FluorA I, II and XI) was further investigated. As mentioned above, all tested FluorAs displayed the same pattern of distribution in the primary root with different the signal intensities when using the same confocal settings (Fig. 1 C, S5 A-B). Moreover, the structures lacking a 2,4-D-like moiety were not taken up (PIP-NBD) or very poorly (FluorA XI) (Fig. S5 A) so the uptake of the compounds appeared to be auxin-dependent. Pre-treatment of plants with the auxin efflux inhibitor NPA led to an accumulation of both FluorA I and II, increasing the overall fluorescent signal in the roots, suggesting that active auxin efflux is involved in regulating the distribution of these FluorA compounds (Fig. 3 A). On the contrary, no significant changes in the intensity or pattern of the fluorescence were observed after affecting auxin influx pathways either by pre-treatment with the auxin influx inhibitor 2-NOA or by using the *aux1-21lax3* auxin transport mutant (Fig. S5 C) suggesting that the compounds bypass active auxin influx by passive diffusion. This implication was supported by a hypocotyl transport assay, wherein decapitated etiolated

hypocotyls were placed just below blocks of agar containing 2 μ M FluorAs (Fig. S5 D). After 3 h, fluorescent signal of both compounds was observed in the hypocotyl in a gradient, being most concentrated near the agar block. NPA pre-treatment of the hypocotyls to block active auxin efflux led to an increased signal close to the agar blocks but the tissue signal pattern was similar to that in non-NPA treated plants. These results suggest that both active transport and passive diffusion contribute to the transport of FluorA I and FluorA II.

PAT contributes to the modulation of plant development by regulating auxin spatiotemporal concentrations in specific tissues such as lateral root initiation sites in the root pericycle, the concave side of the apical hook or the QC of the root apex (8). Therefore, the localization of our fluorescent analogues was evaluated in these specific tissues. Both FluorA I and II established a PAT-dependent maximum in the QC of the root collumela (Fig. 3 B). Moreover, these 2,4-D probes were detected in lateral root primordia and accumulated in early emerged lateral roots (Fig. 3 C-D). Additionally, the generation of a predicted auxin maximum on the concave side of the apical hook was observed after FluorA II treatment, while FluorA I accumulated at the base of the cotyledons (Fig. 3 E). Importantly, FluorA XI did not show any pattern of accumulation the apical hook (Fig. S5 E). These FluorA accumulations in the apical hook were abolished by NPA treatment (Fig. 3 F). Moreover, the auxin-specific asymmetric pattern in the hook was observed after FluorA II treatment also in Lansberg (Ler) WT (Fig. 3 G). In contrast with the situation in the primary root, the uptake of FluorA II in the transport mutant *aux1lax1lax2* was significantly decreased (Fig. 3 G). On the other hand, *pin3pin4pin7* mutant in Col-0/Ler background displayed a strong accumulation of FluorA II in the epidermis on both sides of the hypocotyl (Fig. 3 G), suggesting that PINs play an important role for the further distribution of FluorA II. Overall, the obtained data indicated that the tissue distribution of both FluorA I and II is, aside from simple diffusion, also regulated by the active auxin transport system.

High spatial resolution of FluorA imaging enables the study of subcellular auxin localization

A huge advantage of fluorescently labeled hormones is the high spatiotemporal resolution of their distribution. Whereas other commonly used methods usually provide qualitative information about hormone distribution with an organ/tissue-level resolution, visualization of small fluorescent molecules in real time is possible even at the subcellular level in a minimally invasive manner (46). To investigate the distribution of FluorA I and II compounds at the level of individual organelles, several *Arabidopsis* marker lines were examined for the co-localization of the FluorA NBD signal with the fluorescent label of the respective organelle. Quantification based on Pearson's correlation coefficient showed similar co-localization rates of FluorA I and FluorA II with the cyan fluorescent protein (CFP)-tagged trafficking marker SYNTAXIN OF PLANTS 61 (*pSYP61::SYP61-CFP*) (Fig. 4 A). In addition, both of the chemicals, but especially FluorA II, showed higher co-localization of the NBD signal with the SYP61 marker after treatment with the endomembrane trafficking inhibitor brefeldin A (BFA) (Fig. 4

B). These results confirm that the FluorA compounds localize to the endosomes within the endomembrane trafficking system of the cells. Moreover, the FluorA signals co-localized well with the p24 δ 5-RFP signal of an ER marker line, showing that both FluorA I and FluorA II localize to the ER, with a higher preference for FluorA II (Fig. 4 C). The presence of FluorA compounds was not observed in the cell nucleus under our experimental conditions, as there was no co-localization of the FluorAs with the fluorescent signals of a *p35S::H2B-mCherry* marker, in which the DNA regions of condensed heterochromatin are labeled (Fig. 4 D). Taken together, these data confirm the high spatial resolution of our fluorescent labeling approach. Hence, our compounds can serve as useful research tools to track the dynamics of the transport and distribution of auxins, not only within different tissues, but also at the subcellular level.

Live imaging of FluorA distribution in auxin-mediated developmental processes

PAT also plays an important role in auxin tissue-specific redistribution as a response to different kinds of stimuli such as gravistimulation or light (9). We therefore investigated whether these environmental signals affect FluorA I and II distribution. It is known that gravistimulation promotes asymmetric distribution of auxin in roots and their bending in the direction of gravity (48). In agreement with this, the gravistimulated roots of *Arabidopsis* Col-0 WT treated with FluorA I displayed an uneven distribution of fluorescence, with a stronger signal on the lower side of the root (Fig. 5 A), while the negative control FluorA XI did not show this effect (Fig. S5 F). In addition, it has been shown that the accumulation of auxin in apical hook can be disrupted by light, leading to apical hook opening (49). In order to test whether FluorA compound distribution was also sensitive to an external light signal, etiolated Col-0 WT seedlings with established fluorescent maxima of FluorA II on the concave side of the apical hook were transferred to standard light conditions and scanned at different time-points. This light stimulation led to the redistribution of the fluorescent signal and loss of accumulation at the concave side of the hook (Fig. 5 B). The consistent fluorescence signal in the roots in the same time-points confirmed that the loss of accumulation was tissue-specific, and not due to light-stimulated degradation of FluorA II (Fig. S6). Moreover, FluorA II displayed the changes in distribution in longer time period without any light impulse (Fig. 5 C).

Overall, our data show that the fluorescently labeled auxin analogues FluorA I and FluorA II can be used as probes for visualization of auxin sites of action and auxin redistribution patterns during different developmental processes such as gravistimulation-induced root bending or light-induced apical hook opening.

Discussion

Recently, an extensive interest in imaging of signaling molecules has developed in the plant biology field (46). Fluorescent versions of native and synthetic auxins, resulting in both fluorescently labeled (50–52) and caged

auxins (53–55) have been reported and used for various purposes (50–55). The first attempt to label auxin for live imaging was performed by Sokołowska et al. (51). N1 substitution of IAA was utilized for conjugation with fluorescein isothiocyanate (FITC) or rhodamine isothiocyanate (RITC) using a simple synthetic procedure. Both conjugates were shown to maintain auxin biological activity on oat coleoptiles and *Arabidopsis* roots as well as the native auxin distribution pattern in the latter. However, the stability of the compounds *in vivo* and its link with the auxin effects *in planta* was not discussed. On the contrary, Hayashi et al. (52) argued that elevated auxin concentrations would induce changes in auxin metabolism, such as an increase in GRETCHEN HAGEN 3 (GH3) auxin-inactivating enzymes (56) and altered localization of PIN transporters (57) and thus the exogenous application of active fluorescent analogues would no longer mimic native auxin distribution. The authors therefore employed a synthetic strategy using benzyl-auxin analogues of IAA and NAA, which appeared to be recognized by auxin transporters but not by auxin receptors (58). They focused on the preparation of two conjugates of IAA and NAA with NBD, which are active within the auxin transport system but inactive within auxin signaling (52).

Here we present fluorescent auxin analogues derived from 2,4-D and labeled with NBD using two different linkers, which are attached via the side chain carboxyl group of the 2,4-D with amide bond. Our concurrent study (40) presenting structures similar to FluorA compounds, being 2,4-D and 2,4,5-T derivatives bearing the same PIP linker and aliphatic linker similar to EDA, showed these structures to be sterically favorable for the binding to the TIR1-AUX/IAA7 co-receptor system (40). Moreover, the extensive SPR analysis revealed that various auxin agonists, including set of chlorinated auxin derivatives, can differently stabilize the co-receptor system depending on the F-box-AUX/IAA partners (59). Despite these facts, the same SPR study revealed that none of the FluorA compounds bind to the TIR1 receptor *in vitro*. This was confirmed *in vivo* by treatment of *p35S::DII-Venus* seedlings, when the exogenous application of 2,4-D equivalent to amount from FluorA metabolism promoted the similar response as FluorA treatment.

The presented fluorescent analogues FluorA I and FluorA II were mainly designed as tools for direct visualization of auxin distribution *in planta*. Using both pharmacological and genetic approaches to study the transport mechanisms of these compounds revealed that both of the FluorAs, to a greater extent than free 2,4-D, are able to bypass active auxin uptake into the cells due to the contribution of passive diffusion. It can be rationalized that attaching the linker-NBD hydrophobic moiety (60, 61) to the hydrophilic carboxyl group of 2,4-D significantly increases the hydrophobicity of the molecules, especially in the case of FluorA II, and thus improves their transport across the lipid membranes. The further distribution of the compounds is proposed to be driven by mechanisms of active auxin transport. The increased fluorescence intensity of the FluorAs after NPA treatment is consistent with recent findings that 2,4-D is also a substrate for PIN and ABCB transporters (27, 28). On the contrary, POA-derived FluorA XI was not effectively taken up into the roots of Col-0. This corresponds with the fact that unsubstituted phenoxyacetic acid has a low lipid solubility, while two chlorine

atoms increase this solubility and thus greatly support the uptake of 2,4-D derivatives (62). Furthermore, the PIP-NBD substructure lacking the 2,4-D part displayed no signal in the roots, confirming the 2,4-D moiety to be crucial for the uptake of the compounds into the plant.

In planta, the fluorescent 2,4-D conjugates mimicked the auxin-like asymmetric distribution known to occur in *Arabidopsis* roots and shoots (63, 64). The transport of auxin in lateral root primordia and young developing roots is an efflux-dependent process involving major roles of PIN1, ABCB1 and ABCB19 (15), while the generation of auxin gradients in gravistimulated roots is driven mainly by PIN2 (65) and PIN3 (66) carriers. More specifically, 2,4-D has been shown to be preferentially transported by PIN2, PIN7, ABCB1 and ABCB19 (27, 28). The observed localization of FluorAs in *Arabidopsis* roots suggests that these compounds are also actively transported by PIN and ABCB auxin carriers. Surprisingly, since the passive diffusion was shown to also contribute to the FluorA transport in the root, the distribution was thus more similar to that of native auxin than that of free 2,4-D. This observation confirms the different physical and chemical properties of FluorAs compared to 2,4-D.

The formation of the apical hook depends on asymmetric auxin distribution coordinated by the PIN1, 3, 4 and 7 auxin efflux carriers (66). Light-stimulated redistribution (49) as well as passive diffusion of IAA away from the concave side of the hook (67) then leads to apical hook opening. In this developmental process, FluorA II displayed auxin-like distribution with the concentration maxima on the concave side of the hook. Moreover, since it was shown that PIN3, 4 and 7 are expressed in the epidermis of the hypocotyl during maintenance phase of hook development (67), our observations of FluorA II strongly accumulated in this region is in agreement with this study, suggesting PINs are required for FluorA II to be further distributed. Besides the PIN transporters, the auxin influx carriers AUX1 and LAX3 also play an important role in apical hook development (68). Although our results suggest that FluorA I and II are not primarily transported in the roots by the AUX and LAX influx carriers, the opposite situation was observed in the apical hook. The uptake of FluorA II was abolished in *aux1lax1lax2* mutant proposing the impact of active auxin influx on distribution of FluorA II in the shoots. Since comparing the distinct mode of FluorA II distribution in the root of *aux1lax3* mutant and in the hook of *aux1lax1lax2* mutant, the differences can be discussed to be tissue-specific or FluorA II can represent a preferential substrate for specific influx carriers. Even it can be the combination of both, which must be further studied in more detail.

We also confirmed the localization of FluorA compounds in specific organelles of root cells, showing that both FluorA I and FluorA II are suitable for studies of auxin distribution at the subcellular level. In agreement with previously reported works (47, 52), the fluorescent 2,4-D analogues were present in the ER but not in the nucleus, showing the important role of the ER in the regulation of nuclear auxin uptake (47). Additionally, we revealed the presence of FluorAs in endosomes.

To conclude, although both FluorA I and II – fluorescent conjugates of 2,4-D with NBD - were shown to be inactive for auxin signaling, they mimicked the auxin distribution patterns known to occur *in planta* in distinct developmental processes. The structural modification of the 2,4-D molecule altered the behavior of the compounds compared to free 2,4-D. Thus, despite being 2,4-D derivatives, FluorA compounds were able to bypass active auxin influx mechanisms by passive diffusion similarly to IAA, and moreover they also appeared to be efficiently distributed via the auxin transport system with similar tissue-specific preferences as native auxin. As low molecular mass compounds, FluorAs provided a subcellular resolution of visualization, making them a valuable tool for following subcellular auxin gradients and studies of mechanisms for maintaining auxin intracellular homeostasis. Taken together, the presented fluorescent 2,4-D compounds represent a convenient research toolset to visualize and study the relationship between auxin action and localization *in planta* at both tissue and subcellular levels.

Materials and Methods

For synthesis of FluorA compounds, plant materials and growth conditions, stability measurements, auxin bioassays and microscopic analyses, see SI Materials and Methods.

ACKNOWLEDGMENTS. We greatly thank Dolf Weijers and Che-Yang Liao for sharing the *pDR5v2::Venus* marker line seeds before they were published. We are thankful to Ota Blahoušek for technical assistance with editing of figures and Tomáš Pospíšil for providing stable isotope labeled precursors for synthesis of internal FluorA standards. We also gratefully acknowledge Samsa M. Doyle for critical reading and English correction of the manuscript. This work was supported by the Internal Grant Agency of Palacký University (IGA_PrF_2019_020), by the Ministry of Education, Youth and Sports of the Czech Republic through the European Regional Development Fund-Project ‘Plants as a tool for sustainable global development’ (CZ.02.1.01/0.0/0.0/16_019/0000827), by Vetenskapsrådet and VINNOVA (Verket för Innovationssystemet to T.V., S.R.) and Knut och Alice Wallenbergs Stiftelse via “Shapesystem” grant number 2012.0050 (S.R.), Kempestiftelserna (P.G.), The Carl Tryggers foundation (P.G.) and the Swedish Research Council grant number VR2016-00768 (P.G.), the Olle Engkvist Byggmästare Foundation (S. Ra.), B.P. was partially supported by the Endowment Fund of Palacký University in Olomouc.

References

1. Enders TA, Strader LC (2016) Auxin Activity: Past, present, and Future. *Am J Bot* 102(January 2015):180–196.
2. Ljung K (2013) Auxin metabolism and homeostasis during plant development. *Development* 140(5):943–

950.

3. Sauer M, Robert S, Kleine-Vehn J (2013) Auxin: simply complicated. *J Exp Bot* 64(9):2565–2577.
4. Vanneste S, Friml J (2009) Auxin: A Trigger for Change in Plant Development. *Cell* 136(6):1005–1016.
5. Simon S, Petrášek J (2010) Why plants need more than one type of auxin. *Plant Sci* 180:454–460.
6. Ma Q, Robert S (2014) Auxin biology revealed by small molecules. *Physiol Plant* 151(1):25–42.
7. Woodward AW, Bartel B (2005) Auxin: Regulation, action, and interaction. *Ann Bot* 95(5):707–735.
8. Vieten A, Sauer M, Brewer PB, Friml J (2007) Molecular and cellular aspects of auxin-transport-mediated development. *Trends Plant Sci* 12(4):160–168.
9. Adamowski M, Friml J (2015) PIN-Dependent Auxin Transport: Action, Regulation, and Evolution. *Plant Cell* 27(1):20–32.
10. Lomax TL, Muday GK, Rubery PH (1995) Auxin Transport. *Plant Hormones* (Springer Netherlands, Dordrecht), pp 509–530.
11. Grones P, Friml J (2015) Auxin transporters and binding proteins at a glance. *J Cell Sci* 128(1):1–7.
12. Bennett MJ, et al. (1996) Arabidopsis AUX1 Gene: A Permease-Like Regulator of Root Gravitropism. *Science* (80-) 273(5277).
13. Péret B, et al. (2012) AUX/LAX genes encode a family of auxin influx transporters that perform distinct functions during Arabidopsis development. *Plant Cell* 24(7):2874–85.
14. Geisler M, Murphy AS (2006) The ABC of auxin transport: The role of p-glycoproteins in plant development. *FEBS Lett* 580(4):1094–1102.
15. Zažímalová E, Murphy AS, Yang H, Hoyerova K, Hosek P (2010) Auxin Transporters — Why So Many ? *Cold Spring Harb Perspect Biol* 2(3):1–14.
16. Mitchison G (2015) The Shape of an Auxin Pulse, and What It Tells Us about the Transport Mechanism. *PLoS Comput Biol* 11(10):e1004487.
17. Kubeš M, et al. (2012) The Arabidopsis concentration-dependent influx/efflux transporter ABCB4 regulates cellular auxin levels in the root epidermis. *Plant J* 69(4):640–654.
18. Kamimoto Y, et al. (2012) Arabidopsis ABCB21 is a Facultative Auxin Importer/Exporter Regulated by Cytoplasmic Auxin Concentration. *Plant Cell Physiol* 53(12):2090–2100.
19. Barbez E, et al. (2012) A novel putative auxin carrier family regulates intracellular auxin homeostasis in plants. *Nature* 485(7396):119–122.
20. Ranocha P, et al. (2013) Arabidopsis WAT1 is a vacuolar auxin transport facilitator required for auxin homeostasis. *Nat Commun* 4:2625.
21. Lewis DR, Muday GK (2009) Measurement of auxin transport in Arabidopsis thaliana. *Nat Protoc* 4(4):437–51.
22. Delbarre A, Muller P, Imhoff V, Guern J (1996) Comparison of mechanisms controlling uptake and

accumulation of 2,4-dichlorophenoxy acetic acid, naphthalene-1-acetic acid, and indole-3-acetic acid in suspension-cultured tobacco cells. *Planta* 198(4):532–541.

23. Swarup K, et al. (2008) The auxin influx carrier LAX3 promotes lateral root emergence. *Nat Cell Biol* 10(8):946–954.
24. Yang Y, Hammes UZ, Taylor CG, Schachtman DP, Nielsen E (2006) High-Affinity Auxin Transport by the AUX1 Influx Carrier Protein. *Curr Biol* 16:1123–1127.
25. Hoyerova K, et al. (2017) Auxin molecular field maps define AUX1 selectivity: many auxin herbicides are not substrates. *New Phytol*. doi:10.1111/nph.14950.
26. Petrášek J, et al. (2006) PIN proteins perform a rate-limiting function in cellular auxin efflux. *Science* 312(5775):914–8.
27. Hošek P, et al. (2012) Auxin transport at cellular level: new insights supported by mathematical modelling. *J Exp Bot* 63(10):3815–3827.
28. Yang H, Murphy AS (2009) Functional expression and characterization of Arabidopsis ABCB, AUX 1 and PIN auxin transporters in *Schizosaccharomyces pombe*. *Plant J* 59(1):179–191.
29. Cho M, Lee SH, Cho H-T (2007) P-Glycoprotein4 Displays Auxin Efflux Transporter-Like Action in Arabidopsis Root Hair Cells and Tobacco Cells. *Plant Cell* 19:3930–3943.
30. Lavy M, Estelle M (2016) Mechanisms of auxin signaling. *Development* 143(18):3226–3229.
31. Calderon-Villalobos LI, Tan X, Zheng N, Estelle M (2010) Auxin Perception—Structural Insights. *Cold Spring Harb Perspect Biol* 2:a005546.
32. Parry G, et al. (2009) Complex regulation of the TIR1/AFB family of auxin receptors. *Proc Natl Acad Sci USA* 106(52):22540–5.
33. Pařízková B, Pernisová M, Novák O (2017) What has been seen cannot be unseen – detecting auxin in vivo. (iii):1–26.
34. Tan X, et al. (2007) Mechanism of auxin perception by the TIR1 ubiquitin ligase. *Nature* 446(7136):640–645.
35. Brunoud G, et al. (2012) A novel sensor to map auxin response and distribution at high spatio-temporal resolution. *Nature* 482(7383):103–106.
36. Seifertová D, et al. (2014) Characterization of transmembrane auxin transport in Arabidopsis suspension-cultured cells. *J Plant Physiol* 171:429–437.
37. Grossmann K (2009) Auxin herbicides: current status of mechanism and mode of action. *Pest Manag Sci* 66(2): 113–120.
38. Kaethner TM (1977) Conformational change theory for auxin structure-activity relationships. *Nature* 267:19–23.
39. Farrimond JA, Elliott MC, Clack DW (1978) Charge separation as a component of the structural

requirements for hormone activity. *Nature* 274(5669):401–402.

40. Vain T, et al. (2019) Selective auxin agonists induce specific AUX/IAA protein degradation to modulate plant development. *Proc Natl Acad Sci USA* 116(13):6463–6472.
41. Weijers D, et al. (2005) Developmental specificity of auxin response by pairs of ARF and Aux/IAA transcriptional regulators. *EMBO J* 24(10):1874–85.
42. Oono Y, Chen QG, Overvoorde PJ, Köhler C, Theologis A (1998) age Mutants of Arabidopsis exhibit altered auxin-regulated gene expression. *Plant Cell* 10(10):1649–62.
43. Dharmasiri N, Dharmasiri S, Estelle M (2005) The F-box protein TIR1 is an auxin receptor. *Nature* 435(May):441–445.
44. Kepinski S, Leyser O (2005) The Arabidopsis F-box protein TIR1 is an auxin receptor. *Nature* 435(7041):446–451.
45. Himanen K, et al. (2002) Auxin-Mediated Cell Cycle Activation during Early Lateral Root Initiation. *Society* 14(October):2339–2351.
46. Lace B, Prandi C (2016) Shaping Small Bioactive Molecules to Untangle Their Biological Function : A Focus on Fluorescent Plant Hormones. *Mol Plant* 9(8):1099–1118.
47. Middleton AM, et al. (2018) Data-Driven Modeling of Intracellular Auxin Fluxes Indicates a Dominant Role of the ER in Controlling Nuclear Auxin Uptake. *Cell Rep* 22:3044–3057.
48. Friml J, Wiśniewska J, Benková E, Mendgen K, Palme K (2002) Lateral relocation of auxin efflux regulator PIN3 mediates tropism in Arabidopsis. *Nature* 415(6873):806–809.
49. Liscum E, Hangarter RP (1993) Light-Stimulated Apical Hook Opening in Wild-Type Arabidopsis thaliana Seedlings. *Plant Physiol* 101(2):567–572.
50. Muscolo A, Sidari M, Francioso O, Tugnoli V, Nardi S (2007) The auxin-like activity of humic substances is related to membrane interactions in carrot cell cultures. *J Chem Ecol* 33(1):115–129.
51. Sokołowska K, Kizińska J, Szewczuk Z, Banasiak A (2014) Auxin conjugated to fluorescent dyes - a tool for the analysis of auxin transport pathways. *Plant Biol* 16(5):866–877.
52. Hayashi K -i., et al. (2014) Auxin transport sites are visualized in planta using fluorescent auxin analogs. *Proc Natl Acad Sci USA* 111(31):1–6.
53. Atta S, Jana A, Ananthakirshnan R, Narayana Dhuleep PS (2010) Fluorescent Caged Compounds of 2,4-Dichlorophenoxyacetic Acid (2,4-D): Photorelease Technology for Controlled Release of 2,4-D. *J Agric Food Chem* 58(22):11844–11851.
54. Atta S, et al. (2013) Photoremovable protecting groups as controlled-release device for sex pheromone. *Photochem Photobiol Sci* 12(2):393–403.
55. Atta S, et al. (2015) Nano-pesticide formulation based on fluorescent organic photoresponsive nanoparticles: for controlled release of 2,4-D and real time monitoring of morphological changes induced

by 2,4-D in plant systems. *RSC Adv* 5(106):86990–86996.

56. Ludwig-Müller J (2011) Auxin conjugates: their role for plant development and in the evolution of land plants. *J Exp Bot* 62(6):1757–1773.
57. Petrasek J, Friml J (2009) Auxin transport routes in plant development. *Development* 136(16):2675–2688.
58. Tsuda E, et al. (2011) Alkoxy-auxins are selective inhibitors of auxin transport mediated by PIN, ABCB, and AUX1 transporters. *J Biol Chem* 286(3):2354–2364.
59. Lee S, et al. (2014) Defining binding efficiency and specificity of auxins for SCF(TIR1/AFB)-Aux/IAA co-receptor complex formation. *ACS Chem Biol* 9(3):673–682.
60. Bertorelle F, Dondon R, Fery-Forgues S (2002) Compared Behavior of Hydrophobic Fluorescent NBD Probes in Micelles and in Cyclodextrins. *J Fluoresc* 12(2):205–207.
61. Santa T, Matsumura D, Huang CZ, Kitada C, Imai K (2002) Design and synthesis of a hydrophilic fluorescent derivatization reagent for carboxylic acids, 4-N-(4-N-aminoethyl)piperazino-7-nitro-2,1,3-benzoxadiazole (NBD-PZ-NH₂), and its application to capillary electrophoresis with laser-induced fluorescence detec. *Biomed Chromatogr* 16(8):523–528.
62. Thimann Kenneth Vivian (1977) *Hormone Action in the Whole Life of Plants* Available at: <https://books.google.cz/books?id=n6RiTBhbUOcC&pg=PA230&dq=phenoxyacetic+acid+auxin&hl=cs&sa=X&ved=0ahUKEwjfSL7IzOjTAhVKb5oKHUdIDIsQ6AEILjAB#v=onepage&q=phenoxyacetic acid auxin&f=false> [Accessed May 11, 2017].
63. Friml J (2003) Auxin transport—shaping the plant. *Curr Opin Plant Biol*:7–12.
64. Benková E, et al. (2003) Local, Efflux-Dependent Auxin Gradients as a Common Module for Plant Organ Formation. *Cell* 115(5):591–602.
65. Rahman A, et al. (2010) Gravitropism of Arabidopsis thaliana roots requires the polarization of PIN2 toward the root tip in meristematic cortical cells. *Plant Cell* 22(June):1762–1776.
66. Friml J, Wiśniewska J, Benková E, Mendgen K, Palme K (2002) Lateral relocation of auxin efflux regulator PIN3 mediates tropism in Arabidopsis. *Nature* 415(6873):806–809.
67. Zadnikova P, et al. (2010) Role of PIN-mediated auxin efflux in apical hook development of Arabidopsis thaliana. *Development* 137(4):607–617.
68. Vandenbussche F, et al. (2010) The auxin influx carriers AUX1 and LAX3 are involved in auxin-ethylene interactions during apical hook development in Arabidopsis thaliana seedlings. *Development* 137(4):597–606.

Figures

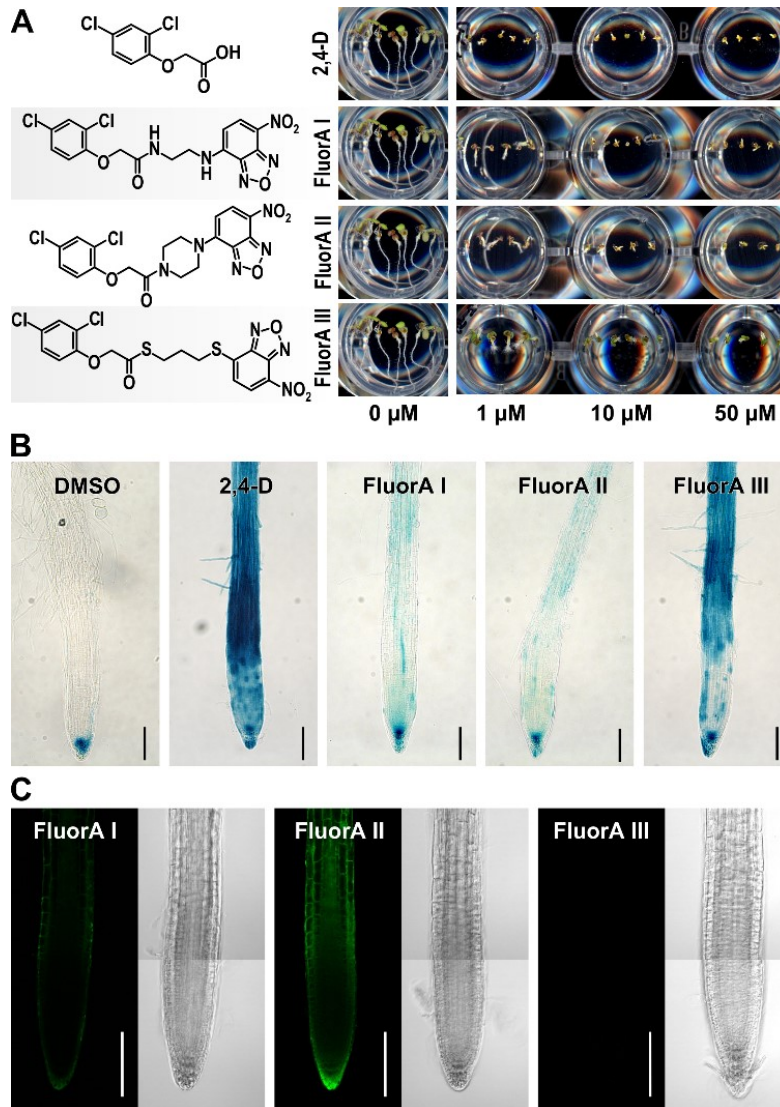


Fig. 1. FluorA screening strategy. The two best candidate compounds were chosen based on their biological activity (A-B) and fluorescent properties (C). (A) Seedlings of *Arabidopsis* Col-0 WT were grown in the presence of 2,4-D or FluorA compounds (1, 10, 50 μM) or DMSO only (0 μM). After 5 days, their effect on primary root growth was evaluated. (B) Five-day-old seedlings of *Arabidopsis pDR5::GUS* marker line were treated with DMSO and 2,4-D or FluorA compounds at 10 μM for 5 h. The expression of *DR5* in the primary root was then assessed by GUS staining. (C) Seedlings of *Arabidopsis* Col-0 WT were incubated in liquid ½ MS media with 2 μM FluorAs for 15 min. The quality of fluorescent signal was visualized with confocal settings optimized for FluorA II. (B-C) Scale bars represent 100 μm.

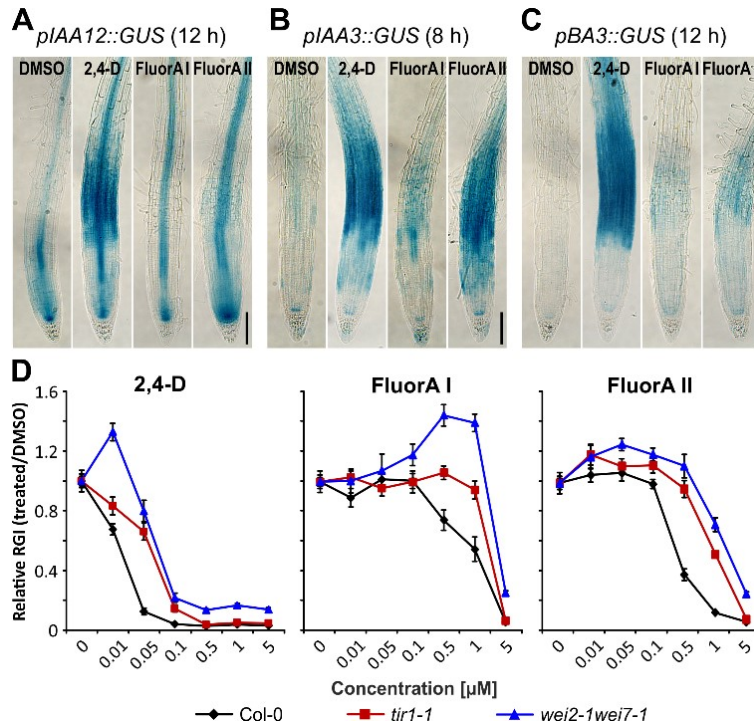


Fig. 2. FluorAs are involved in auxin responses via the TIR1 signaling pathway. (A-C) Five-day-old seedlings of different *Arabidopsis* reporter lines were treated with DMSO or 10 μ M 2,4-D and FluorA compounds for the indicated periods of time. Expression of the *pIAA12* (A), *pIAA3* (B) and *pBA3* (C) auxin-sensitive promoters was evaluated by GUS staining. (D) Seedlings of *Arabidopsis tir1-1* and *wei2-1wei7-1* mutant lines grown in the presence of 2,4-D or FluorAs at defined final concentrations (0-5 μ M). After 5 days, the primary root length was quantified relative to DMSO-treated seedlings and plotted as relative root growth inhibition (RGI). Scale bars represent 100 μ m; values are means \pm SE, n = 10.

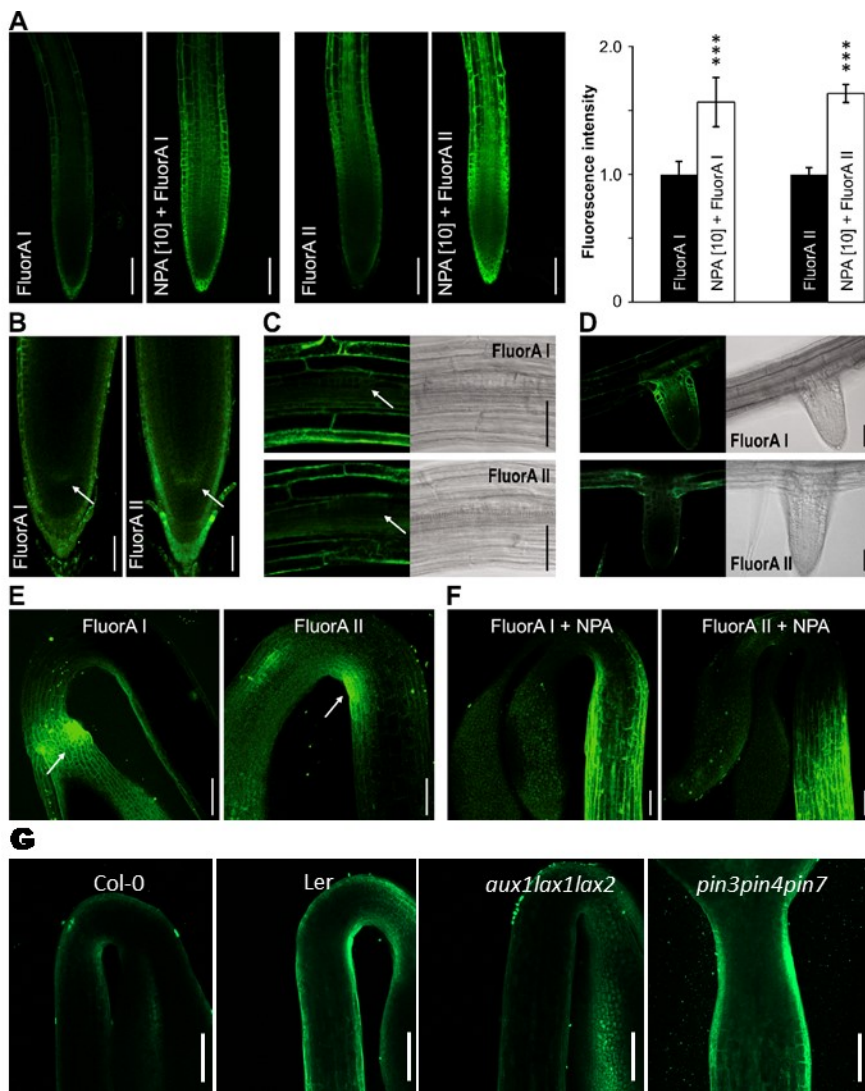


Fig. 3. Distribution of FluorAs *in planta*. (A) Five-day-old seedlings of *Arabidopsis* Col-0 WT were treated with FluorA compounds at 2 μ M for 15 min with or without 10 μ M NPA pre-treatment for 3 h. The intensity of the FluorA fluorescence in roots was then quantified and expressed relative to non-NPA-treated plants. (B) Five-day-old seedlings of *Arabidopsis* Col-0 WT were incubated with 2 μ M FluorAs for 15 min and then transferred on non-treated solid media. After 3 h both FluorA I and FluorA II established concentration maxima in the quiescent centre. The arrows indicate QC centre. (C-D) The presence of FluorAs in lateral root primordia (C) and emerged lateral roots (D) of 5-day-old *Arabidopsis* Col-0 WT seedlings after 15 min treatment at 2 μ M. The arrows indicate lateral root initiation sites. (E) FluorA I accumulated at the base of the cotyledons while FluorA II accumulated in the inner apical hook of 3-day-old dark-grown *Arabidopsis* Col-0 WT seedlings after 15 min treatment at 2 μ M. The arrows indicate tissue-specific accumulation of FluorAs in the hypocotyl. (F) 10 μ M NPA pre-treatment for 3 hours disturbed the localization of FluorA I in cotyledons and FluorA II in apical hooks of 3-day-old dark-grown *Arabidopsis* Col-0 WT seedlings. (G) 2 μ M FluorA II displayed the asymmetric distribution in both Col-0 and Ler WT. The accumulation was completely abolished in *aux1lax1lax2* mutant while *pin3pin4pin7* mutant exhibited significant increase of fluorescent signal in the epidermis of the hypocotyl. (A) Statistical analyses were performed using the Student's *t*-test (values are means \pm SE; $n = 30$ from 3 independent biological replicates; p -values: *** $P < 0.001$). (B-D) Frequency of seedlings showing the specific accumulation was $\sim 50\%$ (E-F) Frequency of seedlings showing the specific accumulation was $\sim 80\%$. (G) Only one biological replicate was performed. (A,C-G) Scale bars represent 100 μ m; (B) scale bars represent 50 μ m.

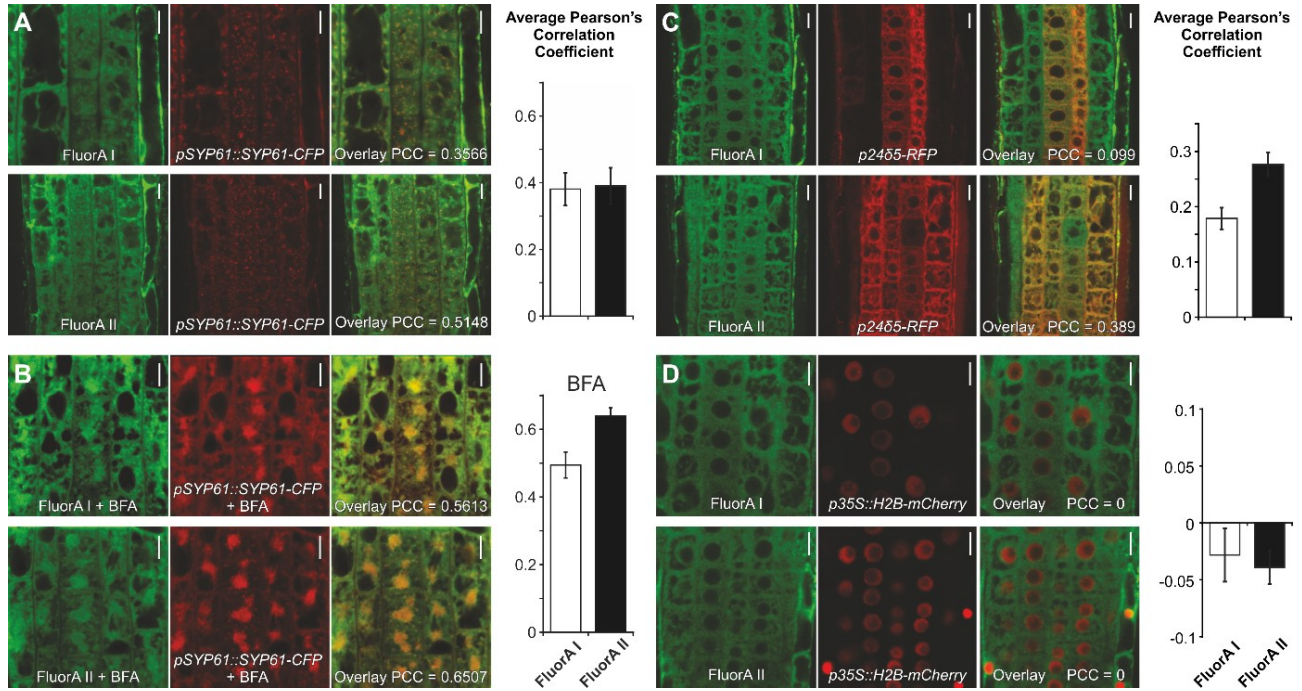


Fig. 4. Subcellular localization of FluorAs. Confocal images of root meristem cells of five-day-old *Arabidopsis* seedlings expressing specific organelle markers, treated with 2 μ M FluorA compounds for 15 min. FluorA localization in endosomes (A-B) without (A) and with (B) treatment of 25 μ M BFA for 90 min, and in ER (C) and nuclei (D) was evaluated based on co-localization of NBD fluorescence signal with $pSYP61::SYP61-CFP$ (A-B), $p24\delta5-RFP$ (C) and $p35S::H2B-mCherry$ (D) marker fluorescence using Pearson's Correlation Coefficient (PCC). Values are means \pm SE, $n = 30$ from 3 independent biological replicates. Scale bars represent 10 μ m.

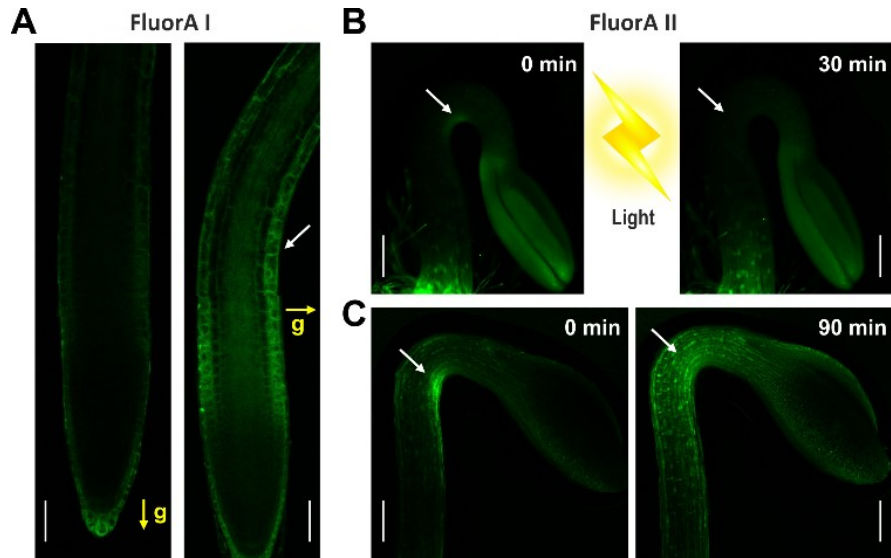


Fig. 5. Distribution of FluorAs in response to auxin-responsive external stimuli. Confocal (A) and a vertical macroconfocal (B-C) images. (A) Roots of five-day-old seedlings of *Arabidopsis* Col-0 WT were gravistimulated for 40 min (g, yellow arrow) and then treated with 2 μ M FluorA I for 15 min. (B-C) Three-day-old dark-grown seedlings of *Arabidopsis* Col-0 WT treated with 2 μ M FluorA II for 15 min. The accumulation of FluorA II in the apical hook was evaluated before (0 min) and 30 min after (B) or without (C) a light stimulus. (A) Frequency of seedlings showing the specific accumulation was ~ 60 %. (B-C). Frequency of seedlings showing the specific accumulation was ~ 80 %. (A) Scale bars represent 100 μ m; (B-C) scale bars represent 1 mm. The white arrows indicate tissue-specific accumulation of FluorAs in gravistimulated root (A) or inner apical hook and its redistribution from the hook zone (B-C).

Supporting Information

SI Materials and Methods

1. Synthesis of FluorA compounds.

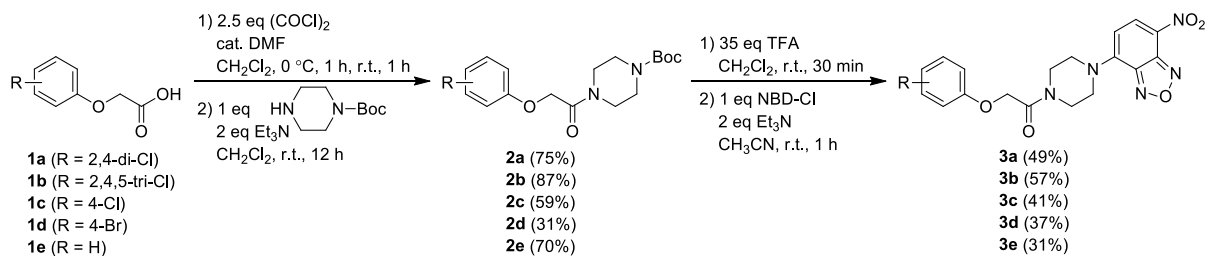
1.1. General methods

Reagents and solvents were purchased from common commercial suppliers and used without further purification. Dichloromethane and acetonitrile were distilled from calcium hydride, while dimethylformamide was dried over molecular sieves before use. The conversion of starting materials was monitored by thin layer chromatography (TLC) on aluminium plates coated with silica gel 60 F254 (Merck, USA) and the components were visualized by UV light (254 and 365 nm) and staining solutions (ninhydrin and potassium permanganate). The purification of the reaction mixtures was performed by column chromatography on silica gel (40-63 micron Davisil LC60A, Grace Davison, UK). ^1H (500 MHz) and ^{13}C (126 MHz) NMR spectra were recorded at room temperature (Jeol ECA-500 NMR, Japan) in deuterated solvents (CDCl_3 or $\text{DMSO}-d_6$) as indicated for each compound. Peak assignments were elucidated *via* APT and HMQC techniques when necessary. The chromatographic purity and mass spectra of the prepared compounds were analyzed using high performance liquid chromatography–photodiode array–mass spectrometry (HPLC–PDA–MS) method. Compounds ($10\ \mu\text{L}$ of $3.10^{-5}\ \text{M}$ in 0.01% DMSO) were injected onto a reverse-phased column (Symmetry C18, $5\ \mu\text{m}$, $150\ \text{mm} \times 2.1\ \text{mm}$; Waters, Milford, MA, USA) equilibrated at $25\ ^\circ\text{C}$ with solvent (A), which consisted of 15 mM ammonium formate adjusted to pH 4.0 and solvent (B), which consisted of methanol. At a flow-rate of $200\ \mu\text{L}/\text{min}$, the following binary gradient was used: 0 min, 10% B; 0-24 min, linear gradient to 90% B; 25-34 min, isocratic elution of 90% B; 35-45 min, linear gradient to 10% B using an Alliance 2695 Separations Module (Waters, Milford, MA, USA). The effluent was then introduced to a 2996 PDA detector (Waters, Milford, MA, USA) (scanning range 210-700 nm with 1.2 nm resolution) and a tandem mass analyser Q-ToF micro Mass Spectrometer (Waters, Manchester, UK) with an electrospray source (source temperature $120\ ^\circ\text{C}$, desolvation temperature $300\ ^\circ\text{C}$, capillary voltage 3 kV). Nitrogen was used as well as cone gas ($50\ \text{l}/\text{h}$) and desolvation gas ($500\ \text{l}/\text{h}$). Data acquisition was performed in the full scan mode (50-1000 Da), with scan time of 0.5 s and cone voltage 20 V. Analyses were performed in positive (ESI+) and negative (ESI-) mode and molecular ions were recorded in $[\text{M}+\text{H}]^+$ and $[\text{M}-\text{H}]^-$ or $[\text{M}+\text{HCOOH}-\text{H}]^-$, forms, respectively.

1.2. General procedure for the synthesis of 2a-e and 3a-e (Scheme 1).

Synthesis of *tert*-butyl 4-(2-(2,4-dichlorophenoxy)acetyl)piperazine-1-carboxylate (**2a**) is representative. 2,4-D (**1a**; 441 mg, 2 mmol) was dissolved in anhydrous dichloromethane (20 mL) and cooled down to $0\ ^\circ\text{C}$. Subsequently, dimethylformamide (30 μL) and oxalyl chloride (0.43 mL, 5 mmol) were added drop-wise with vigorous stirring and the resulting reaction mixture was stirred at $0\ ^\circ\text{C}$ for 1 hour and then at room temperature for the next 1 hour. Evaporation of the solvent under reduced pressure in a cold water bath afforded intermediate 2-(2,4-dichlorophenoxy)acetyl chloride in a quantitative yield, which was used in the next step without further purification or characterization. The residual crude 2-(2,4-dichlorophenoxy)acetyl chloride was dissolved in anhydrous dichloromethane (10 mL) and cooled down to $0\ ^\circ\text{C}$. Subsequently, triethylamine (0.56 mL, 4 mmol) was added drop-wise, followed by *tert*-butyl piperazine-1-carboxylate (1-Boc-piperazine) (372 mg, 2 mmol), allowed to warm up to room temperature and the resulting reaction mixture was stirred for 12 h. Upon completion, the reaction mixture was cooled down to $0\ ^\circ\text{C}$, quenched with water (10 mL) and extracted with ethyl acetate ($3 \times 20\ \text{mL}$). Combined organic fractions were washed with water (10 mL) and brine (10 mL), dried over anhydrous sodium sulphate, filtered and concentrated under reduced pressure. Purification of the residue by flash chromatography on silica gel afforded compound **2a**.

Synthesis of *tert*-butyl 2-(2,4-dichlorophenoxy)-1-(4-(7-nitrobenzo[*c*][1,2,5]oxadiazol-4-yl)piperazin-1-yl)ethanone (**3a**, FluorA II) is representative. Compound **2a** (129 mg, 0.33 mmol) was dissolved in anhydrous dichloromethane (4 mL) and cooled down to 0 °C. Subsequently, trifluoroacetic acid (0.825 mL) was added drop-wise with vigorous stirring, the reaction mixture was allowed to warm up to room temperature and the resulting reaction mixture was stirred for 30 minutes at room temperature. Subsequently, the reaction mixture was cooled down to 0 °C, quenched with saturated aqueous sodium bicarbonate solution (to pH = 7) and extracted with ethyl acetate (3 × 20 mL). Combined organic fractions were washed with water (10 mL) and brine (10 mL), dried over anhydrous sodium sulphate, filtered and concentrated under reduced pressure to afford intermediate 2-(2,4-dichlorophenoxy)-1-(piperazin-1-yl)ethanone in a quantitative yield, which was used in the next step without further purification or characterization. The residual 2-(2,4-dichlorophenoxy)-1-(piperazin-1-yl)ethanone was dissolved in acetonitrile (7 mL), to which triethylamine (92 μL, 0.66 mmol) was added drop-wise, followed by 4-chloro-7-nitrobenzofurazan, NBD-Cl (66 mg, 0.33 mmol) at 0 °C. The reaction mixture was stirred at room temperature for 1 hour. The reaction mixture was quenched with saturated ammonium chloride solution (10 mL) and extracted with ethyl acetate (3 × 20 mL). Combined organic fractions were washed with water (10 mL) and brine (10 mL), dried over anhydrous sodium sulphate, filtered and concentrated under reduced pressure. Purification of the residue by flash chromatography on silica gel afforded compound **3a**.



Scheme I

tert-Butyl 4-(2-(2,4-dichlorophenoxy)acetyl)piperazine-1-carboxylate (**2a**): white solid, *R_f* = 0.29 (petroleum ether/ethyl acetate 3/2), yield 75%. ¹H NMR (500 MHz, CDCl₃): δ 7.36 (d, *J* = 2.45 Hz, 1H), 7.16 (d, *J* = 8.86, 2.45 Hz, 1H), 6.92 (d, *J* = 8.86 Hz, 1H), 4.74 (s, 2H), 3.61 – 3.53 (m, 4H), 3.45 – 3.35 (m, 4H), 1.44 (s, 9H). ¹³C NMR (126 MHz, CDCl₃): δ 165.8, 154.5, 152.0, 130.4, 127.9, 127.1, 123.6, 114.3, 80.6, 68.9, 45.6, 42.2, 28.4. MS (ESI+): *m/z* (%) = 388.7357 ([M+H]⁺, 25). HPLC–UV purity: 99.06%.

2-(2,4-Dichlorophenoxy)-1-(4-(7-nitrobenzo[*c*][1,2,5]oxadiazol-4-yl)piperazin-1-yl)ethan-1-one (**3a**, FluorA II): orange solid, *R_f* = 0.41 (CH₂Cl₂/acetone 20/1), yield 49%. ¹H NMR (500 MHz, DMSO-*d*₆): δ 8.49 (d, *J* = 9.2 Hz, 1H), 7.54 (d, *J* = 2.8 Hz, 1H), 7.30 (dd, *J* = 8.9, 2.8 Hz, 1H), 7.06 (d, *J* = 8.9 Hz, 1H), 6.60 (d, *J* = 9.2 Hz, 1H), 5.05 (s, 2H), 4.29 – 4.10 (m, 4H), 3.80 – 3.67 (m, 4H). ¹³C NMR (126 MHz, DMSO-*d*₆): δ 166.2, 153.2, 146.0, 145.4, 145.3, 136.9, 129.8, 128.3, 125.1, 122.7, 121.8, 115.8, 103.8, 66.9, 49.3, 49.0, 43.3, 41.1. MS (ESI-): *m/z* (%) = 496.2106 ([M+HCOOH-H]⁻, 100). HPLC–UV purity: 99.19%.

tert-Butyl 4-(2-(2,4,5-trichlorophenoxy)acetyl)piperazine-1-carboxylate (**2b**): white solid, *R_f* = 0.29 (petroleum ether/ethyl acetate 2/1), yield 87%. ¹H NMR (500 MHz, CDCl₃): δ 7.44 (s, 1H), 7.06 (s, 1H), 4.73 (s, 2H), 3.64 – 3.51 (m, 4H), 3.49 – 3.36 (m, 4H), 1.43 (s, 9H). ¹³C NMR (126 MHz, CDCl₃): δ 165.2, 154.5, 152.3, 131.6, 131.3, 125.6, 122.1, 115.2, 80.6, 68.8, 45.5, 42.2, 28.4. MS (ESI+): *m/z* (%) = 422.8232 ([M+H]⁺, 20). HPLC–UV purity: 99.74%.

1-(4-(7-Nitrobenzo[c][1,2,5]oxadiazol-4-yl)piperazin-1-yl)-2-(2,4,5-trichlorophenoxy)ethan-1-one (**3b, FluorA VII**): orange solid, $R_f = 0.47$ ($\text{CH}_2\text{Cl}_2/\text{acetone } 20/1$), yield 57%. $^1\text{H NMR}$ (500 MHz, $\text{DMSO}-d_6$): δ 8.49 (d, $J = 9.1$ Hz, 1H), 7.78 (s, 1H), 7.42 (s, 1H), 6.60 (d, $J = 9.2$ Hz, 1H), 5.11 (s, 2H), 4.28 – 4.11 (m, 4H), 3.75 – 3.69 (m, 4H). $^{13}\text{C NMR}$ (126 MHz, $\text{DMSO}-d_6$): δ 165.9, 153.7, 146.0, 145.4, 145.3, 136.9, 131.1, 130.7, 123.4, 121.8, 121.6, 116.3, 103.8, 67.1, 49.2, 49.0, 43.2, 41.1. MS (ESI-): m/z (%) = 530.1920 ($[\text{M}+\text{HCOOH}-\text{H}]^-$, 100). HPLC–UV purity: 98.42%.

tert-Butyl 4-(2-(4-chlorophenoxy)acetyl)piperazine-1-carboxylate (**2c**): white solid, $R_f = 0.29$ (petroleum ether/ethyl acetate 3/2), yield 59%. $^1\text{H NMR}$ (500 MHz, CDCl_3): δ 7.22 (d, $J = 9.0$ Hz, 1H), 6.86 (d, $J = 9.0$ Hz, 1H), 4.66 (s, 2H), 3.59 – 3.48 (m, 4H), 3.43 – 3.33 (m, 4H), 1.44 (s, 9H). $^{13}\text{C NMR}$ (126 MHz, CDCl_3): δ 166.4, 156.4, 154.5, 129.7, 126.8, 116.0, 80.5, 68.0, 45.4, 42.1, 28.4. MS (ESI+): m/z (%) = 354.9385 ($[\text{M}+\text{H}]^+$, 20). HPLC–UV purity: 98.94%.

2-(4-Chlorophenoxy)-1-(4-(7-nitrobenzo[c][1,2,5]oxadiazol-4-yl)piperazin-1-yl)ethan-1-one (**3c, FluorA IX**): orange solid, $R_f = 0.32$ ($\text{CH}_2\text{Cl}_2/\text{acetone } 20/1$), yield 41%. $^1\text{H NMR}$ (500 MHz, $\text{DMSO}-d_6$): δ 8.48 (d, $J = 9.1$ Hz, 1H), 7.28 (d, $J = 9.0$ Hz, 2H), 6.93 (d, $J = 9.1$ Hz, 2H), 6.59 (d, $J = 9.2$ Hz, 1H), 4.88 (s, 2H), 4.18 (d, $J = 40.8$ Hz, 4H), 3.91 – 3.52 (m, 4H). $^{13}\text{C NMR}$ (126 MHz, $\text{DMSO}-d_6$): δ 166.7, 157.5, 146.0, 145.4, 145.3, 136.9, 129.6, 125.1, 121.8, 117.0, 103.8, 66.4, 49.3, 49.0, 43.3, 41.1. MS (ESI+): m/z (%) = 462.3372 ($[\text{M}+\text{HCOOH}-\text{H}]^-$, 100). HPLC–UV purity: 98.97%.

tert-Butyl 4-(2-(4-bromophenoxy)acetyl)piperazine-1-carboxylate (**2d**): white solid, $R_f = 0.23$ (petroleum ether/ethyl acetate 3/2), yield 31%. $^1\text{H NMR}$ (300 MHz, CDCl_3): δ 7.40 (d, $J = 9.1$ Hz, 2H), 6.85 (d, $J = 9.1$ Hz, 2H), 4.70 (s, 2H), 3.64 – 3.51 (m, 4H), 3.48 – 3.34 (m, 4H), 1.48 (s, 9H). $^{13}\text{C NMR}$ (126 MHz, CDCl_3): δ 166.4, 156.9, 154.5, 132.6, 116.5, 114.2, 80.6, 68.0, 45.4, 42.1, 28.4. MS (ESI+): m/z (%) = 398.8239 ($[\text{M}+\text{H}]^+$, 20). HPLC–UV purity: 95.64%.

2-(4-Bromophenoxy)-1-(4-(7-nitrobenzo[c][1,2,5]oxadiazol-4-yl)piperazin-1-yl)ethan-1-one (**3d, FluorA V**): orange solid, $R_f = 0.32$ ($\text{CH}_2\text{Cl}_2/\text{acetone } 20/1$), yield 37%. $^1\text{H NMR}$ (500 MHz, $\text{DMSO}-d_6$): δ 8.46 (d, $J = 9.1$ Hz, 1H), 7.39 (d, $J = 9.1$ Hz, 2H), 6.88 (d, $J = 9.1$ Hz, 2H), 6.57 (d, $J = 9.2$ Hz, 1H), 4.88 (s, 2H), 4.25 – 4.08 (m, 4H), 3.79 – 3.68 (m, 4H). $^{13}\text{C NMR}$ (126 MHz, $\text{DMSO}-d_6$): δ 166.7, 157.9, 146.0, 145.31, 145.27, 136.9, 132.5, 121.7, 117.5, 112.8, 103.8, 66.3, 49.3, 49.0, 43.2, 41.0. MS (ESI-): m/z (%) = 506.1949 ($[\text{M}+\text{HCOOH}-\text{H}]^-$, 100). HPLC–UV purity: <99.9%.

tert-Butyl 4-(2-phenoxyacetyl)piperazine-1-carboxylate (**2e**): white solid, $R_f = 0.29$ (petroleum ether/ethyl acetate 3/2), yield 70%. $^1\text{H NMR}$ (500 MHz, CDCl_3): δ 7.33–7.29 (m, 2H), 6.99 (t, $J = 7.4$ Hz, 1H), 6.93 (d, $J = 8.7$ Hz, 2H), 4.69 (s, 2H), 3.60 – 3.53 (m, 4H), 3.44 – 3.35 (m, 4H), 1.45 (s, 9H). $^{13}\text{C NMR}$ (126 MHz, CDCl_3): δ 166.8, 157.7, 154.6, 129.8, 121.9, 114.6, 80.5, 67.9, 45.5, 42.1, 28.5. MS (ESI+): m/z (%) = 321.0084 ($[\text{M}+\text{H}]^+$, 30). HPLC–UV purity: 97.48%.

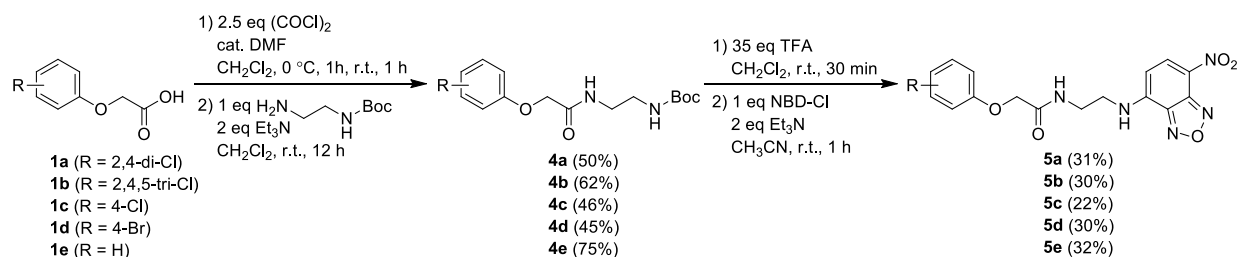
1-(4-(7-Nitrobenzo[c][1,2,5]oxadiazol-4-yl)piperazin-1-yl)-2-phenoxyethan-1-one (**3e, FluorA XI**): orange solid, $R_f = 0.29$ ($\text{CH}_2\text{Cl}_2/\text{acetone } 20/1$), yield 31%. $^1\text{H NMR}$ (500 MHz, $\text{DMSO}-d_6$): δ 8.49 (d, $J = 9.1$ Hz, 1H), 7.39 – 7.10 (m, 2H), 7.06 – 6.83 (m, 3H), 6.60 (d, $J = 9.2$ Hz, 1H), 4.85 (s, 1H), 4.27 – 4.11 (m, 4H), 3.95 – 3.56 (m, 4H). $^{13}\text{C NMR}$ (126 MHz, $\text{DMSO}-d_6$): δ 167.0, 158.5, 146.0, 145.4, 145.3, 136.9, 129.9, 121.8, 121.4, 115.1, 103.8, 66.2, 49.4, 49.0, 43.4, 41.1. MS (ESI+): m/z (%) = 428.3476 ($[\text{M}+\text{HCOOH}-\text{H}]^-$, 100). HPLC–UV purity: 98.13%.

1.3. General procedure for the synthesis of 4a-e and 5a-e (Scheme II).

Synthesis of *tert*-butyl (2-(2-(2,4-dichlorophenoxy)acetamido)ethyl)carbamate (**4a**) is representative. 2,4-D (**1a**; 221 mg, 1 mmol) was dissolved in anhydrous dichloromethane (10 mL) and cooled down to 0 °C. Subsequently, dimethylformamide (15 μL) and oxalyl chloride (0.215 mL, 2.5 mmol) were added drop-wise with vigorous

stirring and the resulting reaction mixture was stirred at 0 °C for 1 hour and then at room temperature for the next 1 hour. Evaporation of the solvent under reduced pressure in a cold water bath afforded the intermediate 2-(2,4-dichlorophenoxy)acetyl chloride in a quantitative yield, which was used in the next step without further purification or characterization. The residual crude 2-(2,4-dichlorophenoxy)acetyl chloride was dissolved in anhydrous dichloromethane (10 mL) and cooled down to 0 °C. Subsequently, triethylamine (278 μL, 2 mmol) was added drop-wise, followed by *tert*-butyl *N*-(2-aminoethyl)carbamate (*N*-Boc-ethylenediamine) (160 mg, 1 mmol), allowed to warm up to room temperature and the resulting reaction mixture was stirred for 12 h. Upon completion, the reaction mixture was cooled down to 0 °C, quenched with water (5 mL) and extracted with ethyl acetate (3 × 15 mL). Combined organic fractions were washed with water (5 mL) and brine (5 mL), dried over anhydrous sodium sulphate, filtered and concentrated under reduced pressure. Purification of the residue by flash chromatography on silica gel afforded compound **4a**.

Synthesis of 2-(2,4-Dichlorophenoxy)-*N*-(2-((7-nitrobenzo[*c*][1,2,5]oxadiazol-4-yl)amino)ethyl) acetamide (**5a**, FluorA I) is representative. Compound **4a** (140 mg, 0.386 mmol) was dissolved in anhydrous dichloromethane (4 mL) and cooled down to 0 °C. Subsequently, trifluoroacetic acid (1 mL) was added drop-wise with vigorous stirring, the reaction mixture was allowed to warm up to room temperature and the resulting reaction mixture was stirred for 30 minutes at room temperature. Subsequently, the reaction mixture was cooled down to 0 °C, quenched with saturated aqueous sodium bicarbonate solution (to pH 7) and extracted with ethyl acetate (3 × 20 mL). Combined organic fractions were washed with water (10 mL) and brine (10 mL), dried over anhydrous sodium sulphate, filtered and concentrated under reduced pressure to afford the intermediate *N*-(2-aminoethyl)-2-(2,4-dichlorophenoxy)acetamide in a quantitative yield, which was used in the next step without further purification or characterization. The residual *N*-(2-aminoethyl)-2-(2,4-dichlorophenoxy)acetamide was dissolved in acetonitrile (15 mL), to which triethylamine (107 μL, 0.771 mmol) was added drop-wise, followed by 4-chloro-7-nitrobenzofurazan, NBD-Cl (77 mg, 0.386 mmol) at 0 °C. The reaction mixture was stirred at room temperature for 1 hour. The reaction mixture was quenched with saturated ammonium chloride solution (10 mL) and extracted with ethyl acetate (3 × 20 mL). Combined organic fractions were washed with water (10 mL) and brine (10 mL), dried over anhydrous sodium sulphate, filtered and concentrated under reduced pressure. Purification of the residue by flash chromatography on silica gel afforded compound **5a**.



Scheme II

tert-Butyl (2-(2-(2,4-dichlorophenoxy)acetamido)ethyl)carbamate (**4a**): white solid, *R_f* = 0.14 (petroleum ether/ethyl acetate 3/2), yield 50%. ¹H NMR (500 MHz, CDCl₃): δ 7.34 (d, *J* = 2.5 Hz, 1H), 7.21 (dd, *J* = 8.9, 2.5 Hz, 1H), 7.17-7.10 (br s, 1H), 6.82 (d, *J* = 8.9 Hz, 1H), 4.86-4.79 (br s, 1H), 4.50 (s, 2H), 3.51-3.46 (m, 2H), 3.33-3.27 (m, 2H), 1.41 (s, 9H). ¹³C NMR (126 MHz, DMSO-*d*₆): δ 167.5, 156.2, 153.0, 129.8, 128.6, 125.6, 123.0, 115.9, 78.2, 68.3, 40.0, 39.1, 28.7. MS (ESI⁺): *m/z* (%) = 362.7133 ([*M*+H]⁺, 20). HPLC-UV purity: 96.77%.

2-(2,4-Dichlorophenoxy)-*N*-(2-((7-nitrobenzo[*c*][1,2,5]oxadiazol-4-yl)amino)ethyl)acetamide (**5a, FluorA I**): orange solid, $R_f = 0.26$ ($\text{CH}_2\text{Cl}_2/\text{acetone } 20/1$), yield 31%. $^1\text{H NMR}$ (500 MHz, CDCl_3): δ 8.48 (d, $J = 8.6$ Hz, 1H), 7.57 – 7.53 (br s, 1H), 7.39 (d, $J = 2.5$ Hz, 1H), 7.32 – 7.28 (br s, 1H), 7.21 (dd, $J = 8.7, 2.4$ Hz, 1H), 6.83 (d, $J = 8.8$ Hz, 1H), 6.18 (d, $J = 8.6$ Hz, 1H), 3.87 – 3.82 (m, 2H), 3.77 – 3.64 (m, 2H). $^{13}\text{C NMR}$ (126 MHz, $\text{DMSO-}d_6$): δ 168.0, 152.5, 145.6, 144.6, 144.2, 138.2, 129.5, 128.1, 125.4, 122.7, 121.1, 115.5, 99.4, 68.1, 43.1, 37.3. MS (ESI-): m/z (%) = 424.1541 ($[\text{M-H}]^-$, 100). HPLC–UV purity: 99.30%.

tert-Butyl (2-(2-(2,4,5-trichlorophenoxy)acetamido)ethyl)carbamate (**4b**): white solid, $R_f = 0.23$ (petroleum ether/ethyl acetate 3/2), yield 62%. $^1\text{H NMR}$ (500 MHz, CDCl_3): δ 7.49 (s, 1H), 7.17 – 7.10 (br s, 1H), 6.98 (s, 1H), 4.85 – 4.78 (br s, 1H), 4.49 (s, 2H), 3.48 (dd, $J = 11.8, 5.8$ Hz, 2H), 3.39 – 3.18 (m, 2H), 1.40 (s, 9H). $^{13}\text{C NMR}$ (126 MHz, CDCl_3): δ 167.3, 156.5, 151.9, 131.8, 131.3, 126.1, 122.3, 115.6, 79.9, 68.5, 40.3, 39.9, 28.4. MS (ESI+): m/z (%) = 396.8232 ($[\text{M+H}]^+$, 20). HPLC–UV purity: 97.97%.

N-(2-((7-Nitrobenzo[*c*][1,2,5]oxadiazol-4-yl)amino)ethyl)-2-(2,4,5-trichlorophenoxy)acetamide (**5b, FluorA VI**): orange solid, $R_f = 0.32$ ($\text{CH}_2\text{Cl}_2/\text{acetone } 20/1$), yield 30%. $^1\text{H NMR}$ (500 MHz, $\text{DMSO-}d_6$): δ 9.35 – 9.27 (br s, 1H), 8.45 (d, $J = 8.6$ Hz, 1H), 8.17 – 8.12 (m, 1H), 7.73 (s, 1H), 7.23 (s, 1H), 6.39 (d, $J = 8.9$ Hz, 1H), 4.64 (s, 2H), 3.56 – 3.50 (br s, 2H), 3.48 – 3.43 (m, 2H). $^{13}\text{C NMR}$ (126 MHz, $\text{DMSO-}d_6$): δ 167.3, 152.7, 145.4, 144.4, 144.0, 137.9, 130.6, 130.2, 123.4, 121.3, 121.0, 115.8, 99.2, 68.1, 42.9, 37.2. MS (ESI-): m/z (%) = 458.1182 ($[\text{M-H}]^+$, 100). HPLC–UV purity: 99.89%.

tert-Butyl (2-(2-(4-chlorophenoxy)acetamido)ethyl)carbamate (**4c**): white solid, $R_f = 0.29$ (petroleum ether/ethyl acetate 1/1), yield 46%. $^1\text{H NMR}$ (500 MHz, CDCl_3): δ 7.27 (d, $J = 9.0$ Hz, 2H), 7.25 – 7.17 (br s, 1H), 6.87 (d, $J = 9.0$ Hz, 2H), 4.92 – 4.70 (br s, 1H), 4.45 (s, 2H), 3.44 (d, $J = 11.2, 5.5$ Hz, 2H), 3.35 – 3.27 (m, 2H), 1.41 (s, 9H). $^{13}\text{C NMR}$ (126 MHz, CDCl_3): δ 168.6, 156.8, 155.9, 129.7, 127.1, 116.1, 80.0, 67.5, 40.5, 40.2, 28.4. MS (ESI+): m/z (%) = 328.9509 ($[\text{M+H}]^+$, 20). HPLC–UV purity: 96.55%.

2-(4-Chlorophenoxy)-*N*-(2-((7-nitrobenzo[*c*][1,2,5]oxadiazol-4-yl)amino)ethyl)acetamide (**5c, FluorA VIII**): orange solid, $R_f = 0.21$ ($\text{CH}_2\text{Cl}_2/\text{acetone } 20/1$), yield 22%. $^1\text{H NMR}$ (500 MHz, $\text{DMSO-}d_6$): δ 9.51 – 9.29 (br s, 1H), 8.57 – 8.39 (m, 1H), 8.38 – 8.21 (br s, 1H), 7.35 – 7.15 (m, 2H), 7.01 – 6.81 (m, 2H), 6.48 – 6.36 (m, 1H), 4.54 (m, 2H), 3.67 – 3.39 (m, 4H). $^{13}\text{C NMR}$ (126 MHz, CDCl_3): δ 168.6, 156.9, 145.9, 144.9, 144.6, 138.5, 129.7, 125.5, 121.5, 117.0, 99.7, 67.8, 43.4, 37.5. MS (ESI+): m/z (%) = 390.1696 ($[\text{M-H}]^-$, 100). HPLC–UV purity: 96.61%.

tert-Butyl (2-(2-(4-bromophenoxy)acetamido)ethyl)carbamate (**4d**): white solid, $R_f = 0.29$ (petroleum ether/ethyl acetate 1/1), yield 45%. $^1\text{H NMR}$ (500 MHz, CDCl_3): δ 7.40 (d, $J = 8.86$ Hz, 2H), 7.25 – 7.18 (br s, 1H), 6.82 (d, $J = 9.17$ Hz, 2H), 4.87 – 4.77 (br s, 1H), 4.44 (s, 2H), 3.47 – 3.41 (m, 2H), 3.35 – 3.27 (m, 2H), 1.41 (s, 9H). $^{13}\text{C NMR}$ (126 MHz, CDCl_3): δ 168.5, 156.9, 156.4, 132.7, 116.6, 114.5, 80.0, 67.5, 40.5, 40.2, 28.4. MS (ESI+): m/z (%) = 372.7887 ($[\text{M+H}]^+$, 20). HPLC–UV purity: <99.9%.

2-(4-Bromophenoxy)-*N*-(2-((7-nitrobenzo[*c*][1,2,5]oxadiazol-4-yl)amino)ethyl)acetamide (**5d, FluorA IV**): orange solid, $R_f = 0.24$ ($\text{CH}_2\text{Cl}_2/\text{acetone } 20/1$), yield 30%. $^1\text{H NMR}$ (500 MHz, CDCl_3): δ 8.47 (d, $J = 8.5$ Hz, 1H), 7.61 – 7.54 (br s, 1H), 7.39 (d, $J = 9.0$ Hz, 2H), 7.14 – 7.06 (br s, 1H), 6.78 (d, $J = 8.9$ Hz, 2H), 6.16 (d, $J = 8.5$ Hz, 1H), 4.54 (s, 2H), 3.81 (dd, $J = 11.1, 6.2$ Hz, 2H), 3.71 – 3.64 (m, 2H), 1.56 (s, 9H). $^{13}\text{C NMR}$ (126 MHz, $\text{DMSO-}d_6$): δ 168.6, 157.4, 145.9, 145.0, 144.6, 138.5, 132.6, 121.5, 117.5, 113.2, 99.7, 67.7, 43.4, 37.5. MS (ESI+): m/z (%) = 434.1277 ($[\text{M-H}]^-$, 100). HPLC–UV purity: 96.21%.

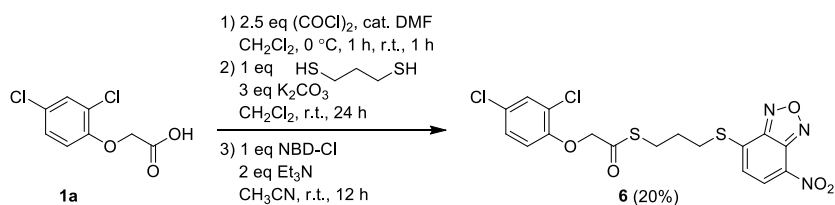
tert-Butyl (2-(2-phenoxyacetamido)ethyl)carbamate (**4e**): white solid, $R_f = 0.11$ (petroleum ether/ethyl acetate 3/2), yield 75%. $^1\text{H NMR}$ (500 MHz, CDCl_3): δ 7.31 (t, $J = 7.7$ Hz, 2H), 7.21 – 7.10 (br s, 1H), 7.01 (t, $J = 7.4$ Hz, 1H), 6.93 (d, $J = 7.8$ Hz, 2H), 4.90 – 4.72 (br s, 1H), 4.48 (s, 2H), 3.45 (dd, $J = 11.5, 5.7$ Hz, 2H), 3.34 – 3.26 (m,

2H), 1.42 (s, 9H). ^{13}C NMR (126 MHz, CDCl_3): δ 169.1, 157.3, 156.7, 129.9, 122.2, 114.7, 79.9, 67.3, 40.3, 40.1, 28.4. MS (ESI+): m/z (%) = 295.0136 ($[\text{M}+\text{H}]^+$, 30). HPLC–UV purity: 92.92%.

N-(2-((7-Nitrobenzo[*c*][1,2,5]oxadiazol-4-yl)amino)ethyl)-2-phenoxyacetamide (**5e, FluorA X**): orange solid, R_f = 0.24 (CH_2Cl_2 /acetone 20/1), yield 32%. ^1H NMR (500 MHz, $\text{DMSO}-d_6$): δ 9.44 – 9.34 (br s, 1H), 8.46 (d, J = 8.9 Hz, 1H), 8.31 – 8.35 (m, 1H), 7.19 (t, J = 7.9 Hz, 2H), 6.89 – 6.85 (m, 3H), 6.41 (d, J = 9.2 Hz, 1H), 4.42 (s, 2H), 3.57 – 3.43 (m, 4H). ^{13}C NMR (126 MHz, $\text{DMSO}-d_6$): δ 168.4, 157.5, 145.3, 144.4, 144.0, 137.9, 129.4, 121.2, 120.9, 114.7, 99.1, 70.0, 42.8, 36.9. MS (ESI+): m/z (%) = 356.2428 ($[\text{M}-\text{H}]^-$, 100). HPLC–UV purity: 99.39%.

1.4. General procedure for the synthesis of **6** (Scheme III).

2,4-D (**1a**; 220 mg, 1 mmol) was dissolved in anhydrous dichloromethane (10 mL) and cooled down to 0 °C. Subsequently, dimethylformamide (15 μL) and oxalyl chloride (0.215 mL, 2.5 mmol) were added drop-wise with vigorous stirring and the resulting reaction mixture was stirred at 0 °C for 1 hour and then at room temperature for the next 1 hour. Evaporation of the solvent under reduced pressure in a cold water bath afforded intermediate 2-(2,4-dichlorophenoxy)acetyl chloride in a quantitative yield, which was used in the next step without further purification or characterization. The residual crude 2-(2,4-dichlorophenoxy)acetyl chloride was dissolved in anhydrous dichloromethane (10 mL) and cooled down to 0 °C. Subsequently, potassium carbonate (414 mg, 3 mmol) and propane-1,3-dithiol (0.1 mL, 1 mmol) were added with vigorous stirring and the resulting reaction mixture was stirred at room temperature for 24 h. Upon completion, the reaction mixture was filtered to remove excess potassium carbonate and the filtrate was evaporated. The resulting intermediate *S*-(3-mercaptopropyl) 2-(2,4-dichlorophenoxy)ethanethioate was dissolved in acetonitrile (10 mL), to which triethylamine (278 μL , 2 mmol) was added drop-wise, followed by 4-chloro-7-nitrobenzofurazan, NBD-Cl (200 mg, 1 mmol) at 0 °C. The reaction mixture was stirred at room temperature for 12 h. Upon completion, the reaction mixture was quenched with water (5 mL) and extracted with ethyl acetate (3 \times 20 mL). Combined organic fractions were washed with water (5 mL) and brine (5 mL), dried over anhydrous sodium sulphate, filtered and concentrated under reduced pressure. Purification of the residue by flash chromatography on silica gel afforded *S*-(3-((7-nitrobenzo[*c*][1,2,5]oxadiazol-4-yl)thio)propyl) 2-(2,4-dichlorophenoxy) ethanethioate (**6**, FluorA III).



Scheme III

S-(3-((7-Nitrobenzo[*c*][1,2,5]oxadiazol-4-yl)thio)propyl) 2-(2,4-dichlorophenoxy)ethanethioate (**6**, FluorA III): orange solid, R_f = 0.31 (petroleum ether/ CH_2Cl_2 /acetone 30/20/1), yield 30%. ^1H NMR (500 MHz, CDCl_3): δ 8.39 (d, J = 7.95 Hz, 1H), 7.43 – 7.40 (m, 1H), 7.20 – 7.15 (m, 2H), 6.80 (d, J = 8.9 Hz, 1H), 4.73 (s, 2H), 3.33 (t, J = 7.3 Hz, 2H), 3.14 (t, J = 7.0 Hz, 2H), 2.14 (p, J = 7.2 Hz, 2H). ^{13}C NMR (126 MHz, CDCl_3): δ 197.1, 152.0, 149.3, 142.6, 140.7, 133.0, 130.7, 130.6, 127.8, 127.7, 124.3, 121.0, 114.6, 73.5, 30.5, 28.1, 26.9. MS (ESI-): m/z (%) = 472.0234 ($[\text{M}-\text{H}]^-$, 100). HPLC purity: 99.49%.

2. Storage and usage of the compounds. The FluorA compounds in powder form were kept at 4 °C. Compounds dissolved in DMSO to obtain 1 or 10 mM stock solutions were stored in -20 °C for approx. 2 weeks.

Aliquots of the powder were made and dissolved one by one to avoid changing ambient conditions and prevent the compounds from precipitating in DMSO or in water solution of ½ MS media. Since the solubility of the compounds in water solutions is limited, final concentrations exceeding 10 µM in liquid media were not used.

3. Plant materials and growth conditions. Seeds of *Arabidopsis thaliana* ecotype Columbia (Col-0) were sown on plates of ½ MS medium (2.2 g/L Murashige and Skoog medium - Duchefa Biochemie, 1% sucrose, 0.05 g/L - morpholinoethanesulfonic acid - Sigma Aldrich and 0.7% agar - Duchefa Biochemie, pH 5.6), stratified for 2 days at 4 °C in the dark and then transferred to long-day light conditions (22 °C, 16 h light/8 h dark) for five days for light-grown seedlings. After 2 days of stratification and 5 h in light (22°C), sown plates were packed into aluminium foil and grown in the dark for 3 days for dark-grown seedlings. All the mutant lines used in this work are in Col-0 background and have been described before: *tir1-1* (1), *axr1-30* (2), *aux1-21lax3* (3), *wei2-1wei7-1* (4), *pDR5::GUS* (5), *pBA3::GUS* (6), *pIAA3::GUS* (7), *pIAA12::GUS* (7), *pCYCB1;1::GUS* (8), *p35S::DII-Venus* (9), *pDR5v2::Venus* (10), *pSYP61::SYP61-CFP* (11), *p35S::H2B-mcherry* (12), p24δ5-RFP (13) and *aux1lax1lax2* (14). *pin3pin4pin7* in Col-0/Ler background was kindly provided by H  l  ne S. Robert, CEITEC, Brno.

4. GUS assays. Five-day-old *Arabidopsis* seedlings of different marker lines expressing GUS were treated with 10 µM fluorescent compounds for defined periods of time (5 h for *pDR5::GUS*, 8 h for *pIAA3::GUS*, 12 h for *pIAA12::GUS* and *pBA3::GUS*, 24 h for *pCYCB1;1::GUS*), fixed with ice-cold acetone for 20 min at -20 °C and washed with distilled water three times. Plants were incubated in the presence of GUS staining solution – 2 mM X-GlcA (Duchefa Biochemie) in GUS buffer (0.1% triton X100; 10 mM EDTA; 0.5 mM potassium ferrocyanide; 0.5 mM potassium ferricyanide in 0.1 M phosphate buffer) – at 37 °C in the dark for 30 min. To stop the staining reaction 70 % ethanol was added for 1 h. The samples were then mounted in a mixture of chloral hydrate:glycerol:H₂O (8:3:1) on a slide glass and examined with a Zeiss Axioplan light microscope.

To perform the *pCYCB1;1::GUS* assay, marker line seedlings were grown in liquid ½ MS media in the presence of 10 µM 1-naphthylphthalamic acid (NPA) for 3 days as described by De Rybel et al. (15) followed by the procedure described above.

5. LC-MS/MS determination of metabolization dynamics. Five-day-old *Arabidopsis* Col-0 seedlings were transferred to liquid ½ MS media with 2 µM fluorescent analogues or only DMSO as a control and treated for defined periods of time (0.5 – 3 h). Non-treated plants were used as a control for time-point 0 h. At distinct time-points, the plants were collected and the roots were harvested to obtain 50 roots per one biological replicate, rinsed with fresh media, frozen in liquid nitrogen and stored at -80 °C until extraction. The one-step purification method based on liquid-liquid extraction was used to remove impurities from the complex plant matrix. Briefly, 900 µL of the extraction solution (hexane:MeOH:H₂O – 1:1:1) was added to plant samples (50 seedlings/sample) together with 2 mm ceria-stabilized zirconium oxide beads. In each extract, 500 pmol of [²H₅]2,4-D (CDN Isotopes, Canada), 1 pmol of [¹³C₂]FluorA I and 10 pmol of [¹³C₂]FluorA II, synthesized from [¹³C₂]2,4-D (16) analogously to that described above for non-labeled conjugates, were added as internal standards to validate the determination. Homogenization was performed using a MixerMill MM 301 bead mill (Retsch GmbH, Haan, Deutschland) for 3 x 3 minutes at a frequency of 27 Hz. Plant extracts were incubated at 4 °C shaking continuously for 30 min, centrifuged (15 min, 23 000 g, 4 °C) and split into 4 technical replicates. The H₂O/MeOH phase was transferred to microspine tubes (VWR[®], Radnor, Pennsylvania), centrifuged again at 12 000 g for 10 min and the flow-through fraction was evaporated to dryness under gentle stream of nitrogen

using a TurboVap® LV evaporation system (Caliper Life Sciences, Hopkinton, MA, USA). Samples were dissolved in 50 µL of 35% methanol and 10 µL was injected onto a reversed-phase column (Kinetex™ C18 100A, 50 x 2.1 mm, 1.7 µm; Phenomenex, Torrance, USA) and analyzed by liquid chromatography–tandem mass spectrometry (LC-MS/MS) using an ACQUITY UPLC® I-Class system combined with a triple quadrupole mass spectrometer Xevo™ TQ-S (Waters, Manchester, UK). The analytes were separated by 9 min linear gradient of 10:90 to 95:5 A:B using 0.1% acetic acid in methanol (A) and 0.1% acetic acid in water (B) as mobile phases at a flow rate of 0.5 mL·min⁻¹ and column temperature of 40 °C. At the end of the gradient, the column was washed with 95% methanol (0.5 min), and re-equilibrated to initial conditions (1.0 min). The effluent was introduced into the MS/MS system with the optimized settings: Source Offset, 60 V; Source Temperature, 150 °C; Desolvation Temperature, 600 °C; Cone Gas Flow, 1000 L·h⁻¹, Collision Gas Flow 0.15 mL·min⁻¹, Nebuliser Gas Flow, 7 Bar; Capillary voltage, 3 kV. For quantification, the multi reaction monitoring (MRM) transitions in positive and negative electrospray modes (ESI⁺ and ESI⁻) were found for each compound as follows: 219 > 161/224 > 163 (ESI⁻), 426 > 246/430 > 250 and 452 > 250/456 > 259 (ESI⁺) for 2,4-D/[²H₅]2,4-D, FluorA I/[¹³C₂]FluorA I and FluorA II/[¹³C₂]FluorA II, respectively. The collision energy and cone voltage were optimized for every transition as well as dwell times for each retention window to obtain a minimum of 15 points per peak. Chromatograms were processed by MassLynx™ V4.1 software (Waters) and quantification was performed by the isotopic dilution method using isotopically labeled standards of each analyte as a reference.

6. *p35S::DII-Venus* and *pDR5v2::Venus* auxin responsive assays. Five-day-old seedlings of *p35S::DII-Venus* and *p35S::mDII-Venus* or *pDR5v2::Venus Arabidopsis* lines were treated in liquid ½ MS medium in the presence of 10 µM fluorescent compounds or DMSO and 10 µM 2,4-D as controls for 15 min or 3 h, respectively. Treatment was followed by 30 min washout of the compounds with a fresh medium, which was changed three times during the washout step. The seedlings were then transferred to a slide glass with a drop of untreated media and confocal images of Venus fluorescence were taken as described above.

7. Root growth inhibition assay. Five-day-old seedlings of *Arabidopsis* Col-0 WT were transferred on vertical plates containing solid ½ MS media supplemented with 2 µM fluorescent analogues or 0.1 µM 2,4-D and DMSO as controls and the bottom of each root was marked (17). Plates were incubated in growth conditions as previously described, images of the roots were scanned at defined time-points with an Epson V600 scanner and the lengths of the roots from the mark to top of the roots were quantified using ImageJ.

8. Root gravitropic response assay. Five-day-old Col-0 seedlings were placed on plates with solid ½ MS medium comprising tested compounds (DMSO, 0.1 µM 2,4-D and 2 µM fluorescent auxin analogues) and incubated vertically under standard growing conditions for 15 min. The plates were then packed into aluminium foil, rotated 90° from the vertical direction and grown for 6 h in the dark (17). At defined time-points, the roots were scanned with an Epson V600 scanner and the curvature angle in response to gravity was quantified for each root using ImageJ.

9. Imaging of fluorescent auxin analogues. Seedlings were typically treated in liquid ½ MS media supplemented by auxin fluorescent analogues at 2 µM concentration for 15 min, and then transferred to microscopic glass slides with a drop of the media containing tested compounds. Confocal images were taken immediately using a Zeiss LSM 780 confocal microscope with a LCI Plan-Neofluar 25x/0.8 Imm Corr DIC M27 objective. NBD-labelled auxins and Venus fluorescent protein were excited at 488 nm, RFP and mCherry

fluorescent proteins at 514 nm and cyan fluorescent protein at 458 nm by an Argon multiline laser. For examination of active polar auxin transport using a chemical genomic approach, 10 μ M NPA or 2-naphthoxyacetic acid (2-NOA) pre-treatment for 3 h followed by 15 min co-treatment with tested compounds was performed. The co-localization studies were achieved based on calculation of Pearson's correlation coefficient using ImageJ plugin Coloc (https://imagej.net/Colocalization_Analysis) after background fluorescent signal threshold was cut off, as described in Dunn et al., 2011 (18). To estimate the co-localization of fluorescent analogues with SYP61 trafficking marker, 90 min pre-treatment of *pSYP61::SYP61-CFP* seedlings with 25 μ M brefeldin A (BFA) was performed.

The basipetal auxin transport assay was performed with decapitated hypocotyls of 3-day-old etiolated seedlings, which were transferred on a $\frac{1}{2}$ MS plate just below a block of agar containing the particular chemical. After 3 or 6 h, images of fluorescence signal were acquired using a Zeiss LSM 780 confocal microscope. As a negative control, hypocotyls were treated with 10 μ M NPA for 3 h and then transferred on a plate with NPA and the particular chemical.

Images of the FluorA II distribution in apical hook of transport mutants *aux1lax1lax2* and *pin3pin4pin7* were acquired using a Zeiss LSM 800 confocal microscope with a Plan-Apochromat 10x/0.45 M27 objective and excitation at 488 nm.

10. Distribution assays of FluorAs in response to light or gravity. To test the distribution of fluorescent analogues in apical hooks, three-day-old etiolated seedlings of *Arabidopsis* were pre-treated with 2 μ M fluorescent analogues in liquid media for 15 min and transferred to vertical plates containing solid $\frac{1}{2}$ MS medium supplemented with 2 μ M compounds. Plates were placed vertically in a humidifying dark chamber to avoid drying of the samples and confocal images were recorded with a Nikon vertical macroconfocal (AZ-C2 vertical) with a AZ100 horizontally mounted microscope with option of 2x/0.2 WD 45 mm or 5x/0.5 WD 15 mm DIC macro-objectives at defined time-points to investigate real time distribution of fluorescent auxins *in vivo*. To achieve the light stimulus for three-day-old etiolated Col-0 seedlings, the plates were transferred to the greenhouse under standard light conditions, and were then placed back into the humidifying dark chamber and the images of fluorescent redistribution recorded immediately every 30 min.

Five-day-old old seedlings of *Arabidopsis* grown on square plates were gravistimulated by 90° rotation for 40 min, then treated with a 2 μ M solution of fluorescent analogues for 15 min and imaged immediately using a Zeiss LSM 780 confocal microscope as described above.

11. Surface plasmon resonance (SPR). The experiments were done according to the protocols described in Lee *et al.*, 2014 (19). TIR1 was expressed in insect cell culture using a recombinant baculovirus. The construct contained sequences for three affinity tags, namely 6 His, maltose-binding protein (MBP) and FLAG. Initial purification using the His tag was followed by clean-up using FLAG chromatography, the purified protein was used for SPR assays by passing it over a streptavidin chip loaded with biotinylated IAA7/IAA17 degron peptides.

The SPR buffer was Hepes-buffered saline with 10mM Hepes, 3 mM EDTA, 150mM NaCl and 0.05% Tween 20. Compounds to be tested were premixed with the protein to a final 50 μ M concentration. Binding experiments were run at a flow rate of 30 μ l.min⁻¹ using 3 min of injection time and 2.5 min of dissociation time. Data from a control channel (biocytin) and from a buffer-only run were subtracted from each sensogram following the standard double reference subtraction protocol.

12. Statistical analysis. Measurements of root lengths and angles after gravistimulation as well as quantification of NBD fluorescence intensity were performed using ImageJ 1.51f software (20). Statistical analysis of data was performed to compare treatment with DMSO control using two-sided independent Student's *t*-tests using Excel (Microsoft Office).

13. Image processing. All adjustments of acquired scanned or confocal images were performed using ImageJ 1.51w software (19) with the same settings for each experimental dataset. Drawings were accomplished by ChemBioDraw Ultra, CorelDRAW X4 and Adobe Illustrator.

SI References

1. Dharmasiri N, Dharmasiri S, Estelle M (2005) The F-box protein TIR1 is an auxin receptor. *Nature* 435(7041):441–445.
2. Hotton SK, Eigenheer RA, Castro MF, Bostick M, Callis J (2011) AXR1-ECR1 and AXL1-ECR1 heterodimeric RUB-activating enzymes diverge in function in *Arabidopsis thaliana*. *Plant Mol Biol* 75(4–5):515–26.
3. Vandenbussche F, et al. (2010) The auxin influx carriers AUX1 and LAX3 are involved in auxin-ethylene interactions during apical hook development in *Arabidopsis thaliana* seedlings. *Development* 137(4):597–606.
4. Stepanova AN, Hoyt JM, Hamilton AA, Alonso JM (2005) A link between ethylene and auxin uncovered by the characterization of two root-specific ethylene-insensitive mutants in *Arabidopsis*. *Plant Cell* 17(8):2230–2242.
5. Ulmasov T, Hagen G, Guilfoyle TJ (1997) ARF1, a transcription factor that binds to auxin response elements. *Science* 276(5320):1865–1868.
6. Oono Y, Chen QG, Overvoorde PJ, Köhler C, Theologis A (1998) *age* Mutants of *Arabidopsis* exhibit altered auxin-regulated gene expression. *Plant Cell* 10(10):1649–1662.
7. Weijers D, et al. (2005) Developmental specificity of auxin response by pairs of ARF and Aux/IAA transcriptional regulators. *EMBO J* 24(10):1874–1885.
8. Himanen K, et al. (2002) Auxin-mediated cell cycle activation during early lateral root initiation. *Plant Cell* 14(10):2339–2351.
9. Brunoud G, et al. (2012) A novel sensor to map auxin response and distribution at high spatio-temporal resolution. *Nature* 482(7383):103–106.
10. Liao C-Y, et al. (2015) Reporters for sensitive and quantitative measurement of auxin response. *Nat Methods* 12(3):207–210.
11. Robert S, et al. (2008) Endosidin1 defines a compartment involved in endocytosis of the brassinosteroid receptor BRI1 and the auxin transporters PIN2 and AUX1. *Proc Natl Acad Sci USA* 105(24):8464–8469.
12. Mao H, Nakamura M, Viotti C, Grebe M (2016) A framework for lateral membrane trafficking and polar tethering of the PEN3 ATP-binding cassette transporter. *Plant Physiol* 172(4):2245–2260.
13. Montesinos JC, et al. (2012) Coupled transport of *Arabidopsis* p24 proteins at the ER-Golgi interace. *J Exp Bot* 63(11):4243–4261.
14. Swarup K., et al. (2008) The auxin influx carrier LAX3 promotes lateral root emergence. *Nat. Cell Biol.* 10: 946–954.
15. De Rybel B, et al. (2012) A role for the root cap in root branching revealed by the non-auxin probe naxillin. *Nat Chem Biol* 8(9):798–805.
16. Eyer L, et al. (2016) 2,4-D and IAA amino acid conjugates show distinct metabolism in *Arabidopsis*. *PLoS One* 11(7):e0159269.
17. Lincoln C, Britton JH, Estelle M (1990) Growth and development of the *axr1* mutants of *Arabidopsis*. *Plant Cell* 2(11):1071–80.
18. Dunn KW, Kamocka MM, McDonald JH (2011) A practical guide to evaluating colocalization in biological microscopy. *Am J Physiol Cell Physiol* 300(4):C723–C742.

19. Lee S, et al., (2014) Defining binding efficiency and specificity of auxins for SCFTIR1/AFB-Aux/IAA co-receptor complex formation. *ACS Chem Biol* 9, 673–682.
20. Schindelin J, Rueden CT, Hiner MC, Eliceiri KW (2015) The ImageJ ecosystem: An open platform for biomedical image analysis. *Mol Reprod Dev* 82(7–8):518–529.

SI Figures

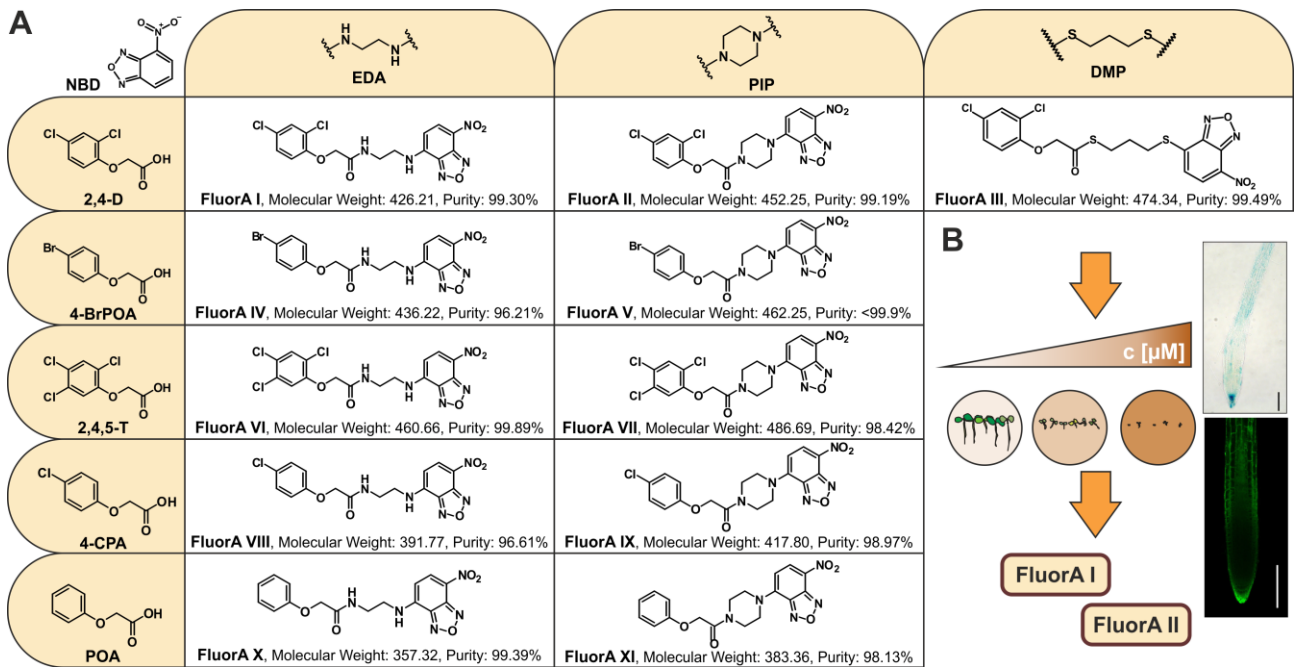


Fig. S1. Library of fluorescent auxin analogues and scheme of screening strategy. (A) The complete list of the FluorA (I-XI) compounds prepared for this study with their structures, molecular weights and purities including structures of the synthetic auxins (2,4-D, 4-BrPOA, 2,4,5-T, 4-CPA and POA), the linkers (EDA, PIP and DMP) and the fluorescent label (NBD) used. No free acids were detected in the stock solutions of the compounds. (B) Scheme of the screening strategy leading to selection of FluorA I and FluorA II. The compounds were evaluated according to their ability to reduce primary root growth of *Arabidopsis* Col-0 WT in a concentration (c)-dependent manner and to induce *pDR5::GUS* expression. In addition, the intensity of the NBD fluorescence signal was assessed.

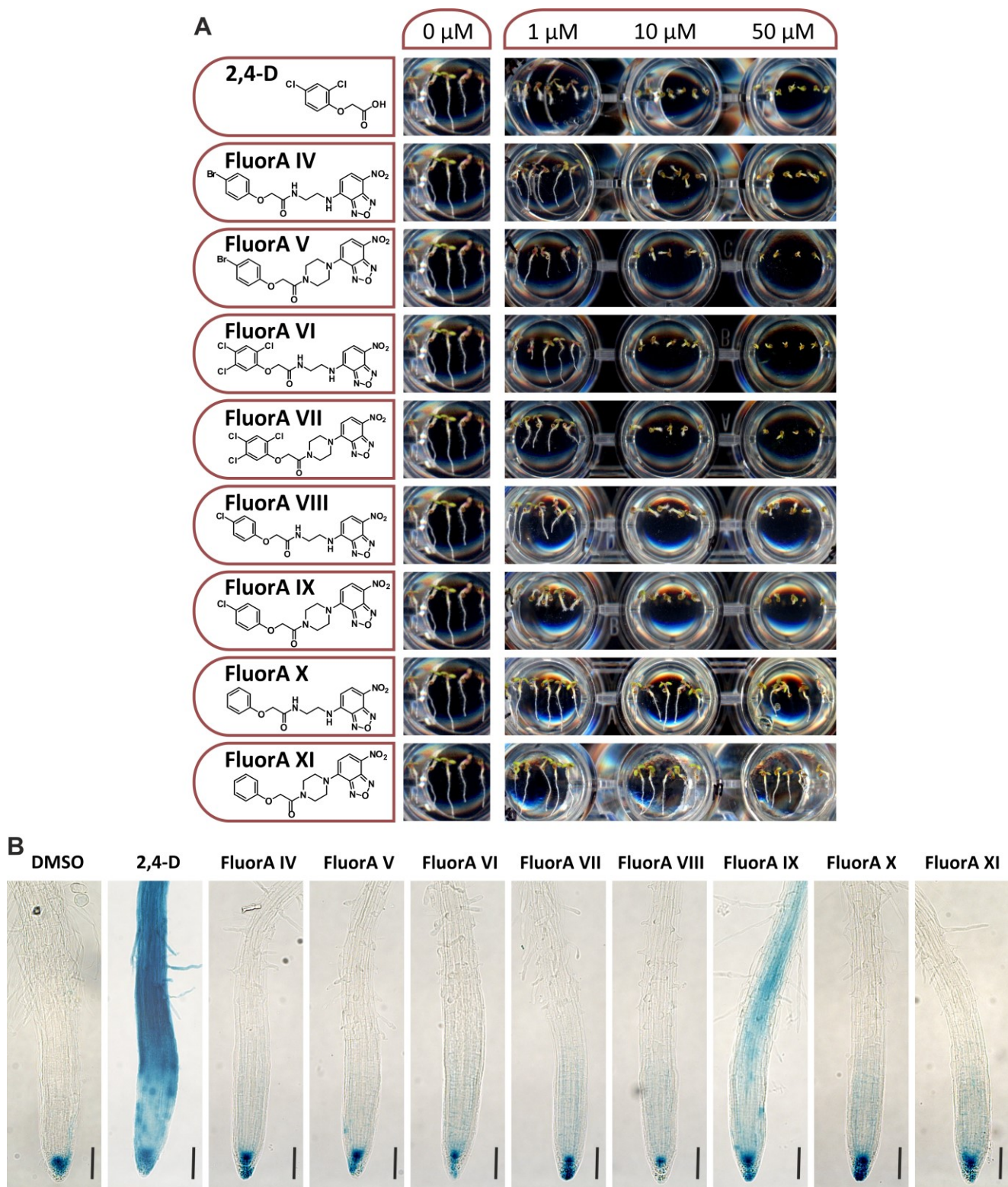


Fig. S2. Testing of the biological activity of the FluorA compounds. (A) Seedlings of *Arabidopsis* Col-0 WT were grown in the presence of DMSO (0 μ M) or different concentrations of 2,4-D or FluorAs (1, 10, or 50 μ M) for five days. The effects of the compounds on primary root growth was then evaluated. (B) Five-d-old seedlings of *Arabidopsis* *pDR5::GUS* marker line were treated with DMSO or with 10 μ M 2,4-D or FluorA compounds for 5 h and *DR5* expression in the primary roots was then examined by GUS staining. (B) Scale bars represent 100 μ m.

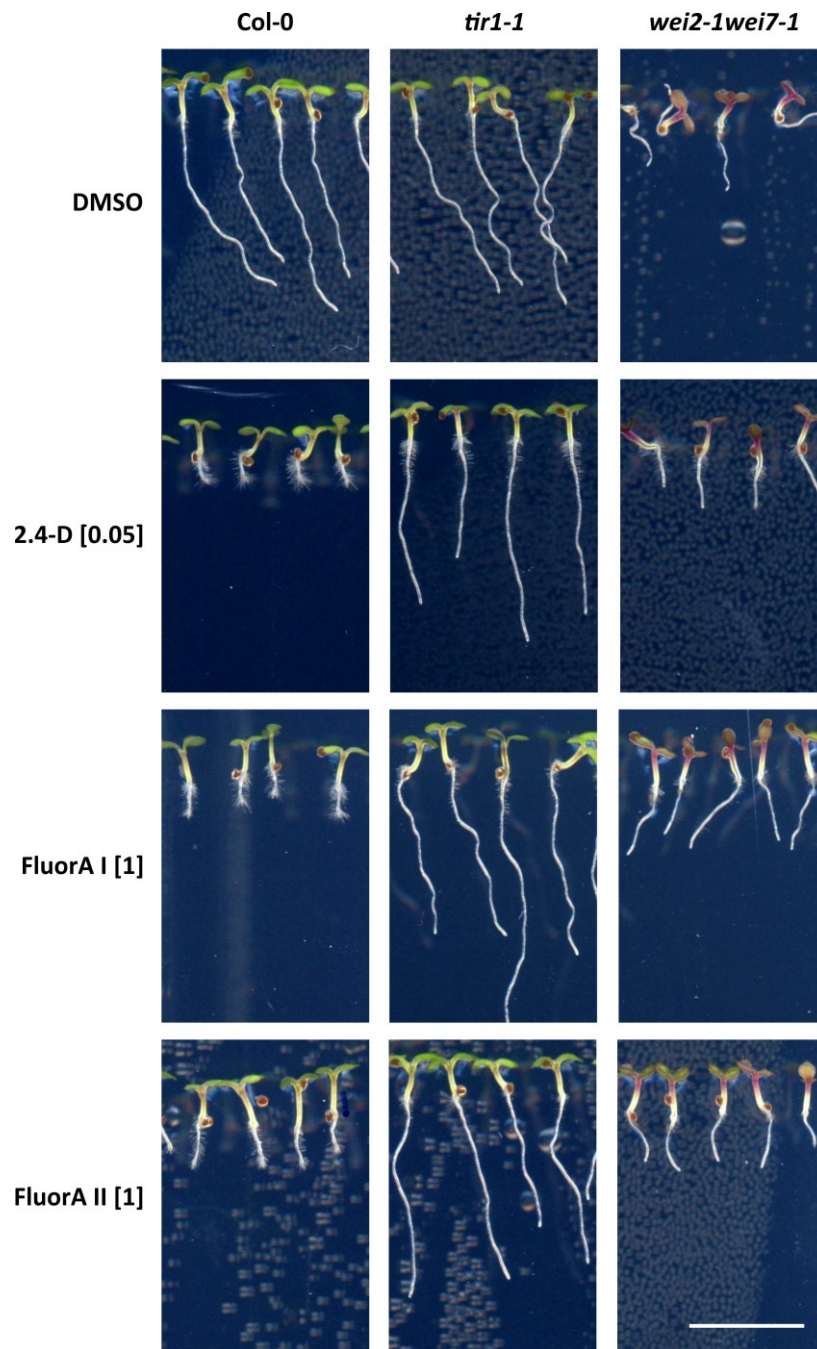


Fig. S3. FluorAs are involved in auxin responses via the TIR1 signaling pathway. The phenotypes of 5-day-old *Arabidopsis* seedlings grown in the presence of 2,4-D, FluorA I and FluorA II at defined concentrations. The *tir1-1* mutant was less sensitive to the compounds than Col-0, suggesting a role of TIR1 in the mode of action of the FluorAs. Moreover, the compounds rescued the agravitropic root phenotype of the *wei2-1wei7-1* auxin biosynthetic mutant. Scale bar represents 1 mm. Concentrations in brackets are in μM .

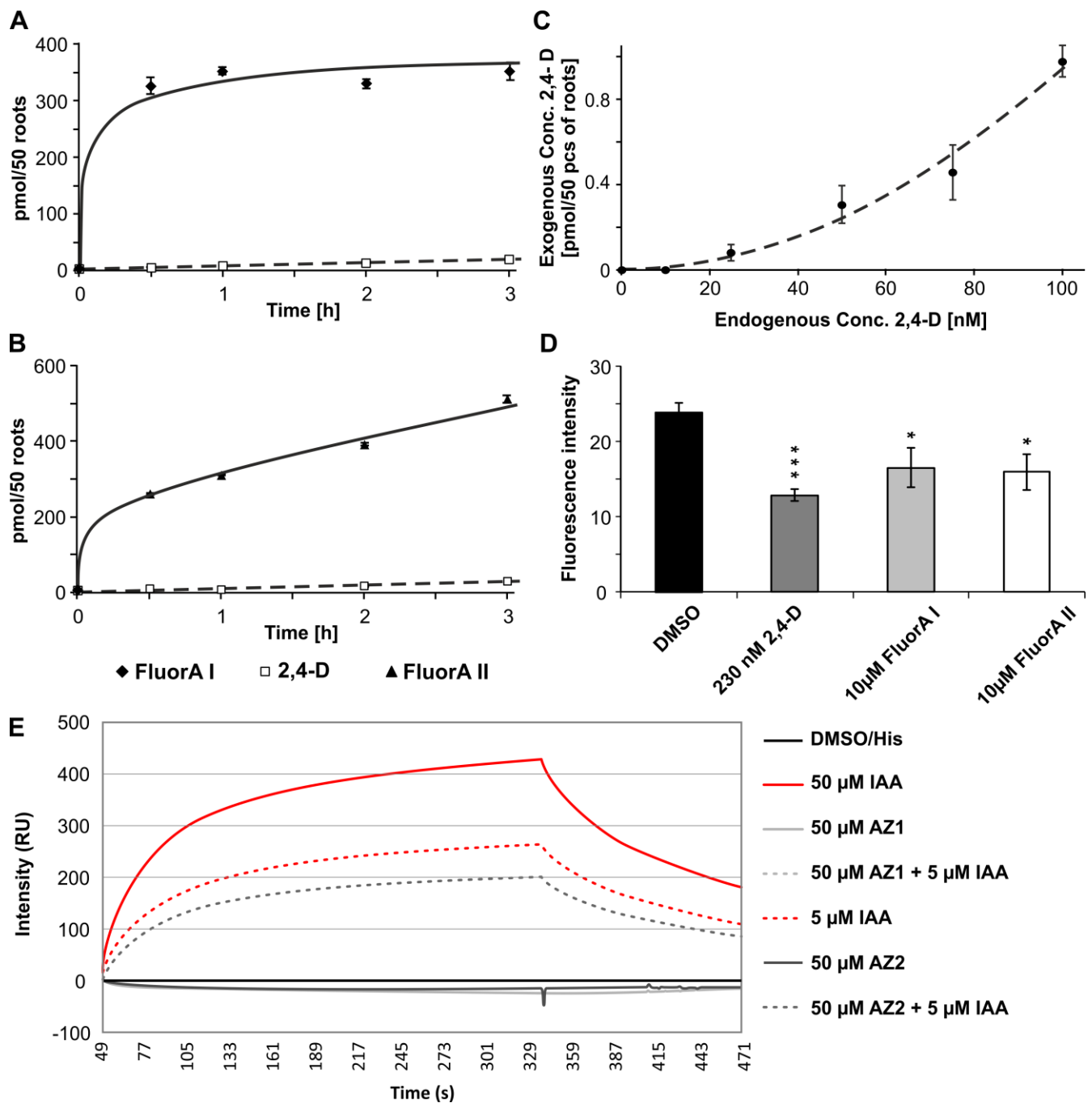


Fig. S4. Biological activity of FluorAs is driven by metabolization *in vivo*. (A-B) Quantitative determination of uptake and metabolization dynamics of FluorA I and FluorA II *in planta* using LC-MS/MS. 5-day-old seedlings of *Arabidopsis* Col-0 WT were treated in liquid media with 10 µM FluorA I (A) or FluorA II (B) and then collected at defined time-points. Both FluorA I and FluorA II displayed similar rates of metabolization, releasing approx. 2.5 pmol/50 roots in 15 min. Values are means \pm SD (n = 5). (C) Determination of endogenous levels of 2,4-D with respect to applied exogenous concentrations after 15 min uptake. Obtained equation was used for calculation of exogenous 2,4-D concentration for achieving 2.5 pmol/50 roots *in planta* (approx. 230 nM). Values are means \pm SD (n = 4). (D) 15 min treatment of *p35S::DII-Venus* seedlings with 10 µM FluorA compounds and 230 nM 2,4-D presuming the equivalent amount of endogenous 2,4-D. Quantification of Venus signal revealed that both treatments displayed similar auxin response suggesting that the bioactivity of FluorA compounds is caused by metabolization of FluorAs *in planta* to free 2,4-D. (E) SPR analysis confirmed *in vitro* that FluorAs do not possess auxin, just very weak anti-auxin, activity to assembly TIR1-IAA7 co-receptor complex.

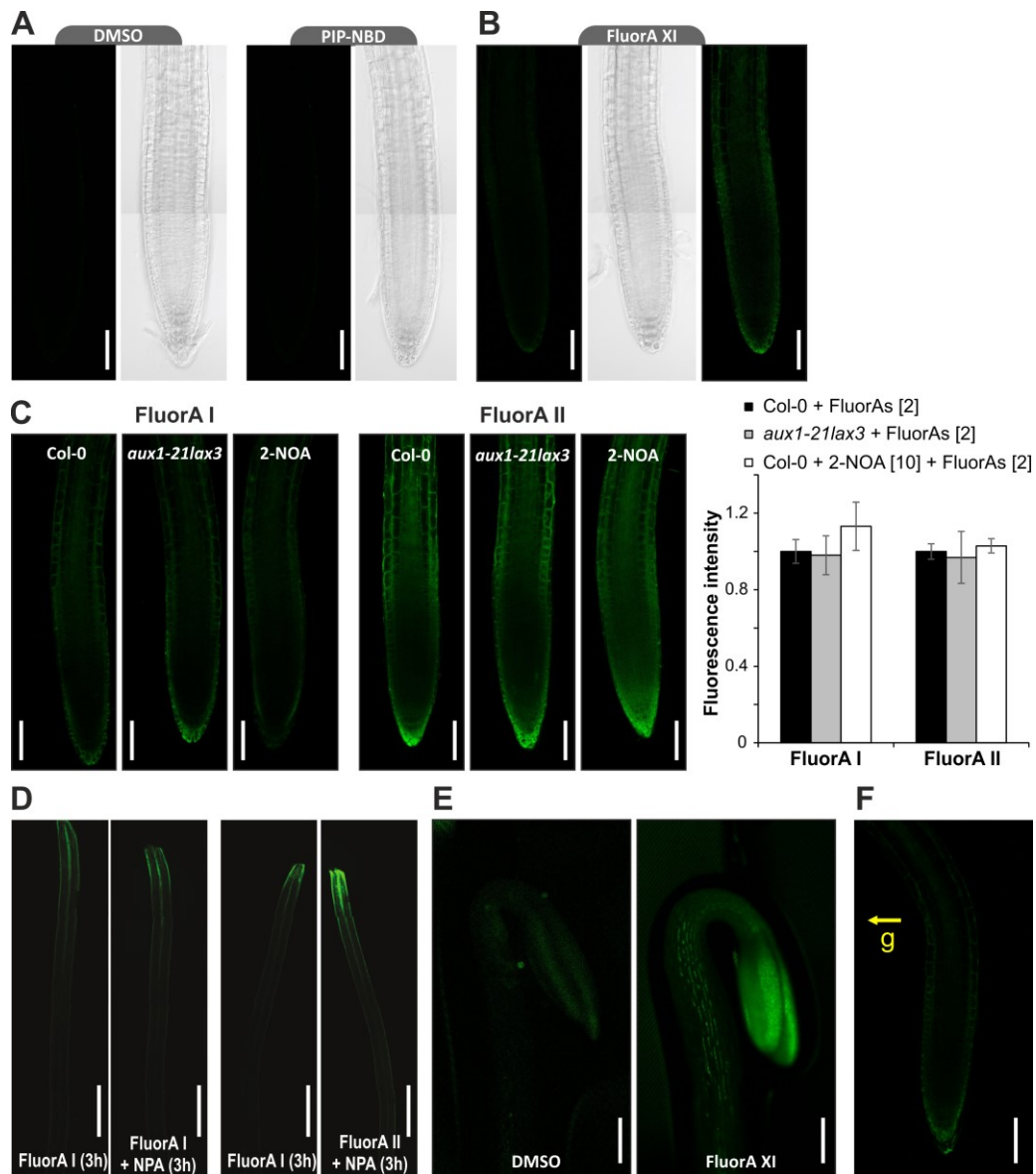


Fig. S5. Distribution of FluorAs *in planta*. (A) Fluorescent pattern of FluorA XI and PIP-NBD structures lacking an auxin-like moiety in 5-day-old *Arabidopsis* Col-0 WT roots under optimized conditions (2 μ M, 15 min). Uptake of compounds appeared to be auxin-dependent. (B) Five-day-old *Arabidopsis* Col-0 WT and *aux1-21/ax3* seedlings were incubated with 2 μ M FluorAs for 15 min. Col-0 seedlings were also pre-treated with 10 μ M 2-NOA for 3 h. No significant effect on fluorescence distribution or intensity of FluorAs was observed after disruption of auxin influx by these chemical genomics or genetics approaches. (C) Agar blocks with 2 μ M FluorA compounds were placed on top of decapitated hypocotyls of x-day-old dark-grown *Arabidopsis* Col-0 WT seedlings and the basipetal transport of the compounds was monitored after 3 h. As a control, pre-treatment with 10 μ M NPA was used to assess the contribution of diffusion. 3-hour treatment with 10 μ M NPA and consecutive decapitation and 3-hour treatment with 2 μ M FluorA I or II agar blocks did not inhibit the transport of the FluorAs. (D) FluorA XI did not exhibit accumulation in apical hooks of 3-day-old dark-grown *Arabidopsis* Col-0 WT seedlings. (E) Gravistimulated roots of 5-day-old *Arabidopsis* Col-0 WT seedlings did not display uneven fluorescence distribution in the root after treatment with 2 μ M FluorA XI for 15 min. (B) Statistical analyses were performed using the Student's *t*-test, values are means \pm SE ($n > 20$ from 3 independent biological replicates); no statistically significant differences were found. (A-B,E) Scale bars indicate 100 μ m; (C-D) scale bars indicate 1 mm. The fluorescent signal was enhanced for FluorA XI in B (right), E and F to emphasize the distribution pattern.

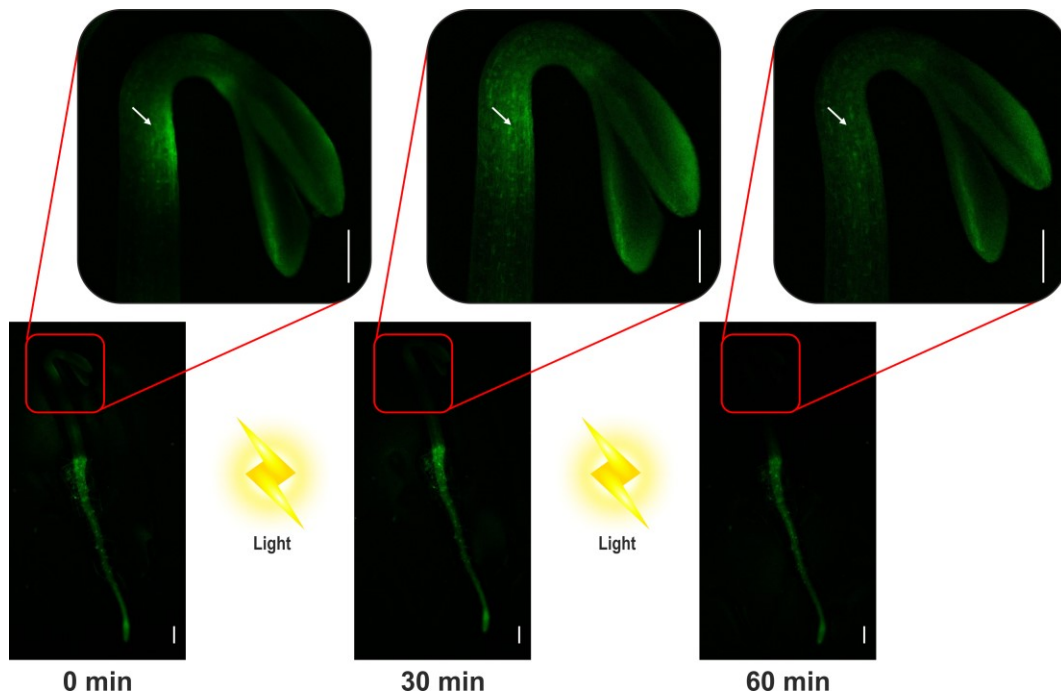


Fig. S6. Distribution response of FluorA II to light in apical hooks is tissue-specific. Apical hooks (upper panels) and roots (lower panels) of 3-day-old dark-grown *Arabidopsis* Col-0 WT seedlings treated with 2 μ M FluorA II for 15 min were imaged using a vertical macroconfocal before (0 min) and 30 and 60 min after a transfer of the plants to standard light conditions. Persistent fluorescent intensity in roots after the light pulse demonstrated that FluorA II re-distribution in apical hooks is tissue-specific and was not due to light-induced degradation of the compound. Scale bars represent 1 mm. The white arrows indicate the redistribution of FluorA II signal in apical hook after light stimulation.



Selective auxin agonists induce specific AUX/IAA protein degradation to modulate plant development

Thomas Vain^{a,1,2}, Sara Raggi^{a,1}, Noel Ferro^b, Deepak Kumar Barange^{a,c}, Martin Kieffer^d, Qian Ma^a, Siansa M. Doyle^a, Mattias Thelander^e, Barbora Pařízková^{f,g}, Ondřej Novák^{a,f,g}, Alexandre Ismail^h, Per-Anders Enquist^c, Adeline Rigal^a, Małgorzata Łangowska^a, Sigurd Ramans Harborough^d, Yi Zhangⁱ, Karin Ljung^a, Judy Callis^j, Fredrik Almqvist^c, Stefan Kepinski^d, Mark Estelleⁱ, Laurens Pauwels^{k,l}, and Stéphanie Robert^{a,3}

^aDepartment of Forest Genetics and Plant Physiology, Umeå Plant Science Centre, Swedish University of Agricultural Sciences, SE-901 83 Umeå, Sweden; ^bInstitute of Physical and Theoretical Chemistry, University of Bonn, 53121 Bonn, Germany; ^cLaboratories for Chemical Biology Umeå, Chemical Biology Consortium Sweden, Department of Chemistry, Umeå University, SE-901 87 Umeå, Sweden; ^dCentre for Plant Sciences, University of Leeds, LS2 9JT Leeds, United Kingdom; ^eDepartment of Plant Biology, Swedish University of Agricultural Sciences, The Linnean Centre for Plant Biology in Uppsala, SE-75007 Uppsala, Sweden; ^fLaboratory of Growth Regulators, Institute of Experimental Botany, The Czech Academy of Sciences, CZ-78371 Olomouc, Czech Republic; ^gLaboratory of Growth Regulators, Faculty of Science, Palacký University, CZ-78371 Olomouc, Czech Republic; ^hSup'Biotech, IONIS Education Group, 94800 Villejuif, France; ⁱSection of Cell and Developmental Biology, University of California, San Diego, La Jolla, CA 92093-0116; ^jDepartment of Molecular and Cellular Biology, University of California, Davis, CA 95616; ^kDepartment of Plant Biotechnology and Bioinformatics, Ghent University, 9052 Ghent, Belgium; and ^lCenter for Plant Systems Biology, Vlaams Instituut voor Biotechnologie, 9052 Ghent, Belgium

Edited by Ottoline Leyser, University of Cambridge, Cambridge, United Kingdom, and approved February 6, 2019 (received for review May 25, 2018)

Auxin phytohormones control most aspects of plant development through a complex and interconnected signaling network. In the presence of auxin, AUXIN/INDOLE-3-ACETIC ACID (AUX/IAA) transcriptional repressors are targeted for degradation by the SKP1-CULLIN1-F-BOX (SCF) ubiquitin-protein ligases containing TRANSPORT INHIBITOR RESISTANT 1/AUXIN SIGNALING F-BOX (TIR1/AFB). CULLIN1-neddylation is required for SCF^{TIR1/AFB} functionality, as exemplified by mutants deficient in the NEDD8-activating enzyme subunit AUXIN-RESISTANT 1 (AXR1). Here, we report a chemical biology screen that identifies small molecules requiring AXR1 to modulate plant development. We selected four molecules of interest, RubNeddin 1 to 4 (RN1 to -4), among which RN3 and RN4 trigger selective auxin responses at transcriptional, biochemical, and morphological levels. This selective activity is explained by their ability to consistently promote the interaction between TIR1 and a specific subset of AUX/IAA proteins, stimulating the degradation of particular AUX/IAA combinations. Finally, we performed a genetic screen using RN4, the RN with the greatest potential for dissecting auxin perception, which revealed that the chromatin remodeling ATPase BRAHMA is implicated in auxin-mediated apical hook development. These results demonstrate the power of selective auxin agonists to dissect auxin perception for plant developmental functions, as well as offering opportunities to discover new molecular players involved in auxin responses.

auxin | chemical biology | selective agonist | prohormone | hormone perception

The survival and reproductive success of all living organisms depend on their ability to perceive and integrate environmental and internal signals. As sessile organisms, plants have developed strategies to adapt to their surroundings, including an extensive developmental plasticity (1). Plant morphological changes are executed through regulation of hormone levels and signaling (2). The phytohormone auxin is involved in almost all aspects of plant development and adaptation. Auxin perception within the nucleus is mediated by the TRANSPORT INHIBITOR RESISTANT 1/AUXIN SIGNALING F-BOX (TIR1/AFB)–AUXIN/INDOLE-3-ACETIC ACID (AUX/IAA) (TIR1/AFB–AUX/IAA) coreceptor complex (3). The TIR1/AFB1–5 F-box proteins are subunits of the S-PHASE KINASE ASSOCIATED PROTEIN 1-CULLIN 1-F-BOX (SCF)-type E3 ligase and act as auxin receptors (4). Formation of the SCF^{TIR1/AFB}–AUX/IAA–auxin complex leads to the ubiquitination of the AUX/IAA transcriptional repressors, targeting them for rapid degradation by the 26S proteasome (4). Removal of AUX/IAAs liberates the auxin response-activating AUXIN RESPONSE FACTOR (ARF) transcription factors from repression (4) and leads to the occurrence of an auxin-

transcriptional response. There is significant variation in auxin-induced degradation rates among different AUX/IAA proteins, and at least some of this variation is attributable to the specificity in the interactions between the 29 AUX/IAAs and 6 TIR1/AFB F-box proteins in *Arabidopsis* (4–6). Amino acids within and outside the degron domain II (DII) of the AUX/IAA proteins determine the interaction strength of the coreceptor and specify AUX/IAA stability (5–7). The multiplicity of the potential coreceptor assembly is the first element mediating the complexity of the auxin response.

Significance

The plant hormone auxin coordinates almost all aspects of plant development. Throughout plant life, the expression of hundreds of genes involved in auxin regulation is orchestrated via several combinatorial and cell-specific auxin perception systems. An effective approach to dissect these complex pathways is the use of synthetic molecules that target specific processes of auxin activity. Here, we describe synthetic auxins, RubNeddins (RNs), which act as selective auxin agonists. The RN with the greatest potential for dissecting auxin perception was RN4, which we used to reveal a role for the chromatin remodeling ATPase BRAHMA in apical hook development. Therefore, the understanding of RN mode of action paves the way to dissecting specific molecular components involved in auxin-regulated developmental processes.

Author contributions: T.V., L.P., and S. Robert designed research; T.V., S. Raggi, N.F., M.K., Q.M., S.M.D., M.T., B.P., A.R., and M.E. performed research; N.F., D.K.B., M.K., B.P., O.N., A.L., P.-A.E., S.R.H., Y.Z., K.L., J.C., F.A., S.K., and M.E. contributed new reagents/analytic tools; T.V., S. Raggi, N.F., S.M.D., M.T., and O.N. analyzed data; and T.V., S. Raggi, S.M.D., and S. Robert wrote the paper.

The authors declare no conflict of interest.

This article is a PNAS Direct Submission.

This open access article is distributed under [Creative Commons Attribution-NonCommercial-NoDerivatives License 4.0 \(CC BY-NC-ND\)](https://creativecommons.org/licenses/by-nc-nd/4.0/).

Data deposition: The whole genome sequencing data of *hkb1* has been deposited at the European Nucleotide Archive, <https://www.ebi.ac.uk/ena> (accession number: PRJEB21529). The RNA sequencing data of *Arabidopsis* cell suspension culture treated with IAA, RN3, and RN4 have been deposited at the European Nucleotide Archive, <http://www.ebi.ac.uk/ena> (accession number: PRJEB31496).

¹T.V. and S. Raggi contributed equally to this work.

²Present address: DIADE, Univ Montpellier, IRD, 34394 Montpellier, France.

³To whom correspondence should be addressed. Email: Stephanie.Robert@slu.se.

This article contains supporting information online at www.pnas.org/lookup/suppl/doi:10.1073/pnas.1809037116/-DCSupplemental.

Published online March 8, 2019.

The ubiquitin-proteasome pathway plays an essential role in plant hormone signaling (8–10). Modification of the relevant components by the ubiquitin-like protein, RELATED TO UBIQUITIN/NEURAL PRECURSOR CELL EXPRESSED DEVELOPMENTALLY DOWN-REGULATED PROTEIN 8 (RUB/NEDD8), which is catalyzed by a cascade of enzymatic reactions analogous to ubiquitination, is critical for the full activity of the proteasome complex (11). In plants, the CULLINs (CUL1, CUL3, and CUL4) are NEDD8-modified proteins that form multimeric E3 ubiquitin ligase complexes (12). CUL1 acts as a scaffold within the SCF-type E3 ligases and neddylation states of CUL1 are essential for the ubiquitin ligase activity of the SCF complex (13). Loss of components of the neddylation pathway, such as the NEDD8-activating enzyme subunit AUXIN RESISTANT 1 (AXR1), reduces the response to several phytohormones, including auxin (14–17).

To understand how auxin perception mediates multiple aspects of plant development, we established an AXR1-dependent developmental defect-based chemical biology screen. Using this approach, we identified small synthetic molecules, RubNeddins (RNs), which selectively promote SCF^{TIR1/AFB}-AUX/IAA coreceptor assembly, allowing local and precise modulation of auxin signaling pathways. Furthermore, these synthetic selective agonists possess the ability to identify and distinguish the molecular players involved in different aspects of auxin-regulated development, thereby dissecting the diversity of auxin action. We demonstrated this by employing these agonists to reveal different roles for specific AUX/IAA proteins during lateral root and apical hook development. In particular, the use of the selective auxin agonist RN4 revealed a role for the chromatin remodeling ATPase BRAHMA in apical hook development.

Results

The Rubylation/Neddylation Pathway Is Required for RNs to Alter Seedling Development. To address the complexity of auxin response, we established a chemical biology screen to isolate synthetic molecules targeting the NEDD8-mediated signaling pathway in *Arabidopsis* (SI Appendix, Fig. S1A and B). We reasoned that some of these molecules might also target the auxin signaling pathway (SI Appendix, Fig. S1A) and we used 1-naphthaleneacetic acid (NAA) as control (SI Appendix, Fig. S1C). This strategy is complementary to previous ones aiming at isolating auxin-related small molecules (18, 19). Compounds affecting auxin-related developmental processes, such as primary root growth, hypocotyl elongation, and gravi- or photo-tropism responses in wild-type but not in *axr1-30* seedlings, were selected (SI Appendix, Fig. S1B). This screening strategy, based on differential effects upon the two genetic backgrounds (Col-0 wild-type vs. *axr1-30*), was essential to filter out chemical activities with general impacts on seedling growth. We hypothesized that a small molecule for which activity was dependent on the AXR1 signaling machinery could be recognized by one or several TIR1/AFB-AUX/IAA coreceptor complexes. Of 8,000 diverse compounds (ChemBridge), we identified 34 small molecules (4.25%) that selectively affected the growth of wild-type compared with *axr1-30* seedlings. Four molecules, named RN1–4, were ultimately selected as they showed a dose-dependent activity and a high potency on wild-type seedling development in the micromolar range (SI Appendix, Fig. S1D). In detail, RN1 activity decreased lateral root number and primary root length, but increased hypocotyl length and adventitious root formation (Fig. 1A and B and SI Appendix, Fig. S2A). RN2 application resulted in the inhibition of primary root growth and lateral root formation, without affecting hypocotyl length (Fig. 1A and C). RN3 promoted the number of lateral roots (Fig. 1A and D). RN4 activity increased hypocotyl elongation and inhibited lateral root formation (Fig. 1A and E). Overall, these structurally similar compounds triggered specific morphological changes in wild-type, while *axr1-30* was resistant to these effects, demonstrating that they require a functional RUB/NEDD8 signaling pathway.

The RNs Act as Developmental Regulators in Several Land Plants. We then analyzed RN effects on *Populus* (poplar) and *Physcomitrella patens* (moss). RN1, which induced hypocotyl elongation and

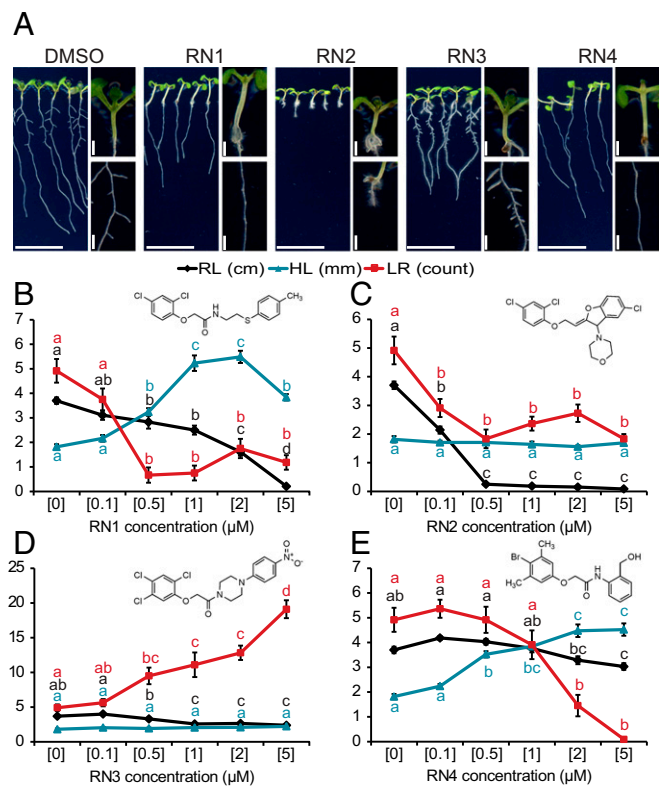


Fig. 1. Four RN chemicals trigger different morphological changes. (A) Col-0 seedlings were grown on RN-supplemented media for 8 d. DMSO was used as control. Images display the effects of the RN at a representative concentration: RN1: 2 μ M; RN2: 0.5 μ M; RN3: 2 μ M; RN4: 5 μ M. (Scale bars, 1 cm.) (B–E) RN1 (B), RN2 (C), RN3 (D), and RN4 (E) selectively affected primary root length (RL), hypocotyl length (HL), and the number of lateral roots (LR). For each graph, the RN structure is reported. Statistics were performed using ANOVA and Tukey's test. Means \pm SEM are shown, $n = 10$ seedlings for each concentration of the dose–response; different letters indicate significant differences at $P < 0.05$. Concentrations in micromolars are indicated in brackets (B–E).

promoted adventitious root formation in *Arabidopsis*, and RN3, which increased lateral root number in *Arabidopsis*, was applied to three different lines of poplar explants (SI Appendix, Fig. S2B–D). The poplar lines were selected for their different rooting abilities; T89 is an easy rooting hybrid while SwAsp19 and -35 have a low rooting capacity even when treated with indole-3-butyric acid, an auxin commonly used as a rooting agent. Interestingly, both RN1 and RN3 promoted adventitious root formation preferentially in the SwAsp lines. Next, the effects of the RNs were investigated in moss and compared with those of IAA (SI Appendix, Fig. S3). Similar to IAA, most of the RNs inhibited caulonemal colony outgrowth (SI Appendix, Fig. S3A). The RN-induced effects on shoots were more diverse. At the tested concentrations, while no effect of RN1 was observed, application of RN2 caused a clear increase in shoot length, RN3 treatment resulted in thinner leaves, and RN4 slightly reduced shoot size (SI Appendix, Fig. S3B). At low concentration, IAA increased the number of buds/shoots per colony after 1 wk (SI Appendix, Fig. S3C), while it reduced bud/shoot formation after 2 wk regardless of the concentrations tested (SI Appendix, Fig. S3D). This dual effect of IAA was mimicked by RN4. RN1 and RN3 treatment resulted mainly in an increase of the bud/shoot number per colony after 1 wk and RN2 only reduced bud/shoot formation after 2 wk. These results demonstrate that the activities of the RNs are mediated by pathways present in several species.

The RNs Partly Function as Prohormones. RN1, RN3, and RN4 share structural similarities with previously described prohormones (19, 20). Because prohormones are hydrolyzed in vivo to release the

active hormone moieties (21), we examined the potential metabolism of the RN compounds in liquid treatment media and *in planta* (SI Appendix, Fig. S4). In RN-supplemented MS media without plants, negligible concentrations of free acids were detected at the 0 h time point, except for 2,4-dichlorophenoxyacetic acid (2,4-D) originating from RN2 and 2,4,5-trichloroacetic acid (2,4,5-T) from RN3 (SI Appendix, Fig. S4D). Importantly, in these plant-free media, no obvious degradation of RN compounds was observed 24 h after treatment. However, in the presence of seedlings, higher levels of the corresponding free acids, 2,4-D, 2,4,5-T, and RN4-1, were found after 24 h in the media treated with RN1, RN3, and RN4, respectively, although the level of 2,4-D in RN2-treated media was not changed (SI Appendix, Fig. S4D). As expected, in *Arabidopsis* seedlings treated by the RNs for 24 h, all free acids were detected in the range from 0.4 to 2% relative to the levels of the corresponding RNs (SI Appendix, Fig. S4E).

These results imply that even though the RN compounds are fairly stable in liquid media, their biological activities might result from their metabolism *in planta* to the free acids 2,4-D (RN1 and RN2) and 2,4,5-T (RN3), which are known to possess auxinic activity and RN4-1 (RN4), which contains a bromo group, an electron-withdrawing substituent that can give rise to a high auxinic activity (22). To address this possibility, we first determined the appropriate treatment concentrations of 2,4-D, 2,4,5-T, and RN4-1 that lead to their accumulation within roots to similar levels as found after treatments with RN1, RN3, and RN4, respectively (SI Appendix, Fig. S5 A, C, and E). Then, using these determined treatment concentrations, we investigated the effects of 2,4-D on primary root length in 5-d-old seedlings (SI Appendix, Fig. S5B) and of 2,4,5-T and RN4-1 on lateral root density in 8-d-old seedlings (SI Appendix, Fig. S5 D and F). The results revealed that 2,4-D, at an *in planta* concentration intermediate to that resulting from treatments with 0.5 and 2 μ M RN1, had an effect on primary root length that was correspondingly intermediate between these two concentrations of RN1 (SI Appendix, Fig. S5B). This suggests that the effect of RN1 on primary root length is likely to be due to the release of 2,4-D. However, in the case of lateral root density, a much weaker effect for 2,4,5-T, or no effect at all for RN4-1, compared with the relevant RN compound was found (SI Appendix, Fig. S5 D and F). These results show that the effects of RN3 and RN4 on lateral root density are only partially, or not at all, due to their degradation to the free acids 2,4,5-T or RN4-1, respectively.

We next performed a structure activity relationship (SAR) analysis by comparing the effects of various RN analogs, 2,4-D, 2,4,5-T, and RN4-1 on plant development and on the expression pattern of the auxin-responsive promoter *DR5* in seedlings of *pDR5::GUS* (23) (SI Appendix, Fig. S6). The SAR analysis indicated that the absence of chlorine at position C2 in the 2,4-D substructure of RN1 (analog RN1-1) or the complete loss of the 2,4-D moiety (analog RN1-2) significantly reduced the effects of RN1 on plant development (SI Appendix, Fig. S6 A and E), implying that the 2,4-D substructure is important for RN1 activity. Modification of the 2,4-D core structure in RN2 (analog RN2-2) abolished its potency, whereas analogs displaying a side-chain modification (RN2-1 or RN2-3) were as potent as RN2 (SI Appendix, Fig. S6 B and F), indicating that the activity of RN2 is most probably attributable to the release of 2,4-D in the growing media. Like RN2, none of the RN2 analogs visibly altered the *pDR5::GUS* expression pattern compared with the DMSO control. RN3 mainly promoted lateral root number, while its effect on primary root elongation was mild (Fig. 1D). Analogs RN3-2 and RN3-3, with modifications on the phenylpiperazine side chain, behaved similarly to RN3 (SI Appendix, Fig. S6 C, G, and H). However, removal of the whole side chain from RN3, generating 2,4,5-T, abolished its positive effect on lateral root number and introduced a strong inhibitory effect on primary root length (SI Appendix, Fig. S6H), suggesting a difference in potency between the two compounds. Moreover, the activity of RN3 was significantly compromised by disruption of the substructure of 2,4,5-T (analog RN3-1) via loss of the three chlo-

rines (SI Appendix, Fig. S6 C, G, and H). These results suggest that the 2,4,5-T substructure is critical for RN3's potency. Further comparisons using analogs only differing in the number of chlorines on the 2,4,5-T substructure, such as between RN3-2, RN3-4, and RN3-6, or between RN3-3, RN3-5, and RN3-7, indicated that C5 chlorination of the 2,4,5-T moiety is crucial for RN3's selective activity. Intriguingly, while RN3 did not alter the *pDR5::GUS* expression pattern compared with the DMSO control, fluorination of the phenyl in RN3 induced *pDR5::GUS* expression in some cases (analog RN3-3 compared with RN3-2), while reducing it in other cases (analogs RN3-5 and RN3-7 compared with RN3-4 and RN3-6, respectively) (SI Appendix, Fig. S6C). These results reinforce the importance of C5 chlorination of the 2,4,5-T moiety for the selective activity of RN3.

We showed that RN4 releases the free acid RN4-1 *in planta* (SI Appendix, Figs. S4 D and E and S5E), possibly by hydrolysis. As expected, considering the presence of a bromo group, this compound strongly induced *pDR5::GUS* expression, in contrast to RN4 itself (SI Appendix, Fig. S6D). While RN4-1 significantly enhanced hypocotyl elongation, it was not as potent in this regard as RN4 (SI Appendix, Fig. S6 D and I). Comparison of the effects of modifications of the RN4-1 substructure (analog RN4-2) and of the hydroxymethylphenylamine substructure (analog RN4-10) of RN4 indicate that while the intact auxinic RN4-1 moiety is indispensable for RN4's effect on the hypocotyl, the nonauxinic side chain is also required to induce maximal hypocotyl elongation (SI Appendix, Fig. S6 D and I). Further comparison between RN4-2 and RN4, as well as their free acids (RN4-3 and RN4-1, respectively), highlight the key contribution of the bromophenoxy methylation to the selective activity of RN4 on hypocotyl rather than primary root (SI Appendix, Fig. S6 D, I, and J). Consistent with the SAR results, even though RN4-2 shows a bipartite structure, it was still able to induce *pDR5::GUS* expression (SI Appendix, Fig. S6D). RN4-10, in which the nonauxinic moiety of RN4 is modified, induced *pDR5::GUS* expression slightly more than RN4 (SI Appendix, Fig. S6D). We also designed RN4 analogs with predicted low hydrolysis capacity (RN4-4, RN4-8, RN4-9, and RN4-11). As expected, none of these analogs could induce hypocotyl growth (SI Appendix, Fig. S6 D and I), indicating that the typical bipartite prohormone structure of RN4 is important for its effect on hypocotyl elongation and that hydrolysis is required to liberate this activity. Moreover, except for RN4-9, these compounds could not induce *pDR5::GUS*. Interestingly, the analog RN4-11, generated by methylation of RN4 on the amide bond, inhibited primary root elongation without affecting hypocotyl length (SI Appendix, Fig. S6J). Because the predicted corresponding free acid RN4-1 did not reduce primary root length, this result indicates that the full, nonhydrolyzed RN4 structure possesses additional auxin-like activity.

Overall, we showed that RN1, RN3, and RN4 function as prohormones, being metabolized *in planta* to release more potent auxin agonists, while the effects of RN2 are most likely due to its degradation to 2,4-D. However, our SAR results also suggest that the nonhydrolyzed forms of RN1, RN3, and RN4 display additional auxin-like effects and therefore might themselves act as selective auxin agonists.

The RNs Act as Selective Auxin Agonists. AXR1 is a component of the neddylation pathway targeting, among others, the CUL proteins (11). To determine which CUL proteins might be involved in mediating the effects of each RN, we tested their potency on the loss-of-function *cul1-6*, *cul3a/b*, and *cul4-1* mutants. We limited these tests to RN1, RN3, and RN4 as we showed that RN2 activity is most probably due to its *in vitro* cleavage into 2,4-D, an already well-described synthetic auxin. All three tested RNs had a lesser effect on the *cul1-6* mutant than on other CUL mutant lines (Fig. 2A), indicating that they function at the level of or upstream of CUL1. Given that signaling pathways mediated by AXR1 and CUL1 converge at the SCF complex, and that the chemical structures and activities of the three RNs are related to auxin, we hypothesized that auxin receptor F-box proteins might

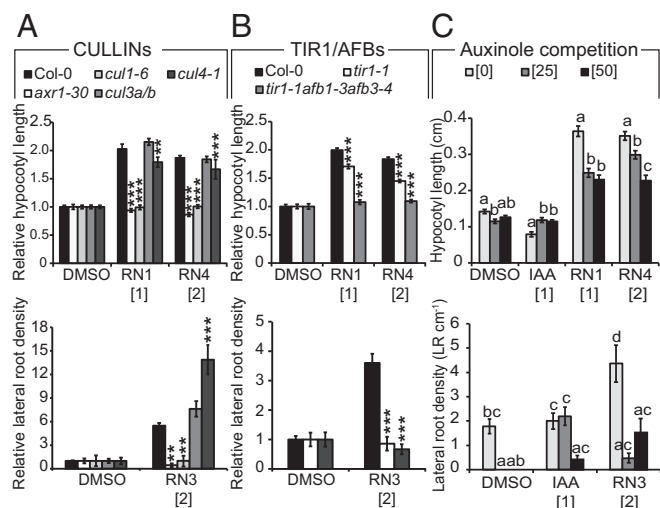


Fig. 2. RN-induced phenotypes require the formation of a functional auxin-SCF^{TIR1/AFB} complex. Relative (treated/DMSO) (A and B) or absolute (C) hypocotyl length (Upper charts) and lateral root density (Lower charts) were measured for wild-type (Col-0) and mutant seedlings grown on media supplemented with RN compounds for 7 d. DMSO was used as control. (A) *axr1-30*, *cul1-6*, *cul3ab*, and *cul4-1*. (B) *tir1-1* and *tir1-1afb1-3afb3-4*. (C) Auxinole competition assay on Col-0. Statistics were performed using ANOVA and Tukey's test. Means \pm SEM are shown, $n = 30$ seedlings across three independent replicates, $**P < 0.01$, $***P < 0.001$ (A and B) or different letters indicate significant differences at $P < 0.05$ (C). Concentrations in micromolars are indicated in brackets.

also be required for RN activities. To test this, we examined *tir1* single and *tir1/afb* multiple mutants and found that the RN-induced phenotypes were strongly reduced when the compounds were applied on *tir1-1* and *tir1-1afb1-3afb3-4* (24, 25) (Fig. 2B). Thus, a functional SCF^{TIR1/AFB} complex is essential for the effects of the RNs. To further confirm this result, we tested the effect of cotreatment of the compound auxinole (26), an auxin antagonist specific for SCF^{TIR1/AFB}, together with each of the three RNs or the endogenous auxin IAA in the wild-type. The RN-induced phenotypes were inhibited by auxinole (Fig. 2C), demonstrating that auxin coreceptor complex formation is essential for RN activities.

Next, we employed a molecular modeling strategy to explore the possible interactions of the RNs with the DII degon of AUX/IAA7 in the auxin-binding pocket of TIR1. Docking experiments validated that the physical property of the auxin-binding pocket was promiscuous enough to accommodate the potential steric hindrance of RN1, RN3, or RN4 (Fig. 3A–C and Movie S1). The calculated free energies (ΔG) of binding also revealed thermodynamic stability for the three RNs inside the auxin pocket of TIR1 (Fig. 3A–C and SI Appendix, Fig. S7A). The positive control IAA was able to bind TIR1 with a $\Delta G_{(IAA-TIR1)}$ of -11.68 , whereas the negative control Tryptophan (Trp) was not, with a $\Delta G_{(Trp-TIR1)}$ of 63.34 (SI Appendix, Fig. S7A). Among the RN analogs, RN4-1 and RN4-2 showed stronger thermodynamic stability compared with IAA. RN2 and the inactive analog RN4-8 could not dock inside the auxin-binding site to stabilize TIR1 (SI Appendix, Fig. S7A). This last result confirmed once again that RN2 activity is most likely due to its cleavage into 2,4-D.

To experimentally confirm the binding of the RNs within the auxin coreceptor complex, we tested their ability to promote the interactions between TIR1 and AUX/IAA proteins using in vitro pull-down assays. First, TIR1-myc protein purified from wheat germ extract and four different GST-AUX/IAA proteins were used (27–29). IAA stimulated the interaction of TIR1-myc with all AUX/IAAs tested (Fig. 3D and SI Appendix, Fig. S7B). All three RNs stimulated the recovery of TIR1-myc in complex with GST-SHY2/IAA3 or GST-AXR2/IAA7 to a similar extent (Fig. 3D and SI Appendix, Fig. S7B). In the case of GST-AXR5/IAA1, RN1 stimulated the interaction with TIR1-myc, while RN3 had

little effect and surprisingly, RN4 decreased the basal interaction (Fig. 3D and SI Appendix, Fig. S7B). When GST-AXR3/IAA17 was used as bait, RN1 strongly promoted the interaction with TIR1-myc, while RN3 had little effect and again, RN4 reduced the basal interaction (Fig. 3D and SI Appendix, Fig. S7B). These data imply that RN3 and RN4 are able to selectively promote the interactions between specific TIR1 and AUX/IAA protein combinations in this system, while RN1 and IAA promoted each interaction, as shown previously for IAA (27–29).

To test that these effects on TIR–AUX/IAA complex formation were not dependent on metabolism of the RN compounds in the wheat germ extract, we next performed a complementary pull-down experiment using insect cell-expressed TIR1 (as a His-MBP-FLAG-TIR1 fusion protein) with bacterially expressed GST-AXR2/IAA7 or GST-AXR3/IAA17 in the presence of the RNs or the RN4 degradation product RN4-1 (SI Appendix, Fig. S7C and D). In this system, the RNs again promoted selective interactions between TIR1 and AXR2/IAA7 or AXR3/IAA17, this time in the absence of potential plant hydrolases (in insect cells). Importantly, the promotion and inhibition of TIR1 interaction with AXR2/IAA7 and AXR3/IAA17, respectively, by RN3 and RN4 were identical in the two in vitro systems. Moreover, the degradation product RN4-1 behaved differently from RN4, by not promoting the interaction between TIR1 and AXR2/IAA7 and slightly promoting the interaction between TIR1 and AXR3/IAA17,

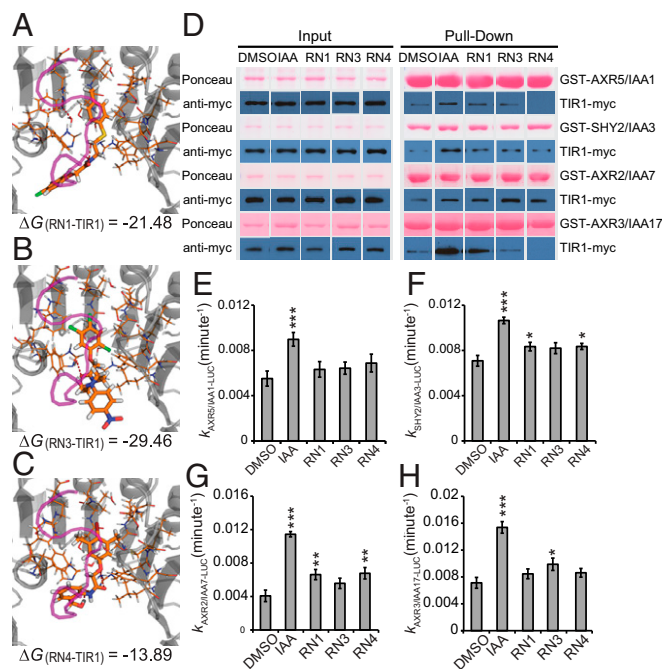


Fig. 3. RN3 and RN4 act as selective agonists of auxin. (A–C) The RNs showed different thermodynamic stabilities from the calculated free energies (ΔG). RN1 (A), RN3 (B), and RN4 (C) were sterically favorable for the binding of the AUX/IAA7 DII degon. TIR1 is presented in gray and the AUX/IAA7 DII degon, which was included afterward to observe any conflict with the RNs, is in purple. Thermodynamic stability was computed within the TIR1 auxin binding pocket and the most stable conformations are represented. (D) The potential of the RNs (at 50 μ M) to promote the formation of the coreceptor complex was performed using in vitro translated TIR1-myc and recombinant GST-AUX/IAAs. Depending on the GST-AUX/IAA translational fusion used for the in vitro GST pull-down, the RNs selectively increased the recovery of TIR1-myc. (E–H) AUX/IAA degradation was assayed in *planta* using *Arabidopsis* lines constitutively expressing different AUX/IAA-LUCs in the presence of RNs at 50 μ M. Effects of the RNs on the in vivo degradation rate k of AXR5/IAA1-LUC (E), SHY2/IAA3-LUC (F), AXR2/IAA7-LUC (G), or AXR3/IAA17-LUC (H) translational fusions. Statistical analyses were performed using the Student's t test. Means \pm SEM are shown, $n = 30$ seedlings across five independent replicates, $*P < 0.05$, $**P < 0.01$, $***P < 0.001$.

which might explain these compounds' different activities *in vivo*. In fact, we were able to confirm that the observed TIR1–AXR/IAA interactions in this system were induced or repressed specifically by the RNs and not by their free-acid degradation products, as no 2,4-D, 2,4,5-T, or RN4-1 could be detected at relevant time points in the pull-down reactions treated with RN1, RN3, or RN4, respectively (*SI Appendix, Fig. S7E*). These data demonstrate that RN3 and RN4 are able to selectively promote the interactions between TIR1 and certain AUX/IAA proteins. Hence, our results suggest that RN3 and RN4 are not just pro-hormones, but also act consistently as selective auxin agonists in two different *in vitro* experimental conditions and their effects on plant development may therefore be attributable to selective auxin agonistic activity.

To test whether the RNs might also act as selective auxin agonists *in planta*, we assayed their potency in promoting the *in vivo* degradation of the AUX/IAA proteins. In a 1-h time course, IAA significantly increased the degradation rate of the four tested AUX/IAA-LUCIFERASE (LUC) proteins, while the RNs had different potency depending on the AUX/IAA proteins used (Fig. 3 *E–H* and *SI Appendix, Fig. S7F*). Therefore, the RN molecules act as selective auxin agonists both *in vitro* and *in vivo*, but the specificity of the interactions seems to be dependent on the experimental conditions, as the predicted behavior of AUX/IAA proteins based on their sensitivity to RN3 and RN4 in our *in planta* LUC assays did not always match that in our *in vitro* pull-down assays. While the conditions tested *in vivo* reflect RN capacity to enhance the interactions of the different SCF^{TIR1/AFB}–AUX/IAA coreceptors within a complex molecular surrounding, those tested *in vitro* reflect the interactions in much simpler conditions. Nonetheless, our results imply that altering interaction affinity within each coreceptor complex with selective auxin agonists might modulate a multitude of specific plant development aspects.

RN3 and RN4 Induce Selective Early Transcriptional Responses. The *in vitro* assays indicated that RN3 and RN4 are the most selective auxin agonists, showing different effects on different AUX/IAA proteins. Moreover, RN3 and RN4 induced distinct developmental processes, particularly on lateral root development. While RN3 enhanced the density of lateral roots without affecting primary root length in the wild-type, RN4 inhibited lateral root development (Fig. 1). Because these RNs promoted fast degradation of AUX/IAA proteins fused to LUC, we investigated how their activities fine-tuned events downstream of coreceptor complex formation. To this end, we performed transcriptome-wide expression profiling of *Arabidopsis* cell suspension cultures treated with IAA, RN3, and RN4, to characterize the early transcriptional responses induced by these compounds (*Dataset S1*). The data have been deposited at the European Nucleotide Archive (www.ebi.ac.uk/ena) under the accession number PRJEB31496 (30). Analysis of the differentially expressed genes (DEGs) revealed subsets that were up- or down-regulated specifically by one, two, or all three chemical treatments (*SI Appendix, Fig. S8A* and *Table S1*). Among the early auxin-responsive genes identified, *AXR5/IAA1*, *IAA2*, *SHORT HYPOCOTYL 2 (SHY2)/IAA3*, and *IAA30* were significantly up-regulated by IAA, RN3, and RN4 (Fig. 4A and *SI Appendix, Table S1*). *IAA5* and *IAA16* expressions were induced specifically by IAA and RN3, while *IAA10* and *IAA29* expressions were up-regulated selectively by IAA and RN4, revealing some differences between RN3 and RN4 in their capacity to induce early-responsive AUX/IAA genes. In total, 121 genes were differentially up-regulated by IAA, RN3, and RN4, such as *LATERAL ORGAN BOUNDARIES-DOMAIN 16 (LBD16)*, *BASIC HELIX-LOOP-HELIX 32 (BHLH32)*, *PINOID-BINDING PROTEIN 1 (PBP1)*, and *PIN-FORMED 3 (PIN3)* (31–34) (Fig. 4A), confirming the potential of the RNs to modulate auxin-related developmental processes. The genes *CINNAMATE 4 HYDROXYGENASE (C4H)*, *TRANSPARENT TESTA 4 (TT4)*, *TT5*, *DEHYDRATION RESPONSE ELEMENT-BINDING PROTEIN 26 (DREB26)*, and *EARLY-RESPONSIVE TO DEHYDRATION 9*

(*ERD9*) were commonly up-regulated by IAA and RN3 but not by RN4. These five genes are known to be tightly regulated in a tissue-specific and auxin-dependent manner to modulate lateral root density and architecture (35–39). Among the genes commonly regulated by IAA and RN4 but not RN3, we identified *MYELOBLASTOSIS 77 (MYB77)* and *BREVIX RADIX (BRX)* transcription factors, which have been shown to control lateral root formation in an auxin-dependent manner (40, 41). These results correlate with the differential effects of RN3 and RN4 on lateral root development. Taken together, these data demonstrate the potential of RN3 and RN4 to specifically identify auxin-responsive genes involved in defined developmental processes, such as lateral root formation. Overall, we showed that RN molecules are able to selectively trigger specific auxin perception machinery, inducing expression of specific sets of genes, and resulting in distinct developmental traits.

RN3 and RN4 Induce Specific Subsets of Auxin Responsive Promoters.

We further investigated the abilities of RN3 and RN4 to selectively induce later auxin responses using various auxin-responsive reporter lines after 45 min, 5 h, or 16 h of RN treatment. We found that neither the auxin-responsive reporter *pDR5::GUS* nor the indicator of nuclear auxin perception *p35S::DII-Venus* (42) showed any response to RN treatment in the primary root (Fig. 4B and *SI Appendix, Fig. S8B* and *D*). However, in the root–hypocotyl junction, the expression of *pDR5::GUS* was promoted by either longer treatment (24 h) or higher concentration (50 μ M) of RN3 or RN4 (Fig. 4C and *SI Appendix, Fig. S8C*). To determine whether these effects were specific to the RNs or rather due to their free-acid degradation products, we first determined the appropriate treatment concentrations of 2,4,5-T and RN4-1 that lead to their accumulation within the roots to similar levels as found after 16-h treatments with RN3 and RN4, respectively (*SI Appendix, Fig. S9A* and *B*). While treatment with 2,4,5-T, similar to RN3, had no effect on *pDR5::GUS* expression in the root (*SI Appendix, Fig. S9C*), treatment with RN4-1, in contrast to RN4, induced *pDR5::GUS* expression in the root (*SI Appendix, Fig. S9D*). For other auxin-responsive reporter lines tested, RN3 and RN4 induced expression patterns that partially overlapped with those induced by IAA (Fig. 4B and C). In the primary root, the RN compounds induced *pSHY2/IAA3::GUS* and *pBODENLOS (BDL)/IAA12::GUS* expression with different patterns compared with that induced by IAA, but did not stimulate *pMASSUGU2 (MSG2)/IAA19::GUS* expression (Fig. 4B). Both compounds also promoted the expression of *pGATA23::GUS*, a marker of lateral root founder cell identity (43). RN4 additionally induced *pSHY2/IAA3::GUS* expression in the hypocotyl and the shoot apical meristem (Fig. 4C). In contrast to the primary root, RN3 and RN4 induced *pMSG2/IAA19::GUS* expression in the hypocotyl (Fig. 4C), although only RN4 induced hypocotyl elongation (Fig. 1B). Treatment of these auxin-responsive reporter lines with 2,4,5-T induced similar expression patterns in the primary root as treatment with RN3 (*SI Appendix, Fig. S9C*), suggesting that the observed effects of RN3 may in fact be due to 2,4,5-T activity. However, as found for the *DR5* promoter, RN4-1 induced the expression of most of the other promoters tested more strongly than RN4 in the primary root (*SI Appendix, Fig. S9D*), suggesting that these two compounds affect auxin-responsive promoter expression rather differently. Despite the release of RN4-1 during RN4 treatment, the effects of RN4 appear to be prominent as this compound did not induce *pDR5::GUS* despite the presence of RN4-1. Our data indicate that RN3 and RN4 may be able to induce specific auxin-regulated promoters, which might be responsible for their selective activities on plant development. Indeed, these RNs activate some but not all modules of the auxin signaling pathway within the same tissue, confirming their selective auxin agonist activities.

A summary of the results obtained for the four RNs is presented in *SI Appendix, Table S2*. In particular, RN3 and RN4 behave as auxin agonists, which selectively promote or inhibit AUX/IAA degradation in a reproducible manner, leading to specific transcriptional regulation and developmental outputs.

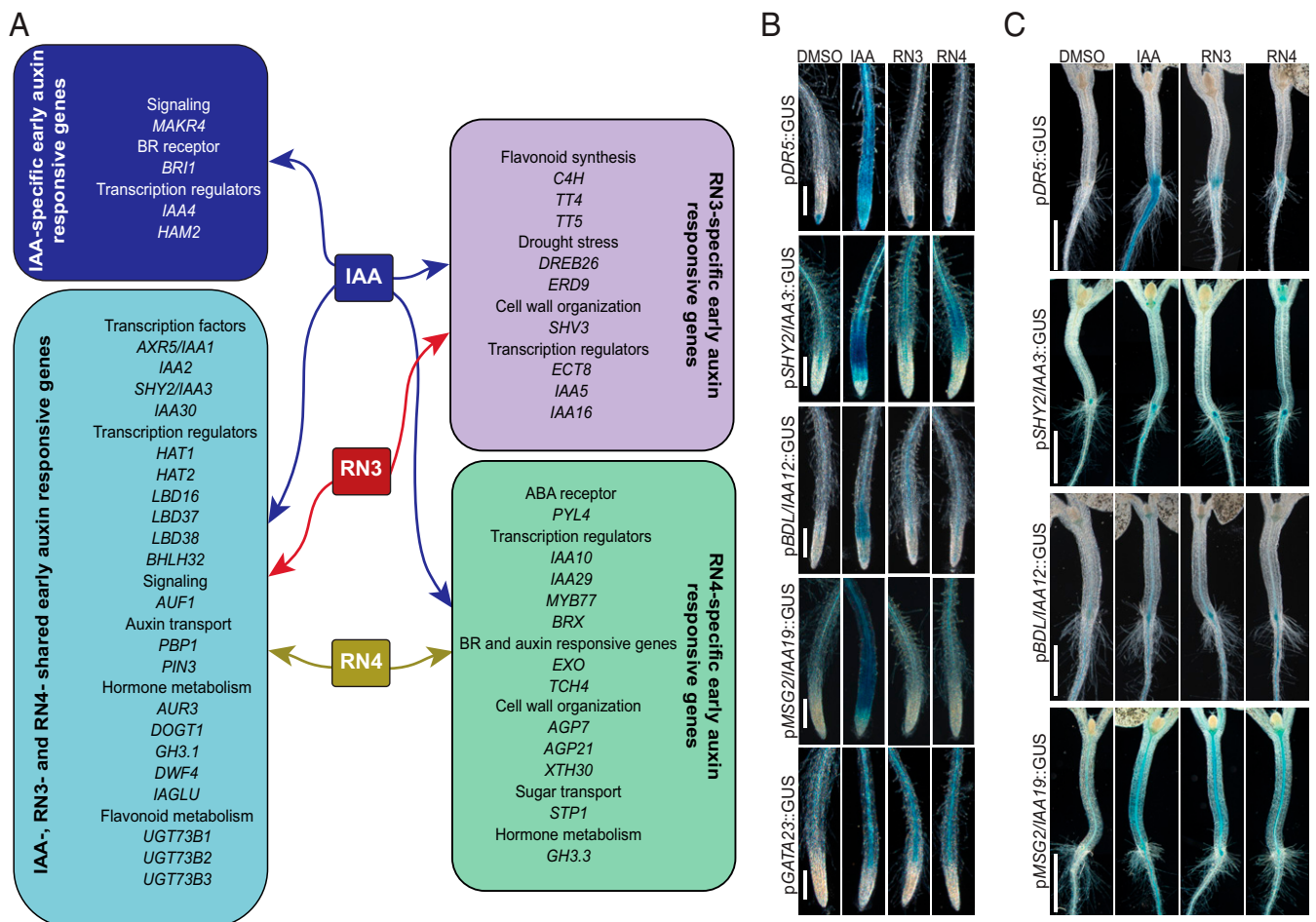


Fig. 4. RN3 and RN4 activate independent auxin responses. (A) Selected sets of up-regulated genes in cell culture representing: IAA-specific induced genes (dark blue); IAA-, RN3-, and RN4-induced genes (light blue); IAA- and RN3-specific induced genes (lilac); and IAA- and RN4-specific induced genes (green) (see Dataset S1 for the complete list of genes and *SI Appendix, Table S1* for fold induction values of the selected genes). (B and C) Five-day-old seedlings expressing pDR5::GUS, pSHY2/IAA3::GUS, pBDL/IAA12::GUS, pMSG2/IAA19::GUS, or pGATA23::GUS transcriptional fusions treated with IAA, RN3, and RN4 at 10 μ M for 16 h. DMSO was used as control. (B) Representative primary roots after GUS staining. (C) Representative hypocotyl-root junctions after GUS staining. (Scale bars, 100 μ m in B and 1 mm in C.)

AUX/IAA Sensitivity to RN3 and RN4 in Planta. We hypothesized that as the RN molecules show selectivity toward the auxin coreceptor complex, they might help to dissect specific functions of individual AUX/IAAs in distinct developmental processes. One approach to achieve this could be to investigate the responses of AUX/IAA gain-of-function mutants to auxin treatment; however, such a genetic approach could prove problematic due to high redundancy among the AUX/IAAs. As a potentially more effective alternative, we challenged such mutants with the specific auxin analogs RN3 and RN4.

We first focused on lateral root development as RN3 and RN4 had opposite effects on this process (Fig. 1 D and E). Furthermore, based on our transcriptomic analysis, RN3 and RN4 induce different sets of IAA-responsive genes that are known to be involved in the regulation of lateral root development (Fig. 4A). We therefore investigated the sensitivities of 8-d-old seedlings of AUX/IAA gain-of-function mutants *axr5-1/iaa1* (28), *axr2-1/iaa7* (44), *shy2-2/iaa3* (45, 46), and *solitary root (slr-1/iaa14)* (47) to treatments of RN3 and RN4 with regards to lateral root development. We tested the sensitivities of these gain-of-function mutants to RN3, which increases lateral root density in Col-0 and Ler, with the Col-0 accession interestingly showing much higher sensitivity to this effect (Fig. 5A). We found that most of the mutants were also sensitive to this effect, with the exception of *slr-1/iaa14* (Fig. 5A). The mutant *shy2-2/iaa3*

was more sensitive to this effect of RN3 than the wild-type (Fig. 5A); however, it is important to note that in this mutant, this compound mainly induced the slight emergence of lateral root primordia rather than the emergence of well-developed lateral roots. These data suggest that apart from SLR/IAA14, the AUX/IAAs we tested are not required for the stimulatory activity of RN3 on lateral root density. We next aimed to characterize RN4 activity on lateral root development in these mutants. RN4 reduced lateral root density in Col-0 and Ler (Fig. 5B). Compared with Col-0, *axr5-1/iaa1* was resistant to this effect of RN4 at 5 μ M, while *axr2-1/iaa7* was sensitive at both tested RN4 concentrations (Fig. 5B). Interestingly, *shy2-2/iaa3* was sensitive to RN4 at 5 μ M, but resistant at 2 μ M, compared with Ler (Fig. 5B). Our results suggest that AXR5/IAA1 and SHY2/IAA3 might be degraded by RN4 to reduce lateral root density.

By using the RN molecules, we revealed potential contributions of specific AUX/IAAs to the complicated process of lateral root development. However, the sensitivities of the *aux/iaa* gain-of-function mutants to the RNs in terms of lateral root development did not exactly match the RN-induced AUX/IAA degradation/stabilization results found with our binding affinity assays. Lateral root development is a complicated process that requires the formation of a new meristem and emergence through several root layers, suggesting that the specific tissue context may affect RN activity and selectivity. We therefore decided to switch our focus to apical hook development in etiolated seedlings, a

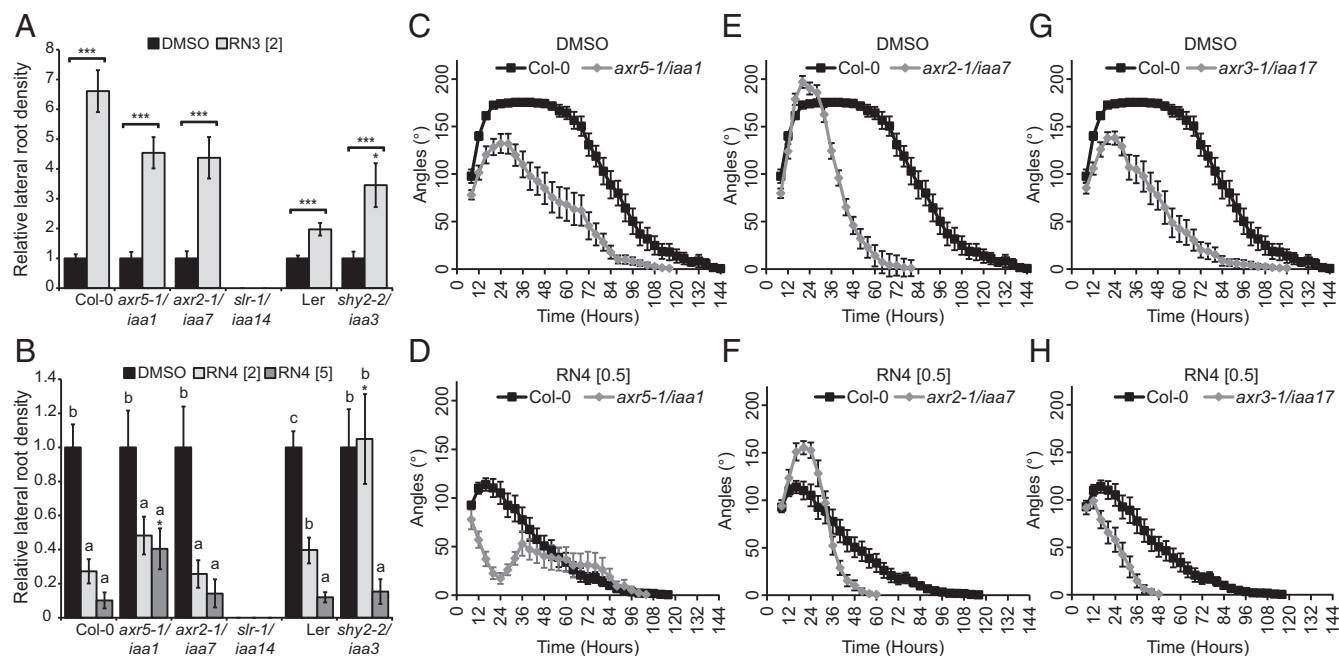


Fig. 5. RN-induced phenotypes require the degradation of specific AUX/IAAs. (A and B) Relative lateral root density (treated/DMSO) was measured for gain-of-function mutants *axr5-1/iaa1*, *axr2-1/iaa7*, *slr-1/iaa14*, and *shy2-2/iaa3* and their respective wild-type grown on media supplemented with RN3 (A) and RN4 (B) for 8 d. DMSO was used as control. Statistical analyses were performed using Student's *t* test (A), or ANOVA and Tukey's test (B) to compare the effect of RN3 (A) or RN4 (B) relative to the DMSO control for each genotype, as indicated with triple asterisks and square brackets (A) or different letters (B). The Student's *t* test was used to compare the relative effect of RN3 (A) or RN4 (B) on the mutants to that on the relevant wild-type, as indicated with single asterisks. (C–H) Gain-of-function mutants *axr5-1/iaa1* (C and D), *axr2-1/iaa7* (E and F), and *axr3-1/iaa17* (G and H) were grown in the dark on DMSO (C, E, and G) and RN4 (D, F, and H)-supplemented media for 6 d. Measurement of apical hook angle was performed every 3 h. Means \pm SEM are shown, $n > 20$ seedlings across three independent replicates; * $P < 0.05$, ** $P < 0.01$, *** $P < 0.001$, different letters indicate significant differences at $P < 0.05$. Concentrations in micromolar are indicated in brackets.

rather simpler process than lateral rooting, but one also regulated by auxin (48). Apical hook development is characterized by differential growth between the two sides of the apical hypocotyl and comprises the formation, maintenance, and opening phases (49, 50). We first tested the effects of RN3 and RN4 on apical hook development in the wild-type (*SI Appendix, Fig. S10A*). While 2 μ M RN3 did not affect apical hook development, RN4 completely abolished hook formation in a dose-dependent manner (*SI Appendix, Fig. S10 A and B*).

We decided to exploit RN4 to understand whether selected AUX/IAAs play specific roles during apical hook development. We tested the effects of 0.5 μ M RN4 on hook development in the gain-of-function mutants *axr5-1/iaa1*, *axr2-1/iaa7*, and *axr3-1/iaa17* for 6 d in the dark. All three mutants showed altered apical hook development compared with the wild-type in control conditions (Fig. 5 C, E, and G). A detailed analysis of these results indicates that AXR5/IAA1 and AXR3/IAA17 need to be degraded for a proper apical hook to develop, while AXR2/IAA7 is likely stabilized during the formation phase and degraded during the maintenance phase. Similar to the wild-type, *axr5-1/iaa1* showed sensitivity to RN4 during the formation phase, with no hook being present at 24 h; however, by 36 h the mutant had attained a slight hook curvature of 50°, which then started opening directly (Fig. 5D). The mutant *axr2-1/iaa7* was resistant to RN4 in the formation phase (Fig. 5F) and *axr3-1/iaa17* was sensitive to RN4 (Fig. 5H). Taken together, these results indicate that all three AUX/IAAs tested here play a role during apical hook development. In particular, our results suggest that AXR2/IAA7 is stabilized during apical hook formation while AXR5/IAA1 stabilization occurs during the maintenance phase.

The effects of 0.5 μ M RN4 on AUX/IAA mutants during the first 24 h of apical hook development (Fig. 5 D, F, and H) correlate strikingly with our *in vitro* pull-down assay results (Fig. 3D). AXR2/IAA7 proteins strongly interacted with TIR1 in the presence of RN4 (Fig. 3 D and G and *SI Appendix, Fig. S7B*), sug-

gesting that a stabilized version of this AUX/IAA should confer resistance to the RN4 auxin agonist, which is indeed what we found with the *axr2-1/iaa7* gain-of-function mutant (Fig. 5F). In contrast, AXR5/IAA1 and AXR3/IAA17 did not interact with TIR1 when RN4 was present in the pull-down assay (Fig. 3 D, E, and H and *SI Appendix, Fig. S7B*) and the corresponding gain-of-function mutants were sensitive to the effects of RN4 on hook development (Fig. 5 D and H).

Overall, our study of the effects of RN4 in particular on the AUX/IAA gain-of-function mutants, distinguishes the involvement of specific AUX/IAAs in lateral root and apical hook development. Thus, we demonstrated the potential of such selective auxin agonists in dissecting auxin perception controlling specific developmental processes *in vivo*.

Mutation in the ATPase Domain of *AtBRM* Confers Resistance to RN4.

RN4 represents a useful tool to investigate the role of auxin during early stages of skotomorphogenesis. To identify new molecular players involved in apical hook development, we performed a forward genetic screen of sensitivity to RN4, using an ethyl methanesulfonate-mutagenized Col-0 population and selected those mutants that were able to form an apical hook in the presence of 0.5 μ M RN4 in the dark, which we named *hookback* (*hkb*) mutants. We then further selected only those of the mutants that were sensitive to the effects of 75 nM 2,4-D on seedling phenotype in the light (*SI Appendix, Fig. S10C*). Using this strategy, we could exclude known auxin resistant mutants that might appear in the screen. Several independent *hkb* lines, each carrying a single recessive mutation, were isolated from the screen and we focused on characterizing one of these, *hkb1*. In contrast to Col-0, *hkb1* had formed well-curved apical hooks in the presence of RN4 24 h after germination, while under mock-treated conditions there were no major differences between the two genotypes (Fig. 6A). Whole-genome sequencing of *hkb1* revealed the presence of one nonsynonymous ethyl methanesulfonate-like mutation (C-to-T

nucleotide substitution) in the coding region of the *AT2G46020* gene that encodes for the SWItch/Sucrose Non-Fermentable (SWI/SNF) chromatin remodeling ATPase *BRAHMA* (*BRM*). The data have been deposited at the European Nucleotide Archive (www.ebi.ac.uk/ena) under the accession number PRJEB21529 (51). To confirm that the mutation in *BRM* is responsible for the resistance of *hkb1* against the negative effect of RN4 on apical hook formation, we carried out several analyses. First, we checked the phenotypes of available T-DNA mutants for *BRM*, including *brm-1*, *brm-2*, *brm-4*, and *brm-5* (*ectopic expression of seed storage proteins3, esp3*) (52, 53). However, we focused our investigations on *brm-5* because both *hkb1* and *brm-5* contain a mutation in the ATPase domain (54) and 4-wk-old plants of the two mutants showed similar phenotypes, including twisted leaves and less siliques than wild-type (Fig. 6B). Importantly, *brm-5* showed similar resistance to the effect of 0.5 μ M RN4 on apical hook formation to that shown by *hkb1* (Fig. 6C and D). These results strongly suggest that the mutation in the ATPase domain of *BRM* in *hkb1* is responsible for the resistance of this mutant to RN4. Next, we crossed *hkb1* with *brm-5* and the F2 generation was analyzed. The *hkb1xbrm-5* mutant showed the same apical hook phenotype and similar RN4 resistance as the single *hkb1* and *brm-5* mutants (Fig. 6C and D), confirming that the mutation that confers resistance against RN4 in *hkb1* is in the *BRM* gene.

Our results suggest that *BRM* may function as a negative regulator of apical hook formation. Considering the resistance of both the *axr2/iaa7* gain-of-function mutant and *hkb1/brm-5* to the effect of RN4 on apical hook formation, we hypothesize that *AXR2/IAA7* might negatively regulate *BRM*-induced gene transcription. We suggest that RN4 induces degradation of *AXR2/IAA7*, which may lead to *BRM*-mediated promotion of transcription of genes negatively regulating apical hook formation, potentially through chromatin remodeling.

Overall, our results show that selective auxin agonists can enable us to dissect the roles of specific AUX/IAAs in developmental processes, leading to the dissection of the molecular mechanisms of these processes.

Discussion

Complicated auxin perception modules translate auxin signals into a multitude of developmental responses (55, 56). Several studies have demonstrated that IAA displays different affinities for different SCF^{TIR1/AFB}-AUX/IAA coreceptor complex combinations (6, 57) and specific auxin perception modules have even been shown to act sequentially during development (58). In this work, we isolated the RNs as selective auxin agonists and revealed their potential to dissect the complex and redundant mechanisms of auxin perception machinery that control specific aspects of plant development. We employed RN4 in particular as a tool to characterize specific auxin perception modules and their potential targets. Remarkably, we even found variability of RN sensitivity between different accessions in both *Arabidopsis* and poplar, pointing to future challenges toward developing the most suitable auxin agonists for specific species and accessions. However, it is important to emphasize that we identified degradation products released from all four RNs *in planta*, which in some cases also induced plant responses. This finding highlights that it is essential to investigate the stability of any such identified auxin agonists and take into account any degradation products released.

Auxin behaves like molecular glue within the SCF^{TIR1/AFB}-AUX/IAA complex (55) by fitting into a space between the TIR1/AFB receptor and AUX/IAA coreceptor and extending the hydrophobic protein interaction surface. It has long been known that the auxin-binding pocket of SCF^{TIR1/AFB} is promiscuous, a feature that was heavily investigated during the early years of auxin research in the 1940s (59, 60). During this time, several auxinic compounds were discovered, including NAA, 2,4-D, and picolinate auxins, such as picloram (61), which are widely used today for basic research and agricultural applications. The 2,4-D and NAA modes of action are similar to that of IAA, as they also enhance the binding affinity between TIR1 and the AUX/IAAs. Their affinity to the coreceptor complex is lower than that of IAA, but they are more stable metabolically, which explains their robust activity. Although the full details of the mode of action of these synthetic auxins are not yet known, they have been instrumental in the discoveries of crucial auxin signaling components, such as *AXR1*, *AXR3/IAA17*, *AXR5/IAA1*, *AFB4*, and *AFB5* (62–66). Thus, synthetic compounds with auxin-like activities hold the potential to dissect the convoluted mechanisms of auxin signaling. Moreover, our isolation and characterization of RN4 revealed different activity and selectivity compared with most of the currently available synthetic auxins, and thus open up new possibilities to identify novel actors in auxin biological responses.

Here, we have shown the selective capacity of RN3 and RN4 to promote the interaction of TIR1 with specific AUX/IAA coreceptors, highlighting a strong potential for such auxin agonists in defining AUX/IAA involvement in specific transcriptional responses and developmental traits. This potential was strongly supported by our genetic approach, showing that different AUX/IAA gain-of-function mutants display defined sensitivities to RN3 and RN4 in terms of lateral root development. Importantly, we uncoupled the effects of RN3 and RN4 on TIR1-AUX/IAA interactions and lateral root development from their free acid degradation products, thus confirming the usefulness of these RN compounds as selective auxin agonists. Multiple AUX/IAA-ARF modules act sequentially over time and space to orchestrate lateral root development (58, 67). Our data indicate that RN3 may promote development of lateral roots through *SLR/IAA14* degradation and the stabilization of *SHY2/IAA3*, but we cannot yet conclude whether degradation of additional AUX/IAAs is also required for this effect. On the other hand, the resistance of the *axr5-1/iaa1* mutant to high concentrations of RN4 revealed a role for *AXR5/IAA1* as a positive regulator of lateral root development.

Moreover, we used the RN with the greatest potential, RN4, as a tool to identify which of several AUX/IAA proteins are directly involved in apical hook development and revealed the implication of auxin-signaling components, such as the SWI/SNF

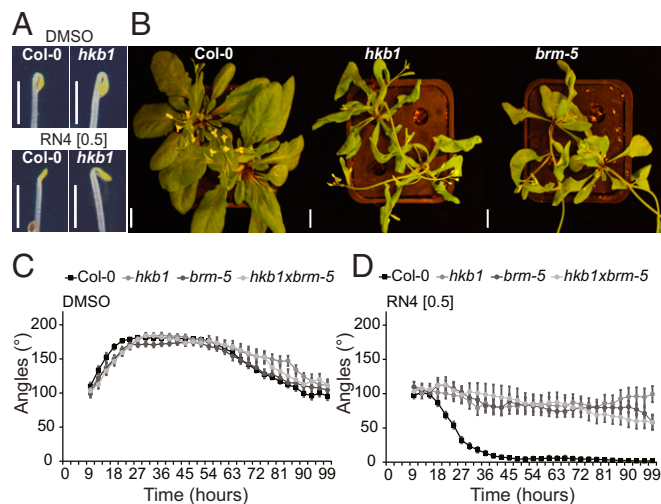


Fig. 6. The *hkb1* mutant is resistant to the RN4 effect on apical hook development and carries a mutation on *BRM*. (A) Comparison of apical hook phenotype in Col-0 and *hkb1* seedlings 24 h after germination in the dark. The seedlings were grown on media supplemented with DMSO (Upper) or RN4 (Lower). (Scale bars, 2 mm.) (B) Four-week-old Col-0, *hkb1*, and *brm-5* grown in long-day greenhouse conditions. (Scale bars, 1 cm.) (C and D) Apical hook angle in Col-0, *hkb1*, *brm-5*, and *hkb1xbrm-5* grown on DMSO (C) and 0.5 μ M RN4 (D) supplemented media for 6 d in the dark. Measurement of apical hook angle was performed every 3 h. Means \pm SEM are shown, $n > 18$ seedlings across two independent replicates. Concentrations in micromolar are indicated in brackets.

chromatin remodeling ATPase BRM. Remarkably, BRM has already been shown to be involved in auxin-dependent floral fate acquisition (68). In the inflorescence, when MONOPTEROS (MP)/ARF5 is free from AUX/IAA repression, it recruits BRM or its homolog SPYED (SYD) to remodel chromatin and thus promote gene transcription. Interestingly, in a yeast three-hybrid assay, AXR3/IAA17 and BDL/IAA12 have been shown to prevent the association of MP to BRM (68). According to these results and our data showing the resistance of *axr2-1/iaa7* and *hkb1/brm-5* to RN4-mediated suppression of apical hook formation, we hypothesize that BRM, by associating with an unknown ARF transcription factor, might promote transcription of genes negatively regulating hook formation. We also hypothesize that AXR2/IAA7 might prevent the association of the ARF to BRM. Application of RN4 prompts the degradation of AXR2/IAA7, which may facilitate the association of the ARF to BRM, promoting transcription of downstream genes negatively regulating apical hook formation, potentially through chromatin remodeling. However, the hypothesis that stabilization of AXR2/IAA7 during apical hook formation blocks BRM activity raises the question of whether MP plays a role during hook development or whether BRM is recruited by other ARFs.

The different affinities of AUX/IAA proteins for IAA, RN3, and RN4 might lie in differences in residues within the DII domain. Our study thus brings us a step closer to a better quantitative understanding of the TIR1–AUX/IAA interaction system of auxin perception in a tissue-specific manner. Besides IAA, several other phytohormones including jasmonate-isoleucine, gibberellin, brassinosteroids, and abscisic acid (ABA), also function by modulating the protein–protein interactions of their coreceptors (69). Isolation of novel molecules modulating such interactions could therefore also be useful in uncovering the signaling components of these phytohormones.

Auxins have many uses in agriculture, horticulture, forestry, and plant tissue culture (59). The selective auxin agonists described here may also find niche applications in these fields. RN activities in the low micromolar range and conservation of their specific developmental effects in land plants enforces this possibility. Moreover, the availability of models for ligand-bound coreceptors may allow rational design of a wider array of auxin agonists using RN structures, in particular RN4, as a starting point. Indeed, a rational design approach has already paved the way for developing agrochemicals interacting specifically with a subset of ABA receptors (70). Such an approach might also have the potential to overcome the limitations of some of the RNs, for example by enhancing stability to eliminate the release of degradation products.

Overall, the isolation and characterization of chemical modulators of plant hormone signaling is an effective way to better understand the specificity of hormonal receptors. Because of the availability of genetic and genomic methods, most chemical biology approaches are performed in model species, such as *Arabidopsis*. However, chemicals that induce well-characterized effects in *Arabidopsis* can be applied to nonmodel species to improve crop and tree value in agriculture and forestry, respectively. The complexity of the genomes of such nonmodel species may also be unraveled by the use of chemicals for which target proteins or pathways are known, giving a better understanding of evolutionary mechanisms.

Materials and Methods

See *SI Appendix* for detailed experimental procedures.

Arabidopsis thaliana seedlings were grown on 1/2 MS medium supplemented with 0.05% Mes, 1% sucrose, and 0.7% agar at pH 5.6. Stock solu-

tions of all compounds were dissolved in DMSO, which was also used in equal volume as a solvent control. Docking experiments were performed using SwissDock (71, 72) with the ZINC ID of the RNs and 2P1Q crystal structure of TIR1 with the DII domain of AXR2/IAA7 (60). The best conformation was chosen according to the FullFitness (kcal/mol). The corresponding binding energies for every conformation of each ligand were calculated using Hybrid-DFT-D3. In vitro pull-down assays, with epitope-tagged TIR1 expressed with TnT-T7 coupled wheat germ extract (Promega), were performed as described previously (29, 73). For the luciferase assay, 7-d-old seedlings were incubated in Bright-Glo luciferase assay system (Promega) luciferine solution (LS) for 30 min before treatment with 50- μ M compounds dissolved in LS. Light emission was recorded for 5 min using a LAS-3000 (Fujifilm) and the natural log of the normalized relative light unit was calculated as described previously (74). The degradation rate k (min^{-1}) was used to compare treatments. The transcriptomic responses induced by the RNs were investigated by RNA sequencing, using *A. thaliana* ecotype Col-0 cell suspension culture (75) treated with 50 μ M RN3, RN4, or IAA for 30 min. Total RNA was extracted from filtered cells using the RNeasy Plant Mini Kit (Qiagen) and sent to the SNP&SEQ Technology Platform in Uppsala University for sequencing. Genes were considered significantly differentially expressed if the adjusted P values after false discovery rate) correction for multiple testing were lower than 0.05. For GUS assays, seedlings were fixed in 80% acetone, washed with 0.1 M phosphate buffer and transferred to 2 mM X-GlcA (Duchefa Biochemie) in GUS buffer (0.1% triton X-100; 10 mM EDTA; 0.5 mM potassium ferrocyanide; 0.5 mM potassium ferricyanide) in the dark at 37 °C before stopping the reaction with 70% ethanol.

ACKNOWLEDGMENTS. We thank the many researchers who kindly provided us with published *Arabidopsis* lines; the *Arabidopsis* Biological Research Center and Nottingham *Arabidopsis* Stock Center for distributing seeds; the Swedish Metabolomics Centre (www.swedishmetabolomicscentre.se/) for access to instrumentation; O. Keech for critical reading of the manuscript; M. Quareshy, V. Uzunova, and R. Napier (University of Warwick) for assistance with insect cell expression of epitope-tagged TIR1; L. Bako, for providing us with *Arabidopsis* cell culture; Pardeep Singh for sharing powder of 2,4,5-T and RN4-1 with us; and R. Bhalerao for sharing the system for time-lapse imaging of dark grown seedlings. J.C. thanks J. Brown for technical assistance, and K. Dreher and J. Gilkerson for helpful discussion and for transgenic line characterization. Sequencing was performed by the SNP&SEQ Technology Platform, Science for Life Laboratory at Uppsala University, a national infrastructure supported by the Swedish Research Council and the Knut and Alice Wallenberg Foundation. RNA sequencing data analysis was in part performed by Bioinformatics Infrastructure for Life Sciences. Amplification of in vitro poplar SwAsp lines was performed by the Poplar Transgenics Facility, Umeå Plant Science Centre. Whole-genome resequencing was performed by Novogene and the results were analyzed with the support of Nicolas Delhomme and Iryna Shutava, Umeå Plant Science Centre Bioinformatics Platform. This work was supported by Vetenskapsrådet VR 2013-4632 and VINNOVA (to T.V., M.E., S.M.D., P.-A.E., and S. Robert); Vetenskapsrådet VR 2016-00768 (to Q.M.); The Knut and Alice Wallenberg Foundation (A.R.); The Knut and Alice Wallenberg Foundation ShapeSystems Grant 2012-0050 (to S.M.D., S. Robert, Q.M., and K.L.); the Olle Engkvist Byggmästare Foundation (S. Raggi); Kempestiftelsen (Q.M., D.K.B., and P.-A.E.); the Carl Tryggers Foundation (Q.M. and M.T.); SweTree Technologies (S.M.D.); an EMBO short-term fellowship (to T.V.); an Seth M. Kempe short-term fellowship (to T.V.); a travel grant from the Bröderna Edlunds Foundation (to T.V.); National Science Foundation MCB-0929100 (to J.C.); National Institutes of Health Grant NIH GM43644 (to M.E.); the Biotechnology and Biological Sciences Research Council BB/L010623/1 (to S.K.); and the Ministry of Education, Youth and Sports of the Czech Republic (European Regional Development Fund-Project “Plants as a tool for sustainable global development” no. CZ.02.1.01/0.0/0.0/16_019/0000827) (to B.P. and O.N.). L.P. was funded by a postdoctoral scholarship and research Grant 1507013N of the Research Foundation Flanders. Chemical Biology Consortium Sweden is primarily funded by the Swedish Research Council (P.-A.E.).

- Teichmann T, Muhr M (2015) Shaping plant architecture. *Front Plant Sci* 6:233.
- Wolters H, Jürgens G (2009) Survival of the flexible: Hormonal growth control and adaptation in plant development. *Nat Rev Genet* 10:305–317.
- Calderon-Villalobos LI, Tan X, Zheng N, Estelle M (2010) Auxin perception—Structural insights. *Cold Spring Harb Perspect Biol* 2:a005546.
- Weijers D, Wagner D (2016) Transcriptional responses to the auxin hormone. *Annu Rev Plant Biol* 67:539–574.
- Dreher KA, Brown J, Saw RE, Callis J (2006) The *Arabidopsis* Aux/IAA protein family has diversified in degradation and auxin responsiveness. *Plant Cell* 18:699–714.
- Calderón Villalobos LIA, et al. (2012) A combinatorial TIR1/AFB-Aux/IAA co-receptor system for differential sensing of auxin. *Nat Chem Biol* 8:477–485.
- Moss BL, et al. (2015) Rate motifs tune auxin/indole-3-acetic acid degradation dynamics. *Plant Physiol* 169:803–813.
- Downes B, Vierstra RD (2005) Post-translational regulation in plants employing a diverse set of polypeptide tags. *Biochem Soc Trans* 33:393–399.
- Hochstrasser M (2009) Origin and function of ubiquitin-like proteins. *Nature* 458:422–429.
- Kelley DR, Estelle M (2012) Ubiquitin-mediated control of plant hormone signaling. *Plant Physiol* 160:47–55.

11. Mergner J, Schwechheimer C (2014) The NEDD8 modification pathway in plants. *Front Plant Sci* 5:103.
12. Hua Z, Vierstra RD (2011) The cullin-RING ubiquitin-protein ligases. *Annu Rev Plant Biol* 62:299–334.
13. Petroski MD, Deshaies RJ (2005) Function and regulation of cullin-RING ubiquitin ligases. *Nat Rev Mol Cell Biol* 6:9–20.
14. Leyser HM, et al. (1993) *Arabidopsis* auxin-resistance gene AXR1 encodes a protein related to ubiquitin-activating enzyme E1. *Nature* 364:161–164.
15. Timpte C, Lincoln C, Pickett FB, Turner J, Estelle M (1995) The AXR1 and AUX1 genes of *Arabidopsis* function in separate auxin-response pathways. *Plant J* 8:561–569.
16. Schwechheimer C, et al. (2001) Interactions of the COP9 signalosome with the E3 ubiquitin ligase SCFTIR1 in mediating auxin response. *Science* 292:1379–1382.
17. Tiryaki I, Staswick PE (2002) An *Arabidopsis* mutant defective in jasmonate response is allelic to the auxin-signaling mutant *axr1*. *Plant Physiol* 130:887–894.
18. Zhao Y, Dai X, Blackwell HE, Schreiber SL, Chory J (2003) *SIR1*, an upstream component in auxin signaling identified by chemical genetics. *Science* 301:1107–1110.
19. Christian M, Hannah WB, Lüthen H, Jones AM (2008) Identification of auxins by a chemical genomics approach. *J Exp Bot* 59:2757–2767.
20. Savaldi-Goldstein S, et al. (2008) New auxin analogs with growth-promoting effects in intact plants reveal a chemical strategy to improve hormone delivery. *Proc Natl Acad Sci USA* 105:15190–15195.
21. Ettmayer P, Amidon GL, Clement B, Testa B (2004) Lessons learned from marketed and investigational prodrugs. *J Med Chem* 47:2393–2404.
22. Aibibili Z, Wang Y, Tu H, Huang X, Zhang A (2012) Facile synthesis and herbicidal evaluation of 4H-3,1-benzoxazin-4-ones and 3H-quinazolin-4-ones with 2-phenoxymethyl substituents. *Molecules* 17:3181–3201.
23. Ulmasov T, Murfett J, Hagen G, Guilfoyle TJ (1997) Aux/IAA proteins repress expression of reporter genes containing natural and highly active synthetic auxin response elements. *Plant Cell* 9:1963–1971.
24. Kepinski S, Leyser O (2005) The *Arabidopsis* F-box protein TIR1 is an auxin receptor. *Nature* 435:446–451.
25. Dharmasiri N, Dharmasiri S, Estelle M (2005) The F-box protein TIR1 is an auxin receptor. *Nature* 435:441–445.
26. Hayashi K, et al. (2012) Rational design of an auxin antagonist of the SCFTIR1 auxin receptor complex. *ACS Chem Biol* 7:590–598.
27. Gray WM, Kepinski S, Rouse D, Leyser O, Estelle M (2001) Auxin regulates SCF(TIR1)-dependent degradation of AUX/IAA proteins. *Nature* 414:271–276.
28. Yang X, et al. (2004) The IAA1 protein is encoded by AXR5 and is a substrate of SCF (TIR1). *Plant J* 40:772–782.
29. Parry G, et al. (2009) Complex regulation of the TIR1/AFB family of auxin receptors. *Proc Natl Acad Sci USA* 106:22540–22545.
30. Vain T, et al. (2019) RNAseq analysis of *Arabidopsis* cell suspension culture treated with IAA, RN3 and RN4. European Nucleotide Archive. Available at www.ebi.ac.uk/ena/data/view/PRJEB31496. Deposited March 1, 2019.
31. Goh T, Joo S, Mimura T, Fukaki H (2012) The establishment of asymmetry in *Arabidopsis* lateral root founder cells is regulated by LBD16/ASL18 and related LBD/ASL proteins. *Development* 139:883–893.
32. De Rybel B, et al. (2014) Plant development. Integration of growth and patterning during vascular tissue formation in *Arabidopsis*. *Science* 345:1252–1255.
33. Vilches-Barro A, Maizel A (2015) Talking through walls: Mechanisms of lateral root emergence in *Arabidopsis thaliana*. *Curr Opin Plant Biol* 23:31–38.
34. Benjamins R, Ampudia CS, Hoojkaas PJ, Offringa R (2003) PINOID-mediated signaling involves calcium-binding proteins. *Plant Physiol* 132:1623–1630.
35. Buer CS, Djordjevic MA (2009) Architectural phenotypes in the transparent testa mutants of *Arabidopsis thaliana*. *J Exp Bot* 60:751–763.
36. Lewis DR, et al. (2011) Auxin and ethylene induce flavonol accumulation through distinct transcriptional networks. *Plant Physiol* 156:144–164.
37. Krishnaswamy S, Verma S, Rahman MH, Kav NNV (2011) Functional characterization of four APETALA2-family genes (RAP2.6, RAP2.6L, DREB19 and DREB26) in *Arabidopsis*. *Plant Mol Biol* 75:107–127.
38. Chen J-H, et al. (2012) Drought and salt stress tolerance of an *Arabidopsis* glutathione S-transferase U17 knockout mutant are attributed to the combined effect of glutathione and abscisic acid. *Plant Physiol* 158:340–351.
39. Jiang H-W, et al. (2010) A glutathione S-transferase regulated by light and hormones participates in the modulation of *Arabidopsis* seedling development. *Plant Physiol* 154:1646–1658.
40. Shin R, et al. (2007) The *Arabidopsis* transcription factor MYB77 modulates auxin signal transduction. *Plant Cell* 19:2440–2453.
41. Li J, et al. (2009) BREVIS RADIX is involved in cytokinin-mediated inhibition of lateral root initiation in *Arabidopsis*. *Planta* 229:593–603.
42. Brunoud G, et al. (2012) A novel sensor to map auxin response and distribution at high spatio-temporal resolution. *Nature* 482:103–106.
43. De Rybel B, et al. (2010) A novel aux/IAA28 signaling cascade activates GATA23-dependent specification of lateral root founder cell identity. *Curr Biol* 20:1697–1706.
44. Nagpal P, et al. (2000) AXR2 encodes a member of the Aux/IAA protein family. *Plant Physiol* 123:563–574.
45. Tian Q, Reed JW (1999) Control of auxin-regulated root development by the *Arabidopsis thaliana* SHY2/IAA3 gene. *Development* 126:711–721.
46. Goh T, Kasahara H, Mimura T, Kamiya Y, Fukaki H (2012) Multiple AUX/IAA-ARF modules regulate lateral root formation: The role of *Arabidopsis* SHY2/IAA3-mediated auxin signalling. *Philos Trans R Soc Lond B Biol Sci* 367:1461–1468.
47. Fukaki H, Tameda S, Masuda H, Tasaka M (2002) Lateral root formation is blocked by a gain-of-function mutation in the *SOLITARY-ROOT/IAA14* gene of *Arabidopsis*. *Plant J* 29:153–168.
48. Abbas M, Alabadi D, Blázquez MA (2013) Differential growth at the apical hook: All roads lead to auxin. *Front Plant Sci* 4:441.
49. Raz V, Ecker JR (1999) Regulation of differential growth in the apical hook of *Arabidopsis*. *Development* 126:3661–3668.
50. Zádorníková P, et al. (2010) Role of PIN-mediated auxin efflux in apical hook development of *Arabidopsis thaliana*. *Development* 137:607–617.
51. Vain T, et al. (2019) DNA sequencing for RN4-resistant *Arabidopsis thaliana* EMS mutant *hookback1* (*hkb1*). European Nucleotide Archive. Available at www.ebi.ac.uk/ena/data/view/PRJEB21529. Deposited June 27, 2017.
52. Hurtado L, Farrona S, Reyes JC (2006) The putative SWI/SNF complex subunit BRAHMA activates flower homeotic genes in *Arabidopsis thaliana*. *Plant Mol Biol* 62:291–304.
53. Tang X, et al. (2008) The *Arabidopsis* BRAHMA chromatin-remodeling ATPase is involved in repression of seed maturation genes in leaves. *Plant Physiol* 147:1143–1157.
54. Farrona S, Hurtado L, Bowman JL, Reyes JC (2004) The *Arabidopsis thaliana* SNF2 homolog AtBRM controls shoot development and flowering. *Development* 131:4965–4975.
55. Wang R, Estelle M (2014) Diversity and specificity: Auxin perception and signaling through the TIR1/AFB pathway. *Curr Opin Plant Biol* 21:51–58.
56. Salehin M, Bagchi R, Estelle M (2015) SCFTIR1/AFB-based auxin perception: Mechanism and role in plant growth and development. *Plant Cell* 27:9–19.
57. Havens KA, et al. (2012) A synthetic approach reveals extensive tunability of auxin signaling. *Plant Physiol* 160:135–142.
58. Lavenus J, et al. (2013) Lateral root development in *Arabidopsis*: Fifty shades of auxin. *Trends Plant Sci* 18:450–458.
59. Jönsson Å (1961) Chemical structure and growth activity of auxins and antiauxins. *Encyclopedia of Plant Physiology*, ed Ruhland W (Springer, Berlin), pp 959–1006.
60. Tan X, et al. (2007) Mechanism of auxin perception by the TIR1 ubiquitin ligase. *Nature* 446:640–645.
61. Ma Q, Grones P, Robert S (2018) Auxin signaling: A big question to be addressed by small molecules. *J Exp Bot* 69:313–328.
62. Maher EP, Martindale SJB (1980) Mutants of *Arabidopsis thaliana* with altered responses to auxins and gravity. *Biochem Genet* 18:1041–1053.
63. Estelle MA, Somerville C (1987) Auxin-resistant mutants of *Arabidopsis thaliana* with an altered morphology. *MGG Mol Gen Genet* 206:200–206.
64. Woodward AW, Bartel B (2005) Auxin: Regulation, action, and interaction. *Ann Bot* 95:707–735.
65. Walsh TA, et al. (2006) Mutations in an auxin receptor homolog AFB5 and in SGT1b confer resistance to synthetic picolinate auxins and not to 2,4-dichlorophenoxyacetic acid or indole-3-acetic acid in *Arabidopsis*. *Plant Physiol* 142:542–552.
66. Prigg MJ, et al. (2016) The *Arabidopsis* auxin receptor F-Box proteins AFB4 and AFB5 are required for response to the synthetic auxin picloram. *G3 (Bethesda)* 6:1383–1390.
67. De Smet I, et al. (2010) Bimodular auxin response controls organogenesis in *Arabidopsis*. *Proc Natl Acad Sci USA* 107:2705–2710.
68. Wu MF, et al. (2015) Auxin-regulated chromatin switch directs acquisition of flower primordium founder fate. *eLife* 4:e09269.
69. Rigal A, Ma Q, Robert S (2014) Unraveling plant hormone signaling through the use of small molecules. *Front Plant Sci* 5:373.
70. Park S-Y, et al. (2015) Agrochemical control of plant water use using engineered abscisic acid receptors. *Nature* 520:545–548.
71. Grosdidier A, Zoete V, Michielin O (2011) SwissDock, a protein-small molecule docking web service based on EADock DSS. *Nucleic Acids Res* 39:W270–W277.
72. Grosdidier A, Zoete V, Michielin O (2011) Fast docking using the CHARMM force field with EADock DSS. *J Comput Chem* 32:2149–2159.
73. Yu H, et al. (2013) Mutations in the TIR1 auxin receptor that increase affinity for auxin/indole-3-acetic acid proteins result in auxin hypersensitivity. *Plant Physiol* 162:295–303.
74. Gilkerson J, et al. (2009) Isolation and characterization of *cul1-7*, a recessive allele of CULLIN1 that disrupts SCF function at the C terminus of CUL1 in *Arabidopsis thaliana*. *Genetics* 181:945–963.
75. Fülöp K, et al. (2005) The Medicago CDKC1-CYCLINT1 kinase complex phosphorylates the carboxy-terminal domain of RNA polymerase II and promotes transcription. *Plant J* 42:810–820.

Supplementary Information for

Selective auxin agonists induce specific AUX/IAA protein degradation to modulate plant development

Thomas Vain, Sara Raggi, Noel Ferro, Deepak Kumar Barange, Martin Kieffer, Qian Ma, Siansa M. Doyle, Mattias Thelander, Barbora Pařízková, Ondřej Novák, Alexandre Ismail, Per-Anders Enquist, Adeline Rigal, Małgorzata Łangowska, Sigurd Ramans Harborough, Yi Zhang, Karin Ljung, Judy Callis, Fredrik Almqvist, Stefan Kepinski, Mark Estelle, Laurens Pauwels and Stéphanie Robert.

Corresponding author: Stéphanie Robert

Email: stephanie.robert@slu.se

This PDF file includes:

Supplementary Materials and Methods

Figs. S1 to S10

Tables S1 to S2

Caption for Movie S1

Caption for Dataset S1

One Supplementary Document “Chemical Synthesis and Characterization”

References for SI Appendix

Other supplementary materials for this manuscript include the following:

Movie S1

Dataset S1

Supplementary Materials and Methods

Plant materials and growth conditions

Seedlings of *Arabidopsis thaliana* were grown at 22°C with 16 h light per day (or in darkness for apical hook analysis) on vertical plates containing growth medium (GM): 1/2 MS (Duchefa Biochemie, Haarlem, The Netherlands); 0.05 % morpholinoethanesulfonic acid (Sigma-Aldrich); 1 % sucrose; 0.7 % agar (Duchefa Biochemie); pH 5.6. Short-term chemical treatments were performed in liquid GM, from which the agar was omitted. Two-day cold stratification of seeds was performed prior to seedling growth. The generation of the *Arabidopsis* lines *axr1-30* (SAIL_904_E06) (1), pDR5::GUS (2), *cul1-6* (3), *cul3a-3cul3b-1* (4), *cul4-1* (5), *tir1-1* (6), *tir1-1afb1-3afb3-4* (7), AXR5/IAA1-LUC (8), AXR3/IAA17-LUC (9), pMSG2/IAA19::GUS (10), pSHY2/IAA3::GUS (11), pBDL/IAA12::GUS (11), GATA23::GUS (12), p35S::DII-Venus (13), *axr5-1* (14), *axr2-1* (15), *slr-1* (16), *shy2-2* (17), *axr3-1* (18), *brm-1* (19), *brm-2* (19), *brm-4* (20) and *brm-5* (20) have been previously described. The SHY2/IAA3-LUC and AXR2/IAA7-LUC transgenic lines and the *hkb1* and *hkb1xbrm-5* mutants were created/identified in this work.

Chemical treatments

For the chemical biology screen, phenotypic screening was performed on a diverse set of 8,000 compounds (ChemBridge) in 24-well plates containing solid growth media supplemented with chemicals dissolved in dimethyl sulfoxide (DMSO) at 17 µM. *Arabidopsis* seedlings of Col-0 and *axr1-30* were grown side by side (in the same well) for 5 days in the wells. DMSO controls were present in each plate. Compounds were selected for their capacity to alter development of Col-0 without affecting *axr1-30*. The 34 hits were repeated three times using DMSO and 1-Naphthaleneacetic acid (NAA) as negative and positive controls. Dose responses were performed in 24-well plates from newly ordered compounds using the ChemBridge identification number (CBID, www.hit2lead.com). Stock solutions of the RNs and all other compounds used were dissolved at 10 mM in DMSO for all further experiments. For the ChemBridge IDs of RN1-4, see Table S2. DMSO treatments were used in equal volume as solvent control. For germination and growth of seedlings on chemicals, seeds were sown directly on chemical-supplemented media. Short-term chemical treatments were performed in liquid GM, from which the agar was omitted.

Chemical synthesis of RN1, RN3 and RN4 and purity assessments of the four RNs

We synthesized the four RN compounds with confirmed chemical identities and their purities in stock solutions were estimated to be higher than 97.99% (Supplementary document 1).

Adventitious root induction in poplar

The poplar lines used in this study were the *Populus tremuloides* x *tremula* hybrid aspen clone T89 (21) and lines number 19 and 35 from the Swedish Aspen (SwAsp) collection of natural populations of *P. tremula* (22). *In vitro* clonal propagation of the lines was performed by transferring shoot cuttings from 4-w-old *in vitro* plants to fresh ½ MS medium (Duchefa Biochemie) at pH 5.6 with 0.27% Phytigel (Sigma) and maintaining the cuttings on a day/night cycle of 16 h at 22 °C / 8 h at 18 °C. Cuttings were kept in shade by covering with white paper until 2 weeks old, after which the paper was removed. Stock solutions of 10 mM indole-3-

butyric acid (IBA), RN1 and RN3 were made in DMSO. For poplar chemical treatments, 7 cuttings per line and treatment were propagated as usual, but to medium supplemented with solvent (control) or 1 μ M or 5 μ M IBA, RN1 or RN3 and 4 biological replicates were performed, on different weeks. Nine days after treatment, all cuttings were transferred to fresh treatment-free medium and growth was continued for 3 more weeks. The number of adventitious roots per cutting was counted 4 weeks after treatment.

Moss growth tests

Physcomitrella patens, subspecies *patens*, strain Gransden 2004, was used. Protonemal tissue was cultivated as described previously (23). Small pieces of protonemal tissue were shaped into 1 mm balls and inoculated on solid BCD medium with supplements as described in the results section, six balls per plate. DMSO solvent controls were included. Buds and gametophores were counted after 1 and 2 weeks of growth using a dissecting microscope. After 4 weeks, colonies were photographed and a subset of large gametophores formed outside the original inoculum of each colony was harvested, examined and photographed.

Stability of the RN compounds

Five-d-old *Arabidopsis* seedlings were transferred to liquid media containing RN-compounds (50 μ M) or DMSO as mock control. Treatment media were collected directly after solubilization of the molecules and after 24 h in the presence or absence of the plants. Whole seedlings were collected in three replicates after 24 h treatments, immediately frozen in liquid nitrogen and stored at -80°C until extraction. For quantification of RNs and their associated free acids, the growing media were diluted 1/10 by methanol, 2 μ l was injected onto a reversed-phase column (Kinetex C18 100A, 50 x 2.1 mm, 1.7 μ m; Phenomenex) and analyzed by liquid chromatography–tandem mass spectrometry (LC-MS/MS), see below. The second set of samples (approx. 100 mg plant material fresh weight) was extracted in 1 ml of methanol using a MixerMill MM 301 bead mill (Retsch GmbH) at a frequency of 29 Hz for 10 min after adding 2 mm ceria-stabilized zirconium oxide beads. The plant extracts were incubated at 4°C with continuous shaking (10 min), centrifuged (15 min, 23 000 g at 4°C), divided into three technical replicates and purified by liquid-liquid extraction using Hexan:Methanol:H₂O (1:2:0.1) to remove impurities and the sample matrix. After 15 min incubation, the methanolic fractions were removed, evaporated to dryness *in vacuo* and dissolved in 100 μ l of methanol prior to LC-MS/MS analysis, using a 1290 Infinity LC system and a 6490 Triple Quadrupole LC/MS system with Jet Stream and Dual Ion Funnel technologies (Agilent Technologies). After injection (2 μ l), the purified samples were eluted using a 5 min gradient comprised of 0.1% acetic acid in methanol and 0.1% acetic acid in water at a flow rate of 0.5 ml min⁻¹, and column temperature of 40°C . The following binary linear gradient was used: 0 min, 10:90 A:B; 9.0 min, 95:5 A:B. At the end of the gradient, the column was washed with 100% methanol (0.5 min), and re-equilibrated to initial conditions (1 min). The effluent was introduced into the MS system with the optimal settings as follows: Drying Gas Temperature, 150°C ; Drying Gas Flow, 16 l min⁻¹; Nebulizer Pressure, 40 psi; Sheath Gas Temperature, 375°C , Sheath Gas Flow, 12 l min⁻¹; Capillary Voltage, 3000 V; Nozzle Voltage, 0 V; Delta iFunnel High/Low Pressure RF, 110/60 V; and Fragmentor, 380 V. Quantification and confirmation were obtained by the various MRM diagnostic transitions of the precursor and the appropriate product ions using optimal collision energies and 50 msec dwell time (Fig. S4B). Chromatograms were analyzed using MassHunter

software (version B.05.02; Agilent Technologies), and the compounds were quantified by according to their recovery listed in Fig S4C.

GUS assays

Seedlings of *Arabidopsis* expressing GUS were fixed in 80% acetone at -20 °C for 20 min and washed with 0.1 M phosphate buffer (Na₂HPO₄ / NaH₂PO₄) at pH 7. Samples were transferred to GUS staining solution: 2 mM X-GlcA (Duchefa Biochemie) in GUS buffer (0.1 % triton X100; 10 mM EDTA; 0.5 mM potassium ferrocyanide; 0.5 mM potassium ferricyanide) in the dark at 37 °C. The staining reaction was stopped using 70 % ethanol and the seedlings were mounted in either 50 % glycerol or a mixture of chloral hydrate: glycerol: H₂O (8:3:1). Samples were observed using a Zeiss Axioplan.

Molecular modeling

Docking experiments were performed using SwissDock (24-25) with the ZINC ID of the RNs (RN1: ZINC2978909; RN2: ZINC19770708, ZINC19770709; RN3: ZINC11461779; RN4: ZINC01160095) and 2P1Q crystal structure of TIR1 with the DII domain of AXR2/IAA7 (26). The best conformation was chosen according to the FullFitness (Kcal/mol). The input geometries of the ligands coming from docking analysis were optimized inside of the auxin binding surface of TIR1 using density functional theory calculations including dispersion correction terms (DFT-D3) to better understand the supramolecular associations (27). The corresponding binding energies for every conformation of each ligand were calculated using Hybrid-DFT-D3. The analysis of the binding energies considered the intrinsic binding energy of the ligand and the binding surface as well as the solvation energies and van der Waals (VdW) forces.

In vitro pull-down assays

The *in vitro* pull-down assays, with epitope-tagged TIR1 expressed with TnT-T7 coupled wheat germ extract (Promega), were performed as described previously (7, 28). TIR1-myc protein was incubated with bacterially expressed GST-AUX/IAA beads in pull-down buffer (25 mM Tris-HCl pH 7.5; 150 mM NaCl; 0.05 % Igepal (Sigma-Aldrich); 10 % Glycerol; 1 mM DTT; 1 mM PMSF; 20 μM MG-132 (Sigma-Aldrich); Protease Inhibitor Cocktail (Roche)) in the presence of DMSO or the compounds at 50 μM for 3 h at 4°C. After washing, proteins were eluted using reduced glutathione (Sigma-Aldrich), separated using SDS-PAGE and visualized using Ponceau staining for the GST-AUX/IAA proteins and anti-c-Myc-peroxydase (Life Technologies) for TIR1-myc. The amount of TIR1-myc in the complex was determined by western blot using anti-myc. The quantity of TIR1-myc pulled down is representative of the strength of co-receptor complex formation.

In-vitro pull-down assays with insect cell-expressed epitope-tagged TIR1 were performed using a similar protocol as described previously (29). His-MBP-FLAG -TIR1 proteins were produced using recombinant baculovirus with *Trichoplusia ni* host cells and purified as previously reported (30). GST-AXR2/IAA7 has been described previously (31). GST-AXR3/IAA17 was constructed by ligating the gene coding sequence as a BamH1-XhoI fragment into pGEX-4T-2 following PCR amplification with the following primers: BHIAXR3 5'-GTGGATCCGGCAGTGTGCGAGCTGAAT-3' and AXR3XHOI 5'-GTCTCGAGTCAAGCTCTGCTCTTGCA-3'. GST-IAA proteins were purified and immobilized on Sepharose 4B beads (GE Healthcare) as described previously (29). Pull-down assays were performed by incubating His-MBP-FLAG -TIR1 protein with Sepharose-GST-IAA

beads in extraction buffer (EB; 150 mM NaCl, 100 mM Tris pH7.5, 0.5% NP-40, 10 mM DTT, 1 mM PMSF, 10 μ M MG-132) in the presence of DMSO or compounds at 50 μ M for 2h at 4°C. After washing, proteins were eluted with hot (70°C) 1 x NuPage LDS sample buffer with 1 x NuPage reducing agent (Life Technologies), separated by SDS-PAGE (NuPAGE Novex 4–12% Bis-Tris gel/ 1 x NuPage MES buffer, Life Technologies) and visualized using Ponceau staining for the GST-AUX/IAA proteins and anti-Flag M2 Peroxidase antibody (Sigma) for His-MBP-FLAG -TIR1.

Creation of the transgenic lines for in vivo AUX/IAA degradation assay

For SHY2/IAA3, site-directed mutagenesis was used to create a silent mutation (coding nt 489 A to C), removing an internal NcoI site in SHY2/IAA3 cDNA (ABRC, C00011). The ORF was then PCR amplified using 5' primer (3-104, GGCGGTACCAATGGATGAGTTTGTAAACC) and 3' primer (3-105, GGCGCCATGGCTACACCACAGCCTAAACC) to introduce a Kpn site 5' of the start site and at the 3' end to remove the stop codon and replace it with an NcoI site. The product was digested with KpnI and NcoI and ligated into a pGREENII-based plasmid containing a KpnI and NcoI site between the 5' UBQ10 flanking region and a luciferase coding region as described previously (8), placing the SHY2/IAA3 ORF in-frame with the LUC coding region. For AXR2/IAA7, site-directed mutagenesis was used to create a silent mutation (coding nt 525 C to T), removing an internal BspHI site in AXR2/IAA7 cDNA (ABRC, C00014). The ORF was then PCR amplified using 5' and 3' primers (3-122, GGCGGTACCAATGATCGGCCAACTTATG) and (3-123, GGCGTCATGACAGATCTGTTCTTGCACTAC), respectively, the PCR product digested with Kpn and BspHI and ligated into the same pGREENII-based plasmid (above). Both ORFs were sequence verified, the plasmids introduced into *Arabidopsis thaliana* ecotype Col and multiple lines segregating for a single insertion were made homozygous as described previously (8). Transgenic lines expressing AXR5/IAA1-LUC (8) and AXR3/IAA17-LUC were described previously (9).

Luciferase assay

Seeds of each genotype were sown individually in flat-bottom white Polystyrene 96-well plates (Fisher Scientific) containing 100 μ L GM. After 7 days, the GM was replaced by 40 μ L Bright-Glo luciferase assay system (Promega) diluted 10 times in GM (luciferine solution; LS) and the plates were incubated for 30 min. At zero time point, compounds dissolved in LS were added to each well to a final concentration of 50 μ M in 50 μ L. Single seedling light emission was recorded for 5 min at the indicated time point using a LAS-3000 (Fujifilm). The natural log of the normalized relative light unit (RLU) was calculated as described previously (32). The degradation rate k (min^{-1}) was used to compare the different treatments, with k being the slope of the degradation curve (Fig. S6) between 5 and 40 min.

RNA sequencing

The transcriptomic responses induced by the RNs were investigated by RNA-Seq, using an *Arabidopsis thaliana* ecotype Col-0 cell suspension culture (33). Treatments were carried out in a 100 ml flask on a shaker at 110 rpm, with 20 ml of a 3-d-old freshly subcultured cell suspension elicited by either RN3, RN4, or IAA at a final concentration of 50 μ M for 30 min. Cells in the liquid medium were harvested by passing the culture through Whatman filter paper in a funnel under vacuum for 10 sec. DMSO (0.5% v/v) treatment was used as the mock control.

Three biological replicates were produced in this way. All the samples were immediately frozen in liquid N₂ upon harvesting and stored at -80 °C. Total RNA was extracted using RNeasy Plant Mini Kit (QIAGEN) and genomic DNA was eliminated using RQ1 RNase-Free DNase I (Promega) on-column digestion. The RNA quality was examined by an Agilent 2100 Bioanalyzer system, with an RNA integrity number (RIN) \geq 8. The construction of the sequencing libraries using the TruSeq stranded mRNA sample prep kit with polyA-selection (Illumina Inc.) and the 125 cycle paired-end sequencing of the 12 libraries in two lanes using the HiSeq system (Illumina Inc.) were performed by NGI (National Genomics Infrastructure) SNP&SEQ Technology Platform at the Uppsala University according to the standard protocols. The reads from each sequencing library were aligned to the *Arabidopsis thaliana* (The Arabidopsis Information Resource 10, TAIR 10) (34) genome using the Subreadalign aligner (35). The mapped reads were converted to gene counts using the featureCounts function (36). These steps were both done using R/Bioconductor package Rsubread version 3.1 (37-39). In order to take into account the difference in the sequencing depth between libraries, the libraries were normalized using a weighted trimmed mean method available from the package edgeR (40). All genes expressed in the 3 replicates and at least two counts per million mapped reads were considered. To estimate differentially expressed genes (DEGs) between the treatment and the DMSO control, data were modeled as a multifactorial experiment and Limma (41) was used to assess differential gene expression. In the modeling, we used the replicate as a batch factor. Genes were considered as statistically significant DEGs if the adjusted p-values after FDR (False Discovery Rate) correction for multiple testing were lower than 0.05. Identified DEGs were clustered using Venn diagrams (<http://bioinformatics.psb.ugent.be/webtools/Venn/>) and expression pattern and auxin response of candidates were analyzed using the Arabidopsis eFP (<http://bar.utoronto.ca/efp/cgi-bin/efpWeb.cgi>).

Confocal microscopy

Seedlings of the p35S::DII-Venus line were transferred to GM without agar containing chemicals. Seedlings were mounted in their treatment medium and images were acquired using a Zeiss LSM 780 confocal microscope with a LCI Plan-Neofluar 25x/0.8 Imm Corr DIC M27 objective. The Venus fluorescent protein was excited at 514 nm with an Argon laser.

Forward genetic screen

Mutagenesis was performed using ethyl methanesulfonate (EMS) at 24 mM final concentration on 10,000 seeds of Col-0 as described previously (42). M1 plants were harvested by bulk of 25 plants per pool. M2 seedlings were first screened for resistance to the effect of 0.5 μ M RN4 on apical hook development in the dark and the isolated mutants were then screened for sensitivity to 75 nM 2,4-D in the light. The *hkb1* mutant, which was selected for resistance to RN4 and sensitivity to 2,4-D, was then backcrossed twice with Col-0. Genomic DNA for whole genome sequencing was extracted from a pool of 25 plants using the E.Z.N.A.® Plant DNA Kit (Omega Bio-tek).

DNA sequencing

The DNA sequencing data has been deposited at the European Nucleotide Archive (www.ebi.ac.uk/ena) under the accession number: PRJEB21529. The construction of the DNA-350 sequencing libraries using the TruSeq Library construction Kit (Illumina Inc.) and the paired-end sequencing of the libraries using the HiSeq PE150 system (Illumina Inc.) were performed by Novogene according to standard protocols. The data pre-processing was performed

as follows: first the quality of the raw sequence data was assessed using FastQC (<http://www.bioinformatics.babraham.ac.uk/projects/fastqc/>), v0.11.4. Data were then filtered to remove adapters and trimmed for quality using Trimmomatic (v0.36; (43); settings TruSeq3-PE-2.fa:2:30:10 SLIDINGWINDOW:5:20 MINLEN:50). After that filtering step, FastQC was run again to ensure that no technical artefacts were introduced. The reads were then aligned to the *Arabidopsis thaliana* (TAIR 10) (34) genome using BWA-MEM version 0.7.8 (44) with the following non-default parameters: -k 32 -M -R. The obtained BAM files were then used as input for variant analysis using GATK version 3.4-46 (45). Briefly, duplicate reads were marked using the Picard (46) library MarkDuplicatesWithMateCigar tool before the reads were further pre-processed using the GATK BaseRecalibrator, RealignerTargetCreator and IndelRealigner tools. BaseRecalibrator used the SNP gold standard for *Arabidopsis thaliana* retrieved on January 26th, 2017. The de-duplicated, recalibrated, realigned BAM files were then used as input to GATK UnifiedGenotyper. The obtained VCF files were further analyzed using ad-hoc R scripts and visualized in JBrowse (47). To identify the causative variant, only SNPs that could have been triggered by the EMS treatment and having an allele frequency of 1 (homozygous) were kept. The effect of these SNPs was then evaluated using snpEff (48) and the remaining candidates manually evaluated.

Plant genotyping

Genomic DNA from *brm-5* and *hkb1* was extracted as previously described (49). PCR was performed using the primers 5'-GAACTTTGCGTGATTACCAGC-3' and 5'-GACCTTCCTTGTCGATTCTCC-3'. The PCR product was purified using the QIAquick PCR Purification Kit (Qiagen). To identify the point mutations in the mutants, the PCR product was sequenced using the primers 5'- CCTTCTTTTTGAAAGGGTTGC-3' and 5'-TGGCCTGTCCTCTGTAGCTT-3' for *brm-5* and *hkb1*, respectively.

Image processing

Figures were designed using Adobe Illustrator. Seedling images were acquired using a flatbed scanner Epson V600 when grown in the light and according to (50) when grown in the dark. Cropping and whole-picture contrast enhancement were done using ImageJ1.50f following the same settings for each panel. Quantification of band intensity in pull-down gel images was performed using ImageJ. Drawings were realized using Inkscape0.48. Movie S1 was realized using Chimera1.10rc.

Statistical analysis

Biological replicates were performed on different days. Primary root length and hypocotyl length were measured on 7-d-old seedlings. Lateral root density was measured on 8-d-old seedlings. Apical hook angle was measured during the first six days of skotomorphogenesis using ImageJ (51). For statistical analyses of data, ANOVA and Tukey's test were performed using R (37), while two sided independent t-tests were performed using Excel (Microsoft Office).

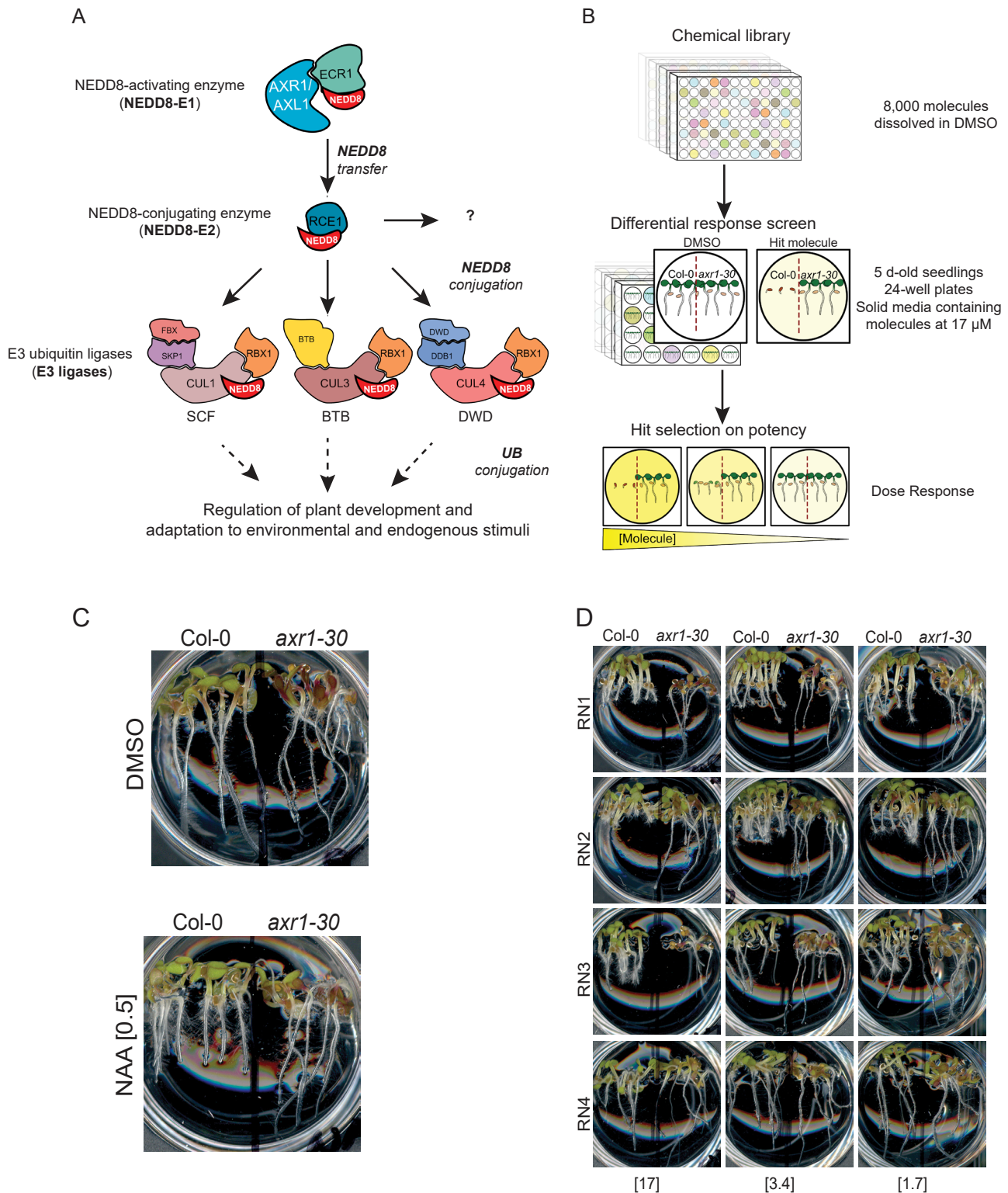


Fig. S1. AXR1-dependent developmental defect based screen. (A) AXR1 mediates the activation of CUL-based E3 ligases by catalyzing attachment of a RUB/NEDD8 protein to the CUL subunit of their respective E3. AXR1 and E1 C-TERMINAL RELATED1 (ECR1) activate NEDD8 that is transferred to RUB1 CONJUGATING ENZYME1 (RCE1) and then to the CUL subunit. These CUL-based E3s are essential for plant development and modulate responses to environmental and endogenous stimuli. (B) Col-0 and *axr1-30* seedlings were grown side by side in 24-well plates for five days in the presence of synthetic small molecules. Thirty-four molecules were identified out of 8,000 as being active on Col-0 development, while affecting *axr1-30* to a lesser extent. Four of these molecules were selected for their strong potency and dose-dependent effect in altering Col-0 development in an AXR1-dependent manner. (C) DMSO and NAA were used as controls. (D) Dose responses of the RNs. Concentrations in micromolars are indicated in brackets.

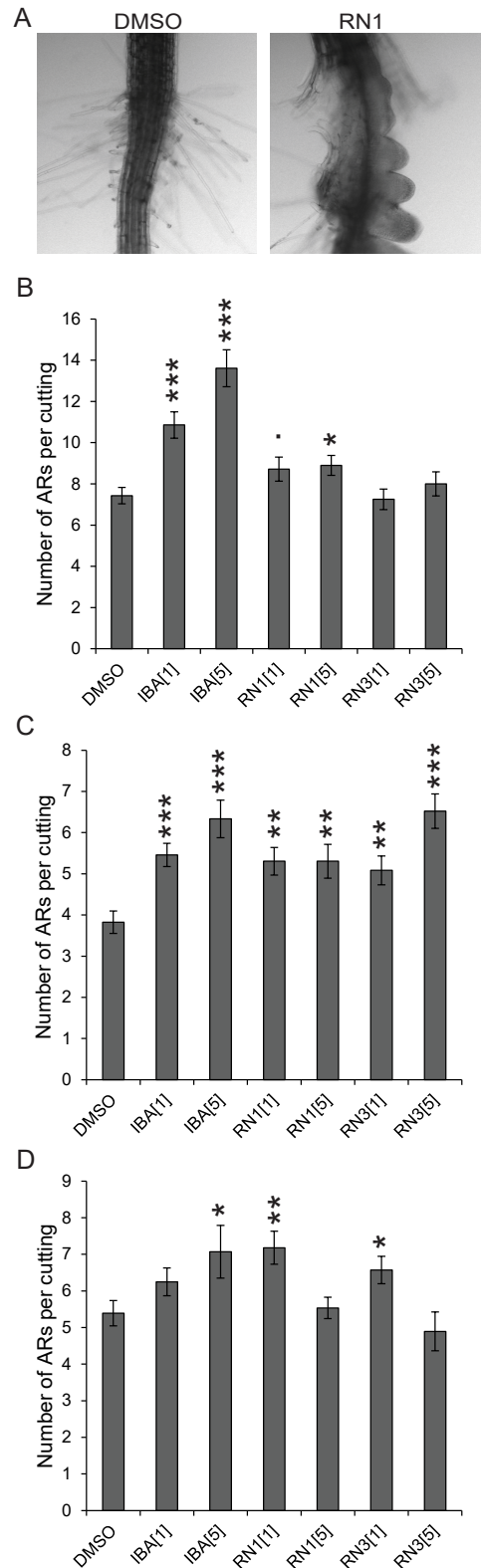


Fig. S2. RN1 and RN3 induce adventitious root (AR) formation. (A) 8-d-old *Arabidopsis* seedlings grown on DMSO or RN1 at 2 μ M. RN1 promoted the formation of amorphous clusters of cells in the hypocotyl base. (B-D) Cuttings of *Populus* lines T89 (B), SwAsp19 (C) and SwAsp35 (D) were propagated in media supplemented with DMSO, IBA, RN1 and RN3 for 9 days to induce rooting. Cuttings were then transferred to fresh medium without treatment. The number of ARs were counted 3 weeks after the transfer. The Student's t-test was performed to compare AR number after mock treatment (DMSO) with that after chemical treatments. Means \pm SEM are shown, $n = 28$ explants across 4 independent replicates, p -value: * $P < 0.05$, ** $P < 0.01$, *** $P < 0.001$. Concentrations in micromolars are indicated in brackets.

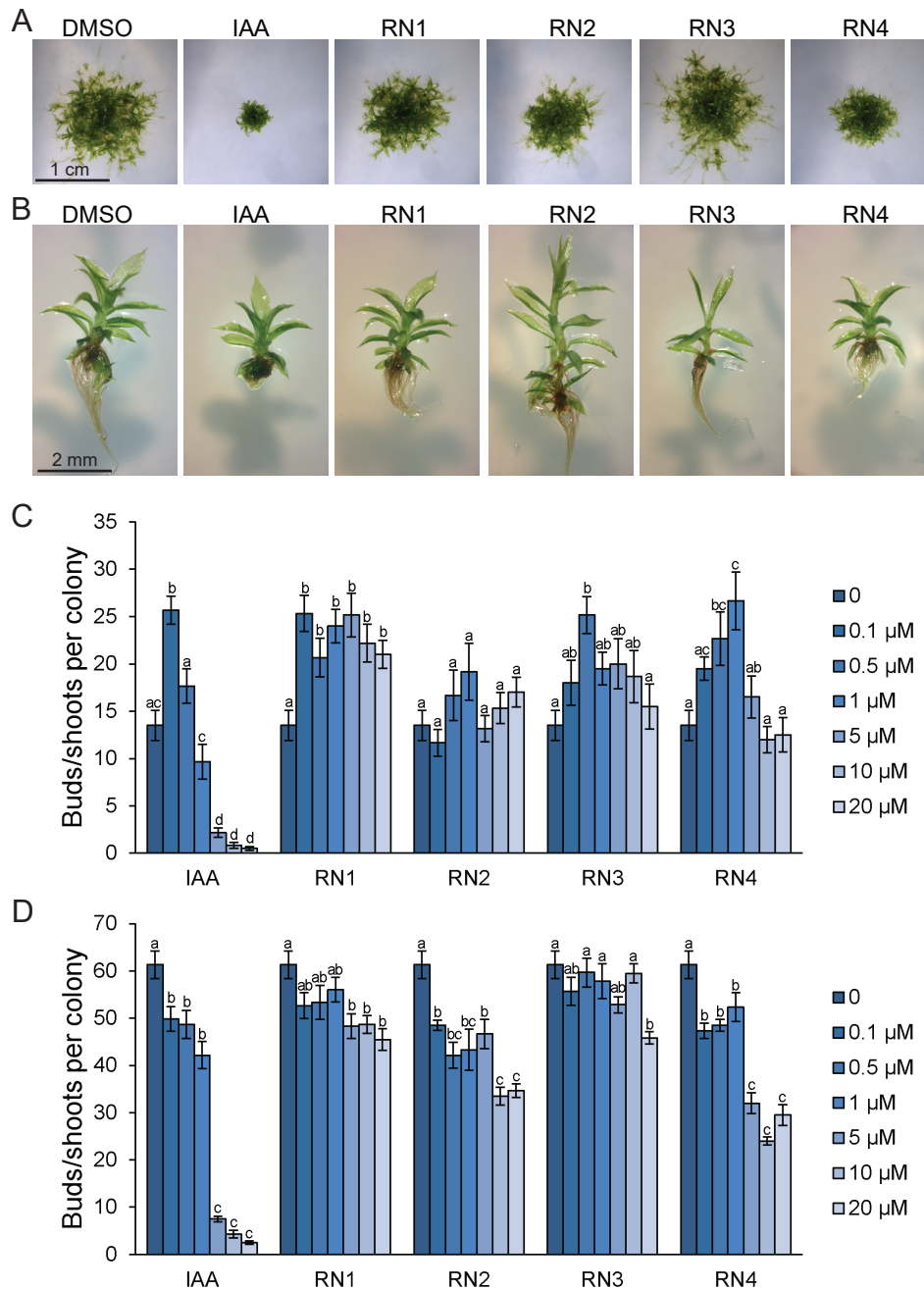


Fig. S3. Auxin-like phenotypes are induced by the RNs in *Physcomitrella patens*. Small pieces of protonemal tissue were transferred to media supplemented with IAA or RN compounds. (A-B) Representative colonies (A) and gametophores (B) after 4 weeks of growth on media supplemented with IAA and RN compounds at 10 μM . DMSO was used as control. (C-D) The number of buds and gametophores was counted for each colony after 1 week (C) and 2 weeks (D) of treatment with concentrations from 0.1 μM to 20 μM . Statistical analyses were performed using ANOVA and Tukey's test. Means \pm SEM are shown, $n = 6$ colonies for each concentration of the dose response. For each treatment, different letters indicate significant differences at $P < 0.05$.

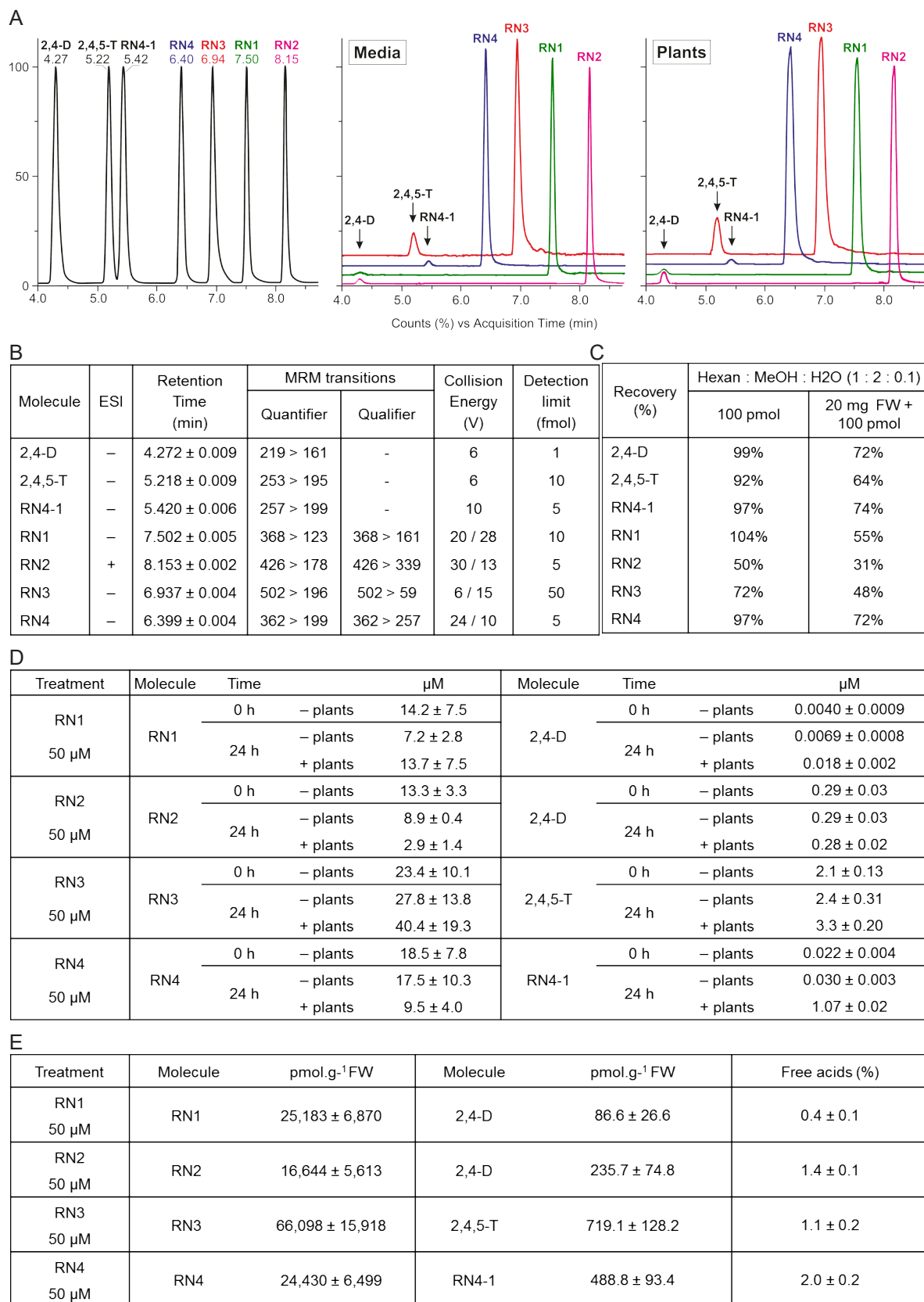


Fig. S4. Analysis of RN stability. Five-d-old *Arabidopsis* seedlings were transferred into liquid media containing RN compounds. Treatment media were collected directly after solubilization of the molecules and after 24 h in the presence or absence of plants. The plants were collected after 24 h treatments. DMSO controls (media and treated plants) were also analyzed in which no RN compounds nor their associated free acids were detected. (A) Multi-MRM chromatograms showing the optimized separation and identification of the analyzed compounds and free acids in liquid media and plants treated by RN compounds. (B) Optimized LC-MS/MS conditions (MRM transitions, retention times, collision energies and limits of detection defined as signal-to-noise ratio 3:1). (C) Liquid-Liquid extraction recovery of the compounds from DMSO treated plant matrix. (D) Molar concentrations of the RNs and their associated free acids in the growing media. (E) Levels of the RNs and their associated free acids in planta after 24 h of treatment. Means ± SD are shown, n = 3 replicates.

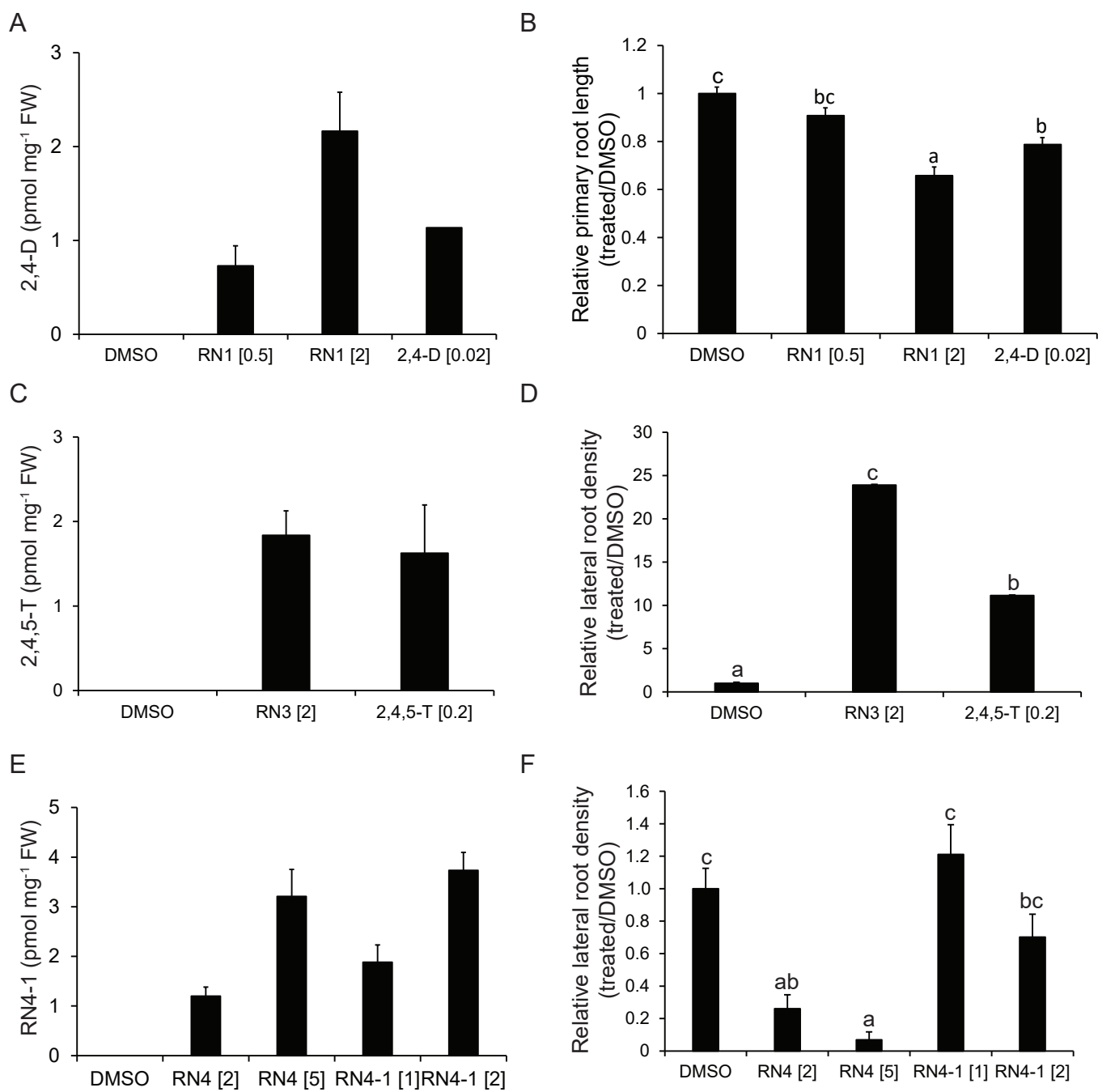


Fig. S5. Quantification of free acids released in roots during long-term RN treatment. Col-0 seedlings were grown on media supplemented with RN1 or 2,4-D for 5 days (A-B) and RN3, 2,4,5-T, RN4 or RN4-1 for 8 days (C-F). DMSO was used as control. The concentration of free acids were quantified in excised roots (A, C, E) after primary root length (B) and lateral root density (D, F) were measured. ANOVA and Tukey's test were performed to compare measurements after mock treatment (DMSO) with that after chemical treatments. Means \pm SEM are shown, $n > 30$ seedlings across 3 independent replicates; different letters indicate significant differences at $P < 0.05$. Concentrations in micromolars are indicated in brackets.

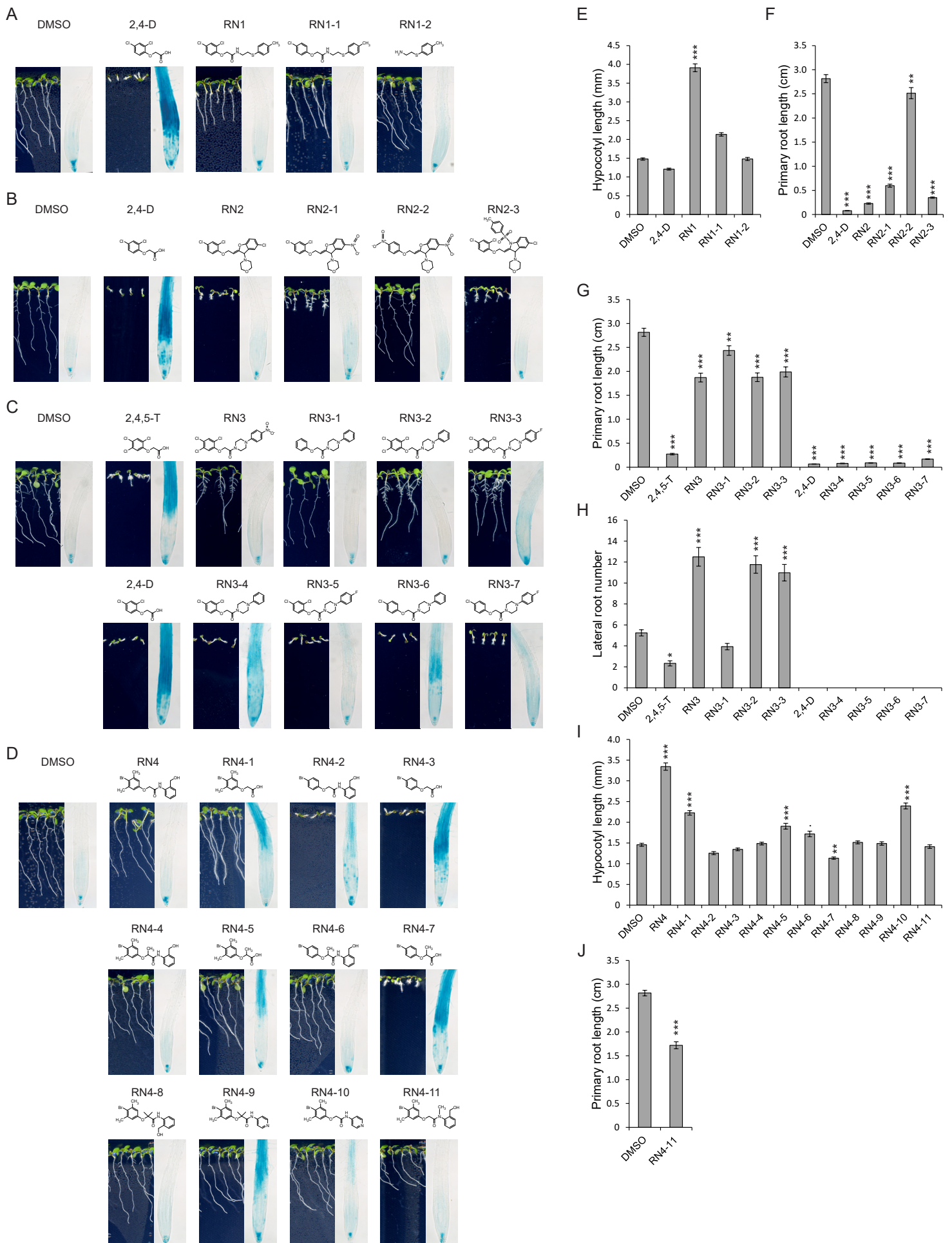


Fig. S6. RN SAR analysis. (A-J) SAR analysis for RN1 (A, E), RN2 (B, F), RN3 (C, G, H) and RN4 (D, I, J). Representative images of eight-d-old seedlings grown on media supplemented with the indicated chemicals, and *pDR5::GUS* expression pattern in 5-d-old GUS-stained seedlings treated with the same chemicals at 10 μ M for 5 h. (E-J) Quantification of RN-induced phenotypes in eight-d-old seedlings grown on media supplemented with the indicated chemicals. Concentrations of the chemicals used (except for GUS-stained seedlings) were (A, E) 1 μ M, (B, F) 0.5 μ M, and (C-D, H-J) 2 μ M. ANOVA and Tukey's test were performed to compare measurements after mock treatment (DMSO) with that after chemical treatments. Means \pm SEM are shown, $n = 50$ seedlings across 3 independent replicates, p -value: $\cdot P < 0.1$, $*P < 0.05$, $**P < 0.01$, $***P < 0.001$.

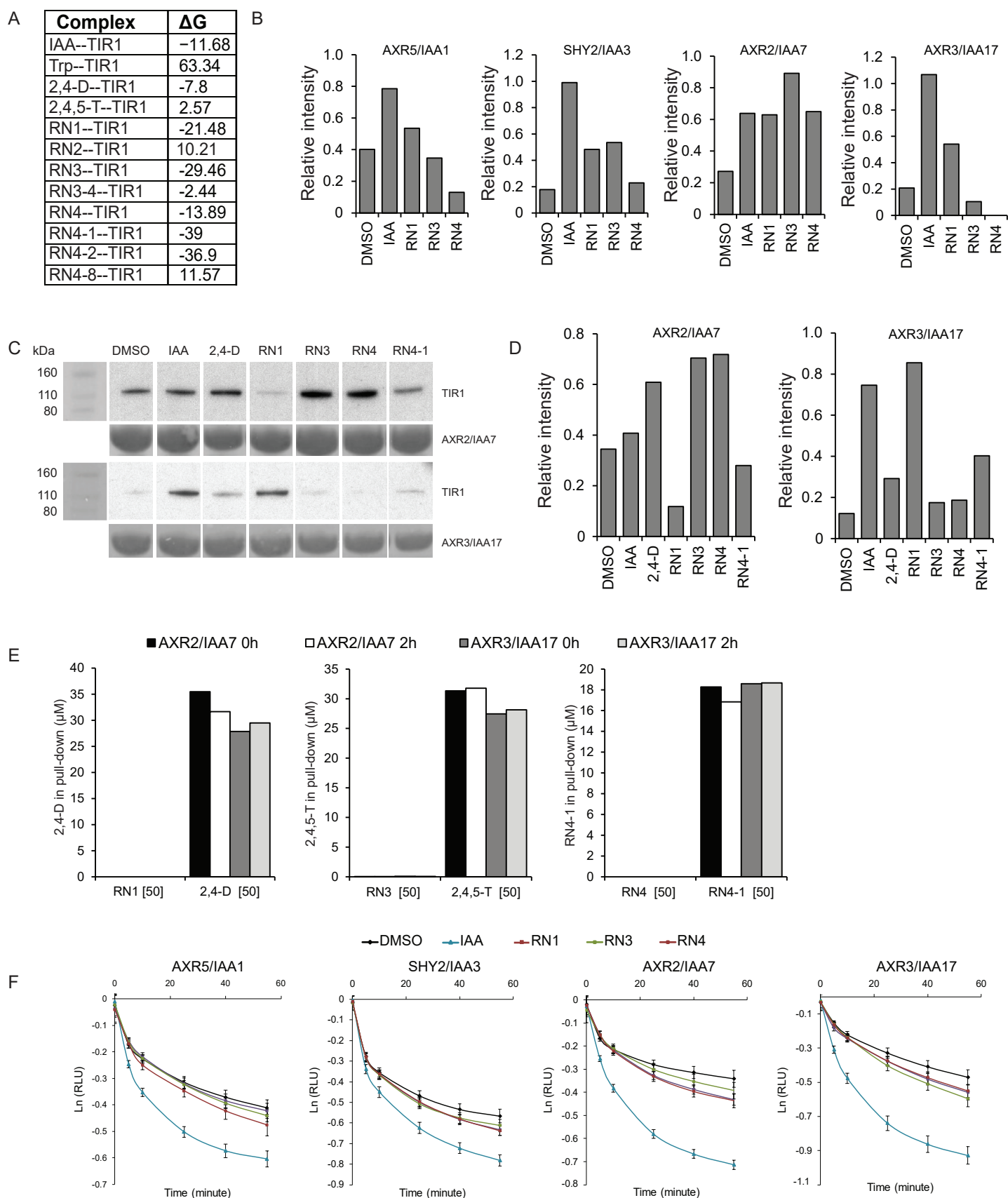


Fig. S7. Thermodynamic stability ($\Delta G_{(\text{chemical-TIR1})}$), in vitro pull-down using insect cell purified TIR1 and AUX/IAA-LUC *in vivo* degradation assay. (A) List of thermodynamic stability values computed for molecules of interest within the TIR1 auxin binding pocket. (B) Quantification of band intensity in the pull-down gel image shown in Fig. 3D. The intensity of each band was normalized to the respective Ponceau staining intensity. (C) Western blot of pull-downs using GSH-Sepharose immobilized GST-AXR2/IAA7 or GST-AXR3/IAA17 against 3XFLAG:MBP:HIS:TIR1 (GST-IAA proteins were produced in *E. coli*, while 3XFLAG:MBP:HIS:TIR1 was produced in insect cells; all were full length proteins and were affinity purified before the pull-downs). All compounds were used in solution at 50 μM . Post pull-down washing was done including the respective compounds at the same concentration. Western blot was hybridized with Anti Flag-HRP antibody. (D) Quantification of band intensity in the pull-down gel image shown in Fig. S7C. The intensity of each band was normalized to the respective Ponceau staining intensity. (E) LC/MS analysis of RN stability in the pull-down buffer before and after 2 h of incubation in the presence of TIR1 and AXR2/IAA7 or AXR3/IAA17. The pull-down was performed as for Fig. S7C. (F) AUX/IAA-LUC degradation over time in 7-d-old seedlings carrying AXR5/IAA1-LUC, SHY2/IAA3-LUC, AXR2/IAA7-LUC and AXR3/IAA17-LUC translational fusions, treated with DMSO and IAA as controls and with the RNs at 50 μM . Time zero represents the first acquisition of light emission directly after treatment. Means \pm SEM are shown, $n = 30$ seedlings across 5 independent replicates. Concentrations in micromolars are indicated in brackets.

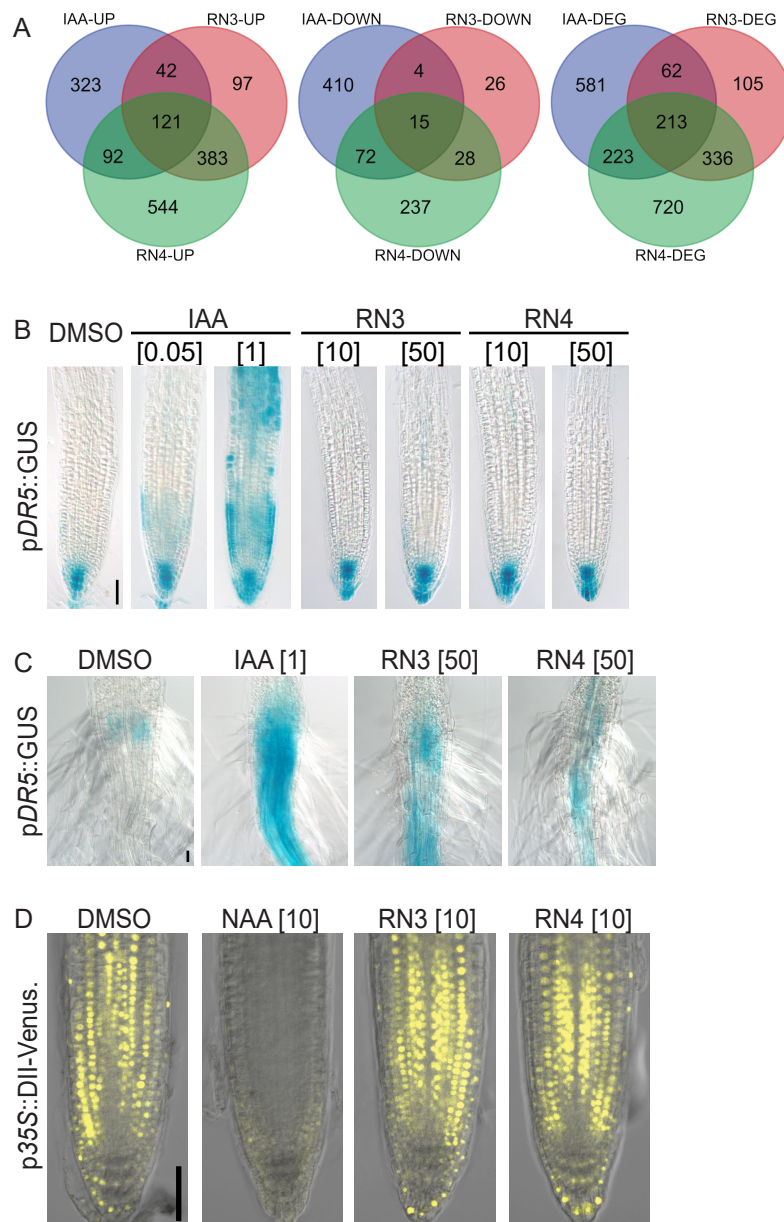
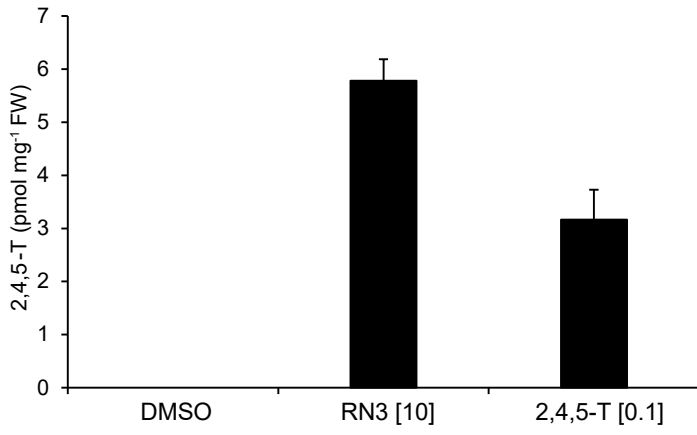
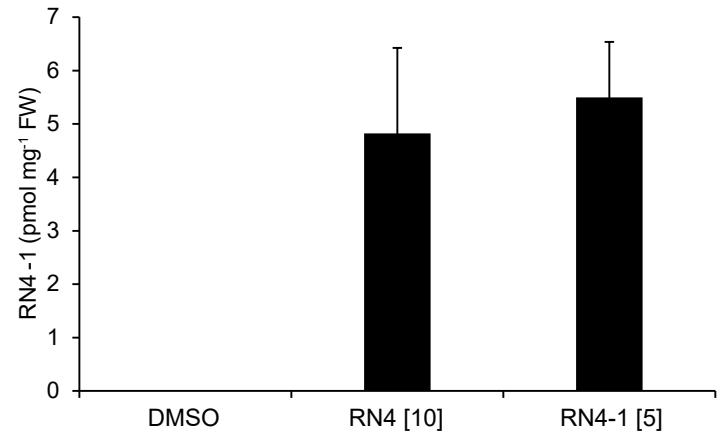


Fig. S8. RN3 and RN4 induce local auxin responses. (A) Venn diagram showing the overlap between genes which were upregulated, downregulated or differentially expressed (DEG) in cell culture after RN3, RN4 or IAA treatments ($n = 3$ culture samples; p -value < 0.05). (B-C) Five-d-old seedlings expressing pDR5::GUS were treated for 5 h with different concentrations of RN3 and RN4. DMSO and two concentrations of IAA were used as negative and positive controls respectively. Representative images of the primary root tip (B) and the root-hypocotyl junction (C) after GUS staining, showing that RN3 and RN4 only induce pDR5::GUS at 50 μ M in the root-hypocotyl junction. (D) Five-d-old seedlings of p35S::DII-Venus were treated for 45 min with RN3 and RN4 at 10 μ M. DMSO and NAA were used as negative and positive controls respectively. Scale bars represent 50 μ m. Concentrations in micromolar are indicated in brackets.

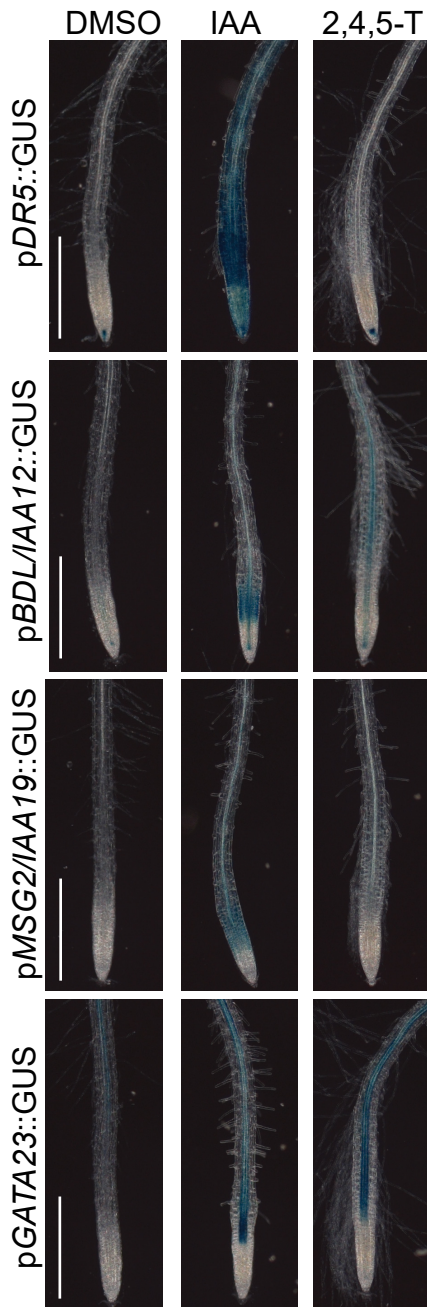
A



B



C



D

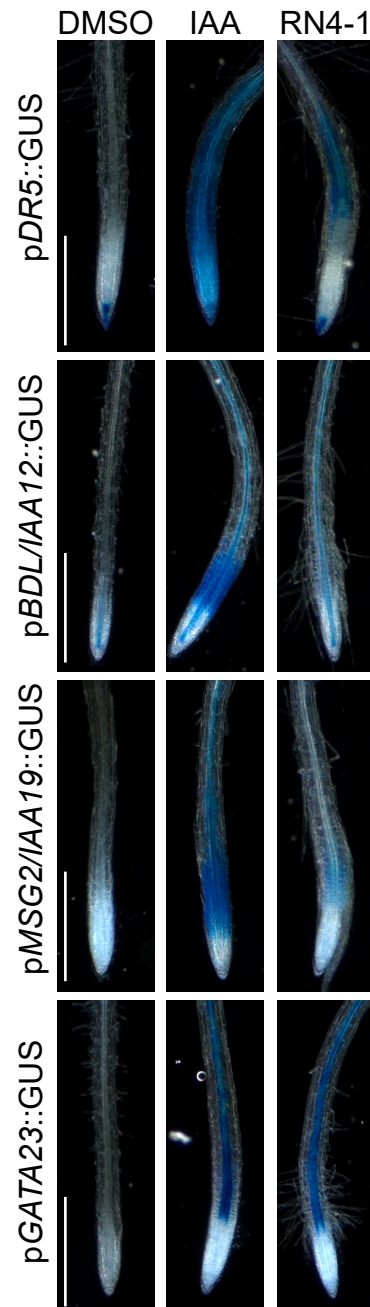


Fig. S9. The effects of 2,4,5-T and RN4-1 on auxin-responsive promoter lines. (A-B) Five-day-old seedlings were treated for 16 h with RN3, 2,4,5-T, RN4 or RN4-1 and the concentrations of free acids released in the excised roots was quantified. DMSO was used as control. (C-D) Representative primary roots of 5-day-old seedlings expressing pDR5::GUS, pBDL/IAA12::GUS, pMSG2/IAA19::GUS or pGATA23::GUS transcriptional fusions treated with 10 μM IAA, 0.1 μM 2,4,5-T or 5 μM RN4-1 for 16 h. DMSO was used as control. Scale bars indicate 500 μm (C-D). Concentrations in micromolars are indicated in brackets.

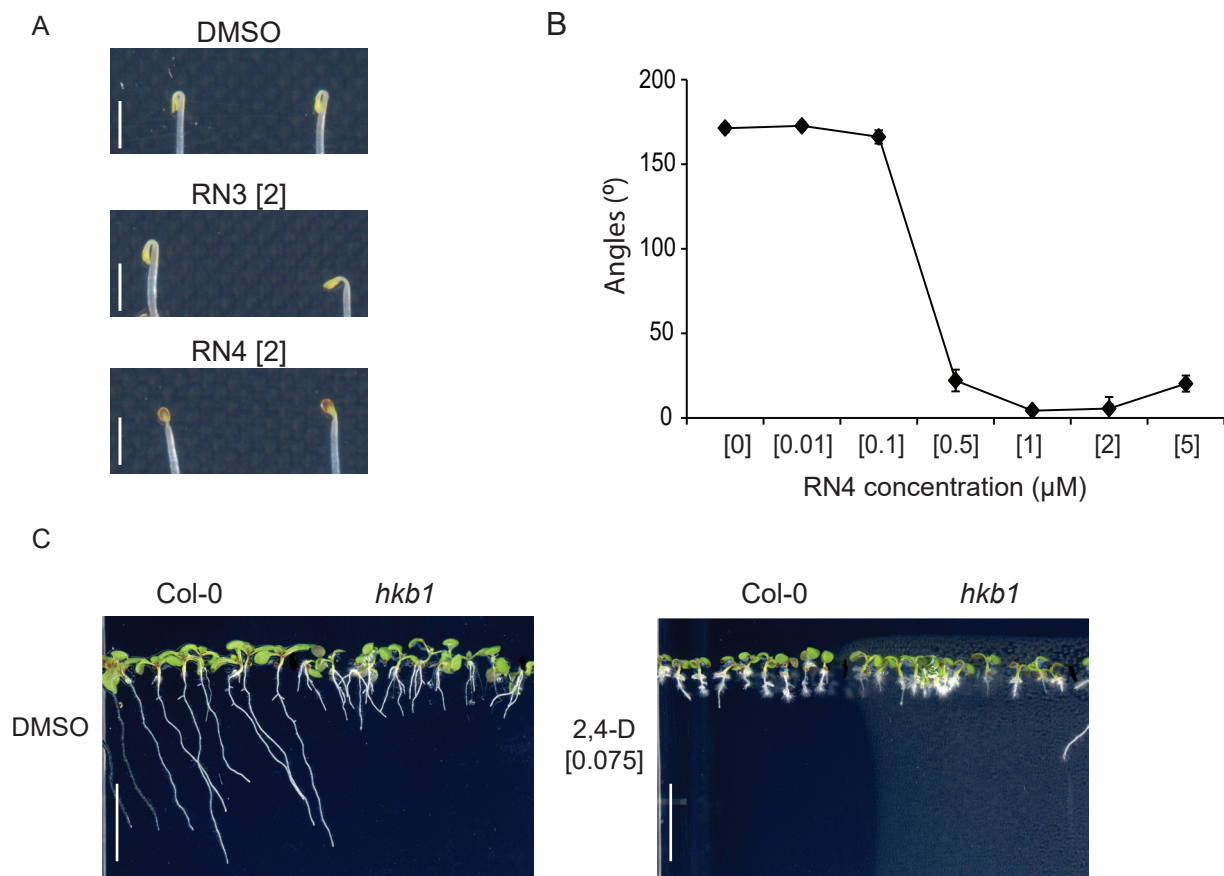


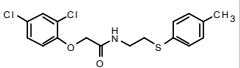
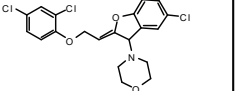
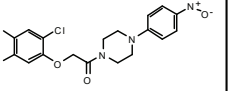
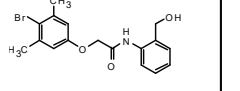
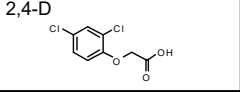
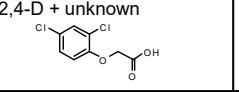
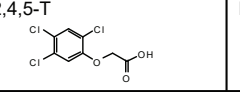
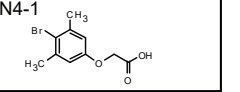
Fig. S10. RN3 and RN4 have distinct effects on apical hook development in *Arabidopsis*. (A) Apical hook phenotypes of 3-d-old Col-0 seedlings grown on media supplemented with DMSO, RN3 and RN4. While RN3 showed a negligible effect, RN4 completely abolished apical hook development. (B) Dose-response graph representing the effect of RN4 on apical hook angle in 4-d-old Col-0 seedlings. (C) Representative images of 8-d-old Col-0 and *hkb1* grown on MS media supplemented with DMSO or 2,4-D. Means \pm SEM are shown, $n = 10$ seedlings for each concentration of the dose response (B). Scale bars represent 2 mm (A) and 1 cm (C). Concentrations in micromolars are indicated in brackets.

Table S1. Selected IAA, RN3 and RN4 up-regulated genes after 30 minute treatments of cell culture. Values indicate fold change upon IAA, RN3 and RN4 treatment compared to DMSO. Statistically significant values (p-value < 0.05) are represented in bold.

IAA up-regulated \cap RN3 not up-regulated \cap RN4 not up-regulated 323 significantly up-regulated genes (4 examples shown)				
AGI	Gene name	IAA	RN3	RN4
AT2G39370	MEMBRANE-ASSOCIATED KINASE REGULATOR 4 (MAKR4)	0.75	0.12	0.22
AT4G39400	BRASSINOSTEROID INSENSITIVE 1 (BRI1)	0.45	-0.01	-0.03
AT5G43700	INDOLE-3-ACETIC ACID INDUCIBLE 4 (IAA4)	0.97	0.23	0.04
AT3G60630	HAIRY MERISTEM 2 (HAM2)	0.39	-0.03	-0.11
IAA up-regulated \cap RN3 up-regulated \cap RN4 up-regulated 121 significantly up-regulated genes (21 examples shown)				
AGI	Gene name	IAA	RN3	RN4
AT1G04240	SHORT HYPOCOTYL 2 (SHY2)	1.59	0.62	1.04
AT1G70940	PIN-FORMED 3 (PIN3)	0.55	0.36	0.22
AT1G78100	AUXIN UP-REGULATED F-BOX PROTEIN 1 (AUF1)	1.47	0.53	0.80
AT2G36800	DON-GLUCOSYLTRANSFERASE 1 (DOGT1)	1.05	1.15	1.47
AT2G42430	LATERAL ORGAN BOUNDARIES-DOMAIN 16 (LBD16)	0.79	0.88	0.96
AT2G14960	IAA-amido synthase (GH3.1)	0.53	0.78	1.28
AT3G23030	INDOLE-3-ACETIC ACID INDUCIBLE 2 (IAA2)	1.23	0.61	1.01
AT3G25710	BASIC HELIX-LOOP-HELIX 32 (BHLH32)	0.99	1.39	1.06
AT3G49940	LOB DOMAIN-CONTAINING PROTEIN 38 (LBD38)	0.61	0.85	1.72
AT3G50660	DWARF 4 (DWF4)	0.43	0.52	0.61
AT3G62100	INDOLE-3-ACETIC ACID INDUCIBLE 30 (IAA30)	1.49	1.53	1.85
AT4G14560	INDOLE-3-ACETIC ACID INDUCIBLE 1 (IAA1)	1.26	0.97	1.53
AT4G15550	INDOLE-3-ACETATE BETA-D-GLUCOSYLTRANSFERASE (IAGLU)	1.72	2.13	1.42
AT4G17460	Homeodomain-leucine Zipper II (HAT1)	2.51	1.04	0.98
AT4G34131	UDP-GLUCOSYL TRANSFERASE 73B3 (UGT73B3)	1.92	2.42	1.86
AT4G34135	UDP-GLUCOSYLTRANSFERASE 73B2 (UGT73B2)	1.66	1.70	1.71
AT4G34138	UDP-GLUCOSYL TRANSFERASE 73B1 (UGT73B1)	0.61	1.07	1.46
AT4G37390	AUXIN UPREGULATED 3 (AUR3)	2.55	1.62	2.59
AT5G47370	Homeodomain-leucine Zipper II (HAT2)	2.08	1.12	1.26
AT5G54490	PINOID-BINDING PROTEIN 1 (PBP1)	0.39	1.07	2.51
AT5G67420	LOB DOMAIN-CONTAINING PROTEIN 37 (LBD37)	0.92	0.84	1.35
IAA up-regulated \cap RN3 up-regulated \cap RN4 not up-regulated 42 significantly differentially up-regulated genes (9 examples shown)				
AGI	Gene name	IAA	RN3	RN4
AT1G10370	EARLY-RESPONSIVE TO DEHYDRATION 9 (ERD9)	1.31	1.08	0.63
AT1G15580	INDOLE-3-ACETIC ACID INDUCIBLE 5 (IAA5)	0.79	0.85	0.59
AT1G21910	DEHYDRATION RESPONSE ELEMENT-BINDING PROTEIN 26 (DREB26)	1.24	0.84	0.45
AT1G79270	EVOLUTIONARILY CONSERVED C-TERMINAL REGION 8 (ECT8)	0.79	0.59	0.08
AT2G30490	CINNAMATE-4-HYDROXYLASE (C4H)	0.55	0.55	0.30
AT3G04730	INDOLEACETIC ACID-INDUCED PROTEIN 16 (IAA16)	0.81	0.57	0.25
AT3G55120	TRANSPARENT TESTA 5 (TT5)	2.05	1.57	1.14
AT4G26690	SHAVEN 3 (SHV3)	0.22	0.24	0.11
AT5G13930	TRANSPARENT TESTA 4 (TT4)	2.34	1.90	1.25

IAA up-regulated \cap RN4 up-regulated \cap RN3 not up-regulated 92 significantly differentially up-regulated genes (12 examples shown)				
AGI	Gene name	IAA	RN3	RN4
AT1G04100	INDOLEACETIC ACID-INDUCED PROTEIN 10 (IAA10)	0.64	0.18	0.34
AT1G11260	SUGAR TRANSPORTER 1 (STP1)	0.44	0.25	0.94
AT1G31880	BREVIS RADIX (BRX)	1.26	0.41	0.67
	XYLOGLUCAN ENDOTRANSGLUCOSYLASE/HYDROLASE			
AT1G32170	30 (XTH30)	0.92	0.35	0.70
AT1G55330	ARABINO GALACTAN PROTEIN 21 (AGP21)	0.37	0.10	0.21
AT2G38310	PYR1-LIKE 4 (PYL4)	0.46	0.21	0.52
AT3G50060	MYB DOMAIN PROTEIN 77 (MYB77)	0.51	-0.13	0.66
AT2G23170	IAA-amido synthase (GH3.3)	0.92	0.23	0.52
AT4G08950	EXORDIUM (EXO)	0.68	0.16	0.41
AT4G32280	INDOLE-3-ACETIC ACID INDUCIBLE 29 (IAA29)	1.13	0.33	0.60
AT5G57560	TOUCH 4 (TCH4)	0.51	0.39	0.95
AT5G65390	ARABINO GALACTAN PROTEIN 7 (AGP7)	0.60	0.03	0.56

Table S2. Summary of the results obtained for each RN molecule described in this work.

Chemical structure of the RubNeddins (RN)				
Chemical name	2-(2,4-dichlorophenoxy)-N-{2-[(4-methylphenyl)thio]ethyl}acetamide	4-{5-chloro-2-[2-(2,4-dichlorophenoxy)ethylidene]-2,3-dihydro-1-benzofuran-3-yl}morpholine	1-(4-nitrophenyl)-4-[(2,4,5-trichlorophenoxy)acetyl]piperazine	2-(4-bromo-3,5-dimethylphenoxy)-N-[2-(hydroxymethyl)phenyl]acetamide
ChemBridge ID	6389186	5742604	6189599	7014462
Degradation product	2,4-D 	2,4-D + unknown 	2,4,5-T 	RN4-1 
Primary effect on <i>Arabidopsis</i> seedlings in presence of the RNs	- Hypocotyl length increase - Primary root growth inhibition - Adventitious root induction	- Primary root growth inhibition	- Lateral root number increase	- Lateral root number decrease - Hypocotyl length increase
Structure Activity Relationship conclusion	Importance of the chlorination in position 2 and 4 and the side chain	Biological activity due to 2,4-D structure	Importance of chlorination in position 2,4 and 5 and the piperazine	Importance of methyl group in position 3 and 5 Hydroxymethylation
Transcriptomic response	N/A	N/A	Tissue and promoter specific	Tissue and promoter specific
Selective formation of the auxin co-receptor complex	Yes	N/A	Yes	Yes
Selective degradation of the AUX/IAA proteins	Yes	N/A	Yes	Yes

Movie S1. Molecular modeling view. The movie represents the crystal structure of TIR1 (Gray), IAA (red), and the DII domain of IAA7 (green). The first sequence shows the best docking probability obtained for RN1 (yellow), RN2 (purple), RN3 (cyan), RN4 (orange) and RN4-8 (pink). The second sequence shows two chosen molecules for RN1 (yellow), RN3 (cyan) and RN4 (orange), corresponding to the best docking conformation, next to the conformation which thermodynamically stabilized TIR1 without the DII-domain of IAA7.

Dataset S1. RNAseq results for *Arabidopsis* cell suspension culture treated with IAA, RN3 and RN4. Column A indicates the gene ID. Column B, C and D indicate the induction ratio between the treatment and DMSO for RN3, RN4 and IAA respectively. Columns E, F and G indicate up-regulation (1), down-regulation (-1) or no difference compared to the DMSO for RN3, RN4 and IAA respectively.

Supplementary Document

Chemical Synthesis and Characterization

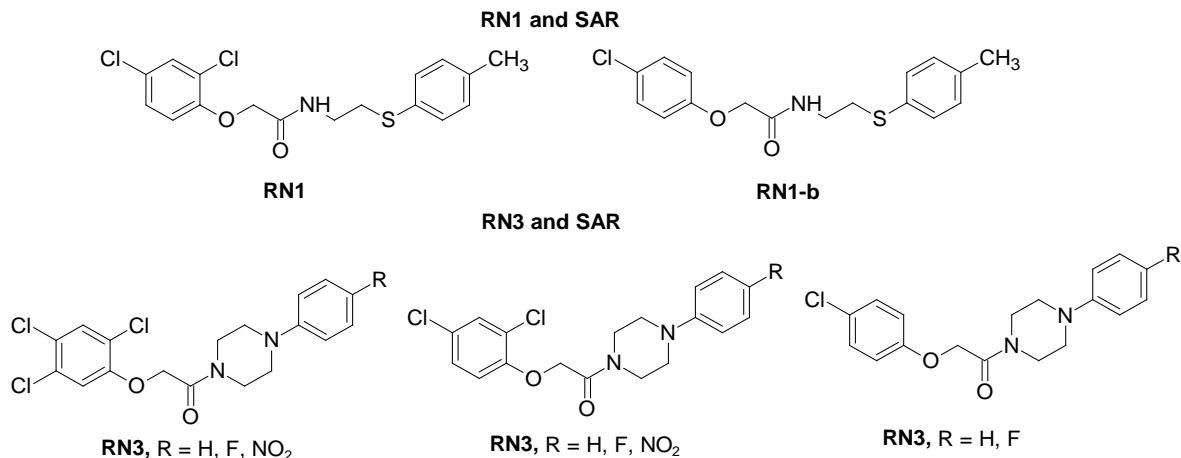
1. General experimental information

Unless stated, all reagents and solvents were used as received from commercial suppliers. All reactions were carried out under an inert atmosphere with dry solvents under anhydrous conditions, unless otherwise indicated. TLC was performed on aluminum backed silica gel plates (medium pore size 60 Å, fluorescent indicator 254 nm) and visualized by exposure to UV light (254 nm) or stained with potassium permanganate (KMnO₄) and ethanolic phosphomolybdic acid (PMA). Column chromatography was performed using silica gel with an average particle diameter 50 µm (range 40–65 µm, pore diameter 53 Å), and eluents are given in brackets. IR spectra were recorded on a spectrometer equipped with an FTIR device. ¹H NMR spectra were recorded on a Bruker AVANCE (at 400 MHz) spectrometer at 298 K, 343 K and calibrated by using the residual peak of the solvent as the internal standard (CDCl₃: δ_H = 7.26 ppm; δ_C = 77.23 ppm. DMSO-d₆: δ_H = 2.50 ppm; δ_C = 39.51 ppm). ¹³C NMR spectra were acquired on a Bruker AVANCE (at 100 MHz) spectrometer and chemical shift (δ ppm) are reported relative to the residual solvent peak. The following abbreviations were used to describe the data of ¹H NMR spectra: chemical shift (δ ppm), s = singlet, d = doublet, t = triplet, q = quartet, m = multiplet, br = broad; coupling constant(s) in Hz. LCMS was conducted on a Micromass ZQ mass spectrometer with ES⁺ ionization. HRMS was performed by using a mass spectrometer with ESI-TOF (ES⁺).

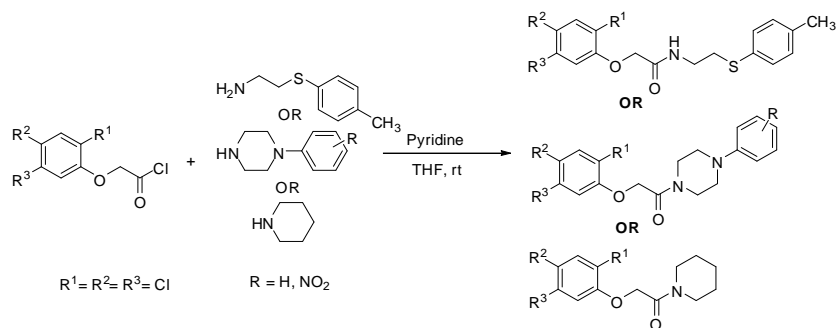
2. Chemical synthesis of hit molecules RN1, RN3, RN4 and their analogs

The hit molecule **RN2** was purchased from ChemBridge and purity data of this molecule is included.

2.1 Synthesis of hit molecules RN1, RN3 and SAR:

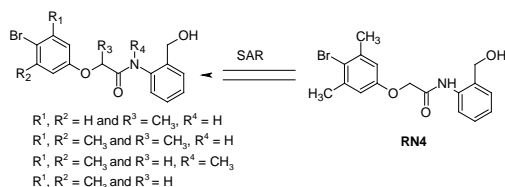


2.1.1 General procedure for the synthesis of hit molecules RN1, RN3 and SAR:

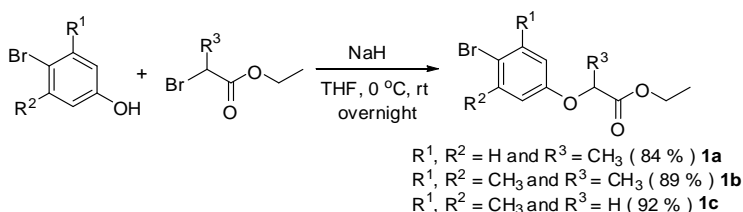


Pyridine (1.2 mmol) was mixed with Amine (1.0 mmol) in anhydrous tetrahydrofuran (5 mL) at 0 °C and stirred for 30 minutes. To this mixture was added a solution of acid chloride (1.2 mmol) in tetrahydrofuran (1 mL) drop wise and the reaction mixture was stirred at room temperature for 4h (monitored by LCMS). The precipitate was washed with ammonium chloride (sat. aq.) and extracted with ethylacetate, and the combined extracts were dried over anhydrous sodium sulfate, concentrated under reduced pressure to give the crude amide. The residue was purified by silica gel column chromatography using *n*-Heptane: Ethyl acetate (20-40 %), to afford pure products (86 % to 92 %).

2.2 Synthesis of hit molecule RN4 and analog:

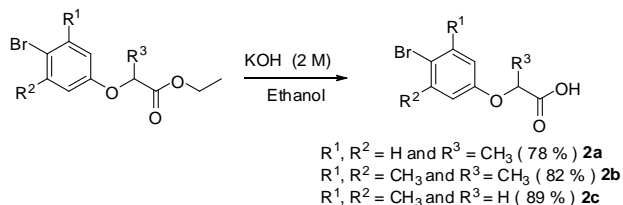


2.2.1 General experimental procedure for the synthesis of substituted phenoxyacetic acid esters (**1a-1c**):



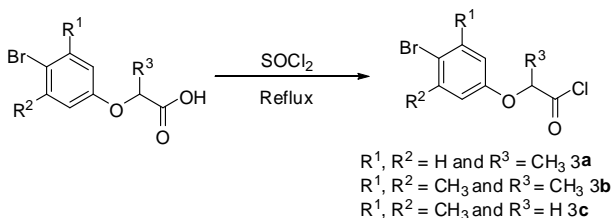
Sodium hydride (60% in paraffin, 2.0 mmol) was stirred for 5 min in hexane under argon atmosphere, and then the solvent was removed by a syringe followed by evaporation with a vacuum pump. This similar process was repeated three times then the sodium hydride residue was suspended in tetrahydrofuran (5 mL) and the mixture was allowed to cool to 0 °C. To this mixture was added a solution of substituted phenol (2.0 mmol) in tetrahydrofuran (3 mL) dropwise over 5 min, and the mixture was stirred for 5 min at the same temperature. Then the mixture was allowed to warm to room temperature and stirred for an additional 15 min. A solution of ethyl-2-bromopropanoate (4.0 mmol) in tetrahydrofurane (2 mL) was added and the mixture was stirred for 14 h. The reaction mixture was acidified by 2 M hydrochloric acid and extracted with EtOAc. The organic layer was washed with brine, dried over anhydrous sodium sulfate, and concentrated in vacuum. The residue was purified by silica gel column chromatography (n-heptane/EtOAc: 9/1) to give pure products (**1a-c**) (52).

2.2.2 General experimental procedure for the synthesis of substituted phenoxyacetic acid (2a-2c):



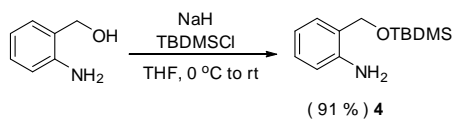
A solution of ester (2.0 mmol) in EtOH (6 mL) was added to an aqueous solution of potassium hydroxide (5 mL, 2 M) at 0 °C. After being stirred for 6-7 h, the reaction mixture was acidified by 3 M hydrochloric acid to afford the white precipitate which was filtered and washed with heptanes to give substituted-2-phenoxypropanoic acid (**2a-c**) in 78-89 % yield.

2.2.3 Experimental procedure for the synthesis of substituted phenoxyacetic acid chloride (3a-3c):



The mixture of phenoxyacetic acid (2 mmol) and thionyl chloride (6–10 mL) was reacted for 3 h under reflux until no further gaseous HCl was released. After completion of the reaction excess of thionyl chloride was distilled off under reduced pressure, giving the corresponding phenoxyacetic chlorides as brown oils. The phenoxyacetic chlorides were used in the next step without further purification.

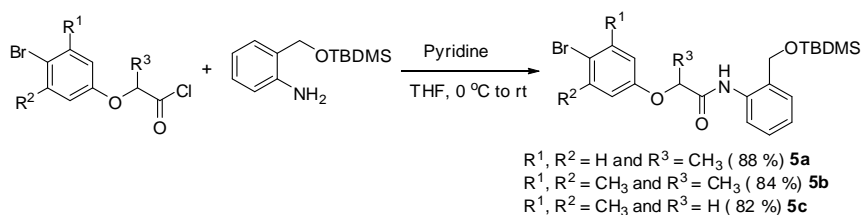
2.2.4 Experimental procedure for the synthesis of 2-((tert-butyl dimethylsilyloxy)methyl)aniline:



To a cooled (0 °C), stirred suspension of NaH (60% dispersion in mineral oil, 1.15 g, 29.05 mmol) in anhydrous THF (5 mL) was added dropwise a solution of 2-aminobenzyl alcohol

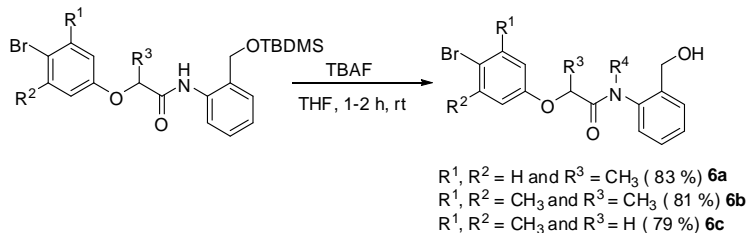
5 (3.25 g, 26.4 mmol) in anhydrous THF (8 mL) and the mixture was stirred at 0 °C for 15 min under nitrogen atmosphere. To this was added dropwise a solution of *tert*-butyldimethylsilyl chloride (4.25 g, 31.65 mmol) in anhydrous THF (12 mL) and the reaction mixture was gradually warmed to room temperature and stirred for 2 h. The reaction mixture was cooled to 0 °C and crushed ice was carefully added to quench the reaction. This was extracted with EtOAc (50 mL) and the combined extracts were washed with brine (10 mL), dried over Na₂SO₄ and concentrated in vacuo. The residue was purified by flash column chromatography (EtOAc/*n*-Heptane 0:100 to 10:90) to yield the title compound (5.5 g, 91%) as a dark yellow, viscous oil.

2.2.5 Experimental procedure for the synthesis of substituted phenoxy)-N-(2-((*tert*-butyldimethylsilyloxy)methyl)phenyl)propanamide:



Pyridine (1.2 mmol) was mixed with 2-((*tert*-butyldimethylsilyloxy)methyl)aniline (1.0 mmol) in anhydrous tetrahydrofuran (5 mL) at 0 °C and stirred for 30 minutes. To this mixture was added a solution of substituted phenoxyacetic acid chloride (1.2 mmol) in tetrahydrofuran (1 mL) drop wise over 5 minutes and the reaction mixture was stirred at room temperature for 4h (monitored by LCMS). The precipitate was washed with ammonium chloride (sat. aq) and extracted with ethylacetate, and the combined extracts were dried over anhydrous sodium sulfate, concentrated under reduced pressure to give the crude amide. The residue was purified by silica gel column chromatography *n*-Heptane: Ethyl acetate (20-40 %), to afford pure products (86 % to 92 %).

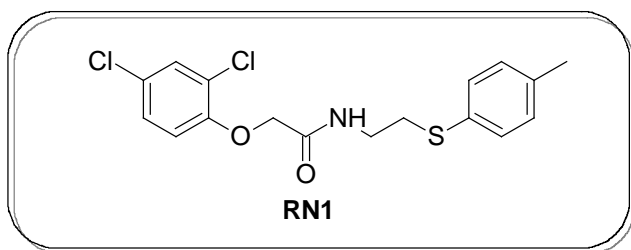
2.2.6 Experimental procedure for the synthesis of 2-(4-bromo-3,5-dimethylphenoxy)-N-(2-(hydroxymethyl)phenyl)acetamide OR 2-(4-bromo-3,5-dimethylphenoxy)-N-(2-(hydroxymethyl)phenyl)-N-methylacetamide:



A mixture of a substituted phenoxy-N-(2-((tert-butyl)dimethylsilyloxy)methyl)phenyl)propanamide (1 mmol) OR 2-(4-bromo-3,5-dimethylphenoxy)-N-(2-(hydroxymethyl)phenyl)-N-methylacetamide (1 mmol), TBAF (1.2 mmol) in THF (10 mL) was stirred at room temperature until the reaction was finished as indicated by thin-layer chromatography (TLC). The reaction mixture was then diluted with dichloromethane (100 mL), washed with brine, dried over sodium sulphate. The solvent was removed in vacuum, and the residue was purified by flash column chromatography.

3. Spectral data for RN1, RN3 and RN4 their analogs:

2-(2,4-dichlorophenoxy)-N-(2-(p-tolylthio)ethyl)acetamide (RN1):

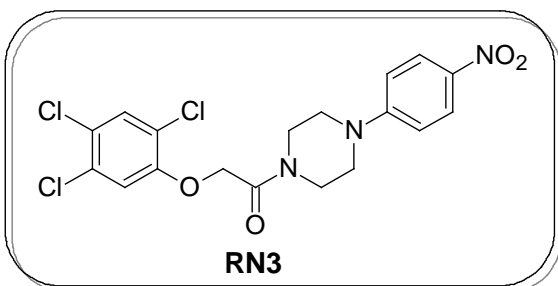


Prepared by following the general procedure 2.1.1 in 89% yield; white fluffy solid; mp 109-111 °C; $R_f = 0.42$ (3:2 of *n*-heptane:EA); IR (KBr) ν 3445, 3293, 2982, 2923, 1669, 1474,

1391, 1259, 1092, 760, 645 cm^{-1} ; $^1\text{H NMR}$ (400 MHz, DMSO-*d*₆) δ 8.16 (t, $J = 4.0$ Hz, 1H, NH), 7.61 (d, $J = 4.0$ Hz, 1H), 7.36 (dd, $J = 8.0, 4.0$ Hz, 1H), 7.29-7.27 (m, 2H), 7.29 (dd, $J = 8.0, 4.0$ Hz, 1H), 7.14 (d, $J = 8.0$ Hz, 2H), 7.05 (d, $J = 8.0$ Hz, 1H), 4.60 (s, 2H), 3.36-3.29 (m, 2H), 3.0 (t, $J = 8.0$ Hz, 2H), 2.26 (s, 3H); $^{13}\text{C NMR}$ (100 MHz, DMSO-*d*₆) δ 166.9, 152.4, 135.5, 131.6, 129.7, 129.3, 129.0, 128.0, 125.1, 122.5, 115.4, 67.8, 38.0,

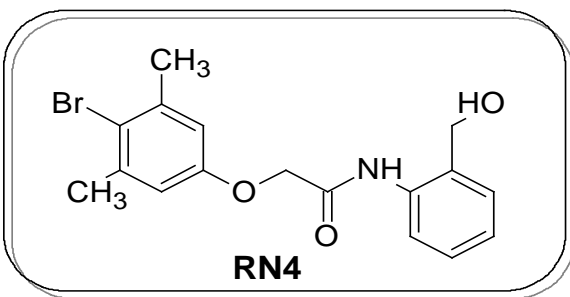
32.0, 20.4 ; **HRMS** (ESI-TOF, $[M + Na]^+$) calcd for $C_{17}H_{17}NO_2NaSCl_2$ 392.0258, found 392.0255.

1-(4-(4-nitrophenyl)piperazin-1-yl)-2-(2,4,5-trichlorophenoxy)ethanone (RN3):



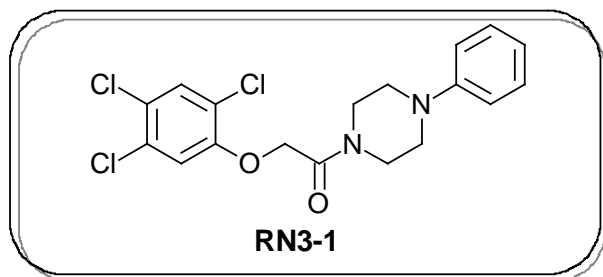
Prepared by following the general procedure **2.1.1** in 84 % yield; yellow solid: mp 236-238 °C; $R_f = 0.52$ (3:2 *n*-heptane:EA); **IR** (KBr) ν 1643, 1546, 1350, 1472, 1391, 1243, 1023, 745, 645 cm^{-1} ; **1H NMR** (400 MHz, DMSO-*d*6) δ 8.09 (d, $J = 12.0$ Hz, 2H), 7.82 (s, 1H), 7.45 (s, 1H), 7.05 (d, $J = 8.0$ Hz, 2H), 5.14 (s, 2H), 3.62 (s, 6H), 3.56-3.52 (m, 2H); **^{13}C NMR** (100 MHz, DMSO-*d*6) δ 165.1, 154.3, 153.1, 136.9, 130.4, 130.1, 125.7, 122.8, 121.0, 115.7, 112.5, 66.5, 45.8, 43.40.5; **HRMS** (ESI-TOF, $[M + H]^+$) calcd for $C_{18}H_{17}N_3O_4Cl_3$ 444.0285, found 444.0285.

2-(4-bromo-3,5-dimethylphenoxy)-N-(2-(hydroxymethyl)phenyl)acetamide (RN4):



Prepared by following the general procedure **2.2.6** in 78 % yield, yellow solid: mp 352.3-352.3, 1647, 1483, 1329, 1259, 1087, 723, 619 cm^{-1} ; **1H NMR** (400 MHz, DMSO-*d*6) δ 10.05 (s, 1H), 7.90 (d, $J = 8.0$ Hz, 1H), 7.33-7.26 (m, 2H), 7.12 (dt, $J = 8.0, 4.0$ Hz, 1H), 6.93 (s, 2H), 5.64 (brs, 1H), 4.68 (s, 2H), 4.54 (s, 2H), 2.34 (s, 6H); **^{13}C NMR** (100 MHz, DMSO-*d*6) δ 166.2, 155.9, 138.6, 136.0, 132.1, 130.1, 127.9, 127.5, 124.2, 122.0, 118.3, 115.0, 67.1, 61.3, 23.5; **HRMS** (ESI-TOF, $[M + Na]^+$) calcd for $C_{17}H_{18}NO_3NaBr$ 386.0368, found 386.067.

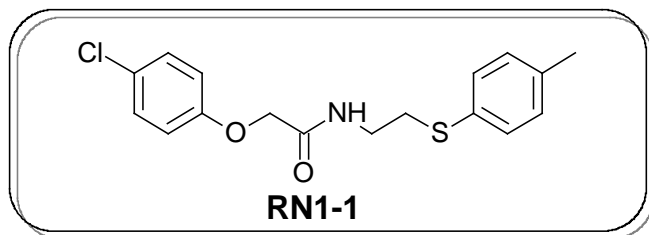
1-(4-phenylpiperazin-1-yl)-2-(2,4,5-trichlorophenoxy)ethanone (RN3-1):



Prepared by following the general procedure 2.1.1 89 %, white solid: mp 186-188 °C; $R_f = 0.53$ (3:2 *n*-heptane:EA); **IR** (KBr) ν 2923, 1642, 1432, 1306, 1221, 1034, 762 cm^{-1} ; **^1H NMR** (400 MHz, DMSO-*d*₆) δ 7.82 (s,

1H), 7.44 (s, 1H), 7.24 (t, $J = 8.0$ Hz, 2H), 6.98 (d, $J = 8.0$ Hz, 2H), 6.82 (t, $J = 8.0$ Hz, 1H), 5.14 (s, 2H), 3.60-3.58 (m, 4H), 3.22-3.20 (m, 2H), 3.18-3.14 (m, 2H); **^{13}C NMR** (100 MHz, CDCl_3) δ 165.1, 152.5, 150.9, 131.6, 131.3, 129.4, 125.6, 120.9, 124.2, 116.9, 118.3, 115.4; **HRMS** (ESI-TOF, $[\text{M} + \text{H}]^+$) calcd for $\text{C}_{18}\text{H}_{18}\text{N}_2\text{O}_2\text{Cl}_3$ 399.0434, found 399.0432.

2-(4-chlorophenoxy)-*N*-(2-(*p*-tolylthio)ethyl)acetamide (RN1-1):

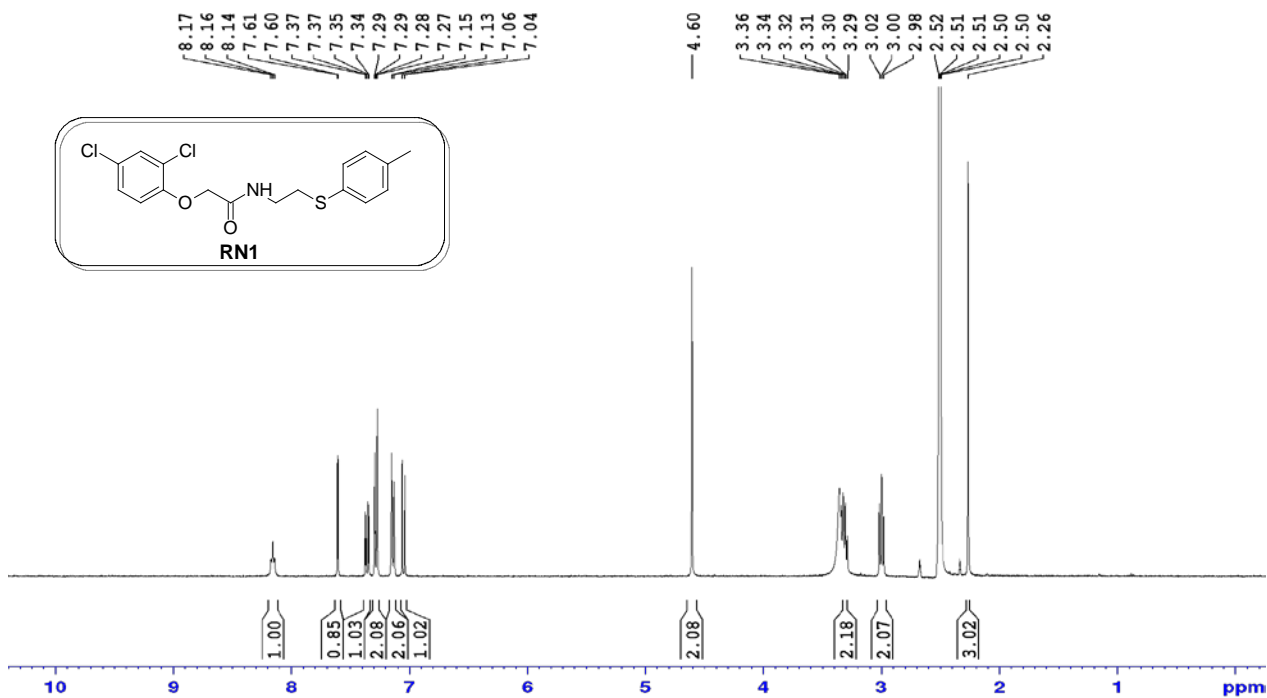


Prepared by following the general procedure. (94%), white solid: mp 101-103 °C; $R_f = 0.51$ (3:2 *n*-heptane:EA); **IR** (KBr) ν 3445, 3293, 2923, 1456, 1316, 1271, 1092, 760,

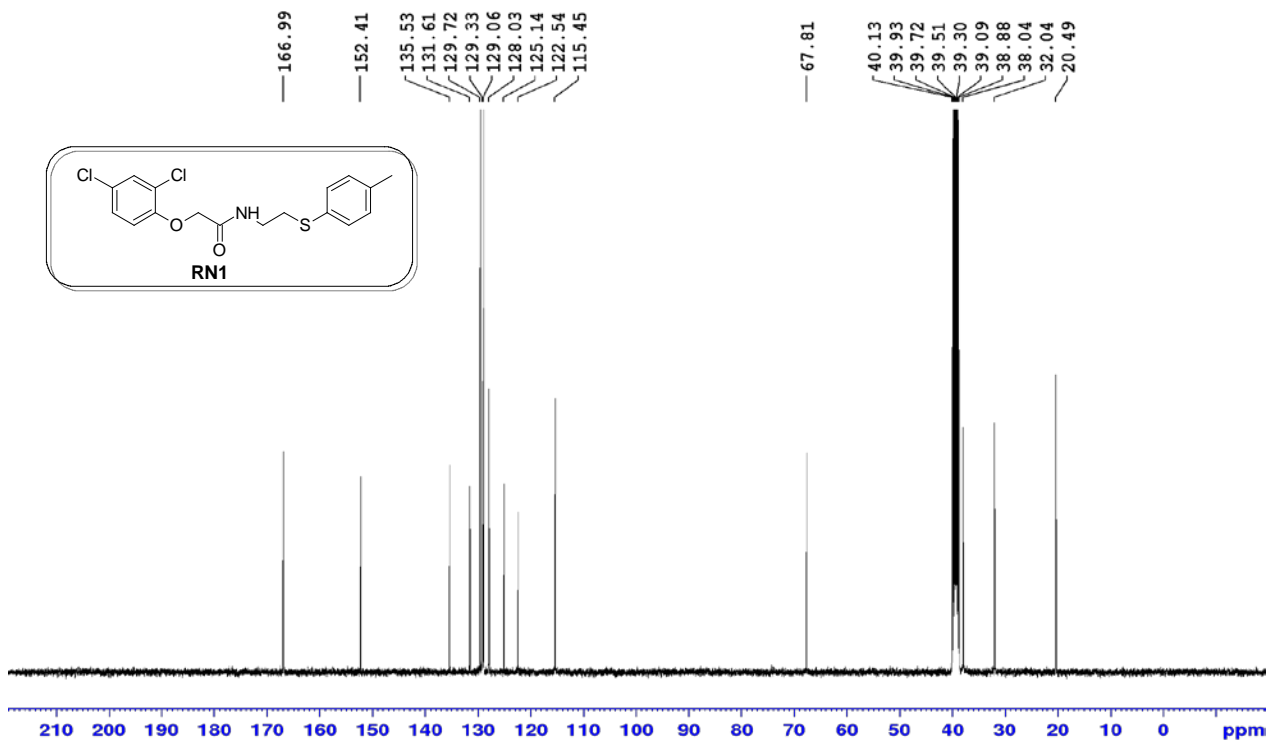
699 cm^{-1} ; **^1H NMR** (400 MHz, CDCl_3) δ 7.28-7.25 (m, 4H), 7.08 (d, $J = 8.0$ Hz, 2H), 6.88 (br s, NH, 1H), 6.85-6.82 (m, 2H), 3.53 (q, $J = 6.2$ Hz, 2H), 3.04 (t, $J = 6.2$ Hz, 2H), 2.28 (s, 3H); **^{13}C NMR** (100 MHz, CDCl_3) δ 167.9, 155.8, 137.2, 131.0, 130.9, 129.8, 127.2, 120.9, 116.1, 67.6, 38.3, 21.1; **HRMS** (ES-TOF, $[\text{M} + \text{H}]^+$) calcd for $\text{C}_{17}\text{H}_{18}\text{NO}_2\text{NaSCl}$ 358.0644, found 358.0644.

3.1. ^1H and ^{13}C NMR spectra

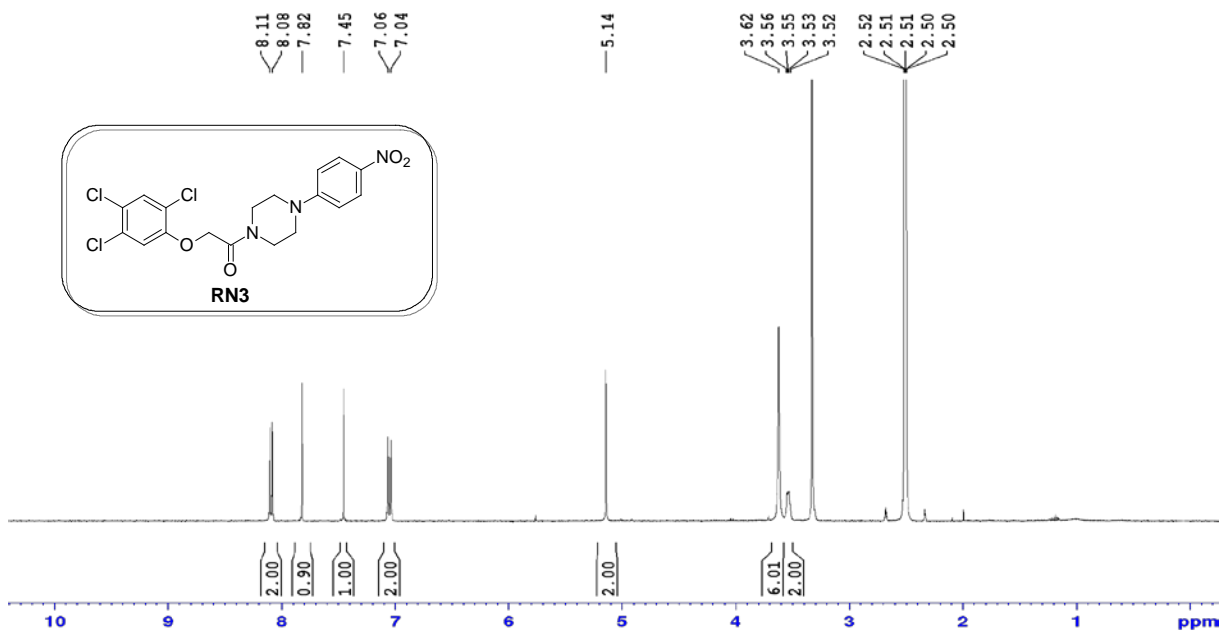
^1H NMR (400 MHz, $\text{DMSO-}d_6$) of 2-(2,4-dichlorophenoxy)-*N*-(2-(p-tolylthio)ethyl)acetamide (RN1):



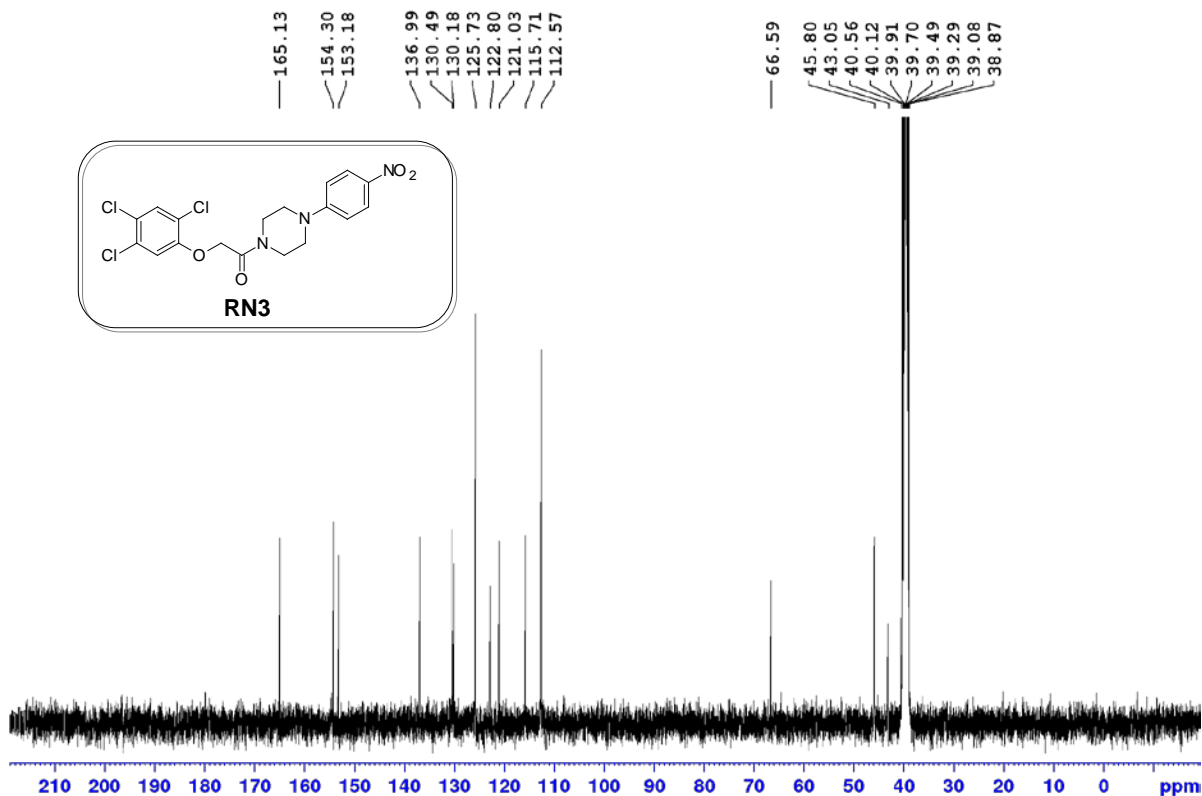
^{13}C NMR (100 MHz, $\text{DMSO-}d_6$) of 2-(2,4-dichlorophenoxy)-*N*-(2-(p-tolylthio)ethyl)acetamide (RN1):



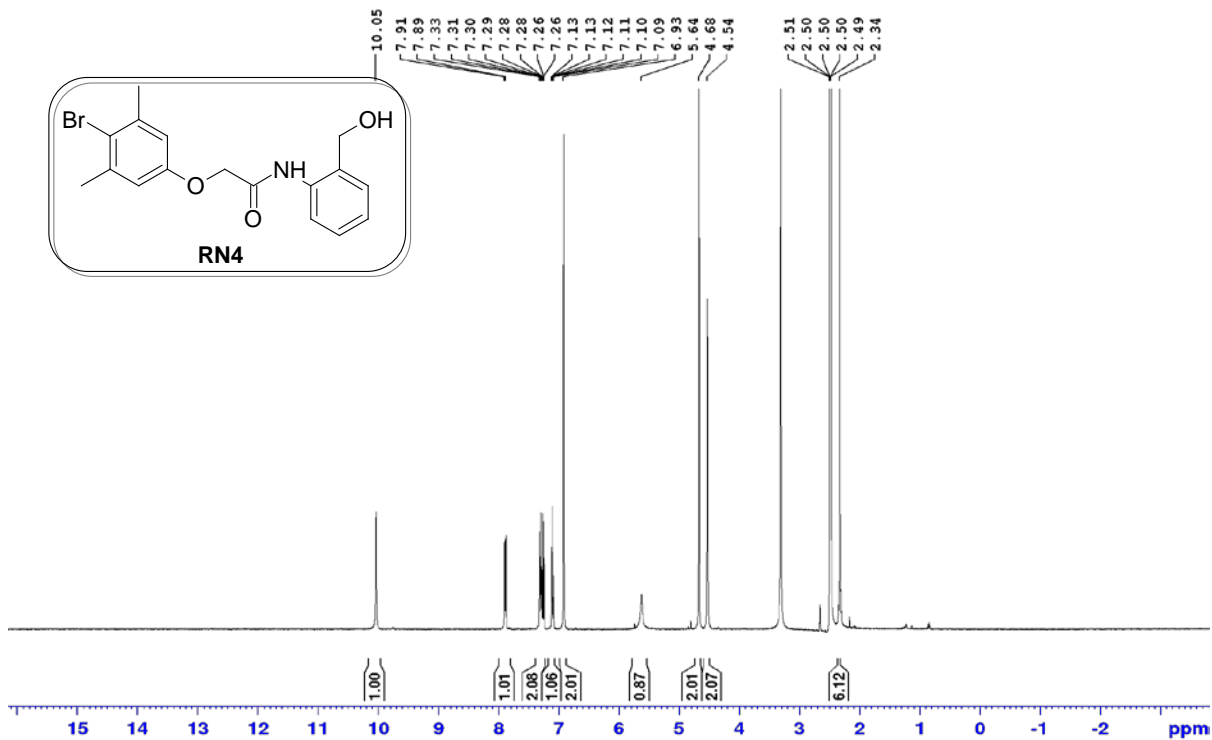
¹H NMR (400 MHz, DMSO-*d*₆) of 1-(4-(4-nitrophenyl)piperazin-1-yl)-2-(2,4,5-trichlorophenoxy)ethanone (RN3):



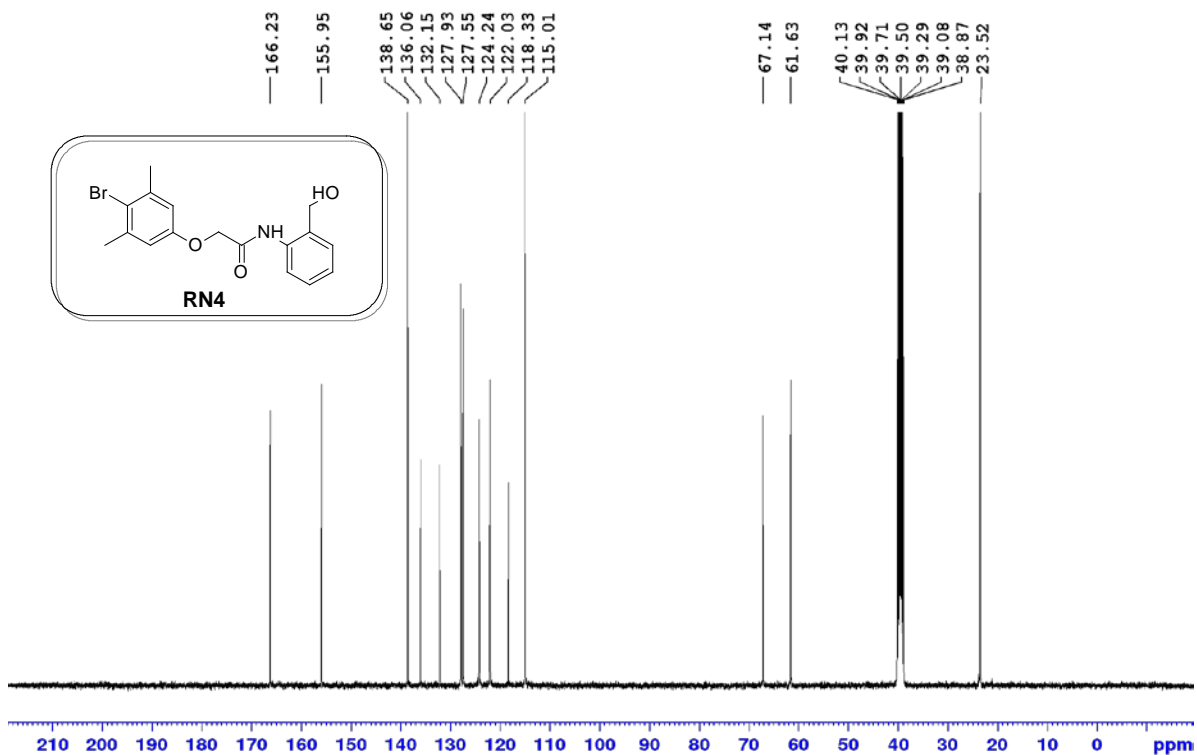
¹³C NMR (100 MHz, DMSO-*d*₆) of 1-(4-(4-nitrophenyl)piperazin-1-yl)-2-(2,4,5-trichlorophenoxy)ethanone (RN3):



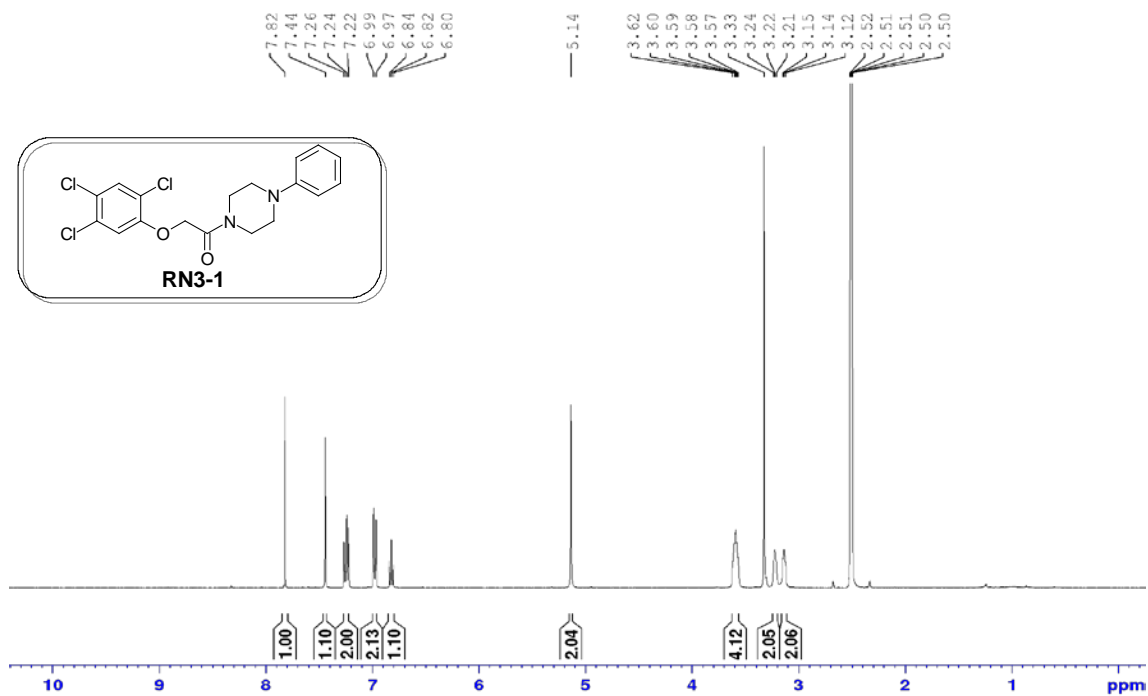
¹H NMR (400 MHz, DMSO-*d*₆) of 2-(4-bromo-3,5-dimethylphenoxy)-*N*-(2-(hydroxymethyl)phenyl)acetamide (RN4):



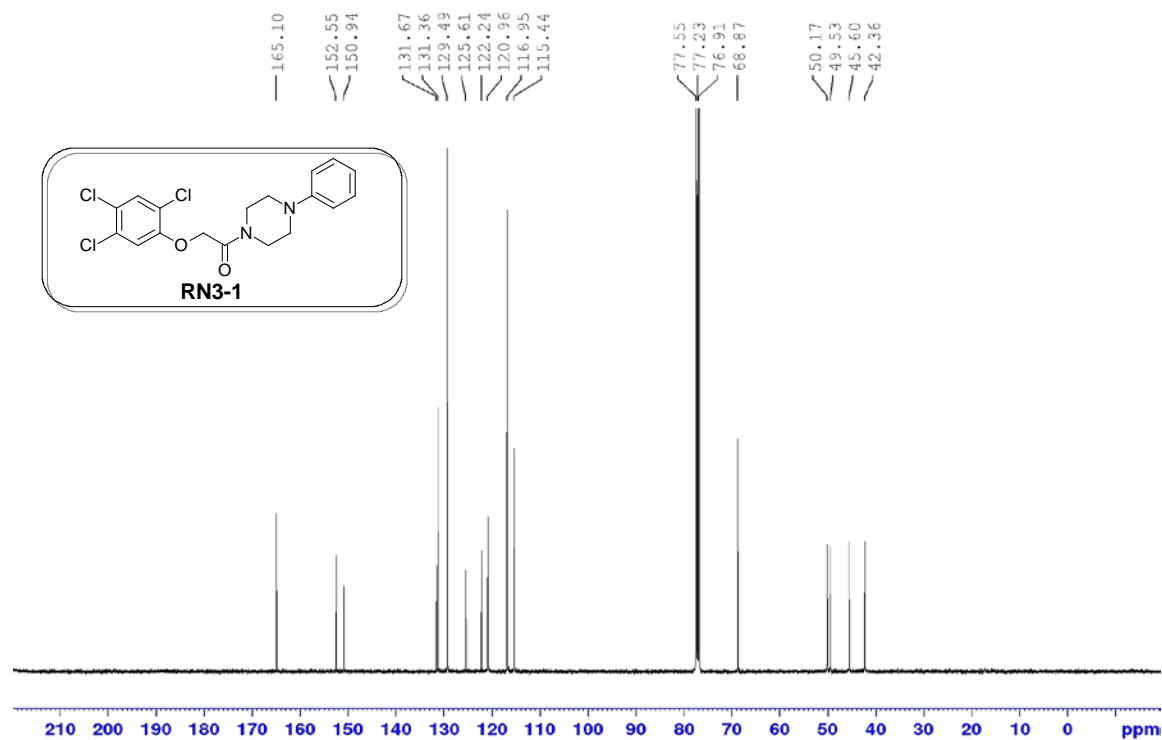
¹³C NMR (100 MHz, DMSO-*d*₆) of 2-(4-bromo-3,5-dimethylphenoxy)-*N*-(2-(hydroxymethyl)phenyl)acetamide (RN4):



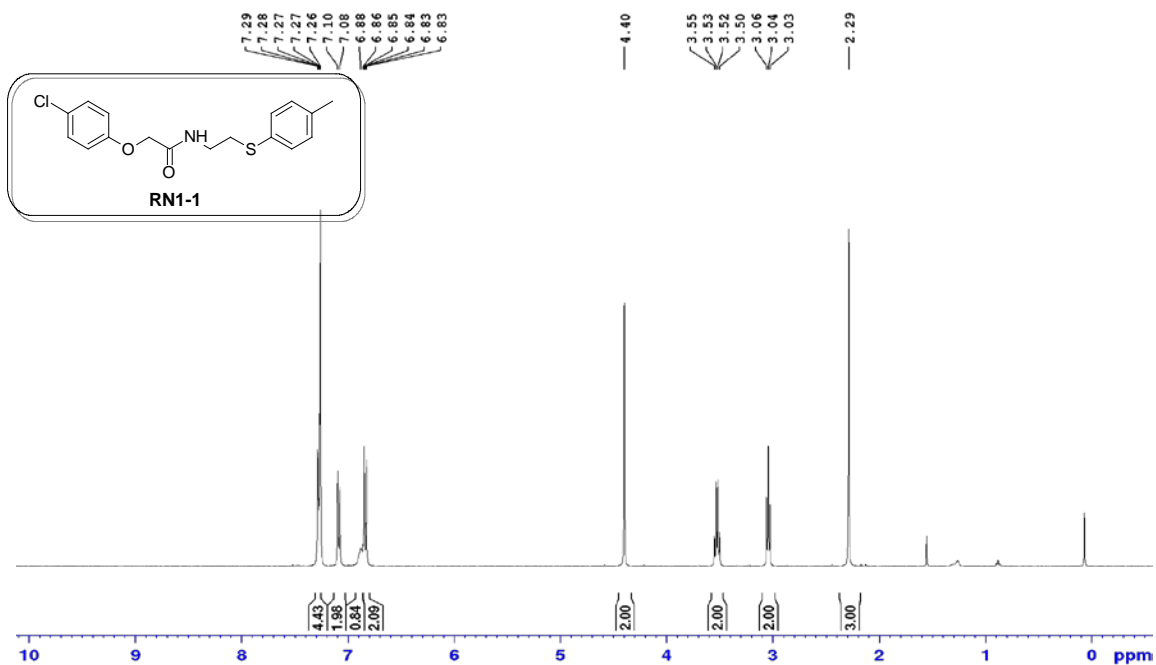
¹H NMR (400 MHz, DMSO-*d*₆) of 1-(4-phenylpiperazin-1-yl)-2-(2,4,5-trichlorophenoxy)ethanone (RN3-1):



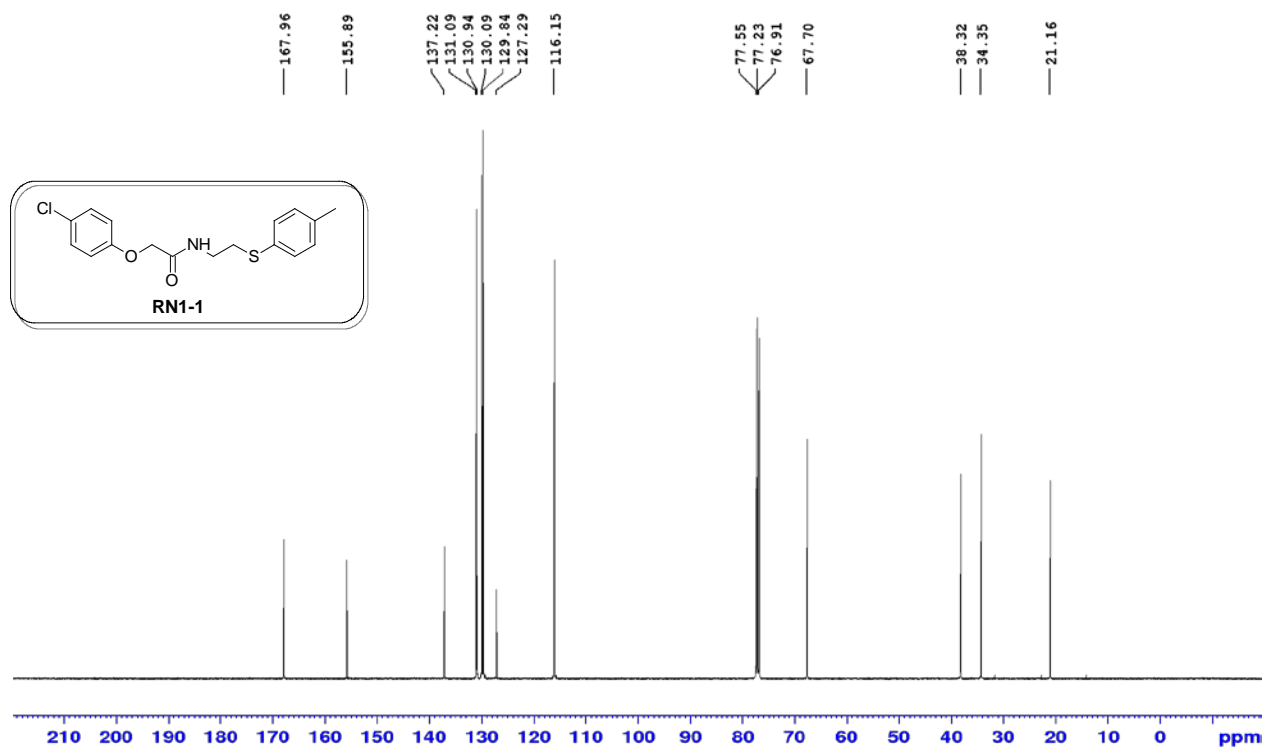
¹³C NMR (100 MHz, CDCl₃) of 1-(4-phenylpiperazin-1-yl)-2-(2,4,5-trichlorophenoxy)ethanone (RN3-1):



¹H NMR (100 MHz, CDCl₃) 2-(4-chlorophenoxy)-N-(2-(p-tolylthio)ethyl)acetamide (RN1-1):

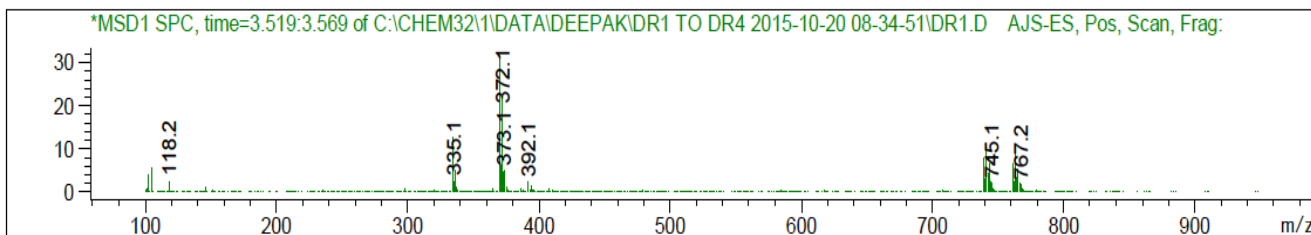
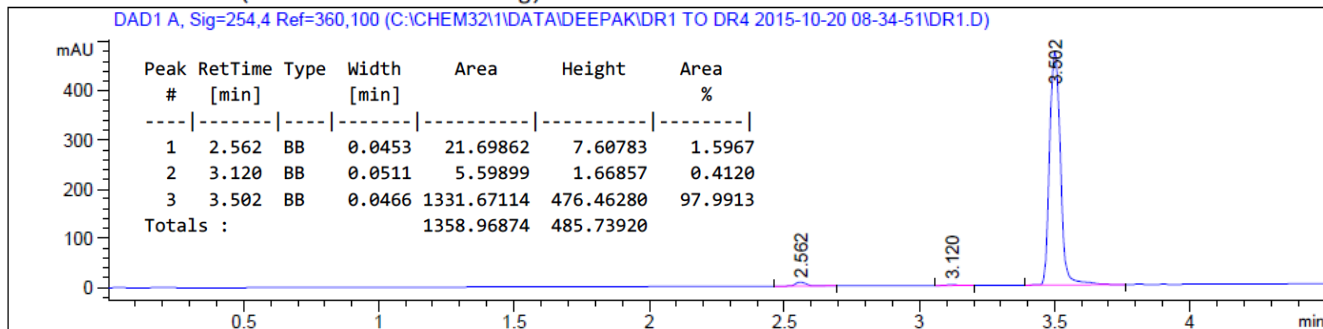


¹H NMR (100 MHz, CDCl₃) 2-(4-chlorophenoxy)-N-(2-(p-tolylthio)ethyl)acetamide (RN1-1):

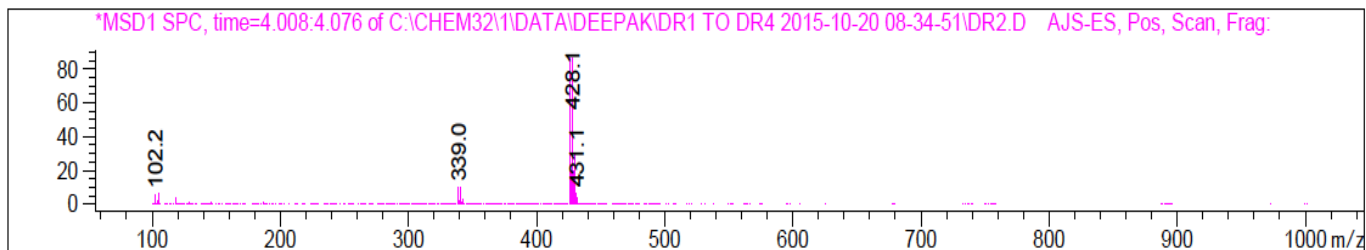
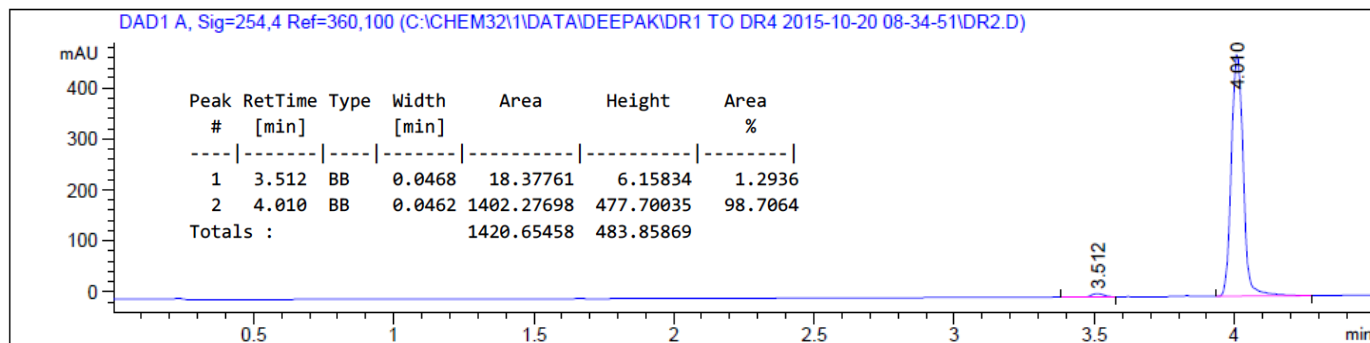


3.1. HPLC-UV-MS analysis of RN compounds

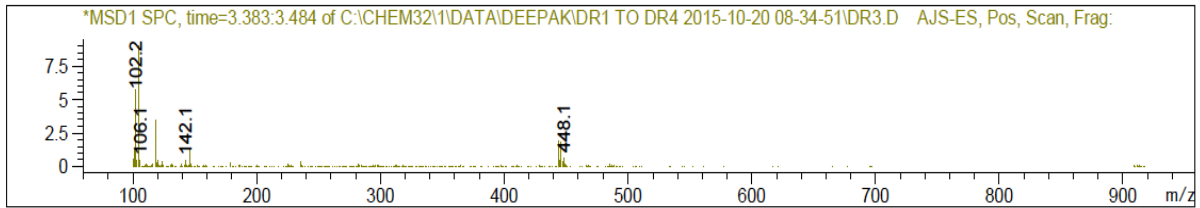
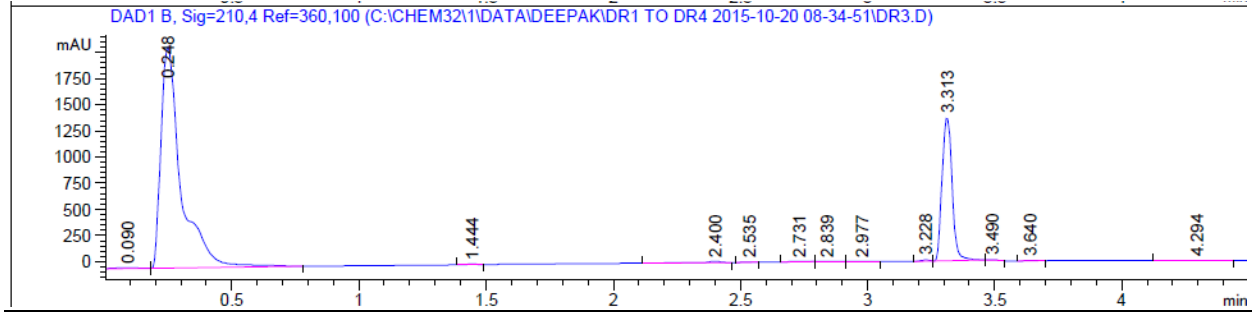
2-(2,4-dichlorophenoxy)-N-(2-(p-tolylthio)ethyl)acetamide (RN1)



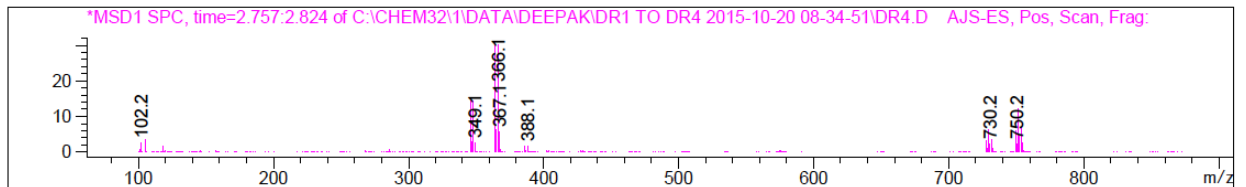
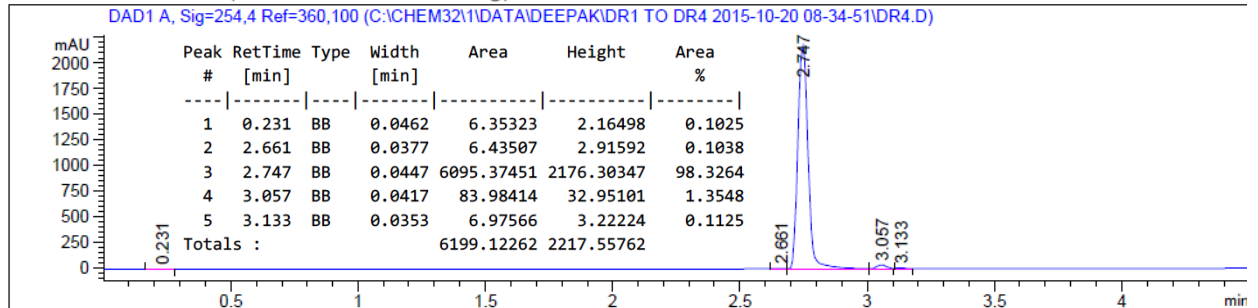
(Z)-4-(5-chloro-2-(2-(2,4-dichlorophenoxy)ethylidene)-2,3-dihydrobenzofuran-3-yl)morpholine (RN2)



1-(4-(4-nitrophenyl)piperazin-1-yl)-2-(2,4,5-trichlorophenoxy)ethanone (RN3)



2-(4-bromo-3,5-dimethylphenoxy)-N-(2-(hydroxymethyl)phenyl)acetamide (RN4)



References

1. Hotton SK, Eigenheer R A, Castro MF, Bostick M, Callis J (2011) AXR1-ECR1 and AXL1-ECR1 heterodimeric RUB-activating enzymes diverge in function in *Arabidopsis thaliana*. *Plant Mol Biol* 75(4–5):515–26.
2. Ulmasov T, Murfett J, Hagen G, Guilfoyle TJ (1997) Aux/IAA proteins repress expression of reporter genes containing natural and highly active synthetic auxin response elements. *Plant Cell* 9(11):1963–71.
3. Moon J, et al. (2007) A new CULLIN 1 mutant has altered responses to hormones and light in *Arabidopsis*. *Plant Physiol* 143(2):684–96.
4. Thomann A, et al. (2009) *Arabidopsis* CULLIN3 genes regulate primary root growth and patterning by ethylene-dependent and -independent mechanisms. *PLoS Genet* 5(1):e1000328.
5. Bernhardt A, et al. (2006) CUL4 associates with DDB1 and DET1 and its downregulation affects diverse aspects of development in *Arabidopsis thaliana*. *Plant J* 47(4):591–603.
6. Ruegger M, et al. (1998) The TIR1 protein of *Arabidopsis* functions in auxin response and is related to human SKP2 and yeast grr1p. *Genes Dev* 12(2):198–207.
7. Parry G, et al. (2009) Complex regulation of the TIR1/AFB family of auxin receptors. *Proc Natl Acad Sci U S A* 106(52):22540–5
8. Dreher KA, Brown J, Saw RE, Callis J (2006) The *Arabidopsis* Aux/IAA protein family has diversified in degradation and auxin responsiveness. *Plant Cell* 18(3):699–714.
9. Worley CK, et al. (2000) Degradation of Aux/IAA proteins is essential for normal auxin signalling. *Plant J* 21(6):553–562.
10. Tatematsu K, et al. (2004) MASSUGU2 encodes Aux/IAA19, an auxin-regulated protein that functions together with the transcriptional activator NPH4/ARF7 to regulate differential growth responses of hypocotyl and formation of lateral roots in *Arabidopsis thaliana*. *Plant Cell* 16(2):379–93.
11. Hamann T, Benkova E, Bäurle I, Kientz M, Jürgens G (2002) The *Arabidopsis* *BODENLOS* gene encodes an auxin response protein inhibiting MONOPTEROS-mediated embryo patterning. *Genes Dev* 16(13):1610–1615.
12. De Rybel B, et al. (2010) A novel aux/IAA28 signaling cascade activates GATA23-dependent specification of lateral root founder cell identity. *Curr Biol* 20(19):1697–706.
13. Brunoud G, et al. (2012) A novel sensor to map auxin response and distribution at high spatio-temporal resolution. *Nature* 482(7383):103–6.
14. Yang X, et al. (2004) The IAA1 protein is encoded by *AXR5* and is a substrate of SCF(TIR1). *Plant J* 40(5):772–82.
15. Timpte C, Wilson AK, Estelle M (1994) The *axr2-1* mutation of *Arabidopsis thaliana* is a gain-of-function mutation that disrupts an early step in auxin

- response. *Genetics* 138(4):1239–49.
16. Fukaki H, Tameda S, Masuda H, Tasaka M (2002) Lateral root formation is blocked by a gain-of-function mutation in the *SOLITARY-ROOT/IAA14* gene of *Arabidopsis*. *Plant J* 29(2):153–68.
 17. Tian Q (2002) *Arabidopsis* SHY2/IAA3 inhibits auxin-regulated gene expression. *Plant Cell* 14(2):301–319.
 18. Leyser HMO, Pickett FB, Dharmasiri S, Estelle M (1996) Mutations in the *AXR3* gene of *Arabidopsis* result in altered auxin response including ectopic expression from the SAUR-AC1 promoter. *Plant J* 10(3):403–413.
 19. Hurtado L, Farrona S, Reyes J C (2006) The putative SWI/SNF complex subunit BRAHMA activates flower homeotic genes in *Arabidopsis thaliana*. *Plant Molecular Biology* 62(1): 291-304.
 20. Tang X, Hou A, Babu M, Nguyen V, Hurtado L, Lu Q, Reyes J C, Wang A, Keller W A, Harada J J, Tsang E W (2008). The *Arabidopsis* BRAHMA chromatin-remodeling ATPase is involved in repression of seed maturation genes in leaves. *Plant Physiol* 147(3): 1143-1157.
 21. Nilsson O, et al. (1992) Spatial pattern of cauliflower mosaic virus 35S promoter-luciferase expression in transgenic hybrid aspen trees monitored by enzymatic assay and non-destructive imaging. *Transgenic Research*, 1(5):209-220.
 22. Luquez V, et al. (2007) Natural phenological variation in aspen (*Populus tremula*): the SwAsp collection. *Tree Genet Genomes* 4(2):279–292.
 23. Thelander M, et al. (2007) The moss genes PpSKI1 and PpSKI2 encode nuclear SnRK1 interacting proteins with homologues in vascular plants. *Plant Mol Biol* 64(5):559–73.
 24. Grosdidier A, Zoete V, Michielin O (2011) SwissDock, a protein-small molecule docking web service based on EADock DSS. *Nucleic Acids Res* 39(suppl_2):W270-7.
 25. Grosdidier A, Zoete V, Michielin O (2011) Fast docking using the CHARMM force field with EADock DSS. *J Comput Chem* 32(10):2149–59.
 26. Tan X, et al. (2007) Mechanism of auxin perception by the TIR1 ubiquitin ligase. *Nature* 446(7136):640–5.
 27. Grimme S (2011) Density functional theory with London dispersion corrections. *Wiley Interdiscip Rev Comput Mol Sci* 1(2):211–228.
 28. Yu H, et al. (2013) Mutations in the TIR1 auxin receptor that increase affinity for auxin/indole-3-acetic acid proteins result in auxin hypersensitivity. *Plant Physiol* 162(1):295–303.
 29. Kepinski S (2009) Pull-down assays for plant hormone research. *Methods Mol Biol* 495:61–80.
 30. Lee S, et al. (2014) Defining binding efficiency and specificity of auxins for SCF(TIR1/AFB)-Aux/IAA co-receptor complex formation. *ACS Chem Biol* 9(3):673–82.

31. Gray WM, Kepinski S, Rouse D, Leyser O, Estelle M (2001) Auxin regulates SCF(TIR1)-dependent degradation of AUX/IAA proteins. *Nature* 414(6861):271–6.
32. Gilkerson J, et al. (2009) Isolation and characterization of *cull1-7*, a recessive allele of CULLIN1 that disrupts SCF function at the C terminus of CUL1 in *Arabidopsis thaliana*. *Genetics* 181(3):945–63.
33. Fülöp K, et al. (2005) The Medicago CDKC;1-CYCLINT;1 kinase complex phosphorylates the carboxy-terminal domain of RNA polymerase II and promotes transcription. *Plant J* 42(6):810–20.
34. Lamesch P, et al. (2011) The Arabidopsis Information Resource (TAIR): improved gene annotation and new tools. *Nucleic acids research*, 40(D1):D1202-D1210.
35. Liao Y, Smyth GK, Shi W (2013) The Subread aligner: fast, accurate and scalable read mapping by seed-and-vote. *Nucleic Acids Res* 41(10):e108.
36. Liao Y, Smyth GK, Shi W (2014) featureCounts: an efficient general purpose program for assigning sequence reads to genomic features. *Bioinformatics* 30(7):923–30.
37. R Core Team (2017). R: A language and environment for statistical computing. R Foundation for Statistical Computing, Vienna, Austria. URL <http://www.R-project.org/>.
38. Huber, W., Carey, V.J., Gentleman, R., Anders, S., Carlson, M., Carvalho, B.S., Bravo, H.C., Davis, S., Gatto, L., Girke, T. and Gottardo, R., 2015. Orchestrating high-throughput genomic analysis with Bioconductor. *Nature methods*, 12(2):115.
39. Liao Y, Smyth GK, Shi W (2013) The Subread aligner: fast, accurate and scalable read mapping by seed-and-vote. *Nucleic acids research*, 41(10):e108-e108.
40. Robinson MD, McCarthy DJ, Smyth GK (2010) edgeR: a Bioconductor package for differential expression analysis of digital gene expression data. *Bioinformatics* 26(1):139–40.
41. Ritchie ME, et al. (2015) limma powers differential expression analyses for RNA-Sequencing and microarray studies. *Nucleic Acids Res* 43(7):e47.
42. Weigel D and Glazebrook J. (2006) EMS Mutagenesis of *Arabidopsis* Seed. *CSH Protoc* 2006(5): pdb-prot4621.
43. Bolger AM, Lohse M, Usadel B (2014) Trimmomatic: a flexible trimmer for Illumina sequence data. *Bioinformatics*, 30(15):2114-2120.
44. Li H (2013) Aligning sequence reads, clone sequences and assembly contigs with BWA-MEM. *arXiv preprint arXiv:1303.3997*.
45. DePristo MA, et al. (2011) A framework for variation discovery and genotyping using next-generation DNA sequencing data. *Nature genetics*, 43(5):491.
46. <http://broadinstitute.github.io/picard/>
47. Buels R, et al. (2016) JBrowse: a dynamic web platform for genome visualization and analysis. *Genome biology*, 17(1):66.

48. Cingolani P, et al (2012) A program for annotating and predicting the effects of single nucleotide polymorphisms, SnpEff: SNPs in the genome of *Drosophila melanogaster* strain w1118; iso-2; iso-3. *Fly*, 6(2):80-92.
49. Edwards K, Johnstone C, Thompson C (1991) A simple and rapid method for the preparation of plant genomic DNA for PCR analysis. *Nucleic Acids Research*, 19(6):1349.
50. Jonsson K, Boutté Y, Singh R K, Gendre D, Bhalerao R P (2017). Ethylene regulates differential growth via BIG ARF-GEF-dependent post-Golgi secretory trafficking in *Arabidopsis*. *The Plant Cell*, 29(5):1039-1052.
51. Rasband, W.S., ImageJ, U. S. National Institutes of Health, Bethesda, Maryland, USA, <https://imagej.nih.gov/ij/>, 1997-2016.
52. Linderman RJ, Binet S, Petrich SR (1999) Enhanced diastereoselectivity in the asymmetric Ugi reaction using a new “convertible” isonitrile. *The Journal of Organic Chemistry*, 64(2):336-337.

RESEARCH ARTICLE

2,4-D and IAA Amino Acid Conjugates Show Distinct Metabolism in *Arabidopsis*

Luděk Eyer¹, Thomas Vain², Barbora Pařízková³, Jana Oklestková³, Elke Barbez^{4na}, Hana Kozubíková⁵, Tomáš Pospíšil⁵, Rokšana Wierzbicka^{1ab}, Jürgen Kleine-Vehn⁴, Milan Fránek¹, Miroslav Strnad³, Stéphanie Robert^{*2}, Ondrej Novak^{3*}

1 Department of Virology, Veterinary Research Institute, Brno, Czech Republic, **2** Department of Forest Genetics and Plant Physiology, Umeå Plant Science Centre, Swedish University of Agricultural Sciences, Umeå, Sweden, **3** Laboratory of Growth Regulators, Centre of the Region Haná for Biotechnological and Agricultural Research, Institute of Experimental Botany CAS & Faculty of Science of Palacký University, Olomouc, Czech Republic, **4** Department of Applied Genetics and Cell Biology, University of Natural Resources and Life Sciences (BOKU), Vienna, Austria, **5** Department of Chemical Biology and Genetics, Centre of the Region Haná for Biotechnological and Agricultural Research, Faculty of Science of Palacký University, Olomouc, Czech Republic

^{na} Current address: Gregor Mendel Institute of Molecular Plant Biology, Austrian Academy of Sciences, Vienna Biocenter (VBC), Vienna, Austria,

^{ab} Current address: Swedish University of Agricultural Sciences, Department of Food Science, Uppsala, Sweden

* novako@ueb.cas.cz (ON); stephanie.robert@slu.se (SR)



OPEN ACCESS

Citation: Eyer L, Vain T, Pařízková B, Oklestková J, Barbez E, Kozubíková H, et al. (2016) 2,4-D and IAA Amino Acid Conjugates Show Distinct Metabolism in *Arabidopsis*. PLoS ONE 11(7): e0159269. doi:10.1371/journal.pone.0159269

Editor: Abidur Rahman, Iwate University, JAPAN

Received: April 7, 2016

Accepted: June 29, 2016

Published: July 19, 2016

Copyright: © 2016 Eyer et al. This is an open access article distributed under the terms of the [Creative Commons Attribution License](https://creativecommons.org/licenses/by/4.0/), which permits unrestricted use, distribution, and reproduction in any medium, provided the original author and source are credited.

Data Availability Statement: All relevant data are within the paper and its Supporting Information files.

Funding: This work was funded by the Czech Science Foundation (Nr. GA14-34792S; ON, JO, BP), by the Ministry of Education, Youth and Sports of the Czech Republic – NPU I program with projects LO1204 (ON, JO, HK, TP, MS) and LO1218 (LE, MF), the “Návrat” program LK21306 (ON, JO), by the Internal Grant Agency of Palacký University (Nr. IGA_PrF_2016_011; BP, HK), by Vetenskapsrådet and VINNOVA (TV, SR), IWT agency for innovation by science and technology (EB), and by the Vienna Science and Technology Fund (WWTF) Vienna Research Group program (JK-V), Austrian Science

Abstract

The herbicide 2,4-D exhibits an auxinic activity and therefore can be used as a synthetic and traceable analog to study auxin-related responses. Here we identified that not only exogenous 2,4-D but also its amide-linked metabolite 2,4-D-Glu displayed an inhibitory effect on plant growth via the TIR1/AFB auxin-mediated signaling pathway. To further investigate 2,4-D metabolite conversion, identity and activity, we have developed a novel purification procedure based on the combination of ion exchange and immuno-specific sorbents combined with a sensitive liquid chromatography-mass spectrometry method. In 2,4-D treated samples, 2,4-D-Glu and 2,4-D-Asp were detected at 100-fold lower concentrations compared to 2,4-D levels, showing that 2,4-D can be metabolized in the plant. Moreover, 2,4-D-Asp and 2,4-D-Glu were identified as reversible forms of 2,4-D homeostasis that can be converted to free 2,4-D. This work paves the way to new studies of auxin action in plant development.

Introduction

The distribution of the phytohormone auxin (indole-3-acetic acid, IAA) mediates most aspects of plant development by triggering molecular processes, which control organogenesis in response to environmental and development cues. Auxin regulation of gene expression occurs by the action of the nuclear-localized F-box proteins TRANSPORT INHIBITOR RESPONSE 1/AUXIN SIGNALING F-BOX (TIR1/AFB), which promote the degradation of the AUXIN/INDOLE-3-ACETIC ACID (Aux/IAA) transcriptional repressors in an auxin-dependent

Fund (FWF) (P26568-B16 and P26591-B16) (JK-V), and the European Research Council (ERC) Starting Grant 639478-AuxinER (JK-V).

Competing Interests: The authors have declared that no competing interests exist.

manner via the ubiquitin-proteasome system (UPS) [1]. Loss of any components of the auxin signaling pathway such as the activity of the upstream elements AUXIN-RESISTANT-1 (AXR1) and CULLIN1 (CUL1) induces resistance to exogenous auxin application [2,3].

The cellular auxin level is regulated by auxin biosynthesis in conjunction with directional auxin transport, degradation and conversion to conjugated forms [4]. The proportion of free active IAA is highly regulated and kept at an optimum level within tissues and inside the cell [5]. Beside free IAA, two alternative forms of IAA arise: the ester-linked and amide-linked IAA conjugates [6], within which IAA-Alanine (IAA-Ala), IAA-Glutamate (IAA-Glu), IAA-Leucine (IAA-Leu) and IAA-Aspartate (IAA-Asp) are the predominant forms [7]. To maintain auxin homeostasis, the abundance of supposedly inactive IAA conjugates differs inside *Arabidopsis thaliana* organs and between ecotypes and is subject to complex regulation to compensate for metabolism change imposed by *SUPERROOT1* (*SUR1*) mutation or *YUCCA1* (*YUC1*) overexpression [8]. At least seven members of the GRETCHEN HAGEN 3 (GH3) protein family have been shown to be involved in IAA conjugation to amino acids and their expression is regulated by auxin [9,10]. This mechanism is reversible and the hydrolysis of IAA conjugates to free IAA is facilitated by the IAA-LEUCINE RESISTANT 1 (ILR1)-like amidohydrolase family [11–13]. Expression patterns of GH3 and ILR1-like genes reveal they might have tissue-specific functions [14,15]. Even though a lot has been recently discovered about IAA conjugate tissue distribution [8,16], the minimal amount of evidence for their bioactivity [17] and low number of associated mutants with a phenotype [14,15,18] have been shown. Therefore their biosynthesis process and biological function remain as complex standing questions in auxin biology.

Synthetic auxins have been used extensively to study auxin-related activities, with the advantage of being more stable than endogenous auxins. Such substances include the canonical 2,4-dichlorophenoxyacetic acid (2,4-D) and other chlorine-substituted phenoxyacetic acid derivatives, which are still the most widely used herbicides for efficient control of broad-leaved weeds in cereal crops and lawns [19,20]. Commonly used, 2,4-D displays an auxinic activity including efficient stimulation of cell division and general plant growth at low concentration, while application of concentrated 2,4-D is toxic for dicot development [21]. The TIR1/AFB machinery has been shown to be the dominant signaling pathway involved in 2,4-D action, with TIR1 being the preeminent receptor within the auxin-related F-Box protein family [22].

The metabolism of 2,4-D in plants shares common features with metabolism of auxins and is based on three main mechanisms: the degradation or chemical modification of the acetic acid side chain, the hydroxylation of the aromatic ring and the conjugation of the 2,4-D molecule, mainly with amino acids and glucose [23]. Most of these molecules are believed to be catabolic products of 2,4-D detoxification metabolism that induce no auxin response and have been found in a broad range of species (wheat, potato, radish, lettuce and apple) [24,25]. In transgenic plants engineered for 2,4-D tolerance, the enzymatic degradation leads to 2,4-dichlorophenol, a less phytotoxic compound than 2,4-D [26]. 2,4-D-Glutamic acid (2,4-D-Glu) and 2,4-D-Aspartic acid (2,4-D-Asp) are two major metabolites, which represent almost 25% of all amide-linked conjugates isolated from 2,4-D treated plants [27]. Furthermore, *in vivo* metabolic conversions of 2,4-D-Glu to free 2,4-D, ring-hydroxylated metabolites and conjugates with other amino acids were observed in soybean cotyledon callus tissues [28]. Biological properties of 2,4-D conjugated with D-amino acids, including stimulation of coleoptile elongation and growth of soybean root callus, have been later reported by Davidonis *et al.* (1982) [29].

The detection and quantification of 2,4-D and its metabolites in plant tissues is still very challenging due to their low abundance. Different herbicide multiresidue screening methods using gas chromatography (GC) and liquid chromatography (LC) linked to mass spectrometry

(MS) were reported for the analysis of residual phenoxy acids in soil, water and foods of animal origin [30–32]. Koesukwiwat *et al.* (2008) [33] applied LC–MS for the analysis of phenoxy acid herbicide residues in rice based on commonly used liquid extraction/partition and dispersive solid-phase extraction (QuEChERS method). The same extraction approach was later employed in an effective simultaneous determination of five plant growth regulators in fruits [34]. To our knowledge, no specific method for isolation of 2,4-D and its metabolites using immunoaffinity chromatography (IAC) has been previously published. However, IAC is the most powerful method for purifying specific classes of growth regulators from complex plant matrices [35].

Using anti-2,4-D monoclonal antibodies (E2/G2), we describe here a novel IAC procedure for efficient isolation of 2,4-D and its conjugated metabolites. We also report the synthesis of two 2,4-D-amino acid conjugates (as synthetic auxin analogs), 2,4-D-Glu and 2,4-D-Asp, and examined their potency to affect root growth in *Arabidopsis* seedlings via the TIR1/AFB auxin-mediated signaling pathway. Further investigation using a sensitive mass spectrometry-based method reveal their activity via the quantification of the catabolic/conversion products of 2,4-D, 2,4-D-Glu and 2,4-D-Asp. These highly specific and sensitive methodologies led us to identify the rate of 2,4-D conversion and will facilitate the development of further approaches to associate plant development and the activity of conjugative enzymes.

Materials and Methods

Preparation of 2,4-D-amino acid conjugates

In order to use 2,4-D conjugates for our research, 2,4-D-Glu and 2,4-D-Asp were synthesized by two-step procedure: (a) preparation of dimethyl-2,4-dichlorophenoxyacetyl-aminodimethyl dicarboxylates using free 2,4-D acid as a starting reagent and (b) hydrolysis of the formed dimethyl-dicarboxylates (esters) to 2,4-D-Glu and 2,4-D-Asp with LiOH (S1 Table; S2 Table).

2-(2,4-dichlorophenoxy)acetic acid (1 mmol) was dissolved in dry dioxane (6.6 ml) and dry ethyl acetate (3.3 ml). Hydrochloride of glutamic/aspartic acid dimethyl ester (1 mmol) was added to the reaction mixture and the mixture was cooled in an ice bath. Then *N,N'*-dicyclohexylcarbodiimide (1 mmol) and *N*-methylmorpholine (1 mmol) were added alternately. The reaction mixture was stirred for 2 h at 0°C and then filtered and the solid material was washed with EtOAc (3x20 ml). The filtrate was washed with 4% aqueous H₃PO₄ (2x10 ml), 5% aqueous NaHCO₃ (2x10 ml) and brine (10 ml) and the organic layer was dried with sodium sulfate and filtered. The solvent was removed *in vacuo* and the residue was purified by column flash chromatography on silica (CH₃Cl:EtOAc, ratio 8:2) to afford a white solid.

Dimethyl ester (0.54 mmol) was then dissolved in tetrahydrofuran (THF; 20 ml). Lithium hydroxide monohydrate (11.5 mmol) was dissolved in water (10 ml) and then added to the reaction mixture at room temperature. After two hours, Et₂O (20 ml) was added and the organic layer was washed with saturated sodium bicarbonate (3x10 ml). Combined aqueous layers were acidified to pH 2–3 with KHSO₄ solution and extracted with dichloromethane (DCM; 3x10 ml). Combined organic layers were dried with Na₂SO₄, filtered and evaporated *in vacuo*. The remaining material was purified by column chromatography on silica, eluting with DCM:MeOH:acetic acid (5:1+1% acetic acid) to afford a white solid.

Nuclear magnetic resonance (NMR) and high resolution mass spectrometry (HRMS) of the products were used to verify the structure of 2,4-D amino conjugates (see S1 Table; S2 Table). The final product purities were 92.6% and 98.6% of 2,4-D-Glu and 2,4-D-Asp, respectively. Importantly, free 2,4-D was not detected as a possible impurity in both new synthetic auxin analogs by ultra-high performance liquid chromatography–tandem mass spectrometry (UHPLC-MS/MS) method as described below.

Plant material and growth conditions

All *Arabidopsis* mutants and transgenic lines employed in this study are in the Columbia (Col-0) background and have been described previously: *axr1-30* [36] (Hotton *et al.*, 2011), *cull1-6* and the auxin reporter line pDR5::GUS [37]. Surface-sterilized seeds were sown on solid medium (half-strength Murashige and Skoog (0.5 MS), sucrose 1%, agar 0.7%, pH 5.7) and stratified for 2 days at 4°C. Plants were grown on vertically oriented plates under a 16 h photoperiod at 21–23°C.

Chemical treatment

Nine-day-old seedlings of *Arabidopsis* were grown on medium supplemented with 2,4-D, 2,4-D-Glu and 2,4-D-Asp at the indicated final concentrations (0.05 µM and 0.5 µM). For pDR5::GUS expression experiments, five-day-old seedlings were treated for 5 hours with the indicated chemicals using a concentration of 10 µM. Stock solutions were 10 mM in 100% DMSO. For quantification measurements, treated and DMSO-treated (control) 9-day-old plants were harvested, weighed and immediately plunged into liquid nitrogen. All samples were stored at -70°C. For short-term metabolization study, seven-day-old seedlings of *Arabidopsis* ecotype Col-0 were incubated for 5 min, 30 min and 3 hours in solid media supplemented with 1 µM of IAA and 2,4-D, and 10 µM of IAA-Asp and 2,4-D-Asp. Seedlings were collected and washed extensively with water to minimize traces of the external compound. All samples were then extracted and analyzed by UHPLC-MS/MS as explained below. 2,4-D and its amino acid conjugates were also analyzed for their short- and long-term stability. Solid media were treated with compounds at the final concentrations 0.05, 0.5, 1 and 10 µM and transferred to microcentrifuge tubes. After 5 min, 30 min, 3 hours and 7 days of incubation in the growth chamber (16/8 h of light/dark, 23°C), the media (200 µl) were melted in a microwave oven, diluted by a factor of 10 and purified by the two-step purification method (see below).

Histochemical analysis, image processing and statistical analysis

Five-day-old seedlings of *Arabidopsis* expressing pDR5::GUS were fixed in 80% acetone at -20°C for 20 min and washed with 0.1 M phosphate buffer (Na₂HPO₄/NaH₂PO₄) at pH 7; 0.1% triton X100; 10 mM EDTA; 0.5 mM potassium ferrocyanide; 0.5 mM potassium ferricyanide (GUS buffer). Samples were transferred to the GUS staining solution (2 mM X-Gluc (Duchefa) in GUS buffer) for 30 min in the dark at 37°C. The staining reaction was stopped using 70% ethanol. Plants were rehydrated progressively and mounted in 50% glycerol. Samples were observed using differential interference contrast microscopy with a Zeiss Axioplan microscope.

Primary root lengths were measured on seven-day-old seedlings using ImageJ software (W. Rasband, National Institutes of Health, Bethesda, MD, <http://rsbweb.nih.gov/ij/>) and statistical analyses of data (ANOVA and Tukey's test) were performed using R software (John Chambers and colleagues, Bell laboratories).

Extraction and purification of 2,4-D metabolites

For quantification of 2,4-D and its metabolites, 15–20 mg fresh weight of treated plant tissues were extracted in 1 ml of cold sodium phosphate buffer (50 mM, pH 7.0) according to the method previously described [8]. In each extract, 100 pmol of [²H₅]-2,4-D (CDN Isotopes, Canada) and 10 pmol of [¹³C₂,¹⁵N]-2,4-D-Asp and [¹³C₂,¹⁵N]-2,4-D-Glu synthesised from [¹³C₂]-2,4-D and [¹⁵N]-Asp/[¹⁵N]-Glu as described above for non-labeled conjugates were

added as internal standards to validate the determination. The samples were purified using a mixed mode reversed phase/strong anion exchange column (Oasis[®] MAX, 1 ml/30 mg, Waters) followed by immunoaffinity chromatography (S1 Fig).

Antibody characterization and immunoaffinity column preparation

The E2/G2 antibodies were prepared previously by Fránek *et al.* (1994) [38]. The binding properties and cross reactivity of the monoclonal E2/G2 antibodies were characterized by direct ELISA format, using E2/G2 as a capture and 2,4-D-HRP conjugate as a detection reagent. Immunoaffinity chromatography columns were prepared and characterized using a modified version of a protocol described by Rolčík *et al.* (2002) [39]. Briefly, the IAG was prepared by coupling of the monoclonal antibodies (25 mg) with 1 ml of Affi-Gel 10 (Bio-Rad, USA) in 5 ml cartridges. Subsequently, the IAG was regenerated with a cycle of 3 ml portions of H₂O-MeOH-H₂O, re-conditioned by 3 ml PBS (50mM NaH₂PO₄, 15mM NaCl, pH 7.2) and finally used for sample enrichment. After methanolic elution, the samples were evaporated to dryness prior to UHPLC-MS/MS analysis. The process efficiency of the two-step isolation method was examined using crude plant extracts (15 mg fresh weight) in quadruplicates, which were spiked with known concentrations of 2,4-D (0.5, 5 and 50 pmol) and the recoveries of analyte were calculated.

UHPLC-MS/MS conditions

For quantitative analysis of 2,4-D and its metabolites/analogues, ACQUITY UPLC[®] I-Class System (Waters, USA) combined with Xevo[™] TQ-S MS (Waters, UK) were used. The samples were injected onto a reversed-phase column (Acquity UPLC[®] BEH C18, 1.7 μ m, 2.1x50 mm; temperature 40°C) and eluted with a linear gradient (0–7 min, 35–65% B; 7–8 min, 100% B; 8–10 min, 35% B) of aqueous 0.1% formic acid (A) and 0.1% formic acid in methanol (B) at a flow-rate of 0.25 ml min⁻¹. Quantification was obtained by multiple reaction monitoring (MRM) mode of precursor ion ([M-H]⁻) and the appropriate product ion. The MRM transitions and the MS settings are listed in S3 Table. The calibration curves ranging from 50 fmol to 250 pmol were constructed by serial dilutions of the authentic standards and the known concentration of the appropriate internal labeled standards. The concentrations of the 2,4-D metabolites were calculated by isotopic dilution method according to a known quantity of an internal standard added during the extraction step.

Quantification of IAA and its amide-linked conjugates

Extraction and purification of auxin metabolites were done as described previously by Novák *et al.* (2012) [8] with minor modifications. Frozen samples were homogenized using a Mixer-Mill (Retsch GmbH, Haan, Germany) and extracted in 1 ml 50 mM sodium phosphate buffer (pH 7.0) containing 1% sodium diethyldithiocarbamate, ¹³C-labeled internal standards. The samples were purified on Oasis HLB columns (30 mg, Waters Corp., Milford, USA), eluates were evaporated to dryness and dissolved in 20 μ l of mobile phase prior to mass analysis using an ACQUITY UPLC[®] I-Class System and Xevo[™] TQ-S MS.

Results

2,4-D metabolite inhibits primary root growth through an auxin-mediated signaling pathway

Initially we tested the potential bio-activity of the 2,4-D amide-linked conjugates. The physiological activities of 2,4-D, 2,4-D-Glu and 2,4-D-Asp were tested in wild-type *Arabidopsis*

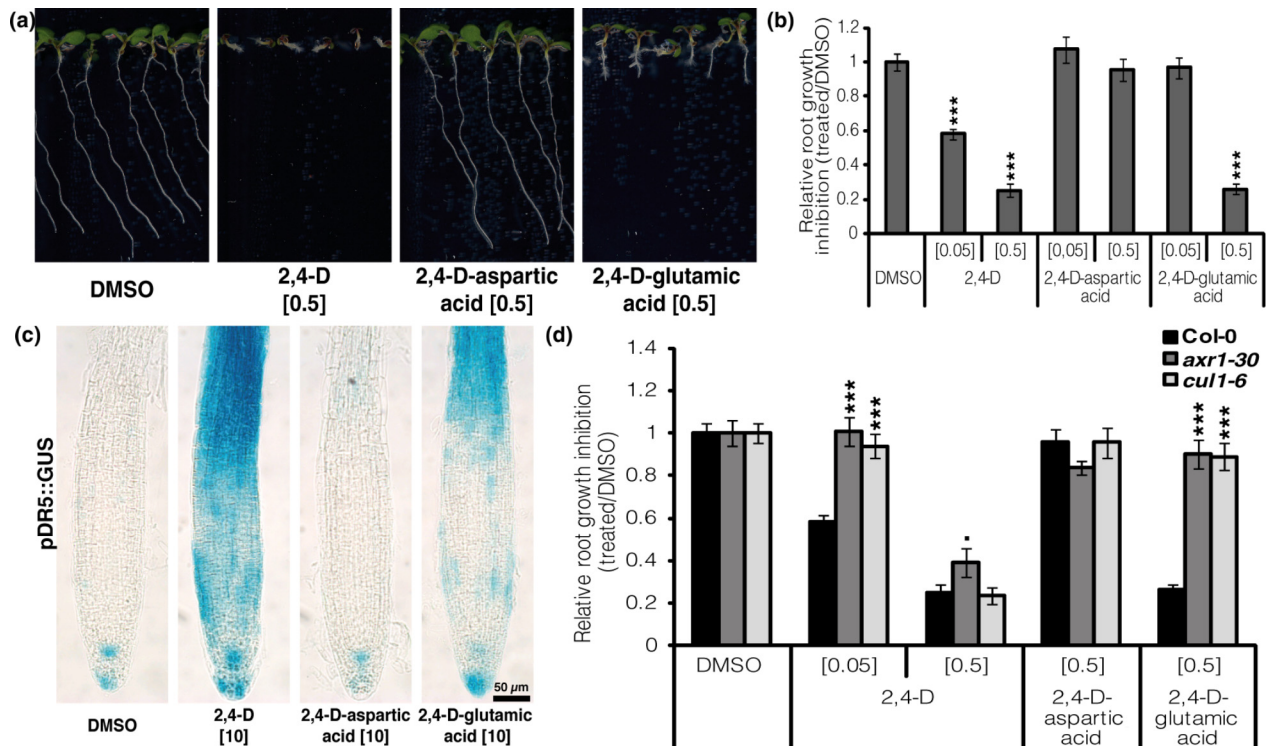


Fig 1. 2,4-D and 2,4-D metabolites act on *Arabidopsis thaliana* through auxin signaling pathway. (A) Col-0 seedlings were grown for 7 days on 2,4-D, 2,4-D-aspartic acid and 2,4-D-glutamic acid. DMSO was used as control. 2,4-D and 2,4-D-glutamic acid induced a clear reduction of primary root growth at 0.5 μM. (B) Relative root growth inhibition quantification. (C) Expression of pDR5::GUS in the primary root meristem after DMSO, 2,4-D, 2,4-D-aspartic acid and 2,4-D-glutamic acid treatments (5 day-old seedlings, 5 h treatment, 10 μM). Similarly to 2,4-D, 2,4-D-glutamic acid strongly induced the expression of pDR5::GUS in the primary root meristem. 2,4-D-aspartic acid slightly induced expression of pDR5::GUS in the elongation zone of the primary root. (D) Col-0, *axr1-30* and *cul1-6* seedlings were grown for 7 days on 2,4-D, 2,4-D-aspartic acid and 2,4-D-glutamic acid. DMSO was used as control. *axr1-30* and *cul1-6* lines showed significantly less sensitivity to the primary root growth inhibition observed in Col-0 with 2,4-D at 0.05 μM and 2,4-D-glutamic acid at 0.5 μM. In (B) and (D), values represent n>30 from three independent experiments. Statistical analysis was performed using ANOVA & comparison of means (Tukey's test) to relative root growth inhibition of DMSO (B) and Col-0 (D). No asterisks indicate p-value < 0.1; * p-value < 0.05; ** p-value < 0.01; *** p-value < 0.001.

doi:10.1371/journal.pone.0159269.g001

seedlings. The seedlings grown in the presence of 2,4-D and to a lesser extent 2,4-D-Glu, displayed dose-dependent inhibition of primary root development and induction of lateral root formation (Fig 1A and 1B). At comparable concentrations, no inhibitory effect on plant growth was observed after 2,4-D-Asp treatment. Overall, these data demonstrate that 2,4-D-Glu displays a potential activity on seedling growth but with a lower potency than 2,4-D. This activity might be directly attributed to 2,4-D-Glu or to a degradation product to free 2,4-D.

2,4-D is known to act through the TIR1/AFB auxin-mediated signaling pathway [22]. In order to understand the mode of action of 2,4-D-Glu, the activities of 2,4-D, 2,4-D-Glu, and 2,4-D-Asp were tested on mutants deficient in the auxin-mediated signaling pathway—*axr1-30* [36] and *cul1-6* [40]. In sharp contrast to the Col-0 wild-type lines, the *axr1-30* and *cul1-6* mutants displayed decreased sensitivity to 2,4-D-Glu (0.5 μM). A similar decrease in sensitivity of *axr1-30* and *cul1-6* mutants was observed in plants treated with low concentration of 2,4-D (0.05 μM). However, at high concentration of 2,4-D (0.5 μM), a strong root growth inhibition occurred equally in the wild-type and the auxin-signaling deficient mutants, suggesting that at 0.5 μM, 2,4-D exhibits a toxic activity (Fig 1D). These data support the idea that the nuclear auxin signaling machinery mediates 2,4-D action as shown before, but also show that this

machinery mediates 2,4-D-Glu derived activities as well. To further investigate the mode of action of 2,4-D-Glu, 2,4-D and both 2,4-D-amino acid conjugates were assessed for their ability to affect the expression of pDR5::GUS, a synthetic auxin-responsive marker line commonly used to image auxin response [37] (Fig 1C). Similarly to 2,4-D, the plants treated with 2,4-D-Glu showed an increased pDR5::GUS expression in the primary root tip after 5 hours. This indicates that 2,4-D-Glu is able to directly or indirectly induce an auxin response. Interestingly, even though no 2,4-D-Asp-induced phenotypes were observed in seedlings, 2,4-D-Asp slightly induced pDR5::GUS expression in the root elongation zone (Fig 1C), suggesting a very low activity.

Class-specific isolation of 2,4-D and its amino acid conjugates

In order to investigate the catabolic/conversion products of 2,4-D and 2,4-D-conjugates, we first established a method to pre-concentrate 2,4-D related compounds from plant tissues. The metabolites of nine-day-old *Arabidopsis* seedlings grown on media supplemented by the respective compounds were extracted. The extracts were subsequently enriched by a solid-phase extraction (SPE) to increase method selectivity (S1 Fig) and immunoaffinity purification to selectively capture trace amounts of 2,4-D and its metabolites from complex plant matrices using the monoclonal antibodies E2/G2 [38]. The IAC is a powerful isolation tool to reduce large proportions of potentially interfering substances and also to increase the sensitivity of the subsequent LC-MS/MS analysis, since interferences by the sample matrix can be reduced, resulting in an increased signal-to-noise ratios. According to the cross-reactivity study, the E2/G2 antibodies preferably recognized compounds with the 2,4-dichlorophenoxyacetic moiety (S4 Table). Moreover, the capacity of the immunoaffinity gel (IAG) is an important parameter, which is defined as the maximum amount of the analyte that can be pre-concentrated by a given volume of immunosorbent [41]. Thus, to test our column capacities, 2,4-D standards ranging from 1 pmol to 1 nmol were applied to 0.5 ml of the gel and the recovery was determined by UHPLC-MS/MS. The IAG capacity was estimated to be around 200 pmol ml⁻¹. Up to this concentration of 2,4-D recovery was still higher than 50% (S2 Fig). Beyond this limit, the immunoextraction recovery declined rapidly. Therefore, the yields of 2,4-D metabolites and selected structural analogs were also tested in a wide concentration range from 1 to 300 pmol (Table 1; S4 Table). The results showed good affinity of the E2/G2 antibodies to specifically bind the 2,4-D-amino acid conjugates and to a lesser extent some structural analogs (2,4-dichlorophenoxybutyric acid, 2-methyl-4-dichlorophenoxybutyric acid and 2,4,5-trichlorophenoxyacetic acid). After SPE and class-specific IAC employing the monoclonal E2/G2 antibodies, the total recoveries for 2,4-D, 2,4-D-Glu and 2,4-D-Asp were 66 ± 17%, 28 ± 8% and

Table 1. E2/G2 monoclonal antibodies and immunoaffinity gel characteristics.

Compound	CR (%)	Recovery (%)					
		1 pmol	5 pmol	10 pmol	50 pmol	100 pmol	300 pmol
2,4-D	100.0	91.5 ± 7.9	75.3 ± 4.3	69.4 ± 4.9	59.2 ± 2.3	47.6 ± 7.9	32.6 ± 5.8
2,4-D-Asp	46.4	48.3 ± 9.6	14.7 ± 2.4	9.3 ± 1.4	7.2 ± 0.2	1.6 ± 0.3	0.8 ± 0.1
2,4-D-Glu	60.0	36.1 ± 6.6	31.8 ± 0.6	19.9 ± 1.5	18.0 ± 1.4	6.8 ± 1.2	4.9 ± 0.1

Percentage of cross reactivity (CR) was calculated using the equation: CR(%) = IC50(2,4-D)/IC50(cross reactant) × 100, where IC50 is the concentration of a competitor (cross reactant) resulting in 50% reduction of alkaline phosphatase conjugate binding in direct ELISA system. Mixtures of 2,4-D structural analogs with concentrations ranging from 1 to 300 pmol were applied onto 0.5 ml of IAG, each spiking level was then determined by UHPLC-MS/MS, compared with the concentration of appropriate standard solution and the recoveries were calculated (values are means ± SD, n = 3).

doi:10.1371/journal.pone.0159269.t001

$16 \pm 6\%$ ($n = 12$), respectively (S5 Table). This result indicates that the method is appropriate for the routine isolation of 2,4-D and its conjugates from plant tissue.

2,4-D metabolite profiling by UHPLC-MS/MS

The newly developed two-step purification procedure has been linked to ultra-high performance liquid chromatography–tandem mass spectrometry (UHPLC-MS/MS). During the MS-based analysis, a mixture of eight 2,4-D metabolites/analogs could be baseline separated over 7.0 min (as shown in S3 Fig). The chromatographic stability was tested in detail by 10 consecutive measurements (S3 Table) and coefficients of variation for the retention times were found to range between 0.08% and 0.30% relative standard deviation (RSD), showing high levels of consistency during the chromatographic separations. 2,4-D and its amino acid conjugates were detected in negative-ion, multi reaction monitoring (MRM) mode with a strong signal from the deprotonated molecule $[M-H]^-$ and high-intensity fragment of 2,4-dichlorophenoxy moiety (m/z 161) (Fig 2). Furthermore, we have used rapid switching between two modes of operation, MRM and product ion confirmation spectrum (PICS) modes for a simultaneous quantification and a structural confirmation by sensitive MS/MS full scan [42]. After optimizing the MS/MS conditions, correlation coefficients between 0.9985 and 0.9995 were calculated in the linear dynamic ranges from the lower limits of detection close to 20 fmol using repeated injection of all investigated 2,4-D metabolites (S3 Table).

We also validated both parts of the analytical method together (purification and quantification) using a spiking experiment of crude plant extracts (15 mg fresh weight of *Arabidopsis* seedlings). The precision and accuracy of the whole procedure is shown in S5 Table. For 0.5 pmol (low), 5 pmol (medium) and 50 pmol (high) concentrations of 2,4-D metabolites, the mean precision was 6.0% RSD (in the range 1.4%–10.6%), and the mean accuracy was 5.9% bias (in the range -3.6% to 18.3%). Overall, these results confirm that our new method is a powerful, precise and accurate tool for the target profiling of 2,4-D metabolites.

In vivo metabolism of 2,4-D and its amino acid conjugates

Having established a specific immunoaffinity-based and sensitive MS-based approach, we studied the 2,4-D metabolism *in vivo*. The extracts purified using a SPE column (Oasis[®] MAX, 1 ml/30 mg, Waters) followed by immunoaffinity chromatography were injected onto a reverse-phase chromatographic column for quantification of the 2,4-D-amino acid conjugates and confirmation of their presence in the plant tissues grown on media supplemented with 2,4-D and 2,4-D-conjugates (Fig 2). In 2,4-D treated seedlings, 2,4-D-Glu and 2,4-D-Asp were detected at 100-fold lower concentrations in comparison with 2,4-D levels (Table 2), confirming the high metabolic stability of 2,4-D. This also clearly demonstrates the relationship between 2,4-D uptake and formation of amide-linked conjugates in *Arabidopsis* seedlings (Fig 3A).

Next we treated 9-day-old seedlings with 2,4-D amino acid conjugates and detected free 2,4-D levels (Table 2). This observation is in good agreement with previous studies [27,28] showing that metabolism of 2,4-D-conjugates results in conversion into the free 2,4-D molecule. This hydrolysis did not occur in the growth media by itself, indicating that it depends on inherent enzymatic activity (S4 Fig). Interestingly, a higher proportion of 2,4-D was observed in the 2,4-D-Glu-treated samples (more than 70% converted as shown in Fig 3C), compared to samples treated with 2,4-D-Asp (only about 35%, Fig 3B), suggesting that both amide-linked conjugate forms are degraded with different metabolic rates and/or catabolic pathways. Alternatively, the cellular uptake of the compounds may differ, because exogenous application of 2,4-D-Glu led to higher compound accumulation in plant tissues as compared to 2,4-D-Asp.

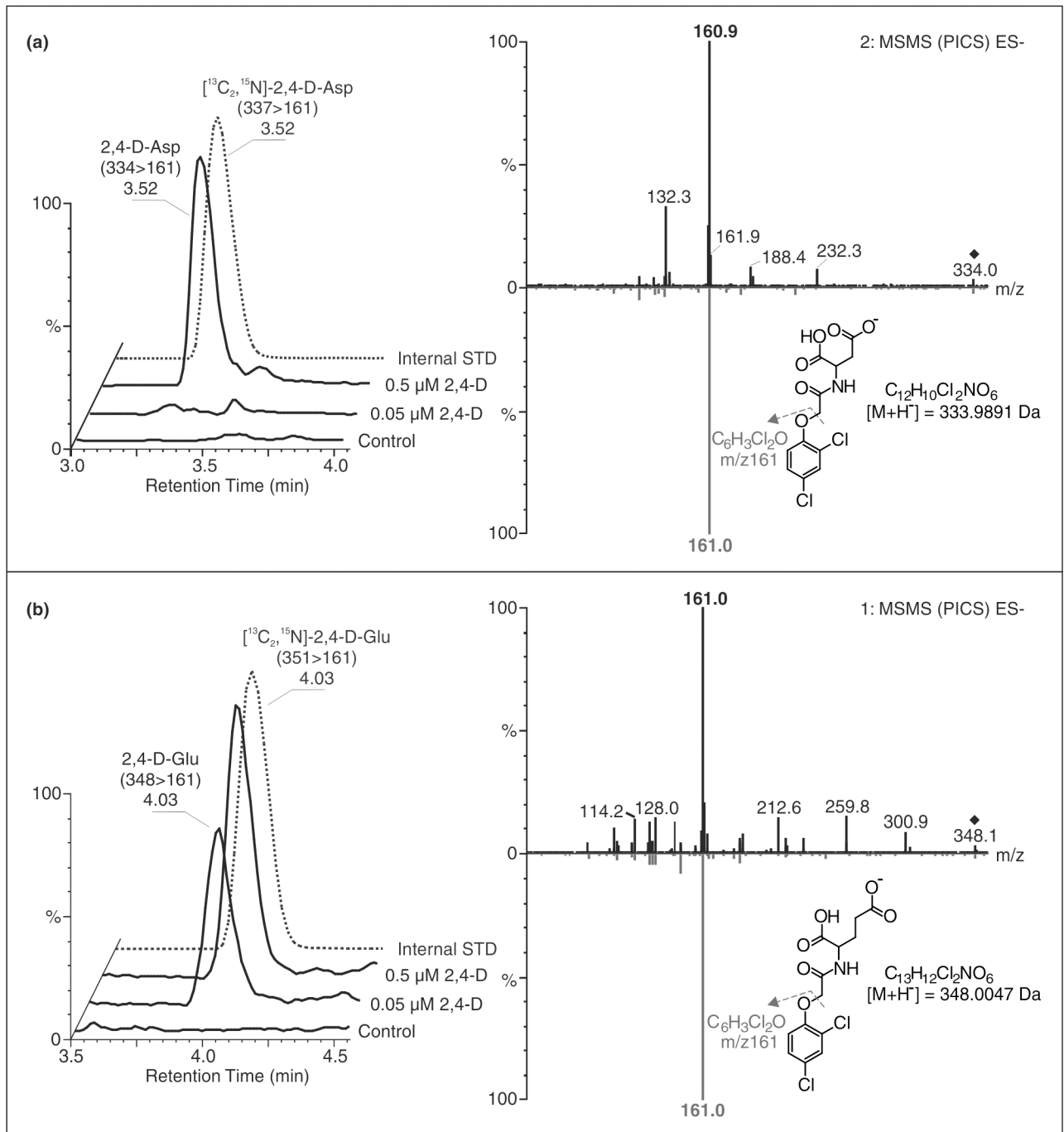


Fig 2. Confirmation of presence of 2,4-D-amino acid conjugates in *Arabidopsis* plant tissues treated with 2,4-D. Left: MRM chromatograms of 2,4-D-Asp (A) and 2,4-D-Glu (B) show their identification in extracts of treated (0.05 μ M and 0.5 μ M of 2,4-D) and untreated (control) plants based on retention time and co-elution with appropriate internal standards (STD, grey color). Right: Product Ion Confirmation Spectra (PICS) of endogenous 2,4-D-Asp (a) and 2,4-D-Glu (b) (black color) in comparison with the standards synthesized (grey color) validates the presence of 2,4-D-amino acid conjugates in plant tissue samples purified by IAC.

doi:10.1371/journal.pone.0159269.g002

Remarkably, the hydrolysis efficiency was independent of the initial concentration of 2,4-D-amino acid conjugates supplemented in the growth medium (Fig 3B and 3C), showing approximately the same proportion of 2,4-D in concentration ranges of 0.05 μ M and 0.5 μ M. Notably,

Table 2. Levels of 2,4-D and its metabolites in 1 g of extracted *Arabidopsis* tissue.

	2,4-D	2,4-D-Asp	2,4-D-Glu
		0.05 μ M	
2,4-D	761 \pm 208	40 \pm 10	133 \pm 31
2,4-D-Asp	n.d.	77 \pm 10	n.d.
2,4-D-Glu	8 \pm 1	n.d.	35 \pm 12
		0.5 μ M	
2,4-D	3258 \pm 85	519 \pm 97	1295 \pm 296
2,4-D-Asp	24 \pm 5	858 \pm 156	19 \pm 1
2,4-D-Glu	59 \pm 3	5 \pm 2	504 \pm 113

The concentration for all metabolites is in pmol g⁻¹ FW. For 0.05 μ M treatment, the amount of 2,4-D-Asp was not detected (n.d.). Samples were analyzed in four independent biological replicates, and error bars represent the SD.

doi:10.1371/journal.pone.0159269.t002

2,4-D-Glu was determined as the minor metabolite in the plant tissues previously treated with high concentration of 2,4-D-Asp (0.5 μ M), indicating that formed 2,4-D is rapidly secondarily metabolized. Similarly, minor amounts of 2,4-D-Asp were detected in plants treated with 0.5 μ M 2,4-D-Glu. These findings arguably favor the possibility that the divergent auxin-like

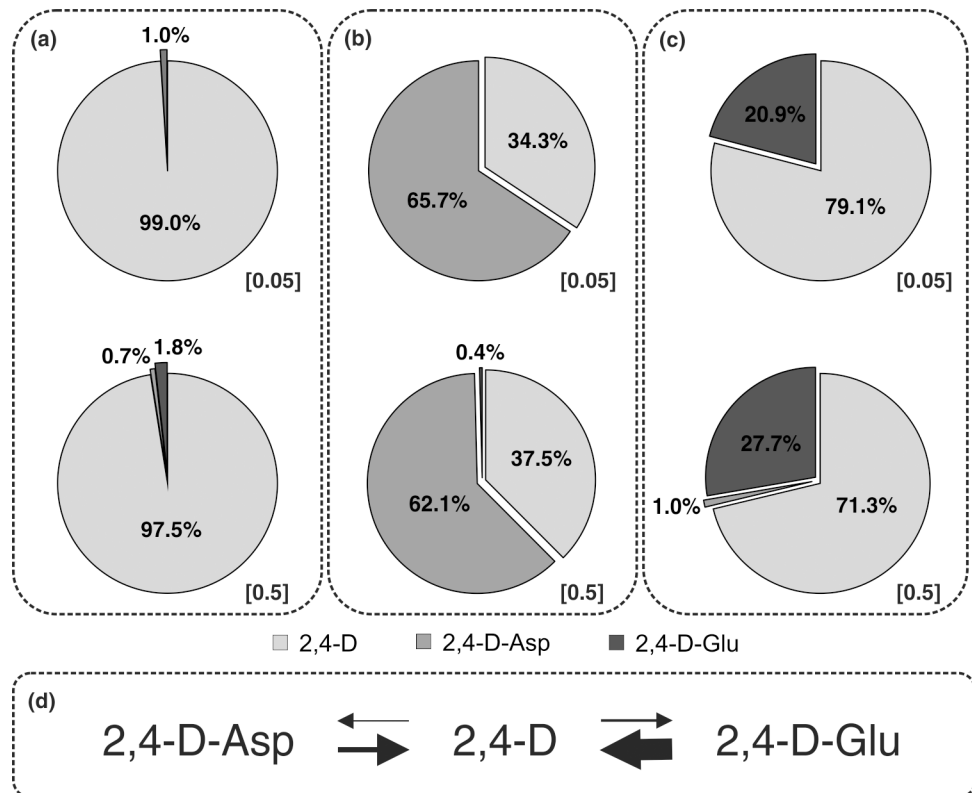


Fig 3. Distribution (%) of 2,4-D and its metabolites in *Arabidopsis* seedlings. Plant tissues were grown on media supplemented with two concentrations (0.05 μ M and 0.5 μ M) of 2,4-D (A), 2,4-D-Asp (B) and 2,4-D-Glu (C), and metabolite distribution in each treatment was calculated from the levels (pmol g⁻¹ FW) detected by UHPLC-MS/MS. In (D), 2,4-D homeostasis and different biosynthetic rates from/to free 2,4-D are indicated (the line thickness illustrates a predicted conversion rate of 2,4-D and its amino acid conjugates).

doi:10.1371/journal.pone.0159269.g003

activities of both 2,4-D amide-linked conjugates are mediated by different cellular uptake and metabolic conversion to free 2,4-D (Fig 3D).

Endogenous and synthetic auxin conjugates show distinct metabolism

Our data reveals that 2,4-D-Asp and 2,4-D-Glu show expressive hydrolysis to 2,4-D, affecting plant growth and development. This is an unexpected finding, because endogenous conjugation of IAA to IAA-Glu and IAA-Asp has been suggested to be non-reversible (reviewed in Ludwig-Mueller, 2011). Accordingly, exogenous application of IAA-Asp does not itself affect plant development [43]. To compare metabolism of synthetic and endogenous IAA conjugates we applied the endogenous compounds IAA and IAA-Asp as well as synthetic 2,4-D and 2,4-D-Asp for 5, 30 and 180 minutes (Fig 4). The initial accumulation of IAA and 2,4-D in plant tissues was comparable during the first 30 minutes. However, while IAA concentration saturated, the 2,4-D accumulation further increased (Fig 4D). IAA saturation correlated with increased abundance in its amide-linked conjugates, such as IAA-Asp and IAA-Glu (Fig 4A), suggesting that auxin conjugation evokes the distinct accumulation rates of IAA and 2,4-D exceeding 30 minutes.

Next we investigated tissue accumulation and metabolism of IAA-Asp and 2,4-D-Asp. In contrast to IAA and 2,4-D, we detected a similar accumulation of both IAA-Asp and 2,4-D-Asp in plant tissues (Fig 4B and 4E). Compared to IAA-Asp, the uptake of 2,4-D-Asp was higher in plant tissues. IAA-Asp treated samples showed only slightly increased endogenous levels of IAA as compared to the control treated samples (Fig 4B). However, 2,4-D-Asp treated samples showed much higher conversion to 2,4-D (Fig 4E), suggesting that not only the metabolism rates of 2,4-D and IAA, but also 2,4-D-Asp and IAA-Asp are distinct. Whereas 2,4-D appears more stable compared to IAA, we propose that 2,4-D amino acid conjugates, such as 2,4-D-Asp, is less stable *in vivo* than IAA-Asp. To confirm our findings, we have tested the short-term stability of 2,4-D and its amino acid conjugates in light and/or in the medium without *Arabidopsis* seedlings (S5 Fig). These results showed no significant change in the exogenous levels of conjugated 2,4-D in 5–180 min after treatment. Accordingly, 2,4-D amide-linked conjugates could be used as a vehicle to intracellularly release 2,4-D.

Our data indicates that amino acid conjugation to synthetic auxins could lead to distinct metabolic turnover as compared to endogenous compounds. This insight could be used to engineer sophisticated auxin compounds to dissect metabolic processes in planta and to establish novel classes of possibly selective herbicides getting released only intracellularly.

Discussion

In plant hormone research, application of synthetic auxin such as 2,4-D has already unraveled the activity of endogenous IAA in specific developmental events [44]. By a multidisciplinary approach combining organic synthesis, chemical biology and quantitative analysis, we deepened the understanding of 2,4-D mode of action and propose a new method using synthetic analogs to monitor auxin action linked to auxin metabolism.

Having established an effective procedure, we first profiled *in vivo* conversion of 2,4-D into conjugated metabolites (Table 2). In plant callus tissues treated with radioactive 2,4-D, amide-linked conjugates have been previously reported as major identified metabolites [45]. 2,4-D, often used for its high metabolic stability, showed under our incubation conditions conjugation with aspartic and glutamic acids—both metabolites were present in very low concentration of only 1–2% of all 2,4-D metabolite contents (Fig 3A), confirming a previous report where they represented only 3% of the conjugated pool throughout the whole *Arabidopsis* plant [46]. The distribution of 2,4-D-amino acid conjugates is also in agreement with previously reported

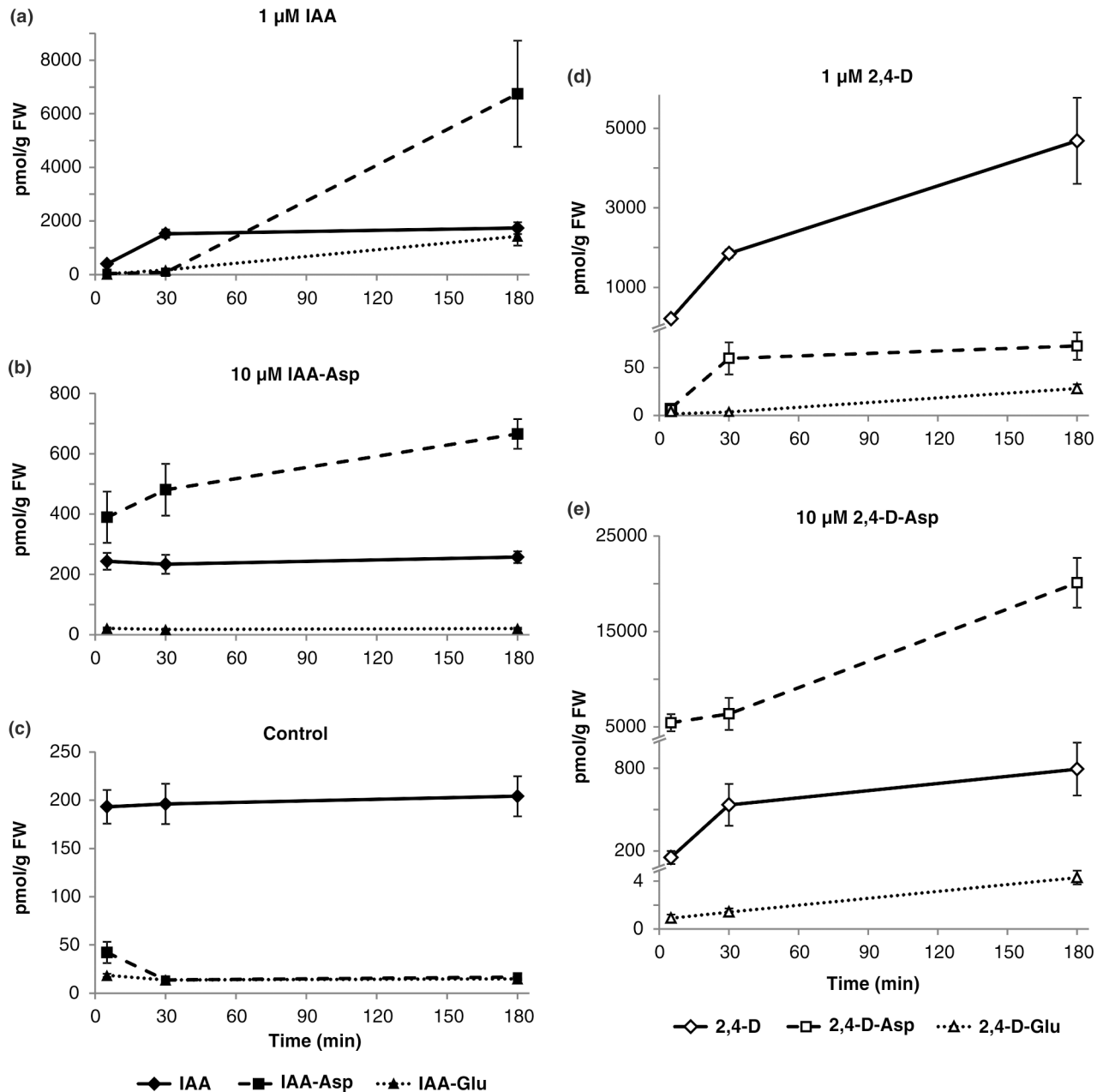


Fig 4. Short-term metabolization of IAA, 2,4-D and their conjugates with aspartate in *Arabidopsis*. Extracts from seven-day-old Col-0 seedlings pre-incubated for 5 min, 30 min and 3 hours with the indicated compounds (A, 1 μ M of IAA; B, 10 μ M of IAA-Asp; D, 1 μ M of 2,4-D; E, 10 μ M of 2,4-D-Asp) were analyzed by UHPLC-MS/MS and compared with an endogenous auxin levels in the control untreated seedlings (C). The concentration for all metabolites is in pmol g^{-1} FW. Samples were analyzed in four independent biological replicates, and error bars represent the SD.

doi:10.1371/journal.pone.0159269.g004

results for treated corn plants (*Zea mays* L.) in which sugar conjugation of 2,4-D was predominant [23]. Interestingly, this result shows the link to auxin metabolism, describing ester-linked sugars as the major conjugate form of IAA in maize kernels [47]. Similarly, in pedicel explants of tobacco, another synthetic auxin, 1-naphthaleneacetic acid (1-NAA), was transformed firstly to a glucose ester and secondly to aspartic acid amide (NAA-Asp) [48]. As a consequence, we propose that 2,4-D homeostasis is controlled by a constant synthesis and breakdown of its

derivatives. Our data further indicate that amide-linked 2,4-D conjugates could be formed and/or accumulated with different biosynthetic rates. Indeed, compared to quantitative measurements of IAA-Asp and IAA-Glu in wild-type *Arabidopsis* lines [8,49], we found the opposite ratio of 2,4-D-Glu to 2,4-D-Asp levels (Table 2). IAA conjugates are generally postulated as being intermediate substrates for the IAA transport machinery, or as IAA storage forms, or as a protection from enzymatic destruction leading to the homeostatic control of IAA [50]. Conversely, in *Arabidopsis*, the most abundant amide-linked IAA conjugates, IAA-Asp and IAA-Glu, are not measurably hydrolyzed to free IAA and are thought to most likely be intermediates in IAA catabolism [6]. It is therefore very difficult to monitor the IAA conjugation/deconjugation ratio *in vivo*. The production and quantification of traceable synthetic auxin and/or auxin conjugates will undoubtedly pave the way to a better understanding of auxin metabolism *in vivo* and could lead to precise *in vivo* characterization of conjugating enzyme activities.

Secondly, to investigate the activity of 2,4-D metabolites, we have successfully synthesized 2,4-D conjugated with L-glutamic and L-aspartic acid (S1 Table, S2 Table). By conducting a chemical biology approach we could show that treatment with 2,4-D conjugates induced a growth phenotype in *Arabidopsis* seedlings, dependent on the SCF hormone signaling pathway (Fig 1). The increase of auxin-responsive reporter expression after 5 hours suggests a fast uptake of the chemical by the plant. Notably, the 2,4-D conjugated with aspartic acid is less potent than 2,4-D-Glu and they are both less active than 2,4-D itself. In previous studies, 2,4-D showed a growth stimulation effect at the optimum concentration of 10^{-6} M, while twenty synthetic amide-linked 2,4-D conjugates also displayed the ability to enhance elongation of *Avena* coleoptile sections but at higher concentrations (10^{-5} – 10^{-6} M) [29,51]. In *Arabidopsis*, seven gene members of the auxin-inducible GH3 family of amido synthetases are able to catalyze the synthesis of IAA amide conjugates [17,52]. As summarized in Westfall *et al.* (2010) [53], most IAA-specific GH3 proteins conjugate IAA to Asp and/or Glu. Similarly in grapevine, modelling of 1-NAA into the active site of GH3-1 suggests that 1-NAA is likely to be a poor substrate for this enzyme [54]. As our data suggest a low conjugation rate of 2,4-D into 2,4-D-Asp and 2,4-D-Glu, it would be relevant to test the capacity of 2,4-D to be a good substrate for the GH3 protein family and compare it to the data already collected for IAA and 1-NAA. Overall, these data offer two possibilities with regard to conjugate activity: (i) the amino acid conjugates of 2,4-D could be the physiologically active forms (as postulated in 51), (ii) only 2,4-D is the active molecule, if it could be formed as a product of the metabolism of the amide-linked 2,4-D conjugates. However, one should not forget to consider the possibility of different uptake capacity relative to the molecule [55].

To further understand the physiological effects of 2,4-D metabolites, we have applied novel analytical approaches to isolate and profile the catabolic/conversion products (S1 Fig). As the concentrations of synthetic auxin metabolites investigated in plant tissues are usually extremely low (pmol.g^{-1} fresh weight), their determination required sample clean-up steps prior to analyte detection. Therefore, the combination of ion-exchange and class-specific sorbents was used for sample enrichment. The Oasis[®] MAX sorbent based on both reverse-phase and anion-exchange has excellent preconditions to separate acidic analytes from neutral compounds [56]. Using previously prepared and characterized E2/G2 monoclonal antibodies [38] (Table 1), we describe here the procedure for efficient sample extraction and purification of 2,4-D and its conjugated metabolites (S1 Fig). All validation parameters (S4 Table; S5 Table), the IAG capacity and the process efficiency, were consistent with phytohormonal IAC-based methods published recently [39,57,58]. We have developed and optimized MS-based method for multiplex confirmation and quantification of 2,4-D metabolites (Fig 2). The MS detection using MRM and PICS modes amplifies the accuracy and precision of trace component analysis

in a complex plant matrix. In agreement with our findings (S3 Table; S5 Table), the overall sensitivity of our analytical method enables analysis of 2,4-D and its amino acid conjugates from minute amounts of plant tissue. Moreover, we have shown the immunoaffinity chromatography gel to be highly specific for 2,4-D, certain 2,4-D metabolites, and other structurally related compounds, making it highly useful for purifying 2,4-D analogs in complex sample extracts (S4 Table). Our approach provides very efficient confirmatory tools that can discriminate auxinic herbicides at ultra-trace levels for reliable and sensitive detection to help ensure food safety.

In auxin metabolism, conjugation is generally considered to be either a reversible or irreversible process of degradation leading to attenuation of auxin activity. Previous studies in soybean cotyledon callus tissue demonstrated that 2,4-D-Glu converts to free 2,4-D and other conjugates [27,29]. Our MS-based data show that 2,4-D-Asp is also hydrolyzed to free 2,4-D as well as glutamic acid conjugate (Fig 3B and 3C). Interestingly, in *Arabidopsis* plants treated with the amino acid conjugates, the level of free 2,4-D was found to be 1.7-fold higher and 3.2-fold lower compared to the concentration of 2,4-D-Glu and 2,4-D-Asp, respectively (Table 2). Based on these results, we conclude that the accumulation of free 2,4-D is connected with the divergent auxin-like activities of both amino acid conjugates. 2,4-D glutamic acid, similarly to 2,4-D, inhibits primary root growth and also acts through an auxin-mediated signaling pathway. Altogether, our quantitative data suggest that 2,4-D-Glu is strongly hydrolyzed to free 2,4-D (<70% of all 2,4-D metabolite levels; Fig 3C) and physiological activity is formed as a product of the amide conjugate metabolism. On the other hand, the lower concentrations of free 2,4-D (>40% of total content; Fig 3B) in the seedlings grown on media supplemented 2,4-D-Asp correspond with no reduction of primary root length and very low activity in the auxin response. These data are consistent with the finding by early studies of auxin metabolism that 1-NAA conjugated with aspartic acid is hydrolyzed very slowly and does not affect the growth of tobacco crown-gall tissues [59]. Furthermore, 1-NAA-Asp acts as an auxin only after hydrolysis to 1-NAA [60]. LeClere *et al.* (2002)[61] tested the ability of IAA-amino acid conjugates to inhibit *Arabidopsis* seedling root growth and compared the *in vitro* enzymatic activity of four *Arabidopsis* IAA-amino acid hydrolases (ILR1, IAR3, ILL1 and ILL2). In accordance with our findings, the aspartic acid conjugate was inactive in root inhibition bioassays and very slightly cleaved by ILR1 and ILL2. However, compared to IAA-Asp, IAA-Glu showed a two-fold increase in substrate specificity of *Arabidopsis* amidohydrolases and a slight activity on root elongation inhibition [61]. According to our finding, we suggest that 2,4-D-Glu is also efficiently hydrolyzed *in vivo* by the amidohydrolases. Taken together, our data strongly indicate that 2,4-D-Asp and 2,4-D-Glu are reversible forms of 2,4-D homeostasis that can be converted to free 2,4-D with different biosynthetic rates (Fig 3D).

Overall, our results demonstrate that 2,4-D is conjugated *in vivo* and that 2,4-D conjugates can be hydrolyzed back to the active form of 2,4-D. Furthermore, free 2,4-D is active on the TIR1/AFB-mediated auxin signaling pathway and not its conjugated forms. As 2,4-D is a poor substrate for ABP1, a discussed potential auxin receptor [62,63], TIR1/AFB and the related auxin signaling pathway have been shown to be the primary signaling machinery targeted by 2,4-D. Moreover and based on structural evidences, 2,4-D-Asp or 2,4-D-Glu would not be able bind to the TIR1-Aux/IAA co-receptor complex. This study paves the way to allow for new experiments linking the nuclear auxin signaling pathway and the regulation of auxin conjugation by the use of traceable synthetic auxin. The hereby technology established to synthesize and quantify *in vivo* 2,4-D forms will lead the way to novel technologies such as the production of 2,4-D-labeled molecules and *in vivo* detection, which would be a specific read-out of TIR1/AFB signaling processes. Expressing inducible amidohydrolases or conjugation enzymes could modulate the cellular 2,4-D amount in a tissue or in a time-controlled manner. This is of

fundamental importance to better understand the auxin effect on plant architecture and also from a more applied point of view. For example, some commercially valuable plants could be genetically manipulated to increase their GH3 level and thus acquire a resistance to the herbicide effect of 2,4-D. Overall, the 2,4-D and 2,4-D metabolites represent fantastic tools for biotechnology approaches.

Supporting Information

S1 Fig. Scheme of a two-step purification protocol for isolation of 2,4-D and its metabolites/structural analogues.

(PDF)

S2 Fig. Capacity of the immunoaffinity gel (IAG) with immobilized E2/G2 antibodies.

(PDF)

S3 Fig. Chromatographic separation of 2,4-D and its metabolites/structural analogs by UHPLC-(ESI-)-MS/MS.

(PDF)

S4 Fig. One-week stability of 2,4-D-amino acid conjugates in growth media.

(PDF)

S5 Fig. Stability of 2,4-D, 2,4-D-Asp and 2,4-D-Glu in short-term chemical treatment.

(PDF)

S1 Table. Preparation scheme and structural characteristics of 2,4-D-Asp.

(PDF)

S2 Table. Preparation scheme and structural characteristics of 2,4-D-Glu.

(PDF)

S3 Table. Optimized UHPLC-(ESI-)-MS/MS parameters.

(PDF)

S4 Table. Characterization of monoclonal E2/G2 antibodies and immunoaffinity gel by 2,4-D structural analogues.

(PDF)

S5 Table. Process efficiency and method validation for the two-step purification procedure.

(PDF)

Acknowledgments

We thank Karin Ljung and Karel Doležal for critical reading of the manuscript and Siamsa M. Doyle for careful revision of the manuscript.

Author Contributions

Conceived and designed the experiments: JKV MF MS SR ON. Performed the experiments: LE TV BP JO EB HK TP RW. Analyzed the data: TV BP JO EB JKV SR ON. Contributed reagents/materials/analysis tools: LE HK TP RW. Wrote the paper: LE TV JO EB JKV SR ON.

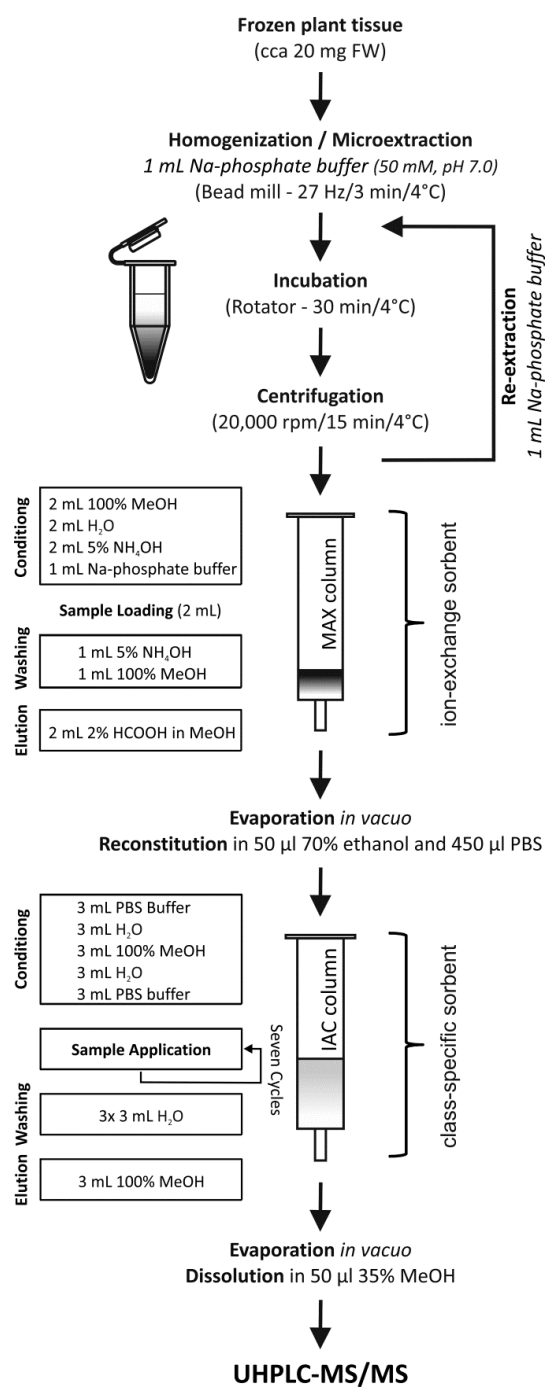
References

1. Santner A, Estelle M. The ubiquitin-proteasome system regulates plant hormone signaling. *Plant J.* 2010; 61: 1029–1104. doi: [10.1111/j.1365-3113X.2010.04112.x](https://doi.org/10.1111/j.1365-3113X.2010.04112.x) PMID: [20409276](https://pubmed.ncbi.nlm.nih.gov/20409276/)

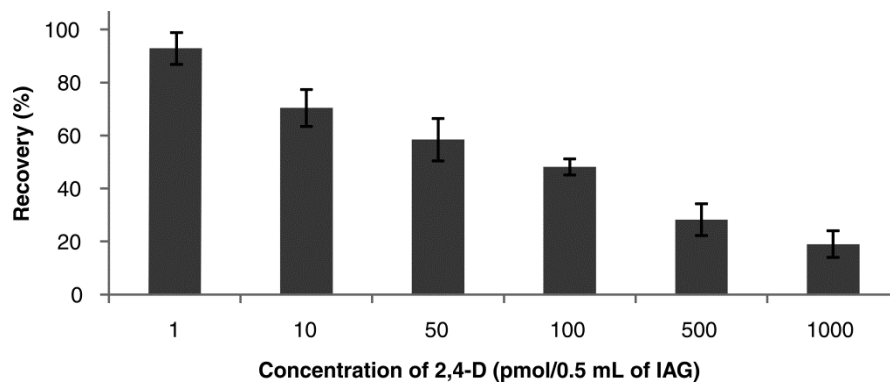
2. Leyser HMO, Lincoln CA, Timpte C, Lammer D, Turner J, Estelle M. Arabidopsis auxin-resistance gene-AXR1 encodes a protein related to ubiquitin-activating enzyme E1. *Nature* 1993; 364: 161–164. PMID: [8321287](#)
3. Hellmann H, Hobbie L, Chapman A, Dharmasiri S, Dharmasiri del Pozo CD, et al. *Arabidopsis* AXR6 encodes CUL1 implicating SCF E3 ligases in auxin regulation of embryogenesis. *EMBO J.* 2003; 22: 3314–3325. PMID: [12839993](#)
4. Sauer M, Robert S, Kleine-Vehn J. Auxin: simply complicated. *J Exp Bot.* 2013; 64: 2565–2577. doi: [10.1093/jxb/ert139](#) PMID: [23669571](#)
5. Petersson SV, Johansson AI, Kowalczyk M, Makoveychuk A, Wang JY, Moritz T, et al. An auxin gradient and maximum in the Arabidopsis root apex shown by high-resolution cell-specific analysis of IAA distribution and synthesis. *Plant Cell* 2009; 21: 1659–1668. doi: [10.1105/tpc.109.066480](#) PMID: [19491238](#)
6. Korasick DA, Enders TA, Strader LC. Auxin biosynthesis and storage forms. *J Exp Bot.* 2013; 64: 2541–2555. doi: [10.1093/jxb/ert080](#) PMID: [23580748](#)
7. Kowalczyk M, Sandberg G. Quantitative analysis of indole-3-acetic acid metabolites in Arabidopsis. *Plant Physiol.* 2001; 127: 1845–1853. PMID: [11743128](#)
8. Novák O, Hényková E, Sairanen I, Kowalczyk M, Pospíšil T, Ljung K. Tissue specific profiling of the *Arabidopsis thaliana* auxin metabolome. *Plant J.* 2012; 72: 523–536. doi: [10.1111/j.1365-313X.2012.05085.x](#) PMID: [22725617](#)
9. Hagen G, Guilfoyle TJ. Rapid induction of selective transcription by auxins. *Mol Cell Biol.* 1985; 5: 1197–1203. PMID: [4041007](#)
10. Staswick PE, Serban B, Rowe M, Tiryaki I, Maldonado MT, Maldonado MC, et al. Characterization of an Arabidopsis enzyme family that conjugates amino acids to indole-3-acetic acid. *Plant Cell* 2005; 17: 616–627. PMID: [15659623](#)
11. Bartel B, Fink GR. ILR1, an amidohydrolase that releases active indole-3-acetic acid from conjugates. *Science* 1995; 23: 1745–1748.
12. Davies RT, Goetz DH, Lasswell J, Anderson MN, Bartel B. IAR3 encodes an auxin conjugate hydrolase from Arabidopsis. *Plant Cell* 1999; 11: 365–376. PMID: [10072397](#)
13. Rampey RA, LeClere S, Kowalczyk M, Ljung K, Sandberg G, Bartel B. A family of auxin-conjugate hydrolases that contributes to free indole-3-acetic acid levels during Arabidopsis germination. *Plant Physiol.* 2004; 135: 978–988. PMID: [15155875](#)
14. Rampey RA, Woodward AW, Hobbs BN, Tierney MP, Lahner B, Salt DE, et al. An Arabidopsis basic helix-loop-helix leucine zipper protein modulates metal homeostasis and auxin conjugate responsiveness. *Genetics* 2006; 174: 1841–1857. PMID: [17028341](#)
15. Takase T, Nakazawa M, Ishikawa A, Kawashima M, Ichikawa T, Takahashi N, et al. *ydk1-D*, an auxin-responsive *GH3* mutant that is involved in hypocotyl and root elongation. *Plant J.* 2004; 37: 471–483. PMID: [14756757](#)
16. Ljung K. Auxin metabolism and homeostasis during plant development. *Development* 2013; 140: 943–950. doi: [10.1242/dev.086363](#) PMID: [23404103](#)
17. Staswick PE. The tryptophan conjugates of jasmonic and indole-3-acetic acids are endogenous auxin inhibitors. *Plant Physiol.* 2009; 150: 1310–1321.
18. Nakazawa M, Yabe N, Ichikawa T, Yamamoto YY, Yoshizumi T, Hasunuma K, et al. *DFL1*, an auxin-responsive *GH3* gene homologue, negatively regulates shoot cell elongation and lateral root formation, and positively regulates the light response of hypocotyl length. *Plant J.* 2001; 25: 213–221. PMID: [11169197](#)
19. Mithila J, Hall JCH, Johnson WG, Kelley KB, Riechers DE. Evolution of resistance to auxinic herbicides: historical perspectives, mechanisms of resistance, and implications for broadleaf weed management in agronomic crops. *Weed Sci.* 2011; 59: 445–457.
20. Grossmann K. Auxin herbicides, current status of mechanism and mode of action. *Pest Manag Sci.* 2010; 66: 113–120. doi: [10.1002/ps.1860](#) PMID: [19823992](#)
21. Sterling TM, Hall JC. Mechanism of action of natural auxins and the auxinic herbicides. In: Roe RM, Burton JD, Kuhr RJ, editors. *Herbicide Activity: Toxicology, Biochemistry and Molecular Biology.* Amsterdam: IOS Press; 1997. pp. 111–141.
22. Parry G, Calderon-Villalobos LI, Prigge M, Peret B, Dharmasiri S, Itoh H, et al. Complex regulation of the TIR1/AFB family of auxin receptors. *Proc Natl Acad Sci U S A.* 2009; 106: 22540–22545. doi: [10.1073/pnas.0911967106](#) PMID: [20018756](#)
23. Feung CS, Loerch SL, Hamilton RH, Mumma RO. Comparative metabolic fate of 2,4-dichlorophenoxyacetic acid in plants and plant tissue culture. *J Agric Food Chem.* 1978; 26: 1064–1067.

24. Loos MA. Phenoxyalkanoic Acids. In: Kearney PC, Kaufman DD, editors. *Herbicides: Chemistry, Degradation, and Mode of Action*. New York: Dekker; 1975. pp. 1–128.
25. Hamburg A, Puvanesarajah V, Burnett TJ, Barnekow DE, Premkumar ND, Smith GA. Comparative degradation of [¹⁴C]-2,4-dichlorophenoxyacetic acid in wheat and potato after Foliar application and in wheat, radish, lettuce, and apple after soil application. *J Agric Food Chem*. 2001; 49: 146–155. PMID: [11170570](#)
26. Laurent F, Debrauwer L, Rathahao E, Scalla R. 2,4-Dichlorophenoxyacetic acid metabolism in transgenic tolerant cotton (*Gossypium hirsutum*). *J Agric Food Chem*. 2000; 48: 5307–5311. PMID: [11087477](#)
27. Feung CS, Hamilto RH, Mumma RO. Metabolism of 2,4-Dichlorophenoxyacetic acid. V. Identification of metabolites in soybean callus tissue cultures. *J Agric Food Chem*. 1973; 21: 637–640. PMID: [4736996](#)
28. Davidonis GH, Hamilton RH, Mumma RO. Metabolism of 2,4-Dichlorophenoxyacetic Acid (2,4-D) in soybean root callus. *Plant Physiol*. 1980; 66: 537–540. PMID: [16661472](#)
29. Davidonis GH, Hamilton RH, Vallejo RP, Buly R, Mumma RO. Biological properties of d-amino acid conjugates of 2,4-D. *Plant Physiol*. 1982; 70: 357–360. PMID: [16662495](#)
30. Santos-Delgado MJ, Crespo-Corral E, Polo-Díez LM. Determination of herbicides in soil samples by gas chromatography: optimization by the simplex method. *Talanta* 2000; 53: 367–377. PMID: [18968122](#)
31. Rodríguez I, Rubí E, González R, Quintana JB, Cela R. On-fibre silylation following solid-phase micro-extraction for the determination of acidic herbicides in water samples by gas chromatography. *Anal Chim Acta* 2005; 537: 259–266.
32. Zanella R, Prestes OD, Friggi CA, Martins ML, Adaime MB. Modern sample preparation methods for pesticide multiresidue determination in foods of animal origin by chromatographic-mass spectrometric techniques. In: Jokanovic M, editor. *The Impact of Pesticides*. Cheyenne: Academy Publishing; 2012. pp. 355–379.
33. Koesukwiwat U, Sanguankaew K, Leepipatpiboon N. Rapid determination of phenoxy acid residues in rice by modified QuEChERS extraction and liquid chromatography-tandem mass spectrometry. *Anal Chim Acta* 2008; 626: 10–20. doi: [10.1016/j.aca.2008.07.034](#) PMID: [18761116](#)
34. Shi X, Jin F, Huang Y, Du X, Li C, Wang M. et al. Simultaneous determination of five plant growth regulators in fruits by modified quick, easy, cheap, effective, rugged, and safe (QuEChERS) extraction and liquid chromatography-tandem mass spectrometry. *J Agric Food Chem*. 2012; 60: 60–65. doi: [10.1021/jf204183d](#) PMID: [22148585](#)
35. Tarkowská D, Novák O, Floková K, Tarkowski P, Turečková V, Grúz J, et al. Quo vadis plant hormone analysis? *Planta* 2014; 240: 55–76. doi: [10.1007/s00425-014-2063-9](#) PMID: [24677098](#)
36. Hotton SK, Eigenheer RA, Castro MF, Bostick M, Callis J. AXR1-ECR1 and AXL1-ECR1 heterodimeric RUB-activating enzymes diverge in function in *Arabidopsis thaliana*. *Plant Mol Biol*. 2011; 75: 515–526. doi: [10.1007/s11103-011-9750-8](#) PMID: [21311953](#)
37. Ulmasov T, Murfet J, Hagen G, Guilfoyle TJ. Aux/IAA proteins repress expression of reporter genes containing natural and highly active synthetic auxin response elements. *Plant Cell* 1997; 9: 1963–1971. PMID: [9401121](#)
38. Fránek M, Kolar V, Granatova M, Nevorankova Z. Monoclonal ELISA for 2,4-dichlorophenoxyacetic acid, Characterization of antibodies and assay optimization. *J Agric Food Chem*. 1994; 42: 1369–1374.
39. Roččík J, Lenobel R, Siglerova V, Strnad M. Isolation of melatonin by immunoaffinity chromatography. *J Chromatogr B* 2002; 775: 9–15.
40. Moon J, Zhao Y, Dai X, Zhang W, Gray WM, Huq E, et al. A new CULLIN 1 mutant has altered responses to hormones and light in *Arabidopsis*. *Plant Physiol*. 2007; 143: 684–696. PMID: [17158585](#)
41. Hennion MC, Pichon V. Immuno-based sample preparation for trace analysis. *J Chromatogr A* 2003; 1000: 29–52. PMID: [12877165](#)
42. Kenny DJ, Worthington KR, Hoyes JB. Scanwave: A new approach to enhancing spectral data on a tandem quadrupole mass spectrometer. *J Am Soc Mass Spectrom*. 2010; 21: 1061–1069. doi: [10.1016/j.jasms.2010.02.017](#) PMID: [20304673](#)
43. Hangarter RP, Peterson MD, Good NE. Biological activities of indoleacetyl amino acids and their use as auxins in tissue culture. *Plant Physiol*. 1980; 65: 761–767. PMID: [16661279](#)
44. De Rybel B, Audenaert D, Beeckman T, Kepinski S. The past, present, and future of chemical biology in auxin research. *ACS Chem Biol*. 2009; 4: 987–998. doi: [10.1021/cb9001624](#) PMID: [19736989](#)
45. Feung CS, Hamilton RH, Witham FH, Mumma RO. The relative amounts and identification of some 2,4-dichlorophenoxyacetic acid metabolites isolated from soybean cotyledon callus cultures. *Plant Physiol*. 1972; 50: 80–86. PMID: [16658138](#)

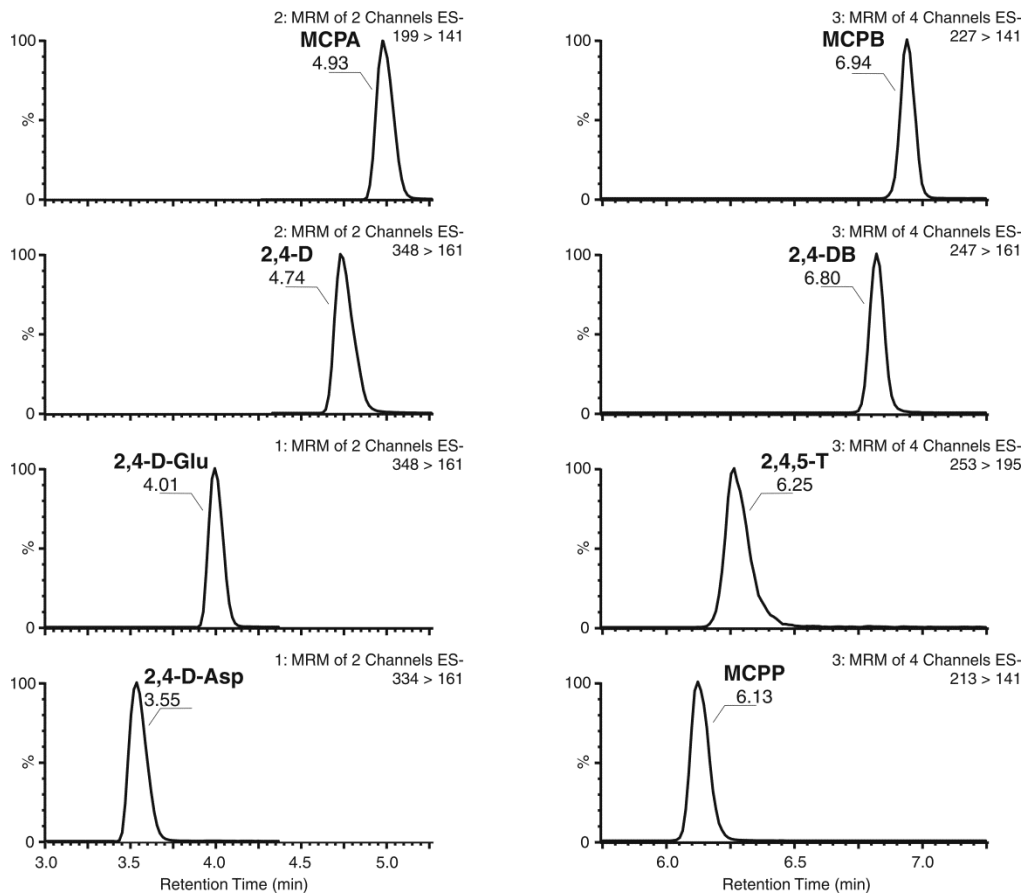
46. Tam YY, Epstein E, Normanly J. Characterization of auxin conjugates in *Arabidopsis*. Low steady-state levels of indole-9-acetyl-aspartate, indole-3-acetyl-glutamate and indole-3-acetyl-glucose. *Plant Physiol.* 2000; 123: 589–595. PMID: [10859188](#)
47. Bandurski RS, Cohen JD, Slovín JP, Reinecke DM. Auxin biosynthesis and metabolism. In: Davies PJ, editor. *Plant Hormones: Physiology, Biochemistry and Molecular Biology*. Dordrecht: Kluwer Academic Publishers; 1995. pp. 39–65.
48. Smulders MJM, van de Ven ETWM, Croes AF, Wullems GJ. Metabolism of 1-naphthaleneacetic acid in explants of tobacco: Evidence for release of free hormone from conjugates. *J Plant Growth Regul.* 1990; 9: 27–34.
49. Stepanova AN, Yun J, Robles LM, Novak O, He W, Guo H, et al. The *Arabidopsis* YUCCA1 flavin monooxygenase functions in the indole-3-pyruvic acid branch of auxin biosynthesis. *Plant Cell* 2011; 23: 3961–3973. doi: [10.1105/tpc.111.088047](#) PMID: [22108406](#)
50. Cohen JD, Bandurski RS. Chemistry and physiology of the bound auxins. *Annu Rev Plant Physiol.* 1982; 33: 403–430.
51. Feung CS, Loerch SL, Hamilton RH, Mumma RO. Metabolism of 2,4-dichlorophenoxyacetic acid. VI. Biological properties of amino acid conjugates. *J Agric Food Chem.* 1974; 22: 307–309. PMID: [4857862](#)
52. Ludwig-Müller J. Auxin conjugates: their role for plant development and in the evolution of land plants. *J Exp Bot.* 2011; 62: 1757–1773. doi: [10.1093/jxb/erq412](#) PMID: [21307383](#)
53. Westfall CS, Herrmann J, Chen Q, Wang S, Jez JM. Modulating plant hormones by enzyme action: the GH3 family of acyl acid amido synthetases. *Plant Signal Behav.* 2010; 5: 1607–1612. PMID: [21150301](#)
54. Peat TS, Bottcher C, Newman J, Lucent D, Cowieson N, Davies C. Crystal structure of an indole-3-acetic acid amido synthetase from grapevine involved in auxin homeostasis. *Plant Cell* 2012; 24: 4525–4538. doi: [10.1105/tpc.112.102921](#) PMID: [23136372](#)
55. Delbarre A, Muller P, Imhoff V, Guern J. Comparison of mechanisms controlling uptake and accumulation of 2,4-dichlorophenoxy acetic acid, naphthalene-1-acetic acid, and indole-3-acetic acid in suspension-cultured tobacco cells. *Planta* 1996; 198: 532–541.
56. Dobrev PI, Havlíček L, Vágner M, Malbeck J, Kamínek M. Purification and determination of plant hormones auxin and abscisic acid using solid phase extraction and two-dimensional high performance liquid chromatography. *J Chromatogr A* 2005; 1075: 159–166. PMID: [15974129](#)
57. Hradecká V, Novák O, Havlíček L, Strnad M. Immunoaffinity chromatography of abscisic acid combined with electrospray liquid chromatography-mass spectrometry. *J Chromatogr B* 2007; 847: 162–173.
58. Liang Y, Zhu X, Zhao M, Liu H. Sensitive quantification of isoprenoid cytokinins in plants by selective immunoaffinity purification and high performance liquid chromatography-quadrupole-time of flight mass spectrometry. *Methods* 2012; 56: 174–179. doi: [10.1016/j.ymeth.2011.08.006](#) PMID: [21867755](#)
59. Vijayaraghavan SJ, Pengelly WL. Bound auxin metabolism in cultured crown-gall tissues of tobacco. *Plant Physiol.* 1986; 80: 315–321. PMID: [16664620](#)
60. Kazemie M, Klämbt D. Studies on the uptake of naphthalene-1-acetic acid and its aspartic acid conjugate into wheat coleoptile tissue. *Planta* 1969; 89: 76–81. doi: [10.1007/BF00386497](#) PMID: [24504352](#)
61. LeClere S, Tellez R, Rampey RA, Matsuda SPT, Bartel B. (2002) Characterization of a family of IAA-amino acid conjugate hydrolases from *Arabidopsis*. *J Biol Chem.* 2002; 277: 20446–20452. PMID: [11923288](#)
62. Sauer M, Kleine-Vehn J. AUXIN BINDING PROTEIN1: The Outsider. *Plant Cell* 2011; 23: 2033–2043. doi: [10.1105/tpc.111.087064](#) PMID: [21719690](#)
63. Gao Y, Zhang Y, Zhang D, Dai X, Etelle M, Zhao Y. Auxin binding protein 1 (ABP1) is not required for either auxin signaling or *Arabidopsis* development. *Proc Natl Aca Sci U S A.* 2015; 112: 2275–2280.



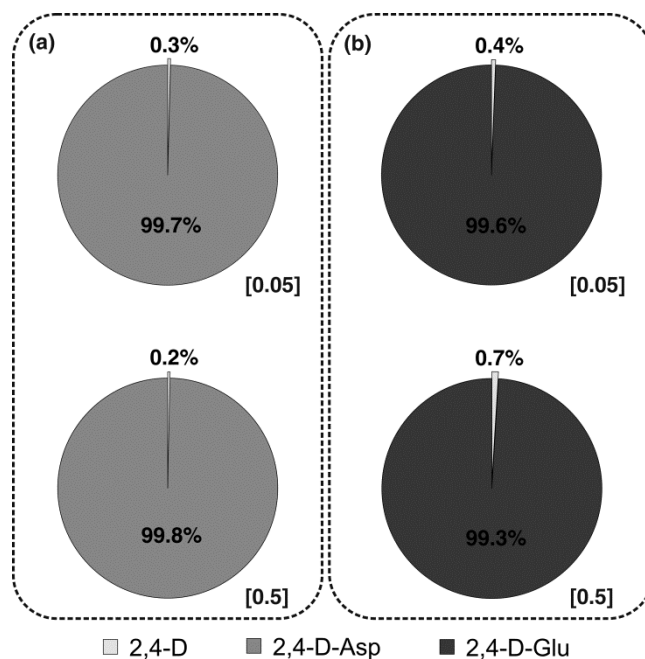
S1 Fig. Scheme of sample preparation process for 2,4-D and its metabolite/structural analogue determination using the ion-exchange and class-specific sorbents in two-step purification protocol. Plant material (20 mg FW) was extracted using 50mM Na-phosphate buffer (pH 7.0) with stable isotope-labelled standards. The extracts were purified using the mixed-mode Oasis® MAX cartridges (1 ml/30 mg). The eluates were evaporated, then reconstituted and repeatedly applied onto immunoaffinity chromatography (IAC) columns. The immunoaffinity gel was subsequently washed and the bound 2,4-D metabolites were eluted by 3ml 100% methanol. All obtained fractions were evaporated to dryness, stored at -20°C until UHPLC-ESI(-)-MS/MS analysis (10 µl of sample injected).



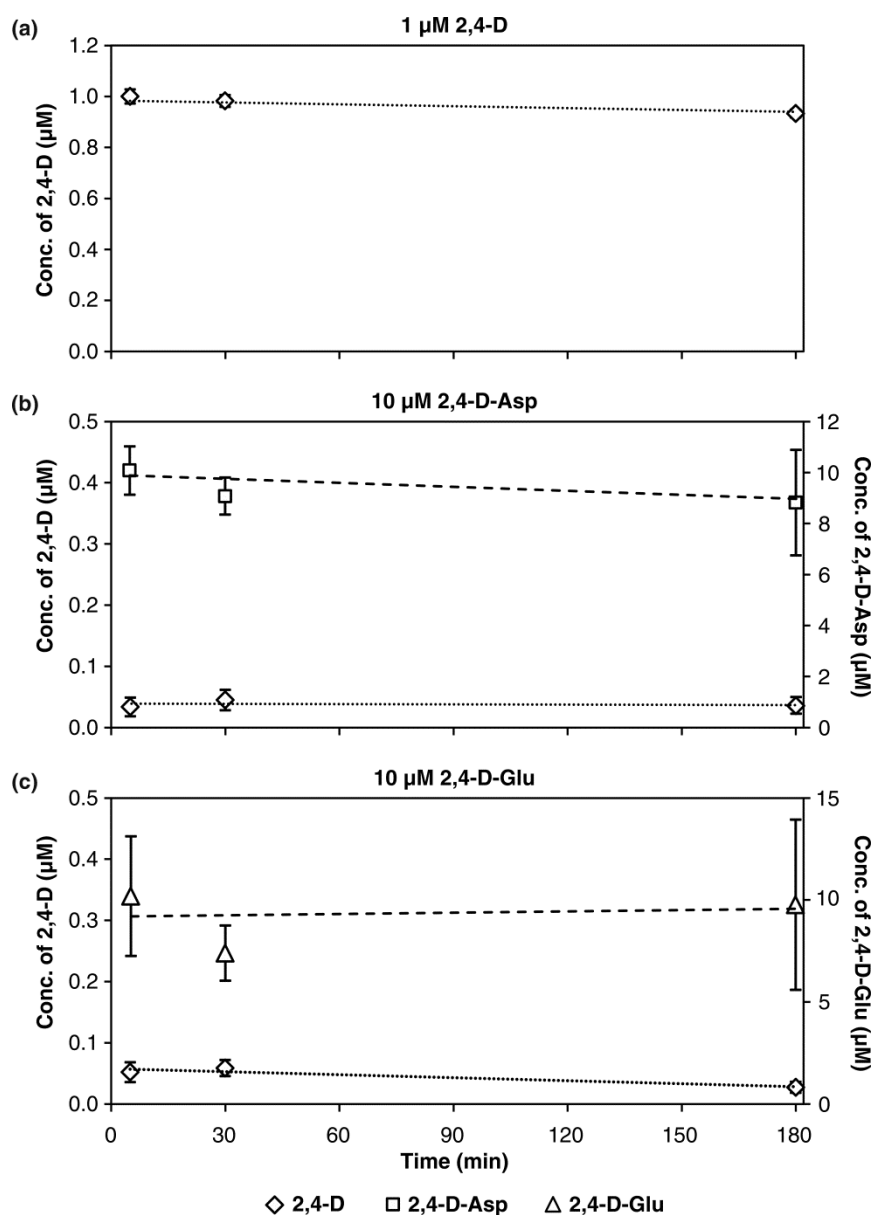
S2 Fig. Capacity of the immunoaffinity gel (IAG) with immobilized E2/G2 antibodies presented as analyte recoveries observed in tests with 0.05–1 nmol of 2,4-D. Solution of 2,4-D with concentrations ranging from 1 to 1000 pmol in methanol:PBS buffer (5:95, v/v) were applied onto 0.5 ml of IAG. The eluates were evaporated to dryness, dissolved in 50 μ L of 35% methanol and analysed by UHPLC-ESI(-)-MS/MS (10 μ L of sample injected). Each spiking level was then determined, compared with the concentration of appropriate standard solution and the recoveries were calculated.



S3 Fig. Chromatographic separation of 2,4-D and its metabolites/structural analogues by UHPLC-(ESI)-MS/MS. The figure shows the MRM chromatograms of 8 analytes represented by 10 pmol of each compound per injection using an Acquity UPLC[®] CSH[™] C18 (2.1x100 mm, 1.7 μ m) column.



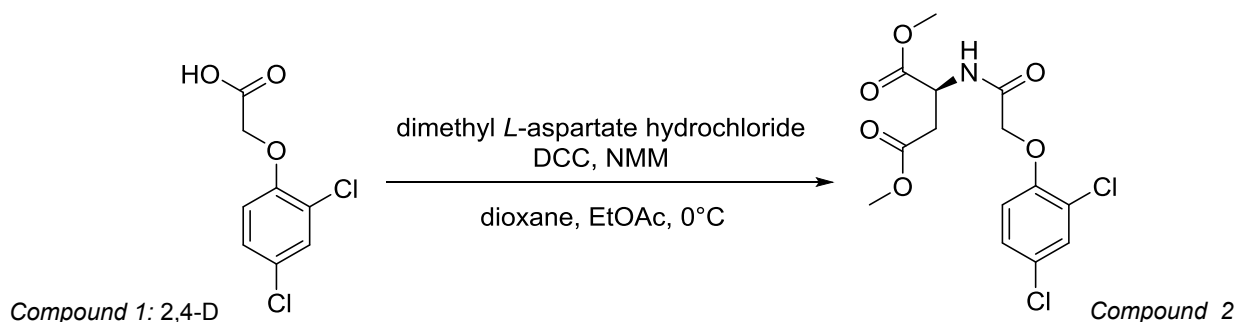
S4 Fig. One-week stability of 2,4-D-amino acid conjugates in growth media. Solid media (half-strength Murashige and Skoog, sucrose 1%, agar 0.7%, pH 5.7) supplemented with 2,4-D-Asp (a) and 2,4-D-Glu (b) at the indicated final concentrations (0.05 μ M and 0.5 μ M) were transferred to microcentrifuge tubes. After 7 days of incubation in the growth chamber (16/8 h of light/dark, 23°C), the media (200 μ l) were melted in a microwave oven, diluted by a factor of 10, purified by the newly developed two-step purification procedure prior to the UHPLC-ESI(-)-MS/MS analysis and distribution (%) of free 2,4-D were calculated.



S5 Fig. Stability of 2,4-D, 2,4-D-Asp and 2,4-D-Glu in short-term chemical treatments. Solid media (half-strength Murashige and Skoog, sucrose 1%, agar 0.7%, pH 5.7) were treated with 2,4-D and 2,4-D-Asp/2,4-D-Glu at the final concentrations 1 μM and 10 μM , respectively, and transferred to microcentrifuge tubes. After 5 min, 30 min and 3 hours of incubation in the growth chamber (16/8 h of light/dark, 23°C), the media (200 μl) were melted in a microwave oven, diluted by a factor of 10 and analyzed by the UHPLC-ESI(-)-MS/MS. The concentration for all metabolites is in pmol g^{-1} FW. Samples were analyzed in four independent biological replicates, and error bars represent the SD. Statistical analysis was performed using ANOVA & comparison of means (Tukey's test) and showed no significant differences in means.

S1 Table. Preparation scheme and structural characteristics of 2,4-D-Asp. The purity of the synthesized compounds was confirmed by high performance liquid chromatography-liquid chromatography-diode array detection (Gold System, Beckman, Switzerland). The elemental composition of the prepared compounds was confirmed by HPLC-(ESI+)-HRMS (Q-TOF micro™ Waters MS Technologies, UK). Accurate masses were calculated and used for the determination of the elemental composition of the analytes with fidelity better than 3 ppm. NMR spectra were recorded on a JEOL ECA-500 spectrometer operating at frequencies of 500 MHz (¹H) and 125 MHz (¹³C) and on a Bruker Avance 300 spectrometer with frequencies of 300 (¹H) and 75 MHz (¹³C). Tetramethylsilane (TMS) was used as the internal standard.

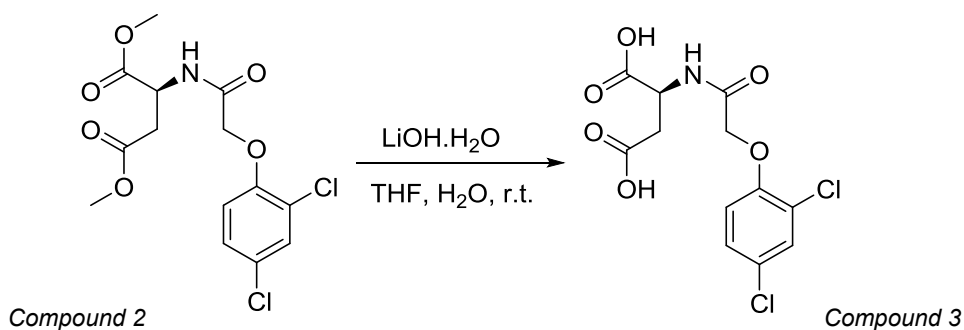
Scheme 1



Compound 2: (S)-Dimethyl-2-(((2,4-dichlorophenoxy)acetyl)amino)butanedioate (obtained in 94 % yield)

¹H-NMR (500 Hz, CDCl₃, δ): 7.75 (1H, d, J = 7.95 Hz, N-H), 7.40 (1H, d, J = 2.45 Hz, H-3'), 7.20 (1H, dd, J = 9.17 Hz, J = 2.45 Hz, H-5'), 6.82 (1H, d, J = 9.17 Hz, H-6'), 4.94 (1H, dt, J = 8.56 Hz, J = 4.28 Hz, H-2), 4.54-4.50 (2H, m, CH₂-O), 3.76 (3H, s, CH₃-O), 3.67 (3H, s, CH₃-O), 3.09 (1H, dd, J = 17.12 Hz, J = 4.28 Hz, H-1a), 2.87 (1H, dd, J = 17.12 Hz, J = 4.28, H-1b).

Scheme 2



Compound 3: (2-((2,4-dichlorophenoxy)acetyl)-L-aspartic acid (obtained in 32 % yield)

¹H-NMR (500 Hz, DMSO-*d*₆, δ): 12.95 (2H, bs, CO₂H), 8.25 (1H, d, J = 7.95 Hz, N-H), 7.59 (1H, d, J = 2.45 Hz, H-3'), 7.33 (1H, dd, J = 9.17 Hz, J = 2.45 Hz, H-5'), 7.06 (1H, d, J = 9.17 Hz, H-6'), 4.66 (2H, s, CH₂-O), 4.58-4.54 (1H, m, H-2), 2.72-2.64 (2H, m, H-3).

¹³C-NMR (125 Hz, DMSO-*d*₆, δ): 172.4 (CO₂H), 172.3 (CO₂H), 167.2 (C-NH), 152.7 (C-1'), 129.7 (CH-3'), 128.3 (CH-5'), 125.8 (C-4'), 123.0 (C-1'), 115.9 (C-6'), 68.0 (CH₂-O), 48.5 (CH-2), 36.3 (CH₂-1).

HRMS: (ESI-), [M-H]⁻, *m/z* 333.9890 (C₁₂H₁₀NO₆Cl₂, Δ 1.5 ppm).

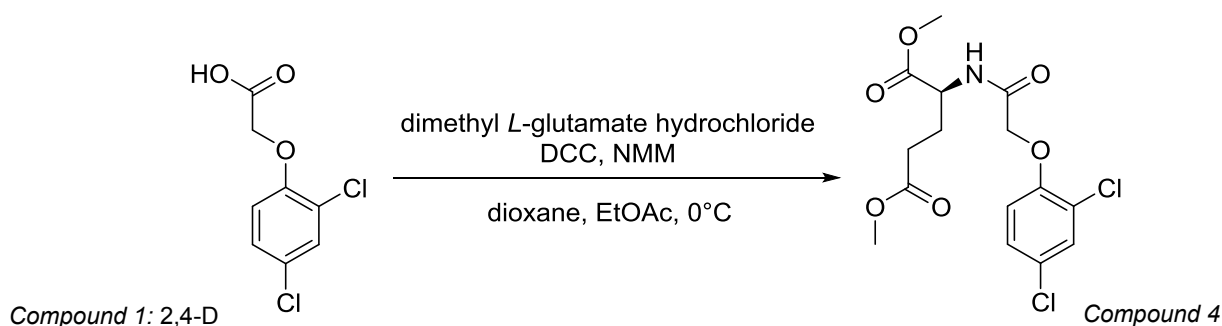
²⁴α_D = 15.3° (in H₂O + NaOH (2.2 equiv., c = 0.5 g/100ml))

Structural characteristics of ¹³C,¹⁵N-2,4D-L-aspartic acid

¹H-NMR (500 Hz, DMSO-*d*₆, δ): 12.90 (2H, bs, CO₂H), 8.29 (1H, ddd, J = 92.6 Hz, J = 8.2 Hz, J = 3.6 Hz, N-H), 7.60 (1H, d, J = 2.4 Hz, H-3'), 7.33 (1H, dd, J = 8.9 Hz, J = 2.4 Hz, H-5'), 7.06 (1H, d, J = 8.9 Hz, H-6'), 4.66 (2H, dd, J = 147.6 Hz, J = 3.7 Hz, CH₂-O), 4.62 (1H, bs, H-2), 2.71 (2H, bs, H-3).

S2 Table. Preparation scheme and structural characteristics of 2,4-D-Glu. The purity of the synthesized compounds was confirmed by high performance liquid chromatography-liquid chromatography-diode array detection (Gold System, Beckman, Switzerland). The elemental composition of the prepared compounds was confirmed by HPLC-(ESI+)-HRMS (Q-TOF micro™ Waters MS Technologies, UK). Accurate masses were calculated and used for the determination of the elemental composition of the analytes with fidelity better than 3 ppm. NMR spectra were recorded on a JEOL ECA-500 spectrometer operating at frequencies of 500 MHz (¹H) and 125 MHz (¹³C) and on a Bruker Avance 300 spectrometer with frequencies of 300 (¹H) and 75 MHz (¹³C). Tetramethylsilane (TMS) was used as the internal standard.

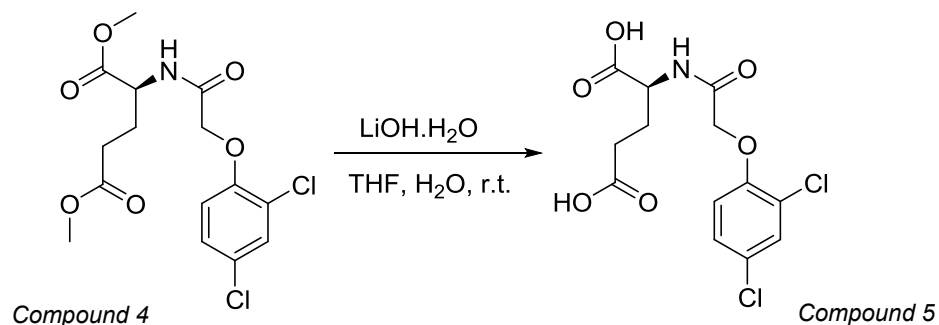
Scheme 3



Compound 4: (S)-Dimethyl-2-((2,4-dichlorophenoxy)acetyl)amino)pentanedioate (obtained in 95 % yield)

¹H-NMR (500 Hz, CDCl₃, δ): 7.41 (1H, d, *J* = 2.45 Hz, H-3'), 7.39 (1H, bs, N-H), 7.21 (1H, dd, *J* = 8.56 Hz, *J* = 2.45 Hz, H-5'), 6.83 (1H, d, *J* = 8.5 Hz, H-6'), 4.72 (1H, dt, *J* = 7.95 Hz, *J* = 5.50 Hz, H-2), 4.56-4.48 (2H, m, CH₂-O), 3.76 (3H, s, CH₃-O), 3.65 (3H, s, CH₃-O), 2.43-2.25 (3H, m, H-4, H-3), 2.10-2.04 (1H, m, H-3).

Scheme 4



Compound 5: (2-((2,4-dichlorophenoxy)acetyl)-L-glutamic acid (obtained in 30 % yield)

¹H-NMR (500 Hz, DMSO-*d*₆, δ): 12.50 (2H, bs, CO₂H), 8.27 (1H, d, *J* = 7.34 Hz, N-H), 7.58 (1H, d, *J* = 3.06 Hz, H-3'), 7.32 (1H, dd, *J* = 8.56 Hz, *J* = 2.45 Hz, H-5'), 7.04 (1H, d, *J* = 9.17 Hz, H-6'), 4.63-4.67 (2H, m, CH₂-O), 4.27-4.23 (1H, m, H-2), 2.25 (2H, t, *J* = 7.34 Hz, H-4), 1.99-1.95 (1H, m, H-3), 1.84-1.80 (1H, m, H-3).

¹³C-NMR (125 Hz, DMSO-*d*₆, δ): 174.3 (CO₂H), 173.3 (CO₂H), 167.4 (C-NH), 152.9 (C-1'), 129.8 (C-3'), 128.4 (C-5'), 125.5 (C-4'), 122.9 (C-2'), 115.8 (C-6'), 67.9 (CH₂-O), 51.6 (CH-2), 30.6 (CH₂-4), 26.9 (CH₂-3).

HRMS: (ESI⁻), [M-H]⁻, *m/z* 348.0037 (C₁₃H₁₂NO₆Cl₂, Δ -1.4 ppm).

²⁴α_D = 12.8° (in H₂O + NaOH (2.2 equiv., *c* = 0.5 g/100ml))

Structural characteristics of ¹³C₂, ¹⁵N-2,4D-L-glutamic acid

¹H-NMR (500 Hz, DMSO-*d*₆, δ): 12.60 (2H, bs, CO₂H), 8.29 (1H, bd, *J* = 91.7 Hz, N-H), 7.59 (1H, s, H-3'), 7.33 (1H, d, *J* = 8.9 Hz, H-5'), 7.03 (1H, d, *J* = 8.9 Hz, H-6'), 4.68 (2H, dd, *J* = 147.9 Hz, *J* = 9.7 Hz, CH₂-O), 4.28 (1H, bs, H-2), 2.26 (2H, t, *J* = 7.3 Hz, H-4), 2.02 (1H, bs, H-3α), 1.82 (1H, bs, H-3β).

S3 Table. Optimized UHPLC-(ESI-)-MS/MS parameters. The precursor and product ions of the studied compounds (MRM transition) and optimized cone/collision energies are listed for each analyte. The retention time stability, limits of detection, dynamic linear range, method linearity (correlation coefficients, R^2) are shown for UHPLC-ESI(-)-MS/MS analysis. The settings of the mass spectrometer in negative electrospray (ESI-) mode were as follows: Capillary Coltage, 3.0 kV; Cone Voltage, 21-30 V; Collision Energy, 10-22 eV; Low/High Resolutions, 3.0/15.0; Desolvation/Source Temperatures, 120/550°C. The gas flows were set to 0.21 ml/min of collision gas (Argon), 1000 l/h of desolvation gas and 70 l/h of cone gas (Nitrogen).

Compound	MRM transition	Cone Voltage [V]	Collision Energy [eV]	Retention time ^a [min]	LOD ^b [fmol]	Linear range [pmol]	R^2
2,4-D	219 > 161	21	10	4.742 ± 0.009	23	0.05–250	0.9995
[²H₅]-2,4-D	224 > 164						
2,4-D-Asp	334 > 161	30	22	3.551 ± 0.011	20	0.05–250	0.9991
[¹³C₂, ¹⁵N]-2,4-D-Asp	337 > 161						
2,4-D-Glu	348 > 161	25	22	4.014 ± 0.006	19	0.05–250	0.9989
[¹³C₂, ¹⁵N]-2,4-D-Glu	351 > 161						
2,4-DB	247 > 161	17	9	6.801 ± 0.008	19	0.05–250	0.9986
MCPA	199 > 141	15	12	4.932 ± 0.004	14	0.05–250	0.9991
MCPB	227 > 141	18	9	6.941 ± 0.005	15	0.05–250	0.9975
MCPP	213 > 141	20	11	6.134 ± 0.008	10	0.05–250	0.9992
2,4,5-T	253 > 195	20	10	6.251 ± 0.006	150	0.5–250	0.9987

^a Values are means ± SD (n = 10); ^b Lower Limit of Detection (LOD) defined as a signal-to-noise ratio of 3:1.

S4 Table. Characterization of monoclonal antibodies E2/G2 and immunoaffinity gel by 2,4-D structural analogues. Percentage of cross reactivity (CR) was calculated using the equation: $CR(\%) = IC_{50}(2,4-D)/IC_{50}(\text{cross reactant}) \times 100$, where IC_{50} is the concentration of a competitor (cross reactant) resulting in 50% reduction of conjugate binding in direct ELISA system. For characterization of an immunoaffinity gel (IAG) with immobilised E2/G2 antibodies, mixtures of selected 2,4-D structural analogues with concentrations ranging from 1 to 300 pmol were applied onto 0.5 ml of IAG. Each spiking level was then determined by UHPLC-ESI(-)-MS/MS, compared with the concentration of appropriate standard solution and the recoveries were calculated. Values are means \pm SD (n = 3); n.d. = not detected.

Compound	CR (%)	Recovery (%)					
		1 pmol	5 pmol	10 pmol	50 pmol	100 pmol	300 pmol
2,4-D	100.0	91.5 \pm 7.9	75.3 \pm 4.3	69.4 \pm 4.9	59.2 \pm 2.3	47.6 \pm 7.9	32.6 \pm 5.8
4-(2,4-dichlorphenoxy) butyric acid (2,4-DB)	0.2	n.d.	10.5 \pm 3.2	14.7 \pm 1.9	8.7 \pm 0.7	2.5 \pm 0.4	1.0 \pm 0.3
2-methyl-4-chlorphenoxy acetic acid (MCPA)	8.04	32.4 \pm 3.5	23.6 \pm 1.0	15.3 \pm 1.6	13.8 \pm 1.5	4.0 \pm 0.4	1.9 \pm 0.3
4-(2-methyl-4-chlorphenoxy) butyric acid (MCPB)	0.9	n.d.	n.d.	n.d.	n.d.	n.d.	0.6 \pm 0.1
2-(2-methyl-4-chlorphenoxy)propionic acid (MCPB)	<0.2	n.d.	n.d.	n.d.	n.d.	0.3 \pm 0.1	0.2 \pm 0.0
2,4,5-trichlorphenoxyacetic acid (2,4,5-T)	3.8	n.d.	n.d.	11.9 \pm 2.8	9.0 \pm 0.4	2.3 \pm 0.5	1.1 \pm 0.3
2,4-D-methylester (2,4-D-Me)	87.73						
2-chlorphenoxyacetic acid	0.9						
2-methyl-4-chlorphenoxyacetic acid	<0.2						
2-methyl-4,6-dichlorphenoxyacetic acid	<0.2						
2-methyl-6-chlorphenoxyacetic acid	<0.2						
4-chlorphenoxyacetic acid	0.9						
2,3-dichlorphenoxyacetic acid	1.6						
3,4-dichlorphenoxyacetic acid	2.7						
2-(2,4-dichlorphenoxy) propionic acid	0.4						
2,4-dichlorphenol	1.72						
2-methyl-4-chlorphenol	0.5						
2,4-dichloranisole	1.5						
3,4-dimethylphenol	<0.2						
pentachlorphenol	0.5						

S5 Table. Process efficiency and method validation (method precision and accuracy) for the ion-exchange and class-specific purification procedure. Extracts of 15 mg FW *Arabidopsis* leaves were spiked with three different concentrations of authentic standards (Low – 0.5 pmol; Medium – 5 pmol; High – 50 pmol) and known concentration of the appropriate internal labeled standards (10 pmol), purified by two-step isolation using the Oasis® MAX sorbent and the immunoaffinity gel, then directly analyzed by UHPLC-ESI(-)-MS/MS.

Compound	Process Efficiency (%) ^a	Method precision (% RSD) ^b			Method accuracy (% bias) ^b		
		Low	Medium	High	Low	Medium	High
2,4-D	66 ± 17	6.2	1.4	4.6	-3.6	3.3	14.6
2,4-D-Asp	16 ± 6	9.6	3.3	10.6	12.9	1.2	6.0
2,4-D-Glu	28 ± 8	8.2	2.3	7.3	18.3	4.6	-3.8

^a Values are means ± SD (n = 12); ^b All analyses were performed in quadruplicate.

Faculty of Science
Palacký University in Olomouc
Laboratory of Growth Regulators

Barbora Pařízková

BIOLOGICAL ACTIVITY OF NOVEL AUXIN SYNTHETIC DERIVATIVES

P1527 Biology
1501V019 Experimental biology

Summary of the Ph.D. thesis

OLOMOUC
2019

This Ph.D. thesis was carried out in the Laboratory of Growth Regulators & *Centre of the Region Haná for Biotechnological and Agricultural Research* within the framework of internal Ph.D. Study of Experimental Biology, guaranteed by the Laboratory of Growth Regulators, Faculty of Science, Palacký University in Olomouc, between the years 2015-2019.

Ph.D. candidate: **Mgr. Barbora Pařízková**

Supervisor: **doc. Mgr. Ondřej Novák, Ph.D.**
Laboratory of Growth, Faculty of Science of Palacký University & Institute of Experimental Botany of the Czech Academy of Sciences, Olomouc, Czech Republic

Consultant: **Assoc. Prof. Stéphanie Robert, Ph.D.**
Umeå Plant Science Centre, Department of Forest Genetics and Plant Physiology, Swedish University of Agricultural Sciences, Umeå, Sweden

Opponents: **Prof. Eva Benková**
Institute of Science and Technology Austria, Klosterneuburg, Austria

Hélène Robert Boisivon, Ph.D.
Mendel Centre for Genomics and Proteomics of Plant Systems, CEITEC – Central European Institute of Technology, Masaryk University, Brno, Czech Republic

The evaluation of this Ph.D. thesis was written by **Prof. Ing. Miroslav Strnad, CSc. DSc.**, Laboratory of Growth Regulators, Faculty of Science, Palacký University in Olomouc.

The oral defence will take place on **26.8.2019** before the Commission for the Ph.D. thesis of the Study Program Experimental Biology, **room.....**, Šlechtitelů 27, Olomouc – Holic.

The Ph.D. thesis and expert reviews will be available 14 days before the defence in the Study Department of Faculty of Science (Mgr. M. Karásková), Palacký University, 17. listopadu 12, Olomouc.

After the defence, the Ph.D. thesis will be stored in the Library of the Biological Departments of Faculty of Science, Palacký University, Šlechtitelů 27, Olomouc – Holic.

Prof. Ing. Miroslav Strnad, CSc. DSc.
Chairman of the Commission for the Ph.D. thesis,
Study Program Experimental Biology,
Faculty of Science, Palacký University in Olomouc

CONTENT

1. INTRODUCTION	4
2. AIMS AND SCOPEs	5
3. MATERIAL AND METHODS	6
4. SURVEY OF RESULTS	10
4.1. Biological characterization of new fluorescent auxins analogues	10
4.2. Method development for studying the metabolic conversion of synthetic auxin analogues <i>in vivo</i>	11
5. CONCLUSION AND PERSPECTIVES	14
6. REFERENCES.....	15
7. LIST OF AUTHOR'S PUBLICATIONS	16
8. SOUHRN (SUMMARY, IN CZECH).....	19

1. INTRODUCTION

Auxins are a class of plant hormones that control almost all physiological processes leading to proper plant growth and development. Indolyl-3-acetic acid (IAA) is considered as the most important naturally occurring auxin (Simon and Petrášek, 2010). Uneven distribution of auxin within specific tissues regulates organogenesis and plant shape in response to exo- and endogenous stimuli (Friml, 2003). The auxin maxima establishment and maintenance are regulated by the coordination of auxin biosynthesis, metabolism and an active polar transport (Ljung, 2013). Furthermore, a wide array of small synthetic molecules with auxin activities has been produced. Biological activity of compounds such as 2,4-dichlorophenoxyacetic acid (2,4-D) or 1-naphtalene acetic acid (NAA) is concentration dependent and therefore they can be used as growth promoters in tissue cultures or inhibiting herbicides in agriculture (Woodward and Bartel, 2005).

The preparation of auxin synthetic derivatives and the study of their structure-activity relationships (SAR) help to unravel the mechanisms of auxin action. With the knowledge on structural requirements, various auxin analogues can be prepared for specific purposes. For example, selective auxin agonists and antagonists of auxin binding proteins can help to evaluate their role in auxin signalling, biosynthesis or transport (Ma and Robert, 2014). The SAR analysis has been extensively used to generate caged and, more importantly, fluorescently labelled plant hormones (Lace and Prandi, 2016). Coupling of auxin molecule with fluorescent probe provides a powerful tool to visualize auxin distribution in plants in minimal invasive manner. *In vivo* and in real time visualization of the compounds enable the study of the relationship between auxin action and localization in plants with a high spatiotemporal resolution at the tissue, cellular and subcellular levels. Moreover, the evaluation of the chemical stability of auxin derivatives *in planta* is a crucial step of the compound characterization. Development of methods employing sensitive detection techniques such as mass spectrometry enables to estimate the potential metabolic conversion rates of tested compounds. The accurate identification of possible metabolites also helps to unravel the molecular mechanisms behind the mode of action of new auxin analogues.

2. AIMS AND SCOPES

The presented Ph.D. thesis has dealt with the SAR study of newly synthesized auxin analogues. A multidisciplinary approach including chemical genomics, reverse genetics and sensitive mass spectrometry (MS)-based methods helped to unravel the mode of action of prepared analogues. Altogether, this work led to the biological characterization of new fluorescent auxin derivatives and selective auxin agonists and into the new insights of 2,4-D metabolism *in planta*.

The main aims of the work described in this thesis were as follows:

- to review the traditional and novel methods for visualization of auxin distribution *in vivo*,
- to perform biological and chemical-physical characterization of new synthetic auxin derivatives in different auxin-responsive assays to estimate their mode of action,
- to study fluorescent properties, tissue-specific distribution and subcellular localization of new fluorescent auxin analogues by confocal microscopy,
- to develop extraction, purification and detection methods for determination and quantification of fluorescently labelled auxin derivatives, novel auxin selective agonists and 2,4-D together with their potential metabolites using MS-based techniques in order to evaluate the metabolic conversion of the compounds *in planta* with respect to their structure.

3. MATERIAL AND METHODS

Chemicals

- All chromatographic solvents and chemicals for hormonal analysis were of hypergrade purity from Sigma-Aldrich Chemie GmbH (Steinheim, Germany), Merck (Darmstadt, Germany) and Roche Diagnostics (Mannheim, Germany).
- Standards of tested chemicals were obtained from Olchemim Ltd (Olomouc, Czech Republic), Sigma-Aldrich Chemie GmbH (Steinheim, Germany), CDN Isotopes (Quebec, Canada), synthesized at the Department of Chemical Biology and Genetics, Centre of the Region Haná for Biotechnological and Agricultural Research, Palacký University, Olomouc or newly ordered using the Chembridge identification number.

Plant materials and growth conditions

- Seeds of *Arabidopsis thaliana* were typically sown on ½ MS medium (2.2 g/L Murashige and Skoog medium - Duchefa Biochemie, 1% sucrose, 0.05 g/L - morpholinoethanesulfonic acid (Sigma Aldrich); and 0.7% agar - Duchefa Biochemie, pH 5.6), stratified for two days at 4 °C in the dark and then transferred to long-day light conditions (22 °C, 16 h light/8 h dark) for five days. To obtain etiolated seedlings, after two days of stratification and 5 h on light (22°C) plates with seeds were packed into aluminium foil and grown in the dark for three days.
- All the mutant lines used in this work are in Col-0 background and have been described before (among others Brunoud et al., 2012; Dharmasiri et al., 2005; Swarup et al., 2008; Ulmasov et al., 1997).

Methods

Auxin-responsive bioassays

Bioassays used to test the auxin activity of synthetic auxin analogues were modified for respective purposes. Times of treatments, concentrations of tested chemicals or concentrations of IAA, used in combination with studied compounds for testing of anti-auxin activity, may differ. More detailed experimental designs of each experiment are described in research papers attached in Supplement sections as mentioned below in brackets. Typically, the assays were performed as follows:

- *Root growth inhibition assay* – Seedlings of *Arabidopsis* Col-0 were grown in the 24-well plates containing solid ½ MS media in the presence of different concentrations of tested compounds in the long-day light conditions. After five days, the lengths of the primary root were measured.
- *Reverse genetics* – Seeds of *Arabidopsis* mutant lines in signalling, transport or biosynthetic pathways were sown on the vertical square Petri dishes with ½ MS medium supplemented by optimized concentration of tested compound and grown for five days in long-day conditions. After that, the primary root growth and the root phenotype were evaluated.
- *GUS assays* - Five-day-old *Arabidopsis* seedlings of GUS marker were treated with 10 µM compounds for defined periods of time, fixed with ice-cold acetone for 20 min at -20 °C and washed with distilled water. Plants were incubated in GUS buffer (0.1% triton X100; 10 mM EDTA; 0.5 mM potassium ferrocyanide; 0.5 mM potassium ferricyanide in 0.1 M phosphate buffer) containing 2 mM X-GlcA (Duchefa Biochemie) at 37 °C in the dark for 30 min. The staining reaction was stopped using 70 % ethanol for one h and the samples were then mounted in a mixture of chloral hydrate:glycerol:H₂O (8:3:1). GUS expression was evaluated using a light microscopy.
- *DII-Venus* - Five-day-old seedlings of *Arabidopsis* DII-Venus marker line were treated with 10 µM chemicals for short time (from 15 to 45 min), the confocal images of the root tips were acquired and the intensity of the Venus signal in the tips was evaluated.

- *Real-time qPCR of early auxin-responsive genes* – Five-day-old *Arabidopsis* Col-0 seedlings were treated in 12-well plate containing ½ MS liquid medium treated with compounds at defined concentrations. 20 fresh seedlings were pre-treated with the first compound for one h followed by two h of co-treatment with the second compound. Seedlings were harvested into liquid nitrogen and frozen to -80°C. Total RNA was extracted using the RNeasy Plant Mini Kit (QIAGEN), with genomic DNA removed by on-column digestion using RQ1 RNase-Free DNase (Promega). 2µg total RNAs was reverse transcribed to cDNA using Oligo(dT)20 primer (Invitrogen) and SuperScript® IV Reverse Transcriptase (Invitrogen). Real-time qPCR analysis was performed using a LightCycler® 480 SYBR Green I Master (Roche) on a LightCycler® 480 Instrument II real-time PCR machine (Roche).

Confocal microscopy

- Seedlings were typically treated in liquid ½ MS media supplemented by auxin fluorescent analogues at optimized concentration, transferred on microscopic slide glass with a drop of the media containing tested compounds. Confocal images were taken immediately using Zeiss LSM 780 confocal microscope or Confocal laser scanning microscope FV1000 (Olympus). NBD-labelled auxins and Venus fluorescent protein were excited at 488 nm, m-cherry fluorescent protein at 514 nm and cyan fluorescent protein at 458 nm by an Argon multiline laser. Live imaging of distribution of fluorescent compounds were performed using Nikon vertical macroconfocal (AZ-C2 vertical) in vertical square Petri dishes containing ½ MS media supplemented with fluorescent compounds.

Extraction and purification methods

- For quantification of 2,4-D and its metabolites, 15–20 mg fresh weight of treated plant tissues were extracted in 1ml of cold sodium phosphate buffer (50 mM, pH 7.0). The samples were purified by performing solid-phase extraction (SPE) using a mixed mode reversed phase/strong anion exchange column (Oasis® MAX, 1 ml/30 mg, Waters) followed by immunoaffinity chromatography (IAC). Isotopically labelled internal standards of each analyte were added to the samples for final quantification.

- For the quantification of fluorescently labelled analogues of 2,4-D and 2,4-D-derived auxin agonists in *Arabidopsis* roots, an one-step extraction and purification method based on a liquid-liquid extraction (LLE) into water:methanol:hexane (1:1:1) mixture was developed. Isotopically labeled internal standards of each analyte were added to the samples for final quantification.

UHPLC-MS/MS methods

- For the quantitative analysis of all tested compounds, ACQUITY UPLC® I-Class system combined with a triple quadrupole mass spectrometer Xevo™ TQ-S (Waters, Manchester, UK) was used. Quantification was obtained by multiple reaction monitoring (MRM) mode of precursor ions ($[M+H]^+$ or $[M-H]^-$) and the appropriate product ions. Concentrations of all compounds were then calculated by an isotopic dilution method using the stable isotope labelled standards by deuterium and/or ^{13}C .
- For the quantification of 2,4-D and its metabolites, the samples were injected onto a reversed-phase column (Acquity UPLC® BEH C18, 1.7 μ m, 2.1x50 mm; temperature 40°C) and eluted with a linear gradient (0–7 min, 35–65% B; 7–8 min, 100% B; 8–10 min, 35% B) of aqueous 0.1% formic acid (A) and 0.1% formic acid in methanol (B) at a flow-rate of 0.25 ml min⁻¹.
- For the quantification of fluorescently labelled analogues of 2,4-D in *Arabidopsis* roots, the samples were injected onto a reversed-phase column (Kinetex™ C18 100A, 50 x 2.1 mm, 1.7 μ m; Phenomenex, Torrance, USA) and eluted with a linear gradient 10:90 to 95:5 A:B using 0.1% acetic acid in methanol (A) and 0.1% acetic acid in water (B) as mobile phases at a flow rate of 0.5 ml min⁻¹ and column temperature of 40 °C. At the end of the gradient, the column was washed with 95% methanol (0.5 min), and re-equilibrate to initial conditions (1.0 min).

4. SURVEY OF RESULTS

Since the precise regulation of auxin distribution is crucial for the proper plant growth and development, a plethora of approaches to visualize auxin transport sites with particular advantages and limits have been developed and reviewed in *Pařízková et al. (2017)*. For this purpose, two groups of synthetic fluorescently labelled auxin analogues derived from IAA (*Bieleszová et al., 2018*) and 2,4-D (*Pařízková et al., unpublished*) were prepared in the Department of Chemical Biology and Genetics (Centre of the Region Haná for Biotechnological and Agricultural Research, Faculty of Science, Palacký University in Olomouc) and characterized in cooperation with Department of Forest Genetics and Plant Physiology of the Swedish University of Agricultural Sciences (SLU) with the Umeå Plant Science Centre (UPSC). Moreover, sensitive LC/MS-based methods were developed to precisely evaluate the stability and metabolic conversion of the fluorescent auxin analogues (*Bieleszová et al., 2018; Pařízková et al., unpublished*), novel auxin selective agonists RubNeddins (RNs) (*Vain, Raggi et al., 2019*) and 2,4-D together with its metabolites (*Eyer et al., 2016*) in plants. Anti-2,4-D monoclonal antibodies (E2/G2) used for efficient isolation of 2,4-D and its analogues from plant matrix were prepared in the Department of Virology, Veterinary Research Institute, Brno.

4.1. Biological characterization of new fluorescent auxins analogues

- The biological activity of four novel fluorescently labelled IAA derivatives differing by the length of the aliphatic linker (C₃ – C₆) between IAA molecule and NBD fluorophore was determined. N1 substitution of the indole ring of IAA was shown not to possess the activity of auxin but *vice versa*, the activity of auxin antagonists, in different auxin bioassays – *Arabidopsis* root growth assay, inhibition effect on auxin-induced root hair formation, DR5::GUS assay and transcription of early auxin-responsive genes. The anti-auxin activity was tightly connected with the length of the linker, making the compound with the longest linker (C₆) the most potent fluorescent anti-auxin. In addition, the length of the linker had a big impact on the fluorescent properties of the

compounds. These characteristics of IAA analogues, such as the fluorescent intensity, fluorescence decay and fluorescence quantum yield, were measured on the Department of Biophysics, Faculty of Science, Palacký University.

All data are summarized in:

Bielešová K., Pařízková B., Kubeš M., Husičková A., Kubala M., Sedlářová M., Doležal K., Strnad M., Novák O., Žukauskaitė A. (2018) New fluorescently labeled auxins exhibit promising anti-auxin activity. N. Biotechnol. 48, 44-52.

- The library of eleven fluorescent auxin analogues derived from five auxin-like compounds in combination with three types of molecular linkers and NBD fluorophore was characterized for biological activity, stability and distribution *in planta*. The screening strategy revealed 2,4-D derivatives (FluorA I and II) as the ones with the best fluorescent and biological properties. However, the evaluation of FluorA metabolization discovered that the biological effect of FluorA compounds is coming from the free 2,4-D released by compound degradation. Importantly, the confocal studies of fluorescent 2,4-D derivatives indicated that distribution of both analogues, aside of simple diffusion, was regulated by active auxin transport system creating the maxima in tissues where the natural auxin is concentrated, such as quiescent centre, concave side of the apical hook or lateral roots and the distribution was affected by exogenous stimuli such as light or gravity. Moreover, the subcellular localization of fluorescent analogues was confirmed in the endosomes and endoplasmic reticulum.

For more detailed information see:

Pařízková B., Žukauskaitė A., Vain T., Grones P., Kubeš M., Kiefferd M., Karel Doležal K., Kepinski S. Napier R., Strnad M., Robert S., Novák O. New auxin fluorescent probes for live imaging of auxin sites of action in plants (in preparation).

4.2. Method development for studying the metabolic conversion of synthetic auxin analogues *in vivo*

- Purification and detection methods were developed for the investigation of metabolism of different auxin structural analogues. Methods based on solid-phase extraction (SPE),

immunoaffinity chromatography (IAC) and liquid-liquid extraction (LLE) together with optimized parameters for liquid chromatography (LC) separation of individual analytes and sensitive tandem mass spectrometry (MS/MS) detection helped to study metabolic conversion and consequent application of auxin derivatives prepared for respective purposes.

- Several purification protocols combining SPE, LLE and/or IAC were tested to efficiently isolate diverse auxin analogues from plant matrix. Rapid one-step purification method using LLE with water:methanol:hexan (1:1:1) mixture as an extraction solvent was chosen during optimization based on its high-throughput, availability and efficiency. The optimized LLE approach was shown to be (with minimal modifications) complex enough for efficient extraction and purification of different organic compounds from plant matrix. Universal LC gradient providing base-line separation of all compounds with sensitive MS/MS detection optimized for each group of derivatives helped to examine the stability characteristics of studied compounds:
 - Fluorescent 2,4-D derivatives FluorA I and II are metabolized *in vivo* to free 2,4-D that provides the auxin response in bioassays.
 - RubNeddins (RNs) are converted *in planta* to corresponding free auxins partially function as prohormones. More detailed dose response analysis of RNs bioactivity coupled with MS quantification of endogenous levels of free auxins released from RN3 and RN4 these RN compounds display different plant response compare to equivalent amount of free 2,4,5-T or RN4-1 respectively. Additional *in vitro* and *in vivo* evidences showed that RN compounds are selective auxin agonists promoting interaction of TIR1 receptor with specific subset of Aux/IAAs.
- Two-step purification protocol employing ion exchange SPE and immuno-specific sorbent based on anti-2,4-D monoclonal antibodies (E2/G2) was combined with a sensitive LC-MS/MS method. Using the target profiling approach, amide-linked metabolites of 2,4-D were detected and identified in 2,4-D treated *Arabidopsis* plants. In addition, the established method helped to unravel that not only the metabolism rates of 2,4-D and IAA, but also metabolisms of their amino acid conjugates (2,4-D-Aspartate and 2,4-D-

Glutamate) are distinct. Whereas 2,4-D appeared more stable compared to IAA with significantly lesser extend of amino acid conjugation, obtained results proposed that amide-linked metabolites of 2,4-D, more pronounced with 2,4-D-Asp, are less stable *in vivo*. Further 2,4-D-Asp can be reversibly converted to free 2,4-D or even secondarily metabolised to 2,4-D-Glu. Moreover, 2,4-D-Glu showed the potency to affect the root growth in *Arabidopsis* via TRANSPORT INHIBITOR RESPONSE1/AUXIN SIGNALING F-BOX (TIR1/AFB) auxin-mediated signalling pathway. Whether the observed auxin effects can be addressed to 2,4-D-Glu itself or to 2,4-D as a hydrolysis product needs to be further investigated.

For more detailed description of experimental design and results see:

Vain T., Raggi S., Ferro N., Kumar Barange D., Kieffer M., Ma Q., Doyle S. M., Thelander M., **Pařízková B.**, Novák O., Ismail A., Enquist P-A., Rigal A., Łangowska M., Harborough S. R., Zhang Y., Ljung K., Callis J., Almqvist F., Kepinski S., Estelle M., Pauwels L., Robert S. (2019) Selective auxin agonists induce specific AUX/IAA protein degradation to modulate plant development. *Proc. Natl. Acad. Sci. USA* **116** (13), 6463–6472.

Pařízková B., Žukauskaitė A., Vain T., Grones P., Kubeš M., Kiefferd M., Karel Doležal K., Kepinski S., Napier R., Strnad M., Robert S., Novák O. New auxin fluorescent probes for live imaging of auxin sites of action in plants (in preparation).

Method development and application of IAC and SPE protocols are described in:

Eyer L., Vain T., Pařízková B., Oklestkova J., Barbez E., Kozubíková H., Pospíšil T., Wierzbicka R., Kleine-Vehn J., Fránek M., Strnad M., Robert S., Novak O. (2016) 2,4-D and IAA Amino Acid Conjugates Show Distinct Metabolism in *Arabidopsis*. *PLoS One* **11** (7), e0159269.

5. CONCLUSION AND PERSPECTIVES

This thesis deals with the characterization of various novel auxin synthetic analogues with respect to their structure so that they can serve as a useful tool for unravelling the mechanisms of auxin physiology. For that reason, such compounds need to be well investigated in term of mode of action, which includes not only evaluation of biological activity but also their metabolism in model systems.

Overall, the most important outcomes of the work are:

- Novel fluorescent derivatives of IAA that display good fluorescent properties and promising anti-auxin activity due the N1 substitution of indole ring, their precise mode of action and distribution need to be studied in more detail.
- Fluorescent analogues of synthetic auxin 2,4-D that are partially metabolized in to free 2,4-D *in planta*. The fluorescent conjugates as such are not active for auxin signalling but display the auxin-like distribution on both tissue and subcellular levels. This distribution is affected in response to exogenous stimuli. The studies of transport mechanisms with focus on the distribution of fluorescent analogues in apical hook are still in progress.
- New purification and detection methods have been developed to evaluate the metabolism of various auxin analogues *in vivo*. They enabled to estimate the stability of FluorA fluorescent 2,4-D-based derivatives and RN auxin agonists in plants as well as helped to uncover the distinct metabolism of 2,4-D and IAA and their respective amino acid conjugates.

In summary, this thesis provides valuable tools for the field of chemical biology in the form of novel auxin synthetic derivatives and techniques how to evaluate their metabolism in plants. The fluorescent auxin analogues with promising biological activity, derivatives mimicking the PAT-driven distribution and selective auxin agonists dissecting different developmental processes, all together with sensitive MS methods to monitor their *in vivo* metabolism represent useful tools for investigation of transport and signalling mechanisms behind plethora of auxin actions.

6. REFERENCES

- Bieleszová K., Pařízková B., Kubeš M., Husičková A., Kubala M., Sedlářová M., Doležal K., Strnad M., Novák O., Žukauskaitė A. (2018) New fluorescently labeled auxins exhibit promising anti-auxin activity. *N. Biotechnol.* **48**, 44-52.
- Brunoud G., Wells D. M., Oliva M., Larrieu A., Mirabet V., Burrow A. H., Beeckman T., Kepinski S., Traas J., Bennett M. J., Vernoux T. (2012) A novel sensor to map auxin response and distribution at high spatio-temporal resolution. *Nature* **482** (7383), 103–106.
- Dharmasiri N., Dharmasiri S., Estelle M. (2005) The F-box protein TIR1 is an auxin receptor. *Nature* **435**, 441–445.
- Eyer L., Vain T., Pařízková B., Okleščková J., Barbez E., Kozubíková H., Pospíšil T., Wierzbicka R., Kleine-Vehn J., Fránek M., Strnad M., Robert S., Novák O. (2016) *PLoS One* **11** (7), e0159269.
- Friml, J. (2003) Auxin transport - shaping the plant. *Curr. Opin. Plant. Biol.* **6**, 7–12.
- Lace B., Prandi C. (2016) Shaping Small Bioactive Molecules to Untangle Their Biological Function: A Focus on Fluorescent Plant Hormones. *Mol Plant.* **9**(8):1099-1118.
- Ljung K. (2013) Auxin metabolism and homeostasis during plant development. *Development* **140**(5):943–950.
- Ma Q., Robert S. (2014) Auxin biology revealed by small molecules. *Physiol. Plant.* **151** (1), 25–42.
- Pařízková B., Pernisová M., Novák O. (2017) What Has Been Seen Cannot Be Unseen—Detecting Auxin *In Vivo*. *Int. J. Mol. Sci.* **18** (12), 2736.
- Pařízková B., Žukauskaitė A., Vain T., Gronos P., Kubeš M., Kiefferd M., Karel Doležal K., Kepinski S., Napier R., Strnad M., Robert S., Novák O. New auxin fluorescent probes for live imaging of auxin sites of action in plants (*in preparation*).
- Simon S., Petrášek J. (2011) Why plants need more than one type of auxin. *Plant Sci.* **180**, 454–460.
- Swarup K., Benková E., Swarup R., Casimiro I., Péret B., Yang Y., Parry G., Nielsen E., De Smet I., Vanneste S., Levesque M. P., Carrier D., James N., Calvo V., Ljung K., Kramer E., Roberts R., Graham N., Marillonnet S., Patel K., Jones J. D., Taylor C. G., Schachtman D. P., May S., Sandberg G., Benfey P., Friml J., Kerr I., Beeckman T., Laplace L., Bennett M. J. (2008) The auxin influx carrier LAX3 promotes lateral root emergence. *Nat Cell Biol.* **10** (8) 946–54.
- Ulmasov T., Murfett J., Hagen G., Guilfoyle T. J. (1997) Aux/IAA Proteins Repress Expression of Reporter Genes Containing Natural and Highly Active Synthetic Auxin Response Elements. *Plant Cell.* **9**, 1963–1971.
- Vain T., Raggi S., Ferro N., Kumar Barange D., Kieffer M., Ma Q., Doyle S. M., Thelander M., Pařízková B., Novák O., Ismail A., Enquist P-A., Rigal A., Łangowska M., Harbrough S. R., Zhang Y., Ljung K., Callis J., Almqvist F., Kepinski S., Estelle M., Pauwels L., Robert S. (2019) Selective auxin agonists induce specific AUX/IAA protein degradation to modulate plant development. *Proc. Natl. Acad. Sci. USA* **116** (13), 6463–6472.
- Woodward A. W., Bartel B. (2005) Auxin: regulation, action, and interaction. *Ann. Bot.* **95**, 707–735.

7. LIST OF AUTHOR'S PUBLICATIONS

Papers published in scientific journals and proceedings

- Eyer L., Vain T., **Pařízková B.**, Oklešťková J., Barbez E., Kozubíková H., Pospíšil T., Wierzbicka R., Kleine-Vehn J., Fránek M., Strnad M., Robert S., Novák O. (2016) 2,4-D and IAA Amino Acid Conjugates Show Distinct Metabolism in *Arabidopsis*. *PLoS One* **11** (7), e0159269.
- Pařízková B., Pernisová M., Novák O. (2017) What Has Been Seen Cannot Be Unseen—Detecting Auxin *In Vivo*. *Int. J. Mol. Sci.* **18** (12), 2736.
- Bielešzová K., Pařízková B., Kubeš M., Husičková A., Kubala M., Sedlářová M., Doležal K., Strnad M., Novák O., Žukauskaitė A. (2018) New fluorescently labeled auxins exhibit promising anti-auxin activity. *N Biotechnol* **48**, 44–52.
- Vain T., Raggi S., Ferro N., Kumar Barange D., Kieffer M., Ma Q., Doyle S. M., Thelander M., **Pařízková B.**, Novák O., Ismail A., Enquist P-A., Rigal A., Łangowska M., Harborough S. R., Zhang Y., Ljung K., Callis J., Almqvist F., Kepinski S., Estelle M., Pauwels L., Robert S. (2019) Selective auxin agonists induce specific AUX/IAA protein degradation to modulate plant development. *Proc. Natl. Acad. Sci. USA* **116** (13), 6463–6472.
- Doyle S. M., Rigal A., Grones P., Karady M., Barange D. K., Majda M., **Pařízková B.**, Karampelias M., Zwiewka M., Pěňčík A., Almqvist F., Ljung K., Novák O., Robert S. (2019) A role for the auxin precursor anthranilic acid in root gravitropism via regulation of PIN-FORMED protein polarity and relocalization in *Arabidopsis*. *New Phytol.* [Epub ahead of print].
- **Pařízková B.**, Žukauskaitė, A., Vain, T., Grones, P., Kubeš, M., Kieffer, M., Doležal, K., Kepinski, S., Strnad, M., Robert, S., Novák, O. (2018) New auxin fluorescent probes for live imaging of auxin sites of action (in preparation).

Published abstracts

- **Pařízková B.**, Oklešťková J., Eyer, L., Fránek M., Strnad M., Novák O. Isolation of 2, 4 – dichlorophenoxyacetic acid and its metabolites by immunoaffinity chromatography from plant tissue. 7th European Plant Science Organisation (EPSO) Conference, Porto Heli, Greece (2013).
- Eyer L., Vain T., **Pařízková B.**, Oklešťková O., Kozubíková H., Fránek M., Strnad M. Robert S., Novák O. Biological activity and quantitative analysis of 2, 4 – dichlorophenoxyacetic

acid and its metabolites *in planta*. Trends in Natural Product Research (TNPR), Olomouc, Czech Republic (2014).

- Eyer L., Vain T., **Pařízková B.**, Oklešťková O., Kozubíková H., Pospíšil T., Fránek M., Strnad M., Robert S., Novák, O. Biological activity and quantitative analysis of 2, 4 – dichlorophenoxyacetic acid and its metabolites *in planta*. Auxin and Cytokinins in Plant Development (ACPD), Prague, Czech Republic (2014).
- **Pařízková B.**, Vain T., Žukauskaitė A., Doležal M., Strnad M., Robert S., Novák O. New tool for unravelling molecular basis of auxin action. Growth Regulators on the way, Malá Morávka, Czech Republic (2016).
- **Pařízková B.**, Vain T., Žukauskaitė A., Doležal K., Strnad M., Robert S., Novák O. New tool for unravelling molecular basis of auxin action. Trends in Natural Product Research (TNPR): A Young Scientists Meeting, Puławy, Poland (2016)
- **Pařízková B.**, Vain T., Žukauskaitė A., Doležal K., Strnad M., Robert S., Novák O. New tool for unravelling molecular basis of auxin action. European Plant Science Organisation (EPSO), Prague, Czech Republic (2016).
- **Pařízková B.**, Vain T., Žukauskaitė A., Kubeš M., Doležal K., Strnad M., Robert S., Novák O. Biological activity and distribution of fluorescently labeled auxin-like compounds. Auxin: Get together in Brno, Czech Republic (2016).
- **Pařízková B.**, Žukauskaitė A., Vain T., Kubeš M., Doležal K., Strnad M., Robert S., Novák O. Determination of metabolization of new fluorescently labeled auxin-like compounds in plant material using UHPLC-MS/MS. Česká chromatografická škola (HPLC 2017), Rožnov p. Radhoštěm, Czech Republic (2017).
- **Pařízková B.**, Žukauskaitė A., Vain T., Kubeš M., Doležal K., Strnad M., Robert S., Novák O. New tool for unravelling molecular basis of auxin action. Chemistry and biology of phytohormones and related substances 2017 (CBPRS), Kouty n. Desnou, Czech Republic (2017).
- **Pařízková B.**, Žukauskaitė A., Vain T., Kubeš M., Doležal K., Strnad M., Robert S., Novák O. New tool for unravelling molecular basis of auxin action. 8th International Symposium on Root Development, Umeå, Sweden (2017).
- **Pařízková B.**, Žukauskaitė A., Vain T., Kubeš M., Doležal K., Strnad M., Robert S., Novák O. Determination of metabolization of new fluorescently labeled auxin-like compounds in plant material using UHPLC-MS/MS. Green for Good 4 (G4G4), Olomouc, Czech Republic (2017).

- **Pařízková B.**, Žukauskaitė A., Vain T., Kubeš M., Doležal K., Strnad M., Robert S., Novák O. New auxin fluorescent probes for live imaging of auxin sites of action. Chemistry and biology of phytohormones and related substances 2018 (CBPRS), Luhačovice, Czech Republic (2018).
- **Pařízková B.**, Žukauskaitė A., Vain T., Grones P., Kubeš M., Kieffer M., Doležal K., Kepinski S., Strnad M., Robert S., Novák O. Biological characterization of new fluorescently labeled auxins. Auxin and Cytokinins in Plant Development (ACPD), Prague, Czech Republic (2018).
- **Pařízková B.**, Žukauskaitė A., Vain T., Grones P., Kubeš M., Kieffer M., Doležal K., Kepinski S., Strnad M., Robert S., Novák O. Determination of metabolization of new fluorescently labeled auxin-like compounds in plant material using UHPLC-MS/MS. XXII International Mass Spectrometry Conference (IMSC), Florence, Italy (2018).
- **Pařízková B.**, Žukauskaitė A., Vain T., Grones P., Kubeš M., Kieffer M., Doležal K., Kepinski S., Strnad M., Robert S., Novák O. Biological characterization of new fluorescently labeled auxins. European Auxin Workshop, Leeds, UK (2018).
- **Pařízková B.**, Žukauskaitė A., Vain T., Grones P., Bielezsová K., Ottová K., Strnad M., Doležal K., Robert S., Novák O. Biological characterization and application of new auxin synthetic derivatives. The Research Centre for Plant Growth and Development (RCPGD) Annual Meeting, Pietermaritzburg, South Africa.
- **Pařízková B.**, Omámková H., Žukauskaitė A., Dzedulionytė K., Strnad M., Novák O., Doležal K. Chiral derivatization and separation of auxinole using automated HPLC purification platform. Česká chromatografická škola (HPLC 2019), Zaječí, Czech Republic (2019).
- **Pařízková B.**, Antoniadi I., Karady M., Poxson D. J., Simon D. T., Petřík I., Strnad M., Novák O., Doležal K., Ljung K. iP & OEiP – a perfect couple to regulate plant development with great specificity. Chemistry and biology of phytohormones and related substances 2018 (CBPRS), Luhačovice, Czech Republic (2019).
- **Pařízková B.**, Antoniadi I., Karady M., Poxson D. J., Simon D. T., Petřík I., Strnad M., Novák O., Doležal K., Ljung K. iP & OEiP – a perfect couple to regulate plant development with great specificity. Green for Good (G4G), Olomouc, Czech Republic (2019).
- **Pařízková B.**, Antoniadi I., Karady M., Poxson D. J., Simon D. T., Petřík I., Strnad M., Novák O., Doležal K., Ljung K. Born to be pumped – cytokinin delivery with high spatial resolution. The International Plant Growth Substances Association (IPGSA) Conference, Paris, France (2019).

8. SOUHRN (SUMMARY, IN CZECH)

Předložená dizertační práce se zabývá studováním biologické aktivity syntetických derivátů auxinů s ohledem na jejich strukturu a současně vývojem citlivých purifikačních a detekčních metod s využitím hmotnostní spektrometrie za účelem studia metabolismu těchto derivátů v rostlinách.

Cílem práce byla biologická charakterizace nových fluorescenčních derivátů odvozených od přirozeného auxinu (indol-3-ylactová kyselina, IAA) a syntetického auxinového analogu (2,4-dichlorofenoxyoctová kyselina, 2,4-D), připravených za účelem vizualizace distribuce auxinů v rostlinách v rámci různých vývojových procesů. Dále byla studována biologická aktivita a látková přeměna nově identifikovaných metabolitů 2,4-D v *Arabidopsis*, konkrétně dvou aminokyselinových konjugátů 2,4-D s kyselinou asparagovou a glutamovou (2,4-D-Asp a 2,4-D-Glu) a nových strukturních analogů 2,4-D působících jako selektivní auxinový agonisté. Za účelem studia metabolismu auxinových derivátů byla vyvinuta purifikační technika na bázi extrakce kapalina-kapalina (LLE), pro studium metabolismu 2,4-D pak purifikace s využitím extrakce na pevné fázi (SPE) v kombinaci s imunoafinitní chromatografií (IAC). Pro všechny skupiny studovaných látek byla optimalizována citlivá detekční metoda využívající propojení kapalinové chromatografie s tandemovou hmotnostní spektrometrií (LC-MS/MS).

Fluorescenční deriváty odvozené od IAA byly připraveny vazbou alifatického molekulárního raménka (linker) s fluorescenční značkou v pozici N1 indolového kruhu. Struktura studovaných derivátů se tak lišila pouze počtem uhlíků, tj. délkou alifatického raménka, od C₃ po C₆. Substituce indolu v N1 pozici překvapivě změnila biologický charakter látek z auxinů na látky vykazující anti-auxinové účinky. Délka linkeru ovlivňovala nejen biologickou aktivitu v různých auxinových biotestech, ale také fyzikálně-chemické vlastnosti studovaných látek. Látka s nejdelším můstkem (C₆) vykazující nejsilnější anti-auxinové účinky a nejlepší fluorescenční vlastnosti byla vybrána pro detailnější studování molekulárních mechanismů jejího účinku.

Na základě SAR analýzy knihovny fluorescenčně značených syntetických auxinů byla vybrána analoga 2,4-D označena NBD fluorescenční próbou prostřednictvím dvou typů můstků jako kandidátní struktury vykazující nejlepší biologické i fluorescenční vlastnosti. Podrobnější studium mechanismu účinku v rámci *in vitro* i *in vivo* experimentů ovšem odhalilo, že fluorescenční analoga jsou v rostlinách metabolizována a biologická odezva je

výsledkem účinku rozpadem vzniklé volné 2,4-D. Naopak tkáňově specifická distribuce fluorescenčních derivátů 2,4-D a jejich redistribuce v rámci odpovědi na exogenní stimuly kopíruje distribuci auxinů přirozených. Mohou tak sloužit jako užitečný nástroj k vizualizaci distribuce auxinů na tkáňové, buněčné i subcelulární úrovni. Apikální háček etiolovaných semenáčků *A. thaliana* byl vybrán jako modelový systém pro detailní studování transportních mechanismů fluorescenčních látek pomocí mutantních linií *Arabidopsis* a chemického ošetření inhibitorů polárního auxinového transportu.

SAR analýza prováděná na signální mutantní linii *A. thaliana axr1-30 (auxin-resistant1)* pomohla také odhalit auxinová strukturní analoga působící jako selektivní auxinový agonisté, tj. látky vyvolávající specifickou interakci mezi konkrétním auxinovým receptorem a inhibitorem exprese auxinových genů Aux/IAA (AUXIN/INDOLE 3-ACETIC ACID INDUCIBLE). Aplikace látky RN4 a následné celogenomové sekvenování mutantních linií *Arabidopsis* rezistentních k účinkům RN4 v rámci vývoje apikálního háčku byla objevena role chromatin remodelující ATPázy BRAHMA (BRM), která hraje významnou úlohu právě v auxinem řízeném procesu tvorby apikálního háčku.

V další části práce byla vyvinuta a validována metoda pro izolaci a kvantifikaci 2,4-D a jejích metabolitů v rostlinné matrici. Tato analýza pomohla identifikovat amino-konjugáty 2,4-D-Asp a 2,4-D-Glu v semenáčcích *Arabidopsis*. Zatímco 2,4-D oproti IAA vykazovala větší metabolickou stabilitu *in vivo*, 2,4-D amino-konjugáty byly v rostlinách méně stabilní a rychle byly konvertovány zpět na volnou 2,4-D, popř. sekundárně v malém rozsahu opět konjugovány s aminokyselinami. 2,4-D-Glu navíc vykazovala auxinovou aktivitu v základních auxinových biotestech prostřednictvím TRANSPORT INHIBITOR RESPONSE1/AUXIN SIGNALING F-BOX (TIR1/AFB) signální dráhy. Zda-li pozorovaná auxinová odezva může být adresována samotnému 2,4-D-Glu konjugátu či volné 2,4-D vzniklé zpětnou konverzí musí být dále studováno.

Předložená práce poskytuje podrobnou charakterizaci nových auxinových analog jakožto užitečných nástrojů chemické biologie společně s novými purifikačními a detekčními metodami, které umožňují studium jejich metabolismu v rostlinách. Fluorescenční deriváty vykazující zajímavé biologické vlastnosti či auxinový profil distribuce, stejně jako selektivní auxinové agonisté umožňující selektivní modulaci vývojových procesů rostlin, představují inovativní přístupy ke studiu molekulárních mechanismů auxinů stojících za jejich širokou škálou fyziologických účinků.